

2015

The Quaternary geomorphological evolution of the River Murray mouth and lakes region, southern Australia

Deirdre Dymphna Ryan
University of Wollongong

Follow this and additional works at: <https://ro.uow.edu.au/theses>

University of Wollongong

Copyright Warning

You may print or download ONE copy of this document for the purpose of your own research or study. The University does not authorise you to copy, communicate or otherwise make available electronically to any other person any copyright material contained on this site.

You are reminded of the following: This work is copyright. Apart from any use permitted under the Copyright Act 1968, no part of this work may be reproduced by any process, nor may any other exclusive right be exercised, without the permission of the author. Copyright owners are entitled to take legal action against persons who infringe their copyright. A reproduction of material that is protected by copyright may be a copyright infringement. A court may impose penalties and award damages in relation to offences and infringements relating to copyright material.

Higher penalties may apply, and higher damages may be awarded, for offences and infringements involving the conversion of material into digital or electronic form.

Unless otherwise indicated, the views expressed in this thesis are those of the author and do not necessarily represent the views of the University of Wollongong.

Recommended Citation

Ryan, Deirdre Dymphna, The Quaternary geomorphological evolution of the River Murray mouth and lakes region, southern Australia, Doctor of Philosophy thesis, School of Earth and Environmental Sciences, University of Wollongong, 2015. <https://ro.uow.edu.au/theses/4539>

UNIVERSITY OF WOLLONGONG

COPYRIGHT WARNING

You may print or download ONE copy of this document for the purpose of your own research or study. The University does not authorise you to copy, communicate or otherwise make available electronically to any other person any copyright material contained on this site. You are reminded of the following:

Copyright owners are entitled to take legal action against persons who infringe their copyright. A reproduction of material that is protected by copyright may be a copyright infringement. A court may impose penalties and award damages in relation to offences and infringements relating to copyright material. Higher penalties may apply, and higher damages may be awarded, for offences and infringements involving the conversion of material into digital or electronic form.

The Quaternary geomorphological evolution of the River Murray mouth and lakes region, southern Australia

A thesis submitted in fulfilment of the requirements of the award of the
degree of

Doctor of Philosophy

from

The University of Wollongong

by

Deirdre Dymphna Ryan

BSc. MSc.

School of Earth and Environmental Sciences

2015

I, Deirdre Ryan, declare that this thesis, submitted in fulfilment of the requirements for the award of Doctor of Philosophy, in the School of Earth and Environmental Sciences, University of Wollongong, is wholly my own work unless otherwise referenced or acknowledged. The document has not been submitted for qualifications at any other academic institution.

Deirdre Ryan

August 2015

Murray Mouth

So this is where it ends at last!

*Half a continent poured out
through the long tide-swept sand –
the snout of bars,
the crunch of wet shells shining,
and at night the swinging stars!*

*No guard of honour from great old trees,
no bustle of ships or wharves,
no city lights, no high bluffs or banks,
not even a nation's thanks.*

*Only the long low beaches on and on,
and in the white sandhills a gap, a smoothness lying,
and a channel, a rip,
a strange wild stir...*

Who would wish it other?

*Alone, unmarred, the spirit of the land
it springs from slips to rest.
Sardonic old saunterer, here at last
Is death and burial in the line of surf –
free as the south wind edged with agate,
no ships or sewers, smoke or smear of oil,
no lumber, roadways or tilled soil...
only a great old river at its end,
silently, unrecognised by light or bell,
swept under the wild hooves of the South
and blessed only by the ponderous pelican's farewell.*

Colin Thiele, 1970



Murray Mouth, South Australia

Abstract

This thesis examines the Quaternary geomorphological evolution of the River Murray Mouth region of southern Australia in the context of increasing aridity and fluctuations in eustatic sea level and climate. The region is located at the northern margin of the Coorong Coastal Plain, which preserves a long terrestrial record of Quaternary sea-level highstands within the Bridgewater Formation, a sedimentary succession of coastal carbonate aeolianites with associated beach and back-barrier lagoon facies. The stratigraphic record within the study area has been obscured by long term regional subsidence due to its location adjacent to the uplifting Mount Lofty Ranges, erosion by the River Murray and the dunefields of siliceous Molineaux Sands deposited under continental conditions during periods of glacially low sea levels. Unravelling the depositional record within this region assists in understanding localised variations in the sea-level record, the position of the River Murray during eustatic sea-level fluctuations and the dichotomy of sedimentary successions between the terrestrial, arid climates of glacial periods and marginal marine, wetter climates of interglacial periods.

The development of the Pleistocene coastline has been extrapolated from the modern beach-barrier-lagoon analogue, following the principle of uniformitarianism. Pleistocene sedimentary successions were recognised by facies architecture and lithology with depositional and diagenetic environments determined through petrographic analyses. The correlation of the sedimentary successions was based on their morphostratigraphic relationships and geochronological analyses using amino acid racemisation, thermoluminescence, optically stimulated luminescence and radiocarbon methods. The results of these analytical techniques were correlated with the Coorong Coastal Plain sea-level highstand record and the oxygen isotope record.

The calcium carbonate content of the Bridgewater Formation aeolianite in the study area is regionally variable and lower than the Coorong Coastal Plain equivalents with consequently higher quartz content. This is attributed to terrestrial sediment input by the River Murray, the quartz-rich character of the offshore shelf environment,

continental siliceous dune development during periods of lowered sea level and the reworking of sediments during sea-level transgressions. Extensive recycling of sediments in the region is reflected in a lack of characteristic features on quartz grains from interglacial and glacial sedimentary successions indicative of depositional environment, the ubiquitous presence of reworked quartz and carbonate skeletal grains throughout interglacial sedimentary successions as revealed by AAR analysis of whole-rock samples and individual foraminifer tests.

This research has revealed an extensive record of Pleistocene deposition, most likely correlating with the earliest recognised deposit of the Bridgewater Formation on the Coorong Coastal Plain. The early Pleistocene barriers are composite features deposited when the orbitally driven cycles of eustatic sea level and climate change transitioned from obliquity (41 ka) to eccentricity (100 ka). The middle Pleistocene record within the study area is best represented by MIS 7 (191-243 ka) aeolianites forming Sturt Peninsula. The remaining middle Pleistocene record is minimal reflecting ongoing rates of subsidence and high potential for erosion in the region, hindering the ability to draw conclusions regarding the height of interglacial sea level. The longest Pleistocene sedimentary succession is found at Point McLeay, a topographic high in the study area since at least MIS 11 (374-424 ka). The last interglacial shoreline (MIS 5e, 130-109 ka) is the best preserved exhibiting regional variability in sedimentary characteristics and preservation as a result of sediment source, environment of deposition, calcrete development and position in the landscape.

The distribution of Bridgewater Formation throughout the Pleistocene and orientation of the coastline has been affected by differential rates of uplift across the Coorong Coastal Plain and dominant longshore drift to the northwest. Both factors have helped to constrain the position of the River Murray to the northern coastal plain where it has been located since its initiation following the demise of Lake Bungunnia. The orientation of the early Pleistocene ranges was also influenced by the granitic basement feature, the Padthaway Ridge. The subsidence in the Murray Mouth has resulted in closely-spaced, onlapping or stacked sedimentary successions of middle to late Pleistocene age that have been subjected to erosion and reworking by the River Murray and Southern Ocean during successive sea-level highstands. The preservation of

interglacial and glacial sedimentary successions reflects the differential rates of uplift in the region, their proximity to the River Murray and the height of successive sea-level highstands which, on the southern Australia coastline, has returned to within 6 m. Sedimentary successions within the region of subsidence are more susceptible to the migration and erosive force of the River Murray and the Southern Ocean during sea-level transgressions. Erosion by the river delivers sediment to the continental shelf which is redistributed within the continental dunefields of siliceous sand during periods of glacially lowered sea level. During sea-level transgressions these dunefields are reworked and the sediment is redelivered to the coastline bringing full circle the sediment recycling characteristic of the region. The low preservation potential of sedimentary successions in the region reaffirms the River Murray Mouth identity as a failed delta.

ACKNOWLEDGEMENTS

First and foremost thanks must go to my supervisors Professor Colin Murray-Wallace, Honorary Professorial Fellow Robert “Bob” Bourman and Associate Professor Brian Jones. It is only with their guidance and many discussions that this work was possible. Thank you Colin for taking me on as a PhD student. Thank you to both Colin and Bob for introducing me to the beautiful and fascinating landscape that is the Coorong Coastal Plain. Thank you Brian for expanding my understanding of the many subdisciplines of geology.

I also must thank Terry Lachlan, AAR and OSL laboratory technician extraordinaire and my “unofficial” supervisor. Terry also provided invaluable guidance and feedback and was kind enough to run my OSL sample. Thank you to Professor Bert Roberts and Dr. Zenobia Jacobs for providing time in the OSL lab for my sample to be run. Many thanks go to David Price for his TL work and morning teas. José Abrantes prepared thin-sections, ran XRD analyses, helped me with SEM analyses and became a great gym buddy. My success in the SAL Laboratory would not have been possible without the assistance of Heidi Brown, Alex Mackcay and Chris Owers. Extra thanks goes to Chris for reading over some of my methodology and the laughs. Thank you Dr. Alan Hogg and Dr. Fiona Petchey from the University of Waikato Radiocarbon Dating Laboratory for conducting radiocarbon analyses.

I’d like to thank Chris Ferguson for helping me to understand some of the finer points of the Terra Australis Orogeny and Solomon Buckman for assistance in interpreting the intricacies of tectonics in the Mount Lofty Ranges. Thank you to Professor Patrick De Deckker for providing sediment samples from the Lacepede Shelf and providing useful feedback. Victor Gostin must also be thanked for helpful feedback and suggestions. I’d also like to express my gratitude to Steve Barnett for showing an interest in my project and providing advice with regards to the drillhole data in the region. Additional thanks to folks at the various government departments of South Australia for providing data and clarifications.

I recognise the Traditional Owners of the region, the Ngarrindjeri Aboriginal people and thank them for access to particular field sites. I am honoured to have been allowed access to these spiritual places. I express my appreciation specifically to the late Tom Trevorrow, Ellen Trevorrow, Clyde Rigney and Daryl Summer.

This work would not be possible without the permission of the following land owners or property managers and I am extremely grateful: the Grundy Family of Mundoo Island, the Irwin Family at Riverside, Annie Lucas, Richard Owen, Barry Hill and Nick Grundy, all on Hindmarsh Island, also Steve at Stratland and Lindy Turner southeast of Lake Albert.

Deserving just as much thanks is the many friends and peers who have been there for laughs and support in the past few years and without whom this experience would not have been the same. Samantha Rowe for the excellent hospitality, laughs and great cooking. The Calera Winery Crew have been the best co-workers I've ever had and given me so many good laughs and memories. The Luis Family of Paso Robles, the Macarthur and Shield Families of Queensland who have taken me in and made me feel like home. The Tuesday Morning Coffee Crew (Florian, Steph, Nathan, Amy, Anna, Brent, Venera, Sarah, Daniela, Tom) and Rafael, Ebbe, and Omar, thank you for all the jocularity and commiseration. I can't wait to catch up with everyone in Illaroy, that wonderful, fantastical place. Additional thanks to Daniela Müller for the fieldwork assistance. You're the best and I hope to return the favour. Extra thanks to Nathan Jankowski, Amy Blakemore, Anna Habeck-Fardy and Sarah Eccleshall who went above and beyond and fantastic people. My non-PhD friends (at UOW at least) Bridget, Julien, Greg, Morgan, Ellen, Kane, Jerom, Laura and Sandy, who have supported me in every which way possible and distracted me when necessary. My housemates, who are my brothers from other mothers, fathers and countries: Jef Pennings and Sebastian Isbanner. Extra special, thanks, love, appreciation and gratitude go to my best girlfriends Nikki Hui, Laila Kerouate and Ellen Kim. You girls have been there from through ups and downs since way before this started and I'm sure long after – let's hope mostly ups.

To my family (Mom, Fiona, Megan and Jake) and extended family (the San Francisco Ryans and the Englanders), thank you for all the support and encouragement. Although I've chosen this adventure in another hemisphere I love and miss you all.

Last but certainly not least, I thank my father James "Jim" Ryan for the unconditional love and support since day one. Words are not enough. You've never once let me down. I love you daddy.

Table of Contents

Abstract.....	i
Acknowledgements.....	v
Table of Contents.....	viii
List of Figures.....	xvii
List of Tables.....	xxiii
List of Equations.....	xxv
Chapter 1: Thesis Introduction.....	1
Chapter 2: Cenozoic Development of the southwestern Murray Basin and Fleurieu Peninsula, southern Australia.....	7
2.1 Introduction.....	7
2.2 Pre-Cenozoic development of southeastern Australia.....	9
2.3 Palaeogene-Neogene development.....	13
2.3.1 Palaeocene-Eocene to Lower Oligocene, 65-34 Ma.....	14
2.3.2 Oligocene through Middle Miocene, 34-11 Ma.....	16
2.3.3 Late Miocene through Pliocene, 11-2.58 Ma.....	18
2.3.4 Neogene tectonics.....	25
2.3.5 The proto-River Murray.....	29
2.4 The Quaternary.....	31
2.4.1 The Quaternary Period.....	32
2.4.2 The Milankovitch Hypothesis.....	33
2.4.3 The oxygen isotope record.....	35
2.4.4 Progression of Quaternary aridity in Australia.....	37
2.5 Murray Basin aridity.....	40
2.5.1 Glacial aeolian landforms.....	41
2.5.2 The glacial River Murray during glacial sea-level lowstands.....	44
2.5.3 Bridgewater Formation: an interglacial aeolian succession.....	47
2.5.3.1 Quaternary sea-level record.....	53

2.5.3.2 The Last Interglacial shoreline: neotectonic and environmental indicator.....	55
2.5.3.3 Murray Lakes record.....	57
2.5.3.4 Discussion.....	60
2.6 Synthesis and Conclusions.....	65
Chapter 3: Physical Environment of the River Murray Lakes Region, Coorong Coastal Plain, South Australia.....	69
3.1 Introduction.....	69
3.2 The Coorong Coastal Plain.....	69
3.3 The Modern shoreline.....	71
3.3.1 The barrier shoreline complex.....	74
3.3.1.1 Barrier development.....	76
3.3.1.2 Murray Mouth location.....	79
3.3.1.3 Barrier sediments.....	80
3.4 The River Murray.....	81
3.5 The Lacepede Shelf.....	81
3.5.1 Macrofacies trend.....	84
3.6 Carbonate Diagenesis.....	87
3.6.1 The sea floor, shallow marine phreatic.....	88
3.6.2 Subaerial exposure, the meteoric zone.....	89
3.6.2.1 Calcrete.....	91
3.6.2.2 <i>Terra rossa</i> soil.....	95
3.7 Lithology of Quaternary Deposits.....	97
3.7.1 St Kilda Formation.....	99
3.7.2 Bridgewater Formation.....	100
3.7.3 Glanville Formation.....	102
3.7.4 Padthaway Formation.....	103
3.7.5 Unnamed Quaternary Dolomite.....	104
3.7.6 Molineaux Sand.....	104

3.7.7 Pooraka Formation.....	104
3.8 Conclusions.....	105
Chapter 4: Stratigraphy and Petrography of the Pleistocene Bridgewater Formation and Holocene successions, River Murray Lakes region, South Australia.....	107
4.1 Introduction.....	107
4.2 Methods of fossil and sediment analysis.....	108
4.2.1 Taphonomic analysis.....	108
4.2.2 Particle size analysis.....	118
4.2.3 Binocular microscope analysis.....	119
4.2.4 Thin section analysis.....	121
4.2.5 X-ray diffraction.....	122
4.2.6 Scanning Electron Microscope.....	122
4.3 Field site descriptions and sedimentary petrography.....	122
4.3.1 Lacepede Shelf.....	122
4.3.1.1 Lacepede Shelf substrate sediments.....	126
4.3.1.2 Discussion.....	132
4.3.2 Early Holocene shoreline.....	132
4.3.2.1 Southern Hindmarsh Island.....	133
4.3.2.2 Discussion.....	139
4.3.3 The Last Interglacial beach-barrier complex.....	140
4.3.3.1 Southeast Lake Albert.....	141
Stratland Field Site.....	141
Sediment Analyses.....	144
Camp Coorong.....	144
Discussion.....	147
4.3.3.2 Hindmarsh Island.....	147
Mundoo Island.....	149
McLeay Road Quarry.....	149

Cheese Factory.....	151
Riverside.....	152
Denver Property.....	153
Discussion.....	159
4.3.3.3 Goolwa.....	160
Goolwa Fossil Assemblages.....	163
Chart House.....	164
Stratco Hardware and Tennis Court.....	169
Goolwa West – MIS 5e aeolianite.....	173
MIS 5c Barrier.....	175
Discussion.....	179
4.3.3.4 Fleurieu Peninsula.....	179
Watson Gap.....	180
Victor Harbor.....	182
Yilki.....	182
Waitpinga.....	184
Discussion.....	185
4.3.3.5 Summary of last interglacial shoreline development.....	185
4.3.4 MIS 7e: Sturt Peninsula, the Alexandrina Coastline.....	187
4.3.4.1 Point Sturt Road and Griffin Road.....	189
4.3.4.2 Clayton Bay Road.....	191
4.3.4.3 Discussion of interpreted MIS 7 sedimentary successions.....	192
4.3.5 Stacked sedimentary successions.....	192
4.3.5.1 Myrtlegrove Road.....	193
4.3.5.2 Knights Beach, Fleurieu Peninsula.....	197
4.3.5.3 Point McLeay, Narrung Peninsula.....	204
4.3.6 Inland locations.....	211
4.3.6.1 Mount Misery.....	212

4.3.6.2 McIntosh Road and Gravel Pit.....	215
4.3.6.3 North Coonalpyn.....	218
4.3.6.4 South Coonalpyn.....	219
4.3.6.5 Emu Springs.....	221
4.3.6.6 Tauragut Well.....	222
4.3.6.7 Carcuma.....	223
4.3.6.8 Tailern Bend.....	224
4.3.6.9 Murray Bridge.....	225
4.3.6.10 Discussion of inland field sites.....	227
4.3.7 Siliceous Sands.....	231
4.3.7.1 Molineaux Sand.....	233
4.3.7.2 Solution pipes, <i>terra rossa</i> and alluvium.....	238
4.3.7.3 Siliceous sands discussion.....	240
4.3.8 Quartz Grains.....	242
4.3.9 Carbonate Grains.....	244
4.3.10 Analysis of drillhole log data within the northern Coorong Coastal Plain.....	245
4.3.11 Conclusions.....	250
Chapter 5: Methodological considerations of Amino Acid Racemisation and its application in dating Pleistocene interglacial sedimentary successions.....	255
5.1 Introduction.....	255
5.2 Amino Acid Racemisation.....	255
5.2.1 The Rate of Racemisation.....	257
5.2.1.1 Hydrolysis.....	258
5.2.1.2 Temperature.....	260
5.2.1.3 Genus-effect.....	263
5.2.1.4 Environmental Factors.....	263
5.2.1.5 Kinetic Models.....	265

5.2.2 Applications of AAR.....	266
5.2.2.1 Resolution of mixed-age populations.....	266
5.2.2.2 Aminostratigraphy.....	267
5.2.2.3 Whole-rock analysis.....	269
5.2.2.4 Numerical age.....	270
5.2.3 AAR analysis method.....	271
5.2.3.1 Sample selection.....	273
5.2.3.2 Sample preparation.....	275
5.2.3.3 Data screening and rejection criteria.....	280
Amino acid abundance.....	280
Serine abundance.....	282
Amino acid covariance.....	282
Analytical uncertainty.....	282
5.3 Complexities of the River Murray Mouth Region.....	285
5.3.1 Low calcium carbonate content.....	285
5.3.2 Carbonate grain origin.....	286
5.4 Summary.....	288
Chapter 6: Geochronological Analysis of the Quaternary sedimentary successions within the River Murray Lakes Region, South Australia.....	291
6.1 Introduction.....	291
6.2 Luminescence techniques.....	291
6.2.1 Luminescence methods used in this research.....	293
6.3 Radiocarbon analysis.....	295
6.3 AAR numerical age determination.....	296
6.4 Results of geochronological analyses in this research.....	298
6.4.1 The Holocene.....	299
6.4.1.1 Holocene shell results.....	299
6.4.1.2 Modern whole-rock results.....	303

6.4.1.3 Modern foraminifers results.....	306
6.4.1.4 Summary.....	308
6.4.2 Siliceous sand deposition.....	309
6.4.3 The Last Interglacial.....	310
6.4.3.1 Depth of Burial.....	311
6.4.3.2 MIS 5e shell record.....	312
6.4.3.3 Late Pleistocene whole-rock and foraminifer.....	315
Southeast Lake Albert.....	315
Hindmarsh Island.....	319
Goolwa.....	321
Fleurieu Peninsula.....	322
Point McLeay.....	323
6.4.3.4 Summary.....	323
6.4.4 Middle to early Pleistocene.....	324
6.4.4.1 MIS 7.....	328
6.4.4.2 Inland sedimentary successions.....	329
6.4.4.3 Summary.....	331
6.4.5 Conclusions.....	333

Chapter 7: Quaternary landscape development of the River Murray terminus, South Australia and correlation to the sea-level record of the Coorong Coastal Plain.....335

7.1 Introduction	335
7.2 Correlating the Bridgewater Formation successions within the Murray Lakes region to the Robe-Naracoorte record.....	336
7.2.1 Early Pleistocene Bridgewater Formation and associated deposits.....	340
7.2.1.1 The Cannonball Hill Range.....	344
7.2.1.2 The Coonalpyn Range.....	345
7.2.1.3 The Murray Lakes Range.....	347
7.2.1.4 The Padthaway Formation and Quaternary dolomite plain.....	350

7.2.1.5 Alluvial fans.....	352
7.2.2 Middle through Late Pleistocene Bridgewater Formation.....	354
7.2.2.1 Point McLeay.....	356
7.2.2.2 Penultimate Interglacial coastline.....	360
7.2.2.3 Last Interglacial coastline.....	363
MIS 5e.....	364
MIS 5c.....	368
7.2.3 Holocene.....	368
7.2.4 Summary.....	369
7.3 Comparison with global interglacial sea-level records.....	371
7.3.1 Early Pleistocene.....	372
7.3.2 Middle and late Pleistocene.....	373
7.3.2.1 Marine Isotope Stage 11.....	374
7.3.2.2 Marine Isotope Stage 9.....	375
7.3.2.3 The Penultimate Interglacial coastline, MIS 7.....	376
7.3.3.3 The Last Interglacial coastline, MIS 5.....	377
7.4 Molineaux Sand deposition.....	379
7.5 The River Murray.....	381
7.6 Conclusions.....	383
7.7 Further Research.....	386
References.....	389
Appendix 1.....	439
Appendix 2.....	443
Appendix 3.....	449
Appendix 4.....	455

List of Figures

Chapter 1: Thesis Introduction

Chapter 2: Cenozoic Development of the southwestern Murray Basin and Fleurieu Peninsula, southern Australia

Figure 2.1: Location of River Murray terminus and depth to Precambrian and Early Palaeozoic bedrock.....	8
Figure 2.2: Structural units controlling the shape and location of the Murray Basin.....	11
Figure 2.3: Distribution of Permian strata beneath the River Murray Lakes region (modified from Gatehouse <i>et al.</i> , 1991) and limits of the Troubridge Basin (modified from Alley and Bourman, 1995).....	12
Figure 2.4: The extent of the Buccleuch Embayment record of Eocene marine transgression.....	15
Figure 2.5: The Loxton-Parilla Sands record of Early Pliocene marine regression from the Murray Basin.....	19
Figure 2.6: Approximate extent of Pliocene mega-lake, Lake Bungunnia.....	22
Figure 2.7: The horst block structure within South Australia with known fault locations.....	27
Figure 2.8: The hierarchy of Quaternary geologic time as defined by the International Commission on Stratigraphy.....	33
Figure 2.9: The orbital rhythms: eccentricity, obliquity and precession.....	34
Figure 2.10: Quaternary oxygen isotope stratigraphy (from Lisiecki and Raymo, 2005).....	39
Figure 2.11 A: Isobaric charts illustrating the approximate 5° latitude shift of westerly winds between the Last Glacial maximum and current Holocene interglacial (modified from Sprigg, 1982b).....	43
Figure 2.11 B: Distribution of aeolian glacial dunes within the Murray Basin.....	46
Figure 2.12: Position of the palaeo-River Murray during periods of lowered sea-level within the Late Quaternary (modified from Hill <i>et al.</i> , 2009).....	46
Figure 2.13: The Bridgewater Formation as mapped in the Portland region of Victoria.....	48
Figure 2.14: The Bridgewater Formation across the Coorong Coastal Plain.....	50

Figure 2.15: Schematic cross-section of the Coorong Coastal Plain with ages of coastal barriers between Robe and Naracoorte shown in relation to the oxygen-isotope record.....54

Figure 2.16: Shoreline elevations of the last interglacial (MIS 5e) coastal deposits in South Australia plotted in relation to their morphotectonics settings (modified from Murray-Wallace, 2002).....56

Figure 2.17: Detail of Quaternary Bridgewater Formation and Molineaux Sands sedimentary successions in the Murray Lakes region.....59

Chapter 3: Physical Environment of the River Murray Lakes Region, Coorong Coastal Plain, southern Australia

Figure 3.1: Location of the River Murray terminus and mouth in the southwestern corner of the Murray Basin.....70

Figure 3.2: Long term temperature and wind data for locations within and surrounding the River Murray Mouth and lakes region.....73

Figure 3.3: Block diagram of the three main geomorphological elements and depositional environments of a barrier shoreline depositional system.....75

Figure 3.4: Holocene barrier evolution along the Coorong Coastal Plain as proposed by Short and Hesp (1984) and modified by Harvey (2006).....77

Figure 3.5: An illustration of the different morphological and neritic environments on the Lacepede shelf (from James and Bone, 2011).....83

Figure 3.6: Major ocean boundary currents and minor currents of the southern Australia continental margin (modified from Murray-Wallace, 2014).....83

Figure 3.7: Sediment megafacies of the Lacepede Shelf and adjacent continental shelf (from James and Bone, 2011).....84

Figure 3.8: The time of deposition for relict, stranded and Holocene carbonate grain assemblages during Late Quaternary sea-level fluctuations (from Rivers *et al.*, 2007)....86

Figure 3.9: Simplified scheme of major diagenetic environments (modified from Flügel, 2010).....88

Figure 3.10: The division of the meteoric zone into the vadose and phreatic zones with the classification of calcretes based upon their hydrological setting within the meteoric environment.....90

Figure 3.11: Calcrete maturity as measured by diagenetic grades reflecting mineralogical, thin-section and relative-age characteristics of the calcrete (from Hearty and O’Leary, 2008).....	93
Figure 3.12: Photograph of solution pipes at Bridgewater Bay (provided by Colin Murray-Wallace, 20 May 2015).....	95
Figure 3.13: Photograph of red <i>terra rossa</i> soil overlying the West Naracoorte Bridgewater Formation (provided by Colin Murray-Wallace, 20 May 2015).....	96
Figure 3.14: Outline of the study area within the Coorong Coastal Plain shown with a chart of stratigraphic units and a rock relation diagram (modified from Rogers, 1979)...	98
Figure 3.15: A representative cross-section of the last interglacial barrier, the Woakwine Range (modified from Belperio <i>et al.</i> , 1995).....	99
 Chapter 4: Stratigraphy and Petrography of the Pleistocene Bridgewater Formation and Holocene successions, River Murray Mouth Region, southern Australia	
Figure 4.1: The study area at the northern margin of the Coorong Coastal Plain with geographic relationship of field sites outlined.....	109
Figure 4.2: Species chosen for AAR analysis due to their common occurrence in fossil assemblages and modern beach deposits.....	117
Figure 4.3: Classification schemes for limestones and mixed siliciclastic and carbonate sediments used in this research.....	121
Figure 4.4: SEM photographs of carbonate grains.....	123
Figure 4.5: Location of vibracore samples on the Lacepede Shelf.....	126
Figure 4.6: Modern shallow substrate sediment samples retrieved from the Lacepede Shelf.....	128
Figure 4.7: Digital Elevation Model of Hindmarsh Island with location of field sites discussed in text.....	134
Figure 4.8: Transect of Hindmarsh Island generated from the DEM in direction of north to south passing through or adjacent to auger holes.....	136
Figure 4.9: Field sites southeast of Lake Albert.....	142
Figure 4.10: Photographs illustrating the variable appearance of deposits within the Lake Albert region.....	143

Figure 4.11: Camp Coorong shell beds.....	146
Figure 4.12: Field sites and locations related to MIS 5e sea-level on Hindmarsh Island.....	148
Figure 4.13: Shell beds at the McLeay Road Quarry on the centre of Hindmarsh Island.....	150
Figure 4.14: The Cheese Factory site faces west with north in the upslope direction....	152
Figure 4.15: Riverside calcretes on northern Hindmarsh Island.....	154
Figure 4.16: Denver Property calcretes on eastern Hindmarsh Island.....	155
Figure 4.17: Photomicrographs of calcrete thin sections from the Denver Property and Riverside Calcrete A.....	158
Figure 4.18: Goolwa Channel region and shell beds.....	161
Figure 4.19: Chart House field site stratigraphy.....	164
Figure 4.20: Tennis Court and Stratco Hardware sediments with photomicrographs....	172
Figure 4.21: Additional field sites west of Goolwa.....	174
Figure 4.22: Features associated with the MIS 5e aeolianite west of Goolwa.....	175
Figure 4.23: Features of the Surfer Beach dune from east to west.....	176
Figure 4.24: Sir Richard Peninsula calcrete inlier and photomicrographs.....	178
Figure 4.25: Fleurieu Peninsula field sites.....	181
Figure 4.26: Photographs of field sites from Fleurieu Peninsula.....	183
Figure 4.27: Field sites associated with MIS 7 interglacial deposition.....	188
Figure 4.28: Photographs from Sturt Peninsula.....	190
Figure 4.29: Myrtlegrove Road field site sedimentary successions.....	194
Figure 4.30: The stratigraphy of the Knights Beach aeolianite succession.....	198
Figure 4.31: The location of Point McLeay on Narrung Peninsula.....	205
Figure 4.32: Sedimentary succession at Point McLeay.....	207
Figure 4.33: The location of the inland sites within the study area and their relationship to the ranges of Bridgewater Formation on the Coorong Coastal Plain.....	213

Figure 4.34: Mount Misery stratigraphy with photomicrographs.....	214
Figure 4.35: B-McIntosh Road and Gravel Pit locations with photomicrographs.....	216
Figure 4.36: North Coonalpyn field site.....	219
Figure 4.37: South Coonalpyn field site with photomicrographs.....	220
Figure 4.38: Emu Springs field site.....	222
Figure 4.39: The Tauragut Well field site.....	223
Figure 4.40: Carcuma field site.....	224
Figure 4.41: Tailem Bend field site.....	225
Figure 4.42: Murray Bridge field site with photomicrographs.....	226
Figure 4.43: Location of Molineaux Sands, terra rossa soil, solution pipes and alluvium field sites.....	232
Figure 4.44: Molineaux Sand field sites.....	234
Figure 4.45: Results of XRD mineralogical analysis of Bridgewater Formation sediments.....	246
 Chapter 5: Methodological considerations of Amino Acid Racemisation and its application in dating Pleistocene interglacial sedimentary successions	
Figure 5.1: Generalised left- and right-handed amino acid enantiomers (Schroeder and Bada, 1976).....	256
Figure 5.2: The breakdown of polypeptide chains to free amino acids by hydrolysis (modified from Wehmiller, 1980).....	259
Figure 5.3: Summary of intrageneric racemisation rates for multiple amino acids illustrating the fast and slow rates of racemisation and different apparent rates of racemisation per amino acid (Wehmiller et al., 2010; 2011; 2012).....	260
Figure 5.4: Aminostratigraphy and kinetic model interpretation of enantiomeric ratio data illustrating the latitudinal trends in D/L values due to latitudinal gradient of effective temperature (Wehmiller, 1982).....	262
Figure 5.5: Stratigraphy and correlation of eight sections in north Eleuthera, Bahamas demonstrating the combined use of lithostratigraphy and aminozones (from Hearty, 1998).....	268

Figure 5.6: lot of the exponential change in D/L valine data against the linear current mean annual temperature for Quaternary marine molluscs (modified from Murray-Wallace, 2000).....	269
Figure 5.7: An example of the sampling and sub-sampling method used in this research.....	272
Figure 5.8: Internal features of the bivalve <i>Spisula trigonella</i>	276
Figure 5.9: Charts illustrating the mean trends in free amino acids (FAA) and total hydrolysable (THAA) D/L values dependent upon the oxidising agent used in preparation of shell for hydrolysis.....	279
Figure 5.10: Example of a chromatograph trace with the interlaboratory comparison (ILC) standard A.....	281
Figure 5.11: The analytical precision for glutamic acid as determined by repeat measurement of inter-laboratory comparison standards (ILC-A, B, and C).....	283
 Chapter 6: Geochronological Analysis of the Quaternary sedimentary successions within the River Murray Lakes Region, southern Australia	
Figure 6.1: Calibration plot of ASX D/L values vs. $\sqrt{\text{Time}}$ (a) for <i>Spisula trigonella</i> shell.....	297
Figure 6.2: Holocene shell and whole-rock samples were retrieved from the modern beaches.....	300
Figure 6.3: Scatter plot of aspartic acid (ASX) D/L values vs. age of Holocene <i>Spisula trigonella</i>	302
Figure 6.4: Scatter plot of mean valine acid (VAL) vs. glutamic acid (GLX) D/L values for 'modern' whole-rock.....	304
Figure 6.5: Graphs of glutamic acid (GLX) and valine (VAL) D/L values for individual <i>Discorbis</i> and <i>Elphidium</i> foraminifers retrieved from modern shoreline sediments alongside mean whole-rock values.....	307
Figure 6.6: The results of analyses from the last interglacial shoreline (<i>sensu lato</i>) are presented with regard to their geographic relationships, from east to west, southeast Lake Albert, Hindmarsh Island, Goolwa and Fleurieu Peninsula.....	310
Figure 6.7: MIS 5e mean GLX D/L values for the bivalve <i>Spisula trigonella</i> with increasing depth of burial with Holocene shell retrieved from the modern shoreline for comparison.....	311

Figure 6.8: Mean glutamic acid (GLX) D/L values with 1 σ for last interglacial mollusc species.....	313
Figure 6.9: Results of last interglacial whole-rock sample (with 1 σ uncertainty terms) and individual foraminifer analyses.....	316
Figure 6.10: Location of middle to early Pleistocene sedimentary successions and field sites.....	325
Figure 6.11: Summary of analytical results of middle to early Pleistocene sedimentary successions with the average GLX D/L values for modern and MIS 5 (<i>sensu lato</i>) whole-rock, shell and foraminifers provided for comparison.....	327
Figure 6.12: Second glow TL glowcurves following 20.07 Gy irradiation demonstrating the different TL energy characteristics of quartz grains from Mount Misery.....	331
 Chapter 7: Quaternary landscape development of the River Murray terminus, South Australia and correlation to the sea-level record of the Coorong Coastal Plain	
Figure 7.1: SRTM image of Coorong Coastal Plain with distinct landforms of the Bridgewater Formation.....	337
Figure 7.2: Northern Coorong Coastal Plain with topographic transects and correlation of Bridgewater Formation sedimentary successions to the oxygen isotope record.....	339
Figure 7.3: Topographic transects of the northern Coorong Coastal Plain derived from SRTM data.....	342
Figure 7.4: The extent of Middle to Late Pleistocene Bridgewater Formation and associated deposits within the Murray Lakes region.....	355

List of Tables

Chapter 4: Stratigraphy and Petrography of the Pleistocene Bridgewater Formation and Holocene successions, River Murray Mouth Region, southern Australia	
Table 4.1: Taphonomic grading scheme developed for fossil molluscs.....	111
Table 4.2: Shell species collected per field site.....	112

Table 4.3: Description of modern substrate sediments retrieved from the Lacepede Shelf.....	130
Table 4.4: Analytical results for auger holes located on southern Hindmarsh Island....	138
Table 4.5: Analytical results for selected aeolianites in the region southeast of Lake Albert.....	145
Table 4.6: Analytical results for northern Hindmarsh Island aeolianites.....	157
Table 4.7: Analytical results at Chart House site.....	167
Table 4.8: Analytical results of the Myrtlegrove siliceous dune succession.....	195
Table 4.9: Analytical results of the Knights Beach Bridgewater Formation dune succession.....	203
Table 4.10: Analytical results of the Point McLeay dune succession.....	209
Table 4.11: Analytical results of the inland site locations.....	228
Table 4.12: Analytical results for Molineaux Sand.....	236
Table 4.13: Analytical results for solution pipe fill, <i>terra rossa</i> and alluvium.....	239
 Chapter 5: Methodological considerations of Amino Acid Racemisation and its application in dating Pleistocene interglacial sedimentary successions	
Table 5.1: THAA and FAA GLX D/L values for shell prepared using either H ₂ O ₂ or NaClO as an oxidising agent.....	279
Table 5.2: Amino acid D/L values of twenty-three interlaboratory comparison standards (ILC-A, B and C) shown with 1 σ	284
 Chapter 6: Geochronological Analysis of the Quaternary sedimentary successions within the River Murray Lakes Region, southern Australia	
Table 6.1: Luminescence ages and analytical results from within the study area.....	295
Table 6.2: Results of AAR analysis of modern and Holocene shell samples.....	301
Table 6.3: Numerical age calibration results for Holocene <i>Spisula trigonella</i>	302
Table 6.4: Results of whole-rock analysis from the modern shoreline of the River Murray Mouth region and Point McLeay aeolianite.....	307

Table 6.5: Average of foraminifer results accepted as Holocene from the modern shoreline within the River Murray Mouth region.....	310
Table 6.6: Summary of mollusc shell analysis from MIS 5e field sites in the River Murray Mouth region.....	314
Table 6.7: Summary of whole-rock sample analyses from MIS 5c (Surfer Beach) and MIS 5e field sites in the River Murray Mouth region.....	317
Table 6.8: Summary of individual foraminifer analyses from MIS 5e field sites in the River Murray Mouth region.....	319
Table 6.9: Summary of whole-rock sample analyses for MIS 7 aeolianite on northern Hindmarsh Island and Sturt Peninsula.....	326
Table 6.10: Summary of individual foraminifer analyses for MIS 7 aeolianite on northern Hindmarsh Island and Sturt Peninsula, Point McLeay and more inland field sites.....	326

List of Equations

Chapter 5: Methodological considerations of Amino Acid Racemisation and its application in dating Pleistocene interglacial sedimentary successions

Equation 5.1: General racemisation reaction for amino acids.....	256
Equation 5.2: Integrated rate expression for the racemisation reaction.....	257

Chapter 6: Geochronological Analysis of the Quaternary sedimentary successions within the River Murray Lakes Region, southern Australia

Equation 6.1: Luminescence dose rate equation.....	292
Equation 6.2: Apparent parabolic kinetic model equation for age determination.....	296
Equation 6.3: Slope of regression line.....	297

Chapter 1

Thesis Introduction

This thesis examines the Quaternary geomorphological evolution of the River Murray Mouth and lakes region in southern Australia within the context of increasing aridity and fluctuations in eustatic sea level and climate. The River Murray, the largest exoreic river in Australia, draining one-seventh of the continent, debouches into the Southern Ocean at the northern margin of the Coorong Coastal Plain. Located far from the periphery of Quaternary ice sheets, not subject to the effects of associated glacio-isostasy and within a continent of relative stability, the record of Quaternary sea-level change within the Murray mouth and lakes region has been subjected to the effects of localised subsidence. Two hundred kilometres to the southeast of the River Murray Mouth, in the region between Robe and Naracoorte, uplift accompanying Quaternary intraplate volcanism has aided the preservation of a succession of beach-barrier-lagoonal shoreline complexes, globally one of the longest records of Quaternary sea-level highstands now preserved in a terrestrial setting. The localised subsidence of the northern-most coastal plain and lateral movement of the River Murray accompanying cycles of glacio-eustatic sea-level and climate change have produced a geomorphologically complex regional landscape surrounding the River Murray Mouth.

The presence of a complex series of Pleistocene coastal landforms within the Murray Mouth region and their relation to the Coorong Coastal Plain, was initially recognised by de Mooy (1959) and Sprigg (1959) but their ages could not be discerned due to a lack of suitable geochronological methods with which to correlate the widely separated stratigraphical successions. Subsequent studies focused on the Holocene and/or the late Pleistocene record (Bourman and Murray-Wallace, 1991; Bourman *et al.*, 2000; Cann *et al.*, 2000). It was not until 2010 that Murray-Wallace *et al.* confirmed the presence of composite coastal barrier structures which were correlated with MIS 5c, 5e and 7. However, the extent of Pleistocene coastal stratigraphic successions within the region was still not fully recognised.

This thesis explores the role of subtle Quaternary neotectonic processes and their influences on sedimentation near the River Murray terminus in relationship to the larger regional context of the Coorong Coastal Plain. It also investigates how global fluctuations of climate and sea level during the Quaternary have impacted on sediment deposition as well as demonstrating how, post-deposition, the sedimentary successions influenced the movement and location of the palaeo-River Murray throughout cycles of glacio-eustatic sea-level change. The impact of fluvial processes on the preservation of sedimentary successions is also investigated, providing an understanding of how the interplay between the river and sedimentary successions has affected long-term landscape development.

The aims of this research are addressed using morphostratigraphical, petrological, geochronological and geographic. Exposures within sedimentary successions were analysed for their mode of formation to infer the depositional palaeo-environment. Subsequent diagenesis and degree of preservation were observed to determine post-depositional processes. A geochronological framework for middle Pleistocene through to Holocene sedimentation within the region has been established by using amino acid racemisation (AAR), thermoluminescence (TL), optically-stimulated luminescence (OSL) and radiocarbon analyses. Early Pleistocene deposits, beyond the range of the geochronological methods applied in this study, are identified, described and correlated to the marine isotope record revealing a longer record than previously recognised for the region.

The remainder of this thesis is organised as follows:

Chapter 2 reviews aspects of Cenozoic history that have influenced development of the southwestern Murray Basin (where the study area is located) and the adjacent uplifting Fleurieu Peninsula, parts of which are included within the study area. The ancient geological features of southern Australia represent antecedent conditions that significantly influenced the Cenozoic development of the region and are reviewed first. The geological and geomorphological development, through the Paleogene and Neogene Periods is subsequently explored, as well as the physical and climatic settings, which characterise the Quaternary in this region. The review of the Quaternary Period

describes how the effects of glacio-eustatic sea-level and climatic oscillations shaped a geomorphologically complex region preserving records of a marginal marine environment and a terrestrially arid environment. This overview includes an extensive review of the Pleistocene Bridgewater Formation which preserves one of the longest records of interglacial high sea levels in the world in the form of aeolian carbonate coastal barriers. The record provided by the Bridgewater Formation was used to quantify the differential tectonism along the Coorong Coastal Plain, the development of the coastline during successive interglacial highstands, river mouth migration and erosion by, the palaeo-River Murray were major foci of this thesis.

The modern physical environment of the River Murray terminus is described in Chapter 3. The processes which have formed the modern coastal sedimentary successions serve as direct analogues for the development of their Pleistocene counterparts. Sediment sources are identified from the River Murray and the offshore Lacepede Shelf, a cool-water temperate carbonate factory (James *et al.*, 1992). The diagenetic processes which affect carbonate sediments and aid in their preservation are reviewed. Finally, lithological descriptions of sediments previously identified within the study area are provided.

Chapter 4 presents the stratigraphical and petrographical analyses undertaken and their results. The spatial distribution of sedimentary successions as identified by their morphostratigraphical features and facies architecture is presented. The coastal Bridgewater Formation, composed of beach and aeolian carbonate dunes deposited during interglacial periods of high sea-level, is most prevalent in the region. Descriptions are presented in an inferred time-transgressive manner beginning with the Lacepede Shelf and early Holocene, followed by aeolian deposits interpreted as being related to MIS 5 and MIS 7 due to geographic locations and previous geochronological information. Subsequent descriptions are made of the stacked sedimentary successions of the Pleistocene Bridgewater Formation located well inland of the modern coastline, followed by discussion of the aeolian siliceous sands associated with glacial aridity and the expansion of arid environments during the Last Glacial Maximum. Fossils and sediments were subjected to taphonomic, particle size, binocular microscope, thin section, X-ray diffraction and scanning electron microscope analyses. Results indicate

environments of deposition and post-depositional processes which acted on the sediments and reveal the magnitude of reworking that occurred in the Murray Mouth region.

The principal geochronological method used in this research to analyse interglacial sedimentary successions was amino acid racemisation (AAR) due to its suitability for analysing carbonate sediments. Chapter 5 provides a review of the AAR reaction, outlining the relevance of this method to the thesis, the applications of the method, sample selection and the analytical procedure. This chapter also discusses the complexities of the Murray Lakes region made evident by sample analyses.

Four geochronological methods were used in this research: amino acid racemisation (AAR), thermoluminescence (TL), optically-stimulated luminescence (OSL) and radiocarbon dating. The results from each method are presented in Chapter 6. A brief review of the methodological principles behind the luminescence techniques (TL and OSL) is also presented. The geochronological results extend the known geographical limits of MIS 5e and 7 sediments within the region, confirm the presence of MIS 11 carbonate aeolianite northeast of the Murray Mouth and substantiate the premise that early Pleistocene sedimentary successions are preserved within the northern Coorong Coastal Plain. Results of AAR analyses illustrate the high potential for reworking within the Murray Mouth region and reveal, that in terms of sediment composition, the successions commonly represent palimpsest deposits.

Chapter 7 combines the results from the previous chapters to provide a synthesis of the development of the River Murray terminus within the Pleistocene and into the Holocene. Neotectonic processes have played a large role in the distribution of Pleistocene sedimentary successions and the location of the River Murray. The Bridgewater Formation in the region is correlated with the record of interglacial sea-level highstands preserved on the southeastern Coorong Coastal Plain between Robe, Naracoorte and Bordertown and is reviewed in the context of eustatic sea-level change. The implications of the distribution and preservation of glacial Molineaux Sand for sediment recycling is discussed and the course and position of the palaeo-River Murray

and its mouth is reviewed. The major conclusions from this research are presented and ideas for further research proposed.

Chapter 2

Cenozoic Development of the southwestern Murray Basin and Fleurieu Peninsula, southern Australia

2.1 Introduction

Much of the Australian landscape reflects the ancient geology of the continent (Doutch and Nicholas, 1978; Wasson, 1982; Twidale and Campbell, 1995; Pillans, 2007). The landscape in which the River Murray terminates is not an exception. Remnants of Permian glaciated terrain are for example preserved on Precambrian and Cambrian bedrock within the Mount Lofty Ranges and on the contiguous Kangaroo Island which led Howchin (1926), Milnes and Bourman (1972) and Twidale (1994; 2000) to comment on the remarkable preservation and exposure of such an ancient landscape. The Quaternary record preserved there, a reflection of the glacio-eustatic sea level and climate change of the most recent geologic period of Australia, is distinct in the landscape.

The study area is located in the southwestern corner of the Murray Basin encompassing the terminus of the River Murray (the longest river of Australia) and the northern end of the Pleistocene Coorong Coastal Plain. The study area also includes the southern margin of the adjacent Fleurieu Peninsula, part of the Mount Lofty-Flinders Ranges, composed of Precambrian and Early Palaeozoic bedrock. The Murray Basin is a Cenozoic sag basin, the bedrock topography of which is a consequence of differential subsidence and uplift along pre-existing Devonian and older fracture sets (Wasson, 1982; Brown and Stephenson, 1991). The majority of depositional sequences in the basin are less than 200 m thick and reach 600 m maximum in the deep, west-central portion of the basin (Brown, 1983). The shallow basement influences sedimentation patterns, groundwater flow and surface drainage patterns (Figure 2.1).

This chapter reviews the aspects of Cenozoic history that bear relevance to understanding landscape development during the Quaternary. Because the bedrock beneath and surrounding the Murray Basin continues to exert influence and control on

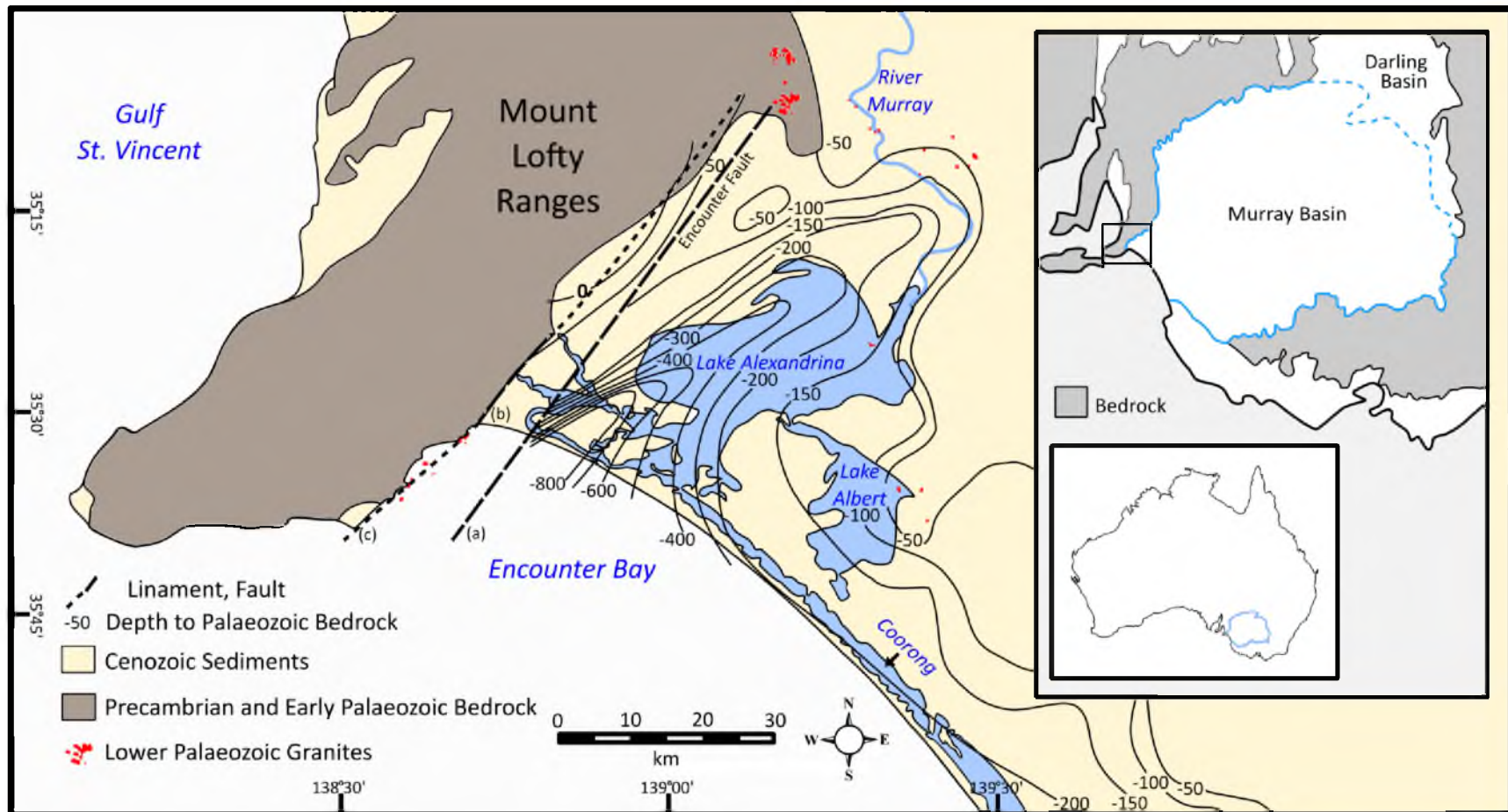


Figure 2.1: The River Murray terminus is located adjacent to the Mount Lofty Ranges comprising at or near surface Precambrian and Early Palaeozoic bedrock which continues beneath the Murray Basin and exerts influence on the modern landscape. The exact location of the Encounter Fault on the western margin of the Murray Basin has not been established. Three representations have been provided here: (a) the location as provided from Gatehouse *et al.*, 1991 in accordance with bedrock contours; (b) normal fault position with dip to the southeast (Thomson and Horwitz, 1962); (c) the Encounter Lineament trends in a northeast-southwest direction parallel to the Mount Lofty Ranges (Twidale *et al.*, 1978, Rogers *et al.*, 1995). Bedrock contours from Gatehouse *et al.*, 1991.

the study area, the first section of this chapter briefly reviews the early cratonisation of eastern Australia as well as the Permian glaciation for which, in some regions, evidence is still visible in the landscape. The second section focusses on the Cenozoic development of the Murray Basin through the Paleogene and Neogene Periods. The tectonic and climatic changes during this time established the physical setting and arid climatic regime which characterises the Quaternary Murray Basin. It was also during this period that the Eastern Highlands and northern tributaries to the proto-River Murray were established. The third section concentrates on Quaternary global climatic oscillations and the increasingly arid nature of the Australian continent. The study area is located in a region considered marginal marine during interglacial periods when eustatic sea-level is high but terrestrial during glacial periods when sea-level is low. The dichotomy of environment has shaped a geomorphologically complex region. An appreciation of the environmental changes produced by global climatic oscillations is required to understand development of the landscape. The more arid glacial environment is reflected, in the Murray Basin, by vast dunefields. The final section renews focus on landscape development within the southwestern corner of the Murray Basin. This includes an extensive review of the Pleistocene Bridgewater Formation. Preserved on the Coorong Coastal Plain, the Bridgewater Formation provides one of the longest terrestrial records of interglacial high sea-levels in the world (Hossfeld, 1950; Sprigg, 1952; Belperio and Cann, 1990; Huntley *et al.*, 1993; Murray-Wallace, 2001).

2.2 Pre-Cenozoic development of southeastern Australia

The structural units controlling the shape and location of the Murray Basin evolved over an extensive period of time. This section reviews the Proterozoic to Mesozoic genesis of the geologic structures which frame the Murray Basin.

The Australian continent is composed of three cratonic regions which formed from west to east (Wasson, 1982; McKenzie *et al.*, 2004; Huston *et al.*, 2012). The western and central cratons are composed largely of Precambrian shield rocks. The eastern craton is composed of accreted Palaeozoic sediments known collectively as the Tasman Orogenic Belt. Accretion of the Tasman Orogenic Belt, known as the Terra Australis Orogen (Cawood, 2005), encompasses the Delamerian, Lachlan, Thomson and

New England Fold Belts of eastern Australia, which have traditionally been divided into a series of separate structural units based on the timing and nature of orogenic activity and the geographic disposition of the units (Cawood, 2005). The margins of the Quaternary Murray Basin and its underlying bedrock are composed of remnants of the Delamerian and Lachlan Orogens.

The Delamerian Orogeny (520-500 Ma) deformed Proterozoic and Cambrian continental rift strata within the ancient Stansbury Basin and Kanmantoo Trough (Miller *et al.*, 2005). The Adelaide Fold Belt, which forms the Mount Lofty-Flinders Ranges (Figure 2.2), is the westernmost expression of the orogeny. The sigmoidal shape of the Adelaide Fold Belt and arcuate fold trends of the entire Delamerian Fold Belt are due to basement trends (Preiss *et al.*, 1981; Paul *et al.*, 2000; Preiss, 2000). Cenozoic sediments of the western Murray Basin unconformably overlie the Kanmantoo Group and Adelaide Fold Belt (Brown and Stephenson, 1991).

Igneous activity associated with the Delamerian Orogeny formed the Padthaway Ridge, a basement horst-like structure of Late Cambrian-Ordovician granitoids trending northwesterly 30-60 km inland from the Coorong (Figure 2.2) (Sprigg, 1952; Rochow, 1971; Hill *et al.*, 2009). Granite intrusion is also visible in Encounter Bay (Figure 2.1). These igneous rocks intruded into the surrounding rocks and sediments of the Adelaide Rift Complex and Kanmantoo Group respectively and many outcrop through Cenozoic sequences today. The Lachlan Fold Belt, the deformation of which began approximately 40 million years after the Delamerian Orogeny (445-440 Ma) (Miller *et al.*, 2005), flanks and underlies the eastern and southern Murray Basin.

Record of the Permian glaciation is preserved within numerous troughs beneath the Murray Basin and across the Fleurieu Peninsula. The Late Palaeozoic Troubridge Basin encompasses the Permian Cape Jervis Formation, deposits of which stretch from the Yorke Peninsula, southeast across the Fleurieu Peninsula, eastern Kangaroo Island and beneath the River Murray terminus and the northern Coorong (Wopfner, 1972; Alley and Bourman, 1995) (Figure 2.3). The Permian sediments within and surrounding the River Murray Mouth region may have served as a sediment source during the Quaternary.

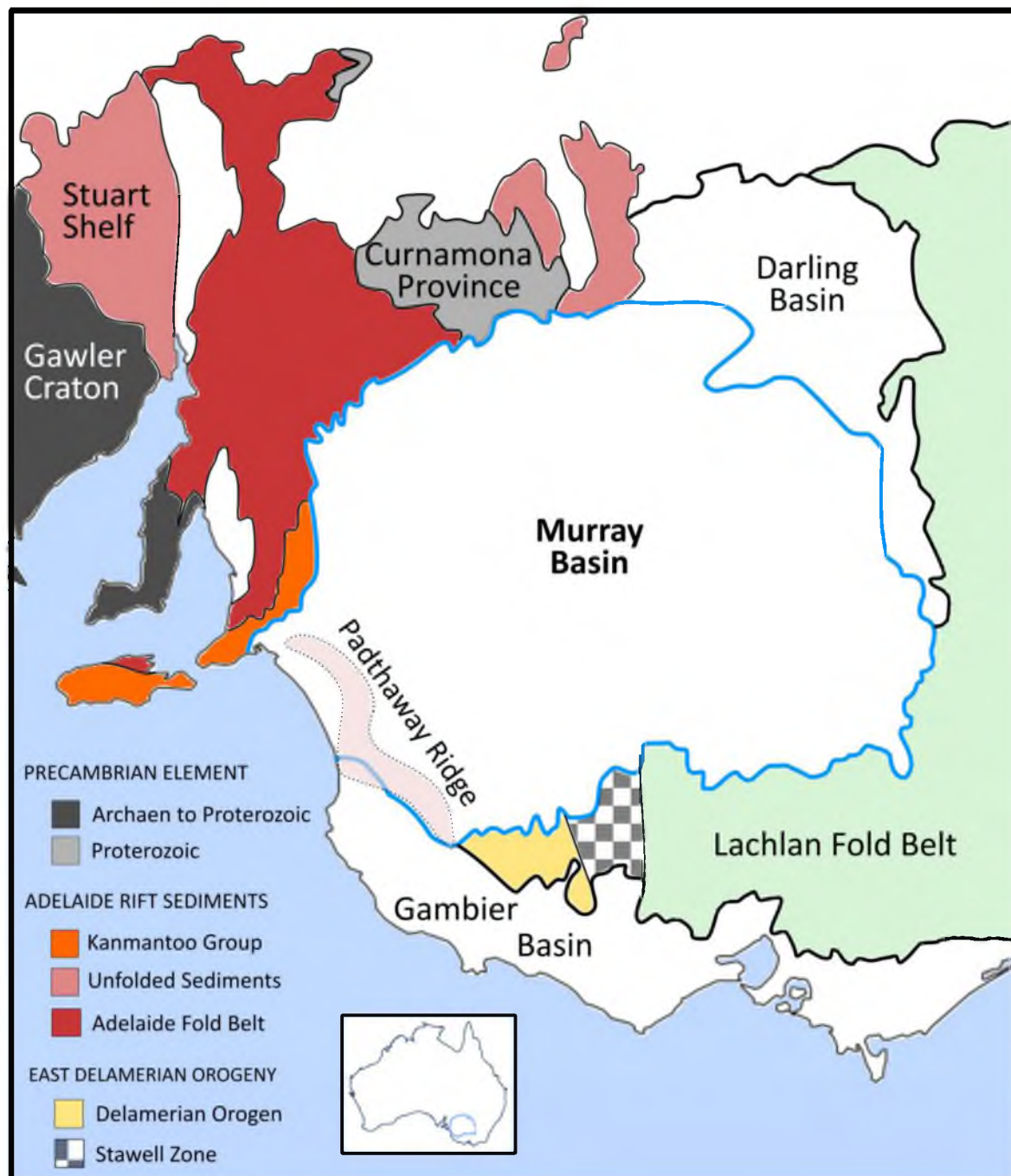


Figure 2.2: The Delamerian Orogeny folded Proterozoic and Cambrian rift sediments to form the Adelaide Fold Belt (Miller *et al.*, 2005; Aitken, 2010). The Delamerian Orogen extends beneath the western Murray Basin and composes part of the Victorian Highlands on the eastern margin of the basin. The Lachlan Orogen is eastward of and occurred after the Delamerian Orogen as part of the greater Terra Australis Orogeny (Cawood, 2005). The resulting Lachlan Fold Belt makes up much of the southern and eastern margin of the basin and continues under the basin. The exact boundary between the Delamerian and Lachlan Orogens is unknown (Glen, 2013). The boundary between the two in the Victorian Highlands is somewhere in the Stawell Zone (Gray and Foster, 2004; Miller *et al.*, 2005).

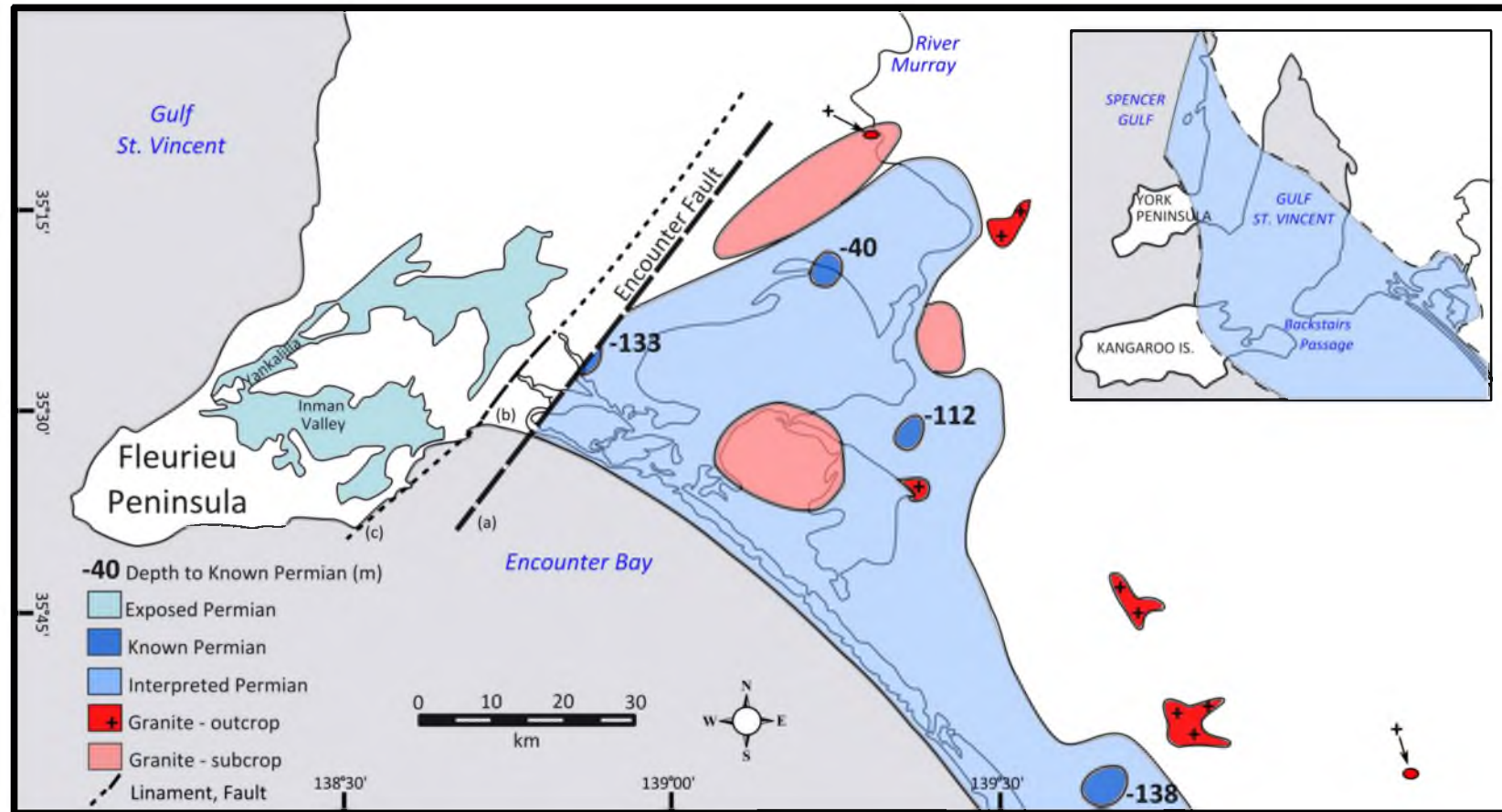


Figure 2.3: Distribution of Permian strata beneath the River Murray terminus and upper Coorong (modified from Gatehouse *et al.* 1991) and on Fleurieu Peninsula (Thompson and Horwitz, 1962). Inset: The approximate limits of the Troubridge Basin (modified from Alley and Bourman, 1995). The exact location of the Encounter Fault on the western margin of the Murray Basin has not been established. Three representations have been provided here: (a) the location as provided from Gatehouse *et al.* 1991 in accordance with bedrock contours; (b) normal fault position with dip to the southeast (Thomson and Horwitz, 1962); (c) the Encounter Lineament trends in a northeast-southwest direction parallel to the Mount Lofty Ranges (Twidale *et al.* 1978, Rogers *et al.* 1995).

The rifting of Australia from the larger continent of Gondwana (Australia, South America, Africa, India and Antarctica) began with seafloor spreading off northwest Australia (160 Ma) (Veevers, 2006) and was complete with the collapse of the continental margin following the initiation of fast spreading at ~44 Ma (Norvick and Smith, 2001). The Australian Southern Rift System (ASRS) encompasses the southern coastal margin rift valleys and their sedimentary fills (Kreig *et al.*, 1995). The strike-slip regimes, developed during the closing stages of the Delamerian Orogeny, served as crustal weaknesses controlling the locus of the Cretaceous-Cenozoic breakup (Gibson *et al.*, 2011). Intra-cratonic subsidence, uplift of the Eastern Highlands, inception of southwestern drainage into the juvenile ocean and emplacement of oceanic crust at the Australia-Antarctic rift created a template for the modern Australian landscape (Norvick and Smith, 2001; Veevers, 2006). These adjustments to the Australian plate coincided with the end of the Mesozoic and the beginning of the Cenozoic at 65 Ma.

2.3 Paleogene-Neogene development

The Murray Basin was created with the relaxation of the Australian platform (Veevers, 2000). Early Cenozoic tectonic movements separated the onshore margin of the basin from the adjacent Cenozoic Gambier Basin (also known as the Gambier Embayment of the Otway Basin) along the diffuse boundary of the Padthaway Ridge (Smith *et al.*, 1995). Brown (1985) identified three major depositional sequences before the Quaternary within the Murray Basin: Palaeocene-Eocene to Lower Oligocene, Oligocene to Middle Miocene, and upper Miocene to Pliocene. These major sequences are explained by tectono-eustatic models and related intrabasinal isostatic adjustments associated with sediment loading (Brown, 1983). The topographically low-lying and low gradient setting of the basin throughout the Cenozoic left it prone to partial flooding by shallow epicontinental seas during periods of high relative sea level. Slow subsidence rates, low rates of sediment supply and minimal compaction resulted in Cenozoic sediments reaching at maximum 600 m thickness in the central-western part of the basin, but averaging less than 200-300 m (Brown, 1983; Brown and Stephenson, 1991). The depositional sequences within the Murray Basin have the potential to serve as indicators of Cenozoic climate and sea level changes. However, as noted by numerous

authors (McGowran *et al.*, 2004; Gallagher and Gourley, 2007; Miranda *et al.*, 2009), access to the depositional sequences, and therefore ability to interpret them, is hampered by their paucity of outcrop. Many deposits are exposed only in the River Murray valley and elsewhere occur only in subsurface, requiring mapping to be based on borehole records. The development of the Cenozoic Murray Basin and how it pertains to the study area will be the focus of the forthcoming section.

2.3.1 Palaeocene-Eocene to Lower Oligocene, 65-34 Ma

With uplift of the Eastern Highlands in the Cretaceous, south-western drainage into the Australian-Antarctic depression began (Veevers, 2006). Uplift of the Mount Lofty-Flinders Ranges (South Australia Highlands), which would have hindered westerly flow, is likely to have begun in the Palaeocene starting at the northern end of the Flinders Ranges and continuing south (Wellman and Greenhalgh, 1988). Half of the total uplift in the middle and southern Mount Lofty Ranges occurred before the mid-Cenozoic (Stephenson and Brown, 1989). The ranges, as an eroded complex of the Adelaide Fold Belt, indicate reactivation of the older structures with some of the uplift occurring along rejuvenated Delamerian fault-trends (Preiss, 1995; 2000) and the formation of neotectonic faults independent of the older zones (Jayawardena, 2013; see Neogene tectonic review below). The uplift of the ranges has been considered a function of compression (as indicated by reverse faults) and regional isostatic compensation (Wellman and Greenhalgh, 1988).

Earliest sedimentation within the Murray Basin occurred at the Palaeocene-Eocene (55 Ma) boundary (Norvick and Smith, 2001). These sediments were predominantly fluvial, composed of undifferentiated sands, clays and siltstones of Palaeocene to Eocene age (Firman, 1973) and spread across the entire Murray Basin (Brown, 1983). They were named the Knight Group by Sprigg (1952) and described in detail by Ludbrook (1961) for the Padthaway Ridge area where it thins out. The Padthaway Ridge would have formed a laterally extensive high at the time of deposition.

At 44 Ma the Australian continent began its fast rate of movement northward with subsequent rapid thermal subsidence and marine transgression into many low lying

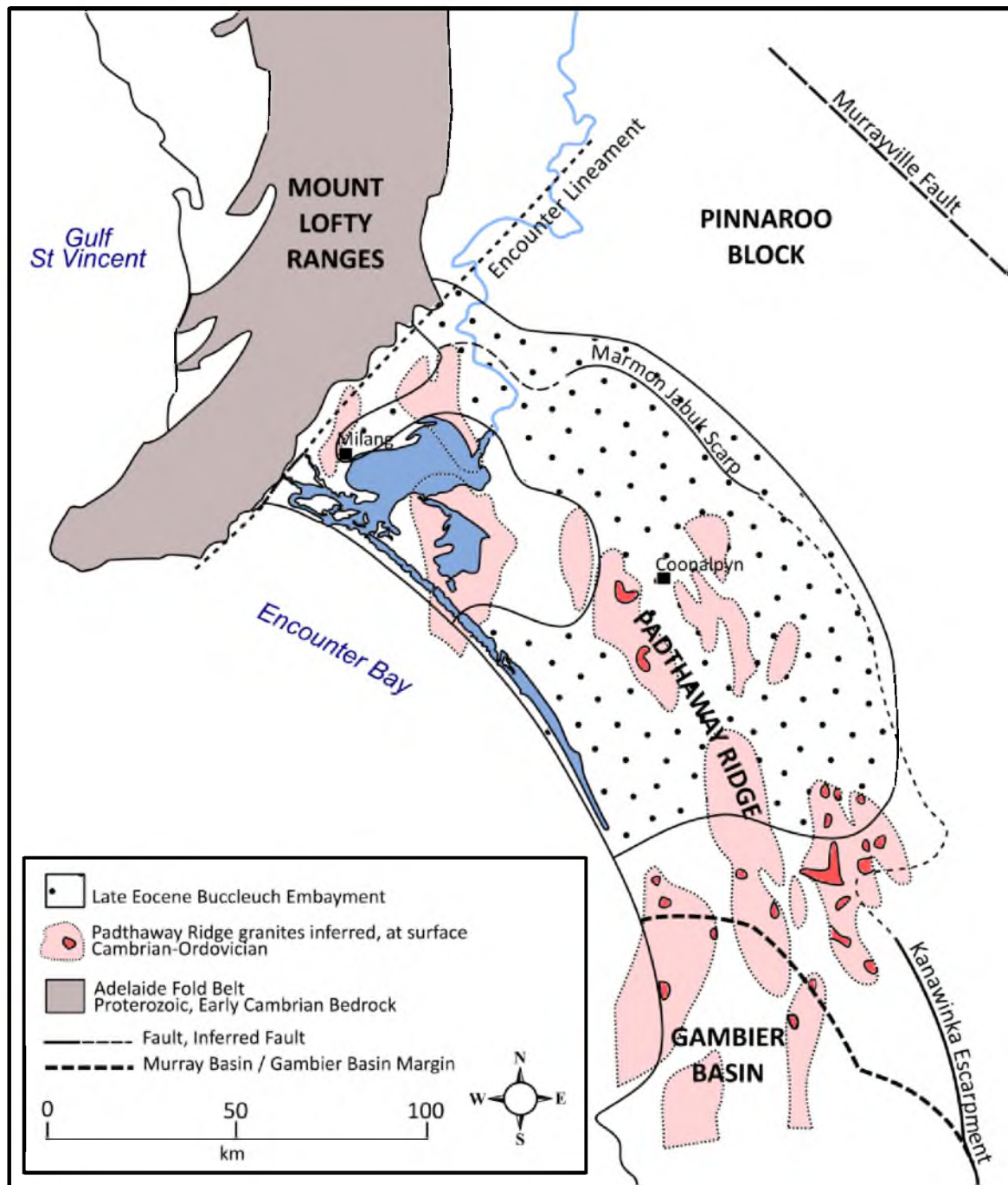


Figure 2.4: The Buccleuch Embayment (Ludbrook, 1961; Brown and Stephenson, 1991). Buccleuch beds are absent over the palaeo-topographic highs of the Padthaway Ridge but extend landward of the later Marmon Jabuk and Kanawinka Escarpments (see discussion below). Location of granitoid intrusives from Preiss, 1995 (figure 7.18). Fault locations from Rogers *et al.*, 1995 (figure 10.6). Both faults are normal with the Murrayville Fault downthrown to the northeast (Rogers, 1979) and Encounter Fault downthrown to the southeast (Thomson and Horwitz, 1962).

areas of the continental margins (Norvick and Smith, 2001). In the Murray Basin the transgression was balanced by a terrigenous sediment supply that restricted marine incursion in the basin to the west and southwest (Brown, 1983). At this time the

Padthaway Ridge would have served as a natural breakwater (O'Driscoll, 1960). The marine sediments of the Buccleuch Group, shallow-marine glauconitic calcareous clays, carbonaceous sands with thin limestone lenses and bryozoan limestone (Ludbrook, 1961) are found within the Buccleuch Embayment, which extends roughly from the Mount Lofty Ranges north to the Marmon Jabuk Range and east beyond Coonalpyn (Figure 2.4) (Brown and Stephenson, 1991). Both the Knights Group and Buccleuch Group have been identified within boreholes in the study area (O'Driscoll, 1960).

The Eocene high sea level marks the initiation of the Leeuwin Current (McGowran *et al.*, 1997a; b). The current has since been associated with 'warm' times when a component of the South Equatorial Current brought warm, low-salinity surface water and biotas to southern Australia due to squeezing in the north and counter-gyral deflection in the south. During cooling times the Subtropical Convergence shifted northwards and the Leeuwin Current decreased in strength. The Leeuwin Current enhanced the differences between the warm/cool, transgressive/regressive stratigraphic and palaeobiological successions on the southern Australian margin (McGowran *et al.*, 1997a; b; 2004). The Leeuwin Current has continued to influence faunal distribution across southern Australia throughout the Quaternary (section 2.5.3).

A trend of global cooling which began after the early Eocene Climatic Optimum (EECO), 52-50 Ma, continued after the transgression and probably reflects the growth of Antarctic ice sheets (Zachos *et al.*, 2001; Fujioka and Chappell, 2010). Establishment of the ice sheets was possible with the development of the Southern Ocean and the Antarctic Circumpolar Current following the opening of the Drake Passage during the late Eocene, which isolated Antarctica from the warmer northern seas (Williams, 2000; Zachos *et al.*, 2001). The deposition of the Buccleuch Group ceased with a fall in sea level during the Early Oligocene. The Eocene-Oligocene boundary is marked by rapid expansion of the Antarctic ice sheet(s) ~35 Ma (Zachos *et al.*, 2001) and opening of the Southern Ocean.

2.3.2 Oligocene through Middle Miocene, 34-11 Ma

The sea level fall during the Oligocene was the largest in 250 Ma (McGowran *et al.*, 1997) but was followed by a substantial rise in the Late Oligocene, which peaked

during the Mid-Miocene (Brown, 1983) to form the Murravian Gulf (Sprigg, 1952). The ingression into the Murray Basin created an expansive (~520 x 410 km) epeiric shallow sea located in the southwest of the basin semi-protected by the Padthaway Ridge archipelago (Lukasik *et al.*, 2000). At that time the Padthaway Ridge served as a diffusive but protective barrier to the Murray Basin (Lukasik *et al.*, 2000). In South Australia the Oligo-Miocene transgression is the source of the Murray Supergroup, the stratigraphic framework of which was established by Ludbrook (1957, 1961), but revised by Lukasik and James (1998) with further revision by Gallagher and Gourley (2007). The strata of the Murray Supergroup outcrop in the Murray Basin along the river cliffs in South Australia where River Murray incision over the past 0.7 Ma has exposed the strata (Ludbrook, 1961; Twidale, 1978; Brown and Stephenson, 1991).

The Oligo-Miocene highstand correlates with another exceptional warm phase (~27 Ma to ~15 Ma) in the otherwise cooling Cenozoic (Zachos *et al.*, 2001; Fujioka and Chappell, 2010; Riordan *et al.*, 2012). The initial warming phase, the Late Oligocene Warming Event (LOWE: 27-26 Ma) is associated with a reduced extent of Antarctic ice, which persisted through the Miocene Climatic Optimum (MICO: 17-15 Ma). During this period global ice volumes remained low. The peak of the warm phase, MICO, coincides roughly with the peak of marine ingression in the Murray Basin (16 Ma) (Fujioka and Chappell, 2010). The warm signal was enhanced by the transport of warm-water organisms into the southern margin by the Leeuwin Current (McGowran *et al.*, 2004). The increase in accumulation rates and carbonate deposition in all Cenozoic basins of southern Australia between the Oligocene-Lower Miocene and Lower-Middle Miocene indicates a warmer, drier climate and higher seawater temperatures by Middle Miocene times (Lukasik and James, 2006). Increasing aridity along all of southern Australia, including the Murray Basin, can be associated with the northwards movement of Australia into drier climatic belts and a decrease in precipitation as ice built up in Antarctica (Kemp, 1978). The warming ended abruptly at ~14 Ma corresponding with a major global cooling (McGowran *et al.*, 2004) and eventual reestablishment of the East Antarctic Ice Sheet (15-10 Ma) (Kemp, 1978; Zachos *et al.*, 2001). Sea level regression was followed by a period of substantial weathering and erosion in the basin and active

entrenchment of adjacent highland valleys. The resulting erosional surface is known as the Mologa Surface (Macumber, 1978; Brown, 1985).

2.3.3 Late Miocene through Pliocene, 11-2.58 Ma

The last major marine transgression, in terms of distance inland, into the Murray Basin occurred during the Late Miocene. The marl, silty clay and minor fine sand of the Bookpurnong Formation are all variably shelly, glauconitic and micaceous and indicative of a shallow-water marine succession (Ludbrook, 1961; Carter, 1985). The marine flooding would have extended over the Padthaway Ridge but was flanked to the west, roughly in the location of the present-day River Murray, by a zone of fluvial and estuarine environments, which were connected to the Southern Ocean (Brown, 1985). The Bookpurnong Formation is present in the central western region of the basin but is absent over the Pinnaroo Block (Figure 2.4) suggesting that the block had uplifted since the last marine transgression and was a submarine platform during the late Miocene transgression (Stephenson and Brown, 1989). The Bookpurnong Formation is flanked to the east and north and is conformably overlain by the shallow to marginal marine Loxton Sands. Shell beds at the base of the Loxton Sands indicate a shallow water or estuarine environment.

The Loxton Sands transition into the Parilla Sands. These sediments are unfossiliferous, non-marine, fine- to medium-grained clayey quartz sand with thin beds of clay (Rogers *et al.*, 1995). The Parilla Sands are recognised as stranded coastal ridges formed by aeolian and fluvial reworking of the Loxton Sands as sea level regressed. They may include lacustrine and fluvial deposits between the coastal ridges (Belperio and Bluck, 1990). The two sands are commonly referred to as the Loxton-Parilla Sands after the suggestion by Brown and Stephenson (1991) and due to the close relation of the two units and difficulties in distinguishing them.

The sea level highstand during the Late Miocene-Early Pliocene extended up to 500 km inland from the modern coast with sea level ~60 m above that of the present day (Brown and Stephenson, 1991; Langford *et al.*, 1995). The subsequent regression is recorded in the Loxton-Parilla strandplain which reaches an across-strike distance of

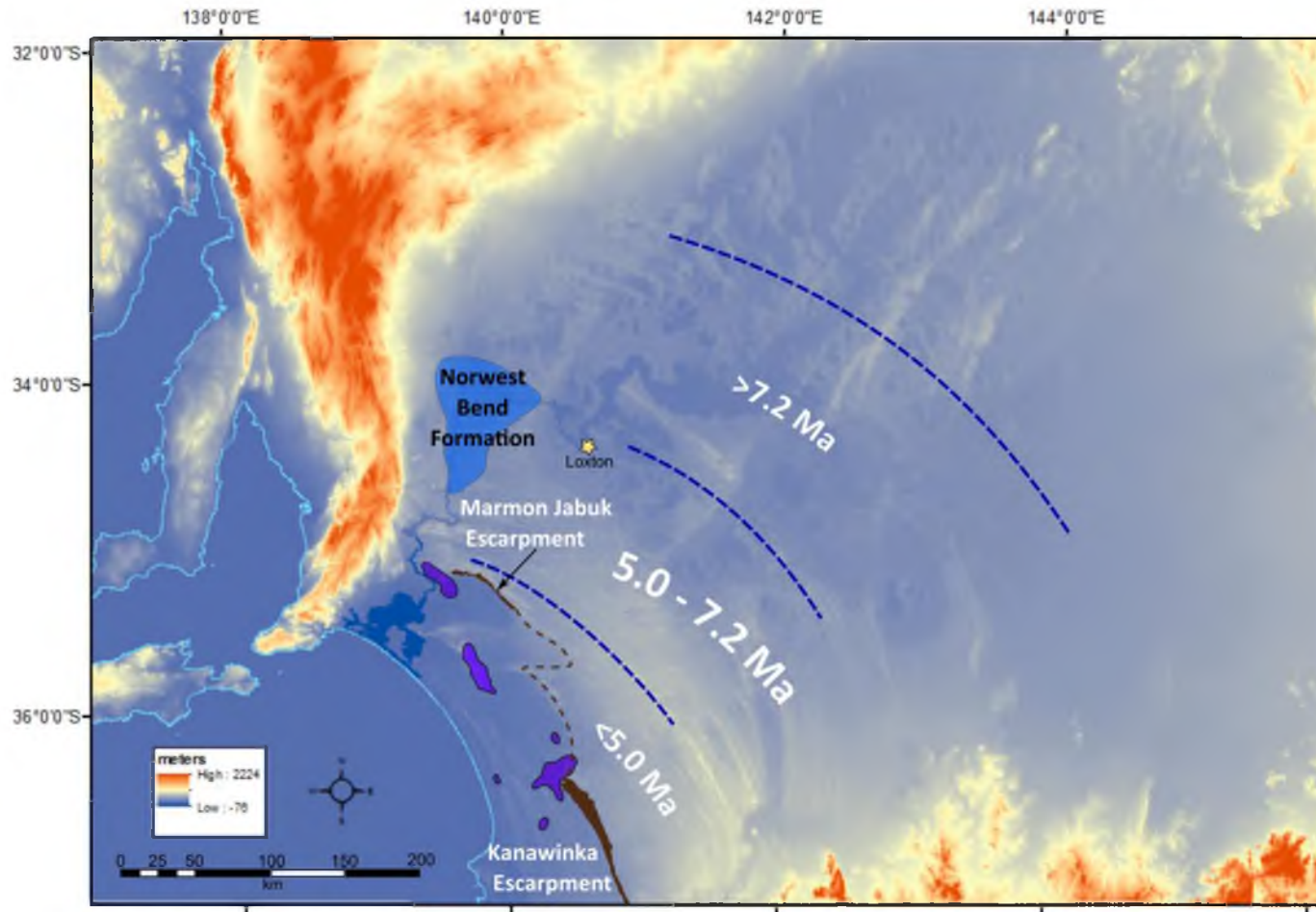


Figure 2.5: The Loxton-Parilla Sands record the regression of the Late Miocene-Early Pliocene sea from the Murray Basin (Brown and Stephenson, 1991; Langford *et al.*, 1995) as indicated by the blue dashed lines. Deposition of the strandlines has been constrained by strontium isotope analysis, beginning by 7.2 Ma and largely complete by ~5 Ma (Miranda *et al.*, 2009). The estuarine Norwest Bend Formation was deposited concurrent with the Loxton-Parilla Sands (Miranda *et al.*, 2008). The strandlines terminate along the Marmon Jabuk – Kanawinka Escarpment. The purple colour indicates where basement rocks of the Padthaway Ridge outcrop through the Cenozoic sediments. The modern coastline and Lakes Alexandrina and Albert are provided for orientation purposes. Location of Marmon Jabuk and Kanawinka Escarpments from Thomson and Horwitz, 1962 and Rogers, 1979. SRTM derived Digital Elevation Model data provided by Commonwealth of Australia, Geoscience Australia (2009).

~350 km and contains a series of more than 600 shore parallel strandlines trending northwest-southeast (Figure 2.5). Kotsonis (1999) suggested that the deposition of the earliest strandlines is comparable to an ice-free Earth. The strandlines fade out on the Padthaway High, terminating at the Marmon Jabuk and Kanawinka Escarpments, which have been interpreted as fault scarps (Sprigg, 1952; Bowler *et al.*, 2006) or a Pliocene coastal erosional feature (Hossfeld, 1950; Belperio and Bluck, 1990; Wallace *et al.*, 2005). The escarpment is truly a continuous geomorphic feature extending more than 600 km from the Mount Lofty Ranges in South Australia to the Portland area of Victoria (McLaren *et al.*, 2011). Relatedly, the structure subject to uplift landward of these escarpments has been given different names, being more commonly referred to as the Pinnaroo Block in South Australia when discussing uplift northeast the Marmon Jabuk escarpment (Twidale *et al.*, 1978; An *et al.*, 1986; Stephenson, 1986) or the Padthaway High (not to be confused with the Padthaway Ridge) when discussing uplift to the southeast and behind the Kanawinka Escarpment (Bowler *et al.*, 2006; McLaren and Wallace, 2010; McLaren *et al.*, 2011).

Strandlines similar to the Loxton-Parilla Sands exist in the southern Victoria Otway, Port Phillip and Gippsland Basins (Wallace *et al.*, 2005). Strontium isotope dating of the coastal strandlines in the southern Victoria basins indicates that deposition occurred from 5.8 – 2.5 Ma and perhaps continued in the offshore Gippsland Basin. This deposition age is somewhat later than that of the Murray Basin where strontium isotope analysis indicates strandline deposition began by 7.2 Ma (Late Miocene) within the central and western part of the basin and was largely complete by ~5 Ma (Miranda *et al.*, 2009).

The strandlines in every basin are capped by a weathering surface produced by subaerial exposure in a climate wetter than present. In the Murray Basin the variably ferruginous and/or siliceous surface is known as the Karoonda Surface (Firman, 1966 b). The surface is characteristic of late Miocene to Plio-Pleistocene weathering and has been correlated with other Pliocene lateritic weathering profiles in southeastern Australia (Firman, 1967 b; 1973; Kotsonis, 1999). The age of the surface has been further confined by palaeomagnetic dating of the overlying sediments of Pliocene Lake Bungunnia (see below, this section). At Loxton the Karoonda Surface of the Loxton-

Parilla Sands indicates that the sands were exposed to weathering as early as 4.6 Ma. Loxton is also the westernmost limit of silcrete in the Loxton-Parilla Sands (Kotsonis, 1999). The younger weathering profiles to the west and south of Loxton consist predominantly of iron accumulation and possibly reflect a change in climate.

The estuarine environment, which developed in the western Murray Basin concurrent with the deposition of the Loxton-Parilla Sands, is preserved in the sediments of the Norwest Bend Formation. The Norwest Bend Formation is recognised in outcrop along the River Murray Gorge by the oyster shell that dominates the succession (Ludbrook,; 1961; Twidale *et al.*, 1978; Brown and Stephenson, 1991). The formation is actually divisible into two informal members (Pufahl *et al.*, 2004). The lower member occurs as a quartzose sand member with matrices, which vary from clayey-silt and fine-to-coarse sand with numerous bivalves present throughout. The upper member is characteristically rich in oyster shells. The oysters form coquinas that in many localities directly overlie the Murray Group Limestone. The lower member resembles a more open and marginal-marine environment, comparable to that of the Loxton-Parilla Sands, and the upper member a more estuarine environment (Pufahl *et al.*, 2004; Miranda *et al.*, 2008). Miranda *et al.* (2008) constrained the deposition of the Upper Norwest Bend Formation to the Late Miocene-Early Pliocene (probably before 5 Ma) with strontium isotope analysis. This age agrees with later strontium isotope analysis on the Loxton-Parilla Sands (Miranda *et al.*, 2009). The upper Norwest Bend Formation is truncated by an unconformity surface laterally equivalent to the Karoonda Surface (Pufahl *et al.*, 2004).

There was a significant drop in sea temperature at the Miocene/Pliocene Boundary (~5 Ma) most likely reflecting rapid expansion of the West Antarctic Ice Sheet (10-6 Ma) (Kemp, 1978; Zachos *et al.*, 2001). In southern Australia the impact would have been a lowering of temperatures and an increased frequency of dry, anticyclonic circulation (Kemp, 1978) with concurrent lowering of sea level recorded in the strandlines of the southern Australian basins. The change in climatic conditions is reflected in the sedimentary style of the lower and upper members of the Norwest Bend Formation (Pufahl *et al.*, 2004). The siliciclastic sediment of the lower quartzose sand

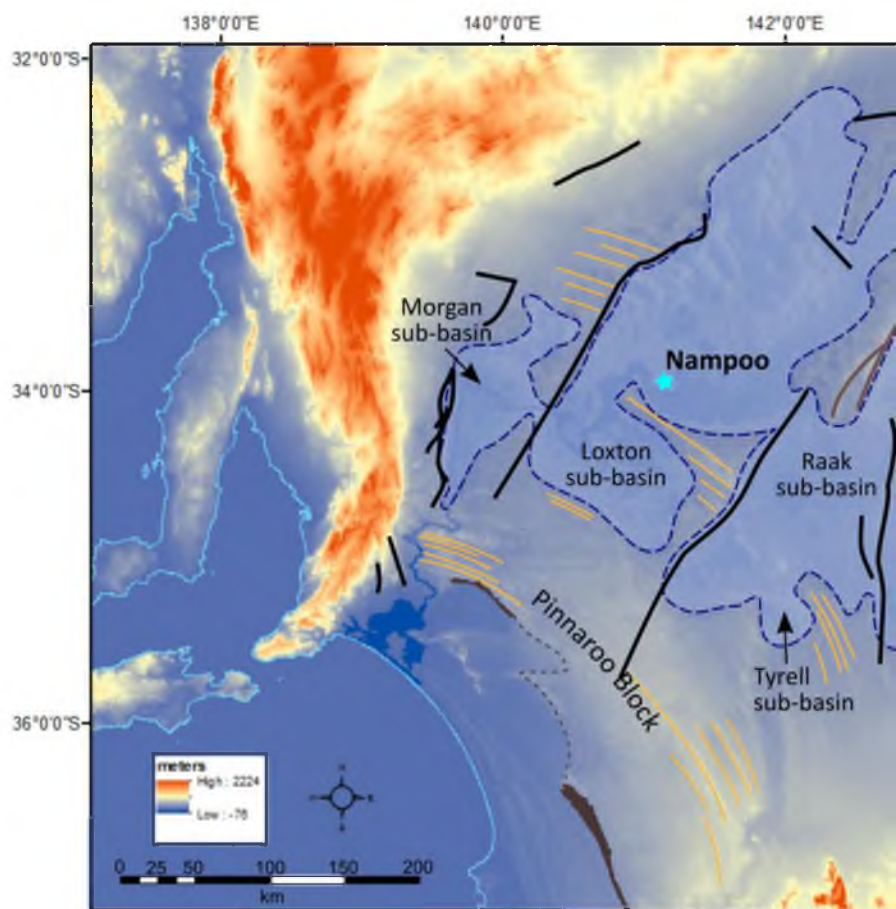




Figure 2.6: The approximate extent of the Pliocene mega-lake, Lake Bungunnia. Lake deposits are thickest in the east and shallow to the west (Stephenson, 1986; McLaren *et al.*, 2009). The top of the Nampoo Station section has an absolute elevation of 56.6 ± 0.5 m above present mean sea-level and likely represents the record of maximum fill of the lake basin (McLaren *et al.*, 2009). The black lines indicate the location of pre-Cenozoic faults underlying the Murray Basin (SA Department for Manufacturing, Innovation, Trade, Resources and Energy (DMITRE), 2014). The ridge locations, indicated by light brown lines, are from McLaren *et al.* (2011). Orange lines represent strandlines of the Loxton-Parilla Sands and dark brown the Marmon Jabuk - Kanawinka Escarpment (see Figure 2.5). SRTM derived Digital Elevation Model data provided by Commonwealth of Australia, Geoscience Australia (2009).

member was derived from prolonged, deep, subaerial weathering and accumulated under an equitable, relatively warm, humid climate. The mollusc assemblage reflects an open-marine environment. As rainfall and river outflow decreased, marine influence increased, promoting oyster growth in a restricted coastal environment. A semi-arid environment in Australia was established by the Pliocene (Fujioka and Chappell, 2010).

The climatic change of the Plio-Pleistocene is recorded in the large inland Lake Bungunnia which occupied an extensive area of the Murray Basin, overlying portions of both the Norwest Bend Formation and the laterally equivalent Karoonda Surface. The lake is one of the largest known Pliocene lakes in the world. At maximum expansion the lake covered an area of over 50,000 km² and was at least 60 m deep (Bowler *et al.*, 2006; McLaren and Wallace, 2010) (Figure 2.6). Reactivation of faults underlying the Murray Basin, most likely the uplift of the Pinnaroo Block, led to the formation of the mega-lake (Stephenson, 1986). The lake was composed of four sub-basins, from east to west: Tyrrell Basin, Raak Basin, Loxton Basin and Morgan Basin. The lake sediments are represented by the Blanchetown Clay (<40 m) and Bungunnia Limestone (1-3 m) (McLaren *et al.*, 2009; McLaren and Wallace, 2010). The distribution and thickness of the clay is dependent upon the topography of the underlying Miocene and Pliocene sediments at the time of lake formation; the lake deposits are thickest in the east and shallow to 1-10 m in the west (Stephenson, 1986; McLaren *et al.*, 2009) possibly following the trend of lake initiation and growth (An *et al.*, 1986). Within the Blanchetown Clay are two members: the basal Chowilla Sand (Firman, 1966b) representing fluvial reworking of the Loxton-Parilla Sands (Firman, 1973) and the Nampoo Member. The Nampoo Member is a basin-wide aeolian-lacustrine silt unit located approximately 46 m above sea level representing wind-blown dust or loess (McLaren *et al.*, 2009).

The age of the lake was first constrained with the use of magnetic reversal stratigraphy by Bowler (1980), who determined lake initiation to be within the Gauss Chron and >2.4 Ma. An *et al.* (1986), also using palaeomagnetic analysis found the basal section of the Blanchetown Clay at Tyrrell and Chowilla sequences to be of normal polarity and in the Gauss Chron. Furthermore, they suggested that displaced sediments from the base of the Blanchetown Clay in the Lake Tyrrell Basin could have been

deposited as early as the Gilbert Chron and lake initiation had begun by 3.5 Ma. Bowler *et al.* (2006) using the dates of An *et al.* (1986) suggested that lake initiation began in the west and expanded east. Later palaeomagnetic analysis (McLaren *et al.*, 2009) of the Blanchetown Clay at Nampoo found the entire section to be of reverse polarity and within the Matuyama-Gauss Boundary implying lake initiation around 2.4 Ma. The conflict in initiation age was resolved by McLaren and Wallace (2010) who showed that the section used by An *et al.* (1986) to represent the Gauss Chron had been interpreted as coming from too far down in the stratigraphy and many of their deduced normal polarity intervals can be explained by overprinting.

Although lake initiation has been resolved to early within the Matuyama Chron, lake demise is not well-defined. Palaeomagnetic analysis dates the youngest Blanchetown Clay deposits within the Matuyama Chron (An *et al.*, 1986; McLaren *et al.*, 2009). However these deposits are truncated by an unconformity and other late lake deposits are unsuitable for palaeomagnetic analysis. The sediments overlying the youngest Blanchetown Clay are all of normal polarity within the current Brunhes Chron.

The extensive but relatively shallow nature of Lake Bungunnia would mean that the sedimentary record was sensitive to climate change with consideration to total evaporation and rates of discharge from feeder-rivers (McLaren and Wallace, 2010). Estimates of rainfall and runoff rates by Stephenson (1986) were determined under the assumption that a permanent outlet stream was unlikely. This view was based upon the longevity of the lake of at least 1.7 Ma. Increased vegetation cover would have tended to decrease runoff but rainfall would have been higher and less seasonal. A conservative estimate (Stephenson, 1986) of the palaeoclimatic conditions necessary to maintain Lake Bungunnia for an extended period is: evaporation 1.5-2.0 m yr⁻¹, average runoff 7-10% and average rainfall between 500 and 940 mm; conditions twice as wet as today. The Nampoo Member reflects a climatic shift ~1.5-1.4 Ma from a wet climate regime towards an arid regime with high average wind speeds (McLaren *et al.*, 2009; McLaren and Wallace, 2010). The Bungunnia Limestone, which sits unconformably above terraces of the Blanchetown Clay at successively lower lake levels, records decreasing lake levels and a progressive increase in the amplitude of arid climatic cycles (McLaren and Wallace, 2010). It has been suggested by An *et al.* (1986) that the desiccation of Lake

Bungunnia provides the starting point for present landscape development in that it marks the full development of arid conditions similar to modern time.

All south Victorian basins (Otway, Port Phillip and Gippsland) show a structural discordance between the deposition of Pliocene and Quaternary sediments (Wallace *et al.*, 2005). In the Murray Basin, along the Padthaway Ridge, this discordance is shown as a possible 4 Ma gap in the depositional record between the Loxton-Parilla Sands and the Quaternary Bridgewater Formation (McLaren *et al.*, 2011). The development of the Karoonda Surface below Lake Bungunnia suggests a substantial lapse in time between marine regression and lake formation (McLaren *et al.*, 2009). The hiatus in deposition is most likely one of many consequences of the Neogene tectonics discussed below.

2.3.4 Neogene tectonics

The movement of the northern margin of Australian continent into the subduction realm in Indonesia and the western Pacific after ~15 Ma resulted in continental tilt which continues to drive uplift on the southern margin (Sandiford, 2007; Sandiford *et al.*, 2009). Northern margin subsidence has placed much of the Cenozoic shorelines 0 to 50 m beneath sea level, whereas on the southern margin exposed mid-Miocene marine sequences imply a differential uplift of approximately 150 m since the mid-Miocene. Ongoing continent-scale tilt is on a WNW-ESE axis. The morphotectonic asymmetry of the tilt explains the dramatic uplift of the Nullarbor Plain in the Eucla Basin and the comparatively slight movement of the Murray Basin. The Mid-Miocene marine sequences in the Eucla Basin are found at ~180 m higher elevation than their counterparts in the Murray Basin (Sandiford, 2007). Differential uplift across the southern margin would have taken place before the Pliocene as contemporary sequences of that age are found at similar elevations, ~70 m or less. The continued subsidence of the northern margin and uplift along the southern margin implies that the continental tilting continues to the present day.

Li *et al.* (2004) recognised three mega-hiatus events (15-16 Ma, 8-9 Ma, 1.5-2.5 Ma) within the Neogene sediments of the Great Australian Bight reflecting tectonic instability across the southern Australian margin and glacio-eustatic sea-level change. This tectonism has been linked to a change in the continental stress regime (Dickinson *et*

al., 2002; Li *et al.*, 2004), reflecting resistance along the collisional boundaries of Australia and intraplate torques due to topographic forces (Coblentz *et al.*, 1995). In south-eastern Australia these changes led to east-west compression. Late Miocene through Pliocene compression was projected as basin inversion and erosion and associated localised folding as older structures were reactivated by the readjustment of older fault networks (Dickinson *et al.*, 2002). The tectonic origin of the unconformities is recognisable in their generally angular nature, the deformation of the deposits, which they overlie and the presence of a planation surface (Dickinson *et al.*, 2002; Li *et al.*, 2004). If the ages of the Mologa Surface, Karoonda Surface and the gap in deposition between the Loxton-Parilla Sands and Quaternary Bridgewater Formation are correct as they have so far been constrained, then their development coincides with these tectonic events.

The Mount Lofty Ranges and the Southern Highlands of Victoria comprise tilted fault blocks bounded by reverse faults and fault-line scarps. The Mid to Late-Neogene uplift has been associated with reverse faulting and the compressional stress regime to create a horst block structure (Bourman and Lindsay, 1989; Dickenson *et al.*, 2001; 2002). Uplift and erosion is recognised in the Miocene-Pliocene unconformity and in the offset of Oligocene-Miocene and Miocene-Pliocene sediments between intramontane and flanking basins (Wellman and Greenhalgh, 1988; Bourman and Lindsay, 1989; Tokarev *et al.*, 1998; Wallace *et al.*, 2005; Dickinson *et al.*, 2001; 2002). The associated scarps define prominent features and illustrate the first-order control that neotectonic fault movements have on the landscape (Tokarev *et al.*, 1998). Downfaulting and downwarping on the margins of Mount Lofty Ranges has formed Gulf St. Vincent to the west, and to the east a depression through which the modern River Murray flows and where Lakes Alexandrina and Albert are situated (Figure 2.7) (Sprigg, 1952; James *et al.*, 1992). Since ~6 Ma localised transpression (due to oblique forcing driven by the collision of the SE Australian and Pacific plates) has driven deformation resulting in sinistral strike-slip movements (Jayawardena, 2013).

The main watershed divide is located on the eastern side of the ranges (Tokarev *et al.*, 1998) indicating differential uplift of the eastern edge of the ranges before a Late

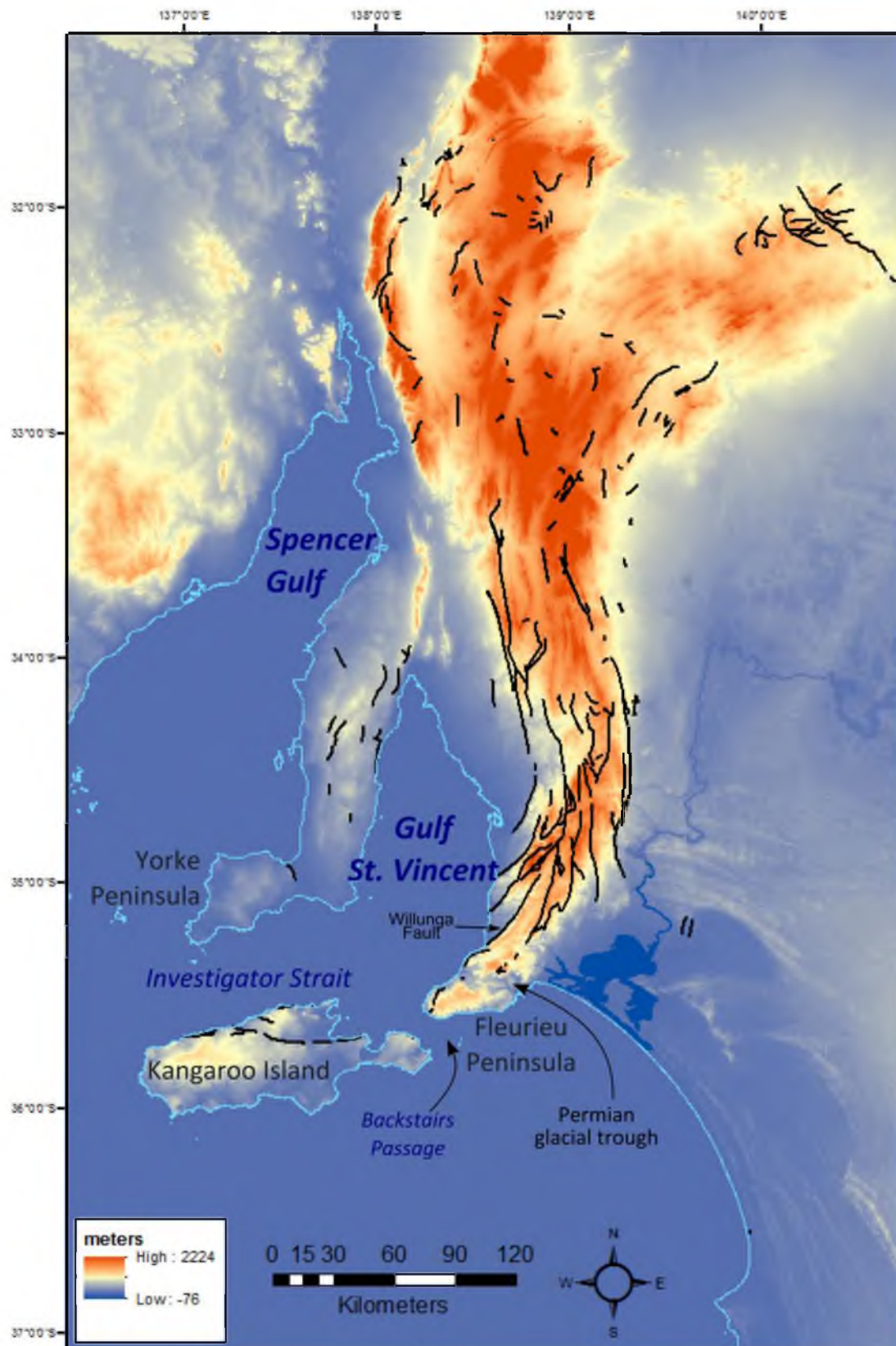


Figure 2.7: The horst block structure of South Australia is due to uplift and associated reverse faulting. The peninsulas are horst-like features of elevated basement rocks with Kangaroo Island an extension of Fleurieu Peninsula (Sprigg, 1952; James *et al.*, 1992). Black lines indicate known fault locations (DMITRE, 2014). SRTM derived Digital Elevation Model data provided by Commonwealth of Australia, Geoscience Australia (2009).

Miocene-Early Pliocene uplift. Uplift on the eastern margin of the ranges along the predominantly north-south trending faults has been east side up producing west-facing scarps and possible down-ward tilting of the western side, typical reverse faulting (Gibson, 2004). Uplift in the Mount Lofty Ranges during the Late Miocene-Early Pliocene was substantial with ~500 m of movement along the Willunga Fault (Tokarev *et al.*, 1998), and concentrated on the western edge of the ranges, which is now at a greater elevation than its eastern counterpart. The uplift disturbed the older established drainage pattern in the Ranges. Uplift of the Mount Lofty Ranges relative to the Murray Basin since the Mid-Miocene is ~200 m (Wellman and Greenhalgh, 1988) with an average slip rate on the major bounding faults of 30-100 m/10⁶ over the past 1-5 Ma (Sandiford, 2003). Continued faulting is made evident by the presence of neotectonic and reactivated Delamerian structures (Jayawardena, 2013). Neotectonic low-angle thrust faulting is clearly evident within faulted and tilted unconsolidated Cenozoic sediments but can also be observed extending into basement rocks. In some instances, Proterozoic basement is observed thrust over younger Quaternary sediments. Quaternary tectonic activity appears to be a result of both compressional reverse and strike slip faulting (Jayawardena, 2013).

Miranda *et al.* (2009) suggested that Neogene tectonic instability influenced the deposition of the Loxton-Parilla strandplain. Increased uplift and erosion after 5.0 Ma, combined with falling sea level, halted deposition of the Loxton-Parilla Sands and allowed development of the Karoonda Surface. McLaren *et al.* (2011) went further and suggested that continual long-term, possibly continent-scale uplift was responsible for progradation rates of the Loxton-Parilla strandplain and the Quaternary Bridgewater Formation. Cessation of the Loxton-Parilla Sands deposition was due to the differential uplift in the southern portion of the Murray Basin.

Faulting within the Murray Basin is most easily recognised by displacement of the Loxton-Parilla Sands. Loxton-Parilla strandlines on top of the Pinnaroo Block are found from west to east at 140 m AHD and 210 m AHD (Kotsonis, 1999) and reach 300 m on the Dundas Tablelands in Victoria (Dickinson *et al.*, 2001). Changes in the Loxton-Parilla strandline orientation can be explained by incremental tectonic movement (i.e. the change in strandline orientation across the Wimmera River in Victoria is consistent with

slight uplift to the southeast; Bowler *et al.*, 2006). Falling sea level and uplift of the Padthaway High and the extending Pinnaroo Block have been interpreted as being responsible for the development of the Kanawinka Escarpment (ranging from 30-100 m above present sea level) (Stephenson, 1986; Miranda *et al.*, 2008; 2009; McLaren *et al.*, 2011) as both a fault scarp and an erosional feature. The uplift would have shifted the shoreface seaward more rapidly than would have occurred by progradation alone (Roy and Whitehouse, 1999). The shift would have been counteracted by reduced rates of deposition and in this case, erosion on the uplifted blocks to form the Kanawinka escarpment. A northwest-southeast trending lineament broadly parallel to and north of the Kanawinka escarpment, the Bordertown-Apsley line, truncates the last Loxton-Parilla strandline and suggests a tectonic origin (Bowler *et al.*, 2006).

Another consequence of the Padthaway High uplift was the formation of Pliocene Lake Bungunnia ~2.4 Ma (section 2.3.3). Lake Bungunnia filled a number of sub-basins within the Murray Basin formed by differential movement along the northeast-trending Hamley, Danyo, Neckarboo, Tyrell and Iona Faults (Sandiford, 2003). Total displacement on the faults measures 50-75 m since the Pliocene. The uplift of the Padthaway High blocked the palaeodrainage to the Southern Ocean to form the large inland lake. Debate continues on the association of Lake Bungunnia to an ancestral River Murray, which is the topic of the next section.

2.3.5 The proto-River Murray

Cenozoic drainage in the central and western Murray Basin is mostly speculative as this part of the basin would have been subject to sediment bypass during sea level lowstands (Stephenson and Brown, 1989) and subject to marine ingression during highstands. However the importance of the River Murray in this thesis requires a review of previous discussion on the existence and location of an ancient River Murray and its tributaries.

Eastern and south-eastern tributaries of the River Murray, including the Murrumbidgee and Lachlan Rivers, developed alluvial fan and distributary channel complexes converging towards the central western geographic low of the Murray Basin as early as the Eocene (Stephenson and Brown, 1989). In the Eastern Highlands, a

coordinated drainage system ancestral to the modern River Murray headwaters was in place as early as the Eocene (Macumber, 1978). The Loddon, Campaspe, Goulburn and Ovens river valleys were subject to major phases of valley incision and river development in the Eocene and Miocene. The presence of this drainage system suggests that an early River Murray valley system was in existence in at least the eastern Murray Basin at the time. To the north, the Darling River most likely precedes Lakes Bungunnia into which it flowed (Stephenson and Brown, 1989; Bowler *et al.*, 2006).

Williams and Goode (1978) proposed that within the Eocene and Miocene the lower reach of the ancient River Murray flowed along basement lineaments across the South Australian Highlands (Mount Lofty - Flinders Ranges) and into Spencer Gulf before uplift of these ranges. Although Veevers (1982) placed uplift of the South Australian Highlands in the Palaeocene, he allowed the possibility of short intervals of drainage across the Southern Highlands in the Eocene and Miocene, in agreement with Williams and Goode (1978). Other authors (Gostin and Jenkins, 1980; Harris *et al.*, 1980) argued against any Cenozoic drainage across the South Australian Highlands based on the timing of highland uplift and the likely flow of any rivers southward across the partial barrier of the Padthaway Ridge in accordance with marine access to the basin during the Cenozoic. Harris *et al.* (1980) further suggested that the first available opportunity for an ancestral River Murray was not until the middle Pliocene, ~3 Ma, as proposed by Twidale *et al.*, (1978). Stephenson and Brown (1989) citing evidence from a comprehensive geological study of the Murray Basin (Brown and Stephenson, 1986; Brown and Stephenson, 1991 – in press at time of 1989 publication) determined that flow across the South Australian Highlands during the Cenozoic would have been unlikely as the uplands would have presented a topographic obstacle, and because the main depocentre of the Murray Basin appears to have been located in the central west of the basin since its development. This is where the earliest sediments, the fluvial Warina Sand of the Renmark Group (Firman, 1973; Lawrence; 1975), are found in the Murray Basin, suggesting the presence of a palaeodrainage directed to that region since the inception of the basin (Brown and Stephenson, 1986; Stephenson and Brown, 1989). Following the development of the northern, eastern and southern tributaries in the Eocene, drainage would have been towards this topographic low point.

There is evidence of drainage occurring sporadically along the western margin of Murray Basin since the Eocene. At the southwestern margin of the basin several small north-south trending coal fields occur within the Late Eocene Olney Formation suggesting that major drainage may have passed through the area (Stephenson and Brown, 1989). Additionally, infill of the Late Eocene Buccleuch Embayment by a progressively increasing proportion of terrigenous clastics up-sequence implies that a major incoming drainage gradually filled the embayment with sediment. This suggests that an ancient drainage system was connected directly to the Southern Ocean at the southwestern margin of the basin and across the Padthaway Ridge (Stephenson and Brown, 1989). Miranda *et al.* (2008) discovered a palaeo-valley system beneath the Norwest Bend Formation trending NNE-SSW 15-20 km east of the modern River Murray. The Miocene surface here is depressed by 10-15 m. The southerly-flowing palaeo-drainage originated north of Morgan and was incised in the Late Miocene or Earliest Pliocene. The authors found no evidence of fluvial input from the east.

McLaren *et al.* (2011) suggested that the Douglas Depression in western Victoria was, at least during early Pliocene time, the major drainage system from the Murray Basin. The Pliocene uplift of the Padthaway High reversed drainage in the Douglas Depression and created tectonic dams along its length initiating the formation of Lake Bungunnia. Continued uplift in the Victorian Highlands allowed the eventual breaching of the tectonic dam in the western part of the basin by an ancestral River Murray. The resurgent tectonics, which occurred in the Neogene (section 2.3.4), and successive phases of river avulsion within the Quaternary determined the course of the modern River Murray (Twidale *et al.*, 1978).

2.4 The Quaternary

The Quaternary period encompasses the past 2.588 Ma of Earth history, containing the Pleistocene and Holocene Epochs (Gibbard *et al.*, 2010; Cohen *et al.*, 2013), and is characterised by marked global climate oscillations and the repeated growth and decay of continental ice sheets associated with substantial fluctuations of eustatic sea-level (Belperio, 1995b; Woodroffe, 2002; Miall, 2010; Murray-Wallace and Woodroffe, 2014). Global fluctuations in sea-level and ice volume have been linked to a

phenomenon explained by the Astronomical Theory of Climate Change (Croll, 1875), later expanded and recognised as the Milankovitch Hypothesis (Emiliani, 1955; Broecker *et al.*, 1968; Imbrie *et al.*, 1984; Plint *et al.*, 1992). Changes in ice volume and sea water temperatures subsequently affect climate (Petit *et al.*, 1999; Barrows *et al.*, 2007; Fujioka and Chappell, 2010; Barker *et al.*, 2011), which, in Australia has also been influenced by the steady northward movement of the continent (Kemp, 1978; Bowler, 1982; Fujioka and Chappell, 2010). The increased aridity of continental Australia during the Quaternary has prompted the deposition of aeolian dunes directly linked to the climate of fluctuating glacial and interglacial periods as well as glacio-eustatic sea-level changes. This record is found on the Coorong Coastal Plain (CCP).

This section will first provide the hierarchy of Quaternary geologic time which provides a framework for the ensuing review. This is followed by a review of the Milankovitch Hypothesis and how it explains the oscillation of sea-level and climate throughout the Quaternary and how that record persists in biological, geomorphological and geological proxies. In southern Australia, climatic fluctuations have been recorded in aeolian dune development: siliceous dunes deposited during glacial periods and carbonate dunes in marginal marine environments during interglacial periods. This section concludes with a description of the climate and sea-level record provided by the aeolian dune record in the Murray Basin and on the Coorong Coastal Plain.

2.4.1 The Quaternary Period

The Neogene/Quaternary Boundary, with which the Pliocene/Pleistocene Boundary is coeval has been placed at 2.588 Ma (within MIS 103) (Gibbard *et al.*, 2010). The base for the Quaternary and Pleistocene marks the initiation of general global cooling, major climatic and environmental oscillations and the establishment of the global physical boundary conditions which characterise the Quaternary (Bowen and Gibbard, 2007; Head *et al.*, 2008; Gibbard *et al.*, 2010). This boundary broadly corresponds with major cooling phases recorded in the North Atlantic, China, northwestern Europe, and New Zealand between 2.8 – 2.4 Ma, closure of the Isthmus of Panama (2.72 Ma), and the Gauss-Matuyama magnetic reversal (2.581 Ma).

The Quaternary is subdivided into the Pleistocene and Holocene Epochs (Figure 2.8), geologic-climatic units based on proxy climatic indicators that provide clear climatic signatures (Walker *et al.*, 2009). The boundary of the Middle and Late Pleistocene corresponds to the Brunhes-Matuyama magnetic reversal at 0.781 Ma (Cohen and Gibbard, 2011). The Holocene includes the present day and has been referred to in literature as *recent* and *post-glacial*. The Pleistocene/Holocene boundary is placed at the end of the Younger Dryas (11.7 ka), the most recent cold episode of the Pleistocene, as defined by the Greenland NGRIP ice-core record (Walker *et al.*, 2009). The global climatic oscillations and sea-level fluctuations of the Quaternary can be explained by the Milankovitch Hypothesis.

Figure 2.8: The hierarchy of Quaternary geologic time as defined by the International Commission on Stratigraphy (Cohen *et al.*, 2011) with palaeomagnetic chrons.

Period	Epoch	Age		Chron	numerical age (Ma)
Quaternary	Holocene			Brunhes	present
	Pleistocene	Late			0.0117
		Middle			0.126
		Early	Calabrian	Matuyama	0.781
			Gelasian		1.80
					2.588

2.4.2 The Milankovitch Hypothesis

The orbital geometry of the Earth is now accepted as a major force behind the fluctuations of long-term global ice volume, global climate and the cyclicity (10^4 - 10^5 years) recognised in the Late Cenozoic sedimentary record (Broecker *et al.*, 1968; Hays *et al.*, 1976; Chappell and Shackleton, 1986; Petit *et al.*, 1999; Zachos *et al.*, 2001). The view that the surface temperature of the Earth varies in response to regular and predictable changes in the orbit of the Earth and movements of its axis was first developed by Croll (1875). However, the phenomenon is recognised as Milankovitch Theory after the Serbian mathematician who carried out the theoretical work (Miall,

2010; Murray-Wallace and Woodroffe, 2014). 'Milankovitch cycles' are the result of three orbital rhythms (Figure 2.9), which control the latitudinal seasonal distribution of incoming solar radiation, also known as insolation, and subsequently global climate (Hays *et al.*, 1976; Plint *et al.*, 1992; Zachos *et al.*, 2001). The orbital rhythms are:

1. *Eccentricity*, the shape of the orbit of the Earth around the sun from near circular to elliptical (400 ka and 100 ka oscillation);
2. *Obliquity*, the tilt of the axis of the Earth relative to the plane in which it orbits the sun, varying between 21.8° and 24.4° (41 ka oscillation); and
3. *Precession*, the wobble of the Earth around its axis of rotation (23 ka oscillation).

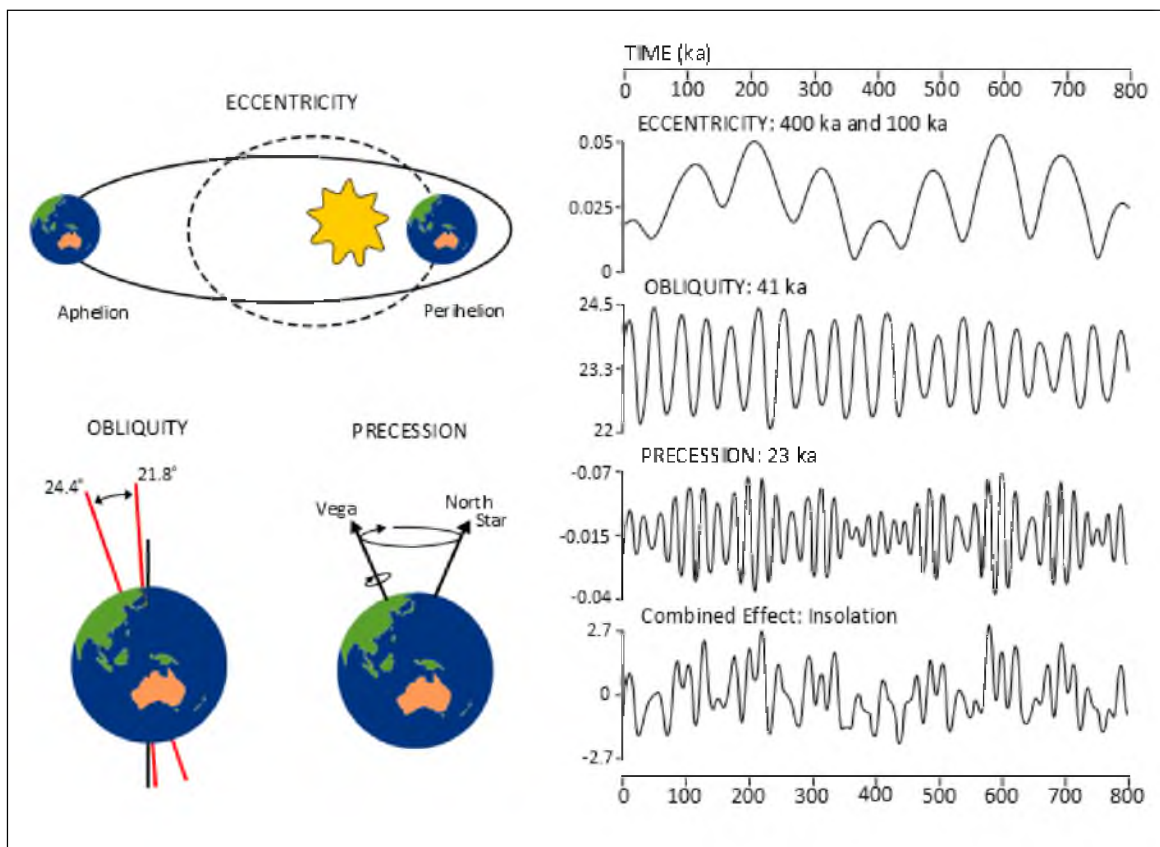


Figure 2.9: The three principal orbital rhythms driving the cyclicity of global climate change are: eccentricity, obliquity and precession. The combined effect of the rhythms determines the insolation (solar radiation) that reaches the surface of the Earth. Variation in eccentricity, obliquity, and precession over the past 800 ka and their combined effect on insolation is from Imbrie (1985). The obliquity scale is in degrees. The insolation scale is in standard deviation units.

Precession alters the structure of the seasonal cycle by affecting where in the orbit around the sun (with relation to aphelion or perihelion) seasons occur, thereby affecting the intensity of insolation during each season and increasing seasonal contrast

in one hemisphere while decreasing it in the other (Imbrie, 1985; Zachos *et al.*, 2001). Obliquity alters the latitudinal distribution of insolation by modulating the intensity of the seasonal cycle (Imbrie, 1985; Zachos *et al.*, 2001, Miall, 2010). For example, when obliquity is high, more energy is delivered to the poles and seasonal contrast is increased (i.e. winter will be colder and summers hotter in both hemispheres). When obliquity is low, more energy is delivered to the equator resulting in decreased seasonality. Eccentricity affects climate by tempering the amplitude of precession, thereby influencing the total annual/seasonal solar energy budget (Ruddiman *et al.*, 1986; Zachos *et al.*, 2001). These orbital rhythms have been shown to produce the climatic variance (at periods corresponding to 23 ka, 41 ka, and ~100 ka) of the Quaternary record through cyclical variation in the intensity and seasonal distribution of incoming solar radiation and to be the cause of the succession of Quaternary ice ages by affecting the summer melt period and ice sheet development (Hays *et al.*, 1976 Imbrie, 1985; Petit *et al.*, 1999; Barrows *et al.*, 2007; Fujioka and Chappell, 2010). The volume of terrestrial ice on Earth is directly linked to the volume of water in the ocean and is one of two factors which control relative sea-level and water depth in a global context, the other being the volume of ocean basins which is predominantly due to the volume of spreading of the oceanic ridges (Plint *et al.*, 1992).

The influence of Milankovitch cycles on the growth and decay of large continental ice sheets, and therefore Quaternary sea-level, are reflected in the record provided by deep sea cores and polar ice sheets. The development of the sea-level and climatic history of the Earth has been made possible by proxy analysis of marine sediment, oceanic oxygen isotopes, and ice cores (Shackleton and Opdyke, 1973; Chappell and Shackleton, 1986; Zachos *et al.*, 2001; Siddall *et al.*, 2007). Changes within these records have been directly correlated to Milankovitch cycles and calibrated to orbital parameters to provide a time-scale (Imbrie *et al.*, 1984; Chappell and Shackleton, 1986, Ruddiman *et al.*, 1986, Martinson *et al.*, 1987 Raymo *et al.*, 1989).

2.4.3 The oxygen isotope record

There are multiple proxies available to assist in understanding palaeosea-level and climate for the Quaternary. Sea-level indicators include biological proxies (coral reefs, mangroves, seagrass, salt-marsh sediments, submerged forests, marine molluscs,

microfossils, etc.) and geomorphological and geological proxies (marine terraces and shore platforms, shoreline notches, beach ridges, aeolianites, calcretes, beachrock, etc.). High-resolution proxy climate indicators are more limited but include tree rings, pollen grains, coral reefs, lake and ocean sediments, periglacial features, and snow and ice deposits. The limitation of many of these proxies, sea-level or climate, is their preservation (or lack thereof) in the geological record and therefore, completeness and the ability to establish adequate geochronological control, especially relating to developing a global record of Quaternary sea-level and climate change. The advent of deep sea and ice sheet coring in conjunction with oxygen isotope analysis, alongside analysis of other stable isotope content and major chemical elements, has made such a global record possible. The cores are used in the development of the oxygen isotope ($\delta^{18}\text{O}$) record which can be dated using orbital tuning by matching the regularities in the record to Milankovitch cycles (Imbrie *et al.*, 1984; Martinson *et al.*, 1987; Lorius *et al.*, 1989).

Ice cores reflect atmospheric temperature and composition (including levels of trace greenhouse gases) and the $\delta^{18}\text{O}$ of water precipitated at the time of snow deposition (Dansgaard and Oeschger, 1989; Lorius *et al.*, 1989; Petit *et al.*, 1999) as well as providing a record of marine and terrestrial aerosols. Ice cores in Antarctica show much larger impurity concentrations during glacial periods than interglacials (Lorius *et al.*, 1989; Petit *et al.*, 1999) reflecting the larger size of continents due to lowered sea level, more extensive arid areas which form at the forefront of ice sheets, more efficient meridional transport linked to higher wind speeds (Petit *et al.*, 1981) and a reduced hydrological cycle (Yung *et al.*, 1996). The record of changes in atmospheric trace gases, variations in atmospheric particulate matter and other trace substances can be used to reconstruct *inter alia* changes in atmospheric circulation, former temperature and precipitation regimes. Furthermore, changes in atmospheric $\delta^{18}\text{O}$ can be used as an indicator of large ice-volume changes (Dansgaard and Oeschger, 1989; Petit *et al.*, 1999).

Deep-sea sediments, through the remains of planktonic and benthic foraminifera, provide a record of the $^{18}\text{O}/^{16}\text{O}$ ratio of sea water during their life (Emiliani, 1955; Shackleton and Opdyke, 1973). The lighter ^{16}O is preferentially stored in continental ice sheets and the oxygen isotope record within marine foraminifera reflects

variations in global ice volume, the isotopic composition of sea water and local water temperature (Emiliani, 1955; Shackleton and Opdyke, 1973; Chappell and Shackleton, 1986; Chappell *et al.*, 1996). The waxing and waning of the Northern Hemisphere and Antarctic ice sheets is the dominant cause for variation within the $\delta^{18}\text{O}$ record, accounting for approximately 70% of variability (Shackleton and Opdyke, 1973; Zachos *et al.*, 2001). Therefore, the oxygen isotope record can be used to infer an ice volume or ocean volume and sea water temperature record.

In 1967, Shackleton proposed that the isotopic composition of the ocean detected in deep-sea sediment cores could be used to provide a global stratigraphic record. Peaks in the record correspond with warmer intervals (interglacial or interstadial) and are assigned an odd Marine Isotope Stage (MIS) number, also known as a marine Oxygen Isotope Stage (OIS). Troughs corresponding to glacial or stadials are assigned an even number. The record provides a framework of standard stages allowing correlation of Quaternary records not only from deep-sea sediments but other proxies as well, including terrestrial records (Shackleton, 2006). The Holocene is assigned MIS 1, the last interglacial (*sensu lato*) MIS 5 with the intervening glacial maximum MIS 2, interstadial MIS 3, and stadial MIS 4; the higher the number, the older the stage (Figure 2.10). The time-scale of the records range from the high-resolution deep-sea chronostratigraphic record for the past 300 ka (Martinson *et al.*, 1987) to the single global deep-sea record representing the entire Cenozoic (Zachos *et al.*, 2001).

2.4.4 Progression of Quaternary aridity in Australia

During the Cenozoic the climate of Australia has been influenced by: 1) the development of Antarctic ice and cooling of the deep ocean and 2) the northward drift of the continent and development of circumpolar circulation in the Southern Ocean (Kemp, 1978; Fujioka and Chappell, 2010). By the Quaternary, Australia had reached lower latitudes and as a consequence the continent largely escaped glaciation. The growth of the Antarctic ice sheets was mirrored by the equator-ward migration and intensification of the anti-cyclonic sub-tropical high pressure belts (Bowler, 1982). The establishment of Northern Hemisphere glaciation (NHG) (~3 Ma) coincided with extensive cooling of the Southern Ocean driving the paths of the anticyclones farther north over Australia and establishing the anticyclone tracks and pressure patterns

characteristic of the Quaternary (Bowler, 1982; Bowler and Sandiford, 2007). This marks a transition period in climatic conditions affecting Australia (i.e. the beginning of winter rainfall and intensified westerly circulation and the development of arid landscapes across the southern margin of Australia). The Plio-Pleistocene cooling also enhanced the thermal gradients surrounding Antarctica and changed Southern Ocean dynamics resulting in a much higher energy coastline along southern Australia (Bowler and Sandiford, 2007).

Bowler and Sandiford (2007) suggested that Pliocene growth of the Antarctic Ice Sheets and early Pleistocene cooling dampened both the precession and obliquity signals and favoured the development of the 100 ka cycle, which has been prominent in the late Quaternary record. The Southern Ocean has been shown to be highly sensitive to climate change, on both orbital and suborbital timescales, in deep-sea records spanning the last glacial-interglacial cycle (Barrows and De Deckker, 2007; Barrows *et al.*, 2007). The record shows a large magnitude of sea surface temperature (SST) change and variability. SST change is felt equally on land and such a regional response reflects a common cause for climate change and close meteorological links between land and sea.

By the end of the Late Pliocene climate change had progressed from the Early Pliocene warm-wet with summer rainfall peak (mean annual temperature (MAT) 2-4°C higher than present, mean annual precipitation (MAP) 50-70% higher than present) to a drier-cooler climate with a winter rainfall peak (MAT 0-2°C higher than present, MAP 0-30% higher than present) (Gallagher *et al.*, 2003). The increase of arid-adapted fauna in the central Australian record at the Pliocene-Pleistocene transition indicates that the region was already becoming comparable to the modern arid zone (Fujioka and Chappell, 2010). Likewise, the landscapes of southeastern Australia were already populated by plant species similar to the present day (Gallagher *et al.*, 2003). Although the modern climatic patterns had been established by the beginning of the Quaternary, Australia was still considerably wetter than today (Martin, 2006). The overall trend throughout the Quaternary has been one of decreasing precipitation, in so much that even the last interglacial period (~120 ka) was wetter than present (Nanson *et al.*, 1992; Bourman *et al.*, 1997; 2010; Fujioka and Chappell, 2010; Cohen *et al.*, 2011).

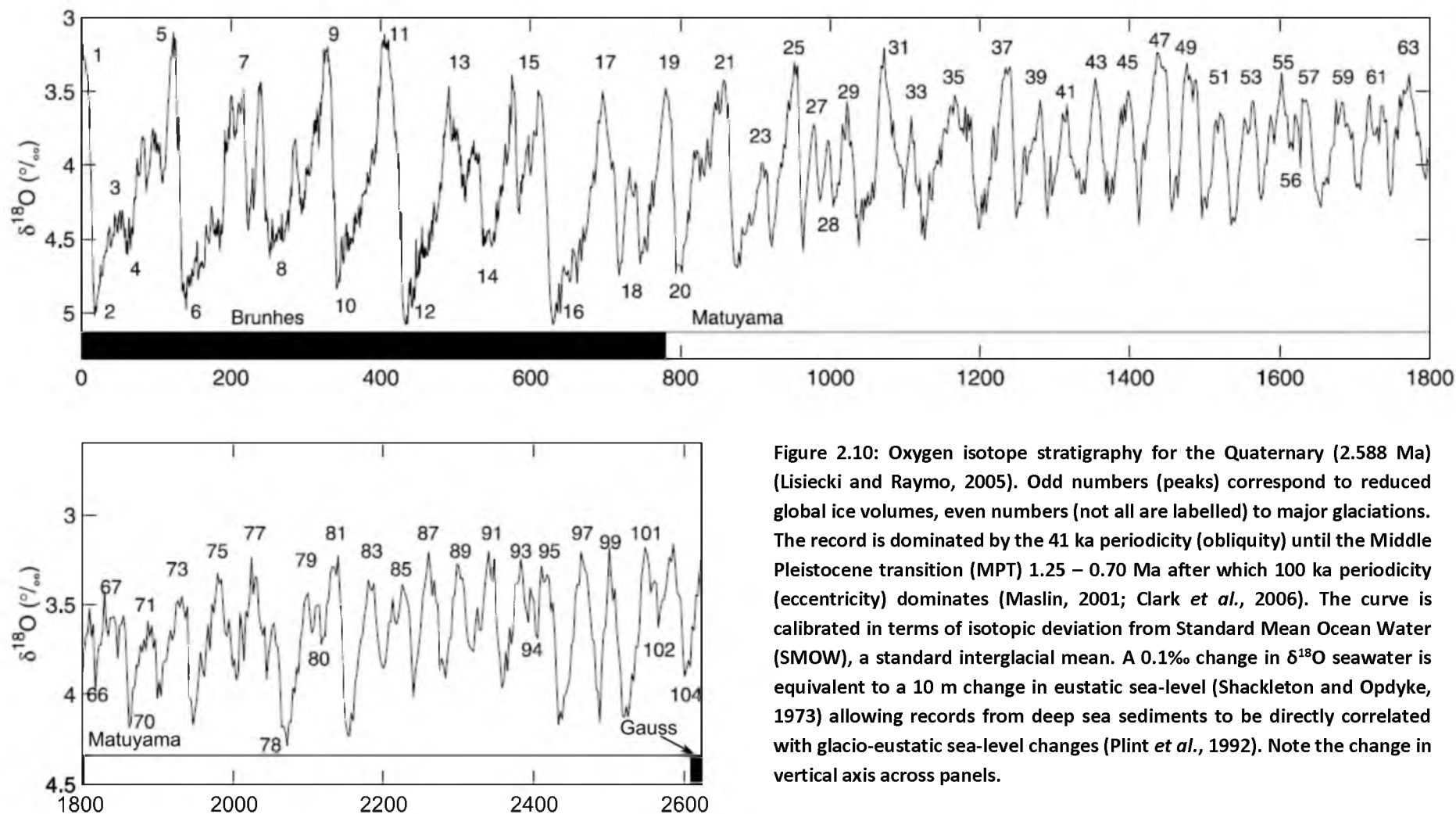


Figure 2.10: Oxygen isotope stratigraphy for the Quaternary (2.588 Ma) (Lisiecki and Raymo, 2005). Odd numbers (peaks) correspond to reduced global ice volumes, even numbers (not all are labelled) to major glaciations. The record is dominated by the 41 ka periodicity (obliquity) until the Middle Pleistocene transition (MPT) 1.25 – 0.70 Ma after which 100 ka periodicity (eccentricity) dominates (Maslin, 2001; Clark *et al.*, 2006). The curve is calibrated in terms of isotopic deviation from Standard Mean Ocean Water (SMOW), a standard interglacial mean. A 0.1‰ change in $\delta^{18}\text{O}$ seawater is equivalent to a 10 m change in eustatic sea-level (Shackleton and Opdyke, 1973) allowing records from deep sea sediments to be directly correlated with glacio-eustatic sea-level changes (Plint *et al.*, 1992). Note the change in vertical axis across panels.

The Middle Pleistocene Transition (MPT) (1.25 – 0.70 Ma) marks the gradual transition of ice age cycles from periods of 41 ka to 100 ka and the intensification of global glacial-interglacial cycles (Maslin *et al.*, 2001; Clark *et al.*, 2006). At the conclusion of the MPT the dominance of the 100 ky cycle was established and the amplitude between warm and cold periods had reached its current maximum (Figure 2.10). By 1 Ma the sub-tropical high pressure belts (STHP) had taken up their present positions over Australia (Bowler, 1982) and the dating of arid landforms in central Australia to 1 Ma indicates aeolian sedimentation and dune activity had commenced by this time (Fujioka *et al.*, 2009). The earliest known glaciation of Tasmania also occurred at ~ 1 Ma (Colhoun and Barrows, 2011). By 900 ka the climate had transitioned from an earlier humid regime to one with phases of fully developed glacial aridity (Bowler *et al.*, 2006). The current pattern of Quaternary climate in Australia appears to have been well established by 500 ka (Bowler, 1982) when an increase in aridity resulted in the initiation of saline-gypseous deposition in the arid zone (Martin, 2006). Accelerated dune formation from the mid-Pleistocene has been accredited to an increasingly arid climate in subsequent glacial cycles (Hesse, 2010).

Aeolian landforms in Australia commonly associated with aridity are dunefields, playas (ephemeral lakes) and associated lunettes, aeolian dust deposits (parna) and stony deserts (gibber pavements). The development of these arid landforms requires significant winds, sparse protective vegetation and a supply of available, unbound surface materials, although not necessarily much lower precipitation than present (Beard, 1982). Enhanced wind activity, and possibly increased evaporation, would have allowed aeolian processes such as deflation and formation of sand dunes and aeolian silt transport to have greater impacts on the landscape (King, 1960; Fujioka and Chappell, 2010). The presence of arid landforms outside the current arid zone attests to the more severe arid conditions associated with glacial periods (Beard, 1982; Hesse, 2010).

2.5 Murray Basin aridity

The southern marginal basins of Australia, being directly impacted by any changes to the boundary conditions of the Cenozoic Southern Ocean, contain sedimentary records reflecting global climate change (Fujioka and Chappell, 2010). The

lower Murray Basin has been a region of fluctuating peaks of fluvial and aeolian activity for the past ~1 Ma (Sprigg, 1982a). An obvious indicator of increasing aridity in the Murray Basin is the demise of Pleistocene Lake Bungunnia (section 2.3.3). Desiccation of the lake has been attributed to a climatic shift from a wet climate regime towards an arid regime with high average wind speeds at ~1.5-1.4 Ma (McLaren *et al.*, 2009; McLaren and Wallace, 2010). The increasing aridity within the basin following the demise of Lake Bungunnia is marked by episodes of lake-lunette building and dunefield development.

The trend of the dunefields deposited during glacial and interglacial periods is determined by the 5° latitude shift of the dominating westerly 'frontal' air stream (Figure 2.11 A). During glacial intervals the 'Roaring Forties' shifted northwards to become the 'Roaring Thirties' (Sprigg, 1982b). In the Murray Basin the intensification of wind strength combined with lowered sea-level and overall drier climate resulted in lunette formation and deposition of west-east trending siliceous desert sands: the Woorinen Formation (Lawrence, 1966), Molineaux Sand (Firman, 1973) and Bunyip Sand (Firman, 1966b) (Figure 2.11 B). During interglacials, with high sea-levels, wind patterns resumed their more southerly position and the southern coastline of Australia became the locus for deposition of aeolian carbonate coastal dunes (Sprigg, 1952; 1979). The Pleistocene interglacial dunes preserved across on the Coorong Coastal Plain, Kangaroo Island and Eyre and Yorke Peninsulas are known as the Bridgewater Formation (Boutakoff, 1963).

2.5.1 Glacial aeolian landforms

Dunes have the potential, depending on degree of preservation, for assisting in the reconstruction of past aridity, wind strength and wind direction once the age of the dune is known (Lomax *et al.*, 2011). The dunefields of the Woorinen Formation, Molineaux Sand and Bunyip Sands provide insights into the aeolian climate of the Quaternary during periods of glacially low sea-levels.

The predominant E-W orientation of the Woorinen Formation and Bunyip Sands is indicative of an environment dominated by westerly winds under conditions more arid than present and a lack of adjustment to modern conditions (King, 1960; Lawrence,

1980; Hesse, 2011). The Woorinen Formation contains an internal structure consisting of five dune members which have been formally recognised, each associated with a sequence of aeolian accretion and except for the uppermost, a degree of soil development (Lawrence, 1966; 1980; Bowler, 1976). The soil development which protects the dune during the next phase of mobilisation, attests to cyclic periodicity in arid and stable, soil-forming phases. If each palaeosol represents a 100 ka glacial-interglacial cycle, dune initiation would be near 500 ka (Bowler *et al.*, 2006).

The Molineaux Sand of South Australia (Firman, 1973), equivalent to the Lowan Sand of Victoria (Lawrence, 1966), is at times referred to as one unit, the Molineaux-Lowan Sand (Brown and Stephenson, 1991) and is here referred to as the Molineaux Sand keeping with the South Australian designation. The Molineaux dunefield is the only glacial dunefield which extends into the study area.

The source of the siliceous sands is contentious with various sources suggested: the underlying Parilla Sand (Lawrence, 1966; 1980; Bowler *et al.*, 2006), the coastal Bridgewater Formation (Crocker, 1946; Sprigg, 1952; 1959; Boutakoff, 1963; Fitzsimmons and Barrows, 2012) and thalassostatic terraces in the River Murray in addition to coastal dunes from the region of the highstand Murray Mouth (Sprigg, 1979). Given that the dunefields extend from the River Murray and its mouth region over the Loxton–Parilla Sands preserved on the Pinnaroo Block and Padthaway High (Figure 2.11 B), all sources are likely to have contributed in some degree to dune formation. Although the dunes trend eastward, they are slightly asymmetric with a steeper northern slope. This is consistent with the existing wind regime which is stronger from the south-west (Lawrence, 1980) indicating reworking during the current Holocene interglacial. The sands were considered to be ‘recent’ in origin by Firman (1973) and it was noted by Bowler *et al.* (2006) that the Molineaux Sand appeared to overprint the Woorinen Formation.

Deposition of the Woorinen Formation was determined by optically stimulated luminescence (OSL) analysis to have been initiated by at least 380 ka (Lomax *et al.*, 2007; 2011). Additional OSL work (Fitzsimmons and Barrows, 2012) has shown Molineaux Sand

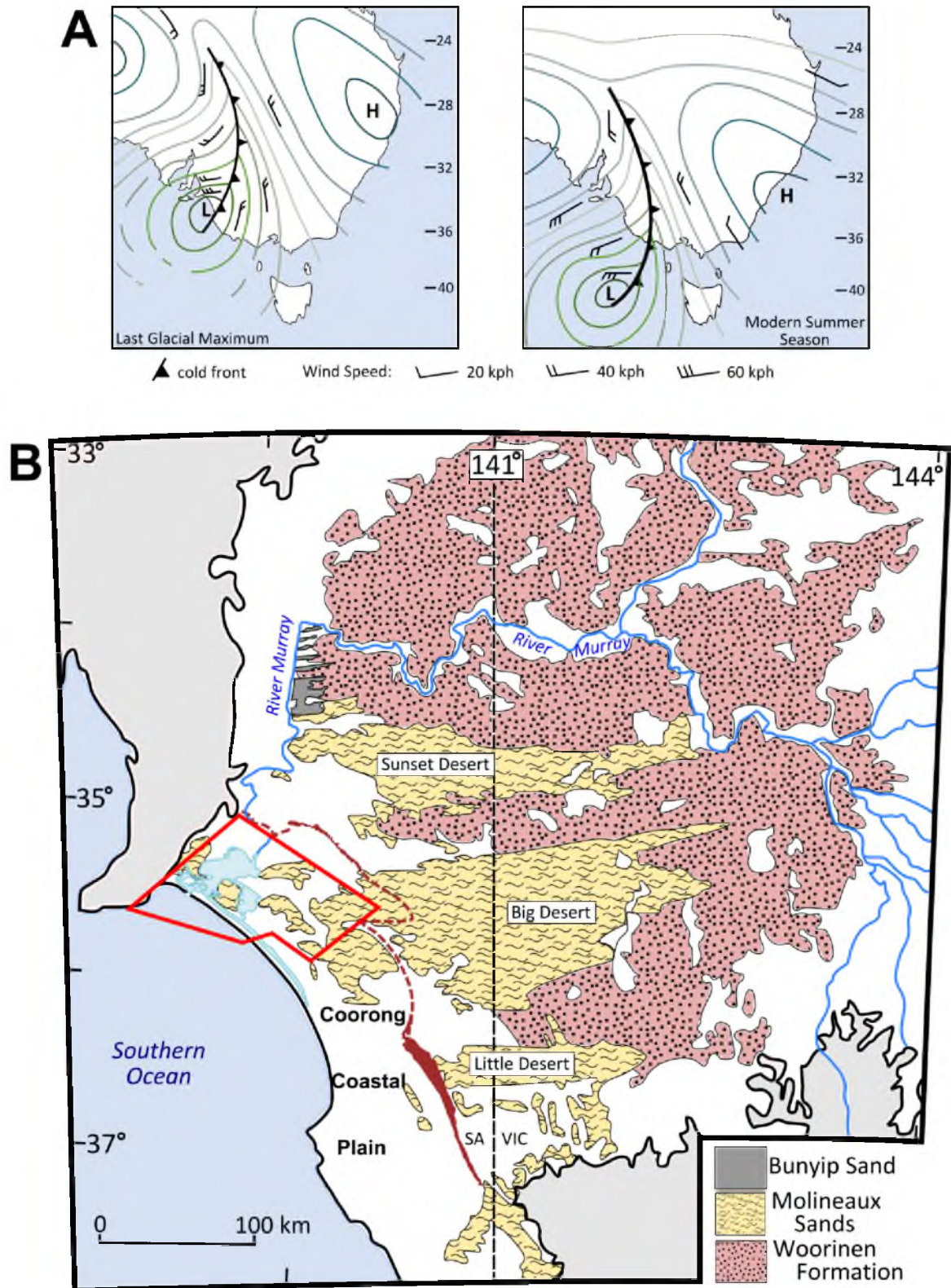


Figure 2.11: A) Isobaric charts illustrating the approximate 5° latitude shift of westerly winds between the LGM and current Holocene interglacial (figure modified from Sprigg, 1982b.) B) Aeolian glacial dunes predominantly trend east-west reflecting the dominant westerly winds during glacial periods (Lawrence, 1966; Firman, 1967; 1973; Sprigg, 1979). The Coorong Coastal Plain, west of the Marmon Jabuk – Kanawinka Escarpment (maroon), is host to interglacial aeolian dunes of the Bridgewater Formation, which trend northwest-southeast. Study area outlined in red. Figure modified from Brown and Stephenson (1991). Bunyip Sand location from DMITRE (2014).

deposition to have begun by 200 ka. Deposition within all of the dunefields appears to have occurred at the same time during defined phases broadly associated with more arid conditions (18-38 ka, 63-72 ka, and 80-111 ka) versus periods of non-deposition coinciding with more humid phases (~40-60 ka and ~75-80 ka). Older phases are present but contain relatively large uncertainties on the OSL ages and are too imprecise to resolve palaeoenvironmental variations (Fitzsimmons and Barrows, 2012). Two modern ages in the Woorinen Formation indicate the dunes are episodically reactivated following bushfires or during severe drought (Lomax *et al.*, 2011). Fitzsimmons and Barrows (2012) found the deposition of Molineaux Sand in their study to be more or less continuous and suggested a lack of available sediment as the principal constraint for deposition.

Intensified glacial aridity is attributed to increased atmospheric circulation, reduced atmospheric moisture and increased size of the continent due to lowered sea levels (Bowler, 1982; Fujioka and Chappell, 2010). The continental shelf, exposed during glacial periods when sea-level was be as much as 120-130 m below present and near the continental margin, serves as a setting for extensive continental dunefield development (Harvey *et al.*, 2001; Hesse, 2010) made possible by the delivery of terrigenous sediment via a glacial River Murray (Sprigg, 1979; Harvey *et al.*, 2001).

2.5.2 The River Murray during glacial sea-level lowstands

The development of the modern River Murray system in South Australia was initiated with the demise of Lake Bungunnia around the time of the Brunhes-Matuyama Boundary (section 2.3.3). The incision of the Murray Valley gorge adjacent to the Mount Lofty Ranges and south of Overland corner, through the calcareous and massive bedding of Miocene Murray Group Limestone, was initiated by the glacio-eustatic lowering of sea level to as much as 120-130 m below present level (Twidale *et al.*, 1978; Harvey *et al.*, 2001; Gingele *et al.*, 2004). Since initial incision, the river has eroded to depths up to 65 m below present sea-level. Bowler *et al.* (2006) suggested that the depth and width of the gorge in which the present Murray meanders, is a grossly underfit stream and indicative of periods of much greater discharge during the wetter climates of the Early to Mid-Pleistocene. However, it could be that the river has had sufficient time to carve the wide valley or even that valley incision had been initiated prior to development of the

Quaternary River Murray by earlier drainage on the western margin of the Murray Basin (section 2.3.5).

During sea-level lowstands a palaeo-River Murray would have flowed across an expansive coastal plain formed on the Lacepede Shelf, a 180 km-wide embayment in the continental shelf, to a coastline located on the margin of the continental shelf approximately 200 km to the south (Hill *et al.*, 2009) (Figure 2.12 A). Harvey *et al.* (2001) and Gingele *et al.* (2004) have suggested that during sea level lowstands Gulf St. Vincent was drained by a palaeo-River Vincent which joined a palaeo-River Murray via the Backstairs Passage. It is likely that the coastal plain was at least partly covered by aeolian sand sheets and dunefields at the time (Bowler, 1976; Sprigg, 1979; Harvey *et al.*, 2001). Glacial period fluvial facies identified on the Lacepede Shelf include in-filled palaeochannels, point-bar deposits and well-stratified, flat-lying lagoonal/lacustrine sediments (Hill *et al.*, 2009). Channels on the shelf reflect at least six downcutting episodes. Channel re-incision in the main Pleistocene channel or valley indicates the return of a palaeo-river to roughly the same place during multiple sea-level cycles.

Channels nearer the modern coastline indicate that the palaeo-River Murray flowed south from Lakes Alexandrina and Albert in the region of the modern Murray Mouth (Hill *et al.*, 2009). Unconsolidated sediments within the modern Goolwa Channel reach depths over 19 m (Oliver and Anderson, 1940) indicating the channel was excavated well below present sea-level since the Last Interglacial (Bourman *et al.*, 2000). During glacial lowstands prior to the Last Glacial Maximum (LGM) the palaeo-mouth of the river was located almost directly to the south of the modern river terminus but it appears to have shifted during the LGM to a position farther to the west-southwest (Gingele *et al.*, 2004; Hill *et al.*, 2009). Sprigg (1979) identified a knickpoint at 100–111 mwd which he interpreted as a palaeo-shoreline formed at the sea-level lowstand of the last glacial maximum. The crest of the escarpment is at 90-100 mwd and the base at 120 mwd marking the inner edge of the outer shelf (James and Bone, 2011).

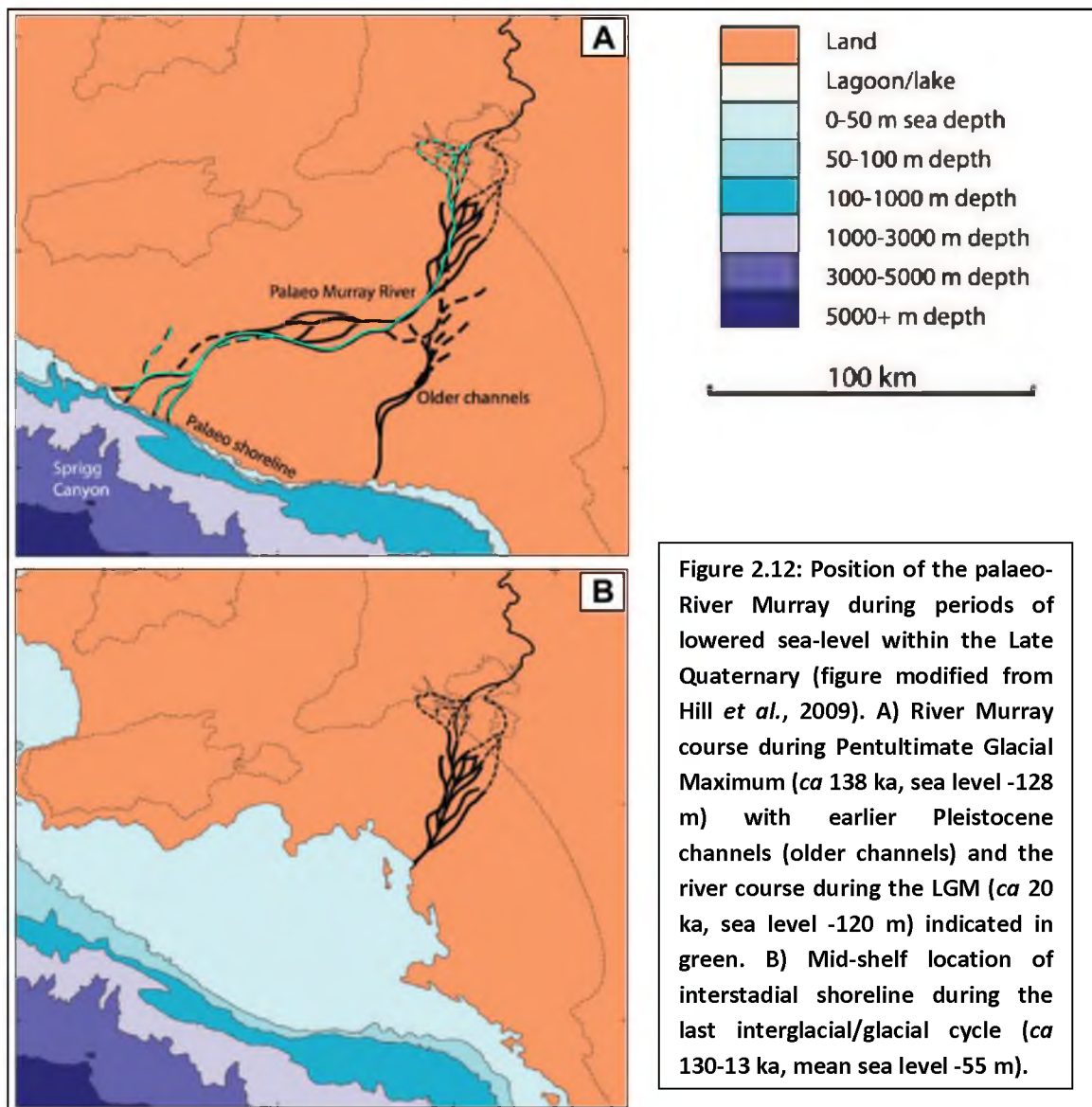


Figure 2.12: Position of the palaeo-River Murray during periods of lowered sea-level within the Late Quaternary (figure modified from Hill *et al.*, 2009). A) River Murray course during Pentultimate Glacial Maximum (ca 138 ka, sea level -128 m) with earlier Pleistocene channels (older channels) and the river course during the LGM (ca 20 ka, sea level -120 m) indicated in green. B) Mid-shelf location of interstadial shoreline during the last interglacial/glacial cycle (ca 130-13 ka, mean sea level -55 m).

The most likely position for the river mouth during interstadials when sea-level would have been located somewhere between the glacial/interglacial extremes is somewhere mid-shelf (Figure 2.12 B) (James *et al.*, 1992; Hill *et al.*, 2009). Intermediate sea-level during interstadials would have resulted in a shallow, relatively low energy shelf with environments ranging from strandline to lagoon to shallow open shelf (James *et al.*, 1992). In the most common palaeogeographic scenario (because sea level for the majority of time, is located between the extreme interglacial maxima and glacial minima), the Lacepede Shelf would have been smaller than its present size with the shoreline and associated banks, shoals and barrier islands, forming somewhere mid-shelf (Hill *et al.*, 2009). Marshes and other wetlands probably would have extended

inland. Mean sea level since ~800 ka has been near -55 m (Siddall *et al.*, 2006; Hill *et al.*, 2009). Former strandlines (marooned beaches) are recognised between 40 and 65 mwd by ridges and sheets of limestone pebbles and gravels and bivalve coquinas (James *et al.*, 1992; James and Bone, 2011) which coincides with the conclusion of Gingele *et al.* (2004) that during MIS 4 and 3 sea level was located between 40 and 70 m below present sea level.

2.5.3 Bridgewater Formation: an interglacial aeolian succession

The Bridgewater Formation is composed of beach and aeolian carbonate dunes deposited as beach barriers during interglacial high sea-levels of the Early Pleistocene or younger ages. Although having been previously reported on (Woods, 1862; Crocker and Cotton, 1946; Hossfeld, 1950; Sprigg, 1952), the Bridgewater Formation was first formally described by Boutakoff (1963) for a type locality at Bridgewater Bay in the Portland region of Victoria (Figure 2.13). Boutakoff described the Bridgewater Formation as calcareous dune-limestones of Upper and Lower Pleistocene age separated by a Middle Pleistocene marine abrasion platform at 27-30 m APSL (above present sea level) at the time of publication, attributed to an exceptionally high global sea-level highstand (the Mindel-Riss Interglacial, MIS 11). He proposed that the dune sands, made up of foraminifers, fragments of molluscs, echinoids, and other marine invertebrates and skeletons, were derived from the weathering and destruction of underlying Tertiary limestones which crop out on the submerged continental shelf. As described by Boutakoff (1963) the Lower Bridgewater Formation lacks any physiographic profile, having been levelled by the Middle Pleistocene highstand, while the ridges of the Upper Bridgewater Formation attain heights of 46-122 m APSL with the greater heights obtained where dunes are stacked. The Upper Bridgewater Formation in the Portland region also contains up to five fossil soil horizons (palaeosols) placed above dune-stabilising calcretes and correlate with cycles of sea-level change (Boutakoff, 1963). These soils are variably pink, pinkish-red, brownish-red and red indicating extensive weathering and pedogenic development.

The stacked dunes of the Bridgewater Formation in the Portland region are spread across the Coorong Coastal Plain (CCP) to the northwest. Hossfeld (1950)

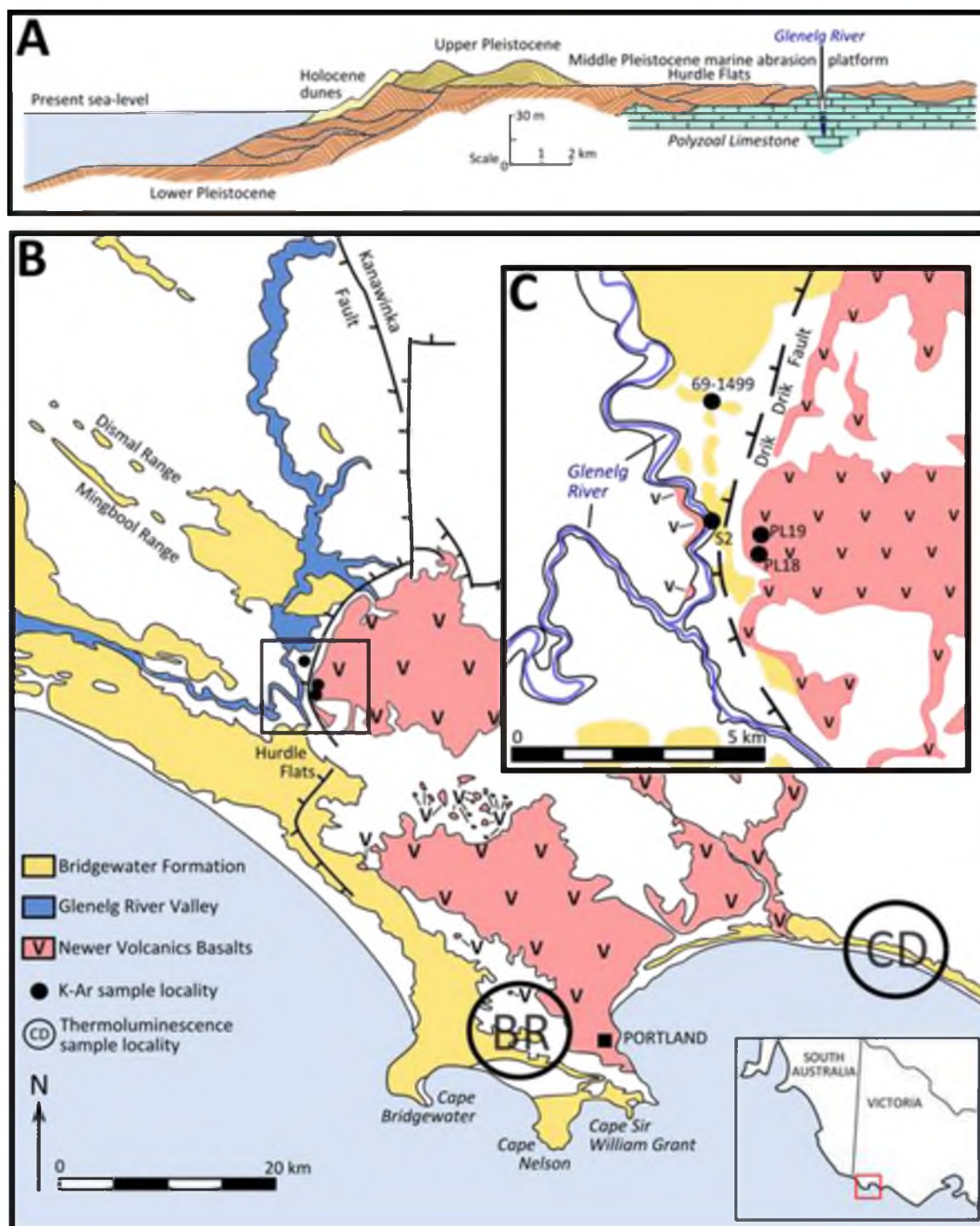


Figure 2.13: The Bridgewater Formation as mapped in the Portland region of Victoria adjacent to the South Australian border. A) A stratigraphic cross-section of the Bridgewater Formation in the terminology of Boutakoff (1963) modified from Boutakoff (1963). B) The Portland region showing the Bridgewater Formation and Newer Volcanics basalts (modified from Singleton *et al.*, 1976). The Glenelg River Valley contains outcrops of the Werriook Limestone. Thermoluminescence sample localities are as provided by White (2000); ages for Codrington Ridge (CD) and Bats Ridge (BR) provided in text. Dismal and Mingbool Ranges have been recently dated (Blakemore, 2014; Blakemore *et al.*, 2015); ages provided in text. The box surrounding the K-Ar sample localities is magnified by inset C. C) K-Ar sample localities along the Glenelg River Valley (modified from Singleton *et al.*, 1976); ages discussed in text. The basalts have been offset ~70 m by movement along the Drik Drik Fault, an extension of the Kanawinka Fault System (Singleton *et al.*, 1976).

identified eighteen dune ranges in a transect from Naracoorte to Robe (Figure 2.14). The separation of the dunes is due to epeirogenic uplift associated with Quaternary volcanism and related igneous intrusions in the Mount Burr-Mount Gambier region which have resulted in broad regional doming and a long-term uplift rate near Mount Gambier of 0.13 mm yr^{-1} . The rates of uplift across the coastal plain are dependent upon the proximity to the centre of volcanism and decrease northwards (Murray-Wallace *et al.*, 1998). Some dunes have been shown to be composite dunes formed over multiple sea-level highstands (Cook *et al.*, 1977; Huntley *et al.*, 1993; Murray-Wallace *et al.*, 1999). This is most likely due to the slow rate of uplift across the coastal plain between Naracoorte and Robe (0.07 mm yr^{-1}) which would require at least two glacial cycles to uplift a former barrier from the influence of marine erosion during a subsequent interglacial (Murray-Wallace, 2002).

The Bridgewater Formation is underlain by older Quaternary deposits, the presence of which is variable across the CCP. In the southeast, the dunes are underlain by the Early Pleistocene Coomandook Formation (Firman, 1967; 1973; Rochow, 1969; 1971; Rogers, 1979; Ludbrook, 1984; Belperio, 1995b). The Coomandook Formation is a fossiliferous, shallow marine limestone recording a marine transgression which transgressed the Padthaway Ridge to reach the Marmon Jabuk – Kanawinka Escarpments. The drilling program of Cook *et al.* (1977), which transversed the CCP from Robe to Naracoorte, shows the Coomandook Formation to be absent to the west of the Reedy Creek Range and the later Quaternary sediments are deposited on the Oligocene-Miocene Gambier Limestone. Farther to the north Quaternary sediments unconformably overlie Early Palaeozoic granites, Eocene (Knight Group, Buccleuch Beds) or Oligocene-Miocene (Ettrick Formation, Murray Supergroup limestones) marine deposits, as well as Coomandook Formation (Cook *et al.*, 1977; Rogers, 1979). Even farther to the north, around the Murray Lakes region, drilling (Barnett, 1991) shows that the Bridgewater Formation and associated back-barrier facies, to be underlain variably by the Oligocene-Miocene limestones of the Murray Supergroup, Late Eocene Buccleuch Beds, and Permian Cape Jervis Formation.

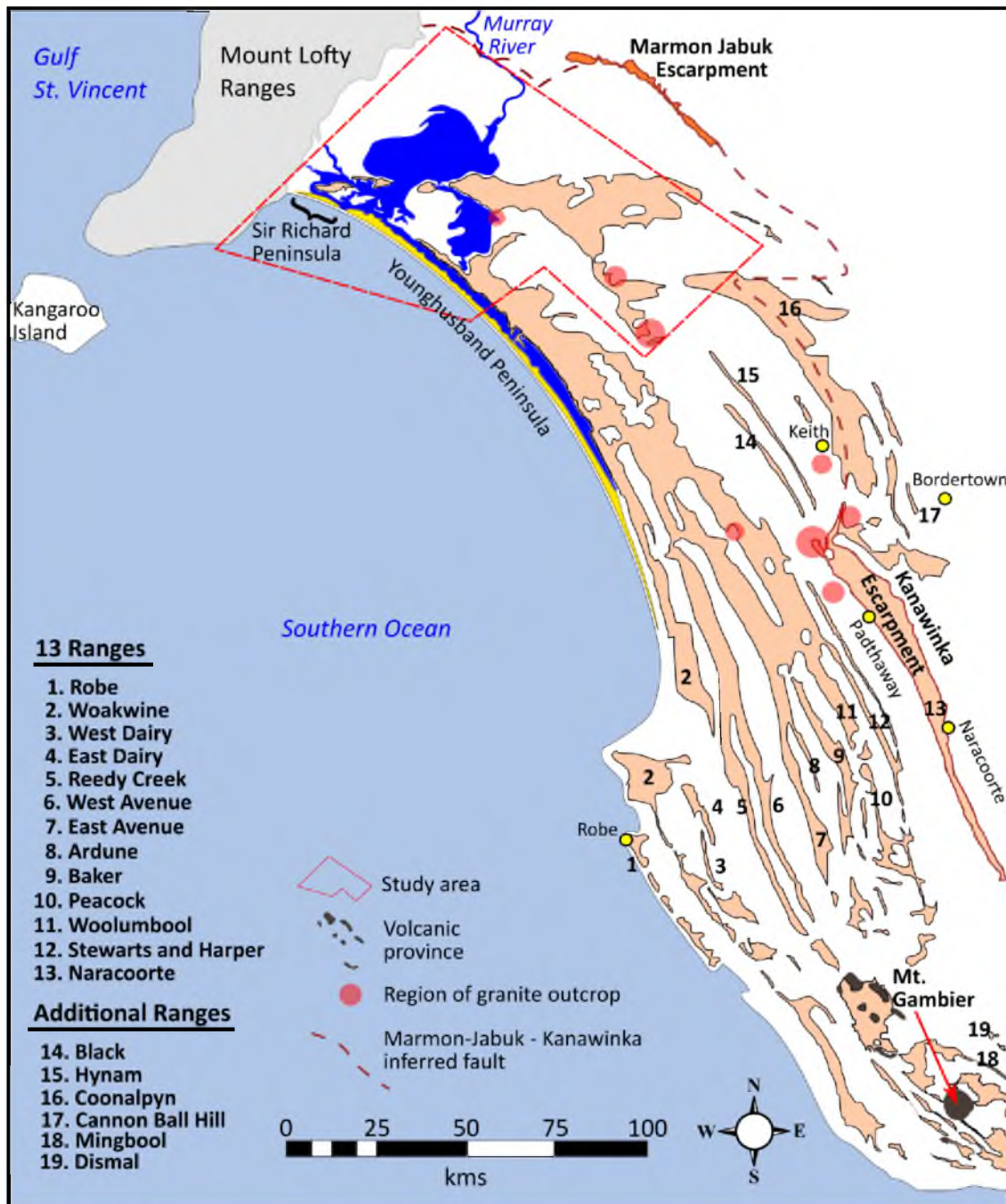


Figure 2.14: The Coorong Coastal Plain in South Australia, extending southeast from the Mount Lofty Ranges and beyond the Mount Burr – Mount Gambier volcanic complex, retains one of the world's longest records of Quaternary interglacial sea-levels preserved in a terrestrial context, recorded by consolidated aeolian dunes of the Bridgewater Formation and associated back-barrier facies. The dunes, trending NW-SE, are known as 'ranges' and occur as successive topographic ridges sub-parallel to the modern coastline increasing in age landwards. Eighteen ranges have been identified between Robe and Naracoorte (Sprigg, 1952; Hossfeld, 1950; de Mooy, 1959; Belperio and Cann, 1990) and many have been dated (Huntley *et al.*, 1993; 1994; Huntley and Prescott, 2001; Murray-Wallace and Belperio, 1991; Murray-Wallace *et al.*, 2001; Belperio, 1995b; Banerjee *et al.*, 2003) to develop a timeline of interglacial deposition and in the determination of palaeo sea-level (Belperio and Cann, 1990; Murray-Wallace *et al.*, 2001). The location of additional ranges discussed in text is also provided.

The lower Bridgewater Formation in Victoria is underlain by the Late Pliocene - Early Pleistocene marine Werrikoo Limestone (Boutakoff, 1963; Singleton *et al.*, 1976), equivalent to the Coomandook Formation in South Australia (Firman, 1967a; 1973; Belperio, 1995b). The Werrikoo Limestone disconformably overlies downthrown basalts (Victorian Newer Volcanics) in the Glenelg River Valley (Singleton *et al.*, 1976). In some areas of the Portland region the aeolian dunes of the lower Bridgewater Formation grade downward into the Werrikoo Limestone. However, in other areas, such as at Cape Nelson and Grant, the Newer Volcanics are overlain unconformably by the upper Bridgewater Formation (Singleton *et al.*, 1976).

The basalts of the Newer Volcanics and the Werrikoo Limestone have helped to constrain the initial deposition of the Bridgewater Formation. Basalts along the Glenelg River valley were dated using the K-Ar radiometric method (Aziz-ur-Rahman and McDougall; 1972; Singleton *et al.*, 1976) to 2.46 ± 0.03 Ma (Sample 69-1499) and between 2.22 ± 0.06 Ma (Sample PL-19) and 2.35 ± 0.04 (Sample PL-18) Ma, respectively (Figure 2.13). The Werrikoo Limestone overlies the downthrown Glenelg River basalt flow with a mean age of 2.24 ± 0.08 (Sample S-2) Ma and contains the foraminifer *Globorotalia truncatulinoides*, which first appeared in the sedimentary record during the Calabrian (Singleton *et al.*, 1976) of the Early Pleistocene. The oldest Bridgewater Formation (in Victoria at least) must then post-date the base of the Calabrian, 1.80 Ma. Three ages have been reported for the Bridgewater Formation in the Portland region. White (2000) used the thermoluminescence technique to date two dune ridges: Codrington Ridge and Bats Ridge (Figure 2.13). Two samples were taken from separate caves within Codrington Ridge providing TL ages of 244 ± 74 (Sample CD-5) ka and 238 ± 45 ka (Sample CD-13). The Bats Ridge sample was also taken from within a cave and returned an age of 290 ± 34 ka (Sample BR-6). Recent (Blakemore, 2014; Blakemore *et al.*, 2015) work has been undertaken to determine the evolution and palaeo-sea-level of the Bridgewater Formation in the Mount Gambier region using amino acid racemisation (AAR) analysis constrained by optically-stimulated luminescence, the results of which link the record between the Coorong Coastal Plain and the Portland region. Two barrier shorelines (the Mingbool and Dismal Ranges) which extend into the Portland region

were assigned AAR numeric ages of 788 ± 118 (MIS 19) and 933 ± 145 (MIS 23), respectively (Blakemore, 2014; Blakemore *et al.*, 2015).

The oldest of the barriers crossing the CCP is the West Naracoorte Range, at the base of the Kanawinka Escarpment. The range contains four well-defined iron-rich, red-brown horizons interpreted to be palaeosols (Sprigg, 1952; Cook *et al.*, 1977; Murray-Wallace *et al.*, 2001). Upslope of the West Naracoorte Range is the East Naracoorte Range of reverse polarity with development placed tentatively at either MIS 21 or 25 (Murray-Wallace, 2002), although, Blakemore *et al.* (2015) correlated it with deposition of the Dismal Range (MIS 23). Between Naracoorte and Padthaway the two ranges coalesce to form a single dune complex (Rogers, 1980) which north of Padthaway divides into four component ridges found east of the Black Range in the Bordertown area (Blackburn *et al.*, 1965; Cook *et al.*, 1977; Bowler *et al.*, 2006). These ridges were built up between the granite headlands of Mt. Boothby and Willalooka (Rogers, 1980) and were considered by Blackburn *et al.* (1965) to predate the Naracoorte Ranges. Rogers (1980) assigned the West Naracoorte Range and ranges to the east as lower members of the Bridgewater Formation and the younger ranges to the west as upper Bridgewater.

Barrier dunes of older age and reversed polarity are located farther inland (Idnurm and Cook, 1980). These dunes begin with the East Naracoorte Range and extend inland towards Bordertown and the last strandlines of the Loxton-Parilla Sands. This region has been identified as the 'Bordertown-Naracoorte transition' (Bowler *et al.*, 2006) and it has been suggested (Murray-Wallace, 2002; Bowler *et al.*, 2006; Bowler and Sandiford, 2007) that this transition zone reflects a shift in the controlling band of the Milankovitch hypothesis from a ~40 kyr obliquity cycle to the ~100 kyr eccentricity cycle. Bowler *et al.* (2006) and Bowler and Sandiford (2007) identified five pre-Naracoorte Bridgewater calcarenites between Keith and Bordertown assigning a tentative age near 1.3 to 1.4 Ma to the earliest range (Cannonball Hill) based upon correlation to marine isotope stages. Each ridge was deposited at a high stand sea-level and by extending the CCP record, provides a systematic chronology for the region (Murray-Wallace *et al.*, 2001; Bowler *et al.*, 2006). Cannonball Hill is separated from the youngest Loxton-Parilla strandline by 20-30 km. The Loxton-Parilla siliceous strandlines reach heights of 50 m

and are on average spaced 1.6 km apart, starkly contrasting with the height (30-40 m) and spacing (10 km) of the carbonate-rich dunes of the Bridgewater Formation and reflect a strong 20 kyr precessional cycle (Bowler *et al.*, 2006; Bowler and Sandiford, 2007). Bowler *et al.* (2006) suggested that the Bordertown-Naracoorte region served as an illustration of dune morphology and sediment transition reflecting change in the controlling dynamics of dune deposition during the Plio-Pleistocene transition on the basis that the last of the Loxton-Parilla Sands were deposited at ~1 Ma. However, Miranda *et al.* (2009) were able to show, using strontium isotope analysis, that deposition of the strandlines was largely completed by ~5 Ma implying a nearly 4 Ma gap in the sedimentary record between final deposition of the Loxton-Parilla Sands and the initial deposition of the oldest Bridgewater Formation. This gap in the sedimentary record corresponds to one of the three mega-hiatus events (2.5-1.5 Ma) recognised by Li *et al.* (2004) in the Great Australian Bight (section 2.3.3).

2.5.3.1 Quaternary sea-level record

To the northwest the Bridgewater Formation on the Coorong Coastal Plain (CCP) provides one of the longest eustatic sea-level records of Pleistocene interglacial highstands in the world (Hossfeld, 1950; Sprigg, 1952; Belperio and Cann, 1990; Huntley *et al.*, 1993; Murray-Wallace, 2001). The dune ranges identified in the transect between Robe and Naracoorte, are in succession progressively younger than the Brunhes-Matuyama geomagnetic polarity reversal (780 ka) (Sprigg, 1952; Belperio and Cann, 1990). Extensive thermoluminescence and optically stimulated luminescence dating of dune sediments (Huntley *et al.*, 1993; 1994; Huntley and Prescott, 2001; Banerjee *et al.*, 2003) and the application of amino acid racemisation analysis to dune and lagoon facies (Murray-Wallace and Belperio, 1991; Belperio, 1995b; Murray-Wallace *et al.*, 2001) provided dune ages and sea-level estimates which could then be related to the oxygen-isotope record (Figure 2.15). Comparison in the height of successive interglacial highstands using the associated back-barrier lagoonal facies (the Glanville and Padthaway Formations) shows that sea-level in the region did not deviate by more than ± 6 m of present sea level for middle and late Pleistocene time (Belperio and Cann, 1990; Murray-Wallace *et al.*, 2001; Murray-Wallace, 2002). This suggests that the sea surface has returned repeatedly to a similar regional elevation with each successive interglacial.

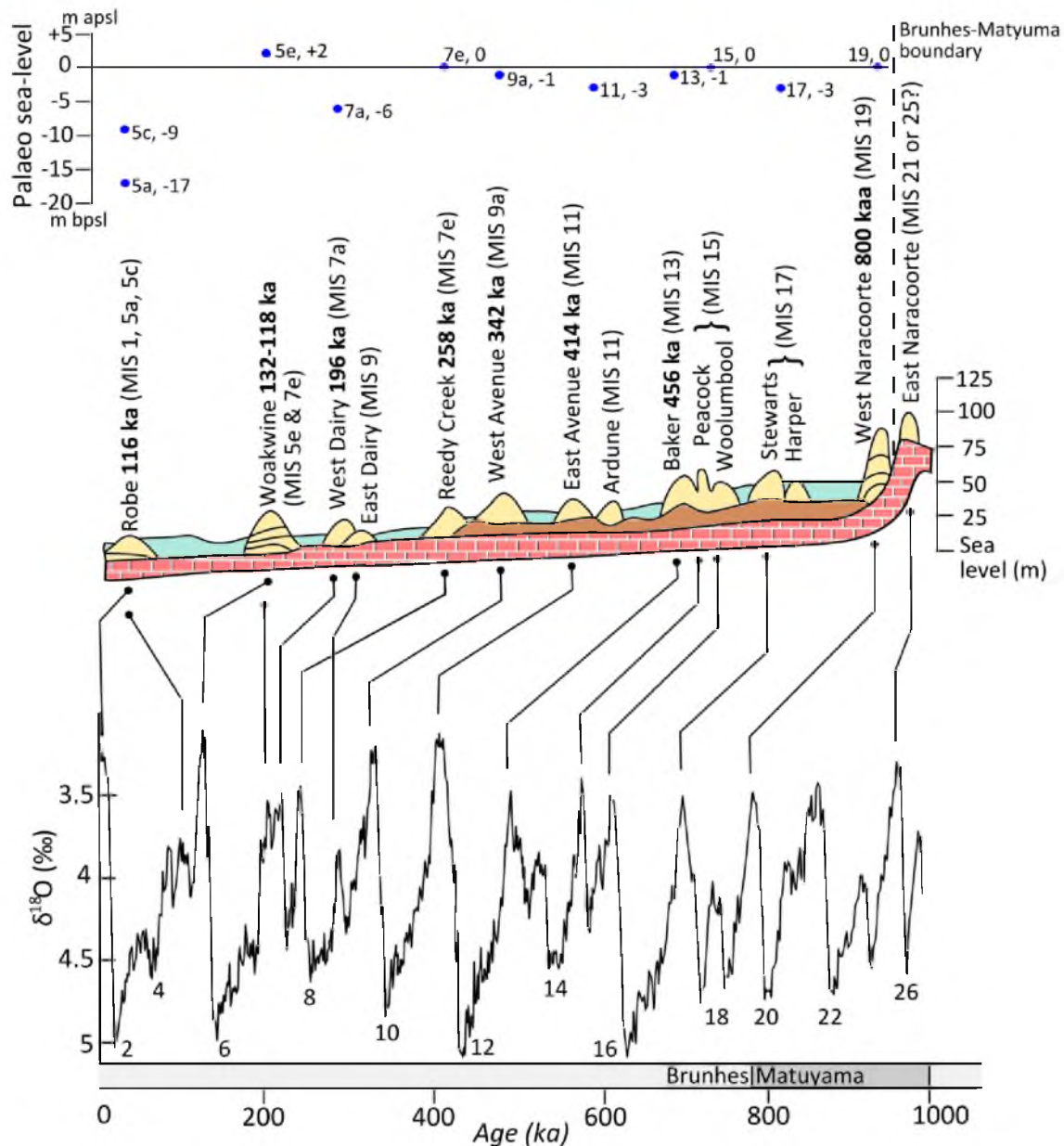


Figure 2.15: Schematic cross-section of the Coorong Coastal Plain with ages of coastal barriers between Robe and Naracoorte shown in relation to the oxygen-isotope record of Lisiecki and Raymo (2005). Also shown is the uplift-corrected palaeo-sea-level for the dune ranges (Belperio and Cann, 1990; Murray-Wallace *et al.*, 2001; Murray-Wallace, 2002). Sea-level has returned to within ± 6 m of present sea-level during each interglacial highstand since the middle Pleistocene. MIS 5e, 9, and 11 are all similarly isotopically light to the current interglacial period, while MIS 7, 13, 15, 17, and 19 are thought to represent interglacials with more ice (Shackleton, 1987). MIS 2, 6, and 12 represent extreme glacial periods (Shackleton, 1987). Figure is modified from Murray-Wallace *et al.*, 1998.

Generally barrier and lagoon systems are a replacement of a previous system; they are a reworking-induced sedimentary system, the spatial distribution of which is related to sea level location (Goa and Collins, 2014). Only when sea level becomes stabilised can the system morphology reach an equilibrium state. Therefore, barrier coastlines provide sedimentary records but they only represent relatively narrow slices of geologic time; i.e. the period of stable sea level (Goa and Collins, 2014). In the context of sea-level highstands, interglacial peaks generally do not exceed 10,000-13,000 yrs in length because interglacial peaks are driven by the incoming solar radiation and radiation cycles are relatively short (Forsström, 2001). Therefore, the strength and length of interglacials (and interstadials) is highly variable because the interplay of the obliquity and precession signals is inconsistent (Forsström, 2001; Jouzel *et al.*, 2007). If both signals peak in phase (within 5 ky) then a stronger interglacial period results (MIS 1, 5, 9, 11 and 19). However, if they are in antiphase then the interglacial is weaker (MIS 7, 13, 15, 17) (Jouzel *et al.*, 2007). It follows that a 'warm' interglacial can only follow a period of extensive glacial melting occurring under the influence of double peaks in solar radiation (Forsström, 2001). Broader peaks (i.e. MIS 11 at least 15,000-16,000 yrs) can be explained by the combined effect of two radiation maxima of varying strengths (Forsström, 2001).

2.5.3.2 The Last Interglacial shoreline: neotectonic and environmental indicator

Marginal marine strata from the last interglacial (LIG) sea-level highstand (MIS 5e) are widely distributed around the Australian coastline. Because of the lack of widespread glaciation in Australia during the Quaternary and a similar degree of hydro-isostatic deformation between interglacials, any lateral variation in the last interglacial shoreline elevation relative to present sea level largely reflects neotectonic modification (Murray-Wallace and Belperio, 1991). In South Australia the back-barrier and peri-tidal facies of the LIG Glanville Formation (Firman, 1966a; Ludbrook, 1976) provide a palaeo-sea level datum (Murray-Wallace and Belperio, 1991; Belperio *et al.*, 1995). Glanville Formation deposits are consistently found at 2 m APSL on the Eyre Peninsula, part of the geotectonically stable Precambrian Gawler Craton; variability from this elevation is

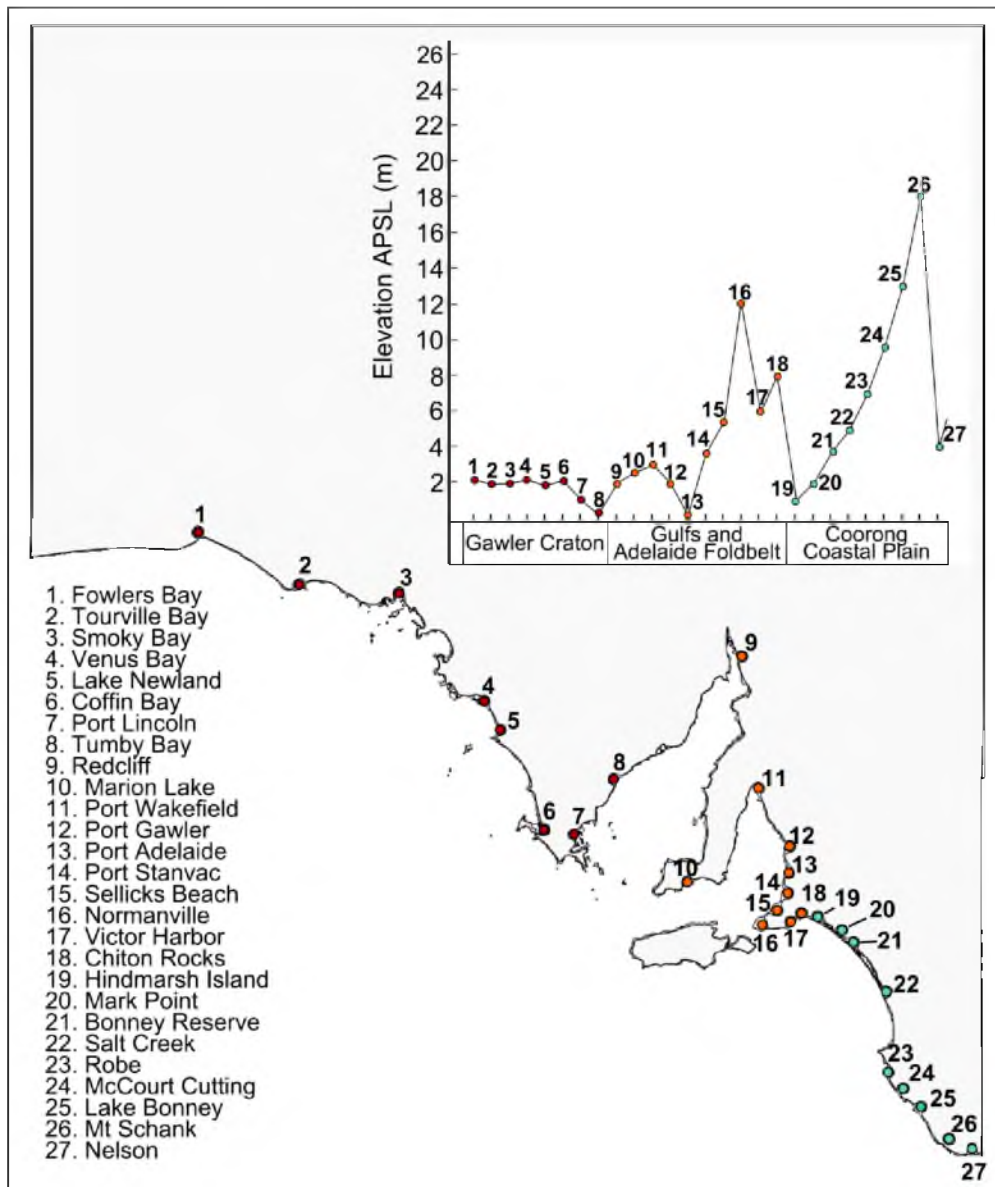


Figure 2.16: Shoreline elevations of the last interglacial (MIS 5e) coastal deposits in South Australia plotted in relation to their morphotectonics settings (figure modified from Murray-Wallace, 2002). Subsidence in the Murray Lakes region at the northern end of the Coorong Coastal Plain has been occurring at a rate of 0.02 mm yr^{-1} over the past 125 ka (Bourman *et al.*, 2000). Uplift of the Coorong Coastal Plain to the southeast in the Mount Gambier volcanic region (includes Mt Schank) at a rate of 0.13 mm yr^{-1} is attributed to intraplate volcanism and magma intrusion (Sprigg, 1952; Cook *et al.*, 1977; Murray-Wallace *et al.*, 1996; 1998).

interpreted as regional neotectonic deformation associated with contrasting pre-Quaternary geotectonic provinces (Murray-Wallace and Belperio, 1991) (Figure 2.16). The high elevation along the Mount Lofty Ranges (Fleurieu Peninsula) reflects the ongoing uplift of the Adelaide Fold Belt, whereas Hindmarsh Island is located in the Murray Lakes region, an area of known subsidence (Bourman *et al.*, 2000).

The Glanville Formation in South Australia is also populated by a fossil fauna of tropical association including the Sydney blood cockle *Anadara trapezia*, the Shark Bay pearl oyster *Pinctada carchariarum* and the foraminifer *Marginopora vertebralis* (Belperio *et al.*, 1995). These species have been identified in the shallow coastal marine sediments of the LIG in Western Australia and South Australia suggesting a stronger Leeuwin Current influence across the continental shelf of southern Australia (Cann and Clarke, 1993). *A. trapezia* molluscs have also been dated in some localities to the penultimate interglacial, MIS 7 (Murray-Wallace *et al.*, 2000). The bivalve has been considered a *prima facie* indicator of the Late Pleistocene interglacial in western and southern Australia (Murray-Wallace and Belperio, 1991; Cann and Clarke, 1993) where the species no longer lives with the documented exception of late Holocene (calibrated amino acid numerical age of 2600 ± 400 yrs BP) specimens identified at Launceston in northern Tasmania (Goede *et al.*, 1993; Murray-Wallace *et al.*, 2000).

The presence of warm water fauna, such as *A. trapezia*, in MIS 5e and 7 deposits, while suggesting a stronger Leeuwin Current, does not necessarily indicate or require a warmer Southern Ocean beyond the continental shelf or warmer terrestrial conditions across southern Australia (Cann and Clarke, 1993). However, given the more extensive distribution of the mollusc during MIS 5e it seems likely that the climate was more humid than at present with more regularly sustained and less seasonally contrasting precipitation patterns and the contraction of the geographic range is a reflection of the increased aridity in Australia over the last glacial cycle (Murray-Wallace *et al.*, 2000). The continued abundance of the tropical foraminifera *M. vertebralis* within refugium at Esperance Bay, West Australia (Cann and Clarke, 1993) and tropical marine fauna as far south as the Great Australian Bight (Garrey *et al.*, 1981) is a testament to the sustained influence of the Leeuwin Current.

2.5.3.3 Murray Lakes record

The record of the Bridgewater Formation is obscured at the north end of the CCP due to the ongoing subsidence and overlying Molineaux Sand. However, this region is significant in understanding the Quaternary development of the Coorong Coastal Plain due to the presence of the River Murray and coastal lowlands and its retention of glacial aeolian deposition.

The Pleistocene record provided by the dune ranges in the region was recognised by both de Mooy (1959) and Sprigg (1959; 1979). The last interglacial coastline, termed the Bonney Coastline (de Mooy, 1959), is an extension of the Woakwine Range to the southeast (Murray-Wallace *et al.*, 1991; Bourman *et al.*, 2000; Murray-Wallace *et al.*, 2010) and runs parallel with the modern coastline following the inner edge of the Coorong (Figure 2.17). De Mooy (1959) suggested multiple stages of Bonney Coastline construction progressing north westwards from southeast of Lake Albert. Initially a river mouth formed directly to the south of Lake Albert and is marked by a recurved spit to the southeast of the lake (de Mooy, 1959). Whether this was the only river mouth or one of multiple is unknown. A chain of swamps to the northwest of Lake Albert on Narrung Peninsula represent the location of a former Coorong behind the last interglacial barrier dune.

North of the former Coorong depressions, Sprigg (1979) recognised a former coastline transecting Narrung Peninsula designated Loveday Bay Beach. Both de Mooy (1959) and Sprigg (1959; 1979) recognised a coastline at the northern shoreline of Lake Albert. Sprigg designated the coastline Lake Albert Beach. De Mooy included the northern shoreline in a much larger coastal complex, which he designated the Alexandrina Coastline encompassing land situated between the two lakes, the northern Narrung Peninsula, Sturt Peninsula, northern Hindmarsh Island and parts of Goolwa (Figure 2.17). This coastline includes strata of MIS 5e, 7, and 9 as determined by thermoluminescence and amino acid racemisation analysis (Bourman *et al.*, 2000; Murray-Wallace *et al.*, 2010). De Mooy (1959) also suggested another former mouth location southwest of Goolwa where a small creek and estuarine deposits converge at a former opening in the present dunes.

The distal end of the LIG coastline, equivalent to the northern end of the Younghusband Peninsula, is preserved along the northern margin of Hindmarsh Island and as a recurved spit on the western end of the island suggesting that the Goolwa Channel has been the major channel of discharge since the LIG (Bourman *et al.*, 2000). A series of barrages in the region, which control the ingress of saltwater into the lakes and river, have been built upon the last interglacial fossil shoreline at 1-3.5 mwd (m water

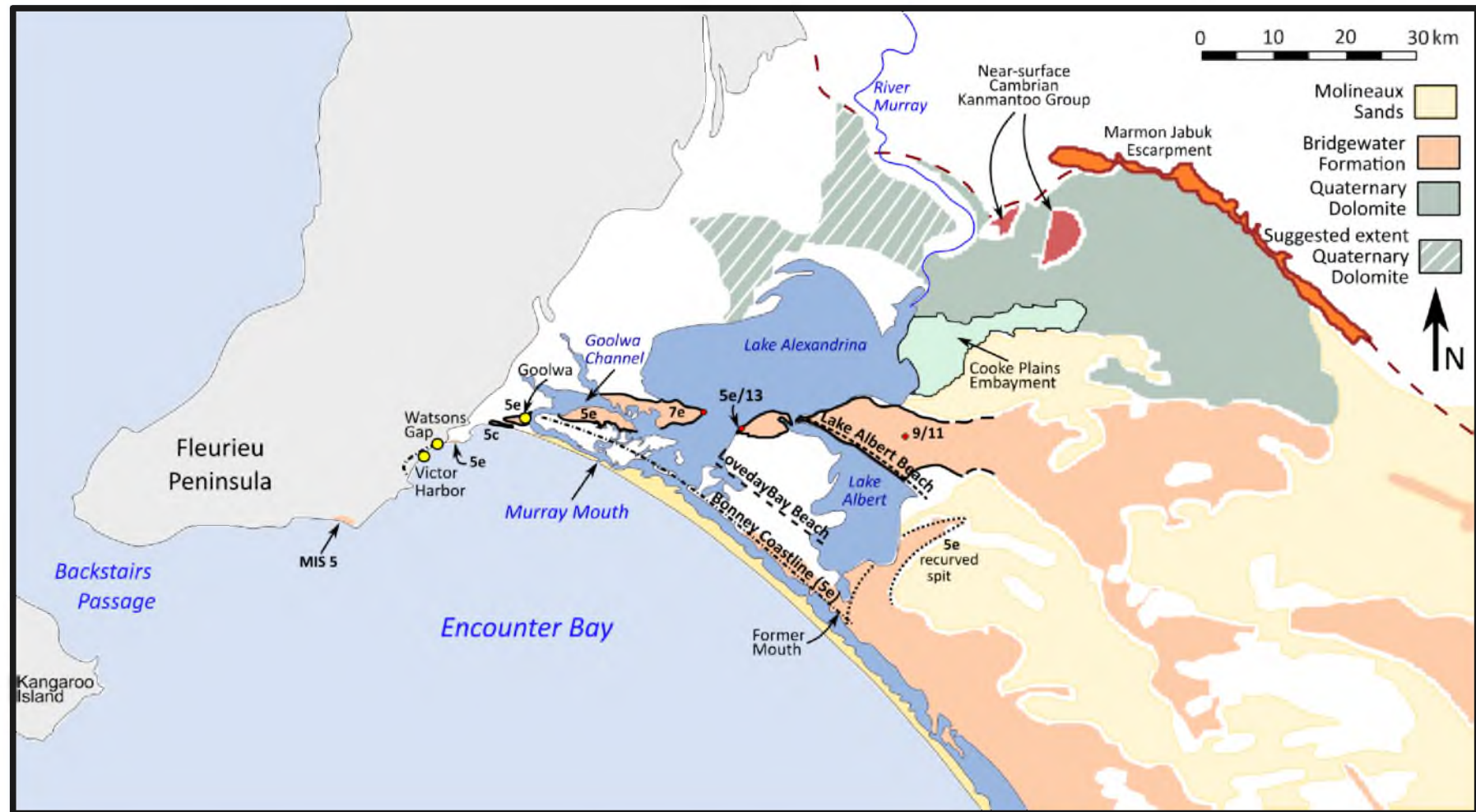


Figure 2.17: The region surrounding the River Murray Lakes. The Molineaux Sand variably overlies the Bridgewater Formation. The Alexandrina coastline (de Mooy, 1959) is delineated by the bold black line and includes strata of MIS 5, 5e, 7e, 9, 11, and 13 (Murray-Wallace *et al.*, 2010). Also included are the Loveday Bay and Lake Albert Beaches (Sprigg, 1959). The Bonney coastline (de Mooy, 1959) corresponds to the last interglacial shoreline (MIS 5e) (Murray-Wallace *et al.*, 2010). The location of a former mouth as proposed by de Mooy (1959) is indicated. Locations of Pleistocene beaches and coastlines as drawn by Murray-Wallace *et al.* (2010).

depth) coinciding with the location of the Bonney Coastline (Oliver and Anderson, 1940; Bourman *et al.*, 2000). However, sediment beneath the Goolwa Channel extends beyond depths of 19 m (Oliver and Anderson, 1940) implying the channel was excavated well below present sea-level during the LGM (Bourman *et al.*, 2000). Relicts of the LIG coastline extend onto Fleurieu Peninsula. The LIG shoreline is found at 6 m AHD (Australian Height Datum) in Victor Harbor and 10 m AHD at Watsons Gap (Bourman *et al.*, 2000). Aeolianite is also present on Fleurieu Peninsula within protected gullies and ranges in age from modern to Last Interglacial (Murray-Wallace *et al.*, 2010).

An additional unit mapped within the region is an unnamed and not formally defined geological unit designated the “Qpu” dolomite on the Pinnaroo 1:250 000 Geological Sheet (Rogers, 1979). Brown and Stephenson (1991) have suggested that the Quaternary dolomite (Rogers, 1979; 1980), which occupies a flat plain at the base of the Marmon Jabuk Scarp (Figure 2.17), is an Early Pleistocene marginal-marine and lagoonal unit formed in a partially protected, low-energy environment. Their premise was built upon the work of Rogers (1980), who showed that the dolomite inter-fingered with colluvial fans adjacent to the Marmon Jabuk Scarp, placing deposition sometime after the Coomandook sea-level high, which is suggested to have created the escarpment (Hossfeld, 1950; Belperio and Bluck, 1990). Deposition of the Qpu dolomite post-dates initial deposition of the Bridgewater Formation as it is separated from the southern margin of the Marmon Jabuk Scarp by a wedge of lower Bridgewater Formation (Rogers, 1979). Brown and Stephenson (1991) tentatively placed deposition of the coastal lagoonal carbonate to at least the age of the East Naracoorte Range based on stratigraphy. It disconformably overlies the Coomandook Formation and is disconformably overlain by the aeolian Molineaux Sand and lacustrine deposits of the Cooke Plains Embayment.

2.5.3.4 Discussion

The initial deposition of the Bridgewater Formation has been constrained in Victoria to post-date 1.80 Ma based on a fossil indicator within the underlying Werriook Limestone and the 2.24 ± 0.08 Ma age for underlying basalt in the Glenelg River Valley (Singleton *et al.*, 1976). The Glenelg River Valley basalt has been displaced by ~70 m along the Drik Drik Fault, a segment of the Kanawinka Fault System, with deposition of

the Werrikoo Limestone on the western downthrown side (Singleton *et al.*, 1976). Singleton *et al.* (1976) placed the fault movement along the Kanawinka Fault system at 2.2 Ma and attributed the marine transgression which deposited the Werrikoo Limestone to the displacement. It is likely the displacement was contiguous along the length of the Marmon Jabuk – Kanawinka lineament as the marine Coomandook Formation of South Australia is equivalent to the Werrikoo Limestone. The movement along the fault at ~2.2 Ma and associated uplift of the Pinnaroo Block and Padthaway High coincides closely with the estimated age of ~2.4 Ma for Lake Bungunnia initiation and supports the notion that uplift of the Pinnaroo Block led to the formation of the lake (Stephenson, 1986). If fault movement had occurred along the entire Kanawinka Fault system at 2.2 Ma, that would imply that the Kanawinka and Marmon Jabuk Escarpments had developed before to the initial deposition of the Bridgewater Formation, and raises questions of how pre-Naracoorte and the East Naracoorte Bridgewater Formation was deposited on an elevated platform, the height of the platform and what height sea-level must have been to achieve that. The subaqueous facies of the Dismal Range (correlated with the East Naracoorte Range) are found at 70 m APSL, a similar height to the East Naracoorte Range but seaward of the Kanawinka Escarpment (Blakemore *et al.*, 2015). At least part of the current elevation of the Dismal Range can be attributed to regional crustal doming of the local basement associated with regional volcanic activity which, although predating formation of the Mingbool Range (i.e. > 788± 118 ka), has not been further constrained (Blakemore *et al.*, 2015).

The age estimate for Cannon Ball Hill (a pre-Naracoorte range) of approximately 1.4-1.3 Ma closely coincides with the climate change record provided by Lake Bungunnia, which suggests a switch to windier, more arid conditions at 1.5-1.4 Ma and also confirms that deposition of the Bridgewater Formation began before the demise of the lake. The dunes of the Bordertown-Naracoorte transition correspond well with the timing of the Middle Pleistocene Transition (1.25-0.70 Ma) marking the gradual transition of ice age cycles from periods of 41 ka to 100 ka and the intensification of global glacial-interglacial cycles (Maslin *et al.*, 2001; Clark *et al.*, 2006). The Bridgewater Formation dunes on the Coorong Coastal Plain (CCP) follow the 100 kyr cyclicity

suggesting that by MIS 19 (~800 ka) the 100 kyr periodicity was fully expressed in southern Australia.

Identifying an easily identifiable marker for the transition between the upper and lower member of the Bridgewater Formation is difficult. Boutakoff (1963) separated the two members by a middle Pleistocene abrasion platform at 27-30 m APSL attributed to a globally high sea-level during MIS 11 and placed the Victorian dunes of Gentle Annie, Kentrbruck, and Jackie Lookout Ranges in the Late Pleistocene member. Unfortunately very little work has been done to determine the age of the Bridgewater Formation in Victoria. Boutakoff linked the dunes to the Mount Ruskin, Burleigh, Caveton and Gambier Ranges in the Mount Gambier Region of South Australia. The latter three have been recently equated to the highstands of MIS 7, 9, and 15 respectively using morphostratigraphy and amino acid racemisation (Blakemore, 2014; Blakemore *et al.*, 2015). Furthermore, sea-level in South Australia during MIS 11 has been placed at 3 m below present sea level (Belperio and Cann, 1990; Murray-Wallace *et al.*, 2001). However, the Compton Range, northeast of Mount Gambier, by the reasoning of Boutakoff (1963), would be part of the lower member of the Bridgewater Formation and is a composite dune (Blakemore, 2014; Blakemore *et al.*, 2015) with MIS 13 Bridgewater separated from overlying MIS 11 by an unconformity formed in a subaqueous environment. The unconformity implies a marine incursion which may be equated to a significantly higher sea level than is recorded by the MIS 11 East Avenue dune on the Coorong Coastal Plain. Palaeo-sea-level for the MIS 11 aeolianite in the Compton Range was calculated to be $+2 \text{ m} \pm 2 \text{ m}$ (Blakemore *et al.*, 2015).

Firman (1973) separated the upper and lower members of the Bridgewater Formation with the middle Pleistocene Ripon Calcrete which crops out along the northern and inland margin of the Padthaway Ridge north of Keith (Figure 2.14). The calcrete does not crop out to the southwest of the Kanawinka Escarpment. Firman (1973) also placed the Ripon calcrete over multiple other surfaces in various environments, using it as a stratigraphic marker: Lake Bungunnia Blanchetown Clay (including Bungunnia Limestone), palaeo-stream channels stranded in the cliffs of the River Murray north of Murray Bridge, and the Mannum Limestone. Similarly, Firman (1964; 1966; 1973) placed the Bakara Calcrete over the Glanville Formation and Ripon

Calcrete but also underlying the Woorinen Formation, which has since been shown to pre-date the Glanville Formation (Bowler *et al.*, 2006; Lomax *et al.*, 2007; 2011). The use of calcrete as a stratigraphic marker is not recommended because lateral facies changes occur in calcrete due to local, mesoscopic, geomorphic and hydrological features and the cyclic repetition of calcrete formation in coastal sequences (Belperio, 1988a; Phillips and Milnes, 1988). The unreliability of calcrete as a stratigraphic marker and the difficulty in identifying a contiguous surface for a mid-Pleistocene highstand suggest neither are favourable as a stratigraphic marker separating lower and upper Bridgewater Formation. Rogers (1980) designated the Naracoorte dunes and anything east as the lower member and anything west as upper member. This designation would place the boundary at a much earlier date than Boutakoff (1963). Placing the stratigraphic marker between the West and East Naracoorte dunes would coincide with the geomagnetic polarity reversal and the establishment of the 100 ka cycle as reflected in the Bridgewater Formation from the West Naracoorte dune to the modern coastline.

Due to the difficulty in discerning the individual barriers of the Bridgewater Formation within the study area, inferences about their development and location must depend on understanding how the southern CCP developed. Equivalents to the pre-Naracoorte dunes are not found on the Marmon Jabuk Scarp. The escarpment, which is formed of Loxton-Parilla Sands, is covered variably by Blanchetown Clay (equivalent to the Coomandook Formation) and a composite calcrete (Rogers, 1979). There are three possibilities for explaining the lower member Bridgewater deposits at the northern end of the CCP:

- 1) they have been completely reworked/eroded by younger dunes as suggested by Bowler *et al.* (2006);
- 2) older dunes are ensconced within younger dunes, forming composite structures; and
- 3) the development of the palaeo- River Murray did not allow the deposition of coastal dunes in the region.

The early Pleistocene dolomite at the base of the Marmon Jabuk Scarp was deposited in a marginal-marine, low-energy environment like a protected carbonate

shelf (Brown and Stephenson, 1991). The preservation of the dolomite suggests that it is unlikely the lower Bridgewater Formation has been completely reworked or eroded. It is more likely that the granite basement highs of the Padthaway Ridge at the northern end of the plain, as in the south, served as headlands and loci for the deposition and formation of a beach barrier that afforded some protection to the dolomite plain. The location of the oldest Bridgewater Formation adjacent to the southern margin of the Marmon Jabuk Scarp, and subsequent successions extending farther to the northwest (Rogers, 1980; Brown and Stephenson, 1991), suggests that development of the Bridgewater Formation progressed northwards. Brown and Stephenson (1991) placed the farthest limits of the dolomite plain north to Murray Bridge and west around the northern shore of Lake Alexandrina matching the extent of a River Murray delta as suggested by de Mooy (1959). If deposition of the dolomite plain does date to the early Pleistocene (alongside Bridgewater Formation) Lake Bungunnia was still in existence and the modern River Murray had not yet developed. However, alluvial sediment thought to be correlative of the Blanchetown Clay has been identified approximately 10 km south of Murray Bridge (Bourman *et al.*, 2010). Although the River Murray as it is recognised today may not have been developed, the increased wetness at the time probably allowed the development of flow off the adjacent Mount Lofty-Flinders Ranges; however, it is not possible to comment on the quantity of sediment being delivered to the region via fluvial transport at the time.

Freshwater flow has been mixing with the Southern Ocean in the vicinity of the modern Murray Mouth for much of the Cenozoic and within the Quaternary at least since the uplift along the Marmon Jabuk – Kanawinka Fault and development of Lake Bungunnia. The six down-cutting episodes recorded by Hill *et al.* (2009) in the centre of the Lacepede Shelf could potentially record sea level lowstands as far back as MIS 12, an extreme glacial event. The multiple channel locations offshore from the modern mouth region, the width of the coastline covered, and de Mooy's (1959) finding of possibly two former LIG mouths separated by a distance of approximately 50 km suggests either much greater discharge during the Last Interglacial or a great capacity for movement of the river mouth. The modern Murray Mouth has been shown to have migrated over a distance of 6 km during the past 3000 years (Bourman and Murray-Wallace, 1991). This

variability in movement may help to explain the presence of Lakes Alexandrina and Albert.

2.6 Synthesis and Conclusions

The Cenozoic succession within the Murray Basin is at its greatest extent in the central-western part of the basin, reaching 600 m below the surface. In the Murray Lakes region, adjacent to the uplift of the Precambrian basement and Permian sediments immediately to the west in the Mount Lofty and Flinders Ranges, basement is as little as 50 m below the surface. The southwestern Murray Basin, underlain by Proterozoic rift passive margin sediments, has been a consistent low topographic point since the reactivation of Delamerian fault trends and uplift of the Mount Lofty and Flinders Ranges in the early Cenozoic. The supply of terrigenous sediments to the Buccleuch Embayment, the presence of a Mid-Miocene palaeo-valley (the Bookpurnong Formation) and the estuarine Norwest Bend Formation below Quaternary sediments are indicative of a fluvial presence along the western margin of the Murray Basin for an extended period of time. The influence of basement features on Cenozoic sedimentation is perhaps most apparent along the Padthaway Ridge. This Palaeozoic basement feature, formed by igneous intrusion associated with the Delamerian Orogeny, has continually served as a topographic high in the landscape throughout numerous marine inundations of the basin and forms the southwest groundwater boundary of the modern basin. Granite outcrops of the Padthaway Ridge are likely to have served as loci for the deposition of sediments, including the Bridgewater Formation.

The Cenozoic has been an era of global cooling. The expansion of the West Antarctic Ice Sheet resulted in a lowering of temperatures and increased frequency of dry, anticyclonic circulation in southern Australia as well as the regression of the last major marine ingression into the Australian continent. The Plio-Pleistocene boundary is also notable for the tectonic uplift along the Pinnaroo Block and Padthaway High that established the mega-Lake Bungunnia and together with the formation of the Marmon Jabuk – Kanawinka Escarpment, initiated the development of the Coorong Coastal Plain.

The climatic and sea-level oscillations which characterise the Quaternary are believed to be a function of orbital forcing as explained by the Milankovitch Hypothesis. In Australia the Quaternary has been marked by increasing aridity as a result of the northward movement of the Australian continent into lower latitudes and the expansion of the Southern Ocean. The development of arid landscapes across southern Australia coincided with the establishment of anti-cyclonic circulation over Australia. Early arid landforms in central Australia date to ~1 Ma, corresponding to a transition in the climate cycle from 41 ka to 100 ka periodicity. Fully developed glacial aridity, established by 900 ka, is associated with a 5° latitude shift northwards of the dominating westerly air stream, reduced atmospheric moisture and increased continentality due to lowered sea level.

Within the Murray Basin the onset of glacial aridity is associated with the desiccation of Lake Bungunnia and deposition of the Nampoo Member, lake-lunette building and extensive dunefield development. The drying of Lake Bungunnia coincides with the establishment of the tectonic and climatic regime which characterises the modern Murray Basin and the establishment of a recognisable (in the 'modern' sense) River Murray. The orientation of the Woorinen Formation and Bunyip Sands reflects the dominant westerly wind direction during glacial periods due to equator-ward compression of anti-cyclonic circulation. During glacial maxima the palaeo-River Murray flowed across the Lacepede Shelf to debouch into the Southern Ocean at or near the continental margin.

The ~100 ka periodicity of interglacial sea-level highstands is documented by the Bridgewater Formation, which is preserved across the Coorong Coastal Plain in southern Australia. Initial deposition on the Coorong Coastal Plain dates to MIS 19 (800 ka) with earlier dunes located west of the Kanawinka Escarpment that may extend the record back as far as 1.4 Ma to coincide with the change in climate that brought about the desiccation of Lake Bungunnia. The Coorong Coastal Plain provides one of the longest terrestrial records of glacio-eustatic sea-level highstands in the world as well as serving as an indicator of regional neotectonics. The record is obscured within the study area due to ongoing subsidence and the presence of vast sheets of glacial period Molineaux Sand. The origin of the siliceous sands is still unresolved. The Murray Lakes region has

been a consistent point of contact between terrestrial water flow and marine environments throughout the Cenozoic and via the River Murray following the demise of Lake Bungunnia. The landscape development of the Murray Lakes region has been influenced by its juxtaposition between two regions of uplift, the environmental change produced as a result of fluctuations of glacio-eustatic sea level and climate (reflected in two aeolian dune formations: the Bridgewater Formation and Molineaux Sand) and the interplay of those successions with the River Murray.

Chapter 3

Physical Environment of the River Murray Lakes Region, Coorong Coastal Plain, southern Australia

3.1 Introduction

This chapter describes the physical environment of the Coorong Coastal Plain. The modern shoreline of the Coorong Coastal Plain, comprising Sir Richard and Younghusband Peninsulas and the back-barrier Coorong Lagoon, are modern analogues of the Bridgewater and Padthaway Formations, respectively. The processes which form the modern coastline inform on the development of their Pleistocene counterparts (Gostin *et al.*, 1988; Bourman *et al.*, 2000; Bourman and Murray-Wallace, 1991; Harvey *et al.*, 2001; 2006; Harvey, 2006). Even though subsidence has resulted in the burial and/or reworking and re-deposition of pre-existing Pleistocene barrier complexes in the study area, the processes which formed that region of coastline can still be inferred by analysis of their modern counterparts.

The chapter begins with a general description of the Coorong Coastal Plain and River Murray Lakes landscape before reviewing the modern shoreline environment and development, which has been influenced by the sediment supply of the modern River Murray and Lacepede Shelf. Following deposition, carbonate sediments undergo diagenesis, which on the Coorong Coastal Plain has aided in the preservation of the Quaternary successions. This important process is reviewed. Lastly, the lithology of modern sedimentary successions and their Pleistocene counterparts within the study area are reviewed as a precursor to Chapter 4 in which the results of stratigraphic and petrographic analysis of this research are presented.

3.2 The Coorong Coastal Plain

The Coorong Coastal Plain (CCP) extends southeast from the eastern slopes of the Mount Lofty Ranges (encompassing most of the study area) past the Mt Gambier volcanic complex and into Victoria (Figure 3.1). The margins of the modern plain are

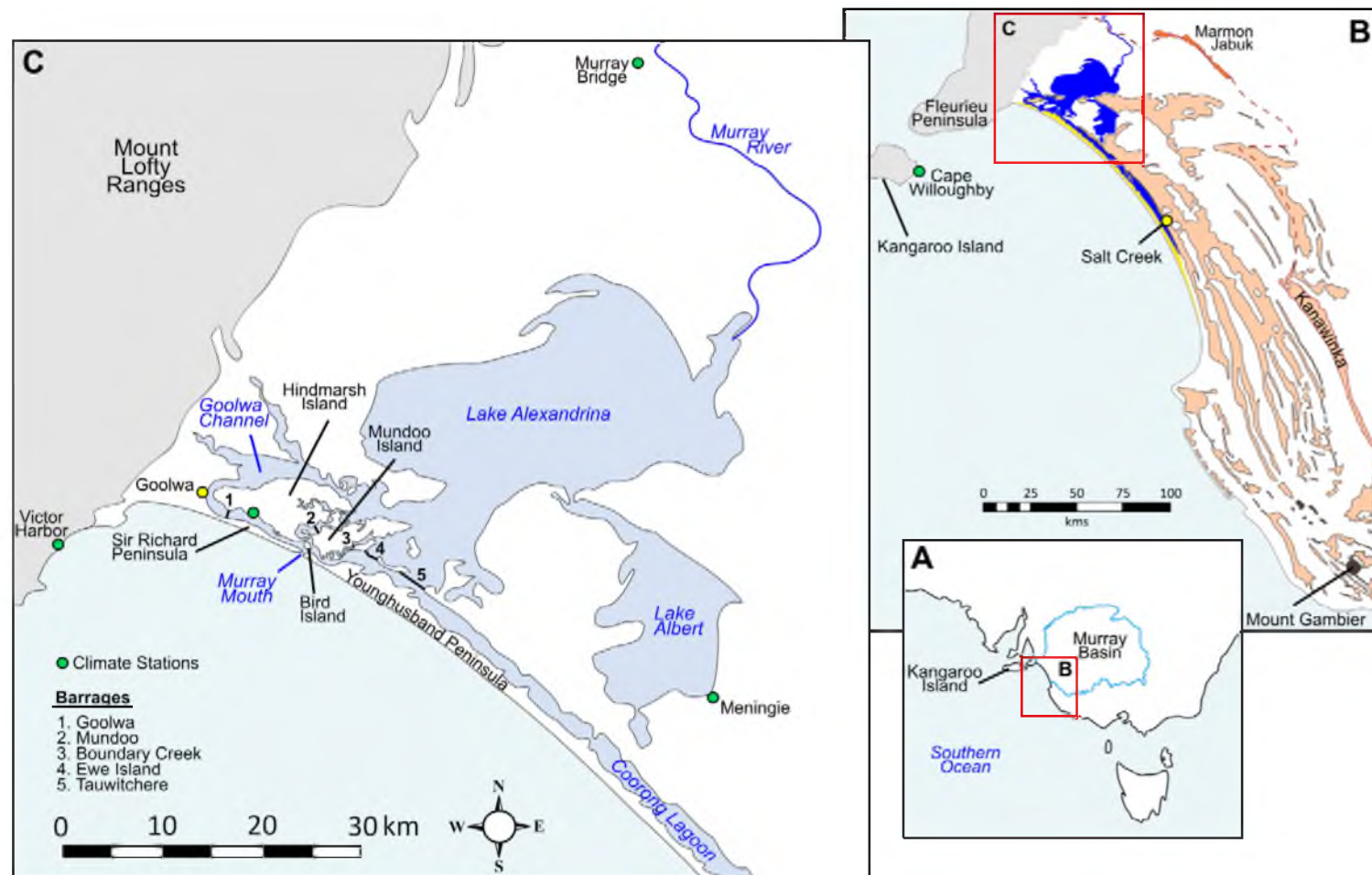


Figure 3.1: The River Murray terminus and mouth is located in the southwestern corner of the Murray Basin (A) at the foothills of the uplifting Mount Lofty Ranges and northern end of the Coorong Coastal Plain (B). The plain, bounded to the east by the Marmon Jabuk – Kanawinka Escarpment, retains a terrestrial record of high sea-level for the past ~800 ka in the dune ridges of the Bridgewater Formation (orange in Inset B). C) The terminus is composed of two broad, shallow lakes: Alexandrina and Albert, and multiple islands and channels. Natural river flow and mouth conditions have been altered by five barrages installed in the 1940s.

defined to the southwest by the Southern Ocean and to the northeast by the Marmon Jabuk-Kanawinka Escarpment which, has been variably interpreted as a fault scarp (Sprigg, 1952; Bowler *et al.*, 2006) or a coastal erosional feature (Hossfeld, 1950; Belperio and Bluck, 1990; Wallace *et al.*, 2005) (section 2.5.3).

The CCP is recognised (Hossfeld, 1950; Sprigg, 1952; Belperio and Cann, 1990; Huntley *et al.*, 1993; Murray-Wallace, 2001) for its long terrestrial record of Quaternary sea-level highstands preserved in the Bridgewater Formation (Boutakoff, 1963) and associated back-barrier estuarine or lagoonal successions (Padthaway Formation) (Sprigg, 1952; Rogers, 1979). The aeolian dunes of the Bridgewater Formation occur as a series of topographic ridges across the coastal plain sub-parallel to the modern coast (Belperio, 1995b). The dunes are spaced on average 10 km apart, up to 30 m above the general level of the plain, with a general increase in age landwards, and are commonly referred to as 'ranges' due to their topographic expression or 'barriers' due to their origin as beach-barrier structures. The barriers exhibit a NW-SE trend reflecting accumulation transverse to the dominant wind regime (Sprigg, 1952; Short and Hesp, 1984). Submerged equivalents are visible in water depths up to 12 m on the offshore Lacepede Shelf near Robe (Sprigg, 1979). The lowlands between the dunes are filled by the back-barrier lagoon and estuarine deposits of the Padthaway Formation (or last interglacial equivalent Glanville Formation). The dunes coalesce and lose topographic expression northwards as they approach the study area in the region of the River Murray terminus.

The river terminus includes two broad and shallow lakes; Lake Alexandrina (58,000 ha) and Lake Albert (18,000 ha), and multiple islands varying in size. Hindmarsh Island is the largest reaching ~15 km in length at its maximum east-west direction and ~7 km width in the north-south direction (Figure 3.1). The river debouches into the Southern Ocean via Encounter Bay onto the Lacepede Shelf.

3.3 The Modern shoreline

Holocene coastal deposition began with rapid sea-level rise (17 to 7 ka BP) following the last glacial maximum (LGM). The shape of the modern coastline was

determined by the geological structures (shelf morphology and bathymetry) encountered by the advancing sea (Gao and Collins, 2014), ongoing neotectonics (Harvey *et al.*, 2001), sediment type and supply, tides, wave and wind energy (Harvey, 2006).

The weather of southeast Australia is Mediterranean in style with generally hot dry summers and cool wet winters (Murray Wallace *et al.*, 2010) (Figure 3.2). Current mean annual temperature (CMAT) varies little in the region: 15.4°C at Victor Harbor on Fleurieu Peninsula, 15.5°C on Hindmarsh Island and 15.6°C at Meningie, although increases inland at Murray Bridge to 16.4°C (Bureau of Meteorology, 2015). Dominant wind directions are from the south, west and north (Bourman and Barnett, 1995). The Murray Mouth and CCP are subject to the progression of anticyclonic and mid-latitude depressional flows, including the prominence of a 5-6 day anticyclonic periodicity of westerlies, southerlies, and southeasterlies (Short and Hesp, 1984). Northwesterlies are more prominent in winter and southwesterlies in the summer. The variation in wind regime and coastal orientation indicates that the significance of processes such as open ocean swell waves, locally-generated storm waves and the effects on onshore winds will vary spatially and temporally (Bourman, 1986).

The shoreline of the CCP is a high energy microtidal (0.8 m) environment dominated by persistent year-round open ocean swell and strong onshore winds. The coast is exposed to waves from the west, southwest, south, and southeast and is subject to the full force of the dominant southwest waves, swell and accompanying winds, although Kangaroo Island provides some protection from westerlies (Harvey and Chappell, 1992). Moderate- to high-energy swell waves of 2 - 4 m (commonly exceeding 3 m) approach from the southwest for 62% of the year (Short and Hesp, 1984) with wave periods ranging from 6 to 15 seconds (Harvey and Chappell, 1992). This can be further enhanced by wind waves. High-energy winter storm waves from the south and southwest over 2.5 m occur 12% of the year (Short and Hesp, 1984). Reissen and Chappell (1991) analysed storm data for 3,849 individual storms in the 51 year period leading up to 1991, which had sufficient wave energy to move significant quantities of sand. The results show the maximum significant wave heights and corresponding period

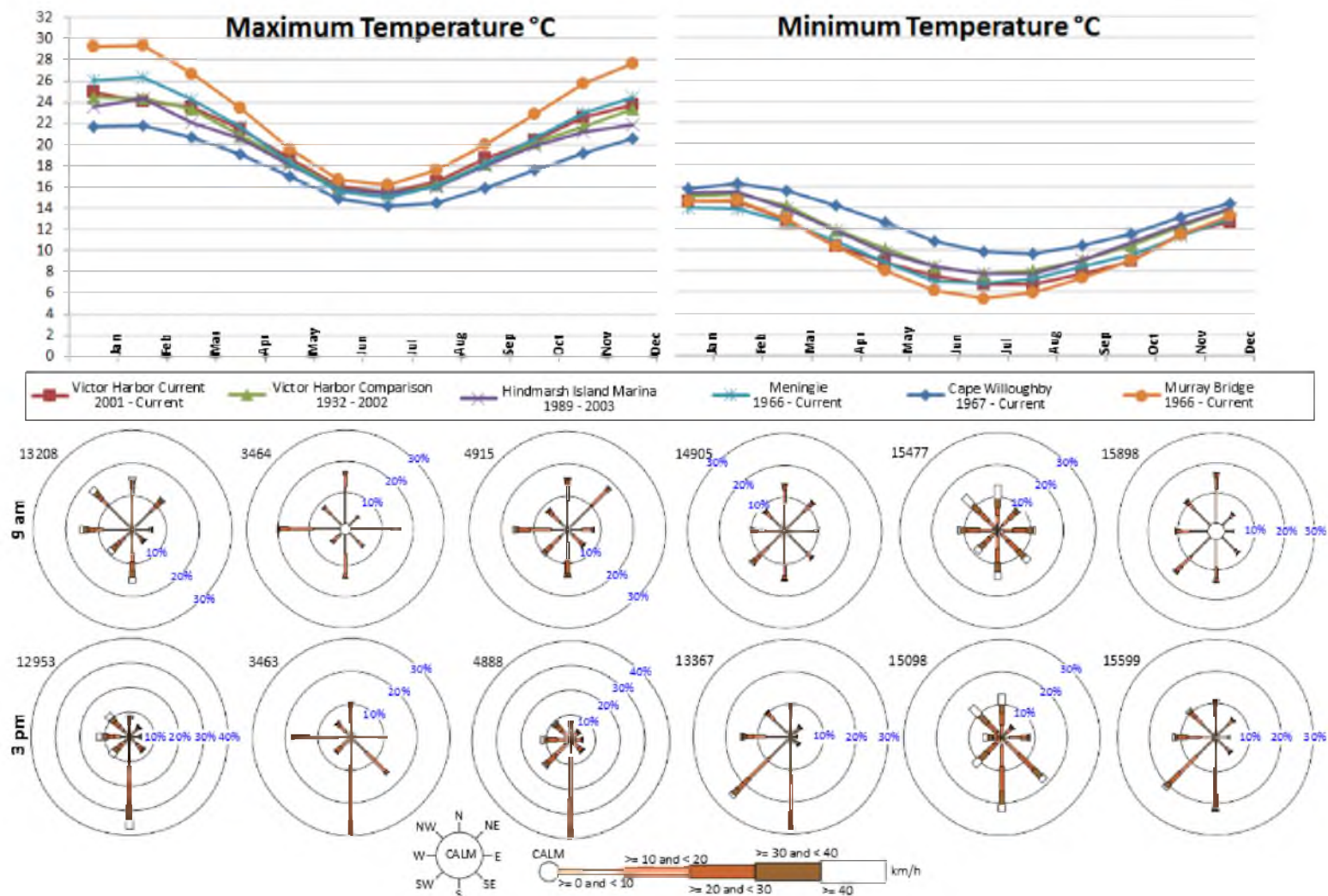


Figure 3.2: Long term temperature and wind data and years recorded for locations within and surrounding the River Murray Mouth and lakes region (climate station locations provided in Figure 3.1). Wind roses plot wind speed and direction taken at 9 am and 3 pm. The value to upper left-hand corner of a wind rose records the number of total observations for each wind rose (Bureau of Meteorology, 2015).

for waves approaching the Murray Mouth from four directions:

- west: 2 m and 12 seconds;
- southwest: 5 m and 12 seconds;
- south: 5 m and 12 seconds; and
- south, southeast: 4 m and 8 seconds.

A low beach gradient (0.03 m) accounts for the dissipative nature of the shoreline; however, due to high wave energy there is only a 20% loss in wave power meaning that more sediment is capable of being moved on shore (Short and Hesp, 1984). Spring high tide at Victor Harbor near the Murray Mouth reaches 0.8 m, although a maximum amplitude of 1 m may be reached during a storm surge (Short and Hesp, 1984).

3.3.1 The barrier shoreline complex

Wave-dominated shorelines are characterised by elongate, shore-parallel sand deposits (Reinson, 1992). The modern CCP shoreline is composed of two narrow transgressive barriers, the Younghusband and Sir Richard Peninsulas, separating the open sea from the Coorong Lagoon and mainland Australia. There are three main geomorphological elements to a barrier shoreline: 1) the sandy barrier, 2) the back-barrier lagoon or estuary, and 3) the tidal channel(s) that cuts through the barrier(s) and connect the lagoon to the open sea (Reinson, 1992). Relatedly, the system contains three major clastic depositional environments (Figure 3.3) which form a composite depositional system: 1) the subtidal to subaerial barrier-beach-dune complex, 2) the subtidal-intertidal lagoon, tidal flats and marsh, and 3) the subtidal-intertidal channels and tidal delta complexes. These geomorphological elements/depositional environments are recognised within the study area as the 1) Younghusband and Sir Richard Peninsulas (including shallow subtidal and littoral facies), 2) the Coorong Lagoon, and 3) the River Murray terminus (including associated tidal channels and Lakes Alexandrina and Albert).

Sir Richard Peninsula extends for approximately 10 km southeast from Goolwa (Figure 3.1) to the Murray Mouth. Width is greatest in its central section (up to 1 km

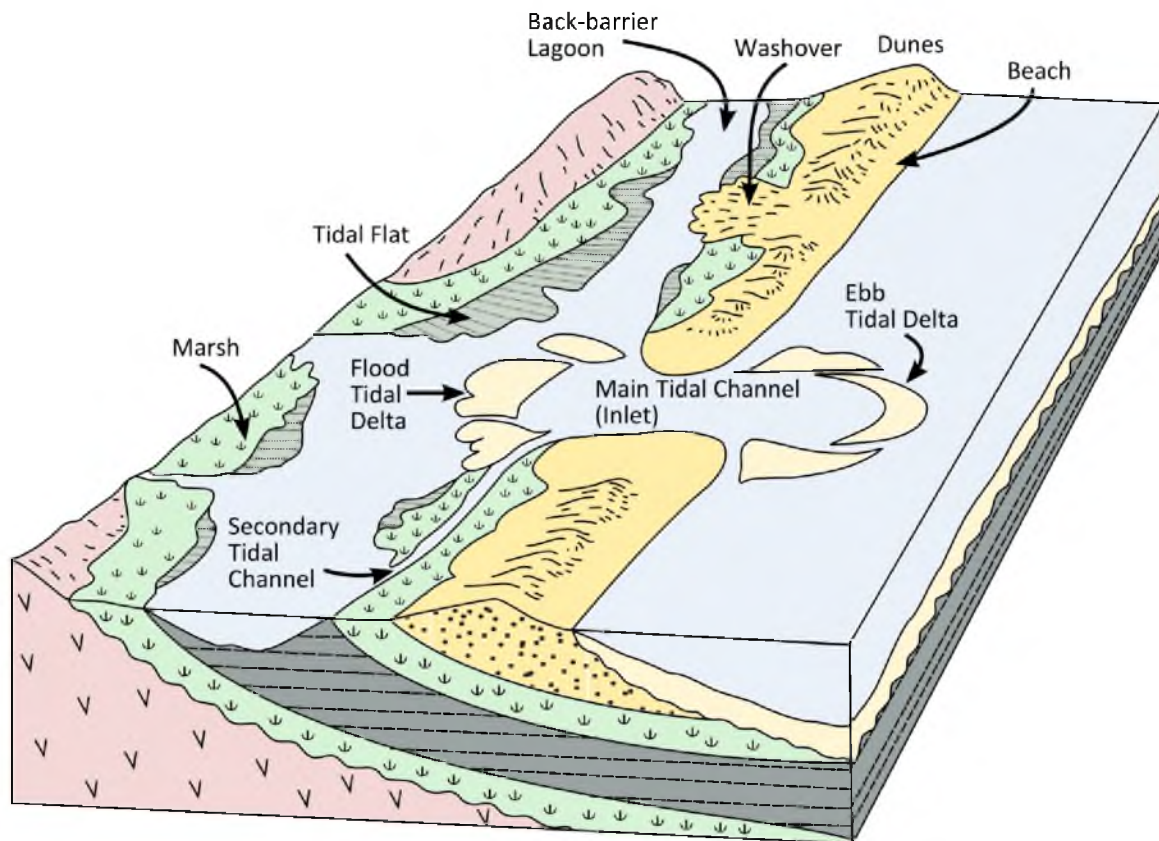


Figure 3.3: Block diagram illustrating the three main geomorphological elements (1. sandy barrier, 2. back-barrier lagoon or estuary, 3. tidal channels) and depositional environments (1. barrier-beach-dune complex, lagoon, 2. tidal flats and marsh, and 3. channels and delta complex) of a barrier shoreline depositional system. Undulating lines mark the development of bounding discontinuities below transgressing marsh and in the shoreface. Figure modified from Reinson, 1992.

wide) and narrowest at the proximal and distal ends. Dunes reach heights of 25 m. Dune morphology consists of transverse frontal dunes backed by older secondary transverse dunes, parabolic dunes and sand flats (Bourman and Murray-Wallace, 1991). Younghusband Peninsula is approximately 180 km long, up to 2 km wide with dunes up to 40 m in height. The peninsula is characterised by transgressive dune sheets, large-scale parabolic and transverse dunes and deflation basins extending to sea level (Short and Hesp, 1984; Belperio, 1995b). Landward of Younghusband Peninsula, extending some 130 km from the Murray Mouth, is the Coorong, a saline lagoon. Water reaches the lagoon via the Murray Mouth, the River Murray, Salt Creek (~95 km southeast of the Murray Mouth, Figure 3.1), seasonal rainwater and unconfined groundwater. Salinity and water levels vary seasonally; ~1 m higher during winter due to high sea levels, winter rainfall and decreased evaporation (Belperio, 1995b). The lagoon becomes increasingly restricted, hypersaline and ephemeral away from the mouth.

3.3.1.1 Barrier development

The development of the Younghusband and Sir Richard Peninsulas is attributed to the Holocene sea-level transgression and peak at ~7000 calendar years BP (Harvey, 1981; 2006). The shoreline at the culmination of the transgression was located along the present eastern shore of the Coorong Lagoon which has formed at the calcrete-capped barrier complex of the last interglacial ~2 km inland (Bourman *et al.*, 2000). Sediment for dune development was sourced from the Lacepede Shelf during the transgression (Harvey, 1981; 2006; Bourman and Murray-Wallace, 1991). A 100,000-years-old calcreted barrier complex corresponding to the sea-level high during MIS 5c (~9 m below present level) would have formed islands and intertidal platforms serving as loci for the development of the modern shoreline; parts of which are likely to form an inliers of Younghusband Peninsula (von der Borch, 1975; Harvey, 1981; 2006; Huntley and Prescott, 2001). Segments of this complex form a linear array of islands, which lie within the modern Coorong parallel to the Younghusband Peninsula and last interglacial Woakwine Range coastal barrier complex (Cann and Murray-Wallace, 2012). Development of the Holocene barriers was first proposed as a five-step process by Short and Hesp (1984) with later modification by Harvey (2006) (Figure 3.4):

1. Island development on offshore bars and, in places, older calcreted barriers;
2. Beach ridge progradation, dune development, and island expansion;
3. Closure of tidal entrances and development of continuous barrier with dunes;
and
4. Barrier migration by continued dune transgression and foreshore erosion.

Radiocarbon ages of charcoal from Aboriginal campfires (Leubbers, 1982) and transgressive basal deposits (Short and Hesp, 1984) and a thermoluminescence age (Harvey *et al.*, 2006) from Barkers Knoll (~1.5 km southeast from the Murray Mouth) suggest the initiation of Younghusband Peninsula occurred simultaneously along the length of the peninsula, suggesting simultaneous deposition along the length of Younghusband Peninsula approximately 6000 - 5500 calendar years ago (Harvey *et al.*, 2006). Progradation would have continued until the nearshore sand supply was depleted followed by foredune erosion and the initiation of dune transgression. A radiocarbon

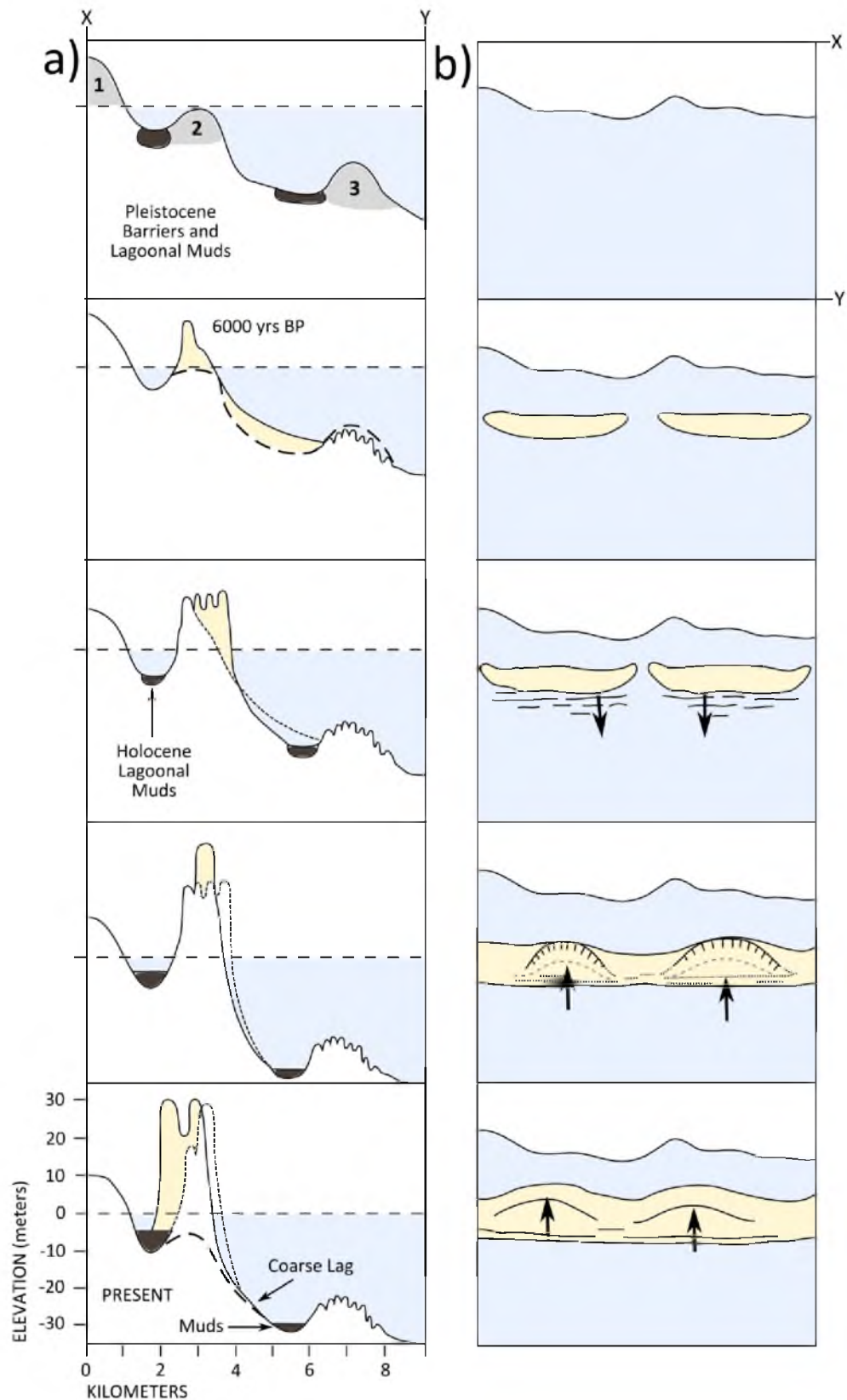


Figure 3.4: Holocene barrier evolution as a) proposed by Short and Hesp (1984) and b) modified by Harvey (2006). Barrier evolution began with early Holocene sea-level rise followed by development of offshore bars, beach progradation, development of a continuous barrier, barrier transgression, and dune transgression as nearshore sand supply was depleted. Figure modified from Harvey, 2006.

age of 1000 ± 80 radiocarbon yr BP (Lab Code SUA-2122) for an exhumed soil horizon (part of a previously buried foredune crest) 5 km southeast of the Murray Mouth had been cited to indicate that dune transgression, at least on that part of the coast, has been active for at least 1000 years (Short and Hesp, 1984). However, it should be noted that the exhumed horizon may reflect localised dune reworking. Laboratory records of the N.W.G. MacIntosh Centre for Quaternary Dating, University of Sydney now stored at the University of Wollongong, Centre of Archaeological Science reveal SUA-2122 to correspond to a *Donax* shell with a reported age of 1020 ± 70 radiocarbon years BP. This age was converted to sidereal age of 1470 ± 180 cal yr BP using the CALIB 7.1 program (Reimer *et al.*, 2013) strengthening the initiation age of Short and Hesp (1984). Landward migration of the dune led to differential loading of muds in the back-barrier lagoonal sediments resulting in folding and changed elevations as the dune sands spilled into the Coorong (Brown, 1965; Bourman *et al.*, 2000; Harvey *et al.*, 2006).

The modern Sir Richard Peninsula has developed on a foundation of weakly cemented calcareous sandstone and back barrier lagoonal facies (Bourman and Murray-Wallace, 1991; Bourman *et al.*, 2000). *Katelysia* sp. shell fragments (SRP#7) within these facies were dated using amino acid racemisation to a numerical age of 8600 ± 1300 years BP (Bourman and Murray-Wallace, 1991). Exposure of these back-barrier strata on the seaward side of the peninsula indicates landward migration of the barrier from an earlier position. The distal half of Sir Richard Peninsula appears to be much younger than the proximal half (Bourman and Murray-Wallace, 1991; Bourman *et al.*, 2000). Aboriginal shell middens, dated by radiocarbon to between 3000 and 200 calendar years, occur only on the proximal half of the peninsula while aeolian sediments have been dated by thermoluminescence to 3000 - 4000 years of age. The smaller size of the dunes on the distal end, the lack of shell middens there, and the possible remnants of a former flood tidal delta behind the peninsula indicate that mouth migration is responsible for the variability in age along the peninsula (Bourman and Murray-Wallace, 1991). The former flood tidal delta sediments are found on the southern margin of Hindmarsh and Mundoo Islands occurring at elevations up to 2 m above present sea-level (APSL) with shell in the upper 60 cm radiocarbon dated to 6410 ± 190 cal yr BP (Lab Code Wk-4784) (Bourman *et al.*, 2000). These sands were deposited while the Sir

Richard and Younghusband Peninsulas were still forming and indicate the presence of a much larger, as well as a migrating, Murray Mouth.

3.3.1.2 Murray Mouth location

The position and morphology of the Murray Mouth is a result of the interplay between littoral drift, wind drift, waves, ocean currents, tidal prisms, freshwater flow and supply of sediment (Reissen and Chappell, 1991). Mouth migration is consistent with the direction of sand movement, which, in turn, is determined by wind direction. The direction of movement between years can be highly variable due to a high rate of sand movement and major directional shifts in potential sand movement (Harvey, 1996). Maintenance of the mouth is related directly to river discharge, wave action and tidal flushing (Bourman and Harvey, 1983).

Between 1936 and 1940 a series of barrages was built across the tidal channels of the river terminus in order to create and maintain a freshwater source for irrigation and navigation purposes (Figure 3.1). The barrages reduced river flow by 75% and contracted the tidal prism by 90%, as well as greatly reducing the width of the mouth and transforming the mouth from a river-dominated to a wave- and tidally dominated outlet (Bourman and Harvey, 1983; Reissen and Chappell, 1991; James *et al.*, in press). This had significant consequences for the river mouth. The barrages allowed stabilisation of flood tidal delta sediments and the creation and growth of Bird Island directly inland from the mouth within five years of barrage completion. Prior to barrage completion shoals were present most years in the vicinity of the Murray Mouth representing exposed flood tide delta plumes, lobes or associated features that were constantly changing and never vegetated (James, 2004). After barrage completion there was no longer sufficient energy during low tide to prevent the development of a more permanent shoal (Bourman and Harvey, 1983; James *et al.*, in press).

The development of Bird Island has made the maintenance of an open Murray Mouth more difficult. In 1981 the Murray Mouth closed, requiring artificial clearance and continued maintenance. Mouth migration has been predominantly to the west following the 1981 reopening (Harvey, 1996) which has provided protection to Bird Island from direct wave exposure and erosion (Bourman *et al.*, 2000; James *et al.*, in

press). In total the mouth has migrated over a range of 1.6 km since the first survey in 1839 (Johnston, 1917; Bourman and Harvey, 1983; Bourman *et al.*, 2000) and up to 6 km over the past 3000 years (Bourman and Murray-Wallace, 1991). Currently the mouth is moving in an eastward direction.

3.3.1.3 Barrier sediments

The sediments which make up the modern coastline are predominantly bioclastic and quartzose sands with minimal heavy minerals. Sprigg (1952) found that the percentage of silicate sediments increased towards the Murray Mouth while carbonate content decreased. Later analyses of beach sediments along Sir Richard Peninsula found no significant or consistent variation in silica vs. carbonate content; SiO₂ varied from 72.7% to 64.0% and CaCO₃ from 20.7% to 27.0% (Bourman and Murray-Wallace, 1991). Short and Hesp (1984) in their analysis of Younghusband Peninsula found carbonate content to increase away from the mouth with 20% at the Murray Mouth to more than 50% 100 km to the south. This was attributed to a decrease in quartz sediment input from the mouth and an increase in shell content. They also found dune, beach, and surf zone grain size to be consistently fine and uniform (2.0 – 2.5 ϕ) from 0-30 km, coarse (0 – 1.0 ϕ) between 30 and 60 km, and fine again from 60-100 km. In comparison, the sands along Sir Richard Peninsula are bi-modal and vary in size from very coarse sand (-1 – 0 ϕ) to very fine sand (3 – 4 ϕ) (Bourman, 1986). Analysis of sediments (Murray-Wallace *et al.*, 2001) to the southeast of the Murray Mouth, from the Pleistocene barrier shorelines of the Coorong Coastal Plain and modern Holocene equivalents at Guichen Bay, showed the carbonate sand to be medium to coarse grained, derived primarily from the shallow inner continental shelf. Grains were represented by comminuted molluscs, echinoids, bryozoans, foraminifers and red algal fragments. The presence of Pleistocene bioclasts within modern sediments as well as the apparent erosion and composite structure of some barriers suggests that older barriers have been sediment sources for younger barrier development (Murray-Wallace *et al.*, 2001). It has been suggested that the increased quartz content to the north near the Murray Mouth is due to the presence of the River Murray (Sprigg, 1959) with the other source of sediment being the offshore Lacepede Shelf (Short and Hesp, 1984).

3.4 The River Murray

The River Murray is part of the largest exoreic drainage network of Australia, the Murray-Darling. Although the Murray-Darling is the fifth largest drainage network globally, river discharge is very low compared with other major global catchments and highly variable; long term average runoff is 11,250 GL but has varied between 2500 GL and 40,000 GL (Eastburn, 1990). A large portion of the River Murray drainage basin is of low topographical relief, 2560 km (89%) of the river channel has a gradient of less than $0.00017 \text{ m km}^{-1}$ (Thoms and Walker, 1992). Erosional scouring during glacial periods and lowered base levels has entrenched the river, at times more than 50 m below present sea level, into Tertiary limestones and Quaternary sediments (Sprigg, 1952; Twidale *et al.*, 1978). The low gradients along the final 600 km stretch of the river contribute to the sluggish flow and the majority of the bedload is trapped in the upstream point bar systems (James *et al.*, 1992). Only a minimal portion of the suspended load reaches the Murray Mouth from which it is quickly and widely dispersed by the longshore and tidal currents. The construction of barrages across the tidal channels inside the Murray Mouth has accelerated the sedimentation of mud on the lake side (Barnett, 1993; Bourman and Barnett, 1995). The lack of sediment delivery and the strong reworking potential at the mouth of the river are the causes for the lack of river delta on this coastline (Bourman and Murray-Wallace, 1991). Although sediment supply to the Mouth is restricted now, it is possible that during more pluvial periods of the late Pleistocene a greater amount of terrestrial sediment was delivered to the coast (Bourman and Murray-Wallace, 1991; James *et al.*, 1992).

3.5 The Lacepede Shelf

The paucity of terrigenous sediment reaching the Lacepede Shelf, coupled with the arid environment and cool water temperatures of southern Australia, permit the growth of carbonate-secreting organisms and the accumulation of bioclastic debris (Gostin *et al.*, 1988). The Lacepede shelf is a low gradient 30,000 km² embayment within the continental shelf situated southeast of Kangaroo Island and Fleurieu Peninsula and west of the Murray Mouth and Sir Richard and Younghusband Peninsulas (James *et al.*, 1992; Hill *et al.*, 2009). The shoreface of Sir Richard and Younghusband Peninsulas is

relatively steep, dropping to 40 mwd (metres water depth) in less than 5 km (James *et al.*, 1992; Hill *et al.*, 2009). However, the shelf itself is fairly shallow; 60% lies within a depth of 40-70 mwd. The shallow neritic zone extends from sea-level to 60 mwd (James and Bone, 2011) (Figure 3.5). The remainder of the shelf, comprised of the middle and steeper deep shelf, is between 60 to 140 mwd and 140 to 200 mwd deep respectively. The continental slope, approximately 80 km wide, drops off sharply to the abyssal plain at depths of 5000-5300 m.

Two coastal current systems flow along the south Australian continental margin affecting the Lacepede Shelf: the Flinders Current System and the Leeuwin Current System (Figure 3.6). The Flinders Current is sourced from the Antarctic Circumpolar Current to the south and consists of cool, well oxygenated water flowing year-round from south of Tasmania and along the coast from east to west as far as Cape Leeuwin (Bye, 1983; Cirano and Middleton, 2004; James and Bone, 2011). The Leeuwin Current brings warm waters from the Northwest Cape in northern Australia south to Cape Leeuwin and eastwards along southern Australia to Tasmania, merging with the South Australian Current in the Great Australian Bight (Godfrey and Ridgway, 1985; James and Bone, 2011). This warm (17-19°C) low-salinity (35.7-35.8‰) water flows over the top of the cooler water of the Flinders Current. The Leeuwin Current is strongest in the winter when westerlies drive the current farther east and inhibit the upwelling of the Flinders Current.

Water temperatures on the western Lacepede Shelf are generally warm (19-20°C) due to the influx of warm water from the South Australian Current through Backstairs Passage, but it cools to the east in the direction of the Bonney Shelf and under the increased influence of the cool Flinders Current (Bye, 1983; James *et al.*, 1992; James and Bone, 2011). Salinity matches this trend, decreasing eastwards from the 35.7-35.8‰ on the western Lacepede Shelf. Upwelling occurs during the summer months off southern Kangaroo Island and on the southeast Lacepede Shelf. The shelf is a region of cool-water Heterozoan carbonate production (James *et al.*, 1992; Hill *et al.*, 2009). Carbonates are produced up to a depth of -400 m and largely consist of non-phototrophic organisms: bryozoans, foraminifers, and molluscs. Phototrophic coralline

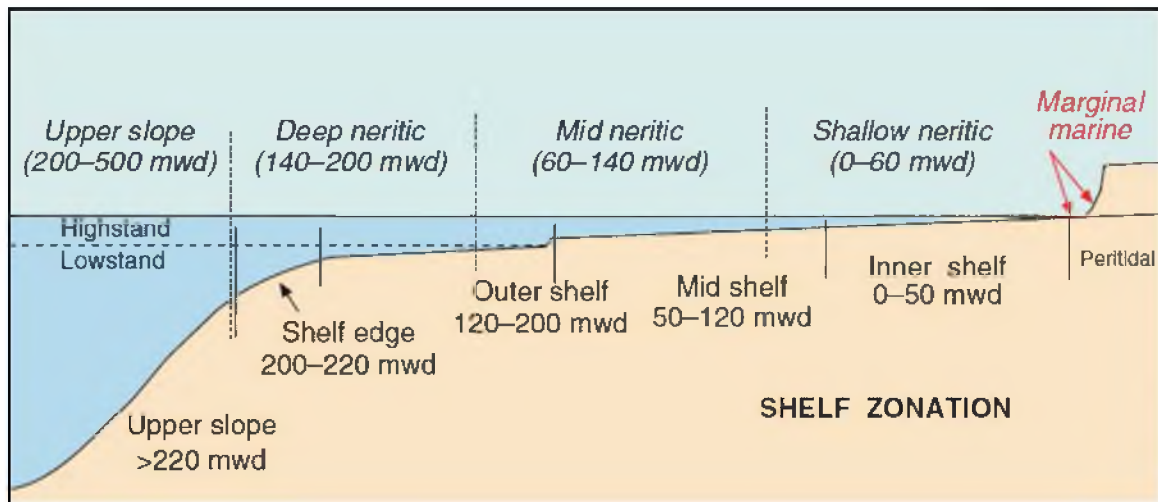


Figure 3.5: An illustration of the different morphological and neritic environments on the shelf (figure 7.1 from James and Bone, 2011).

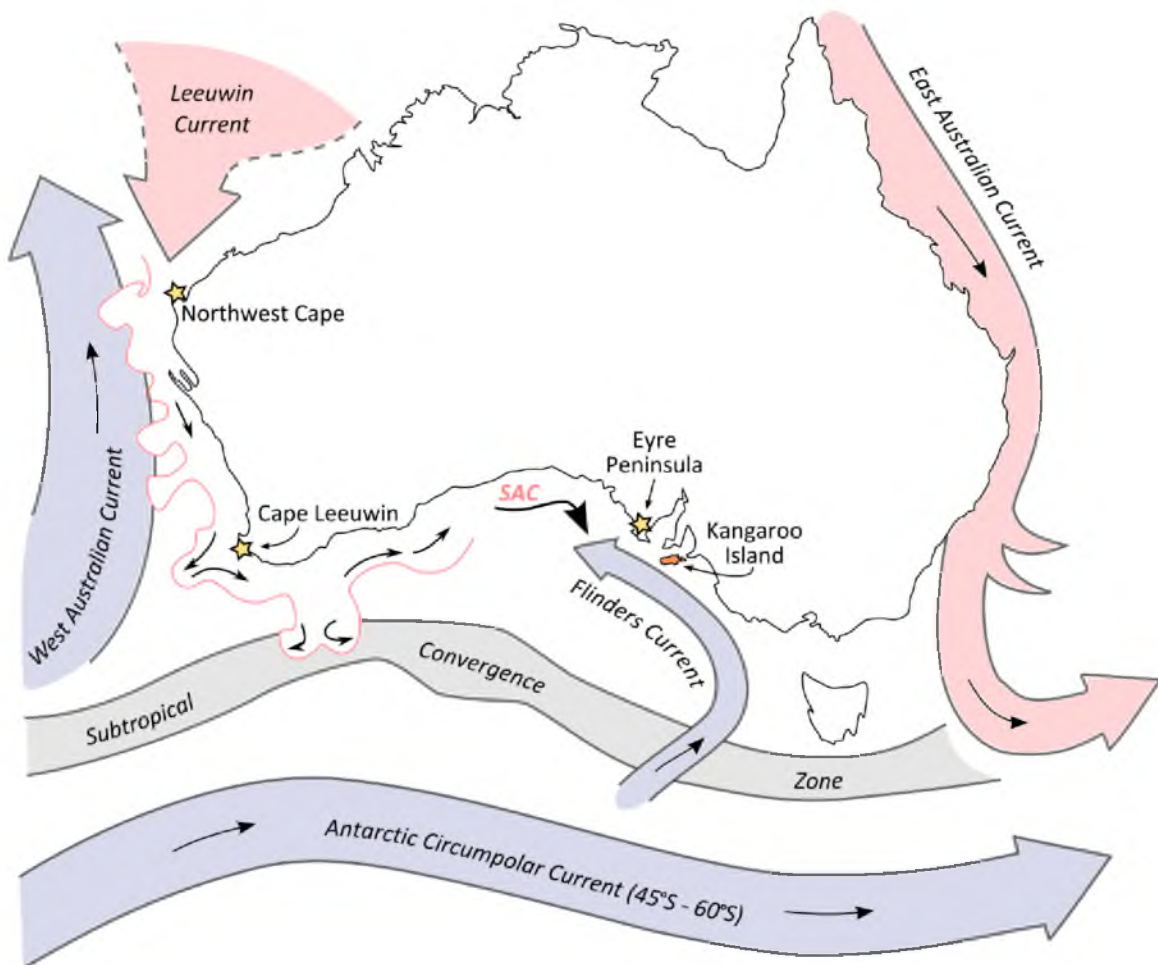


Figure 3.6: Major ocean boundary currents and minor currents of the southern Australia continental margin mentioned in text; SAC, South Australian Current. Blue represents cold water temperature currents, red denotes warm water currents. Stars indicate locations mentioned in text in addition to Kangaroo Island. Figure modified from Murray-Wallace (2014).

algae contribution is notable only in shallow water (<70 m) (James *et al.*, 1992). The shelf here lacks many of the characteristics typical of the tropical Australian shelf (e.g. major coral reef structures, large foraminifera, giant clams and gastropods, and green alga *Halimedi*) (Gostin *et al.*, 1988).

3.5.1 Macrofacies trend

There is a macrofacies trend across the Lacepede shelf from predominantly siliciclastic sediments in the shallow neritic zone to relict sediment in the middle neritic zone, which becomes gradually mixed with recent carbonate outboard until the deep neritic environment is predominantly recent carbonate sediment (Figure 3.7) (James and

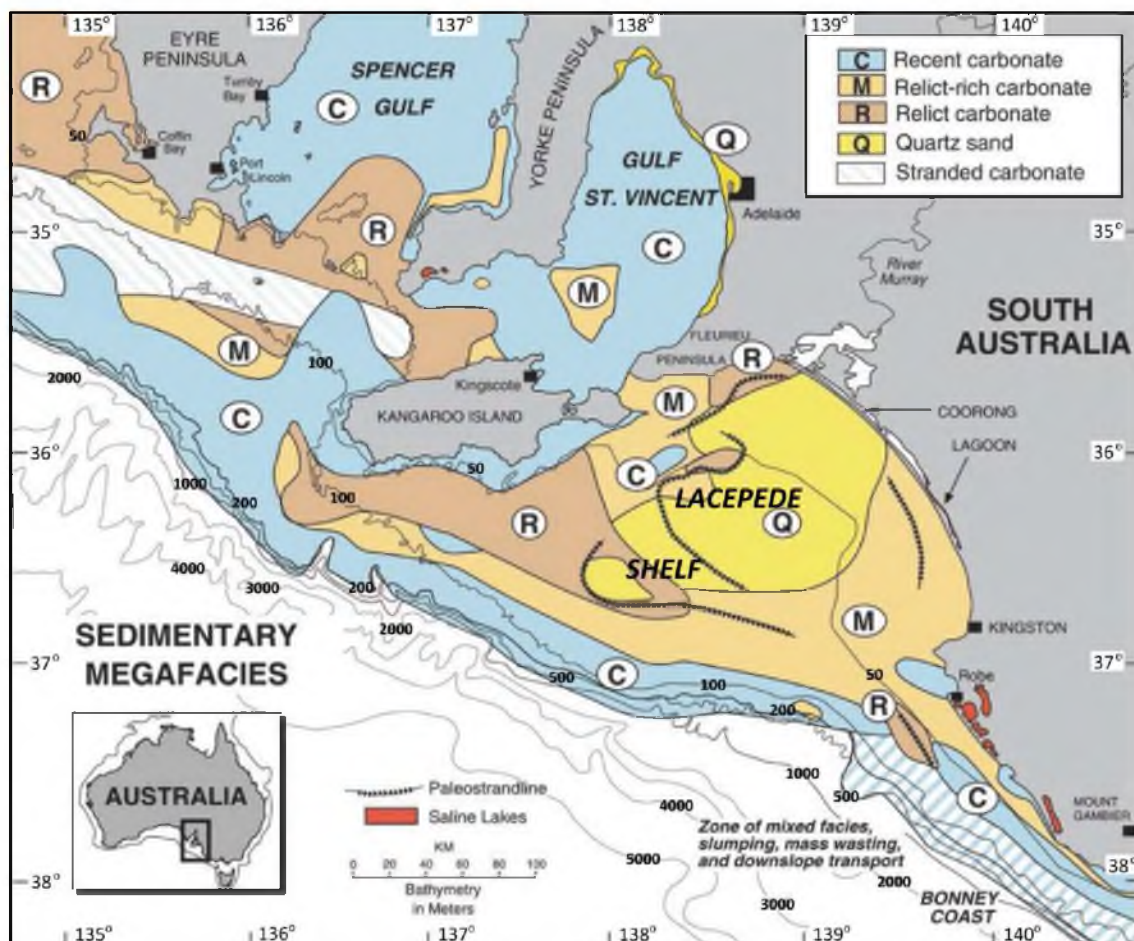


Figure 3.7: The sediment megafacies of the Lacepede Shelf and adjacent continental shelf. Megafacies are determined by their constituents: recent carbonate (>50% carbonate), relict-rich carbonate (25-50% relict grains), relict carbonate (>50% relict), and quartz sand (>50% quartz) (James and Bone, 2011). Note the quantity of quartz sand on the Lacepede Shelf compared with the surrounding continental shelf. The palaeo-River Murray would have delivered quartz to the shelf during periods of lower sea-level (James *et al.*, 1992; Hill *et al.*, 2009) (figure 9.3 from James and Bone, 2011).

Bone, 2011). Active carbonate sedimentation also occurs adjacent to Kangaroo Island due to the upwelling of nutrient-rich waters. Recent and relict carbonate particles are generally distinguishable by their appearance (James *et al.*, 1992; Rivers *et al.*, 2007). Holocene skeletal particles are white or buff and their pores are generally empty but may contain high-Mg calcite cements. Relict grains are stained brown or red-brown and pores are filled with high-Mg calcite cement and/or iron oxide and/or clay. Terrigenous clastic grains are either clean or stained brown. All sediments landward of 80 mwd contain significant amounts of quartz. The predominant facies here are calcareous quartz sand (>50% quartz) and relict-rich skeletal sand and gravel of which 10-50% is quartz. The siliciclastic sediments constitute the largest region of quartzose sand on the southern margin of the continent (James and Bone, 2011). The siliciclastic grains are fine to medium grained and generally very well sorted. These sands would have been delivered to the continental shelf via the palaeo-River Murray or equivalent during periods of lowered sea-level (James *et al.*, 1992; Hill *et al.*, 2009).

The quartz-rich sands which make up the centre of the shelf are mostly surrounded by sediments composed of 25-50% relict grains. Relict grains are defined by James *et al.* (1997) as MIS 3 and 4 skeletons and intraclasts generated when the shelf was partially flooded (Rivers *et al.*, 2007; James and Bone, 2011) (Figure 3.8). They differ from stranded grains which are younger Pleistocene grains formed during the sea-level rise after the last glacial maximum (MIS 2). Stranded grains accumulated in shallow-water environments but are now marooned at water depths much greater than at which they were produced (James and Bone, 2011).

Westward, adjacent to Fleurieu Peninsula, seafloor sediments are composed of relict-rich skeletal carbonate sand and gravel (25-50% relict grains) and mollusc-rich relict sand (>75% relict grains) (James and Bone, 2011). The middle neritic zone south of Kangaroo Island is covered by recent carbonate, as well as isolated bedrock banks and a rocky reef located off Robe. The remaining middle neritic facies range from relict-rich skeletal sands and gravels (25-50% relict grains) to mollusc-rich relict sand, bryozoan-rich relict sand or relict sand, all of which are at least 50% relict grains (James *et al.*, 1992; Li *et al.*, 1998; James and Bone, 2011). The sediments have a speckled brown and

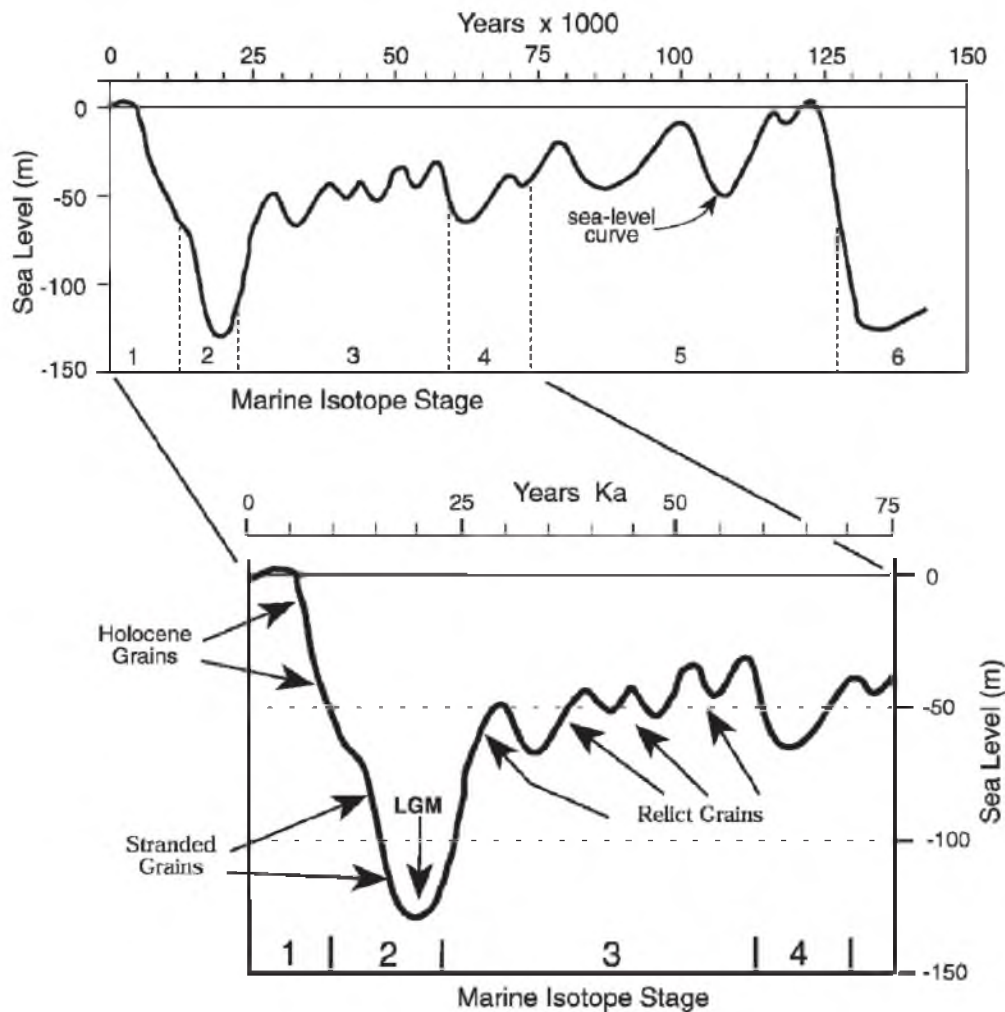


Figure 3.8: The time of deposition for relict, stranded and Holocene carbonate grain assemblages during Late Quaternary sea-level fluctuations (Rivers *et al.*, 2007, figure 4). Relict sediments were deposited when the coastline was located mid-shelf between -30 to -60 m. Stranded sediments were deposited during the sea level rise from -120 m to -60 m. Sea-level fluctuation after Chappell and Shackleton (1986).

cream appearance and are found with either worn bivalve fragments or worn, small brown lithoclast pebbles derived from marooned beach facies. The carbonate species which make up the relict component suggest that lagoonal environments were prevalent on the midshelf during the lower sea-level in the late Pleistocene (Li *et al.*, 1998).

The relict grain component on the shelf decreases with water depth. Between 70 and 90 mwd sediments are largely relict-rich bryozoan or skeletal sands and gravels (25-50% relict grains). The outer shelf beyond 70 m was submerged for most of Late Pleistocene time and most of the carbonate sediments developed beyond 80 mwd are

modern (James *et al.*, 1992). Li *et al.* (1998) also suggested that the strength and depth of wave abrasion on the shelf has limited modern carbonate sedimentation on the present midshelf. Beyond 80 mwd and into the deep neritic zone the recent bryozoan sand and gravel facies dominates (James *et al.*, 1992). This facies is composed of diverse but robust and variably abraded bryozoans. Eventually it gives way to poorly-sorted green fine sand and mud at the outer shelf.

The carbonate sediments produced on the Lacepede shelf are found in open marine and coastal sub-environments including peritidal areas, transgressive aeolianite sheets, and interdune ephemeral saline lakes (Gostin *et al.*, 1988). The high-energy marine setting allows sediment accumulation to occur only in protected gulfs and at depths greater than 60 m. Pre-Holocene lagoonal muds and clays are first encountered at a depth of 25 m (~4.5 km offshore). The swell base is at ~140 mwd with constant movement of sediments above 70 mwd (James *et al.*, 1992). The substantial increase of bryozoan growth beneath 60 mwd suggests it is a good approximation of the depth of wave abrasion above which significant accretion of carbonate does not take place. The relative flatness of the shelf suggests that the late Pleistocene sediments deposited there were reworked during the most recent post-glacial transgression and helps to explain the mix of modern and relict sediments which make up the modern shoreline (James *et al.*, 1992; Hill *et al.*, 2009). The dunes on the shelf would have been incorporated with marine shell hash by the advancing sea, providing sediment for the development of the peninsulas and the extensive Holocene sand flat inland from the barriers forming the southern half of Hindmarsh and Mundoo Islands (Bourman *et al.*, 2000) and may also explain the higher quartz content of the modern peninsulas near the Murray Mouth. In effect, the modern coastline is composed of palimpsest sediments.

3.6 Carbonate Diagenesis

The carbonate sediment deposited on the Coorong Coastal Plain is composed of skeletal grains, foraminifera, coralline algae and intraclasts of older, iron-stained calcarenite (Cook *et al.*, 1977; Colwell, 1978; Murray-Wallace *et al.*, 2001). Calcium carbonate (CaCO_3) occurs as either calcite or aragonite (Scoffin, 1987). Calcite is further divisible by magnesium content into low-magnesium (Mg) calcite or high-magnesium

calcite. Both high-Mg calcite and aragonite are metastable and diagenesis will eventually convert all carbonate sediments to low-Mg calcite (James and Choquette, 1984; Hearty and O'Leary, 2008).

Diagenesis of carbonate grains (the dissolution, redistribution and reprecipitation of carbonate) begins with deposition (Milnes and Hutton, 1983; Wright and Tucker, 1991). The interaction between carbonate and water is the primary driving force in carbonate diagenesis and therefore, an important factor in diagenesis is the composition of surface and subsurface fluids that carbonates come into contact with (James and Choquette, 1983). Hence, a depositional environment (and any post-depositional environments) imparts a unique diagenetic signature which is reflected by the carbonate (Purdy, 1968; James and Choquette, 1983). There are three major diagenetic environments: the sea floor, the meteoric and the deep subsurface (Figure 3.9). The Quaternary sediments of the Coorong Coastal Plain and within the study area have not been exposed to the deep burial environment and consequently that diagenetic environment will not be reviewed here. The meteoric environment is reviewed in two parts reflecting the subdivision within the environment into the vadose phreatic zones. This review begins with the shallow marine phreatic zone, which involves the mixing zone where saline water mixes with freshwater.

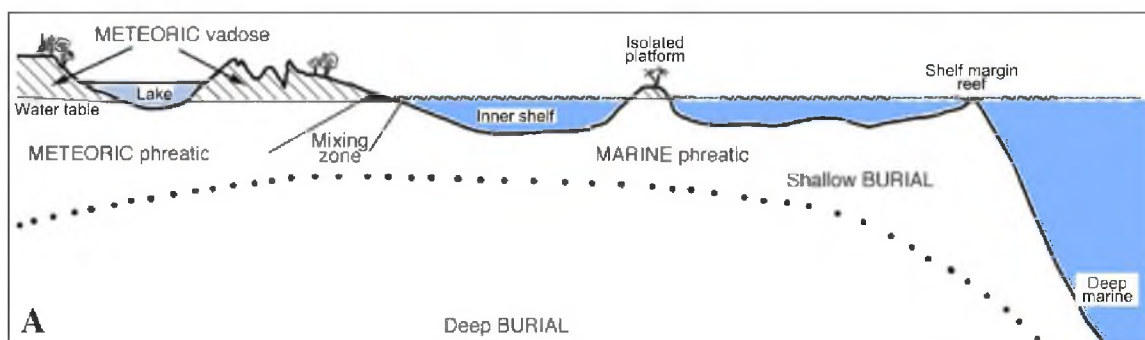


Figure 3.9: Simplified scheme of major diagenetic environments (figure modified from Flügel, 2010).

3.6.1 The sea floor, shallow marine phreatic

Diagenesis in the marine environment takes place at, or slightly below, the sediment-water interface, and on tidal flats and beaches (Purdy, 1968; Flügel, 2010). The

predominant diagenetic process is cement precipitation, aragonite dissolution and the main biological processes are boring by endolith organisms and predation (James and Choquette, 1983; James and Bone, 2011). These processes are visible in the production of ooids, peloids, the lithification of loose carbonate sediments and the destruction of the depositional fabric. Cement precipitation requires adequate porosity and permeability, the ability for CO₂ degassing, the supersaturation of marine water with CaCO₃ and sufficient water circulation (but maintained stability) (Bathurst, 1978; Moore, 1989). The cements precipitated in the marine environment are fine-grained aragonite needles, high-Mg calcite equant fibres or rhombs or microcrystalline (<5 µm) calcite (micrite) which fill intraparticle pore space by first lining voids and subsequently infilling them or binding grains together to form grapestone (Purdy, 1968; Bathurst, 1978; Scoffin, 1987; Adams and MacKenzie, 1998). Grain aggregates on the shelf to ~100 m water depth (mwd) are cemented by high-Mg microcrystalline calcite which is also found in intraskeletal pore space. Hardgrounds are present locally and formed of particles cemented by fibrous high-Mg calcite. The lack of aragonite in Cenozoic deposits, even though aragonite is present in Holocene skeletal particles, implies that aragonite dissolution is taking place in the shallow subsurface within a time span of ~20,000 years (Rivers *et al.*, 2007; 2008; James and Bone, 2011).

Tidal flats, beaches and the underlying shallow subsurface are mixing zones where marine phreatic sea water mixes with the meteoric environment. The marine-meteoric interface in the intertidal zone is where beach rock cementation often occurs under a thin (10-30 cm thick) cover of unconsolidated sediment (Bathurst, 1974; Moore, 1989). Beach rock cements are usually composed of aragonite and high-Mg calcite (Bathurst, 1974) but display diagnostic characteristics typical of meteoric and marine environments (Flügel, 2010). Beach rock may form at an extremely rapid rate (Bathurst, 1974) and is more likely to form and be preserved in protected beaches (Scoffin, 1987).

3.6.2 Subaerial exposure, the meteoric zone

The meteoric environment is divisible into vadose and phreatic settings (James and Choquette, 1983; 1984); the vadose setting is above the water table and the phreatic setting is within the saturated zone (Figure 3.10). The vadose zone is further divisible into the zone of infiltration (soil moisture zone) and zone of gravity percolation

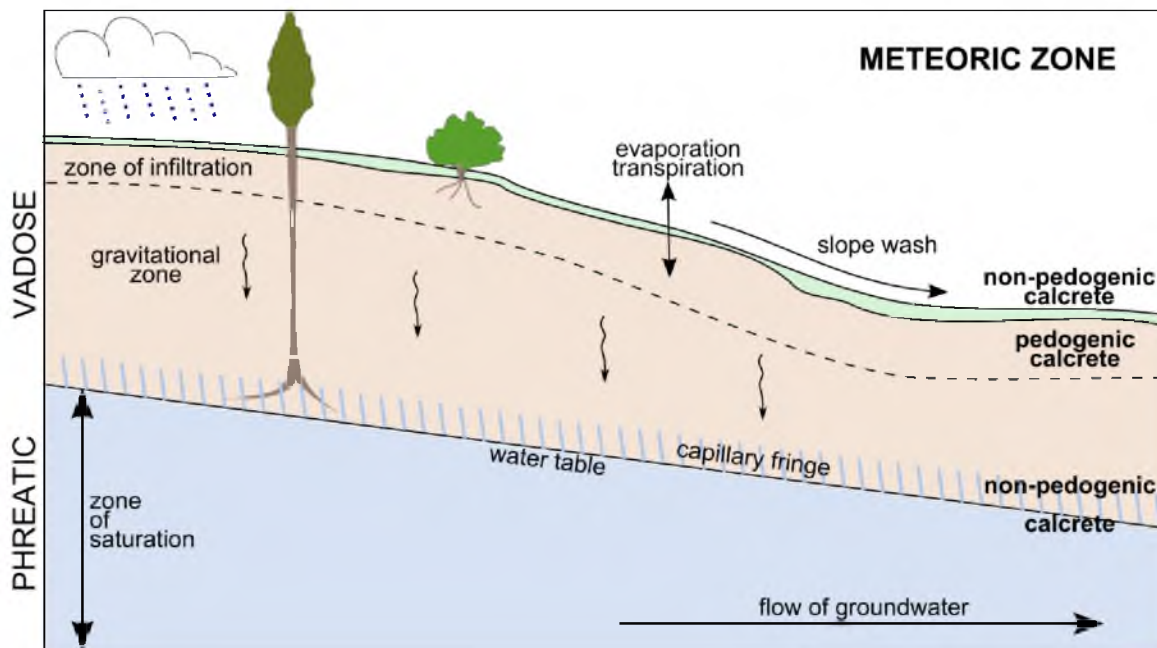


Figure 3.10: The meteoric zone is divisible into the vadose zone (above water table) and phreatic zone (within water table). Calcretes (reviewed below) can be classified based upon their hydrologic setting within the meteoric environment (Carlisle, 1983; Wright and Tucker, 1991).

(Semeniuk and Meagher, 1981; James and Choquette, 1984; Moore, 1989). The zone of infiltration is the location of the air-sediment interface and where rainwater, meltwater or runoff enters the carbonate sequence and as such can be an environment of intense diagenesis. This zone generally includes a soil profile and associated biological activity which alters the composition of fresh water and often induces carbonate precipitation. The underlying zone of gravity percolation is thicker and composed of pore space, variably filled with water and/or air, or organically produced gas; it includes the capillary fringe just above the water table.

Marine carbonate, when exposed to the meteoric environment, undergoes whole-scale mineralogical changes bringing about alteration of grain microstructure or, in some cases, dissolution to create new porosity and permeability (James and Choquette, 1983). Vadose zone and phreatic zone cements have different morphologies reflecting pore space water content (James and Choquette, 1984). Vadose cements grow from pore walls where varying quantities of air and water within the pore space and inconsistent water percolation results in an irregular distribution of cements. The cements are generally equant in shape and exhibit relatively small crystal sizes (Moore,

1989). The partial water content is commonly reflected by meniscus and/or pendant cements that follow capillary water-air interfaces reducing the angularity of pore space (James and Choquette, 1984; Frébourg *et al.*, 2008; Flügel, 2010). Phreatic cements, grown within pores always filled with water, grow unimpeded producing isopachous layers of equant-rhombohedral calcite crystals around pore walls and blocky calcite (James and Choquette, 1984; Moore, 1989; Flügel, 2010). The crystals of the phreatic zone are generally larger than their vadose zone counterparts. Both vadose and phreatic zones can produce epitaxial overgrowth cements, most commonly on echinoderm fragments, but growth is more rapid in the phreatic zone.

In semi-arid warm regions, alteration in the vadose zone is relatively rapid and very subdued or absent in the phreatic zone (James and Choquette, 1984). The low-Mg calcite formed in the meteoric environment (Purdy, 1968) leads to widespread cementation which will, with sufficient time or re-exposure, be subjected to widespread dissolution and the development of karst features (James and Choquette, 1984). These processes are strongly influenced by local surface temperatures and rainfall (James and Choquette, 1983). Calcrete is an outcome of the subaerial exposure and pedogenesis of carbonate sediments in semi-arid to arid environments (Esteban and Klappa, 1983; James and Choquette, 1983; 1984; Frébourg *et al.*, 2008). The development of calcrete has been integral in the preservation of the Bridgewater, Padthaway and Glanville Formations by providing resistance to reworking and other erosional processes (Murray-Wallace *et al.*, 1998). Subaerial weathering also results in the development of *terra rossa* soils. These soils are red in colour and form over stable, non-accreting areas of carbonate sands or limestones.

3.6.2.1 Calcrete

Calcrete is a near surface, terrestrial, accumulation of predominantly calcium carbonate (mainly calcite and dolomite) of variable thickness (centimetres to metres thick) resulting from the alteration of underlying host sediment (Semeniuk and Meagher, 1981; James and Choquette, 1984; Wright and Tucker, 1991). The distribution of calcrete is a factor of the climatic regime (most likely surviving in a semi-arid environment with minimal leaching) and the proximity and availability of an extensive and long-term carbonate source (Milnes, 1982). The solubility of dissolved carbonate in

calcrete is decreased by the removal of H_2O , CO_2 and by the addition of Ca^{2+} (the common ion effect) through processes of evaporation, evapotranspiration, degassing and biological activity, all of which to some extent, are controlled by climate (Wright and Tucker, 1991) and possibly by seasonal effects (Milnes and Hutton 1983).

The formation of calcrete begins with the downward percolation of carbonate-rich soil water (Arakel, 1982). The progression of calcrete formation within the vadose zone is from mottled to massive and then laminar (Semeniuk and Meagher, 1981) with the progressive precipitation or *in situ* development of low-Mg calcite within the regolith (Arakel, 1982). Following precipitation, calcretes can be altered by the modification of calcrete fabrics through chemical and/or mechanical weathering to produce brecciated calcretes (Arakel, 1982). Calcretes mature with age, CaCO_3 recrystallisation (the development of low-Mg calcite), secondary mineral precipitation (which increases rock density and hardness) and dissolution and cavernous weathering (Hearty *et al.*, 1992; Hearty, 1998; Hearty and O'Leary, 2008; Kindler and Hearty, 1996) (Figure 3.11). Soils overlying limestones also display an increase in richness, hue and chroma with age.

The morphology and sedimentological characteristics of calcretes indicate the mode and environment of formation (Milnes, 1982) and is dependent upon the maturity of the profile (Semeniuk and Meagher, 1981). Calcretes can form in both the phreatic (within the water table) and vadose (above the water table) zone with those developed in the phreatic zone referred to as groundwater calcretes (Wright and Tucker, 1991). Groundwater calcretes form from groundwater with a high concentration of carbonate, which is precipitated in the capillary fringe zone or below the water-table (Semeniuk and Meagher, 1981; Wright and Tucker, 1991). Vadose zone calcretes are further identified as either pedogenic (soil profile) or non-pedogenic (Figure 3.10). Pedogenic calcretes form within the soil moisture zone beneath the land surface. Non-pedogenic calcretes form at the surface as laminar crusts or cementation-case hardened surfaces, or within the gravitational zone or at the capillary fringe (Semeniuk and Meagher, 1981; Carlisle, 1983; Wright and Tucker, 1991). However, differentiating pedogenic from non-pedogenic can be very difficult (Wright and Tucker, 1991).

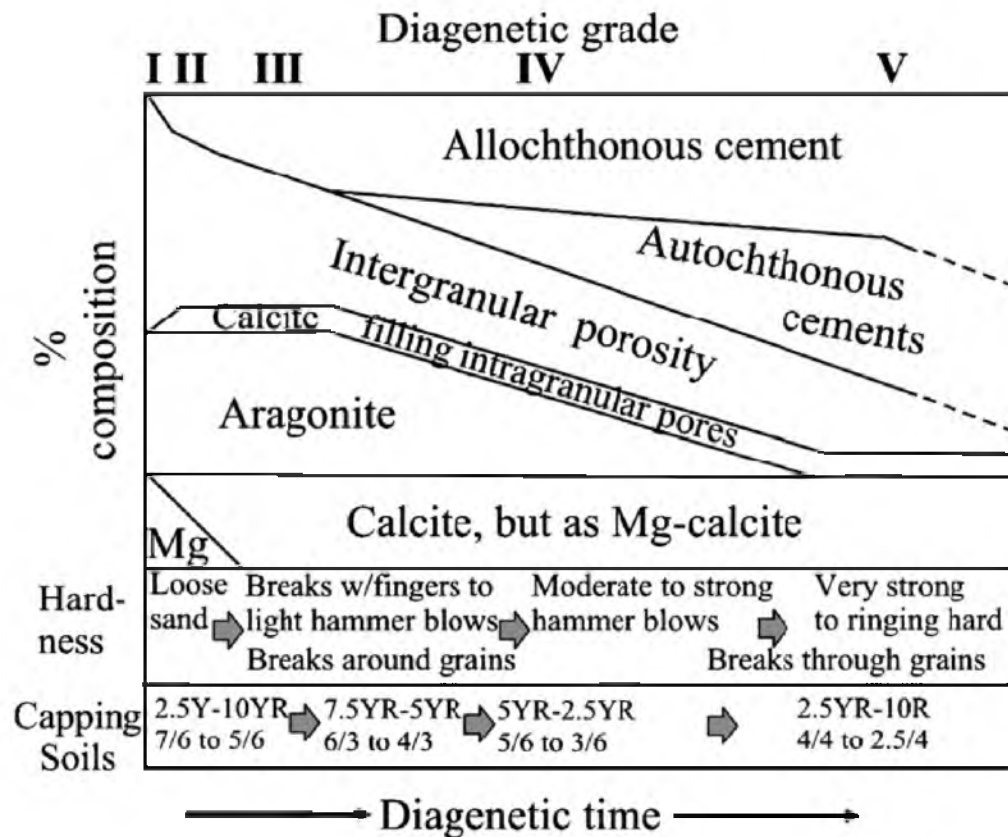


Figure 3.11: Calcrete maturity can be measured using diagenetic grades which reflect mineralogical, thin-section and relative-age characteristic (rock hardness and Munsell (2002) soil color) of the calcrete (Hearty and O'Leary, 2008, figure 5).

The principal morphological types of calcrete common in Australia are: powdery, nodular, pisolitic, tubular (most commonly present as carbonate rhizoliths), laminar, boulder/cobble, hardpan, and carbonate mottles (Chen, 2002). Calcrete profiles are vertically zoned and can contain one or more of these morphological types (James and Choquette, 1984). Other components within calcrete include detrital minerals such as quartz, feldspars and clay minerals, which comprise the normal weathering products of rock (Milnes, 1982).

Warren (1983) concluded that the Bridgewater Formation calcretes had developed in a vadose environment due to their presence within and capping dunes up to 80 m APSL and because sea-level in South Australia had never been more than 5 m APSL (since shown to have been no more than 6 m APSL (Belperio and Bluck, 1990; Murray-Wallace, 2002). The Bridgewater Formation calcrete forms as a pedogenic calcrete in the surficial layers of the calcareous dunes by impregnation and cementation of secondary carbonate. The carbonate component of mature Bridgewater Formation

calcrete is commonly solely low-Mg calcite (from the dissolution of calcareous sand grains in the overlying soil) and to a lesser extent, from Ca^{2+} and HCO_3^- in rainwater. Warren (1983) studied calcrete development on the Bridgewater Formation by comparing the extent of calcrete formation in the Holocene dunes with the more mature development in older Pleistocene dunes. Calcrete development begins with incipient case hardening or capping within the soil moisture zone where some plant roots and rootlets are surrounded or replaced by thin sheaths or tubules of micrite, the first stage of rhizoconcretion. Sand grains within the older Pleistocene dunes can be completely surrounded by meniscus cements of micrite or micrite envelopes. Micrite rinds on quartz grains suggest that most micrite is deposited during diagenesis in a vadose environment. Warren (1983) attributed the development of micrite rinds to the volume and salinity of a film of attached water left on all grains in the vadose zone after gravitational water has passed through the sediment and before evapotranspiration. With time the micrite accumulates in thickness and is deposited throughout the vadose zone but is greatest within pedogenic calcretes due to the presence of the soil-moisture zone. The two morphological types of calcrete common to the coastal zone of Australia are hardpan calcretes and tubular calcretes (Chen *et al.*, 2002). Hardpan calcretes have variable forms from massive and structureless to complex, containing re-cemented nodules, pisoliths, and breccias. Tubular calcretes contain carbonate rhizoliths, which are the carbonate root casts and moulds. Root moulds can also occur in hardpan calcretes.

Common to the hardpan calcretes capping the Bridgewater Formation are the dissolution features known as solution pipes (Blackburn *et al.*, 1965; Warren, 1983). Solution pipes are formed by the ponding of rainwater in subsurface depressions on the calcrete causing redissolution of the calcrete until the water breaks through (Warren, 1983). Voids created by solution are lined with cement that binds the deformed calcrete layers (Arakel, 1982). Any existing solution pipe becomes the preferred drainage conduit for infiltrating rainwater. Boutakoff (1963) mistakenly identified solution pipes on Cape Bridgewater as fossilised tree stumps (Blackburn *et al.*, 1965) (Figure 3.12). Solution pipes are near vertical in orientation and in South Australia generally range from 30-60

cm in diameter and have been observed reaching depths up to 7.5 m (Blackburn *et al.*, 1965). Solution pipes are usually infilled with varying types of soils.

Calcrete has been used as a stratigraphic marker (Firman, 1964; 1966; 1973; Belperio, 1985) to separate the Upper and Lower Bridgewater Formation and the last interglacial Glanville Formation from overlying younger deposits. However, the thickness, topographic expression and calcrete type can be highly variable dependent upon the varying lithologies and landforms in which or upon which it forms; therefore, it is not recommended as a stratigraphic marker (Phillips and Milnes, 1988).



Figure 3.12: Solution pipes at Bridgewater Bay (Cape Bridgewater) were mistaken for fossilised tree stumps by Boutakoff (1963). Photograph provided by Colin Murray-Wallace (20 May 2015).

3.6.2.2 *Terra rossa* soil

Blackburn *et al.* (1965) identified two soil types common to the region of South Australia associated with the calcareous sands of the Bridgewater Formation; podzol and *terra rossa*. The podzols are formed on siliceous sands with practically no carbonate content, which Blackburn *et al.* (1965) thought to have been sourced from the leaching of carbonate from the Bridgewater sands and subsequent reworking. The siliceous sands are actually late Pleistocene desert dunes, the Molineaux Sand (Sprigg, 1959; Firman, 1973), leaving only the *terra rossa* soil as truly developed from underlying calcareous sands.

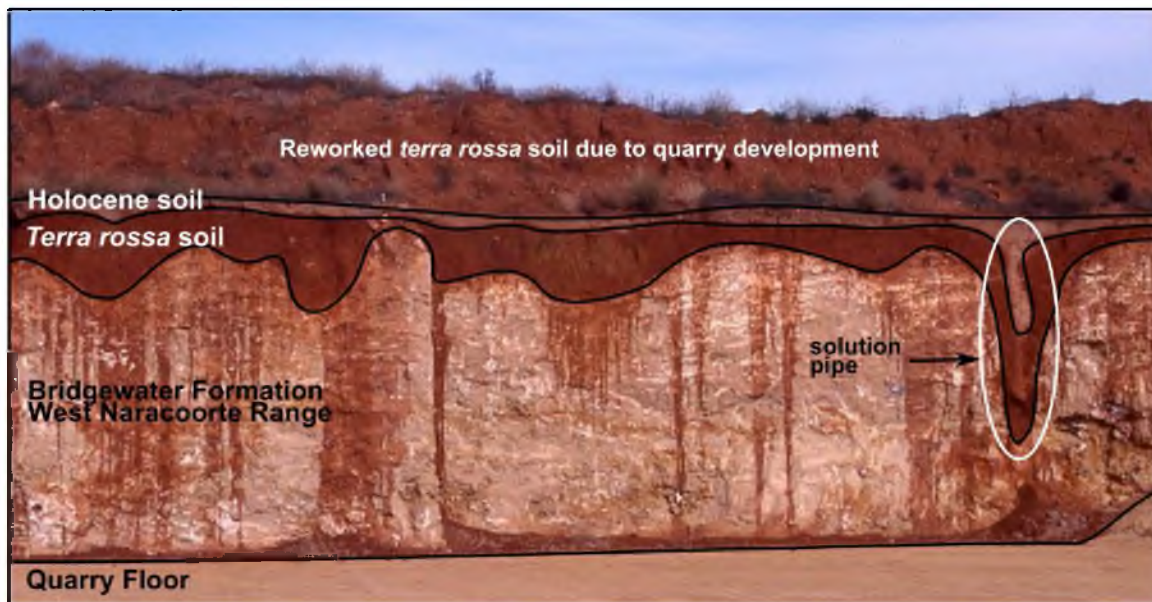


Figure 3.13: Picture of red *terra rossa* soil overlying the West Naracoorte Bridgewater Formation at the former Wrattenbully Quarry. The *terra rossa* infills an eroded surface on the Bridgewater Formation, including a solution pipe. The *terra rossa* is in turn overlain by a Holocene soil. Photograph provided by Colin Murray-Wallace (20 May 2015).

Terra rossa refers to soils of relatively uniform red earth associated with highly calcareous rocks (Blackburn *et al.*, 1965). The *terra rossa* palaeosols found interbedded within the Bridgewater Formation in stable non-accreting areas represent a hiatus in deposition and potentially an extensive period of subaerial exposure related to oscillation of Quaternary sea-level (Boutakoff, 1963; Sprigg, 1979; Milnes, 1982; Brooke *et al.*, 2014). *Terra rossa* is usually found overlying limestone, infilling solution pipes and has been associated with calcrete development (Blackburn *et al.*, 1965) (Figure 3.13). Some authors (Milnes and Hutton, 1983; Zhou *et al.*, 1994) have suggested *terra rossa* possibly formed from the insoluble residues of calcrete weathered *in situ*. However, analysis of *terra rossa* on the southeast Coorong Coastal Plain (Mee *et al.*, 2004) found the residual origin theory (at least for the region) to be unlikely due to insufficient insoluble residue in the underlying calcareous material and a lack of any significant genetic relationship between the soils and the insoluble residues. Instead, an aeolian input was found to be more likely due to a similarity between *terra rossa* sediments and surrounding geology. Blackburn *et al.* (1965) found it unlikely for the Bridgewater Formation to be the parent material citing the presence of calcrete between the calcareous sediments and the overlying *terra rossa*. Mee *et al.* (2004) proposed that weathering of the nearby Palaeozoic Kanmantoo meta-sediments produced fine-grained

detritus which was carried by wind to be redeposited in lagoonal systems where further remobilisation and weathering occurred to produce *terra rossa*. The development of *terra rossa* is not restricted to only lagoonal regions as they are found interbedded with and overlying the Bridgewater Formation (Boutakoff, 1963; Blackburn *et al.*, 1965; Zhou *et al.*, 1994).

3.7 Lithology of Quaternary Deposits

This section provides a lithological description of the sedimentary successions that have been identified and/or mapped within the study area (see section 2.5.3 Murray Lakes Record) (Figure 3.14). The lithology of the successions thus far described, provided aid in their recognition throughout the field studies of this research.

There are five sediment facies associated with the beach-barrier deposits of Quaternary interglacial highstands (Belperio and Cann, 1990; Belperio *et al.*, 1995; Murray-Wallace *et al.*, 1998; 1999): shallow marine (including basal transgressive and shallow subtidal facies), littoral sediments, transgressive aeolian dune facies, and estuarine or lagoon facies (Figure 3.15). Many of the barriers upon the Coorong Coastal Plain have been shown to be composite with interbedded calcretes and unconformity surfaces suggesting more than one major phase of development with longer term hiatus of deposition (Cook *et al.*, 1977; Belperio *et al.*, 1995; Murray-Wallace *et al.*, 1999). The Bridgewater Formation encompasses the dune sediments. Beach facies are labelled as stratigraphically undefined units or as Glanville Formation. The estuarine, lagoonal and additional lacustrine facies are identified as the Glanville Formation (Last Interglacial), the Padthaway Formation and an older unnamed dolomite. In addition to the beach-barrier successions, the study area also contains the siliceous sands of the Molineaux Sand and the alluvial Pooraka Formation. However, the first sedimentary succession to be described is the modern St Kilda Formation, which includes all Holocene coastal sediments and has already been partially described above (section 3.3).

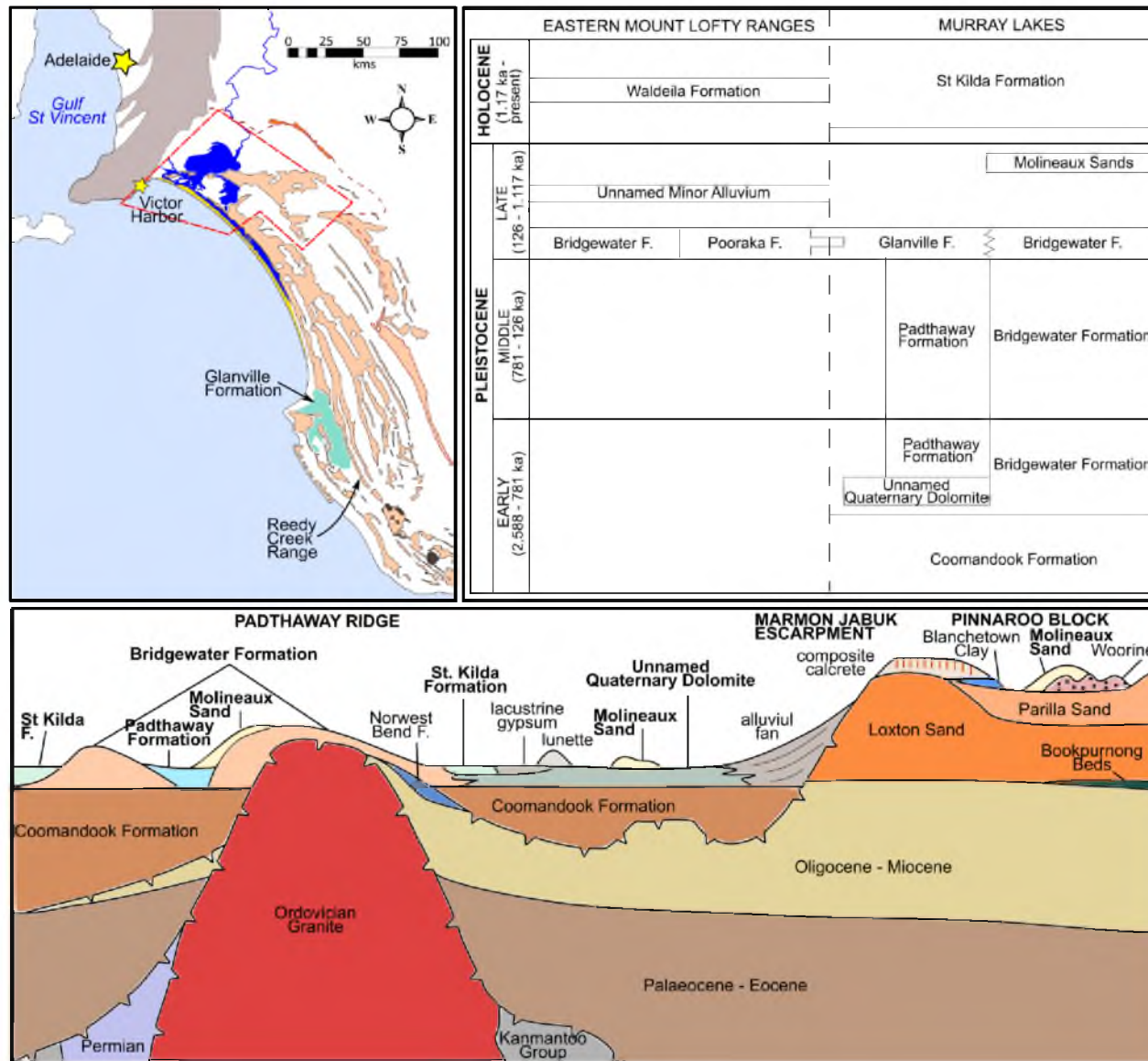


Figure 3.14: The study area (outlined in red dashed line), located at the northern margin of the Coorong Coastal Plain contains sedimentary successions associated with the development of the modern beach-barrier shoreline and Pleistocene equivalents. The St Kilda, Bridgewater and Glanville Formations are also found (Bourman *et al.*, 2000; Murray-Wallace *et al.*, 2010) on the adjacent Fleurieu Peninsula of the Mount Lofty Ranges. Similarly, the last interglacial alluvial Pooraka Formation has been found to interfinger and overlie the Glanville Formation (Firman, 1966a, Bourman *et al.*, 1997; 2010). Later alluvium (50-40 ka and the 6-4 ka Waldeila Formation) have also been identified on the ranges (Bourman *et al.*, 2010). The rock relation diagram (modified from Rogers, 1979) illustrates the relationship of sedimentary successions from the Murray Lakes region southeast of the lakes and includes the major structural elements: the Padthaway Ridge, Marmon Jabuk Escarpment and Pinnaroo Block. The lithology of the sedimentary successions labelled in bold are described in text. Place names and features described in text are also provided in the Coorong Coastal Plain image (top left).

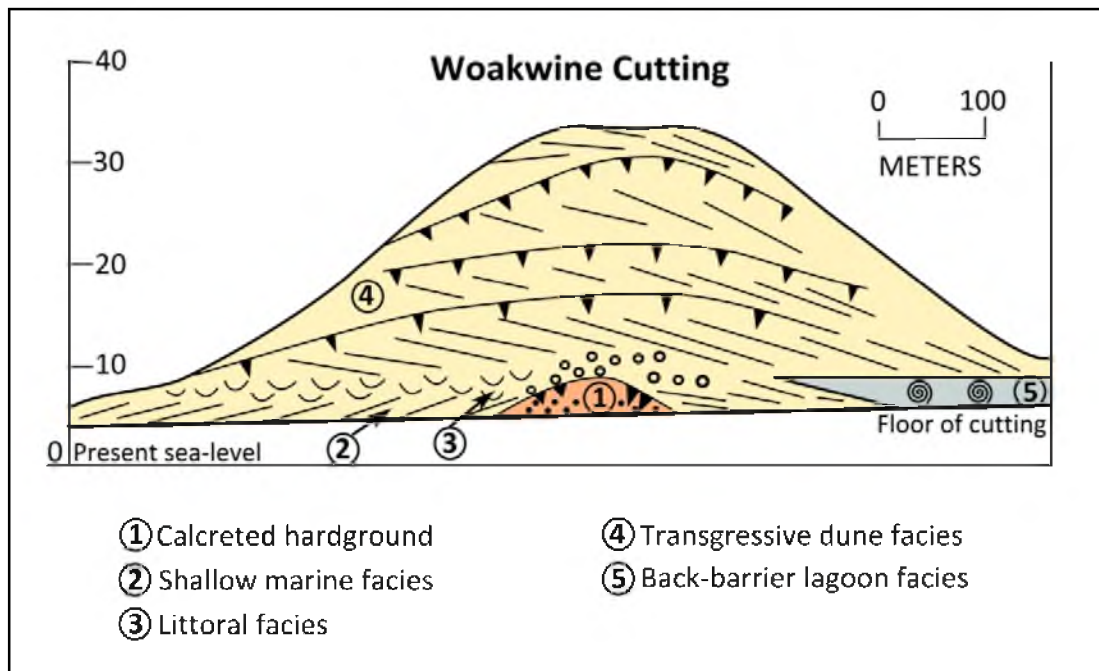


Figure 3.15: A representative cross-section of the last interglacial barrier, the Woakwine Range, based on a deep cutting. The section displays the common sedimentary facies associated with beach-barrier deposits in the region. Figure modified from Belperio *et al.*, 1995.

3.7.1 St Kilda Formation

The St Kilda Formation was originally defined by Firman (1966a) in reference to a low-lying swampy tract inland of the modern coast near St Kilda and found elsewhere in Gulf St. Vincent. He also related the unit to raised sea beds and marine deposits of an earlier high sea level. Cann and Gostin (1985) to clarify confusion over the designation of the St Kilda Formation as either modern or Holocene or both, redefined the unit to “include all Holocene sediments deposited under the influence of marine processes, including estuarine deposits, coastal dunes and storm ridges” (page 122). Accordingly, the St Kilda Formation overlies Pleistocene marine or continental sediments and encompasses the previously named Semaphore Sand (Firman, 1966a) as a member (Belperio, 1995b).

Firman (1973) expanded the definition of the Semaphore Sand to include the most recent dune fields of coastal sand. The Semaphore Sand forms the modern beach and dune complexes (i.e. Sir Richard and Younghusband Peninsulas) and is composed of dominantly unconsolidated, locally mobile, white to pale-grey, calcareous, quartz sand

with variable carbonate content (Brown and Stephenson, 1991). Carbonate occurs in the form of calcite and aragonite and is composed of grains of comminuted molluscs, echinoids, bryozoans, foraminifers and red algal fragments with calcareous rhizoliths and Pleistocene bioclasts also present (Murray-Wallace *et al.*, 2001).

The St Kilda Formation also includes intertidal, estuarine, lacustrine and lagoonal sediments. Lagoonal sediments within the Coorong are composed of a black, sticky, aragonite and Mg calcite mud and generally consist of two distinct phases of deposition (Harvey, 1981; Gostin *et al.*, 1988). The first phase is characterised by bivalve mollusc shells typical of sheltered marine environments. As the lagoon becomes more restricted and increasingly saline, the fauna shifts to those more adapted to hypersaline conditions. The southern half of the lagoon is now considered to be hypersaline (Belperio and Cann, 1990). High groundwater results in precipitates of aragonite, dolomite, and hydromagnesite muds (Gostin *et al.*, 1988). Shallow water or sub-aerial exposure can produce crusts, polygonal cracks, tepees and mud-chip breccias.

Estuarine and lacustrine deposits associated with Lakes Alexandrina and Albert include formerly (within the Holocene) inundated areas adjacent to the Murray Lakes, the largest extension of which is the Cooke Plains Embayment (Stephenson and Brown, 1991). Lake expansion has been attributed to a ~1 m higher than present sea-level ~6500 years ago (Belperio, 1995b) identified by basal eutrophic lagoon facies, lacustrine facies and regressive lake facies which infill former embayments around the lake (von der Borch and Altmann, 1979). The estuarine and lacustrine deposits associated with lake expansion are composed of unconsolidated lacustrine mud, silt, sand, and organic detritus (calcareous and carbonaceous) (Stephenson and Brown, 1991).

3.7.2 Bridgewater Formation

The aeolian dune sediments of the Bridgewater Formation consist predominantly of calcareous sands and quartzose calcarenites composed of skeletal carbonate, quartz, minor feldspar and trace amounts of heavy minerals (Cook *et al.*, 1977; Colwell, 1978). Carbonate content is variable, from <10% to 100 %. The skeletal material typically consists of comminuted shell fragments, coralline algae, bryozoan, variable amounts of whole and fragmented foraminifer and echinoid plates, spines and other components.

Intraclasts from older, indurated, iron-stained calcarenite and bryozoan limestone are also common. Staining or partial replacement by iron oxides in the upper part of the formation imparts a yellowish orange to light brown colour to the sediment that decreases with depth to a pale grey near the base (Cook *et al.*, 1977; Colwell, 1978).

Each of the sedimentary facies within a beach-barrier complex has distinct characteristics. The shallow subtidal facies are seaward-dipping, coarse, clean to muddy carbonate sands with abundant broken shells of marine gastropods and bivalves, with foraminifers and coralline algae also present (Belperio and Cann, 1990; Belperio *et al.*, 1995). The basal transgressive facies is directly overlain by the sublittoral facies, separated by an irregular scour surface with small trough-style depressions (Murray-Wallace *et al.*, 1999). The sublittoral facies consist of seaward-dipping planar cross-beds (clinoforms) with a typical dip of 6- 9° (Murray-Wallace *et al.*, 1999). Littoral sediments are well-sorted, medium- to coarse-grained, quartzose and skeletal carbonate sand, occurring as shoestring sand bodies subparallel to the present coast (Belperio and Cann, 1990). The littoral facies contains seaward-dipping clinoforms and bidirectional trough cross-beds (Belperio *et al.*, 1995; Murray-Wallace *et al.*, 1999). The beach deposits, up to 3 m thick, extend into the core of the ranges as distinctive bidirectional trough cross-bedded strata (Belperio and Cann, 1990; Murray-Wallace *et al.*, 1998). The land-ward migrating aeolianite facies forms the majority of the visible Bridgewater Formation. The dunes comprise weakly cemented, fine- to medium-grained skeletal sand, of well-sorted and rounded molluscan, foraminiferal and algal grains within large-scale crossbeds up to 10 m thick dipping consistently landward at 3-30° (Belperio and Cann, 1990; Belperio *et al.*, 1995). Multiple cosets of crossbeds are separated by reactivation surfaces, made apparent by weakly developed palaeosols and rhizolith concentrations (Murray-Wallace, *et al.*, 1998). The shape of the dune forms has been preserved by laterally persistent indurated calcretes. To their lee side, the dune facies interfinger or overlie sediments of the lagoon facies (Belperio and Cann, 1990).

The carbonate content in the dunes decreases inland, although some older inland dunes show an increase of carbonate content with depth (Cook *et al.*, 1977; Colwell, 1978). This is most likely due to leaching of carbonate from the upper portion of the dune. Barrier sediments to the east of Reedy Creek (MIS 7e) are significantly less

calcareous than those to the west, potentially reflecting the possible contribution of eroded Pliocene sands; although it may also be a function of increased diagenetic alteration to the east (Cook *et al.*, 1977). Cementation has occurred in both the vadose and phreatic zones of the dunes, with cemented framework components commonly enclosed by a thick envelope of micrite (Cook *et al.*, 1977; Colwell, 1978; Warren, 1983). Pores in the vadose zone are commonly lined with meniscus cements of sparry calcite while those in the phreatic zone are commonly filled. In the phreatic zone this envelope commonly outlines the moulds of skeletal fragments. Cementation increases in occurrence with the age of the dune (and therefore increases landward alongside the general trend of age). Increased diagenesis of older dunes is reflected in an inland decrease in magnesium (Mg) and strontium (Sr) content. In general, the dune deposits west of Reedy Creek Range consist predominantly of low-Mg calcite, quartz, and aragonite while those to the east consist mainly of low-Mg calcite and quartz (Cook *et al.*, 1977; Colwell, 1978). Low-Mg calcite is often the only recognisable carbonate in mature calcrete horizons (Warren, 1983).

3.7.3 Glanville Formation

The Glanville Formation is named after the Adelaide suburb of Glanville, where the original section was described by Howchin (1888) at “Fletcher’s New Graving Dock” (Firman, 1966a; Ludbrook, 1976). Howchin (1888) recognised the presence, in a shallow marine unit, of marine fossils, which had become extinct along the entire coast of South Australia; the cockle *Anadara trapezia* and the foraminifer *Marginopora vertebralis* (Ludbrook, 1984). The original type section is now submerged in the Glanville dock excavation in Port Adelaide (Ludbrook, 1976; Cann, 1978). The Glanville Formation on the CCP refers to the last interglacial estuarine/lagoon facies on the lee side of the Woakwine and Dairy Ranges (Belperio and Cann, 1990), which Crocker and Cotton (1946) and Sprigg (1952) referred to as the *Anadara* high sea level.

The Glanville Formation comprises last interglacial back-barrier lagoon facies with sediments that are typically very shelly and sandy to muddy (Ludbrook, 1984; Belperio and Cann, 1990). The facies display a distinctive regressive sedimentary sequence manifested as an upward change in fossil biota from shallow-water subtidal molluscan species that inhabit seagrass meadows to species more characteristic of

intertidal sand flats (Belperio *et al.*, 1995). It is characterised by elements of warm water fauna that are no longer typical in South Australian waters; bivalves: *Anadara trapezia*, *Pinctada carchariarum*, *Macra eximia*, the conical-fusiform gastropod *Euplica bidentata*, and the foraminifers *Marginopora vertebralis* and *Quinqueloculina polygona* (Ludbrook, 1984; Belperio and Cann, 1990; Belperio *et al.*, 1995). Shell beds are most commonly composed of bivalves *Anadara*, *Katelysia*, *Ostrea*, *Chlamys*, and *Anapella* (Cook *et al.*, 1977; Belperio *et al.*, 1995). This unit has provided a useful datum for reconstructing last interglacial sea level to ± 2 m along the tectonically more stable portion of the coast of South Australia (Belperio and Cann, 1990; Belperio *et al.*, 1995; Murray-Wallace and Belperio, 1991; Murray-Wallace *et al.*, 1998; 2001; Murray-Wallace, 2002).

3.7.4 Padthaway Formation

Sprigg (1952), in his description of the southeast region, recognised that sea-floor deposits and planes of marine erosion occur in the interdune corridors but described them as “mostly flats of accumulation sloping gently seaward and harbouring extensive lakes and lagoons which tail off into marshes and flats only periodically flooded” (Sprigg, 1952 p. 65). However, he left the deposits of the interdune corridors unnamed. Firman (1973) labelled the deposits Coonambidgal Formation after Lawrence (1966) for streams or their recent ancestors in the Murray Basin. Rogers (1979; 1980) gave the dolomite, sand and clay occurring between the Bridgewater dune complexes the informal name of Padthaway Formation, which continues to be used (Belperio and Cann, 1990; Brown and Stephenson, 1991; Belperio, 1995b).

The lacustrine sediments are not necessarily coeval with the deposition of beach-barrier and lagoonal sediments and may reflect inter-dune corridor flooding with the return of sea-level highstands during successive interglacials; fluvial and lacustrine sedimentation continues today in some inter-dune corridors (Brown and Stephenson, 1991). However, the basal sediments of these interdune flats, can be considered to follow the trend of the Bridgewater Formation and increase in age inland. The sediments are predominantly pale grey and white calcareous muds typically 1-2 m thick (but can be up to 7 m thick) with variable amounts of calcite, aragonite and dolomite (Cook *et al.*, 1977; Belperio and Cann, 1990). They can contain beds of greenish clay, clayey quartz

sands, calcareous clay, and shell detritus (Belperio and Cann, 1990; Brown and Stephenson, 1991). They may also contain fossils of a variety of fresh to brackish water molluscs, foraminifers and ostracods. Cook *et al.* (1977) recorded the presence of coquinas and scattered individuals of the gastropod *Coxiella striata*.

3.7.5 Unnamed Quaternary Dolomite

This undefined sedimentary unit occupies the plain at the base of the Marmon Jabuk Scarp (Rogers, 1979; 1980; Brown and Stephenson, 1991). It is an Early Pleistocene marginal-marine and lagoonal unit overlying the marine Coomandook Formation and underlying the Molineaux Sand and the Cooke Plains St Kilda Formation. The dolomite is pale-grey, fine-grained, and well-cemented containing intraclasts of sandstone, calcarenite, and dolomite, and is locally capped by calcrete (Brown and Stephenson, 1991).

3.7.6 Molineaux Sand

The glacial Molineaux Sand blankets the Bridgewater and Padthaway Formations at the northern end of the CCP (Rogers, 1980) and interfinger with the St. Kilda Formation and alluvium (Brown and Stephenson, 1991). The Molineaux Sand dunes are composed of unconsolidated aeolian quartz sand grading from pale yellow near the crest of the dune to dark yellow with depth, with soft columnar carbonate nodules (Firman, 1973). The pale yellow sand is veneered by pale grey sand reflecting removal of iron oxide coatings on quartz grains during periods of reworking (Rogers, 1980). Quartz grains, usually more than 98% of the sand by mass, are well-sorted, highly spherical with frosted grain surfaces (Lawrence, 1966). The most common minor accessory minerals are tourmaline, zircon, muscovite, and iron oxide (Brown and Stephenson, 1991). Thermoluminescence ages of dunes in the Murray Mouth and lakes region returned ages indicating deposition 16 -18 ka during the Last Glacial Maximum (LGM) (Bourman *et al.*, 2000).

3.7.7 Pooraka Formation

The Pooraka Formation is a sedimentary succession found on the margins of the Mount Lofty Ranges and on Kangaroo Island underlying river terraces and alluvial fans (Bourman *et al.*, 2010). It is alluvial clay named from the Pooraka Railway Station in

Adelaide (Firman, 1966a) with a reddish-brown colour and weakly developed calcareous pedogenic horizons containing nodules and vertical cylindroids of pedogenic calcium carbonate (Williams, 1969; Bourman *et al.*, 1997; 2010). The clay consists of prismatic and blocky structures within gravel, sand, clayey sand, clay and residual material from weathered basement highs contributing to a variable lithology (Williams, 1969; Brown and Stephenson, 1991). It has variable stratigraphic relationships; it is intermixed with the Glanville Formation at Victor Harbor but in other locations rests directly on the Glanville Formation or an overlying calcrete if present, or is absent from the sedimentary record (Firman, 1966a, Bourman *et al.*, 1997). Bourman *et al.* (1997) suggested the relationship between the Glanville and Pooraka Formations may be dependent upon whether there is sufficient supply of terrestrial sediments to the coastline. During the Last Interglacial, wetter conditions inland would have facilitated aggradation of sediments, whereas the drier conditions of a glacial environment would have promoted dissection. A total of five luminescence ages (mixed thermoluminescence and optically stimulated luminescence) puts deposition of the Pooraka Formation within the Last Interglacial maximum (132-118 ka) (Bourman *et al.*, 1997; 2010).

3.8 Conclusions

The modern shoreline of the CCP is a result of cool-water carbonate production made possible by a reduced supply of terrigenous clastic sediment to the shelf, strandline reworking during successive episodes of sea-level fluctuation, modern reworking of sediment deposited during previous highstands and periods of globally lower sea level and continued Holocene sea floor sediment production (James *et al.*, 1992). Shallow-marine carbonate-producing shelves, such as the Lacepede Shelf, are required for the production of extensive carbonate aeolianite such as that which is found along southern Australia (Brooke, 2001).

Deposition along the Coorong Coastal Plain (CCP) has occurred in a high-energy wind- and wave-dominated environment where the ongoing uplift in the southeast has resulted in the preservation and separation of multiple barrier/lagoon complexes but subsidence in the northwest, which has led to a stacking of deposits and loss of topographic expression (Huntley *et al.*, 1993; Belperio *et al.*, 1995; Murray-Wallace *et*

al., 1996; Bourman *et al.*, 2000; Murray-Wallace *et al.*, 2010). The seasonally wet climate in the region has allowed the development of the extensive Coorong Lagoon and ephemeral lakes in the interdune depressions of older aeolianites (Gostin *et al.*, 1988). On sections of the coast where there has not been progressive uplift, the return of sea-level results in reworking and re-deposition of pre-existing beach/dune systems (Milnes and Ludbrook, 1986; Harvey *et al.*, 2001). The early-mid Holocene sea level highstand, which reached as much as 2 km farther inland to the present eastern shoreline of the Coorong Lagoon (formed of the last interglacial beach-barrier) (Bourman *et al.*, 2000), would have reworked any encountered Last Interglacial or glacial deposits present. The preservation of the older aeolianites (and associated back-barrier deposits) and their resistance to reworking is dependent upon their degree of lithification and calcrete development.

Sea-level fall following interglacial highstands exposes coastal and submarine carbonate sediments to the same diagenetic processes as aeolian carbonate dunes. Any marine carbonate, once subaerially exposed, stabilised and dried out, undergoes identical diagenetic processes and development of an underlying alteration zone regardless of the environment of formation, assuming sufficient residence time for diagenetic processes to proceed (Esteban and Klappa, 1983). It can be expected then, that within the study area, indicators of subaerial diagenesis can be found as overprinting indicators of marine diagenesis. Diagenesis in the region has also been responsible for the development of *terra rossa* soils.

The lithology of the sedimentary successions within the study area reflects the environmental history of the region, which alternates between coastal and terrestrial environments with glacio-eustatic sea level change and its position adjacent to the uplifting Mount Lofty Flinders Ranges.

Chapter 4

Stratigraphy and Petrography of the Pleistocene Bridgewater Formation and Holocene successions, River Murray Mouth Region, southern Australia

4.1 Introduction

The study area is host to carbonate sediments deposited during Quaternary interglacial highstands (Bridgewater Formation), fluvial and estuarine deposits (Glanville and St Kilda Formations) and siliceous sands (Molineaux Sand) associated with periods of low sea level. This chapter provides descriptions of the field relationships of these principle stratigraphic units including the identification of their stratigraphical units, sedimentary structures and measurements of unit thickness, sediment colour and bedding characteristics. It was found that the bedding structure of many of the units had been obliterated either by bioturbation, diagenetic processes or erosion; strike and dip measurements of aeolian bedding were taken where adequately preserved using a Brunton Compass. The formations were recognised on their lithological characteristics and are described in relationship with stratigraphically adjacent units. Fossil assemblages were recorded. Sediments retrieved from the field were analysed for mineral composition, grain morphology and textural characteristics and dry sediments were assigned a Munsell (1994) soil colour. Methods used for sediment analysis include: binocular microscope analysis, particle size analysis, thin section analysis, X-ray diffraction and scanning electron microscopy. Field observations and sediment analyses are used in the reconstruction of depositional and climatic environments and subsequent diagenesis.

This chapter begins with a description of the methods of fossil and sediment analysis used in this thesis. Site descriptions begin with the modern Lacepede Shelf and early Holocene shoreline successions located on Hindmarsh Island before proceeding with the last interglacial shoreline *sensu lato* (MIS 5) and aeolianites of the penultimate

interglacial (MIS 7). Exposures of stacked units representing several interglacials are described before more inland sample sites. Siliceous sands and samples taken from within solution pipes are subsequently described. Digital elevation models (DEMs) have been created to aid in conceptualising the complexity of the landscape and to demonstrate the topographic relationships of the field sites (Figure 4.1; see *Appendix 1* for construction method). The chapter concludes with a comprehensive interpretation of the depositional environments within the River Murray Mouth region and diagenesis that the sedimentary successions have undergone. The conclusions are evaluated and are provided a timeframe by geochronological analysis (Chapter 6).

4.2 Methods of fossil and sediment analysis

Fossil deposits identified in the field were considered for their taphonomic history with emphasis placed on the assemblage mode, taxonomic composition, bioclastic fabric (i.e. packing), geometry and, if possible, internal structure. Sediment samples were analysed for their mineral and carbonate contents and textural relationships in the laboratory using the variety of methods described below.

4.2.1 Taphonomic analysis

Taphonomy is the study of how a fossil becomes preserved in the sedimentary record (biostratinomy) and the diagenesis that occurs after burial (Behrensmeier and Kidwell, 1985; Brett and Baird, 1986). Johnson (1960) described three examples for formation of fossil assemblages which were further elaborated by Kidwell *et al.* (1986):

1. *I, Census assemblage*: a life assemblage which is rapidly buried with little or no chance of transportation (largely autochthonous);
2. *II, Low-energy parautochthonous assemblage*: parautochthonous meaning a time-averaged assemblage in which autochthonous components have been moved, disarticulated, reorientated and/or concentrated from an original position by bioturbation, predation and/or scavengers but not transported from another community (includes hard parts that exhibit some degree of wear and movement through agents such as waves, currents and bioturbation; and

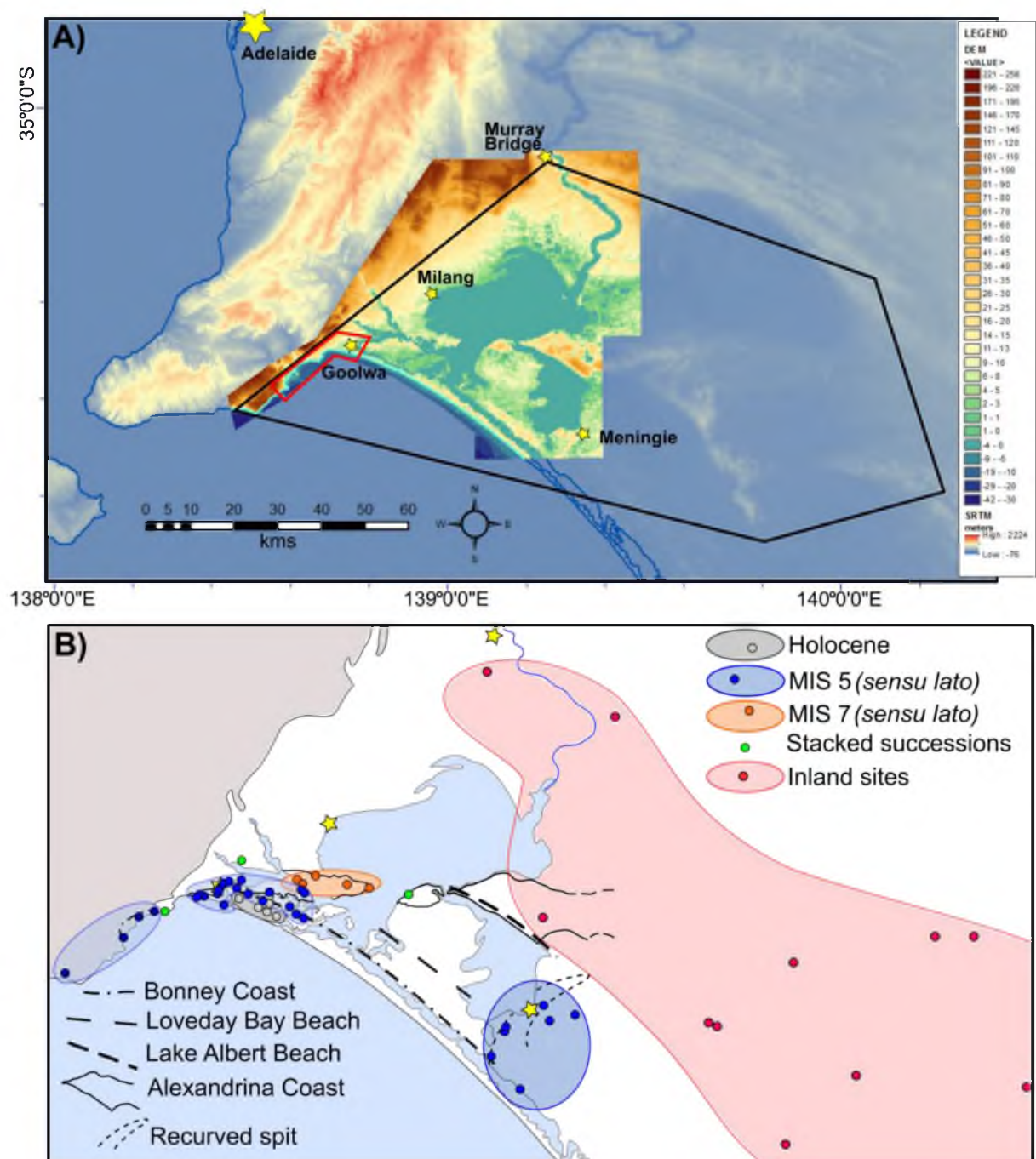


Figure 4.1: The study area at the northern margin of the Coorong Coastal Plain. A) Digital elevation model (DEM) overlaying SRTM (Geoscience Australia, 2011) built from 1:10,000 contour data and spot heights provided by the South Australia Department of Environment, Water and Natural Resources (DEWNR). DEM extent does not cover the entire study area (black box) due to lack of digitised topographic data. Higher spatial resolution (1:2500) was available for built-up areas (red box). Bathymetric data were unavailable for lakes. B) A line drawing of the study area with the location of field sites and their geographic relationships to each other and previously recognised features in the region as drawn by Murray-Wallace *et al.* (2010): the Bonney and Alexandrina coastlines and recurved spit of De Mooy (1959) and the Loveday Bay and Lake Albert beaches of Sprigg (1959). The Alexandrina coast crosses west over northern Lake Albert, Narrung Peninsula, Sturt Peninsula and northern Hindmarsh Island to Goolwa including strata of MIS 5e, 7 and 9.

3. *III, High-energy assemblage*: consists largely of parautochthonous remains but includes allochthonous hard parts.

The mode of formation influences fossil assemblage characteristics: faunal composition, morphological composition, fossil density, fossil size-frequency distribution, articulation, surface conditions of hard parts, chemical and mineralogical composition of hard parts, orientation of fossils, dispersion of fossils and the texture and structure of the sedimentary aggregate (Johnson, 1960). These characteristics serve as qualitative tools from which the rate of burial and general environmental energy at the time of burial can be discerned (Brett and Baird, 1986). Of the three examples described above, an assemblage formed by *I. census assemblage* was not identified in this thesis. Shell was retrieved from nine sites where the assemblage had been excavated or dredged from nearby locations; this represents nearly 30% of the total sites (38) from which shell was sampled. When possible, conclusions regarding the mode of assemblage for the fossils were inferred from the assemblage characteristics that remained following alteration and/or transport.

Four processes, generally occurring in a sequential manner, affect mollusc shell in a marine environment prior to burial: reorientation, disarticulation, fragmentation and corrasion (a combination of mechanical abrasion and biogeochemical corrosion) (Brett and Baird, 1986). These processes work to breakdown skeletal hard parts. Skeletal concentrations in the sediment record are formed by biologic, physical sedimentologic, diagenetic processes or a mixture of two or more processes (Kidwell *et al.*, 1986). The diagenetic processes, which shell is subject to following burial, are dissolution, sediment infilling and mineralisation (Brett and Baird, 1986).

A taphonomic grading scheme was developed for mollusc shell based on general appearance. The grading scheme (Table 4.1) is based on whether or not the shell is articulated (if bivalve) and the condition of individual valves (i.e. whole or fragmented, level of corrasion, and level of preservation of distinguishing features). The highest possible score is a '7', where the shell is articulated (if bivalve) and both valves exhibit no corrasion and can be considered pristine. The only shells given this grade were modern or Holocene. The lowest possible score is a '1', where the shell is a fragment with a high

Table 4.1: Taphonomic grading scheme developed for fossil molluscs reported in this thesis.

Grade	Valve(s) Description
1	Fragment with a high level of corrosion*. Little to no distinguishing features.
2	Fragment with minimal-moderate corrosion maintaining at least some distinguishing features.
3	Whole valve with minimal-moderate corrosion maintaining at least some distinguishing features.
4	Articulated fragments with a high level of corrosion. Little to no distinguishing features.
5	Articulated; whole valve with minimal-moderate corrosion maintaining at least some distinguishing features with partner fragment having little to no distinguishing features.
6	Articulated; both valves whole with minimal-moderate corrosion maintaining at least some distinguishing features.
7	Articulated; both valves whole and in pristine condition with no apparent corrosion.
Grade	Gastropod Description
1	At least half of the shell is missing. May or may not be identifiable.
2	Missing only small portion of shell and identifiable.
3	Whole, pristine in appearance with no apparent corrosion.
*Corrosion: term used to encompass the undifferentiated combination of mechanical abrasion, bioerosion, and biogeochemical solution processes on fossils (Brett & Baird, 1986)	

Table 4.2: Shell species collected per field site. Species listed in blue prefer a low energy environment. 'sp.' indicates the shell could not be differentiated between two possible species; for example, *Irus crenatus* or *Irus griseus*. Species environment information was compiled from Ludbrook (1984) and Grove (2014).

[illegible]

FIELD CODE	MM	GB	GB	GC	CC-b	HSF	AL-BH1	AL-BH2	ALW	ROB	MI	MRQ	MRQ	BH-D	BC-GB	TQ	CC-sh	CC-D	BR	GW	CS	OW	WC	HA	TC	SH	CHR	CSM-D	CSP	MR	CF	WG	VHR
<i>Soletellina biradiata</i> sand and mud in sheltered bays and estuaries, in the intertidal	X							Sp.						X						X								X					
<i>Katelysia rhytiphora</i> sandy beaches in the lower littoral zone or intertidally in mud on																											X						
<i>Katelysia peronii</i> intertidally & subtidally in sand and mud on sheltered shores																																X	
<i>Irus crenatus</i> (variant <i>crebrelamellatus</i>) mud in mangrove swamps and tidal inlets, subtidally in hard sediments such as compacted mud								Sp.									Sp.									?	X					X	
<i>Tellina (Macomona) deltoidalis</i> mud and muddy sand in the middle to lower littoral zone in	X							Sp.			X									X	X	X					X	X	X		X	X	
<i>Irus (Notopaphia) griseus</i> subtidally in sand and mud in moderately sheltered								Sp.									Sp.											X				?	
<i>Telinella albinella</i> lives subtidally in sand, particularly near the mouth of			X					Sp.					X																				
<i>Sunetta aliciae</i> lives subtidally and offshore in sand																																X	
<i>Paphies elongata</i> intertidally in sand in mod. exposed env. Active burrower	X							X			X	X	X	X	X				X						X	X			X			X	
<i>Mactra rufescens</i> sand and mud w preference for ocean beaches	X	X	X	X					X	X	X	X	X	X	X												X		X				

[illegible]

[illegible]

level of corrosion and with no remaining distinguishing features. The grading for gastropods followed the same general structure, with scores ranging from '3' to '1'. This grading scheme was used in the application of amino acid racemisation analysis (AAR; Chapter 5) to ensure that the highest quality shell was subjected to analysis.

A list of mollusc species identified per site in this thesis and their preferred environments is provided in Table 4.2. Mollusc species were identified by reference to *Quaternary Molluscs of South Australia* (Ludbrook, 1984) which provides description of living and fossil molluscs preserved within Quaternary marginal marine sediments in South Australia. In some cases shell was identified to the genus level with two possible species. This is indicated in the table by 'sp.'. The presence of the bivalve *Anadara trapezia* is indicative of the Glanville Formation, although also occurs in MIS 7 and reworked sediments (see sections 2.5.3.2 and 3.7.3). From the field samples containing mollusc shell, twenty different bivalve species and ten gastropod species were identified. Species most commonly encountered were chosen for use in amino acid racemisation analysis, a geochronological method (see Chapter 4). These species are the bivalves *Spisula* (*Notospisula*) *trigonella*, *Paphies* (*Amesmodesma*) *elongata*, *Mactra rufescens* and *Donax deltoides* and gastropods *Hydrococcus brazieri*, *Coxiella striata* and the opercula of *Turbo* sp. (Figure 4.2). The presence of these species was recorded at multiple sites and they are indicative of contrasting physical environments.

Spisula trigonella valves were the most prevalent among Pleistocene and Holocene sedimentary successions. This species is typical of mud and sandy mud environments of estuaries and river mouths (Ludbrook, 1984) in all Australian states (Grove, 2014). *S. trigonella* is a surface dwelling suspension feeder, prefers salinity greater than 10‰ (Jones *et al.*, 1988), and population densities can reach 6000 m⁻² (Green, 1968). The sediment specificity of this species is low although the effect of water depth (found in depths of 3 m to >10 m) and sediment grade on larval distribution and/or food supply probably influences adult abundance (Jones *et al.*, 1988). *S. trigonella* is a hardy species, not very susceptible to changes in salinity, river discharge or water temperature; however, salinity and sediment changes associated with severe flooding can decrease abundance (Jones *et al.*, 1988).



Figure 4.2: Species chosen for AAR analysis due to their common occurrence in fossil assemblages and modern beach deposits. *Cokiella striata* and *Hydrococcus brazieri* photos are taken alongside the same ruler as other shells; the scale bars are millimetres. *Turbo* opercula were always found separate from the rest of the shell. The *Turbo* gastropod shell pictured is *Turbo (Subninella) undulatus*.

Paphies elongata was, of the shell species chosen for AAR analysis, the species most commonly found in association with *S. trigonella*. *P. elongata*, an active burrower in sandy intertidal zones (Ludbrook, 1984), was present at nine of the twenty *S. trigonella* sites. However, this does not indicate a biocenose relationship as the concurrence is within deposits of high-energy environments (Mode III), where reworking and mixing would have occurred. *P. elongata* has multiple synonyms but is recognised as *Paphies elongata* by the World Register of Marine Species (Huber, 2014). This species has been previously referred to as *Amesmodemsa angusta* in South Australia (Ludbrook, 1984).

Mactra rufescens and *Donax deltoides* are bivalve species typical of high energy environments. *M. rufescens* lives in sand and mud and has a preference for ocean

beaches (Ludbrook, 1984). *D. deltoides*, also commonly known as the Goolwa cockle, is an active burrower living intertidally in sandy exposed environments (Grove, 2014). The shells of *D. deltoides* are a common find on the beaches of Encounter Bay (Ludbrook, 1984). Where *D. deltoides* was positively identified, it was in association with *M. rufescens*.

Hydrococcus brazieri and *Coxiella striata* are two small gastropods found in abundance in the Coorong, generally together (Ludbrook, 1984). *H. brazieri* prefers marginal salt lakes, back dune swamps, estuaries and tidal flats and tolerates a wide range of temperature and salinity. *C. striata* is found in both muddy and sandy sediments.

Turbo operculum are most likely to be of the species *Turbo (Subnirina)* *undulatus*, which is found intertidally and subtidally (to 6 m depth) amongst rocks, boulders and seaweed on reefs and platforms on a medium to high energy coast (Ludbrook, 1984, Grove, 2014). The species was positively identified from shell at the McLeay Road shell bed and at Goolwa Beach.

4.2.2 Particle size analysis

Particle size distribution for chosen samples was determined using a Malvern Mastersizer 2000. The Malvern uses laser diffraction to calculate the particle size distribution of a sediment sample. Samples were analysed for their clay-, silt- and sand-sized fractions. The difference in sand particle size between deposits is a factor of sorting, generally through transport (Folk, 1980; Pettijohn *et al.*, 1987). The grain size of aeolian transported desert sand generally ranges from silt (0.060 mm) to coarse sand (2 mm) with clay and silt generally accounting for less than 5% of wind-deposited sands (Glennie, 1970). Carbonate aeolian deposits have variable grain sizes with good to poor sorting depending on the nature of the carbonate particles, which can also lead to less well developed sedimentary structures (Frébourg *et al.*, 2008), however fine and medium grain sizes are most commonly represented (McKee and Ward, 1983). Generally coastal barrier and beach deposits display a distinct coarsening-upward sequence, reflecting the offshore silts and muds at the base through fine sand to coarser, well-

sorted sand at the top (Pettihohn *et al.*, 1987). Complete particle size analysis results are provided in *Appendix 2*.

4.2.3 Binocular microscope analysis

Binocular microscope analysis was used for the description of loosely consolidated and unconsolidated sediment. The sediment was analysed for degree of sorting and particle size using the Malvern Mastersizer (section 4.2.2) except for the Lacepede Shelf sediments where there was insufficient sediment. Quartz grains were described for their degree of sorting, roundness and sphericity and for surface features including staining of grains. These features indicate the modification of grains as an effect of the transport process (Pettijohn *et al.*, 1987) and are dependent upon the structure of the grain (internal properties), process (depositional environment) and stage (time available for modification) (Folk, 1980). The roundness of a quartz grain in particular reflects abrasion history (either aeolian or fluvial transport); although well-rounded grains are usually grains of a large diameter (Glennie, 1970; Pettijohn *et al.*, 1987). Typically, the angularity of aeolian sand grains increases with a decrease in particle size making roundness a function of size (Glennie, 1970). Well-rounded grains are the result of either many cycles of transport or intensive abrasion (Folk, 1980; Pettijohn *et al.*, 1987). Frosting of quartz grains is considered a typical characteristic of many aeolian dunes and polished surfaces as typical of an aqueous environment (Kuenen and Perdok, 1962; Glennie, 1970; Folk, 1980). However, frosting can also be caused by chemical etching or the incipient development of quartz overgrowths (Kuenen and Perdok, 1962; Folk, 1980) and is limited to grains above a certain size; frosting is absent below 0.15 mm (Kuenen and Perdok, 1962). A red iron oxide stain or coating on quartz grains is considered evidence of deposition in a continental environment or subsequent weathering in a terrestrial environment (Glennie, 1970).

The carbonate fraction was analysed for fauna and degree of preservation. Fauna was split into three categories: mollusc, foraminifer and 'other fauna'. Other fauna most commonly included bryozoan fragments, echinoderm fragments, sponge spicules, algae and ostracods. Where possible, species present were recorded. Fauna were analysed for indications of reworking: comminuted fragments of mollusc shell and other fauna, worn or abraded foraminifer tests, and staining. Shell fragments abrade more rapidly than

quartz within aeolian transport showing an increase in the quartz to limestone ratio with transport distance from the quartz/limestone source (Glennie, 1970). The frequency of quartz and carbonate grain features was recorded using the adjectival terms suggested by Flugel (2010): very rare (<2% grains), rare (2-5%), sparse (5-10%), common (10-30%), very common (30-50%), abundant (>50%).

Carbonate content of the 250-500 μm sand-size fraction (medium grain size) by mass was determined for sediments chosen for whole-rock AAR analysis. The reason and methodology for this are reviewed in Chapter 5. Although this fraction is not necessarily representative of an entire sediment sample, it can be indicative of the carbonate content, especially in sediments where the 250-500 μm particle-size fraction is dominant (>50%). The remaining fine, coarse and very coarse particle size fractions can be visually appraised by binocular microscope.

Carbonates are commonly classified under one of two different limestone classification schemes (Adams *et al.*, 1984; Adams and MacKenzie, 1998; Scoffin, 1987; Tucker, 1991; Coe, 2010; Flugel, 2010). The schemes, proposed by Folk (1959, 1962) and Dunham (1962), are based on textural and compositional criteria. The classification of Folk (1959, 1962) is built upon the premise that the depositional method of carbonate rocks is essentially similar to sandstones and shales and their textures are a result of the energy regime at the site of deposition. The Dunham (1962) classification focuses on textural properties and what they may indicate about the depositional environment. The classification scheme of Dunham (1962) was preferred for use in this research because the Folk classification (1959, 1962) assumes a subaqueous depositional environment and tries to evaluate hydrodynamic conditions which are not entirely suitable for aeolianite analysis. The Folk classification scheme also relies heavily on thin sections or peels. Peels were not used in this research and thin sections analysis was limited to moderately to strongly consolidated sediments (section 4.2.4) and not used for every sediment sample. The Dunham classification scheme was expanded by Embry and Klovan (1971) (Figure 4.3) and was used in this research.

An additional scheme used in this research was the Mount (1985) classification scheme for mixed siliciclastic and carbonate sediments (Figure 4.3). This classification is

EXPANDED DUNHAM (1962) LIMESTONE CLASSIFICATION SCHEME (EMBRY AND KLOVAN, 1971)

ALLOCHTHONOUS LIMESTONE ORIGINAL COMPONENTS NOT ORGANICALLY BOUND DURING DEPOSITION						AUTOCHTHONOUS LIMESTONE COMPONENTS ORGANICALLY BOUND DURING DEPOSITION		
Less than 10% >2 mm components				Greater than 10% >2 mm components		Boundstone		
Contains lime mud (<0.03 mm)			No lime mud	Matrix supported	>2 mm component supported	by organisms which act as bafflers	by organisms which encrust and bind	by organisms which build a rigid framework
Mud supported		Grain supported						
Less than 10% grains (>0.03 mm and <2 mm)	Greater than 10% grains							
MUDSTONE	WHACKSTONE	PACKSTONE	GRAINSTONE	FLOATSTONE	RUDSTONE	BAFFLESTONE	BINDSTONE	FRAMESTONE

MOUNT (1985) SCHEME FOR MIXED SILICICLASTIC AND CARBONATE SEDIMENTS

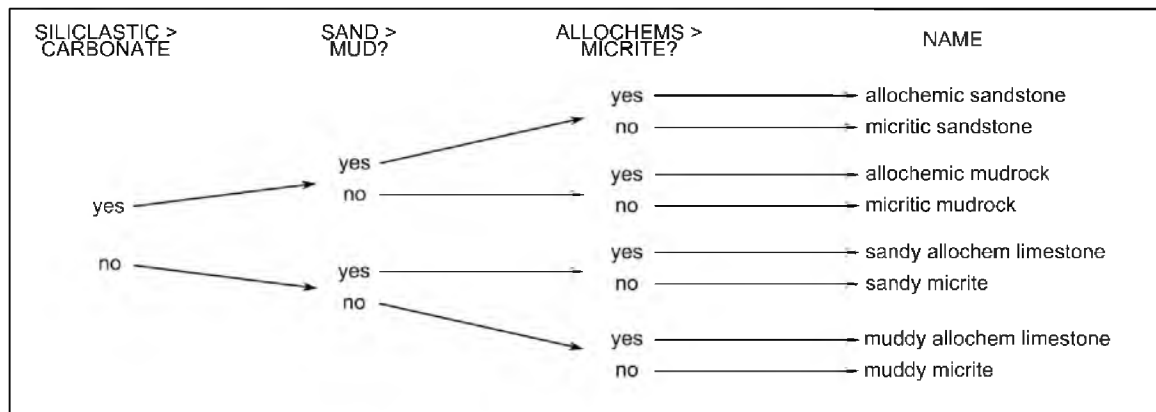


Figure 4.3: Classification schemes used in this research. The Dunham (1962) classification scheme was used in thin section analysis and where the carbonate component constituted >50% of the total sediment. The expansion of Embry and Klován (1971) provided the size aspect and distinguished grains smaller or larger than 2 mm. The Mount (1985) classification scheme was applied to all loose to moderately consolidated sediments, whereas the Dunham scheme was only applied to sediments with >50% carbonate.

used to describe and categorise sediments consisting of four primary components: siliciclastic sand, siliciclastic mud, carbonate sand and carbonate mud. This use of this classification scheme was felt to be necessary because the Dunham (and Folk) classification schemes are intended for pure carbonate sediments whereas, all of the sediments within this research were found to be mixed, consisting predominantly of less than 50% carbonate and at times, to contain less than 10% carbonate.

4.2.4 Thin section analysis

Thin sections were made from samples of moderately to strongly consolidated sediments representing aeolian and fluvial environments of deposition. Thin sections were cut perpendicular to bedding to a thickness of ~30 µm. Binocular analysis under

plain- and cross-polarised light determined the composition and texture of grains as well as the type of cement binding grains together and the contacts between grains. Cements in aeolianites are generally composed of low-Mg calcite but can differ in texture, fabric and mode of cementation (Pye, 1983).

4.2.5 X-ray diffraction

Powder X-ray diffraction (XRD) analysis was used with the CSIRO software package Siroquant to determine the mineralogy of selected samples, including the content of aragonite, high-Mg calcite and low-Mg calcite, which can be indicative of the degree of diagenesis that has occurred in carbonate sediments. Other mineral phases recorded were quartz, feldspars and clays. Feldspars give an indication of the igneous derived component. Clays can be used as environmental and diagenetic indicators. Complete XRD analysis results are provided in *Appendix 3*.

4.2.6 Scanning Electron Microscope

Carbonate grains from selected sediment samples were hand-picked for SEM analysis to allow identification and illustration of the variety of carbonate bioclasts within the sediments and is provided here for direct comparison across all depositional environments and ages (Figure 4.4). Species were identified where possible and the habitat of most foraminifer is indicated based on the distribution of foraminifera from New South Wales, southeast Australia (Yassini and Jones, 1995). The region is temperate (like the study area, although with wetter summers) and there is likely to be minimal variation in a species' preferred environment.

4.3 Field site descriptions and sedimentary petrography

Field site descriptions and associated sedimentary petrography will be presented in a time-transgressive manner, beginning with the most recent and moving back farther in time and generally landward. Field sites are presented and grouped based on temporal and/or physical depositional relationships.

4.3.1 Lacepede Shelf

Since the initiation of the 100 ka eccentricity cycle of sea-level and climate change in the middle Pleistocene, the environment of the Lacepede Shelf has

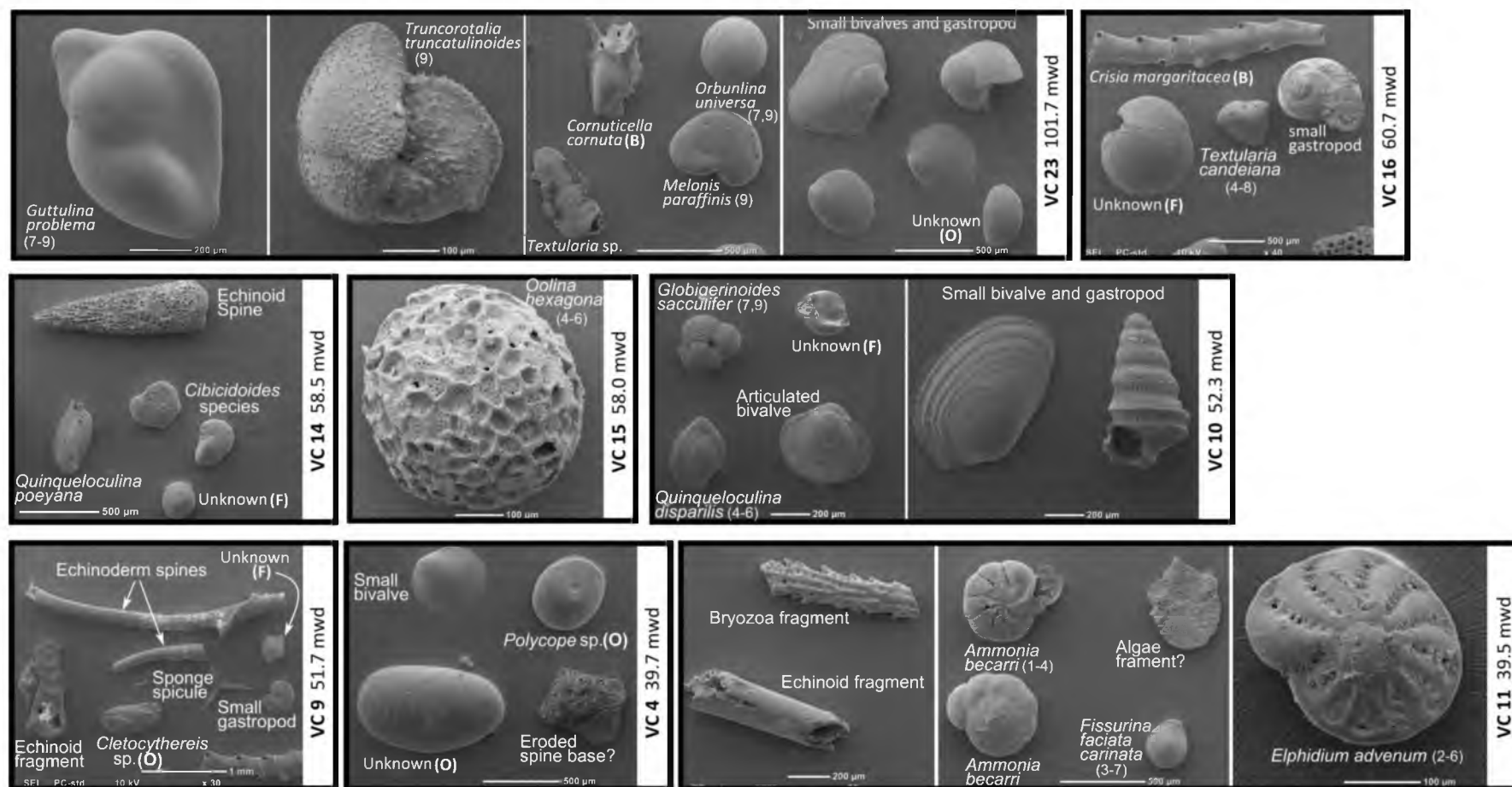


Figure 4.4: SEM photographs of carbonate grains plucked from selected sediment samples retrieved off the Lapcepede Shelf and terrestrial deposits described in this chapter. The SEM photos for each site are contained within the black outline with the field code for the site at the right hand margin. Field codes beginning with 'VC' are from the Lapcepede Shelf and 'mwd' indicates the water depth in metres from which the sediment was retrieved. All other sites are terrestrial with depth of burial provided. Numerals in parentheses following foraminifer indicates distribution: 1) saline lake, 2) lagoon, 3) lagoon inlet channel and intertidal zone, 4) open estuaries, 5) sheltered oceanic embayment, 6) inner shelf, 7) middle shelf, 8) Bass Strait, 9) continental slope (Yassini and Jones, 1995). (F) = foraminifer, (B) = bryozoa, (O) = ostracod.

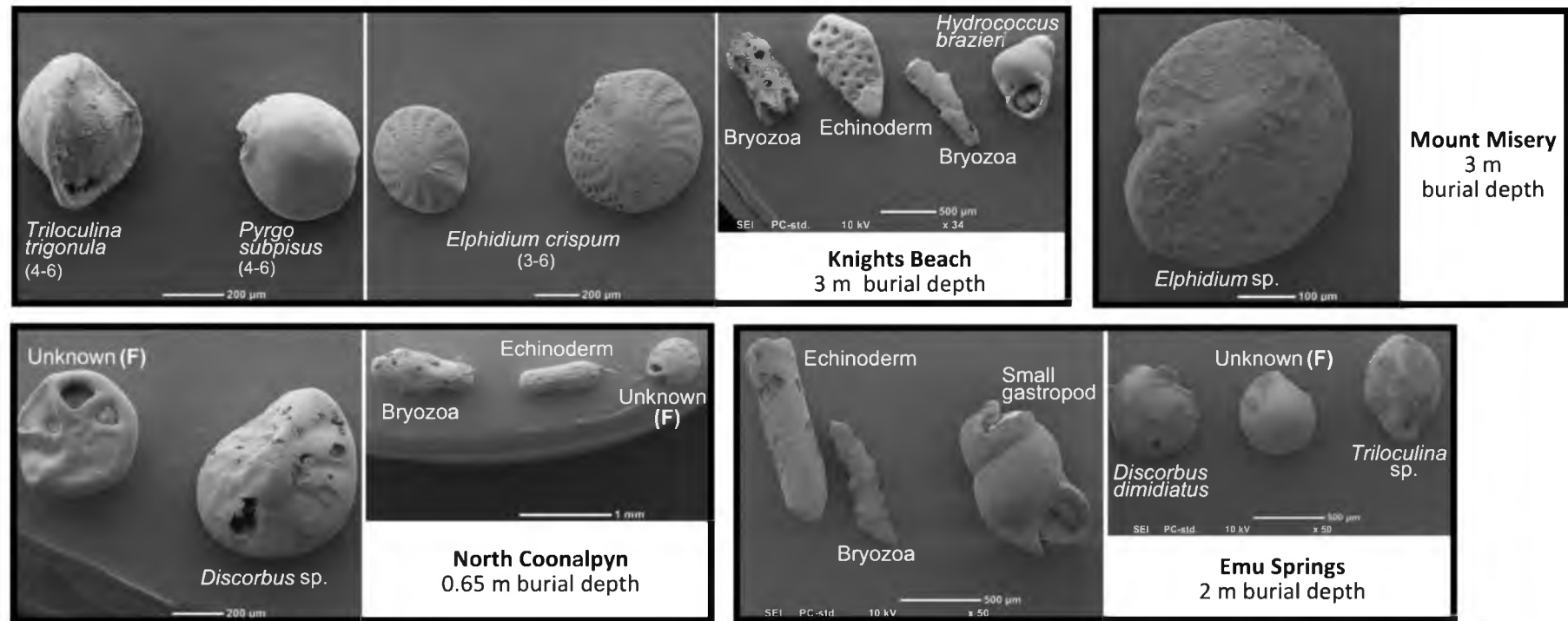


Figure 4.4 continued: SEM photographs of carbonate grains plucked from selected sediment samples retrieved off the Lacepede Shelf and terrestrial deposits described in this chapter. The SEM photos for each site are contained within the black outline with the field code for the site at the right hand margin. Field codes beginning with 'VC' are from the Lacepede Shelf and 'mwd' indicates the water depth in metres from which the sediment was retrieved. All other sites are terrestrial with depth of burial (depth of burial) provided. Numerals in parentheses following foraminifer indicates distribution: 1) saline lake, 2) lagoon, 3) lagoon inlet channel and intertidal zone, 4) open estuaries, 5) sheltered oceanic embayment, 6) inner shelf, 7) middle shelf, 8) Bass Strait, 9) continental slope (Yassini and Jones, 1995). (F) = foraminifer, (B) = bryozoa, (O) = ostracod.

transitioned from carbonate factory, coastal with wetlands (James *et al.*, 1992; Siddall *et al.*, 2006; Hill *et al.*, 2009), river plain (Bowler, 1976; Sprigg, 1979; Harvey *et al.*, 2001) and back again with the fluctuation of eustatic sea-level. The terrestrial and coastal sediments deposited on the Lacepede Shelf during periods of lowered sea-level associated with glacial maxima and interstadials (respectively) are reworked by the rising sea in the prelude to the eustatic sea-level high of an interglacial period. The macrofacies trends of sediments across the Lacepede Shelf (Rivers *et al.*, 2007; James and Bone, 2011) indicate that remnants of these former environments remain within the shallow substrate of the shelf. The analysis of quartz and carbonate grains retrieved from the Lacepede Shelf, through comparison with their coastal and terrestrial counterparts within the study area, has the potential to assist in determining if recycled quartz and carbonate are recognisable across environments.

4.3.1.1 Lacepede Shelf substrate sediments

Modern substrate sediment samples, taken from the tops of vibracores retrieved from a range of water depths across the Lacepede Shelf (see Figure 4.5 for locations), were provided by Professor Patrick De Deckker of the Australian National University and were analysed under a binocular microscope. All samples come from less than 70 m water depth (mwd) on the mid- to inner-shelf except for Sample VC23, which was taken from near the edge of the outer continental shelf at 101.7 mwd. This sample reflects the carbonate factory of the outer shelf as reviewed in section 3.5.1 and differs markedly from the other Lacepede Shelf sediments in not only its location but also its sediment composition.

The surface sediment from VC23 is pale yellow (2.5Y 8/2) reflecting the dominance of carbonate (~100%), which consists of foraminifers, bryozoans and juvenile mollusc valves and gastropods (Figure 4.6). Unlike the remainder of Lacepede Shelf sediments, the mollusc fraction does not dominate and foraminifers and other fauna are strongly represented. Quartz in VC23 is very rare (<2%); only five very fine angular quartz grains exhibiting vitreous lustre were identified under the binocular microscope.

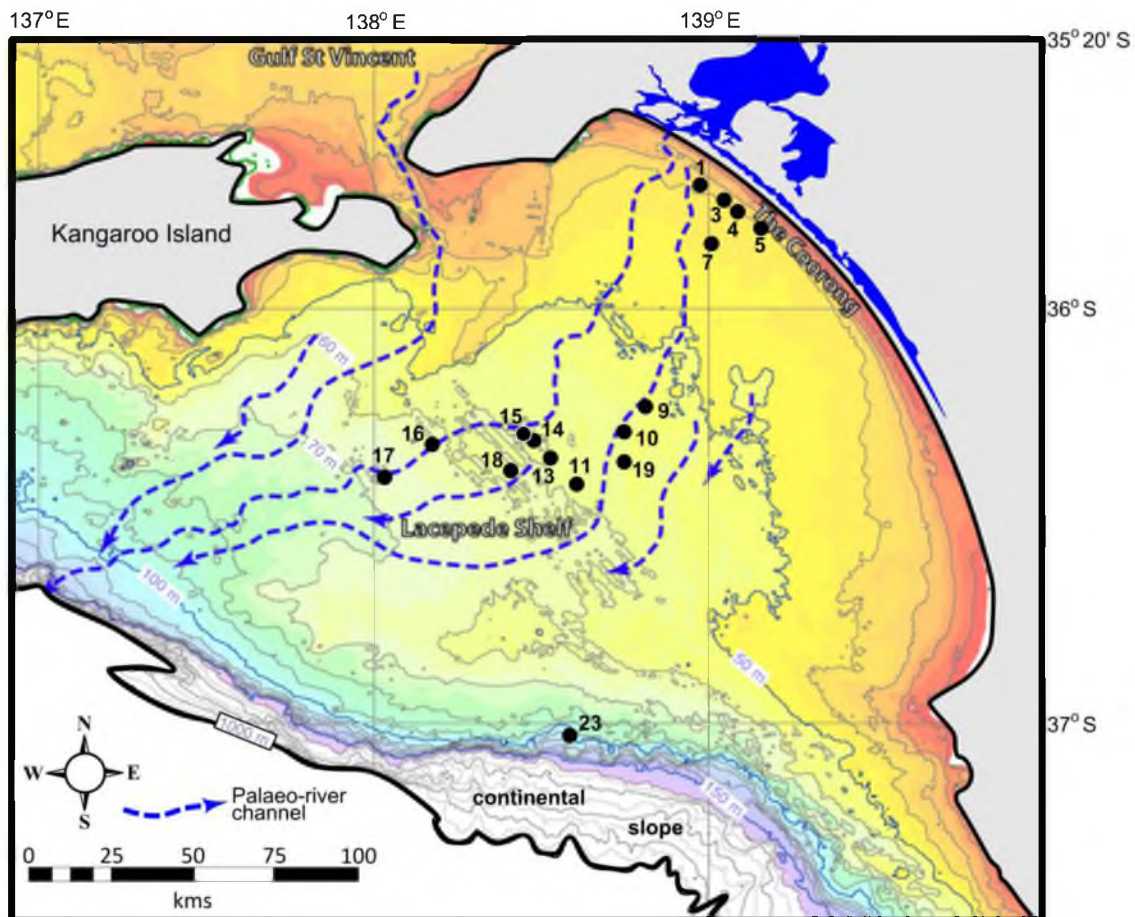


Figure 4.5: Location of vibracore samples on the Lacepede Shelf. All samples (except VC23) were retrieved from the quartz-rich (>50%) sediment megafacies of Lacepede Shelf (James and Bone, 2011; see section 3.5.1). VC23 was retrieved from a zone of carbonate development. Former strandlines are located at water depths between 40 and 65 mwd (James *et al.*, 1992; James and Bone, 2011).

Munsell colour for the remainder of the samples is of hue 10YR with very pale brown the dominant colour, especially below water depths of 50 m, colour otherwise being a variant of yellowish brown except for Sample VC1 which is greyish brown (Table 4.3). This colour reflects the matrix of Sample VC1 which is muddy clay. Sample VC4, although predominantly clean, contains a minor fraction of grains within a thin clay matrix as well as lightly cemented grains forming pebble-size aggregates. The remainder of the samples were clean with no matrix.

The quartz grains are most abundantly present as irregularly-shaped angular to subangular grains (Figure 4.6, Table 4.3). Subrounded to rounded grains were present in greater quantity (10-30%) amongst the larger (medium to very coarse) grain sizes. The quartz sand fraction was used to determine particle size and sorting of the sediments

with resulting particle size consistently fine-medium or very fine-medium with rare exceptions. Exceptions to the particle size trend are samples VC3 and VC7 from 40 and 42 mwd respectively. VC3 consists of poorly-sorted fine to very coarse grains with a clear lustre, whereas VC7 is composed of well-sorted medium grains with variable surface features. Many of the quartz grains of VC7 have black speckles, which may be traces of pedogenic development. The samples are moderately to well-sorted (Table 4.3). Iron-stained grains are present in most samples in either common (10-30%) or very common (30-50%) amounts. Quartz grains with inclusions of ilmenite were common and were identified in most samples. Grains of what appeared to be heavy minerals were plucked for XRD analysis, but the results were inconclusive because the sample size was too small.

Mollusc shell is the most abundant component of the carbonate fraction regardless of the total amount of carbonate within the sample, except for VC23. The shell is mostly present as comminuted fragments although most samples included small disarticulated valves and/or gastropods, VC10 contains small articulated molluscs (Table 4.3). Foraminifer and other fauna are less common. The most commonly encountered foraminifera species are: *Ammonia beccarii* (benthic), *Elphidium* sp. (benthic), *Triloculina* sp. (benthic) and *Globigerinoides* sp. (planktonic) (Table 4.3). *A. beccarii* is common in coastal lagoons, inlet channels of coastal lagoons and open estuaries (Yassini and Jones, 1995) and its presence on the Lapede Shelf is influenced by the presence of the River Murray (Li *et al.*, 1998). The distributions of *Elphidium* sp. and *Triloculina* sp. are more extensive including sheltered oceanic embayments, the intertidal zone and (for *Triloculina* sp.) the inner shelf. Only *Globigerinoides* sp. is found in the middle to outer shelf with some species extending to the continental slope (Yassini and Jones, 1995). Other fauna commonly included bryozoan fragments, with other constituents made up of echinoid fragments, sponge spicules, coralline algae, ostracods and crustacean exoskeletons. This fraction may be larger than interpreted because small fragments of comminuted fauna could be indistinguishable from shell fragments.

Iron-stained carbonate of every fauna type is present in nearly every sample. Mollusc fragments appear to be commonly stained by iron oxides, varying in colour from

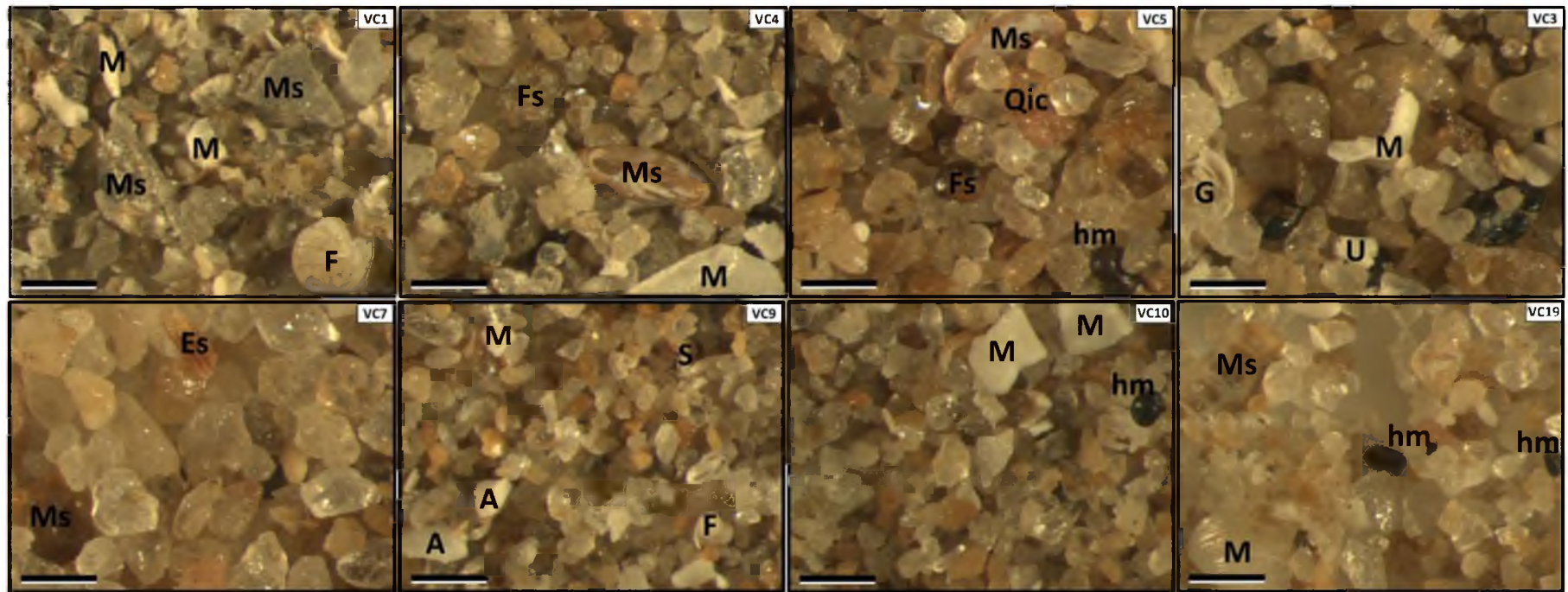


Figure 4.6: Modern shallow substrate sediment samples retrieved from the Lapcepede Shelf in order of increasing water depth (see Figure 4.4 for locations and water depths) and corresponding to descriptions in Table 4.3 and in text. SEM photographs (Figure 4.3) were taken of fauna from samples VC4, VC9, VC10, VC11, VC14, VC15, VC16 and VC23. Scale bar is 500 μ m in length. M = mollusc fragment, G = gastropod fragment, F = foraminifer, E = echinoderm fragment, B = bryozoan, S = sponge spicule, A = algae fragment, U = unknown, hm = heavy mineral, Qic = quartz with inclusion, 's' in association with a carbonate grain label indicates staining.

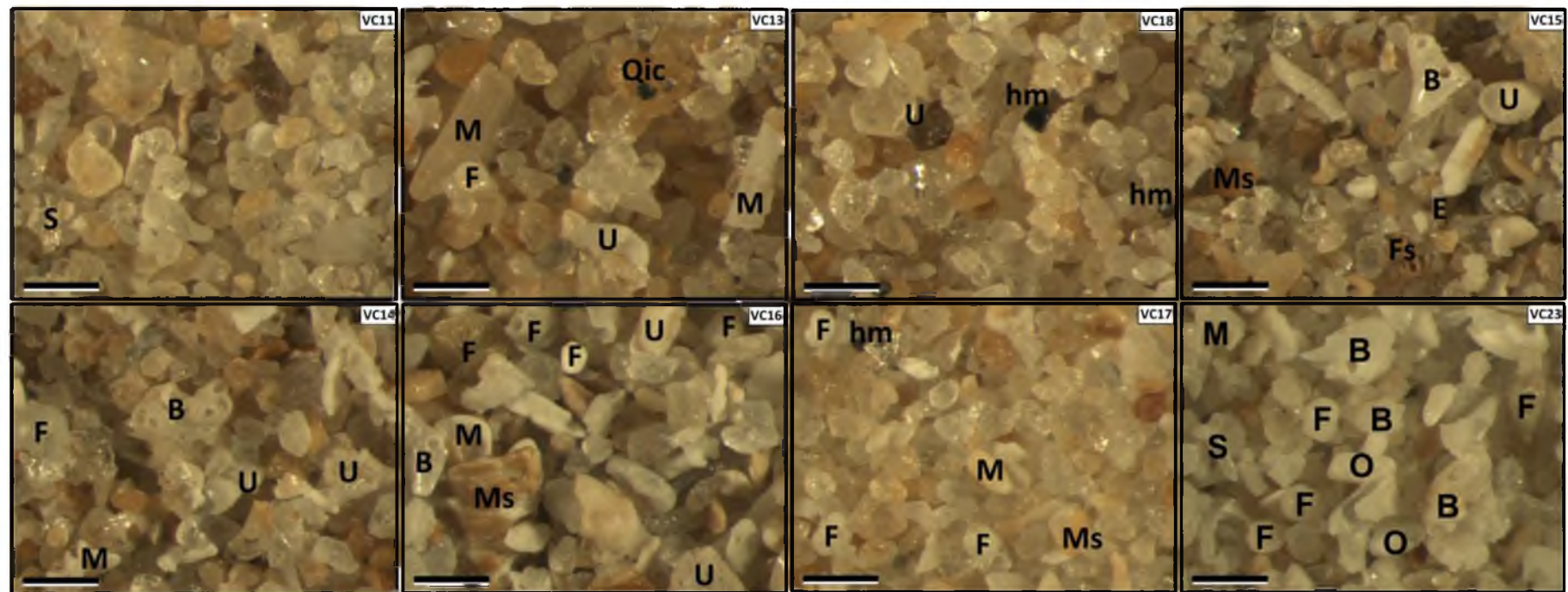


Figure 4.6 continued: Modern shallow substrate sediment samples retrieved from the Lacepede Shelf in order of increasing water depth (see Figure 4.4 for locations and water depths) and corresponding to descriptions in Table 4.3 and in text. SEM photographs (Figure 4.3) were taken of fauna from samples VC4, VC9, VC10, VC11, VC14, VC15, VC16 and VC23. Scale bar is 500 μm in length. M = mollusc fragment, G = gastropod fragment, F = foraminifer, E = echinoderm fragment, B = bryozoan, S = sponge spicule, A = algae fragment, U = unknown, hm = heavy mineral, Qic = quartz with inclusion, 's' in association with a carbonate grain label indicates staining.

Table 4.3: Description of modern substrate sediments retrieved from the Lacepede Shelf. Molluscs are the dominant fraction of carbonate for every sample except VC23 (**). Maximum size of mollusc shell indicated under 'Molluscs' heading. The phrase 'juveniles present' indicates the presence of whole disarticulated valves and/or gastropods. Sediment descriptions correspond to images in Figure 4.6. Foraminifers species *Ammonia beccarii* (benthic), *Elphidium* sp. (benthic), *Triloculina* sp. (benthic) and *Globigerinoides* sp. (planktonic) are indicated by 'A', 'E', 'T' and 'G' respectively.

Lacepede Shelf Samples			Quartz				Carbonate			
ID	Water Depth (m)	Munsell	Particle size	Sorting	Roundness	Surface texture	Carbonate	Molluscs	Foraminifer	Other fauna
VC1	39.5	10YR 5/2 grayish brown	fine - medium	poor	angular	frosted	abundant	≤ 2 mm; juveniles present	common (A, E)	very common
VC4	39.7	10YR 5/4 yellowish brown	fine - medium	moderate	abundantly angular, rarely subrounded	fine grains are variably clear and frosted, very commonly iron-stained; medium grains predominantly have a clear lustre, commonly iron-stained	common	≤ 2 mm; juveniles present	rare (A, E)	sparse
VC5	39.8	10YR 6/6 brownish yellow	medium - fine	very well	abundantly subangular to angular, commonly subrounded	variably have a vitreous lustre or frosting and iron-stained	sparse	≤ 1 mm	very rare (A)	very rare
VC3	40.0	10YR 6/4 light yellowish brown	fine - very coarse	poor	abundantly angular	abundant clear lustre, very commonly iron-stained	very common / abundant	≤ 2 mm; juveniles present	sparse (A, E)	very rare / rare
VC7	42.0	10YR 7/4 very pale brown	medium	well	abundantly subangular to angular, commonly subrounded	clear lustre and iron-staining is very common, remaining grains are commonly translucent	sparse / common	≤ 2 mm	very rare (A, E)	very rare
VC9	51.7	10YR 6/4 light yellowish brown	very fine - medium	well	abundantly subangular to angular	variably having a clear lustre, translucent lustre, or frosting; iron-staining common	very common	≤ 1 mm; juveniles present	very rare (E, T)	sparse
VC10	52.3	10YR 6/4 light yellowish brown	very fine - medium	well	abundantly subangular to angular	abundantly having a clear or translucent lustre and iron-staining; frosting is rare	very common	≤ 3 mm; juveniles present	rare / sparse (A, E, T)	sparse / common
VC19	53.5	10YR 6/3 pale brown	very fine - medium	moderate	abundantly angular with larger grains more commonly rounded	abundant clear or translucent lustre, commonly iron-stained	common	≤ 1 mm; juveniles present	very rare (A, E, T, G)	very rare

Table 4.3 continued: Description of modern substrate sediments retrieved from the Lacepede Shelf. Molluscs are the dominant fraction of carbonate for every sample except VC23 (**). Maximum size of mollusc shell indicated under 'Molluscs' heading. The phrase 'juveniles present' indicates the presence of whole disarticulated valves and/or gastropods. Sediment descriptions correspond to images in Figure 4.6. Foraminifers species *Ammonia beccarii* (benthic), *Elphidium* sp. (benthic), *Triloculina* sp. (benthic) and *Globigerinoides* sp. (planktonic) are indicated by 'A', 'E', 'T' and 'G' respectively.

Lacepede Shelf Samples			Quartz				Carbonate			
ID	Water Depth (m)	Munsell	Particle size	Sorting	Roundness	Surface texture	Carbonate	Molluscs	Foraminifer	Other fauna
VC11	55.3	10YR 8/3 very pale brown	very fine - medium	moderate	angular to subrounded with rounding more common among larger grains	very fine grains very commonly have clear lustre with translucent lustre and iron-staining common; larger grains are abundantly frosted or translucent lustre, rarely iron-stained	sparse	≤ 3 mm	very rare (T)	very rare
VC13	57.5	10YR 7/4 very pale brown	fine - medium	well	angular to subrounded with rounding more common among larger grains	clear or translucent lustre, very commonly iron stained with rare smoky quartz	very common	≤ 1 mm; one whole gastropod 3 mm	very rare (E)	very rare
VC18	57.9	10YR 8/3 very pale brown	fine - medium	moderate	abundantly angular with larger grains more commonly rounded	abundant clear or translucent lustre, commonly iron-stained	rare	≤ 1 mm	very rare	very rare
VC15	58.0	10YR 7/4 very pale brown	very fine - medium	moderate	abundantly subangular to angular, commonly subrounded	abundant clear or translucent lustre, commonly iron-stained	very common / abundant	≤ 2 mm; juveniles present	rare (E, T, G)	sparse
VC14	58.5	10YR 7/4 very pale brown	very fine - medium	well	abundantly angular to subangular	variably clear or frosted, very commonly iron-stained	very common	≤ 1 mm	common (E, T, G)	common
VC16	60.7	10YR 7/3 very pale brown	fine - medium	poor	abundantly angular to subangular	clear lustre abundant, sparse translucent lustre, iron-staining is rare	abundant	≤ 3 mm; juveniles present	common (E, T)	abundant
VC17	67.5	10YR 7/4 very pale brown	very fine - medium	moderate	angular and subangular	abundant clear or translucent lustre, commonly iron-stained	common / very common	≤ 1 mm	very rare (E, T, G)	sparse / common
VC23	101.7	2.5Y 8/2 pale yellow	very fine	well	angular	clear lustre	abundant**	≤ 2 mm; juveniles present	common (G)	abundant

yellow to dark orange. Foraminifer and other fauna also show evidence of iron staining but could also be present in dark brown and dark grey colours from potential algal staining. In some instances the degree of staining inhibited identification of species. Foraminifers are predominantly found as whole tests, although the foraminifers in sample VC18 are abraded. The distribution of Holocene lagoonal, estuarine and intertidal foraminifers in water depths beyond their preferred environment is indicative of stranding and reworking during the postglacial marine transgression (PMT). Li *et al.* (1998) also found relict grains concentrated in samples from 50-100 m water depths on the Lacepede Shelf to consist mainly of shallow water foraminifer species. *A. beccarri* tests can be relatively strong indicators of stranding; shallow-water grains that are found in greater water depths than that in which they were produced following PMT (James and Bone, 2011). The tests are delicate and seem unlikely to survive intact in transport.

4.3.1.2 Discussion

The shallow substrate vibracore samples from the Lacepede Shelf, with the exception of VC23, were retrieved from the quartz-rich region of the shelf characterised by marooned beaches, shoals, barrier islands and wetlands (James *et al.*, 1992; Hill *et al.*, 2009; James and Bone, 2011). The dominant quartz grain size of fine to medium. The dispersal of iron-stained quartz grains throughout the shelf deposit indicates extensive reworking and redistribution of grains, which had been in a terrestrial environment. This is also made apparent by the mixture of clear and frosted quartz grains within many of the samples indicating both aeolian and fluvial sources.

The faunal record is also indicative of reworking and flooding of coastal environments. This is most evident in the mixture of relict grains (stained various shades of orange and brown by iron), stranded post-LGM grains (white or buff) and by the distribution of species such as *A. beccarri* outside of their preferred environments.

4.3.2 Early Holocene shoreline

Before the complete development of the modern Sir Richard and Younghusband Peninsulas, sea level extended farther inland than present, reaching the barrier complex of the Last Interglacial ~2 km inland (Bourman *et al.*, 2000). Within the study area, a mid-Holocene high sea-level is recognised in the former shorelines of Lake Alexandrina

at heights ~2.7 m above present sea level (APSL) (de Mooy, 1959; von der Borch and Altmann, 1979) and sand flat sediments, which make up the southern half of Hindmarsh and Mundoo Islands occurring at elevations up to 2 m APSL (Bourman *et al.*, 2000). The relationship of the early Holocene sand flat sediments with the last interglacial coastline is unestablished. The limit of the transgression onto Hindmarsh Island is also unknown and could be indicated by the extent of remaining last glacial maximum (LGM) dunes on the island; i.e. those that were beyond the erosional reach of the mid Holocene high sea-level. Eight auger holes on Hindmarsh Island were analysed to assist in establishing the relationship of early Holocene sediments to LGM sands and the last interglacial shoreline.

4.3.2.1 Southern Hindmarsh Island

Hindmarsh Island is the largest of the islands located south of Lake Alexandrina and inland of the Murray Mouth. The island is approximately 15 km long at its maximum east-west direction and approximately 7 km maximum width in the north-south direction, covering an area ~50 km² (Figure 4.7). The island is surrounded on three sides by the main channel of the River Murray, the Goolwa channel. It is separated from Mundoo Island, directly to the east, by the Mundoo Channel. The northern half of the island has been shown to be composed of at least two interglacial aeolianites (Murray-Wallace *et al.*, 2010). The southern half of Hindmarsh Island is composed of a sand flat with small coastal dunes located on its southern margin reflecting the early Holocene sea-level maximum (≤ 2 m) and movement of the Murray Mouth during the Holocene (Bourman *et al.*, 2000). The northern half of the island is composed of Pleistocene aeolianite capped by calcrete.

Six auger holes were dug by hand auger for this thesis and sediment was provided from two additional auger holes by Robert (Bob) Bourman (AL-BH1 and AL-BH2). Sediment from the auger holes was retrieved beneath the topsoil where a change in colour occurred and at the bottom of the hole. A whole rock sample (ALW) was also retrieved from one of the coastal dunes on the southern margin of the island, approximately 125 m from the shoreline of the Goolwa Channel.

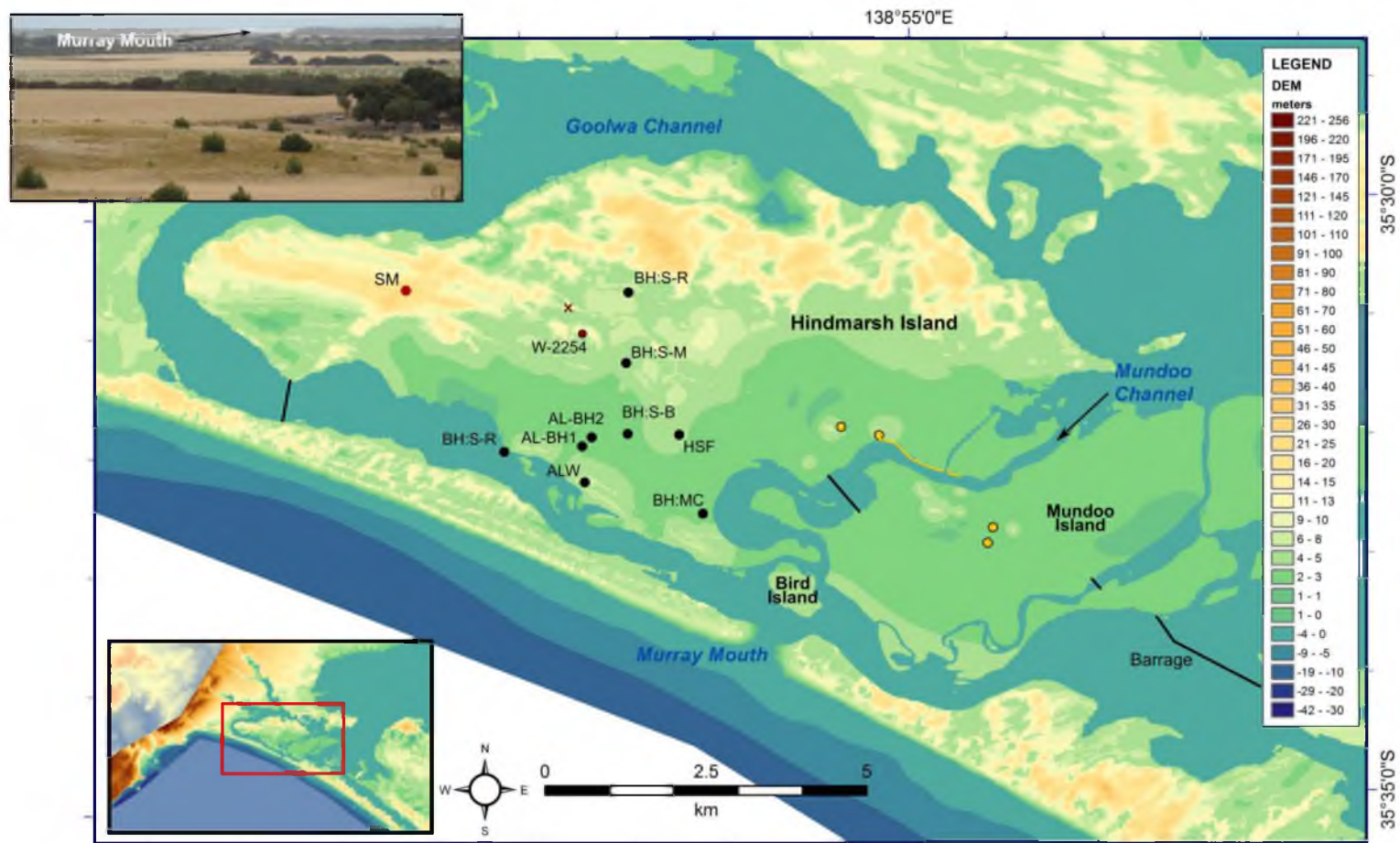


Figure 4.7: Digital Elevation Model of Hindmarsh Island with location of field sites discussed in text indicated by black circles. The northern half of the island is composed of Pleistocene aeolianite giving the island greater topographic expression. Siliceous sands overlying a calcreted aeolianite ridge are indicated by maroon circles with the 'x' signifying the location of a siliceous dune as indicated by a property owner. Calcrete is absent in auger and outcrop south of BH:S-M except to the west (section 4.3.3.2) as indicated by yellow circles and line. Calcrete ridges were removed from the centre of the island by council (personal communication Robert Bourman 21 May 2015). Inset view from Sturt Monument (SM) to Murray Mouth.

Auger holes BH:S-R and BH:S-M (Figure 4.7) revealed siliceous sands which terminated on calcrete at depths of 1.20 m and 0.45 m, respectively. No sample was taken from BH:S-M as it was composed completely of topsoil similar to BH:S-R, but it was noted that clay content increased with depth. Auger holes BH:MC and BH:S-B (Figure 4.7) terminated beneath the water table when the bioclastic sand became too water saturated for removal at depths of 1.74 m and 1.60 m respectively. The land surface at both auger holes was levelled to height above present sea level (APSL) (Figure 4.8). AL-BH1 and AL-BH2 reached depths of 1.5 m and 9 m, respectively. A sample was retrieved from the bottom of AL-BH1 and from every depth of AL-BH2. Two auger holes (HSF-50 and HSF-57; Figure 4.7) were attempted in close vicinity to each other approximately 800 m to the east of AL-BH1 but the sand beneath the soil horizon was too fine for the auger to hold and the holes were terminated at 0.50 m and 0.57 m.

The dominant particle size fraction for all auger holes as determined by hand sieving, is fine (125-250 μm), except for BH:S-R which had a nearly equal quantity of medium grains (250-500 μm). Four sub-samples were taken from the ALW whole-rock sediment and from AL-BH2 (at depths of 1 m, 5 m and 9 m) for particle size analysis and confirmed the dominant grain size to be fine (Table 4.4), although it should be noted that at 1 m depth AL-BH2 contained a significant quantity of silt (~13%) whereas the remainder of the samples contained 5% or less. The larger grain size fractions shown within Table 4.4 likely reflect the carbonate fraction of the sediment. Calcium carbonate was present in all auger holes, although unknown from BH:S-M and questionable in BH:S-R where no shell was found but acid digestion suggests a minor quantity (Table 4.4).

The calcrete beneath BH:S-R and BH:S-M is located at 1.69 m and 1.41 m APSL, respectively, but was not encountered beneath the remaining auger holes located in a more southerly position on the sand flat. The water table was encountered in auger holes BH:S-B and BH:MC at depths of 1.6 m (0.20 m APSL) and 0.95 m (0.30 m APSL), respectively (Figure 4.8). Bioclastic sand beneath the water table is grey due to the anaerobic conditions. Grey sand indicates that the water table is located somewhere above 1.5 m burial at AL-BH1 and between 3 and 4 m at AL-BH2. The bioclastic sands

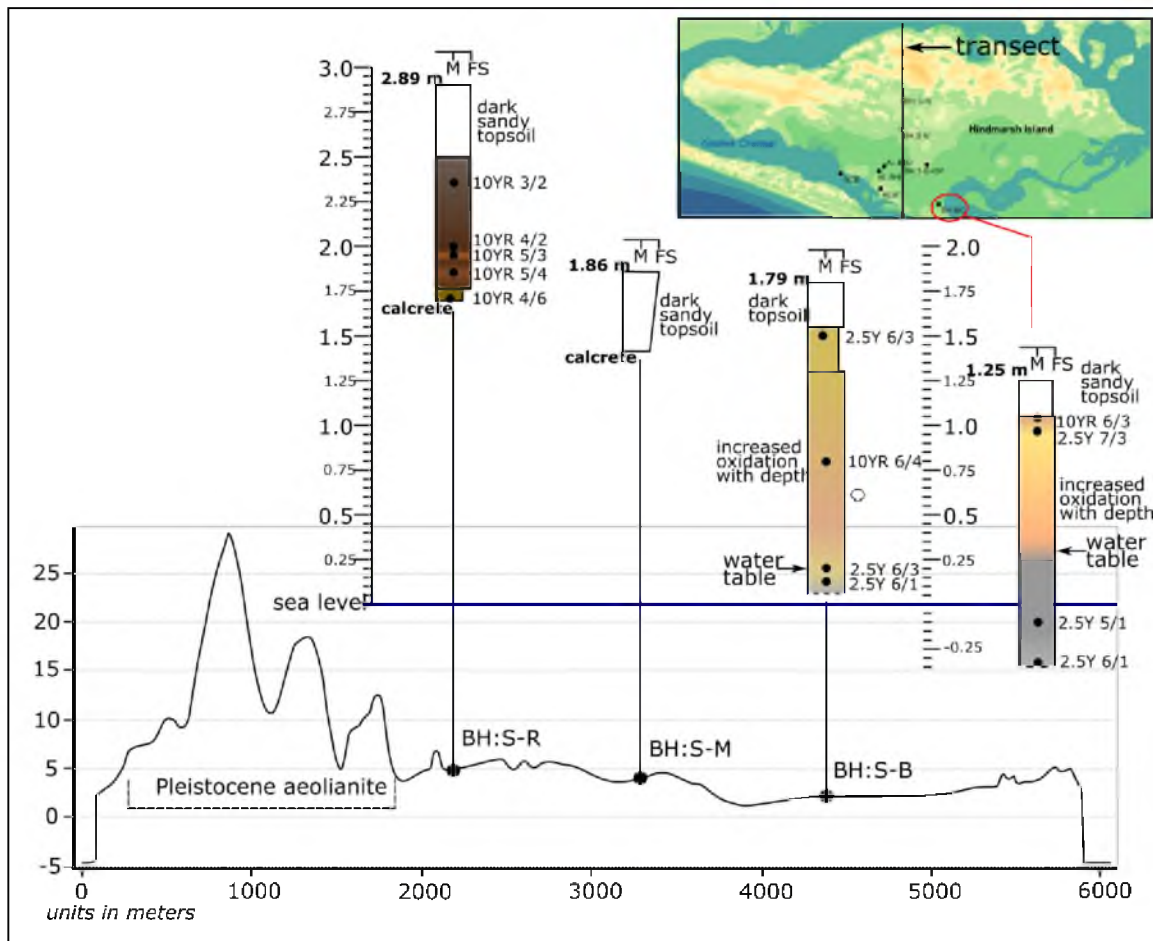


Figure 4.8: Transect of Hindmarsh Island generated from the DEM in direction of north to south passing through or adjacent to auger holes BH:S-R, BH:S-M and BH:S-B. These auger holes and BH:MC were surveyed to height above present sea-level and corresponding log diagrams are provided. The increased oxidation within BH:S-B and BH:MC was interpreted from increased orange mottling throughout the bioclastic sand with depth. BH:S-R and BH:S-M contained siliceous sand.

above the water table tended to be a light yellowish brown or very pale brown except at BH:S-R. Beneath the topsoil, the darker, siliceous sands of BH:S-R take on a banded appearance (Figure 4.8), most significantly below ~ 0.94 m depth of burial where the sands lighten to brown, darken, then lighten to yellowish brown before darkening to a dark yellowish brown sand with a higher clay content at 1.14 m depth of burial.

The uniqueness of the sand from BH:S-R in both grain size and carbonate content suggests a different source for these sediments in comparison to the other auger holes. The position of the sand over calcrete (as with the similar BH:S-M) places deposition of these sands post Last Interglacial. A last glacial maximum (LGM) sand dune composed of

similarly coloured sand, 10YR 6/6 brownish yellow, with a TL age of 20 ± 2 ka (W-2254; Murray-Wallace *et al.*, 2010) is located between and slightly west of the two auger holes (Figure 4.7). A house has been built on a similar sand dune between the LGM dune and BH:S-R (personal communication with property owner Nick Grundy 21 November 2013). Both locations are visible from BH:S-R. An additional siliceous dune (SM) with a similar colour (10YR 4/4 dark yellowish brown) is identified in this thesis farther to the west (Figure 4.7) and described in detail in Section 4.3.7. This dune and the TL dated dune are both found overlying calcreted aeolianite.

All auger holes were analysed for mollusc species content (Table 4.2). The gastropod *Coxiella striata* was identified in AL-BH1, and the gastropod *Hydrococcus brazieri* was identified, in both HSF-50 and HSF-57. AL-BH2 contained the greatest quantity and variety of fauna. Fauna are most abundant between burial depths of 5 m and 8 m and include fragmented, whole disarticulated and articulated valves of juvenile bivalves as well as fragmented and whole gastropods including species typical of the sheltered environment of an estuary (cockles: *S. trigonella*, *Eumarcia fumigata*, *Tellina (Macomona) deltoidalis*, *Soletellina biradiata*; gastropods: *C. striata*, *H. brazieri*) and exposed intertidal and subtidal coastal environments (cockles: *M. rufescens*, *D. deltoides*, *P. elongata*, *Nuculana (Scaeolada) crassa*, *Brachiodontes (Austromytilus) rostratus*; gastropod: *Polinices incei*). The faunal assemblage of mixed species indicates a high-energy environment of deposition (section 4.2.1).

The size of shell fragments decreases above 5 m depth of burial until at 1 m shell fragments are the same size as the fine-grain quartz component, although carbonate content is still comparatively high, 62% (Table 4.4). The auger hole was also analysed for the presence of foraminifera, which were absent in the top 3 m of sediments but present throughout the rest of the sediments. *S. trigonella* valves were selected from depths of 5 m, 8 m, and 9 m for amino acid racemisation (AAR) analysis. One valve from 9 m depth of burial was split with half for AAR analysis while the other half was sent to the Radiocarbon Dating Laboratory at Waikato University in New Zealand for analysis. Shell was also retrieved for AAR analysis from both HSF auger holes and a Holocene beachrock (ROB). These results are presented in Chapter 6.

Table 4.4: Analytical results for auger holes located on southern Hindmarsh Island.

Field Code	DOB (m)	Munsell	% Carbonate	Particle Size Analysis					Mollusc
				VF	F	M	C	VC	
BH:S-R	2.893	land surface height apsl							
	0.54	10YR 3/2 very dark greyish brown	2*						N
	0.90	10YR 4/2 dark greyish brown	2*						N
	0.94	10YR 5/3 brown	0						N
	1.04	10YR 5/4 yellowish brown	0						N
	1.20	10YR 4/6 dark yellowish brown	4*						N
BH:S-M	1.864	land surface height apsl							
	0.45	no sample							
BH:S-B	1.798	land surface height apsl							
	0.30	2.5Y 6/3 light yellowish brown	45						N
	1.00	10YR 6/4 light yellowish brown	48						N
	1.20	shell fragment							Y
	1.60	2.5Y 6/3 light yellowish brown	80						N
	1.74	2.5Y 6/1 grey	84						N
BH:MC	1.248	land surface height apsl							
	0.20	10YR 6/3 pale brown	38						N
	0.30	2.5YR 7/3 pale yellow	42						N
	1.35	2.5Y 5/1 grey	57						N
	1.60	2.5Y 6/1 grey	48						N
AL-BH1	1.50	2.5Y 5/1 grey	12						Y
AL-BH2	1**	10YR 7/4 very pale brown	62	28	55	17			N
	2.00	10YR 7/4 very pale brown	56						Y
	3.00	2.5Y 6/2 light brownish grey	56						Y
	4.00	2.5Y 6/1 grey	38						Y
	5.00	2.5Y 6/1 grey	25	8	54	35	1	2	Y
	6.00	2.5Y 6/1 grey	29						Y
	7.00	2.5Y 6/1 grey	33						Y
	8.00	2.5Y 6/1 grey	30						Y
	9.00	2.5Y 6/1 grey	29	13	60	27			Y
HSF-50	0.50	2.5Y 6/4 light yellowish brown	15						Y
HSF-57	0.57	2.5Y 7/3 pale yellow	30						Y
ALW	0.04	10YR 5/3 brown	26	20	64	16			Y
*No visible reaction by these sediments to HCl and result may reflect loss of silt and/or clay in washing.									
**Contains 13% silt, remainder of samples contain ≤5% silt.									

4.3.2.2 Discussion

The spatial extent of calcrete on northern Hindmarsh Island is easily discernible as it caps the aeolianite succession which makes up that part of the island. The subsurface extent of the calcrete on the middle and southern part of the island is largely unknown. At some point between BH:S-M and BH:S-B (Figure 4.7) the calcrete disappears. Subsequent discussion (section 4.3.3.2) will show that shell beds less than 500 m to the southwest of BH:S-M lack a calcrete capping. However, calcrete does appear again to the southeast on Hindmarsh Island and the adjacent Mundoo Island (Figure 4.7). Calcrete ridges, formerly located in the centre of Hindmarsh Island, have been removed by Council for road cement (personal communication, Robert Bourman, 21 May 2015). As calcrete does not occur in the 9 m deep AL-BH2 it is believed that calcrete related to the late Pleistocene does not extend across the southern margin of the island. A probable explanation for the lack of calcrete is that the area now forming southern Hindmarsh Island was the location of a river valley carved during the LGM.

The siliceous sand, which is found across the middle of the island from the west to the centre of the island is absent from the southern portion of the island. These sands are interpreted to have been reworked into the sandflat deposit as sea level peaked during the mid-Holocene. The siliceous sands rest on calcreted surfaces, which would have aided in the preservation of the easily eroded material during the Holocene. The current extent of the LGM sands is an indicator of the limit of the mid-Holocene sea-level transgression.

The fauna deposit at 5 to 8 m depth of burial within AL-BH2 indicates high energy deposition and most likely reflects the sea level peak of the postglacial marine transgression (PMT). Above that depth mollusc content is limited to the small gastropods *C. striata* and *H. brazieri*, which are no longer present at 2 m depth of burial and foraminifers are also absent in the top 3 m of sediment reflecting altered depositional environment conditions as the modern Sir Richard and Younghusband peninsulas reached full development and the Murray Mouth migrated position. Recognisable carbonate grain content (beyond fine fragments) is not present above 2 m depth of burial. The decreasing content of mollusc shell and foraminifers in these

sediments reflects the increasingly restricted environment as Sir Richard and Younghusband Peninsula barriers developed and the Murray Mouth migrated.

4.3.3 The Last Interglacial beach-barrier complex

Benthic (Shackleton, 1987) and Antarctic ice cores (Jouzel *et al.*, 2007; Masson-Delmotte *et al.*, 2010) indicate that the last interglacial maximum (MIS 5e) was similar in strength to the present Holocene interglacial, although sea level in southern Australia is believed to have been up to 2 m APSL (Murray-Wallace and Belperio, 1991; Belperio *et al.*, 1995). The sedimentary record of the last interglacial maximum on the Coorong Coastal Plain is identified as the Woakwine Range, a predominantly single barrier structure, sub-parallel to the modern coastline forming the landward margin of the Coorong Lagoon for the length of the coastal plain (Murray-Wallace *et al.*, 1999). Variations in the height of the MIS 5e shoreline across South Australia have been attributed to ongoing neotectonics (Murray-Wallace *et al.*, 1996; 1999; section 2.5.3.2) the record of which indicates downtilting towards the Murray Mouth region from both westerly and south-easterly directions and a rate of subsidence of 0.02 mm yr^{-1} for the past 125 ka (Bourman *et al.*, 2000). Aeolianite deposited during the MIS 5c and MIS 5a interstadials form an erosional rocky coastline southeast from Robe (Figure 2.14) (Huntley *et al.*, 1993; 1994; Cann *et al.*, 1999; Murray-Wallace *et al.*, 2002). Thermoluminescence (TL) and sedimentological analysis indicate that a linear array of islands, composed of aeolianite and calcrete, extending north towards the study area within the modern Coorong and sub-parallel to the modern coastline were deposited during MIS 5c (Cann and Murray-Wallace, 2012).

Previous work within the study area (Bourman *et al.*, 2000; Murray-Wallace *et al.*, 2010) identified sedimentary successions related to both MIS 5c and MIS 5e. A cross-bedded aeolianite at Surfer Beach (within the study area, 6 km west-southwest of Goolwa), analysed by thermoluminescence, provided an age of $105 \pm 5 \text{ ka}$ (W-2348, Murray-Wallace *et al.*, 2010) indicating deposition during MIS 5c. The previous research also confirmed the presence of an MIS 5e coastal barrier complex with associated beach and estuarine facies on northern Hindmarsh Island and extending west onto the Mount Lofty Ranges (section 2.5.3.3). However, the extent and preservation of these sedimentary facies was not fully explored and this thesis builds upon the earlier work to

further identify and record the last interglacial sedimentary successions within the study area and provide a geochronological framework for the development of the shoreline. Due to the spatial extent of the last interglacial shoreline within the study area and the number of associated field sites, presentation of analyses is split into four geographic regions: southeast Lake Albert, Hindmarsh Island, Goolwa and Fleurieu Peninsula.

4.3.3.1 Southeast Lake Albert

This region, located ~40 km southeast of the Murray Mouth, is composed of the Bridgewater Formation overlain by extensive deposits of the siliceous Molineaux Sand deposited during a period of glacial aridity. The eastern shoreline of the Coorong Lagoon in this region is composed of last interglacial shelly foreshore deposits. De Mooy (1959) suggested that the southern portion of Lake Albert was open to the sea during the Last Interglacial and that the coastal barrier (referred to as the Bonney coastline) grew in three stages of construction from the eastern side of the lake in a northward direction with lagoon deposits behind each barrier (Figure 4.9). The field sites, all located at less than 20 m APSL, overlap the stages of barrier construction, extending from the eastern shoreline of the Coorong (Stratland, SL, and Camp Coorong, CC-sh) nearly 16 km inland to McIntosh Road (MRC). This latter field site is located ~7 km due east of the easternmost shoreline of Lake Albert (Figure 4.9). The aeolianites at Woolshed Road, Yarindale and Stockcrete all have associated overlying siliceous sands.

At Camp Coorong, shelly facies of the last interglacial foreshore dip seaward into the Coorong Lagoon. The remaining field sites within southeast Lake Albert region are allochemical sandstones as indicated by their low content (4-29%) of calcium carbonate with variable calcrete development (Figure 4.10).

Stratland Field Site

The aeolianite at Stratland, ~0.7 km inland from the Coorong shoreline and in the vicinity of the proposed former mouth (de Mooy, 1959), is unique to the other aeolianites southeast of Lake Albert in its well-preserved bedding (Figure 4.10) and lenses (1-3 cm thick) of shell-rich sand. Nearly horizontal bedding ~1 m thick caps gently southeast (azimuth 044) dipping (9°) beds indicating the stoss side of the dune and

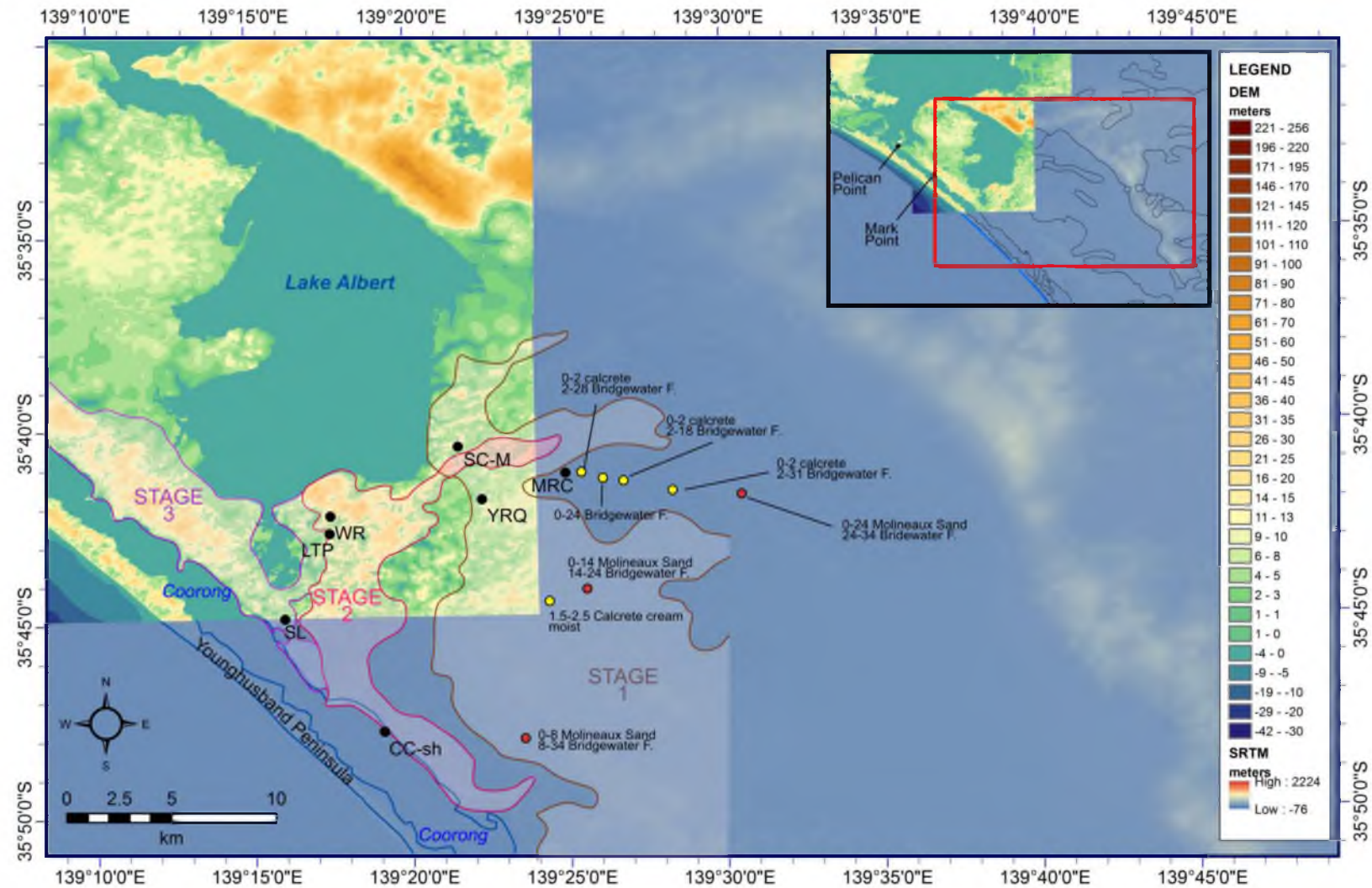


Figure 4.9: Field sites southeast of Lake Albert. The three stages of barrier construction for this region as envisioned by de Mooy (1958) have been included. Yellow circles are boreholes that encountered calcrete at the surface or near-surface. Red boreholes indicate Monlineaux Sand overlying Bridgewater Formation (SARIG).

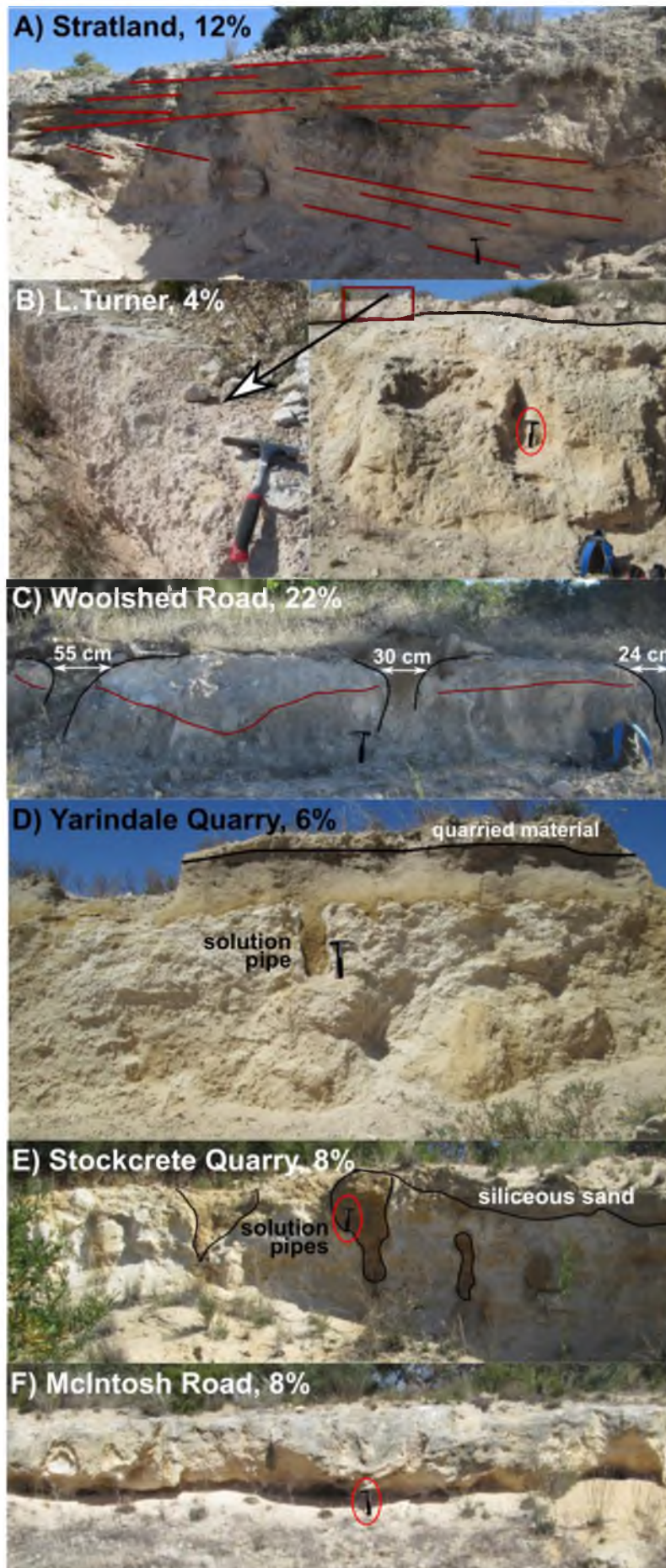


Figure 4.10: Photographs illustrating the variable appearance of deposits within the Lake Albert region and carbonate content in the 250-500 μm fraction. All photos contain rock hammer for scale. A) Calcrete has been disturbed by quarrying. Moderately indurated bedding is interspersed by well indurated shelly lenses. B) A thin laminar (<1 cm) calcrete overlies a variably present indurated pisolitic lens (≤ 10 cm) which grades into a calcrete with rhizoliths (≤ 40 cm). Bedding is not discernible in the loosely consolidated sediment (2.5 m thickness) beneath the calcrete. C) A massive calcrete profile containing a single lamina (red line) at base overlies lightly indurated sediment. Rubbly calcrete is associated with the margins of solution pipes (diameters provided). D) A weakly developed calcrete profile in which a thin (at most centimetres thick) hardpan calcrete overlies lightly indurated slightly nodular calcareous sediment (1.4 m thick). The calcrete is overlain by 45 cm of siliceous sand which grades upwards into a dark pedogenic layer. E) Solution pipes and variably present rhizoliths in weakly indurated sediment overlain by up to 2 m of siliceous sand. F) Low-lying 1 m thick moderately indurated massive calcrete with minor rhizolith development.

winds from the southeast. The quarry also contains a pit, which extends ~6.1 m from the dune surface and exposes iron-stained sediment near the base of the pit reflecting water movement through the deposit. Sediment samples for analysis were taken from the base of the pit (6.1 m depth of burial) and from a shelly lens located at 1.0 m depth of burial. The shelly lenses, the large range in particle size and poor sorting of the Stratland sediments imply a high-energy near-shore environment (Table 4.5). The silt and clay content increase up the profile is indicative of an increase in aeolian sediment input.

Sediment analyses

Sediment samples were also analysed from the Woolshed Road and Yarindale Road aeolianites for particle size distribution and by binocular microscope (Table 4.5). These field sites were chosen because, along with the Stratland field site, they represent a geographic transect normal to the shoreline, have contrasting calcrete development providing a representation of the variability within the landscape and the overlying siliceous sands at Woolshed and Yarindale Roads exhibited the least amount of disturbance. The results of siliceous sand analyses are presented and discussed in section 4.3.7.

The aeolianites (including the Stratland sediments) consist of a predominantly fine to medium grain size typical of carbonate aeolianites (McKee and Ward, 1983). Calcium carbonate in the aeolianites is dominantly represented by mollusc fragments, which in every case are well rounded and abraded (Table 4.5). Other fauna include bryozoan and echinoid fragments and foraminifers. The latter were generally too recrystallised for positive identification, however, small tests of the species *Elphidium macelliforme* and genus *Discorbis* were positively identified. The tests do not necessarily provide a strong indication of palaeoenvironment as small tests of foraminifer are more easily winnowed from their initial environment (Cann *et al.*, 1988).

Camp Coorong

The Camp Coorong shell beds (CC-sh) to the southeast of the Stratland aeolianites are an extension of the MIS 5e foreshore facies ~35 and ~25 km northwest at Pelican Point and Mark Point, respectively (Murray-Wallace *et al.*, 2010). Shallow,

Table 4.5: Analytical results for selected aeolianites in the region southeast of Lake Albert. The percentage of sand-sized particles is based on the total sand-size fraction and not the total sediment.

SITE	Stratland	Stratland	Woolshed Road	Yarindale Road
Field Code	SL (top hash)	SL (orange sand)	WR	YRQ
Calcrete	no	no	yes-massive	yes-laminar
Calcrete thickness	-	-	>1 m	≤5 cm
SEDIMENTS				
Depth of burial (m)	1.0	6.1	0.9	1.4
Munsell Colour	10YR 8/3 very pale brown	10YR 7/8 yellow	10YR 8/3 very pale brown	10YR 7/3 very pale brown
% CaCO ₃ (250-500 µm)	12	29	22	6
Heavy minerals	common	rare	common	sparse
Particle Size Analysis (Malvern Mastersizer)				
clay	2	0	3	2
silt	12	0	20	9
sand	86	100	77	90
very fine	9	3	13	20
fine	30	32	56	51
medium	33	34	31	24
coarse	12	19	0	2
very coarse	16	11	0	2
QUARTZ (binocular analysis)				
Sorting	poor	poor	moderate	moderate
Particle size	very fine-very coarse	very fine-very coarse	fine-medium	fine-medium
Roundness	angularity decreases as size increases	abundantly subangular to subrounded	angular to subrounded	angular to subangular
Surface texture	frosted grains common to very common; milky grains common	abundantly Fe-stained with a clear appearance; frosting is sparse	Fe-staining sparse to common. Abundantly clear with very coarse grains sparsely frosted/milky	abundantly clear but frosting is very common
CARBONATE (binocular analysis)				
	sparse	common	common	sparse
Molluscs	≤ 2.5-3 mm; well rounded, abraded	well rounded, abraded	≤ 1 mm; well rounded, abraded	≤ .05mm, rounded
Foraminifer	very rare	sparse to common	common	very rare
Other fauna	none identified	sparse to common	sparse to common	one fragment

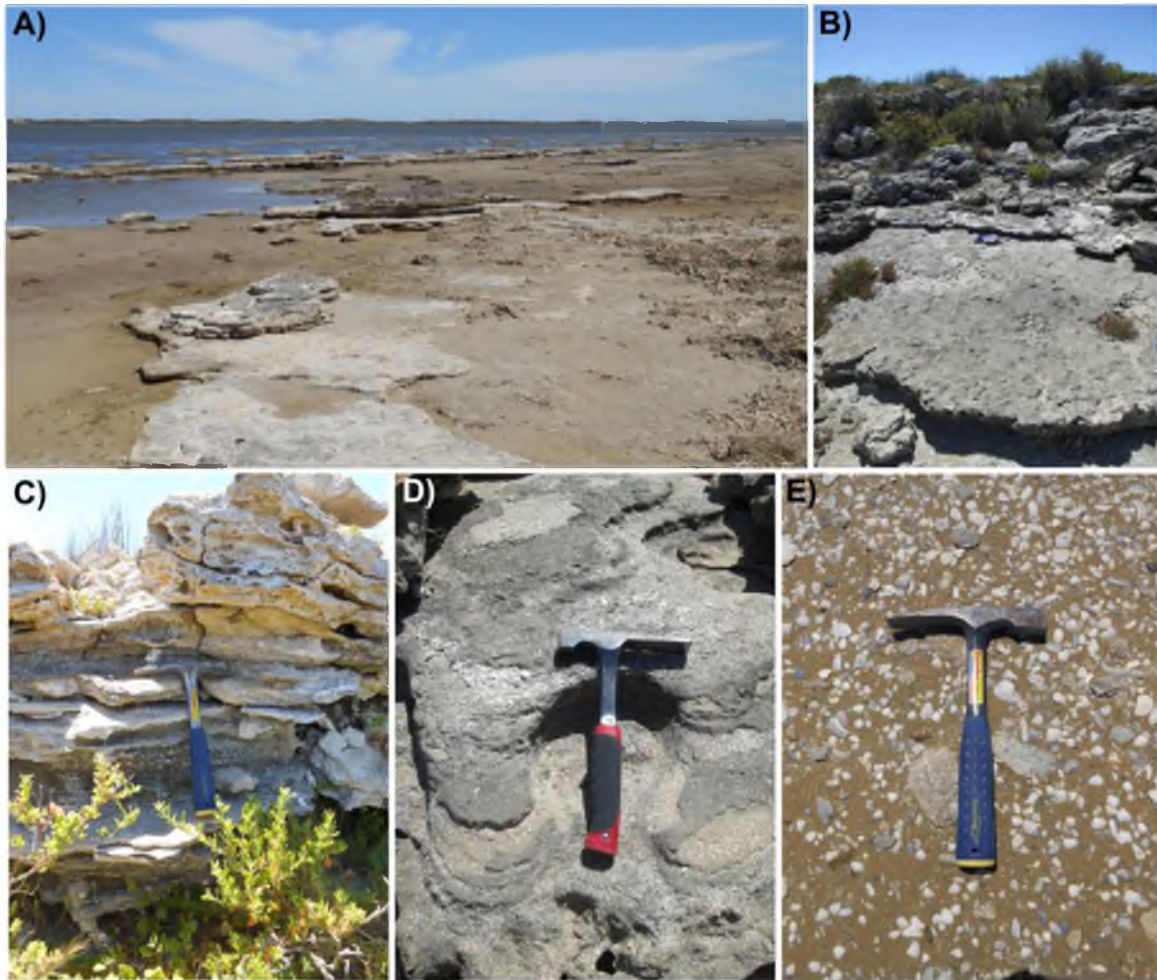


Figure 4.11: The Camp Coorong shell beds are shallow seaward dipping beds (A and B) of cemented shell hash (C and D). The modern shoreline also hosts sandy sediment containing whole disarticulated and fragmented valves of *Spisula trigonella*, *Anadara trapezia*, *Macra rufescens* and *Donax deltoides* and small beaches with deposits of disarticulated *S. trigonella* and the estuarine bivalve *Hydrococcus brazieri*.

seaward dipping planar beds composed of cemented shell hash form an erosional platform (on average 7-8 m in width) extending beneath the water surface (Figure 4.11). The shell is too small (<1cm and in many cases, too weathered) for positive identification (Taphonomic Grade 1). A mixture of fragmented marine (*Macra rufescens* and *Donax deltoides*, Taphonomic Grades 1 and 2) and abraded, disarticulated valves of estuarine (*Spisula trigonella* and *Anadara trapezia*, Taphonomic Grades 2 and 3) mollusc species are deposited loose on the shoreline. The nature of the cemented shell beds and the mollusc species identified indicates a *III, high-energy assemblage*, which differs from the lower energy foreshore counterparts to the northeast.

Discussion

The low carbonate content in the region southeast of Lake Albert is likely a reflection of the offshore environment which is characterised by a quartz-rich zone on the Lacepede Shelf (section 3.5.1). Siliceous sediment would also have been provided by a palaeo-River Murray if present. Although both the Camp Coorong foreshore facies and shelly lenses within the aeolianite at Stratland are indicative of a high-energy environment potentially influenced by a river mouth, a conclusion regarding the presence of palaeo-mouth cannot be made at this point.

The lack of carbonate within the sediments is a likely explanation for the minimal calcrete development in the region. The comparatively thick calcrete (~1 m) at McIntosh Road (MRC, Figure 4.10) suggests a possibly greater age for the sediment there than at the other field sites with the low carbonate content reflecting a greater length of time for calcrete development and the loss and/or degradation of indigenous amino acids. Drillhole logs, provided sedimentological descriptions, on the South Australian Resource Information Geoserver (SARIG) (Department for Manufacturing, Innovation, Trade, Resources and Energy, 2014) to the east of McIntosh Road indicate the presence of Bridgewater calcrete at surface and at depth beneath overlying Molineaux Sand (Figure 4.9).

The record of predominantly aeolian deposition in the region southeast of Lake Albert differs from that of Hindmarsh Island, which indicates a highly complex environment of deposition.

4.3.3.2 Hindmarsh Island

The remains of a prograding recurved spit forms the northern half of Hindmarsh Island indicating both dominant longshore transport from the southeast and the presence of a palaeo-Goolwa Channel in the same location as present (Figure 4.12) (Bourman *et al.*, 2000; Murray-Wallace *et al.*, 2010). AAR analyses of shell from estuarine facies on the northern margin of the spit and sandflat facies to the southeast indicate deposition during MIS 5e (Murray-Wallace *et al.*, 2010). Murray-Wallace *et al.* (2010) also identified an older inlier of aeolianite to the island which TL analysis provided a minimum age of 330 ka (W-2256, Murray-Wallace *et al.*, 2010).

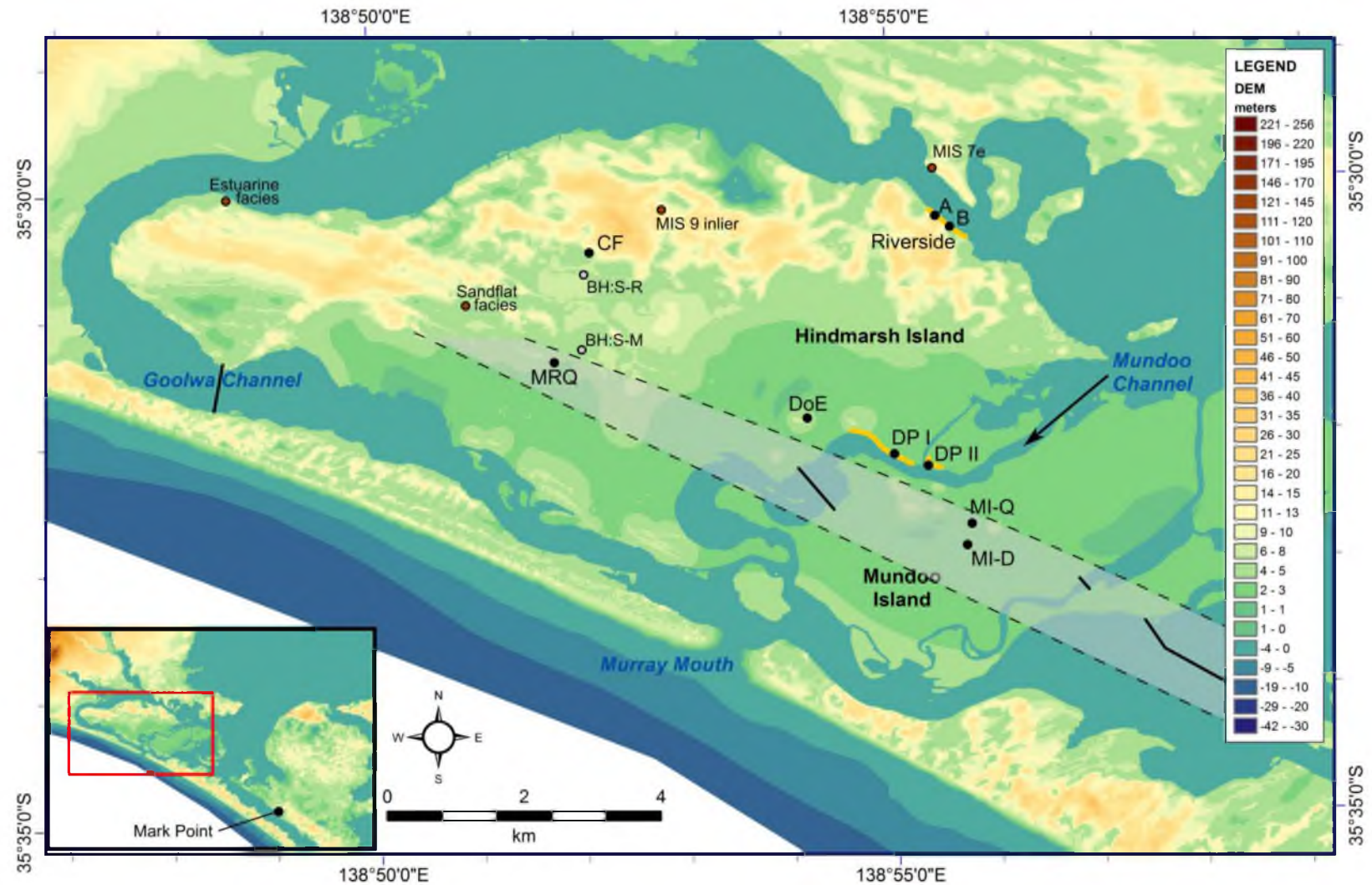


Figure 4.12: Field sites (black circles) and locations related to MIS 5e sea-level on Hindmarsh Island. Last Interglacial shell beds extend across Mundoo and Hindmarsh Islands (grey band). The extent of calcrete at the Denver Property (DP) and Riverside field sites is indicated in orange. Red circles denote facies and aeolianites identified and analysed using TL and AAR by Murray-Wallace *et al.* (2010) referred to in text.

Last interglacial aeolianite is absent from the River Murray terminus region from the northeastern margin of Hindmarsh Island southeast to approximately Mark Point, directly south of the gap between Sturt Peninsula and Point McLeay through which the River Murray flows (Figure 4.12). The absence of nearly 17 km of aeolianite is indicative of the erosive ability of the River Murray in the mouth region. The shell beds upon which barrages are built (except the Goolwa Barrage) are the only remaining indication of the last interglacial deposition in the absence of the barrier dunes (section 2.5.3.3).

This research located additional shell beds on Hindmarsh Island (McLeay Road Quarry and Cheese Factory field sites) and the adjacent Mundoo Island, which due to their geographic location in alignment with the barrages and position seaward of last interglacial aeolianite, are likely to have been deposited during MIS 5e. In addition to the shell beds, calcareous sediments were examined on the northern margin (Riverside) and the eastern margin (Denver Property) of Hindmarsh Island.

Mundoo Island

The shell beds on Mundoo Island were retrieved from two different localities, Mundoo Island Quarry (MI-Q) and Mundoo Island Dredge (MI-D) (Figure 4.12), in the centre of the island. The quarry had been infilled and the dredge shell was taken from a waterway and therefore, the shell was not observed *in situ*. Both sites contained coquinas composed of the intertidal bivalves *Macra rufescens* and *Paphies elongata* with the addition of *Donax deltooides* at the dredge site (Table 4.2) indicating deposition as part of the LIG fossil shoreline. However, the dredge site also contained estuarine mollusc species, *Spisula trigonella*, *Eumarcia fumigata*, *Tellina deltooidalis* (bivalves), *Coxiella striata* and *Hydrococcus brazieri* (gastropods). This mixed fossil assemblage indicates either a change in depositional environment or location in a zone of mixing, implying a nearby mouth. Without having observed the original stratigraphic relationship of the shell deposits, it is not possible at this point to make a conclusion.

McLeay Road Quarry

The McLeay Road Quarry (MRQ) is located ~6.6 km to the northwest of the Mundoo field sites (Figures 4.12 and 4.13). The shell bed, located near the centre of



Figure 4.13: Shell beds at the McLeay Road Quarry on the centre of Hindmarsh Island. Bedding is preserved within the quarry walls at varying degrees (A and B). The nearly planar thick shell beds in A are within a well cemented sediment, whereas in B the thinner shell deposits are found within a lightly cemented sand perhaps reflecting shell content. Solution pipes (C) and bedding (D) was also preserved in the quarry floor.

Hindmarsh Island and approximately 450 m southwest of the previously described auger hole BH:S-M (section 4.3.2), is dominated by disarticulated valves of *P. elongata*, *M. rufescens*, *D. deltoides*, *Nuculana crassa* and *Tellina albinella* (Table 4.2), species typical of exposed intertidal to subtidal environments. One *Turbo* (*Subninella*) *undulatus* shell was also identified and four valves of *S. trigonella* which are interpreted to have been transported from their preferred habitats. The shell is exposed in the quarry walls (which vary between 1 to 1.5 m in height) with some minor bedding preserved in which the shell displays a uniformity of orientation (Figure 4.13). A capping calcrete is not present and the presence of topsoil is variable. Shell is also visible in the quarry floor alongside

solution pipes. The floor of the quarry was levelled to 0.337 m APSL and the top of the shell bed to 1.303 m APSL.

The fossil assemblage here is similarly composed to the last interglacial sandflat facies identified by Murray-Wallace *et al.* (2010) located ~1.5 km to the northwest (Figure 4.12). The alignment with the barrages and the Mundoo Island shell beds further suggests deposition during the LIG.

Cheese Factory

Late Pleistocene lagoonal facies are located ~1.7 km north-northeast of the McLeay Road shell beds at the Cheese Factory site (CF) (Figure 4.12) and ~5 km almost directly east of the lagoon estuarine facies on the northern margin of the Hindmarsh Island recurved spit (Figure 4.12). The site (CF) is a ~20 m long exposure (Figure 4.14) containing shallow (<50 cm) standing water across its floor and located on the seaward margin of the coastal barrier complex of northern Hindmarsh Island. The lagoonal facies is located beneath the seaward toe of the aeolianite dune complex on northern Hindmarsh Island.

The exposure faces west and is parallel to the downhill slope in which it is found. It contains three massive units with no apparent bedding (Figure 4.14). A shell deposit at the base of Unit 1 (between 2 and 2.5 m burial) is made up of species typical of an estuarine environment; *S. trigonella*, *T. deltoidalis* and *E. fumigata* are present as whole disarticulated and fragmented valves. The top of the shelly deposit had been measured to 0.9 m APSL (Bob Bourman, personal communication 24 February 2012). Unit 1 transitions into a yellowish brown (10YR 5/4) sand (Unit 2) in turn overlain by the sand of the aeolian dune (Unit 3) (Figure 4.14). Unit 2 protrudes from the cutting ~30 cm marking a change in composition of sediments between Units 1 and 2. Unit 3 contains multiple solution pipes and is capped by a thin (≤ 15 cm) pale brown laminar calcrete. The height of the profile at its northern extent is ~2.2 m to the top of the scree with the overlying calcrete at roughly 3 m APSL.

The Cheese Factory position in relation to other deposits on the island indicates migration of barrier dunes, located to the south, northwards over the lagoon deposit.

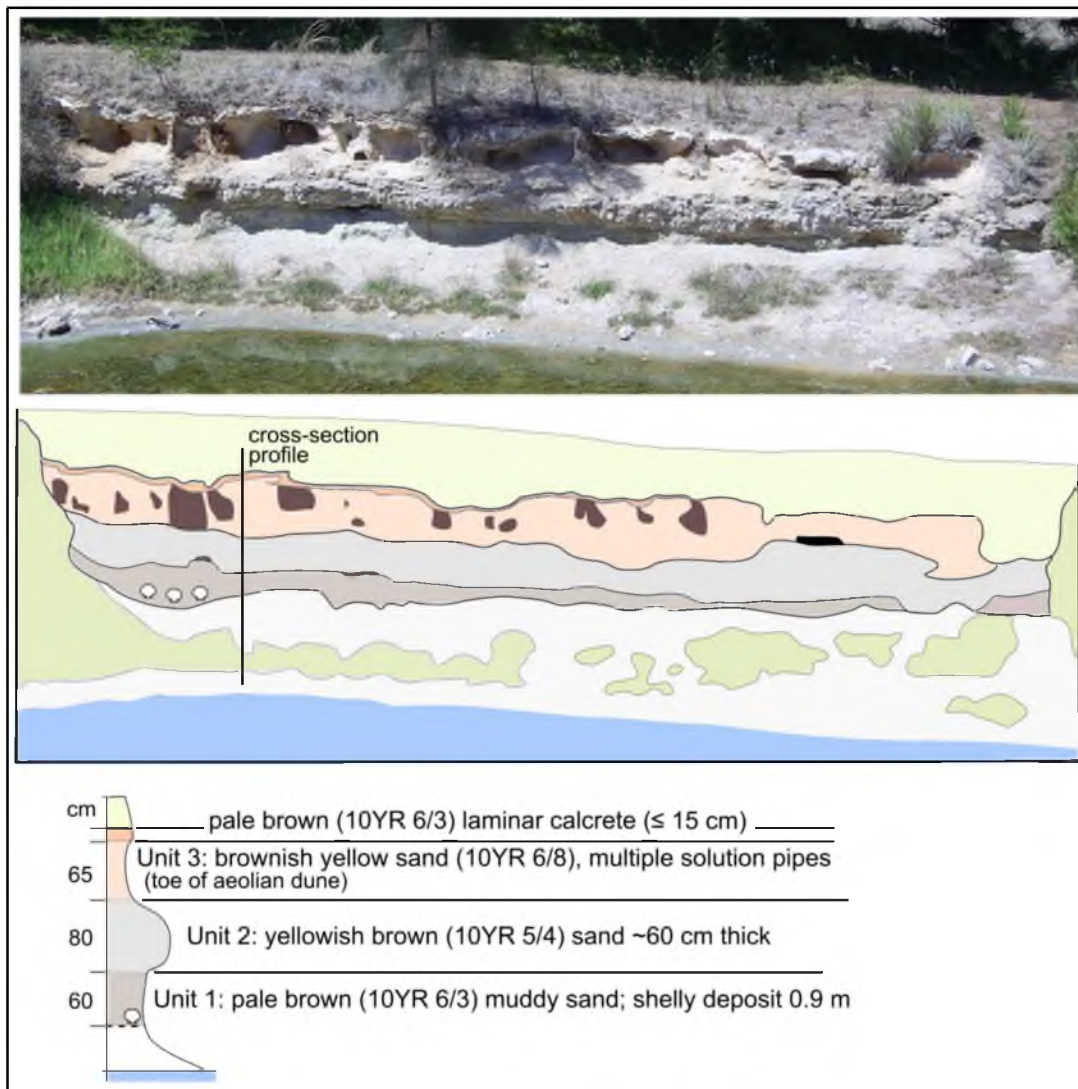


Figure 4.14: The Cheese Factory site faces west with north in the upslope direction. The sand of the last interglacial aeolianite (Unit 3) and the overlying calcrete thin to the south. Scree obscures the shell deposit which is most visible at the northern margin of the quarry.

Migration of coastal barrier dunes inland has been shown to occur as evidenced by deformed back-barrier lagoonal muds (Brown, 1965; Bourman *et al.*, 2000; Harvey *et al.*, 2006) and the presence of back-barrier strata on the seaward side of Sir Richard Peninsula (Bourman and Murray-Wallace, 1991; Bourman *et al.*, 2000; Section 3.3.1.1).

Riverside

Riverside is located on the northeastern shoreline of Hindmarsh Island across the Goolwa Channel from a MIS 7 aeolianite (215 ± 15 ka, TL Sample W-2346, Murray-Wallace *et al.*, 2010) (Figure 4.12) which extends up to 18 m in height with a

superimposed calcrete and sediment of no more than 1 m thickness. The Goolwa Channel is between 400-450 m in width at this point. Along the island shoreline for a distance of 1 km, two distinct calcretes have been identified (Figure 4.15) referred to as Calcrete A (the older) and Calcrete B (the younger). Calcrete A is located relatively low in the shoreline profile, dipping beneath the water level of the Goolwa Channel to the west. The calcretes give the shoreline a hummocky appearance, reflecting the control of calcrete in shaping the landscape.

Calcrete A is a thick (>1 m in places) alternatively massive or nodular, very pale brown (10YR 7/4) calcrete with an overlying laminar calcrete, brecciated in some areas, with minor rhizolith development (Figure 4.15). To the northwest the calcrete surface displays incipient solution pipe development in the form of clay pot karsts. Sediment beneath the calcrete is strongly indurated up to a thickness of 1 m before continuing beneath the modern land surface. At its exposure farthest to the southeast, Calcrete A is massive with faint traces of bedding at its base and extensive rhizolith development (Figure 4.15). The brownish yellow (10YR 6/6) sand beneath the calcrete is lightly consolidated. Sediment samples were taken of the strongly indurated sediments to the west and from the loosely consolidated sediment beneath the calcrete to the east.

The younger Calcrete B makes up the crest of the dune along the margin of the island and is superimposed onto Calcrete A at the eastern extent (Figure 4.15). At the sample location the calcrete is a predominantly nodular, poorly developed calcrete with an underlying lightly indurated light yellowish brown (10YR 6/4) sandstone exhibiting minor calcite development. The results of sediment analysis are discussed below in comparison with the Denver Property sediment samples.

Siliceous sand drapes a portion of the slope with a very different appearance to the underlying calcrete. The sand is a dark yellowish brown (10YR 4/4) and will be discussed in greater detail below (Section 4.3.7).

Denver Property

The Mundoo Channel has eroded through a low-lying, calcreted dune located ~2 km northwest of the Mundoo Island shell beds and ~1 km north of the Mundoo Barrage



Figure 4.15: The northern Hindmarsh Island shoreline contains two calcretes traceable along the steep slope; neither is well exposed and outcrop intermittently. Numbers in profile refer to calcrete photographs. Photograph 2 is of the superimposed calcretes (contact at red line) with the overlying calcrete containing clasts of reworked calcrete (in boxes). Photograph 4b was taken slightly farther to the west of 4a and shows brecciated calcrete beneath laminar. Further description in text.

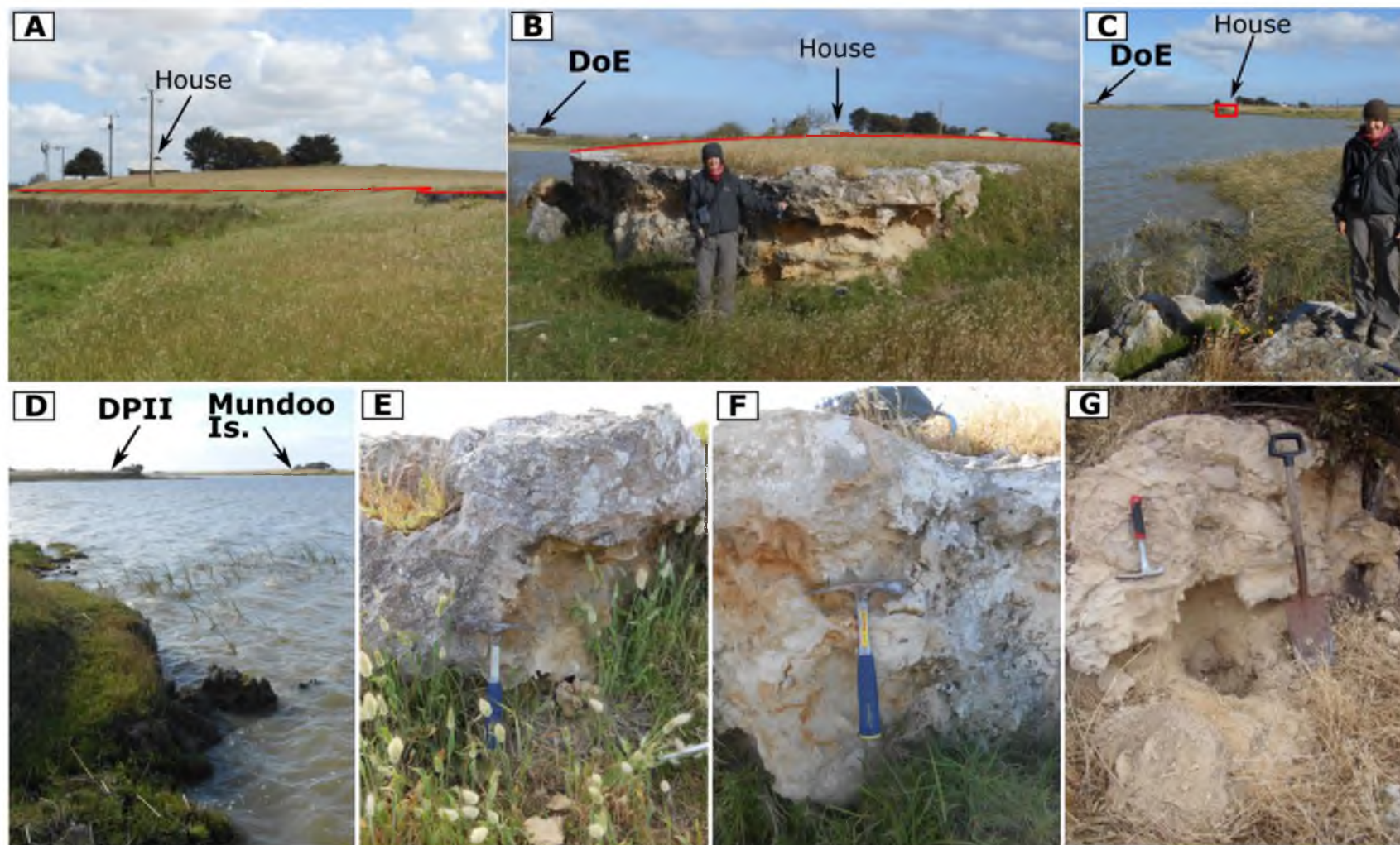


Figure 4.16: The Denver Property (DP) calcrete extends for nearly 280 m along the Mundoo Channel with the dune cresting to the north of the exposure (A and B). The calcrete is truncated by a smaller channel before continuing to the east (C and D). Another calcrete (DoE) is located ~600 m to the west (B and C). Sediment samples were taken from the calcrete on both sides of the channel, west DPI (E) and east DPII (F). Sediment was retrieved from the base of the massive DoE calcrete (G).

(Figure 4.12). Low-lying topography extends to the north and west. The presence of the low-lying calcrete was reported by Bourman *et al.* (2000) with a TL age of 85 ± 7.1 ka (W-2258) of the underlying sediment indicating deposition during substage 5a. Concern over the validity of the age arises when it is considered under the context of sea level during MIS 5a which is thought to have been as much as 17 m below present sea level in the region (Belperio and Cann, 1990; Murray-Wallace *et al.*, 2001). The exposure reaches ~280 m in length (west to east) before being truncated by a small tributary channel of the Mundoo Channel. The dune reaches its greatest height at the truncation, 1.3 m, which is ~2 m above the channel water level (Figure 4.16). The calcreted surface continues on the opposite shoreline of the smaller channel and farther along the margin of the Mundoo Channel for an unknown distance. The sediments on both sides of the channel are highly indurated, massive with bedding having been obliterated by rhizolith development.

Approximately 600 m to the west of the Mundoo Channel dune, an additional calcrete (DoE) is located in association with a small rise in the landscaper (Figure 4.12). This exposure reaches a height of only 90 cm with sediments beneath the calcrete only moderately indurated (Figure 4.16).

Samples from the Denver Property calcrete and the western extent of the Riverside Calcrete A were subjected to thin section analysis (Table 4.6). The Denver Property samples are from either side of the small truncating tributary to the Mundoo Channel. The sample from the west is referred to as DPI and the sample to the east as DPII (Figure 4.12). The sediments retrieved from beneath the Riverside Calcretes A (eastern extent) and B were analysed by binocular microscope (Table 4.6). Particle size analysis was performed on the less indurated sediments beneath Riverside Calcretes A and B and sediment from the Denver calcrete after gentle grinding by mortar and pestle to loosen grains.

Thin section analysis shows the calcretes to be fossiliferous allochemical sandstones (Mount, 1985). Under Dunham (1962) classification, DPI and Riverside Calcrete A (W) are grain-supported skeletal packstones, while DPII is classified as a

Table 4.6: Analytical results for northern Hindmarsh Island aeolianites. The percentage of sand-sized particles is based on the total sand-size fraction and not the total sediment. Analysis was by either thin section or binocular analysis as noted. See Figure 4.12 for location of sample sites.

SITE	Denver I	Denver II	Denver DoE	Riverside	Riverside	Riverside
Field Code	DPI	DPII	DoE	Calcrete A (E)	Calcrete A (W)	Calcrete B
Calcrete	massive-minor rhizolith	massive-minor rhizolith	massive-extensive rhizolith	massive-extensive rhizolith	massive or nodular	weak, nodular
Calcrete thickness (m)	0.75	1	0.9	≤ 1 m	> 1 m	≥ 0.50 cm
SEDIMENTS						
Depth of burial (m)	0.6	1	0.9	1.57	1	1
Munsell Colour	10YR 7/4 very pale brown	10YR 8/3 very pale brown	10YR 8/3 very pale brown	10YR 6/6 brownish yellow	10YR 7/4 very pale brown	10YR 6/4 light yellowish brown
% CaCO ₃ (250-500 µm)	60	59	76	64		54
Heavy minerals	present	present		rare	present	rare
Particle Size Analysis (Malvern Mastersizer)						
clay		1	1	1		0
silt		5	5	7		4
sand		94	94	92		96
very fine		9	11	22		16
fine		58	61	55		50
medium		33	28	23		28
coarse		0	0	0		4
very coarse		0	0	0		3
QUARTZ	thin section	thin section		binocular	thin section	binocular
Sorting	poor-moderate	poor-moderate		moderate	moderate-well	moderate-poor
Particle size	medium-fine	medium-fine		abundantly fine	fine-medium	abundantly fine
Roundness	abundantly subrounded	abundantly subrounded		abundantly subrounded to rounded	subangular-subrounded	abundantly subrounded to rounded
Surface texture				abundant clear lustre or translucent; frosted or milky grains sparse but Fe-stained		abundant clear lustre or translucent; frosted or milky grains sparse
CARBONATE	abundant	abundant		abundant	abundant	very common

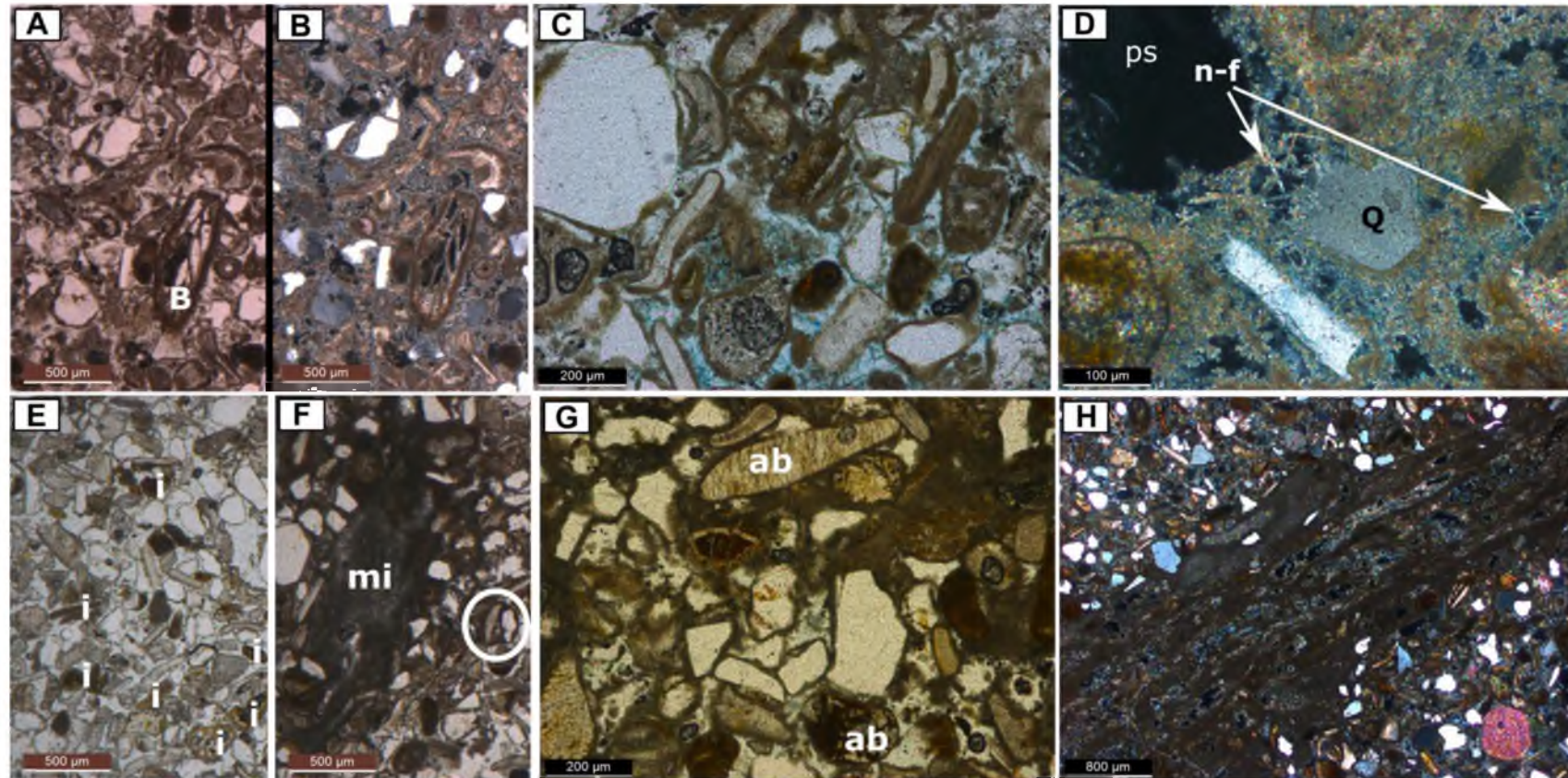


Figure 4.17: Photomicrographs of calcrete thin sections from the Denver Property and Riverside Calcrete A (west). A-D) Photomicrographs of DPI, A and B) Plain and cross-polarised light view of the same section illustrating the degree of micrite development. The bryozoan (B) retains intraskeletal pore space but the majority of intergranular pore space has been filled. C) Close-up of grains; both quartz and carbonate exhibit micrite cement fringes. D) Needle-fibre development within intergranular space. E-F) Photomicrographs of DPII. E) DPII retains much of its primary porosity. Numerous iron-stained grains (i) are present in both samples indicating a reworked component. F) A small region of dense micrite development most likely infilling an animal burrow or rhizolith. White circle surrounds an intraclast of a quartz grain and mollusc fragment bound by micrite. G-H) Photomicrographs of Calcrete A, G) Calcrete A demonstrated greater degree of micrite development than DPI or DPII. Carbonate grains showing evidence of algal boring (ab), the grain structure at the bottom of the image has been nearly obliterated. H) A rhizolith structure infilled by micrite and needle-fibre calcite under cross-polarised light.

grainstone due to a decreased quantity of cement. The DPI and DPII calcretes are similar in quartz and carbonate content (Table 4.6). The carbonate component is a mixture of reworked and iron-stained grains and grains with angular or minimally rounded corners indicating minimal transport. Mollusc fragments reach up to 1 mm in length. The DPI calcrete is more consolidated than the DPII calcrete and this is reflected in the cement content. DPI exhibits more extensive micrite development with needle-fibre calcite and retains little of its original porosity (Figure 4.17). Needle-fibre calcite is a biogenic feature and secondary cement indicative of micrite precipitation (Phillips and Self, 1987). In contrast, DPII retains most of its primary porosity in both intergranular and intraskeletal spaces with only minimal micrite development and no needle-fibre calcite (Figure 4.17). There is a concentration of micrite mud which is likely to be associated with the boring evident throughout the sample. The difference in cement content does not necessarily require different diagenesis but likely reflects the different sampling depths within the calcrete profile (Table 4.6). In comparison, Riverside Calcrete A (W) (Figures 4.12 and 4.15) has a more consistent grain size than the Denver Property samples with carbonate skeletal grains generally not exceeding 500 μm (rare exceptions are present). Iron-staining of carbonate is very common to abundant. Porosity decreases near laminar crusts and rhizoconcretions due to micrite infill (Figure 4.17). Intergranular porosity increases away from these features where meniscus microspar dominates. Intragranular pore space is low with most space infilled by micrite or microspar.

The sandy sediments found beneath Calcrete A (E) (lightly consolidated sand from the east) and Calcrete B are both abundantly fine-grained sandy allochemical limestones (Mount, 1985). Quartz grains are similar between the deposits (Table 4.6). Calcrete A has higher carbonate content in the 250-500 μm fraction (64% versus 54%) and is moderately better sorted. Carbonate grains from both are abundantly comminuted, abraded and iron-stained; however, the Calcrete B sediment contained much larger fragments, up to 1.5 mm. Both samples contain disarticulated juvenile bivalves.

Discussion

The location of and fossil assemblages associated with the shell beds identified on Hindmarsh and Mundoo Islands in this research indicate the location of the LIG fossil

shoreline extending across both islands. Their preservation within the landscape indicates that the erosion, which was sufficiently strong to remove the LIG aeolianite between Hindmarsh Island and Mark Point, did not remove the fossil shoreline.

The large quantity of carbonate within DPI and DPII, even though partially reworked, indicates an environment of deposition near to the inner shelf and makes deposition during MIS 5a unlikely. The location of the field sites directly landward of the last interglacial shoreline suggests a beach environment. The preservation of the fossil shoreline and the low-lying dune at the Denver Property could be attributed to protection from erosion by the river provided by the northerly located aeolianite which was eroded.

The presence of two calcretes on northern Hindmarsh Island, across the Goolwa Channel from a confirmed MIS 7 deposit with superimposed calcrete, indicates that northern Hindmarsh Island is built by a succession of MIS 7 and MIS 5e Bridgewater Formation. The similarity in sediments beneath the calcretes and the reworked clasts of calcrete within Calcrete B where the two calcretes are in direct contact implies a reworked component to the younger Calcrete B sediment.

The record of the recurved spit and back-barrier estuarine deposition continues to the west of the modern Goolwa Channel in the Goolwa region.

4.3.3.3 Goolwa

The Goolwa region encompasses the area of the modern and last interglacial shoreline that extends west from the modern Goolwa channel to the base of the Mount Lofty Ranges, ~7 km distant. The presence of a palaeo-channel in Goolwa is recorded in a series of fossil assemblages found west of and parallel to the modern Goolwa shoreline. To the west of this feature is an aeolianite that an MIS 5e rocky shoreline facies on its seaward margin (Murray-Wallace *et al.*, 2010) indicates is last interglacial in age. To the southwest of this feature, the modern shoreline has formed a cliff within an aeolianite that TL analysis has indicated is MIS 5c in age. This discussion moves west through this landscape beginning with the Goolwa Channel deposits, followed by the MIS 5e aeolianite and a review of the MIS 5c aeolianite. The palaeo-Goolwa Channel record is

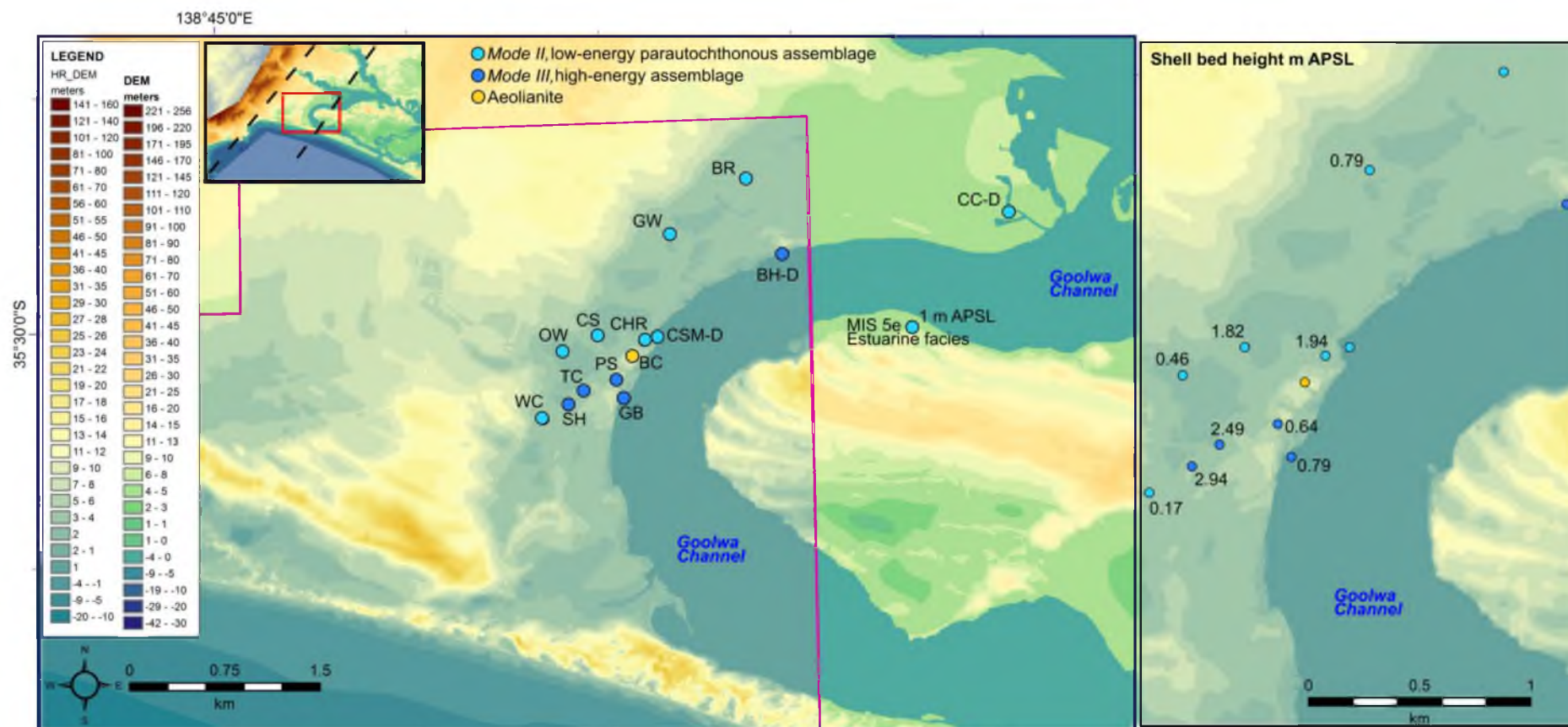


Figure 4.18: Goolwa Channel region and shell beds. From right to left field codes correspond to field sites described in text: CC-D: Currency Creek Dredge, BH-D: Birks Harbour Dredge, BR: Byrnes Road, GW: Goolwa Wetlands, CSM-D: Captain Sturt Marina Dredge, CHR: Chart House Railway, CS: Cadell Street, BC: Bridge Calcrete, PS: Porter Street, OW: Oval Wetlands, TC: Tennis Court, GB: Goolwa Boardwalk, SH: Stratco Hardware, WC: Wakool Court. The MIS 5e estuarine facies was identified by Murray-Wallace *et al.* (2010). Inset top left includes proposed locations of the Encounter Fault (Thomson and Horwitz, 1962; Twidale *et al.*, 1978; Gatehouse *et al.*, 1991; Rogers *et al.*, 1995). Image to the right provides height of shell beds as surveyed in this research. High-resolution DEM overlies low-resolution DEM; margin indicated by pink line. Note different scale of each DEM in the legend.

divided into three parts, Goolwa fossil assemblages, Chart House and the Stratco Hardware and Tennis Court field sites, which illustrate the different depositional environments represented in the record.

Goolwa Fossil assemblages

Two fossil assemblage types are found in Goolwa: *II, low-energy parautochthonous assemblage* and *III, high-energy assemblage* (Figure 4.18). The low-energy assemblages are flanked to the south and east, in the direction of the Hindmarsh Island recurved spit, by assemblages of high-energy deposition. Low-energy assemblages are composed primarily of the estuarine species *Spisula trigonella*, although other species are present (Table 4.2; Figure 4.18), with the fossil molluscs in a generally good state of preservation, taphonomic grades 3-6). The high-energy assemblages in comparison are composed of fossil molluscs with generally poor preservation, taphonomic grades 1-3. Unfortunately all of the sites have been disturbed (either by excavation or by dredging) minimising the conclusions that could be made regarding fossil assemblage characteristics. Disarticulated valves of the bivalve *Anadara trapezia*, generally considered an indicator of the last interglacial Glanville Formation in southern Australia, was identified within both a low energy fossil assemblage, Goolwa Wetlands (GW) and a high energy fossil assemblage, Stratco Hardware (SH).

The fossil assemblages are all located within low-lying topography, at or near surface level and were levelled to present height above sea level (Figure 4.18) except for the mollusc shell retrieved from dredged material, Birks Harbour Dredge (BH-D) and Captain Sturt Marina Dredge (CSM-D). The Cadell Street, Oval Wetlands and Wakool Court field sites had associated calcretes which assisted in constraining the height to which the shell beds were levelled.

The species content of the high-energy fossil assemblages at Birks Harbour Dredge (BH-D), Porter Street (PS) and Goolwa Boardwalk (GB) (Table 4.2) are indicative of a marine environment. Shell from the Porter Street and Goolwa Boardwalk locations was collected by Robert Bourman. The Porter Street shell (estuarine species *Spisula trigonella* and *Nassarius buchardi*) was collected ~150 m west of the Goolwa Channel from a depth of 4.2 m (Robert Bourman, personal communication 10 March 2014). The

shell is predominantly disarticulated whole and broken valves of *S. trigonella* in what appears to be a coarse beach sediment with rounded pebbles and comminuted fragments of *Brachiodontes* sp. and other unidentified gastropods. The shell bed was levelled, in this research, to 0.638 m APSL (Figure 4.18). The Goolwa Boardwalk shell (*Macra rufescens*, *Paphies elongata*, and *Brachiodontes rostratus*) was collected from the Goolwa Channel during a period of lowered water level and levelled to 0.792 m APSL (Robert Bourman, personal communication 23 February 2012).

The fossil assemblages found at Stratco Hardware (SH and SR), Tennis Court (TC) and Chart House (CHR) field sites (Figure 4.18) help to constrain the location of the palaeo-channel. The former two sites are indicative of a mouth environment, whereas the Chart House site transects the margin of a recurved spit deposit. The Chart House site is described first.

Chart House

The Goolwa Railway line cuts through a dune deposit situated to the west of the low-energy fossil assemblages and directly east of the Hindmarsh Island recurved spit (Figure 4.18). The railway cutting extends for ~120 m. The northern end of the cutting exposes a shell deposit and well-preserved planar bedding, both set in calcrete (Figure 4.19.1). The shell deposit, on the western side of the railway cutting, consists of articulated and disarticulated valves and fragments (Figure 4.19.1) of *S. trigonella*, *T. deltoidalis*, *M. rufescens*, *Katelsia rhytiphora*, *Irus crenatus* (or the variant *crebrelamellatus*), and possibly *Eumarcia fumigata*. Most of these species prefer mud and can be found in tidal inlets (Table 4.2). The shell extends from the northernmost extent of the cutting for ~2 m towards the south mostly on top of or within the top 30 cm of the calcrete.

The planar bedding on the eastern side of the railway cutting, exhibits a gentle undulation, with minor solution pipe development (Figure 4.19.1). To the south it transitions into a laminar calcrete overlying two units of indurated silty sand, Units 1 and 2 (Figure 4.19.2). Unit 1, a very pale brown (10YR 8/3) sand, grades upwards into a more consolidated very pale brown (10YR 8/4) sand. The sandy units extend for ~32 m along

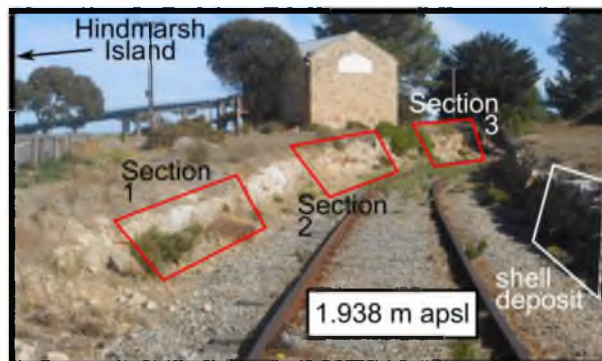
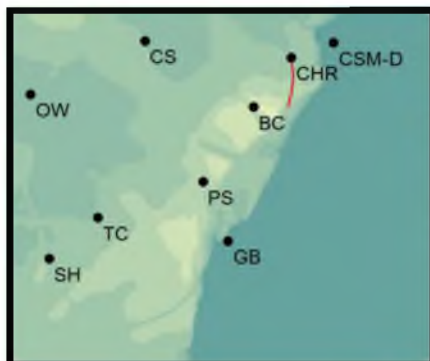
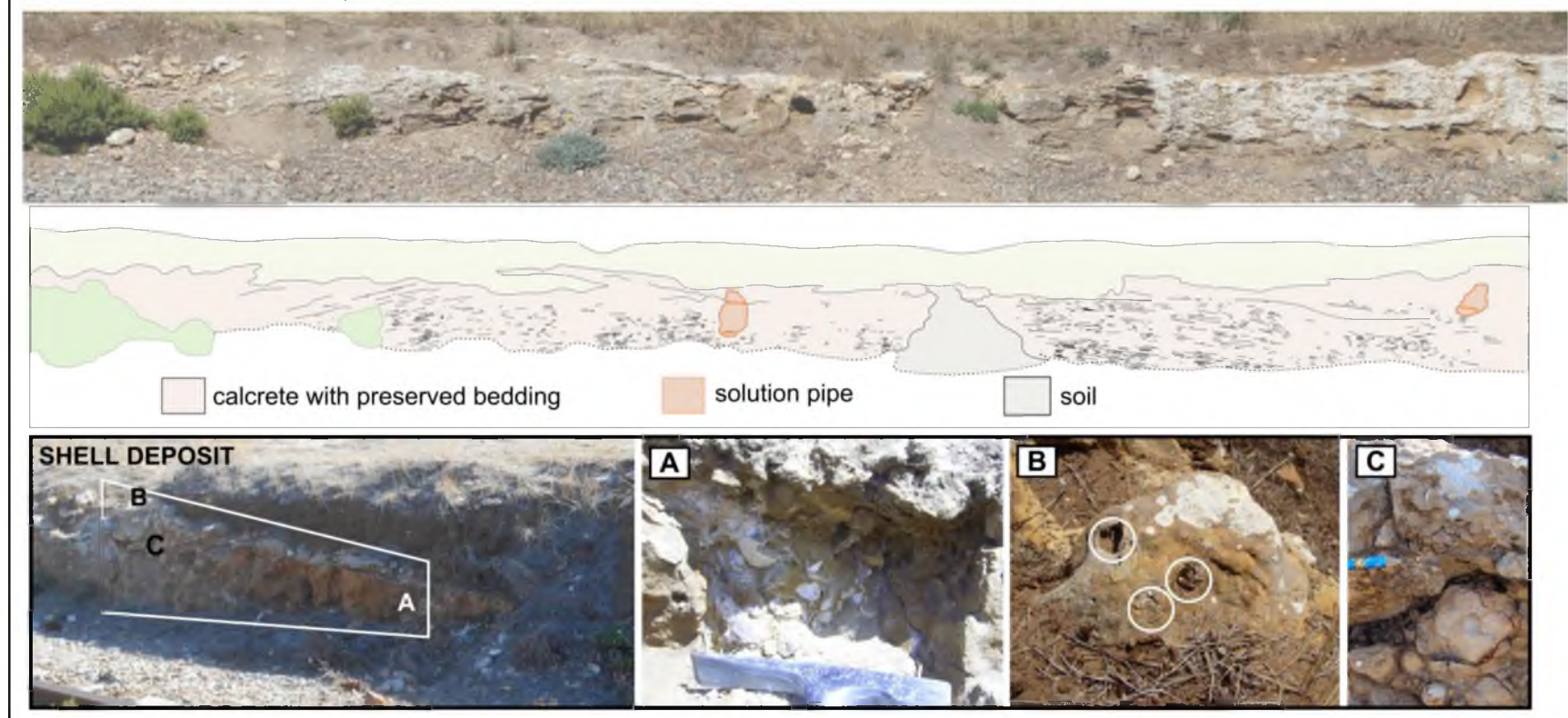
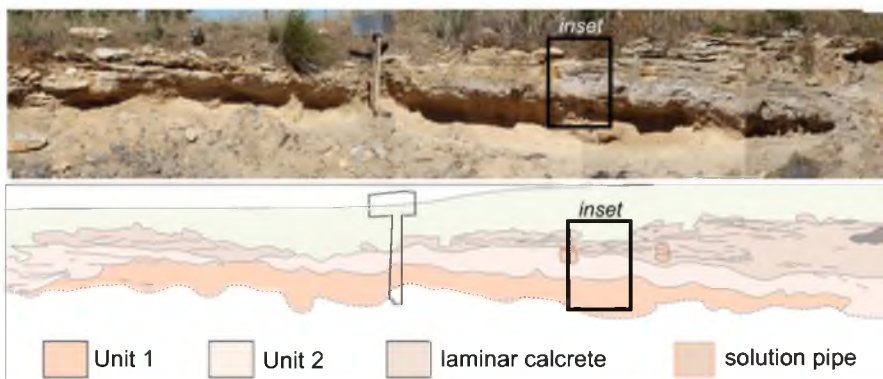


Figure 4.19.1: The three sections at Chart House. The top left image is a close-up of Figure 4.18 showing the location of CHR and extent (red line) in relation to surrounding field sites. Photograph to the right is of the railway exposure looking south. The railway cutting floor was levelled in front of the shell bed. Section 1 below shows the gently undulating preserved bedding opposite the shell deposit as well as photographs of the shell deposit. A) The most dense accumulation of shell. B) Articulated shells in life position at the top of the calcrete. C) Fragmented shell in calcrete.

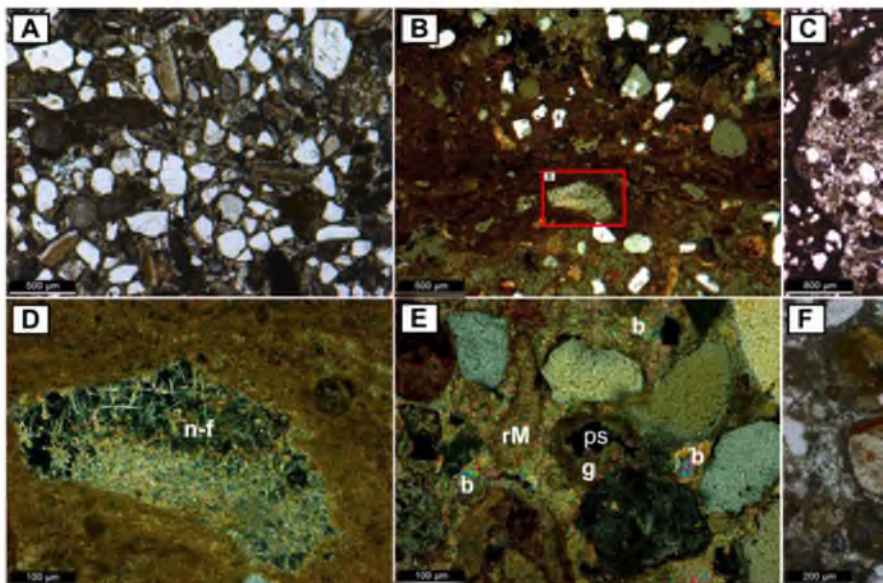
SECTION 1 and shell deposit

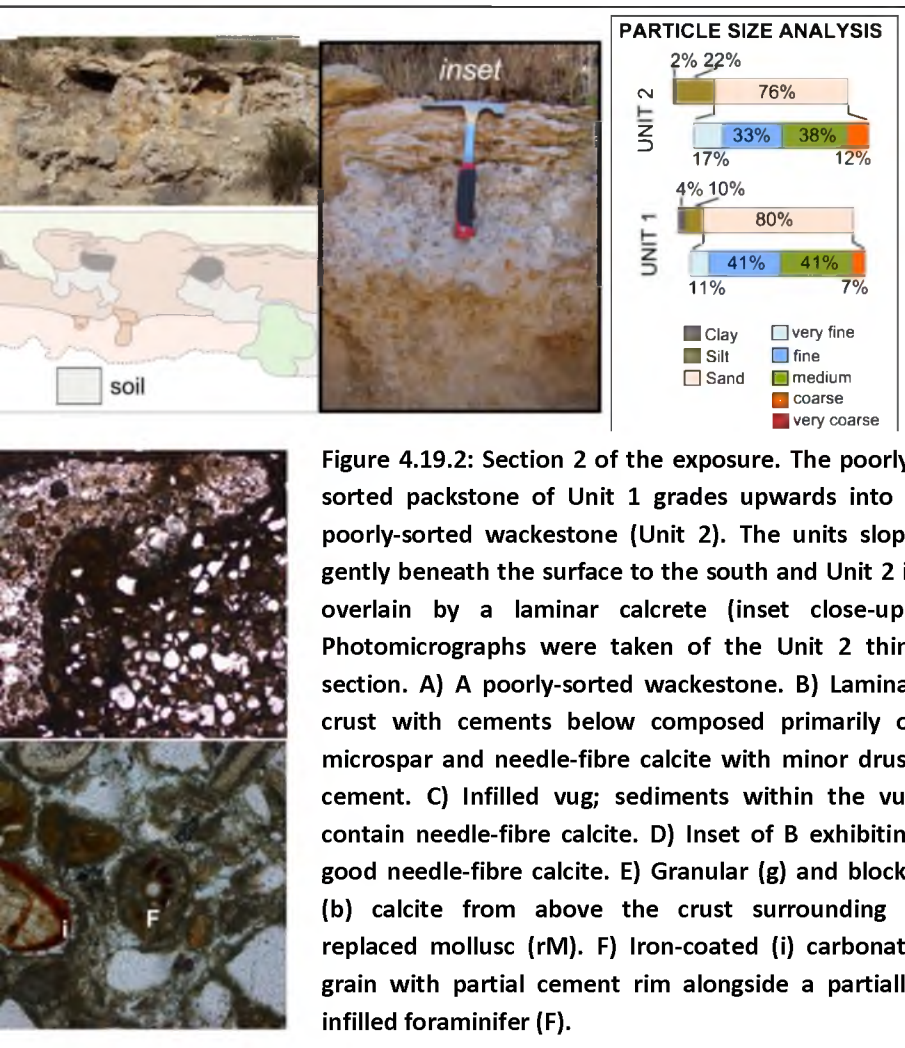


SECTION 2

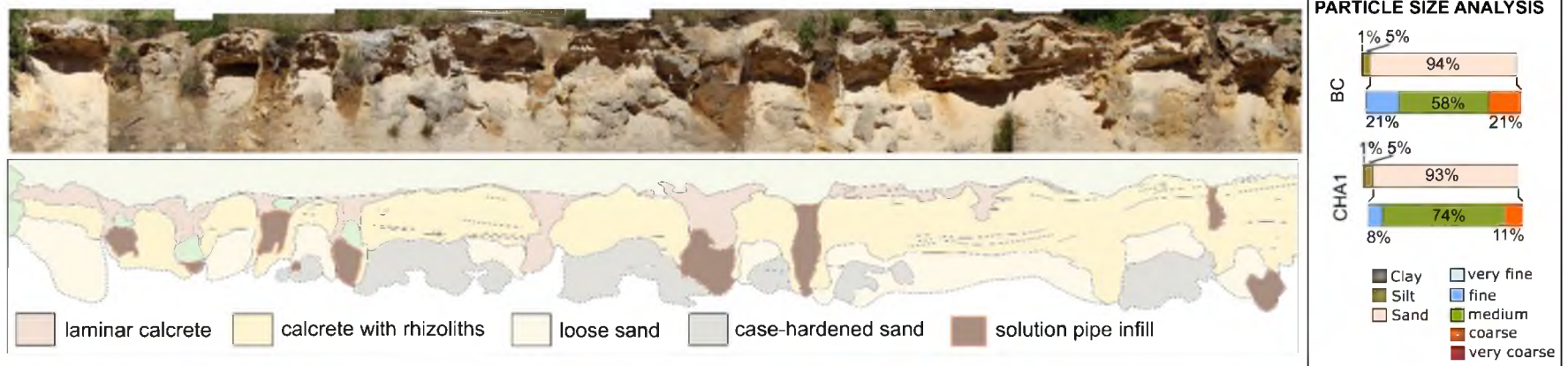


UNIT 2 PHOTOMICROGRAPHS





SECTION 3



CHA1 AND CHA2 PHOTOMICROGRAPHS

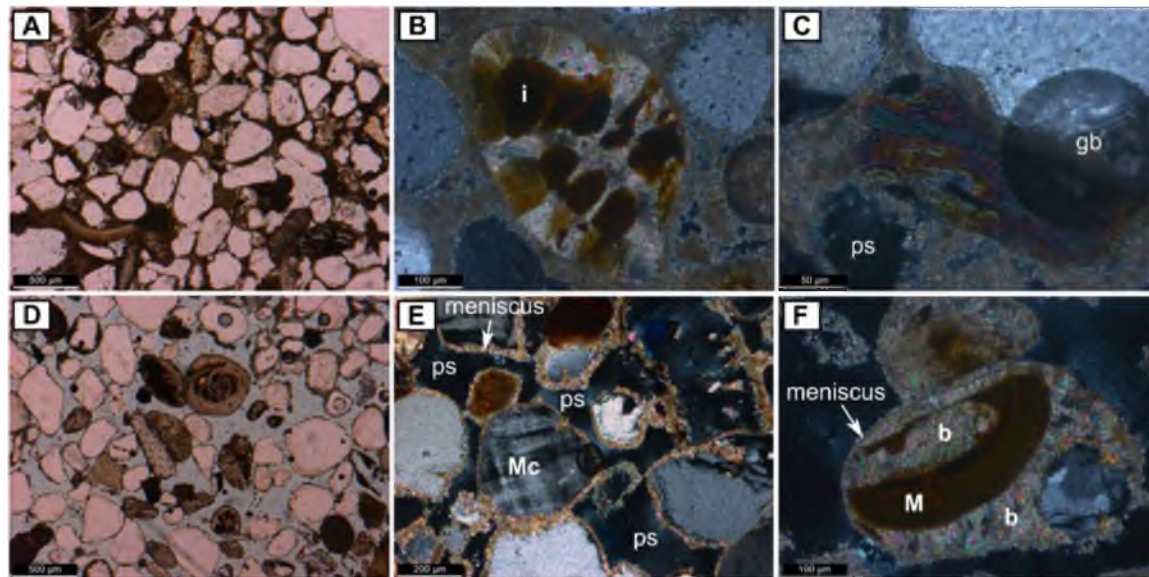


Figure 4.19.3: The exposure of solution pipe-slump sequence at the Chart House site. Note samples CHA1 and BC were analysed for particle size. Photomicrographs of CHA1 (A-C) and CHA2 (D-F): A) CHA1 is more compacted than CHA2 and has greater cement development (which may be a factor of packing). B) Foraminifer with infill of iron-stained micrite. C) Meniscus micrite having nearly filled the pore space (ps) surrounding an unknown mineral. 'gb' = gas bubble. D) CHA2 has a variable fauna content with mollusc, foraminifera and bryozoan present. E) Meniscus cements surrounding quartz, iron-stained carbonate grains, and a microcline (Mc) grain resulting in rounded pore spaces (ps). F) An intraclast of a mollusc and quartz grain and blocky cement with meniscus cement surrounding.

Table 4.7: Analytical results at Chart House site. The percentage of sand-sized particles is based on the total sand-size fraction and not the total sediment. Analysis by thin section or binocular analysis as noted.

SITE	CHART HOUSE	CHART HOUSE	CHART HOUSE	CHART HOUSE	BRIDGE CALCRETE
Field Code	CH Unit 1	CH Unit 2	CHA1	CHA2	BC
Calcrete	laminar	laminar	laminar, massive with rhizoliths	laminar, massive with rhizoliths	massive with rhizoliths
Calcrete thickness (m)	<0.10 - 1	<0.10 - 1	≤1.5	≤1.5	1
SEDIMENTS					
Depth of burial (m)	1.2	1	1.5	1.5	1.5
Munsell Colour	10YR 8/3 very pale brown	10YR 8/4 very pale brown	10YR 8/2 very pale brown	10YR 7/3 very pale brown	10YR 7/3 very pale brown
% CaCO ₃ (250-500 µm)	35	64	21	21	18
Heavy minerals	rare	present	present	present	sparse
Particle Size Analysis (Malvern Mastersizer)					
clay	4	2	1		1
silt	10	22	5		5
sand	86	77	94		93
very fine	11	17	0		0
fine	41	33	21		9
medium	41	38	58		80
coarse	7	12	21		12
very coarse	0	0	0		0
QUARTZ	binocular	thin section	thin section	thin section	binocular
Sorting	poor	poor	moderate-well	moderate	well
Particle size	very fine- coarse	very fine- coarse	fine-coarse	fine-coarse	medium-coarse
Roundness	coarse grains well rounded to subangular with rare angular grains; angularity increases with size decrease	angular to subrounded	abundantly subrounded	abundantly rounded	abundantly rounded/subro unded; commonly subangular
Surface texture	well rounded grains are abundantly frosted; otherwise vitreous lustre or frosted				abundantly clear or translucent, commonly frosted; commonly Fe- stained
CARBONATE	very common	abundant	sparse	common	common
Molluscs	≤1.5 mm angular fragments	subrounded fragments	subrounded - rounded fragments	rounded fragments	≤1.5 mm well rounded fragments
Foraminifer	rare	yes	yes	yes	very rare
Other fauna	very common	yes	yes	yes	common
Primary porosity		low	variable	high	
Cements		microspar, dogtooth, needle-fibre	micrite, microspar	micrite, meniscus microspar	

the exposure before sloping beneath the surface. The laminar calcrete grows in thickness and transitions into a thin laminar calcrete (at most 10 cm thick but generally ≤ 3 cm) overlying a hardened calcrete with extensive rhizolith development reaching a thickness up to 1.5 m (Figure 4.19.3). The calcrete exhibits extensive solution pipe development with the intervening spaces marked by loose very pale brown (10YR 8/2) sand slumping out from beneath the calcrete. The well-defined solution pipe-slump sequence continues for ~20 m before becoming more irregular. As with the northernmost extent of the exposure, the southern margin of the dune slopes down to the modern surface. The sand here is also very pale brown (10YR 7/3) and case-hardened. At its greatest height, midway through the cutting, the aeolian dune reaches 2.8 m on its eastern side. The aeolianite continues to rise to the west on the opposite side of the cutting and is capped at the crest by a 1 m thick similarly massive calcrete with extensive rhizolith development over free flowing very pale brown (10YR 7/3) sand identified as field site Bridge Calcrete (BC) (Figure 4.18).

Sediment samples were taken from Units 1 and 2, the indurated sand from within a slump structure (CHA1), the case-hardened sand at the southern end of the railway cutting (CHA2) and the loose sand beneath the Bridge Calcrete for either thin section or binocular analysis. A summary of the results is provided in Table 4.7. A sediment sample was also taken from the solution pipe infill material and is described in Section 4.3.7.

Unit 1, analysed under binocular microscope, is a poorly-sorted packstone (Dunham, 1962) or fossiliferous allochemical sandstone (Mount, 1985). Unit 2, with a higher carbonate content, was analysed by thin section and is a poorly-sorted wackstone (Dunham, 1962) or fossiliferous sandy allochemical limestone (Mount, 1985). The grains in Unit 1 are commonly coated by cement. Molluscs fragments are either whiter or iron-stained. The remaining fauna is composed of foraminifers (rare), bryozoan fragments (very common) and echinoid fragments (sparse), which are generally stained by iron and coated by calcite cement. Skeletal carbonate grains within Unit 2 are abundant with mollusc, foraminifers and algae very common. Very little primary porosity remains with most intergranular space filled by cement. Intraskelatal space is variably filled (Figure 4.19.2). Iron-coated grains and iron-filled skeletal pore space indicate the presence of

reworked grains. Cement types vary between microspar, blocky spar, dogtooth spar and needle-fibre calcite (Figure 4.19.2). The cement types indicate a meteoric-vadose, meteoric-phreatic or near-surface meteoric diagenetic environment. Sediments deposited in the mixing zone where phreatic and vadose environments meet, such as tidal flats, beaches and underlying shallow subsurface typically contain cements diagnostic of both environments (Flügel, 2010).

The aeolianites represented by samples CHA1, CHA2 and BC are moderately to well sorted allochemical limestones (Mount, 1985) (Table 4.7). Quartz grains within the three deposits are abundantly subrounded to rounded. The carbonate content is composed predominantly of rounded mollusc fragments. Sample CHA2 contains the most variable content with mollusc, foraminifers, bryozoans and echinoids recognised. Iron-stained carbonate grains in all three deposits indicate a reworked component. CHA1 exhibits more extensive development of microspar cement than CHA2 (Figure 4.19.3) and likely reflects sampling location from the base of a calcrete, comparatively CHA2 retains much of its primary porosity. Cements are composed of meniscus dogtooth spar except for the occasional grain ensconced within larger blocky cement crystals (Figure 4.19.3). However, smaller, meniscus type cements surrounding these grains suggest they may be reworked. The cements of CHA1 and CHA2 suggest diagenesis in a meteoric-vadose, meteoric-phreatic or near-surface meteoric zone consistent with Chart House Units 1 and 2 described above.

XRD analysis of all four samples shows Units 1 and 2 to have double the content of low Mg calcite (46% and 57% versus 19% and 24%) but also higher contents of high Mg calcite and aragonite, which is absent in both aeolian deposits. The difference in mineralogy is likely a reflection of the higher original content of carbonate skeletal grains within the sediments of Unit 1 and 2 over CHA1 and CHA2 and not necessarily a reflection of the amount of time elapsed since the initiation of diagenetic processes. The mineralogy is also typical of beach rock cements.

Stratco Hardware and Tennis Court

The Tennis Court (TC) site is located ~330 m nearly directly west from the modern Goolwa Channel and the high-energy fossil assemblage at Goolwa Boardwalk

(Figure 4.18). The exposure here consists of a low-lying calcrete reaching at most 1 m in height and extending for only a few metres in length. The calcrete transitions in that short space from pale with minor rhizolith development to a very thin (cm thick) laminar calcrete overlying an indurated very pale brown (10YR 8/4) fine to very coarse, poorly-sorted sand with comminuted shell fragments throughout (Figure 4.20). Large very coarse quartz grains are visible within hand samples. The shell bed is at least 30 cm thick, disappearing beneath the surface and has been levelled to 2.488 m APSL. The majority of mollusc shell is of taphonomic Grade 1 but includes Grades 2 and 3 disarticulated valves of a mixed species assemblage indicating a high energy, reworking zone. An extension of the shelly deposit (as inferred by similarity in both composition and height above sea level) appears in exposure again less than 160 m to the southwest at the Stratco Hardware site.

The Stratco Hardware site is bisected by a small berm which reaches a height of 1.75 m and is ~3 m wide. The western side of the berm has been excavated to form the corner of the Stratco Hardware yard (SH; Figure 4.20). The cutting exposes a pale brown (10YR 6/3) fine to very coarse, poorly-sorted indurated sand containing comminuted shell fragments. Large very coarse quartz grains are visible within hand samples. A concentrated layer of shell, ~30 cm thick which reaches to the base of the exposure, contains a large, fragmented (Grade 2) *Anadara trapezia* disarticulated valve. The top of the shell lens was levelled to 2.944 m APSL. The eastern side of the berm has been excavated for the railway line exposing a very pale brown (10YR 8/3) indurated fine to very coarse sand (also containing comminuted shell fragments) capped by a laminar calcrete and is indicated in Figure 4.20 as Stratco Railway (SR) for clarity. The railway cutting is at most 75 cm high with a thin (5-8 cm) shell layer at 50 cm depth of burial which extends along the bottom of the cutting for ~40 m (Figure 4.20). Small solution pipes (≤ 20 cm diameter) have developed. The floor of the railway cutting was levelled to 2.706 m APSL.

As with the Tennis Court site, the majority of mollusc shell within the exposures is not identifiable (Grade 1), however the few identified species indicate a mixed species assemblage. Thin sections were prepared from indurated sediment samples on both sides of the berm for comparison.

The thin section from within the Stratco Hardware yard (SH) was prepared from shelly sediment above the shell lens. Quartz grains consist of poorly-sorted fine to very coarse rounded to sub-angular grains (Figure 4.20). Carbonate is very common including molluscs, foraminifers, bryozoans and echinoid fragments; the largest carbonate grain is 9 mm in width. The sediment also includes multiple intraclasts, chert grains and composite quartz grains. Primary porosity is high. The cement type is meniscus spar. The sediment from within the railway cutting (SR) is very similar, however exhibiting a palaeo-surface marking a pause in deposition (Figure 4.20). The surface crust contains micrite cement marking the boundary between the two depositional facies. Microspar cement is in general further developed below the crust with minimal pore space preserved, the majority infilled by granular cement. The grains are also more closely spaced, perhaps reflecting compaction due to the weight of the overlying sediments. Pore space above the crust is greater with meniscus spar well-developed and granular cement moving into the intergranular space. Both sides of the crust contain large mollusc fragments, intraclasts, chert grains, feldspars and iron-stained grains. The thin sections confirm the environment of deposition as a high energy zone of reworking and the subsequent zone of diagenesis as meteoric-vadose, meteoric-phreatic or near-surface meteoric zone.

The sediments at the Tennis Court and Stratco Hardware sites are classified as grainstones (Dunham, 1962) and fossiliferous allochemical sandstones (Mount, 1985). The visual appearance of the shell lenses is reminiscent of the modern Murray Mouth flood tidal delta where comminuted shell fragments and whole disarticulated valves are dispersed amongst a poorly-sorted sand with very coarse quartz grains. The position of the two sites seaward of the recurved spit deposits in Goolwa assist in this conclusion.

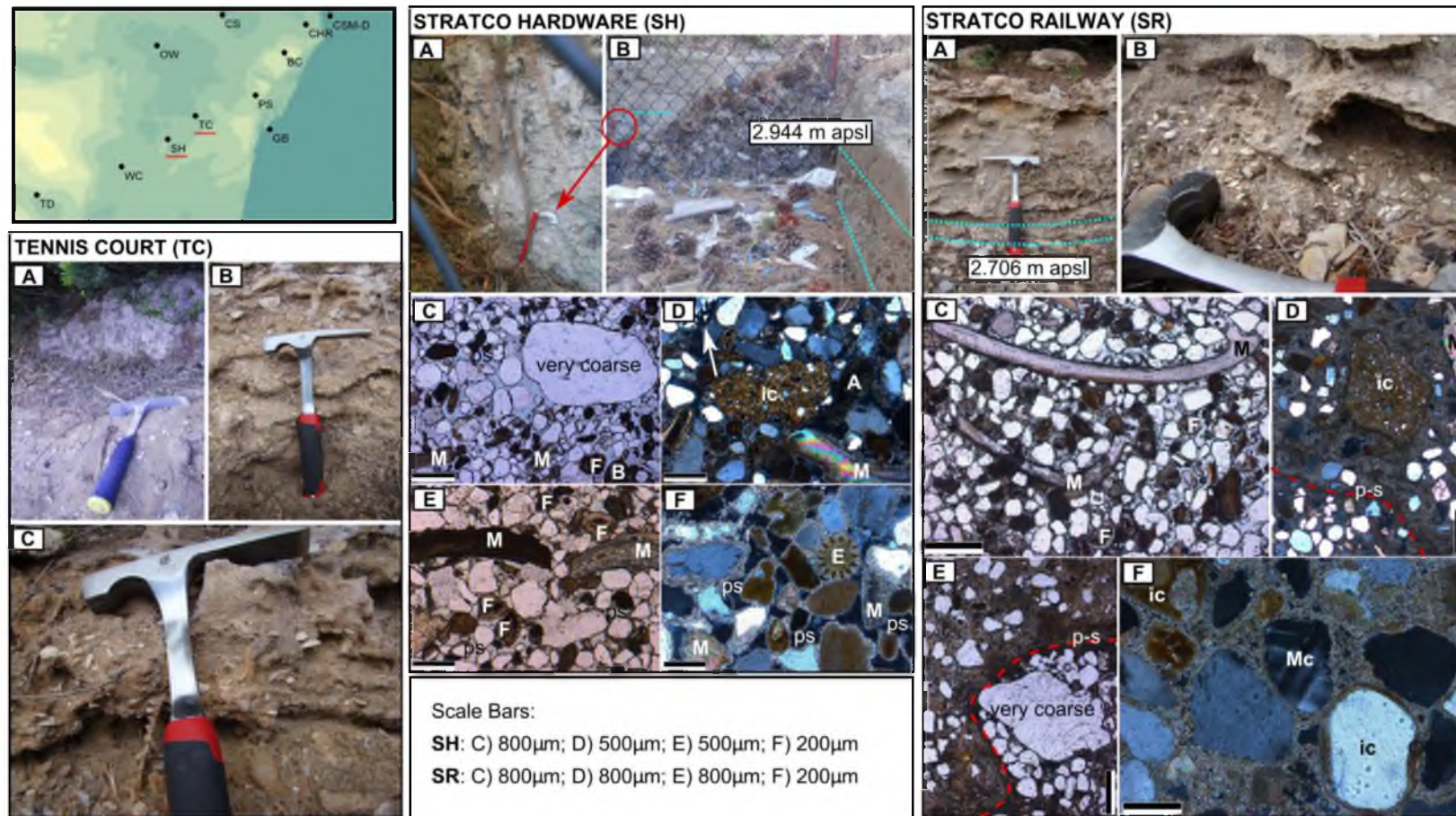


Figure 4.20: Tennis Court and Stratco Hardware sediments. Tennis Court: A) Pale calcrete with minor rhizolith development transitions to a thin laminar calcrete (B) overlying fossiliferous sandy sediment (C). Stratco Hardware: A) and B) Exposure of a shelly lens (dashed line) which contains *A. trapezia* (pointed to by arrow). Photomicrographs: C) A very coarse quartz grain. D) Intraclast (ic) of very fine sediment. Arrow points to a composite quartz grain. E) Large mollusc (M) fragments and foraminifera (F). F) Meniscus spar coats grains with high primary intragranular porosity. Stratco Railway: A) and B) A 40 m long shelly lens is exposed at the base of the cutting. C) Large mollusc (M) fragments and foraminifers (F). D) Intraclast (ic) of very fine sediment located just above the base of the palaeo-surface (p-s). E) A very coarse quartz grain below the palaeo-surface. F) Microcline (Mc) and additional intraclasts (ic). Intergranular pore space mostly filled by granular spar.

Goolwa West – MIS 5e aeolianite

The aeolianite to the west of the field sites described so far trends in a northwest to southeast direction for ~3 km reaching a maximum width of ~1.3 km in north-south transect at its eastern extent. On its seaward margin ~0.75 km inland from the modern coastline the aeolianite is interbedded with a raised rocky shoreline deposit at Traegers Quarry (TQ, Figure 4.22), identified and determined by AAR mollusc shell and whole-rock analyses to be MIS 5e in age. The aeolianite retains similar features visible in the DEM to the prograding shoreline on western Hindmarsh Island and is surrounded by low-lying topography. Mollusc shell has been found in the low-lying region to the north (Robert Bourman, personal communication 8 November 2012) but was not located in the course of this research. A low-lying but inaccessible calcrete was identified to the south (TSP) and additional calcretes were identified at Heinicke Avenue (HA) and the Drain (TD) (Figures 4.21 and 4.22).

The Heinicke Avenue and the Drain calcretes are seaward of the aforementioned channel deposits and potentially overlie either channel or beach deposits. The Heinicke Avenue calcrete is exposed in excavated wetland ~550 m south of Wakool Court. The calcrete is white and marly; no shell bed was located and the only shell found was a valve of *S. trigonella* on the surface (Figure 4.22). The Drain is located approximately 390 m to the southwest of Wakool Court. The calcrete is pale yellow (2.5Y 8/2) and finely laminated with extensive solution pipe development. The diameter of exposed solution pipes range from 25 cm to 70 cm. The calcrete has been exposed by a drain which flows off of a slope of the MIS 5e aeolianite to the north suggesting this calcrete is the older feature. However, additional work is needed to confirm the relationship of the two deposits. Directly above the exposed calcrete is a 50 cm thick unit of yellowish red (5YR 4/6) sandy silt in turn overlain by a recent very pale brown (10YR 7/3) siliceous sand which has been stabilised by vegetation. These sands are described in section 4.3.7.

The low-lying topography surrounding the MIS 5e aeolianite to the north and west suggest the potential for an estuarine/lagoon deposit to the north and outlet to Encounter Bay to the west, however further research is needed in the area.

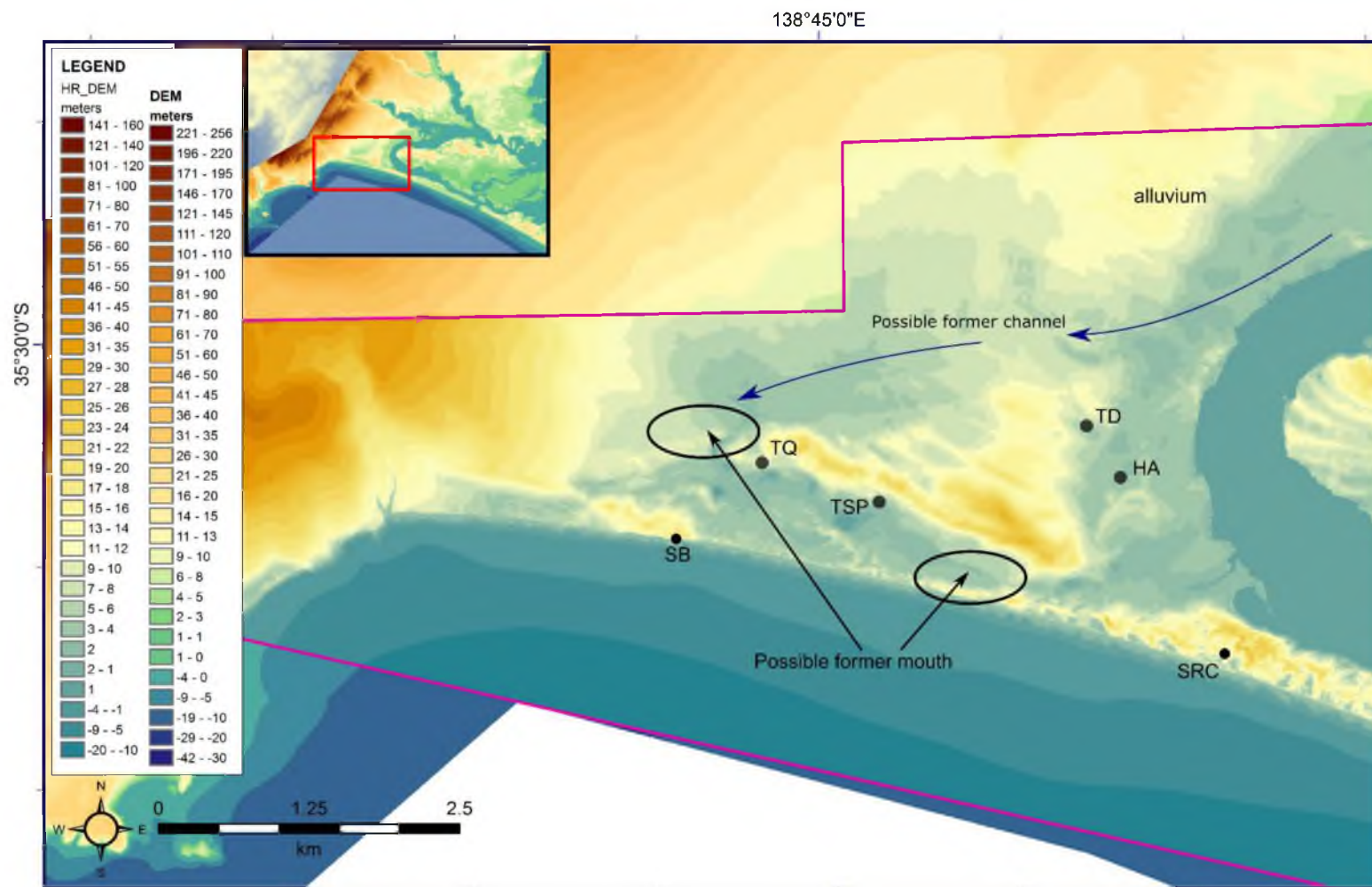
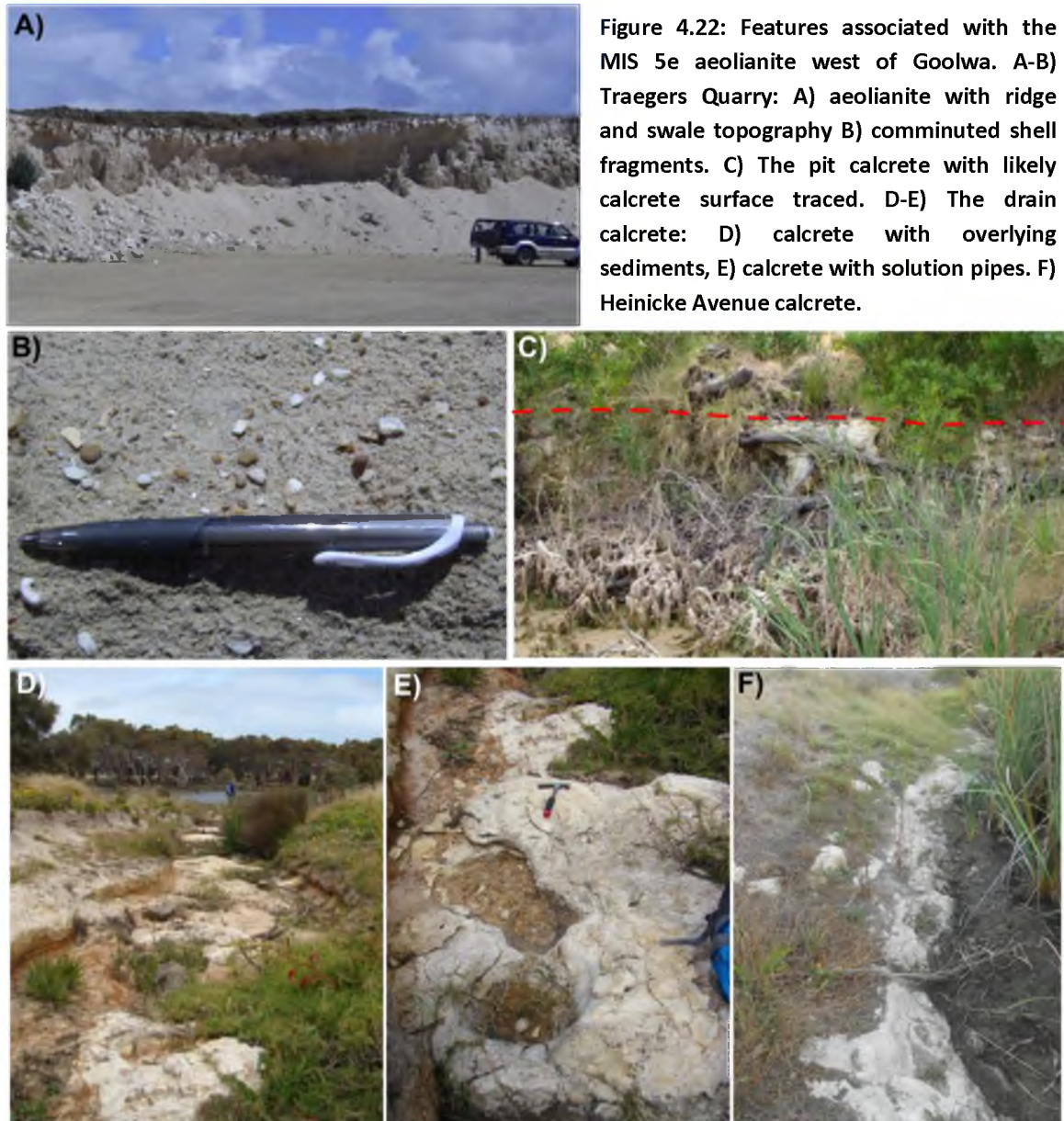


Figure 4.21: Additional sites west of Goolwa. The more seaward location of a possible former mouth was proposed by De Mooy (1959) and may be related to the MIS 5c highstand. Field codes correspond to field sites discussed in text: Surfer Beach (SB), Traegers Quarry (TQ), low lying calcrete (TSP) The Drain (TD), Henicke Avenue (HA) and Sir Richard Peninsula calcrete inlier (SRC).



MIS 5c barrier

Directly to the southwest of the MIS 5e aeolianite west of Goolwa is the Surfer Beach dune (Figure 4.21), an aeolian remnant of the MIS 5c highstand as suggested by a TL age of 105 ± 5 ka (Murray-Wallace *et al.*, 2010). The MIS 5c highstand on the Coorong Coastal Plain, as indicated by the sea-level record at Robe to the southeast, was 9 m BPSL and the aeolianite at Surfer Beach is the first recorded evidence of the interstadial within the study area warranting further description. An additional calcrete was found as an inlier to the Sir Richard Peninsula ~ 4.5 km to the east. The position of this calcrete

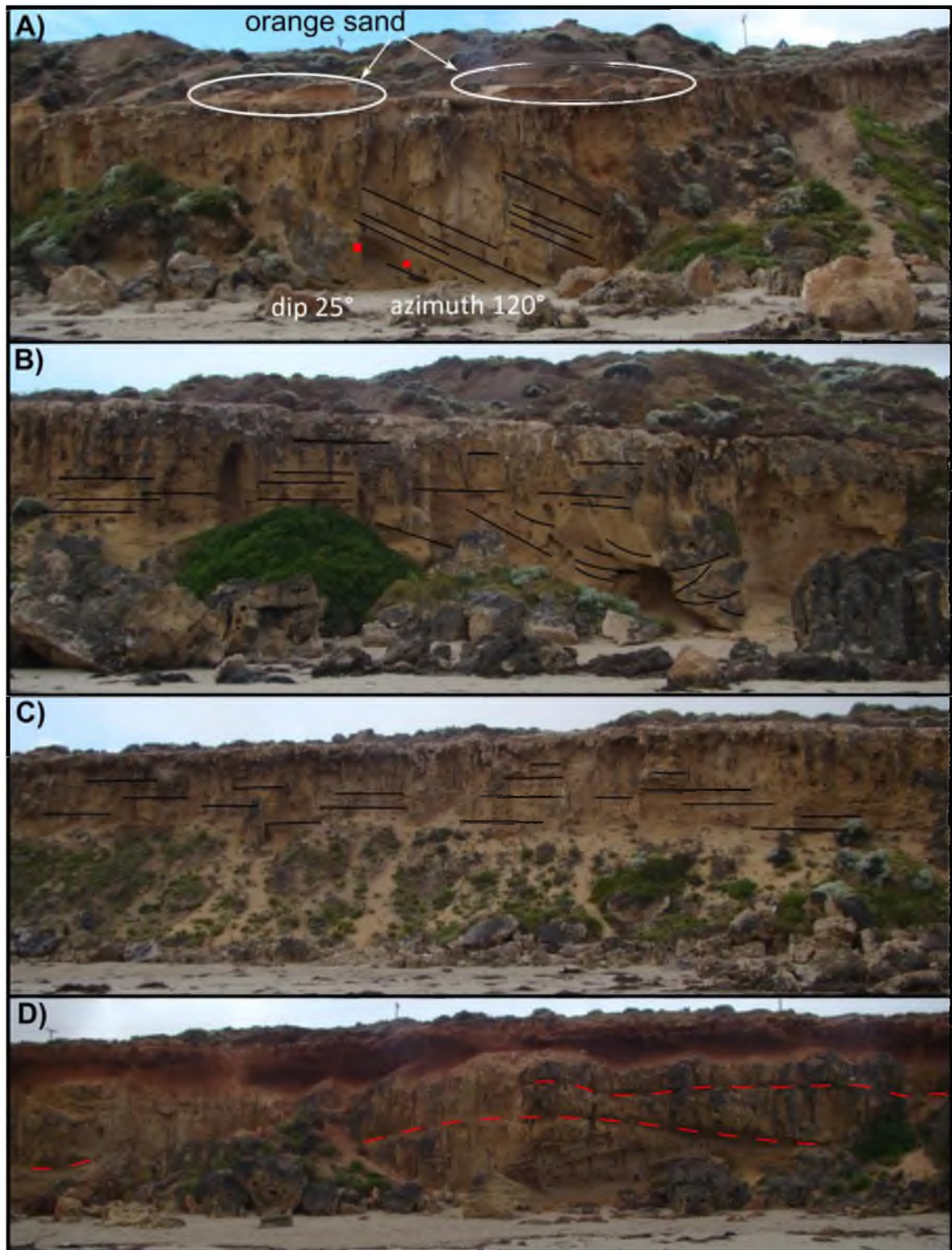


Figure 4.23: Features of the Surfer Beach dune from east to west. A) Location of TL sample (red circle, Murray-Wallace *et al.*, 2010) and sediment sample (red square). Dune here reaches 8 m height. The dune bedding dips in a northeast direction with migration to the northeast. Orange calcrete-capped sand overlies the MIS 5c dune in the west. The entire complex is draped by dark brown sands. B) Bedding features within the dune reveal former interdune swales. C) The dune is predominantly composed horizontal planar bedding indicating the exposure is of the dune crest. D) To the west reactivation surfaces (red dash lines) are visible. The dune in the west also contains a red sand unit beneath the calcrete reminiscent of *terrs rossa* soil.

seaward of the MIS 5e shoreline sedimentary succession is indicative of later deposition most likely in association with the Surfer Beach aeolianite. Both features are described here.

The aeolianite at Surfer Beach forms a 500 m long cliff set back 20-25 m from the reach of high tide. Slightly west (~1.3 km) of Surfer Beach at Middleton, the beach has been subject to nearly 200 m of erosion since 1900 that has exposed distal alluvial fan successions. Because erosion of the coastline appears to be localised in the Middleton-Surfer Beach region, Bourman *et al.* (2000) concluded that the main cause of erosion may be related to tectonic subsidence with a slight sea-level rise being as a minor contributing factor. Sand has accumulated at the base of Surfer Beach only where it is set back farthest from the beach; the remainder of the beach is still likely subject to erosion.

The Surfer Beach aeolianite is capped by a calcrete of variable thickness (although relatively thin, <1 m) and type (massive and rubbly). Rhizolith and solution pipe development is evident throughout the length of the dune. The eastern end of the exposure is overlain by a younger orange aeolian sand with a very thin (<10 cm) calcrete crust (Figure 4.23). The entire complex is draped by dark brown sands, which have been stabilised by vegetation. Reactivation surfaces are exposed at the western end of the cliff (Figure 4.23). The dune also contains a unit of dark red sediment (reminiscent of a *terra rossa* soil) capped by a thin indistinguishable calcrete. This sediment was inaccessible and a sample was not taken. Much of the central portion of the cliff is obscured by loose sand, which has accumulated at the base of the cliff (Figure 4.23). The base of the exposure is littered with large blocks of aeolianite (≤ 6 m, long axis) and calcrete that have fallen from the face of the cliff. A sediment sample was taken from above the TL auger hole of Murray Wallace *et al.* (2010) at a location where the dune reaches 8 m in height (Figure 4.23). The sand is very pale brown (10YR 7/4) and contains 72% CaCO₃. The bedding here has a dip of 25° and azimuth of 120°. The dune has a northwest to southeast orientation (indicating a landward migration to the northeast) which parallels the MIS 5e recurved spit located approximately 1 km inland.

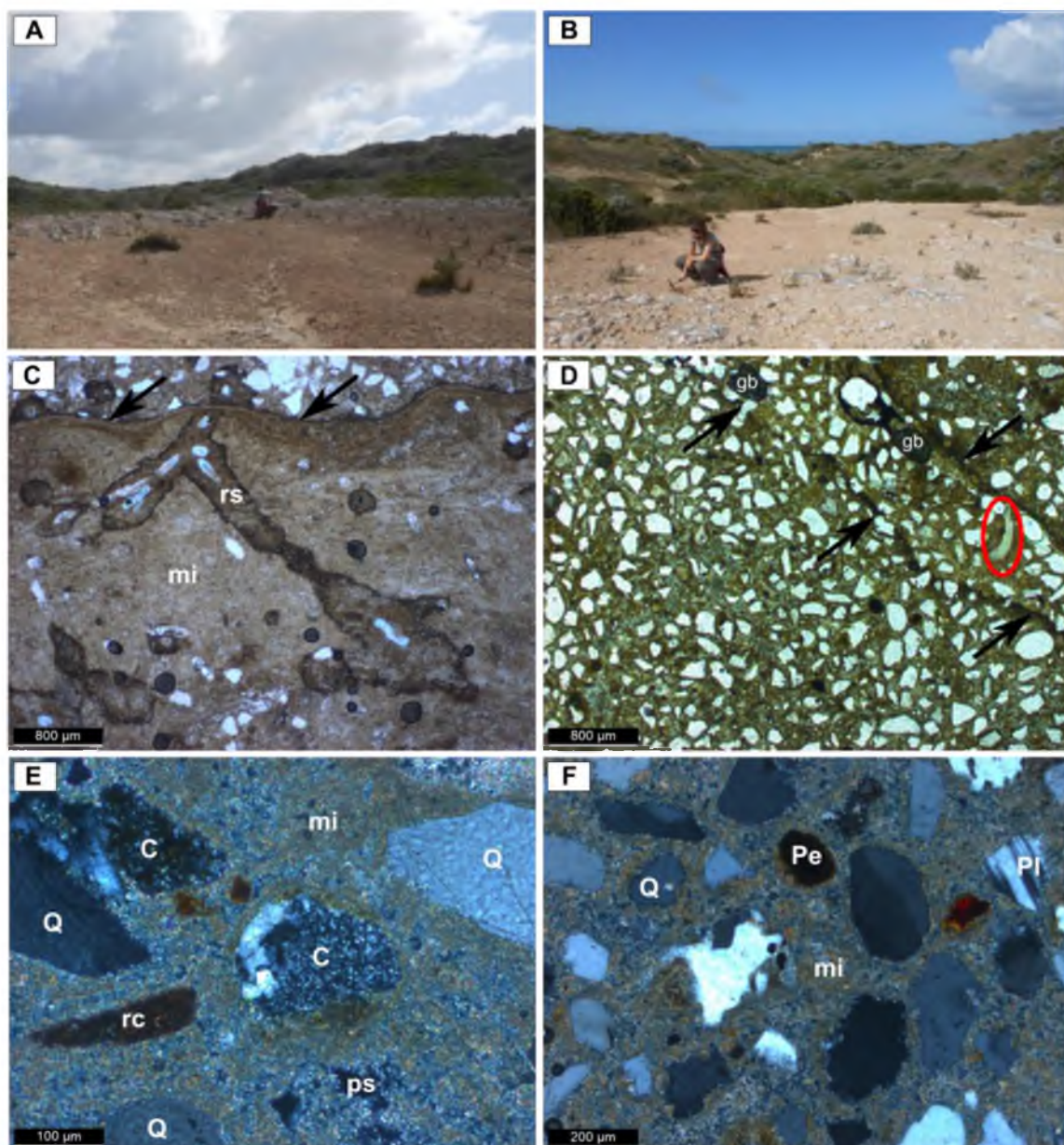


Figure 4.24: Sir Richard Peninsula calcrete inlier and photomicrographs. Photographs look across the calcrete inlier: A) upslope and inland, B) downslope and seaward. C) Laminated crust (indicated by arrows) containing rhizolith structure partially infilled by micrite (mi). The palaeosurface was formed by accretion as indicated by the lack of quartz grains within the crust. Overlying sediment was deposited following dune reactivation. D) Micritic sandstone with a single mollusc fragment circled in red. Black arrows point to the margin of a solution channel, which cuts across quartz grains. E) and F) illustrate different grain types identified: chert grains (C), the central grain containing micro- and macro-crystalline quartz, replaced carbonate grain (rc), peloid (Pe) and plagioclase (Pl), one of four identified within the thin section.

The calcrete inlier within Sir Richard Peninsula was located during this research on the proximal end of the peninsula, seaward of the modern crest (Figure 4.21). The rubbly very pale brown (10YR 8/2) calcrete is exposed in a swale of the modern dunes

and is roughly 30 m in length with a variable width averaging approximately 7 m (Figure 4.24). As there is no cutting within the calcrete a whole rock sample was taken from beneath the calcrete by prying loose a piece of the overlying calcrete of which a sample was also taken. The sandy sediment beneath the calcrete is light yellowish brown (10 YR 6/4) with a CaCO₃ content of 8%. The calcrete itself is composed predominantly of fine-grained angular to sub-angular quartz grains and micrite cement with very little original porosity (Figure 4.24) and is considered a micritic (quartz arenite) sandstone (Mount, 1985).

Discussion

The Goolwa region contains a complex depositional record. Low-lying topography, fossil assemblages, recurved spit and deltaic sediments outline the location for a palaeo-Goolwa Channel and river mouth slightly to the west of its current location, which was established by the end of the last glacial maximum. The migration of the channel may reflect the change in base level as sea level began to recede following the MIS 5e highstand. The channel potentially extended farther west earlier in the interglacial to debouch adjacent to the Mount Lofty Ranges.

A remnant of the MIS 5c barrier at Surfer Beach indicates dune migration to the northeast with a potential record of glacial period sedimentation and pedogenic development preserved at the crest of the aeolianite. To the east a calcrete inlier of Sir Richard Peninsula is of the same age. The lack of MIS 5c barrier connecting the two sedimentary successions could be due to shoreline erosion during the Holocene marine transgression. Alternatively, de Mooy (1959) has suggested the position of a former river mouth in the low-lying region between the two barrier deposits and seaward of the MIS 5e aeolianite west of Goolwa (Figure 4.21) which would explain a lack of barrier between the Surfer Beach aeolianite and the Sir Richard Calcrete inlier.

4.3.3.4 Fleurieu Peninsula

The record of the last interglacial highstand in the Mount Lofty Ranges is preserved within the south and southeast facing bedrock valleys of the Fleurieu Peninsula where sediments of the Bridgewater and Glanville Formations are preserved (Figure 4.25). Mollusc shell retrieved from the Glanville Formation at Victor Harbor and

Watsons Gap have been previously analysed by shell indicating deposition during MIS 5e (Bourman *et al.*, 2000; Murray-Wallace *et al.*, 2010). The sites were also levelled in the previous research to 6 m and 10 m APSL, respectively, illustrating the general trend of uplift away from the Murray Mouth zone of subsidence. The minimal record of last interglacial sedimentary successions warranted the return to previously analysed field sites to provide further description of the sediments and a better understanding of the regional context in which they were deposited. The Knights Beach field site, which is indicated in Figure 4.25, as a composite feature is described later in this chapter (section 4.3.5.2).

Watson Gap

The Watson Gap (WG) field site is located within a railway cutting less than 100 m from the modern shoreline. The cutting is on the seaward side of a topographic high which rises to a height of more than 20 m, separating the modern beach from an unnamed basin (Figure 4.26a). Shell-rich sediment within the cutting has been previously levelled to 10 m APSL (Bourman *et al.*, 2000). A mixed species assemblage of both estuarine (including *Anadara trapezia*) and marine species (Table 4.2) is found in association with angular quartz pebbles and rounded sedimentary rocks (Figure 4.26c) in brown sandy sediment indicating a reworked assemblage, however construction of the railway cutting would have disturbed the original nature of the succession. The shell ranges between taphonomic Grades 1 and 3. At least some of the *Donax deltoides* found at the base of the railway cutting appear to have come from a *Donax* midden located upslope. *Turbo* sp. opercula retrieved from the site have also been subject to burning (Katherine Szabo, personal communication 15 April 2014).

The shelly sediment on the southern side of the railway cutting is overlain by a calcrete-capped aeolianite exposed ~4 m above the floor of the cutting, which is in turn overlain by ~2m of modern sand, soil and vegetation. The calcrete shows massive and blocky morphology and is ≤ 0.75 m thick. The aeolian sand beneath the calcrete is loosely consolidated and very pale brown (10YR 7/4) (Figure 4.26b). The contact between the aeolianite and underlying shelly sediments is obscured by vegetation and the movement of sand downslope but the two successions indicate a transition from a

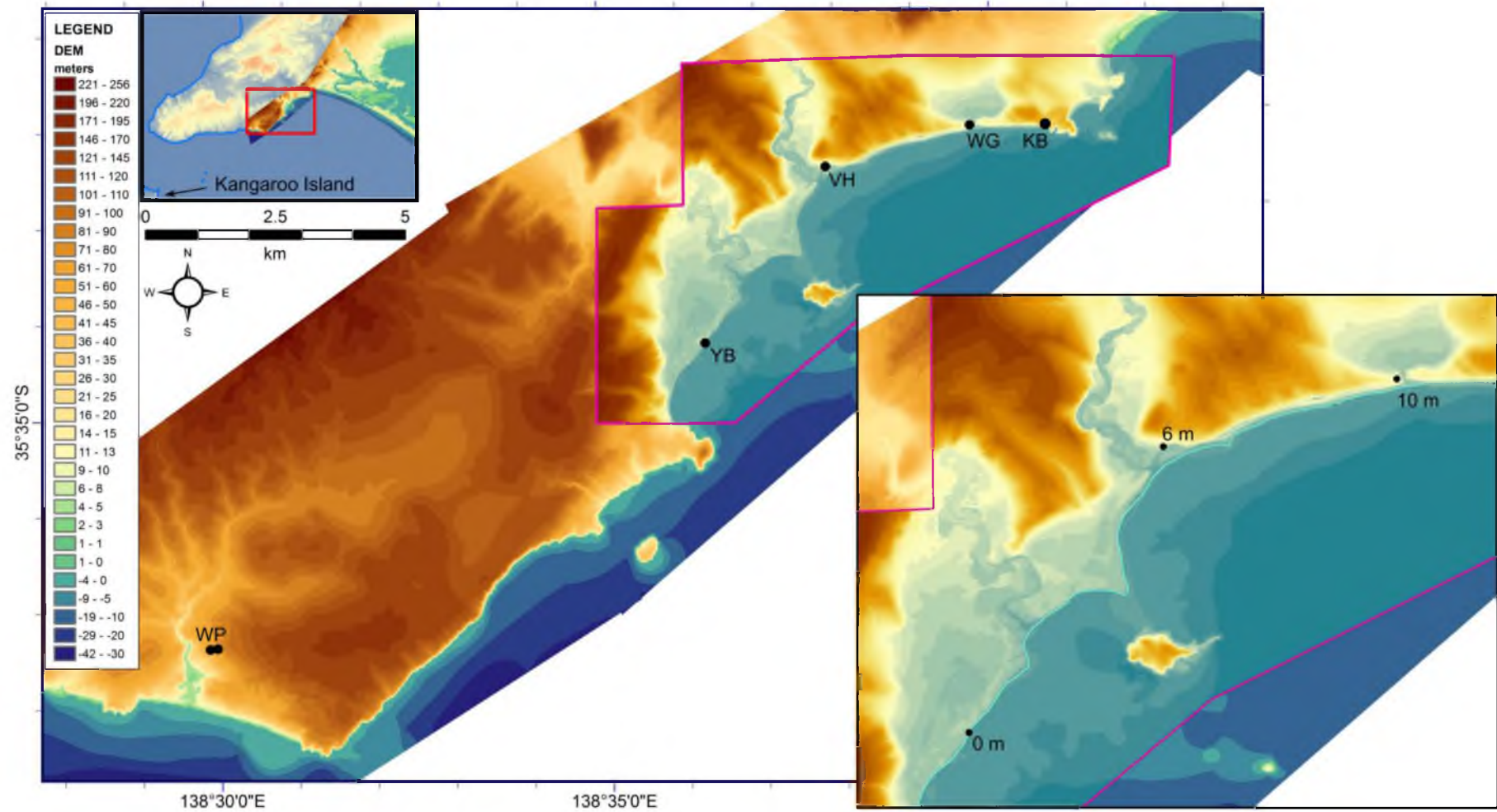


Figure 4.25: Fleurieu Peninsula sites are located on differently orientated coastlines which affect deposition; the offshore Kangaroo Island would also provide some protection from dominant swell. Field sites from east to west are: Waitpinga (WP), Yilki Beach (YB), Victor Harbor (VH), Watsons Gap (WG) and Knights Beach (KB). The close-up inset provides the heights above present sea-level of the latter field sites. Knights Beach is described in Section 4.3.5.2.

fluvial environment to a terrestrial one reflecting a change in base level. This suggests that the aeolianite may be related to the later MIS 5c interstadial. Sand from beneath the calcrete was taken for AAR analysis but the sediment in which the shell deposit is found is too altered for adequate analyses and was not sampled.

Victor Harbor

The Victor Harbor (Field Code VH) field site is located ~2.8 km to the southwest of Watson Gap. The two field sites are separated by bedrock. The Victor Harbor site is on the margin of the Hindmarsh River valley and also within a railway cutting (~2 m high) which has been levelled to 6 m APSL (Bourman *et al.*, 2000). The cutting is ~190 m from the beach and separated from it by a modern dune and small lagoon. This site also contains a fossil assemblage (Grades 1-3) with large angular quartz pebbles in brown sandy sediment (Figure 4.26d, e). The fossil assemblage is predominantly estuarine (including *Anadara trapezia*), but also includes *Ostrea* shell (Table 4.2). This site does not contain a calcrete; however, calcrete nodules are found within the deposit and could be reworked into the deposit.

Samples were not taken of the sediment associated with fossil assemblages at Watson Gap or Victor Harbor as it was deemed that the sediments were too altered by construction of the railway line.

Yilki

Farther to the southwest (~4 km from the beach at Victor Harbor) a highly consolidated carbonate sediment extends from Yilki beach (YB) through the intertidal zone and into the subtidal zone (Figure 4.25) to form a Holocene shore platform (Figure 4.26f). The platform is characterised by numerous solution pipes. Because the margins of the pipes are well-indurated and more resistant to erosion than the surrounding sediments, many of the solution pipes appear as stand-alone atoll-like structures (Figure 4.26g). A sample was taken from the platform at sea-level during low tide. The pale yellow (2.5Y 7/3) sand was coated in modern fauna and flora and contained recent boreholes from burrowing organisms. Thin section analysis shows a poorly-sorted

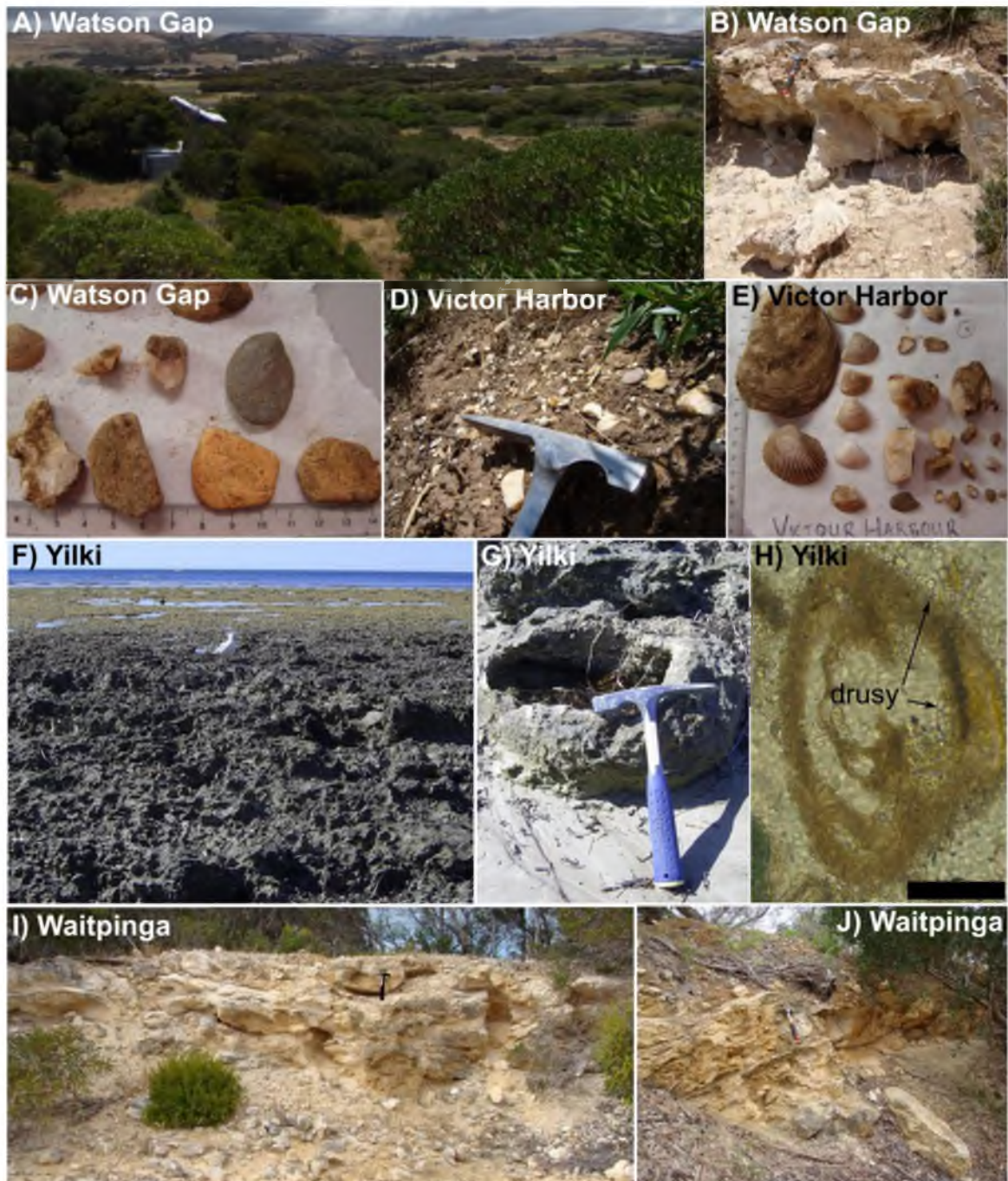


Figure 4.26: Photographs from Fleurieu Peninsula. A-C) Watson Gap: A) the unnamed basin landward of the Watson Gap Railway Cutting with Mount Lofty Ranges in the background. B) Calcrete at Watson Gap with free flowing sand overlies the fossil assemblage which contains angular quartz grains and rounded sedimentary rocks (C). D-E) Victor Harbor hosts a similar assemblage. F-H) Yilki: F) The Holocene shore platform exposed at low tide. G) Solution pipes form atoll-like structures within the platform. H) Micrite and drusy cement with a lack of orientation characterise the sediment surrounding a miliolid foraminifer, the wall of which has been completely micritised. I-J) Waitpinga calcrete: I) massive and blocky and subject to pedogenesis. J) The calcrete preserves steep (23°) bedding dipping to the north-northwest.

packstone (Dunham, 1962) with abundant carbonate content represented by diverse types of fauna; iron-staining of grains is common. Mollusc fragments are less than 1 mm. Quartz grains range from fine to coarse and angular to sub-rounded. Grains exhibit point contacts and primary porosity is moderate. The grains have a thin rim of micrite from which sparry calcite has begun to grow, infilling the available pore space. The infilling cements are drusy in behaviour with crystal size increasing towards the centre of the void. The lack of orientation and in places, lack of substrate control, micritic cement fringes and drusy cement indicate diagenesis in the near surface meteoric environment.

Waitpinga

Nearly 10 km to the southeast of Yilki, the coastline of Fleurieu Peninsula turns sharply to the west exposing the coastline to southern swell and winds allowing the accretion of aeolian dunes in bedrock valleys (Figure 4.25). Waitpinga Beach is one such location where multiple stages of dune formation have accreted. Aeolianites at Waitpinga, set back from the modern beach 700 m and 1.4 km, were analysed by AAR whole-rock and correlated to MIS 5c and MIS 5e, respectively (Murray-Wallace *et al.*, 2010), although the latter determination was made on stratigraphic interpretation as the whole-rock results were poor. The modern aeolianite at Waitpinga has encroached inland and drapes over the MIS 5c aeolianite.

The MIS 5e aeolianite is set farther back in the valley. The crest of the dune (WP) has been bisected by a road cutting trending roughly west-east along the strike of the dune (076°) exposing the calcrete which caps the deposit. The calcrete on the southern side of the cutting is variable in appearance (Figure 4.26i): massive and blocky with laminations and overlain by nodular calcrete. The calcrete reaches a maximum thickness of 1.55 m extending to the base of the cutting. The road surface is composed of calcrete. The northern side of the cutting exposes steep bedding (23°), dipping to the north-northwest (Figure 4.26j). The extensive pedogenesis of the displayed by the sediment and the poor AAR whole-rock results of previous analyses indicate that this aeolianite may pre-date MIS 5e.

Discussion

The preservation of sedimentary successions within bedrock valleys on Fleurieu Peninsula is influenced by the orientation of the coastline and the local neotectonics. Waitpinga Valley, fully exposed to the southern swell and winds has completely infilled with aeolianite deposited over successive stages. In contrast, the bedrock valleys which contain Yilki Beach, Victor Harbor and Watsons Gap sedimentary successions have not been infilled.

Victor Harbor and Watson Gap both retain evidence of an estuarine environment. The large intraclasts of quartz and other rock types were likely introduced to the system by fluvial runoff from the Mount Lofty Ranges which would have contributed to the reworked nature of the sedimentary successions. The basin landward of Watson Gap most likely held a coastal lagoon with protection provided by the beach ridge on the seaward side.

The Yilki Beach shore platform is most likely formed of a MIS 5e aeolianite that has been subject to erosion by both the Hindmarsh River and the Southern Ocean indicating a lack of uplift in comparison to the more easterly Victor Harbor and Watsons Gap.

4.3.3.5 Summary of last interglacial shoreline development

The characteristics of last interglacial deposits within the study area are dependent upon their geographic location. To the southeast of Lake Albert, aeolianite and calcrete extend as much as 16 km inland from the preserved foreshore facies at Camp Coorong. Drillhole data (DMITRE, 2014) also suggests that the Bridgewater Formation extends for a considerable depth (tens of metres) beneath the surface, possibly indicative of stacking of successive periods of deposition, but its exposure at the surface has been limited by the deposition of Molineaux Sands and the subsidence in the region. The recurved spit features in the region as outlined by De Mooy (1959) and the low carbonate content of the sediments imply that the River Murray met the Southern Ocean via southern Lake Albert for at least some of the Last Interglacial.

In the Goolwa/Hindmarsh Island region preservation of the last interglacial beach-barrier complex has been constrained by the erosive force of the River Murray.

The multiple channels of the River Murray appear to have eroded nearly 17 km of aeolianite between Mark Point and Hindmarsh Island leaving only shallowly buried (1-3.5 m) shell beds upon which the four of the five barrages have been built (Goolwa Channel being the exception). These shell beds are shown to extend across the length of Hindmarsh Island. Erosion by the Goolwa Channel on the northern margin of the island has exposed two calcretes on the northern shoreline. The exposure of the two calcretes opposite the MIS 7e dune at Clayton Water Tower on Sturt Peninsula implies that northern Hindmarsh Island is a composite succession consisting of MIS 7e and MIS 5e aeolianite.

The down-cutting and entrenchment of the Goolwa Channel during the LGM has allowed the preservation of a last interglacial recurved spit to the east (Bourman *et al.*, 2000; Murray-Wallace *et al.*, 2010) and a palaeo-channel and mouth to the west. The digital elevation model of the Goolwa region shows an additional aeolian deposit to the west to have features similar to the Hindmarsh Island recurved spit. The low-lying topography behind the aeolianite could be the location of a palaeo-channel as well implying that a former Murray Mouth was located directly north of the location of the MIS 5c aeolianite at Surfers Beach.

The movement of the palaeo-Goolwa Channel would be due to natural variability as exhibited by the modern Murray mouth as a result of the interplay between littoral drift, wind drift, waves, ocean currents, tidal prisms, fresh water flow and sediment supply. The eastward shift of the palaeo-channel could be related to localised neotectonics or a consequence of reduced river flow and sediment supply as precipitation decreased towards the end of the last interglacial. Channel volume would be further diminished with the reduced strength of the flood tide as sea level fall following the last interglacial decreased wave energy along the coastline.

On Fleurieu Peninsula, the orientation of the coastline has controlled deposition within coastal bedrock valleys. Deposition is also likely to have been influenced by the offshore Kangaroo Island which would provide protection from the dominant wind and swell. At Waitpinga, well exposed to the southern swell and winds, the valley has been completely infilled by MIS 5 (*sensu lato*) aeolianite. Farther to the northeast, the

Hindmarsh and Inman River valleys host reworked MIS 5 aeolian, lagoon and beach deposits. Unlike the Waitpinga Valley, these valleys have not been infilled with sediment most likely due to the change in coastline orientation and the protection provided by Rosetta Head from the dominant southwest swell and southerly winds (section 3.3).

4.3.4 MIS 7e: Sturt Peninsula – the Alexandrina Coastline

The Alexandrina coastline was first described by de Mooy (1959) as a steep former coastal dune range with an aeolianite core stretching from along the northern margin of Lake Albert, west across the top of Narrung Peninsula, to Sturt Peninsula, northern Hindmarsh Island and beyond Goolwa (Figure 4.27). Murray-Wallace *et al.* (2010) were able to show that the Alexandrina coastline was a composite feature with the identification of MIS 5e strata (Hindmarsh Island), MIS 7 strata (Sturt Peninsula) and MIS 9 strata (Hindmarsh Island). This is in accord with the trend of the dune ranges (MIS 5e – MIS 17) on the Coorong Coastal Plain which coalesce northwards to form a single composite feature.

Sturt Peninsula forms a neck of land (~4.5 km wide at its widest point, ~1.2 km at its narrowest) and extends for ~9.5 km to form a southern shoreline to Lake Alexandrina (Figure 4.27). The lake narrows between Sturt Peninsula and the eastern Narrung Peninsula to a width of ~5.5 km, forming a passage through which the River Murray waters flow before entering the channel and lagoon system landward of the Murray Mouth. The shoreline at the most eastern extent of Sturt Peninsula (Point Sturt) is composed of a vertical cliff capped by a massive calcrete which reaches up to 1.5 m thickness. The undulating topography of the calcrete reflects the original aeolian form (Figure 4.28). From Point Sturt, both Narrung Peninsula and the Holocene equivalent Younghusband Peninsula (~10.5 km south) are visible. Two localities on Sturt Peninsula, Point Sturt (PTS, the peninsulas most eastern tip) and Clayton (CWT, on the southern margin) (Figure 4.27), were correlated with MIS 7e using TL and AAR analysis (Murray-Wallace *et al.*, 2010). Additional localities (Figure 4.27) on Sturt Peninsula were identified in this thesis and are correlated, based on their geographical relationship to Point Sturt and Clayton, to be part of the MIS 7e coastline. These localities (Point Sturt Road, Griffin Road and Clayton Bay Road) are described here.

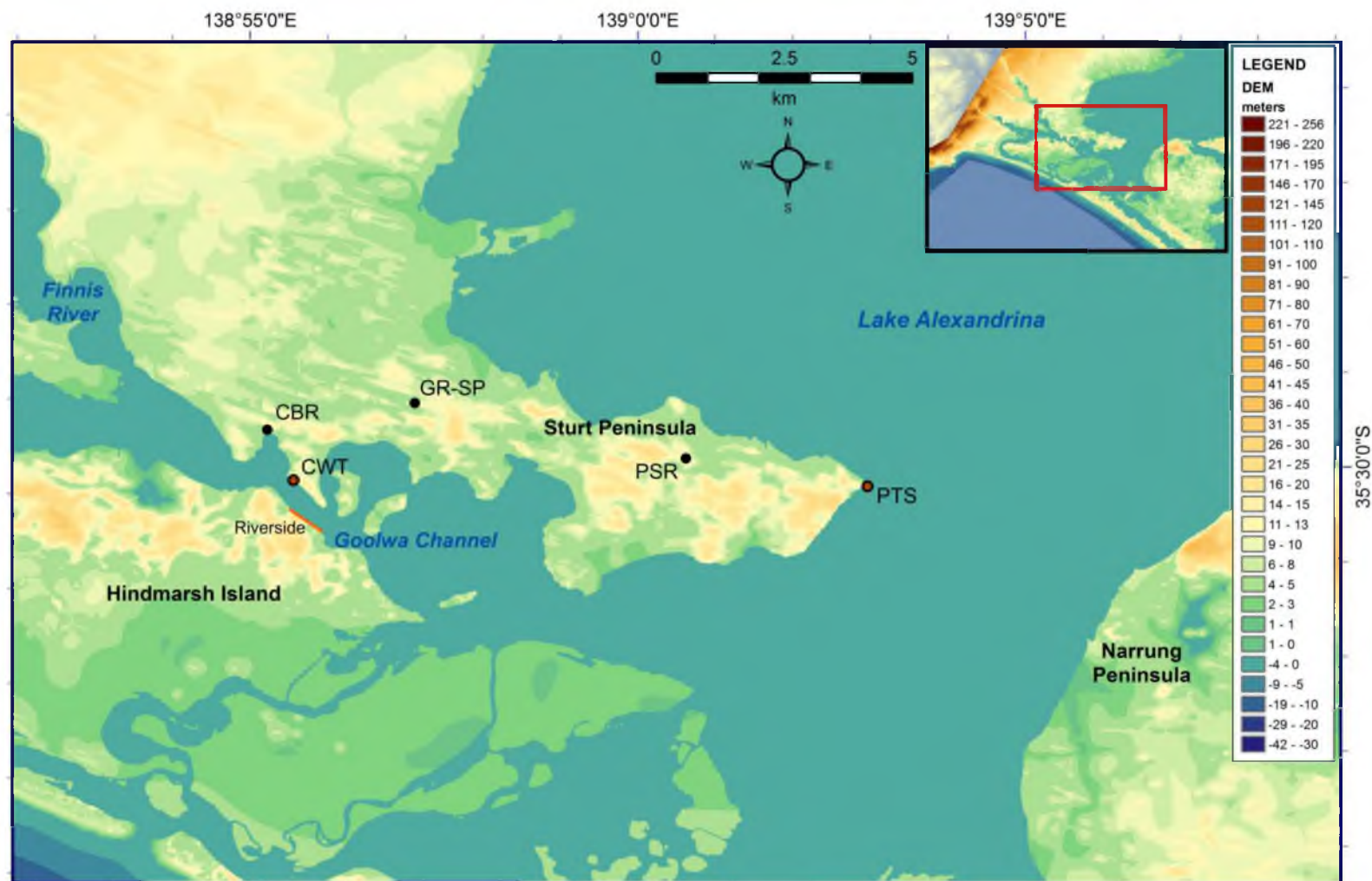


Figure 4.27: Two MIS 7e deposits have been identified previously by TL analysis on Sturt Peninsula: Point Sturt (PTS) 230 ± 50 ka and Clayton Water Tower (CWT) 215 ± 15 ka (Murray-Wallace *et al.*, 2010). The additional sites described here are Point Sturt Road (PSR), Griffin Road (GR-SP) and Clayton Bay Road (CBR). The location of the Riverside calcretes located on northern Hindmarsh Island at is indicated.

4.3.4.1 Point Sturt Road and Griffin Road

The Point Sturt Road (PSR) and Griffin Road (GR) sites are exposures of allochemical sandstones (Mount, 1985) located within small quarries 5.4 km apart, near the crest of Sturt Peninsula and between the two MIS 7e sites of Murray-Wallace *et al.* (2010) (Figure 4.27). While it is likely, given their position on Sturt Peninsula, that the two sedimentary units are aeolianites they differ greatly in their appearance and sediment content.

The Point Sturt Road aeolianite is capped by a rubbly-blocky calcrete with only very faint planar bedding visible near the base of the exposure at its greatest height (~3 m) (Figure 4.28). Any other bedding in the moderately indurated brownish yellow (10YR 6/6) sediment has been obscured by pedogenic processes and the development of minor solution pipes and rhizoliths. The dune is overlain by a vegetated siliceous dune ~1 m thick. The sand fraction (77% of the total sediment) is composed predominantly of fine-medium grains (both 35%) but also contains noticeable quantities of very fine (17%) and coarse grains (13%). Calcite development is extensive and may be reflected by the silt content, 22%. Carbonate content in the 250-500 μm fraction is low (8%). The high quantity of calcite and low carbonate percentage within the medium grain-size fraction suggests that significant leaching of carbonate grains may have occurred. However, this is not conclusive as the medium grain size fraction accounts for only 27% of the total sediment.

In contrast, the Griffin Road aeolianite has no calcrete development (although there are pieces of calcrete in the quarry rubble) and it displays faint but extensive foreset and topset bedding in the 3.7 m deep exposure. The dune has a nearly west-east strike (azimuth 087°) and foreset bedding dips at 20° in north-northwest direction (Figure 4.28). The sediment is also moderately indurated and brownish yellow (10YR 6/6) but contains 44% carbonate in the 250-500 μm fraction and displays no evidence of solution pipe or rhizolith development. Griffin Road is composed of 93% sand-sized grains (silt content is only 6%), predominantly fine-medium grains (45% each). Very fine and coarse grains combined account for less than 10% of the total sediment. The sand is moderately- to well-sorted. Abundant quartz grains are clear to translucent, subrounded

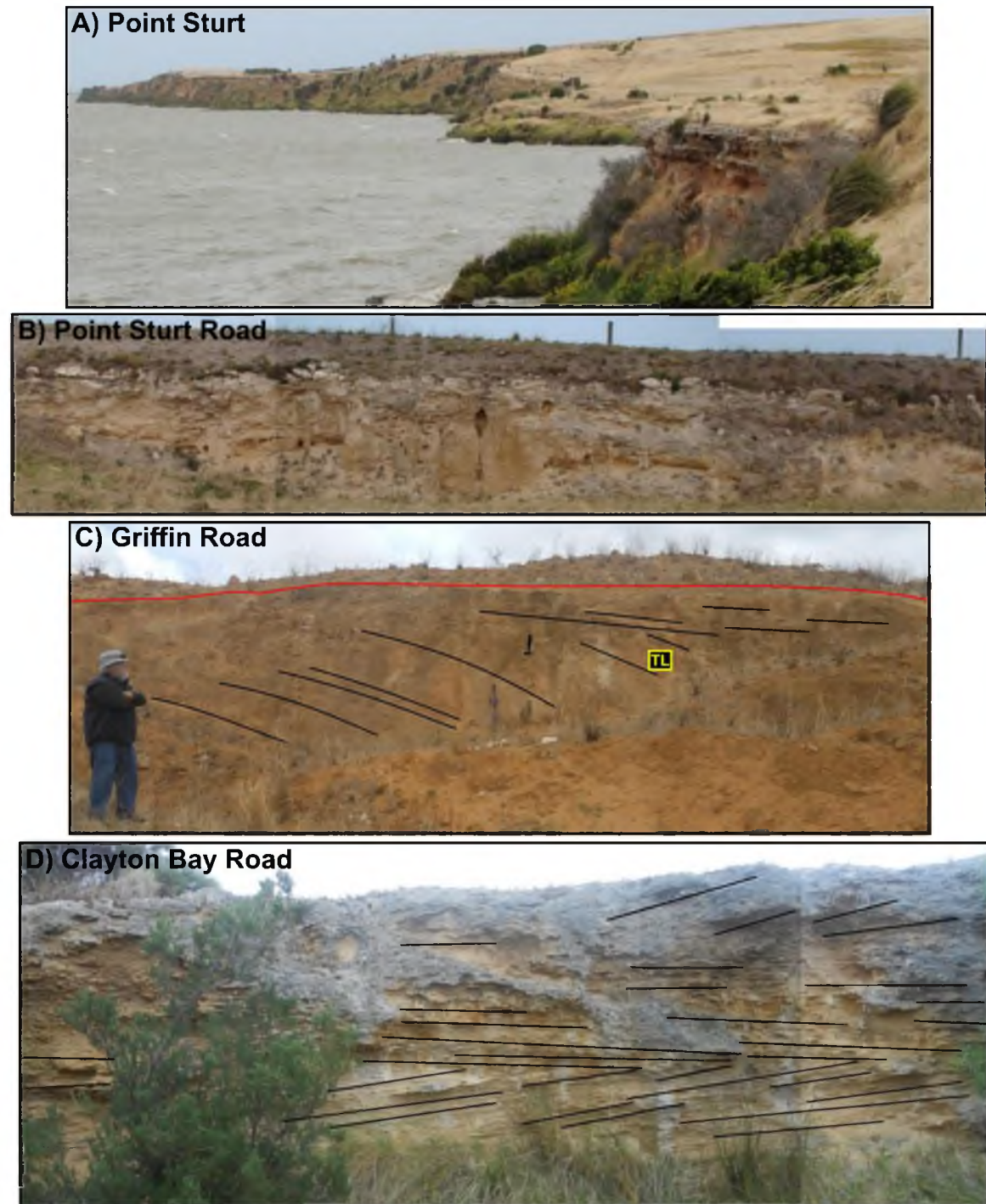


Figure 4.28: Photographs from Sturt Peninsula and of sites described in the text. A) Looking south from the easternmost point of Point Sturt the shoreline reflects the original dune topography. B) The exposure at Point Sturt Road retains negligible amounts of the original stratigraphy beneath a blocky calcrete and overlying siliceous sand. C) Griffin Road retains faint traces of foreset and topset bedding. A TL sample was taken from this dune where indicated. D) Clayton Bay Road displays herringbone cross stratification indicative of bi-direction deposition.

to rounded and commonly subangular. Milky grains are very rare but iron-staining is very common. Well-rounded shell fragments are abundant, reaching a maximum diameter of 1 mm and are variably white or iron-stained. Foraminifer and other fauna are sparse to rare, appear to be recrystallised and are very commonly stained by iron oxide. Foraminifers include tests of *Elphidium macelliforme*, other *Elphidium* sp. and *Discorbis* sp. XRD analysis shows the sediment to be composed of 50% CaCO₃ with low Mg calcite accounting for 42%, followed by aragonite (4%), high Mg calcite (3%) and other types of CaCO₃ cement (1%).

4.3.4.2 Clayton Bay Road

The Clayton Bay Road (CBR) site is situated 1.1 km northwest of the second MIS 7e locality described by Murray-Wallace *et al.* (2010) (Figure 4.26). The exposure is located within 100 m of the Clayton Bay shoreline on the Goolwa Channel and runs parallel to the shoreline for 72 m. The northern shoreline of Hindmarsh Island and the Riverside calcretes (Section 4.3.3) are visible. The exposure of very pale brown (10YR 8/2) moderately indurated sediment reaches 3 m in height but the dune crests towards the northeast. Calcrete and rhizolith development is minimal and confined to the eastern extent of the dune where bedding has been partially obscured by modern root development. Two sets (each ~1.5 m) of planar cross-stratification reflect opposing directions of dune development (Figure 4.28). The strike of the dune shows little variation between the two sets of strata; the lower set azimuth is 051° and the upper set azimuth is 056° giving the dune a general southwest-northeast strike. However, the dip in the lower set is 5° in a northwesterly direction whereas the upper set dips to the southeast at 19°.

A sample was taken from the top of the lower set of cross-strata at a depth of burial of ~1.5 m. The sediment is composed of 87% sand-size particles with medium-fine particles dominant (41% and 34%, respectively). The sediment is poorly sorted as reflected in the additional content of very fine (7%), coarse (15%) and very coarse (3%) particle size. Under a binocular microscope carbonate is shown to be a common to very common component (42% of the 250-500 µm fraction) with rounded and abraded shell fragments reaching up to 2 mm in diameter. Foraminifers and other fauna are rare. *Elphidium macelliforme*, other *Elphidium* sp. and unidentified species are present but are

discoloured and many are abraded and broken. The nature of the carbonate grains suggests a high energy depositional environment near to the carbonate source. Quartz grains are rounded to sub-angular and commonly frosted implying an aeolian component. Fine and very fine grains are increasingly angular to very angular.

The two sets of dune within the succession and sediment petrology indicate near-shore environment for the aeolian succession subject to changing environmental conditions.

4.3.4.3 Discussion of interpreted MIS 7 sedimentary successions

Aeolianites at Point Sturt and Clayton Water Tower on Sturt Peninsula have been confirmed as being deposited during MIS 7e. Given their locations on near the crest of the peninsula and between the MIS 7e aeolianites, it is likely that the Griffin Road and Point Sturt Road dunes are MIS 7e. However, the discovery of an MIS 9 or older aeolianite within the dunes of Hindmarsh Island (Murray-Wallace *et al.*, 2010) means that the two aeolianites could possibly predate MIS 7e. The different petrological characteristics between the sediments, suggests different depositional and post-depositional diagenetic processes at the two locations.

The record on the Coorong Coastal Plain suggests that sea-level in the region during MIS 7e was similar to current sea-level (Belperio and Cann, 1990; Murray-Wallace *et al.*, 2001; Murray-Wallace, 2002). However, more recent work (Blakemore *et al.*, 2015) has placed sea-level during MIS 7 as much as -9 ± 2 m below present. Global sea-level records for MIS 7, which includes up to three separate sea-level peaks (Martinson *et al.*, 1987), are subject to large uncertainties and there are conflicts amongst different sea-level proxies (Siddall *et al.*, 2007). If Sturt Peninsula is composed predominantly of MIS 7 aeolianite, it would be supportive of higher estimates of sea level during the interglacial.

4.3.5 Stacked sedimentary successions

Three field sites are discussed within this section. The sites were chosen because they contain multiple units representing more than one phase of deposition (i.e. multiple interglacials) and for their contribution to understanding the complexity of the landscape. The first site described, Myrtlegrove Road, is situated on the margin of the

uplifting Mount Lofty Ranges and provides evidence of a larger Currency Creek. The Knights Beach site is an embayed beach on the uplifting Fleurieu Peninsula, the coastal cliffs of which are formed by the erosion of Pleistocene coastal aeolianites. The final site examined is Point McLeay, situated on Narrung Peninsula, where the longest record of deposition in the region is exposed in a prominent coastal cliff section.

4.3.5.1 Myrtlegrove Road

Myrtlegrove Road is uniquely positioned between two tributaries to the Goolwa Channel (Currency Creek and Finnis River) and on the margin of an alluvial plain (Figure 4.29). The field site is within 700 m of the nearest shoreline of Currency Creek. There are two areas of interest at this site, a complex consisting of multiple phases of siliceous sand deposition (Figure 4.28a) and slightly farther north (~200 m) a lagoonal deposit (Figure 4.28b); both sites have been exposed by quarrying.

The lagoonal unit has been exposed by shallow digging to a maximum depth of 65 cm (Figure 4.29) which has been surveyed to 1.931 m APSL. The top 50 cm of the exposure has formed a massive hardened calcrete beneath which is a pale yellow (2.5Y 8/3) limestone showing extensive iron oxide staining throughout. A sample of limestone taken from the base contains 97% CaCO₃ (whole sediment). Adjacent to the exposure, within the area where the overlying calcrete had been removed and the wet land surface had been disturbed by cattle, disarticulated valves (Grade 3) of *S. trigonella* were found. The shell had been disturbed and a shell bed or source was not identified. Disarticulated valves partially stained by iron oxide and three were coated with cemented limestone.

The lagoon unit is situated between two northwest-southeast trending dunes which appear to merge to the northwest. The more southerly of the two dunes is truncated by a former shoreline of Currency Creek. It is within this dune that the siliceous sands are exposed.

There are four units of siliceous sand exposed in the quarry reaching a height of 4.5 m (Figure 4.29). The contacts (where exposed) between Units 4 and 3 and Units 3 and 2 are distinct. Unit 2 and 1 are separated by a palaeosol. There is no bedding

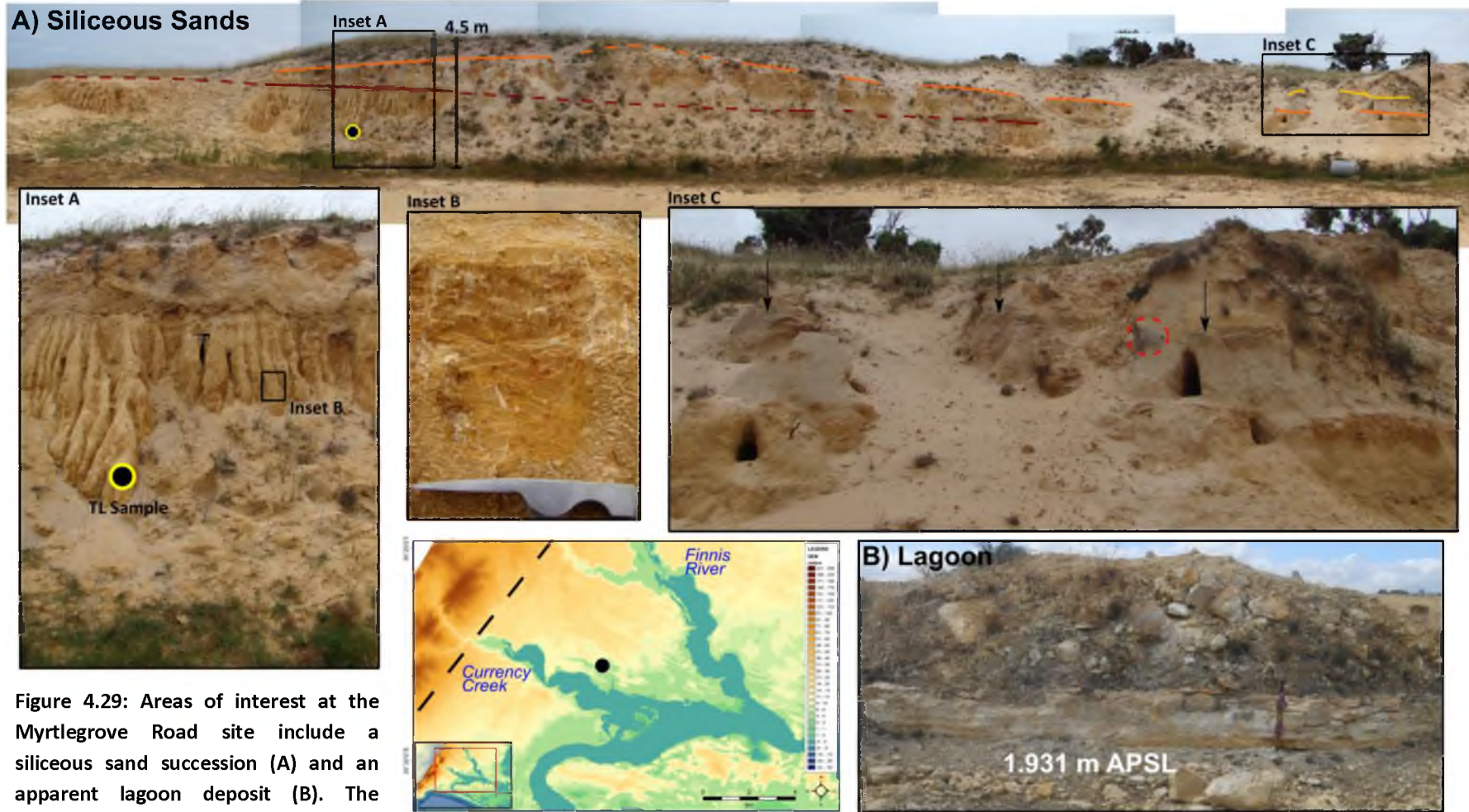


Figure 4.29: Areas of interest at the Myrtlegrove Road site include a siliceous sand succession (A) and an apparent lagoon deposit (B). The photomontage shows the location of contact between units. Unit 2 only

outcrops to the north (right hand side and Inset C). A TL sample was taken from Unit 4 (Inset A). Unit 4 has concentrations of calcite and iron oxide (Inset B). The marly calcrete associated with an apparent lagoon deposit reaches 65 cm in height (B) with quarried material overlying the calcrete.

Table 4.8: Analytical results of the Myrtlegrove siliceous dune succession. The percentage of sand-sized particles is based on the total sand-size fraction and not the total sediment.

SITE	MYRTLEGROVE ROAD (MR)		
Field Code	Unit 4	Unit 3	Unit 2
Calcrete	no	no	no
SEDIMENTS			
Depth of burial (m)	3.5	3.5	0.6
Munsell Colour	7.5YR 5/6 strong brown	10YR 7/6 yellow	10YR 7/4 very pale brown
% CaCO ₃ (250-500 µm)	8	0	0
Heavy minerals	very rare	very rare	very rare
Particle Size Analysis (Malvern Mastersizer)			
clay	7	1	0
silt	40	7	2
sand	53	92	98
very fine	11	21	12
fine	38	51	40
medium	42	28	40
coarse	8	0	8
very coarse	0	0	0
QUARTZ (binocular analysis)			
Sorting	poor	moderate	poor
Particle size	silt and sand	very fine-medium	very fine-coarse
Roundness	abundantly subrounded to rounded with subangular grains very common	fine-medium grains abundantly rounded to subangular; very fine grains abundantly subangular to subrounded but commonly angular	fine-medium grains abundantly rounded to subangular; very fine grains abundantly subangular to subrounded but commonly angular
Surface texture	abundantly frosted	variably frosted or translucent; very commonly opaque; very commonly Fe-stained	variably frosted or translucent; very commonly opaque; very commonly Fe-stained
CARBONATE (binocular analysis)			
	calcite concentrations	none	none

been preserved. The dune succession builds towards the north with later units onlapping the earlier units. Unit 4 loses appears to extend farther to the south outside the margins of the quarry, although the top of the unit may have been truncated by erosion at this end.

Unit 4 is composed of a strong brown (7.5YR 5/6), well indurated silty-sand with concentrations of calcite and iron oxide (Figure 4.29a inset B). Unit 3 is a soft, lightly indurated yellow (10YR 7/6) sand which reaches a maximum thickness of ~2 m (Figure 4.29a inset C). Unit 2 is very pale brown in colour (10YR 7/4) and reaches 75 cm is thickness where it is overlain by a palaeosol. The palaeosol includes evidence of fire: an area of 'blackened' sand with charcoal *in situ*. The last unit is a recent, pale, vegetated sand which drapes the entire succession. Sediment samples from Units 2-4 were analysed under the binocular microscope and for particle size (Table 4.8). Units 2 and 4 were also subjected to XRD analysis.

Staining only occurs on ~10% of the quartz grains. Unit 4 also contains small, fragile calcite concentrations. Units 3 and 2 appear very similar under the microscope (Table 4.8) but Unit 2 contains an overall larger grain size population. Given the softness of the Unit 3 sand and the similarity in characteristics of Unit 2, it is possible that Unit 2 is composed of reactivated Unit 3 sand with a reworked Unit 1 component. Thus, explaining the slight colour and grain size discrepancies between the two units.

These sands are not Bridgewater Formation but the calcite within Unit 4 suggests some association with the adjacent lagoonal unit. The lack of carbonate grains within Unit 4 eliminates carbonate dissolution from the sediment as a source of CaCO_3 . However, the evaporation of CaCO_3 saturated water through Unit 4 could have facilitated the deposition of carbonate within the unit. The close proximity to the margin of the Mount Lofty Range suggests the sands are a distal alluvial deposit and its similarity to the Pooraka Formation, which is generally described as reddish-brown clay in colour containing pedogenic calcium carbonate nodules (Williams, 1969; Bourman *et al.*, 1997; 2010; section 3.7.7), indicates that Unit 4 is Pooraka Formation.

4.3.5.2 Knights Beach, Fleurieu Peninsula

Knights Beach is an embayed south-southwest facing beach located on the uplifting Fleurieu Peninsula (Figure 4.30). It, like Myrtlegrove Road, is also located near the proposed location for the Encounter Fault. Unlike like the nearby Victor Harbor and Watson Gap (section 4.3.3.3) Knights Beach does not retain a record of beach or lagoon deposition. The beach has formed by erosion into a 15 m thick succession of coastal aeolianite which forms the cliff surrounding the beach. A disconformity surface is visible within the aeolianite along the back of the beach indicating two phases of deposition but is obscured at the eastern end of the cliff by calcrete development, pedogenesis and honeycomb weathering (Figure 4.30a-d). The aeolianite succession drapes a headland to the southeast of Cambro-Ordovician Port Elliot granite. The granite bears the striations from Permian glaciation and a wedge of Permian silts separate the crest of the granite from the aeolianite (Milnes and Bourman, 1972). The beach is roughly segregated from Boomer Beach to the west by well indurated aeolianite (~30 m in width) which dips into the Southern Ocean and also protrudes from the intertidal beach face of Knights Beach (Figure 4.30a). Aeolianite outcropping within the intertidal zone continues for at least another 190 m to the west as a shore platform.

The disconformity within the aeolianite follows the undulating crest of the well-indurated Unit 1. Bedding within Unit 1 generally consists of well-preserved planar cross-stratification (Figure 4.29c, d) with variable angles of dip indicating dune swales. The disconformity at the western side of the aeolianite forms an erosional truncation surface with dune migration to the northeast (Figure 4.30b).

The calcrete capping the second unit, Unit 2, is massive displaying extensive rhizolith development. This unit is composed of numerous troughs, the base of which coincide with the disconformity capping Unit 1, implying that the unit was well indurated and resistant to erosion prior to the deposition of Unit 2. The trough cross-bedding is overlain by planar beds over which the calcrete has developed. Sections of this unit have undergone a great deal of erosion creating areas where the unit recedes back from the face of the cliff. There are also locations where the top planar bedding and calcrete remain but large areas of the underlying bedding, including Unit 1, have

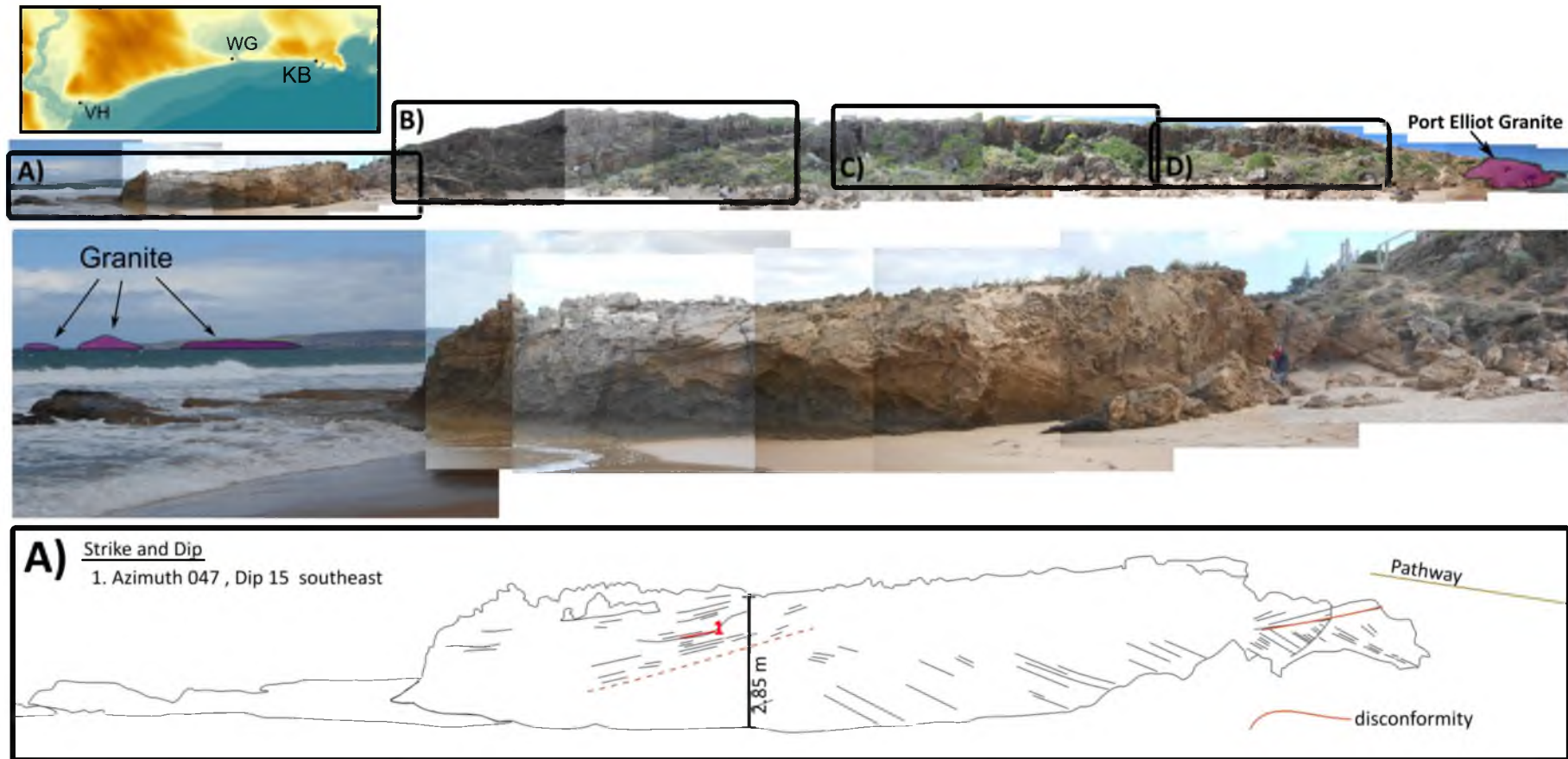


Figure 4.30: The stratigraphy of the Knights Beach (KB) aeolianite succession. Digital elevation model provides location on Fleurieu Peninsula. Photograph montage is a panorama of the beach with the location of insets outlined. Inset A) These photographs are looking in a southeast direction. Only minimal bedding is retained here as the aeolianite has been subjected to intensive weathering by the Southern Ocean. Strike and dip A1 indicate a northeast to southwest trending dune.

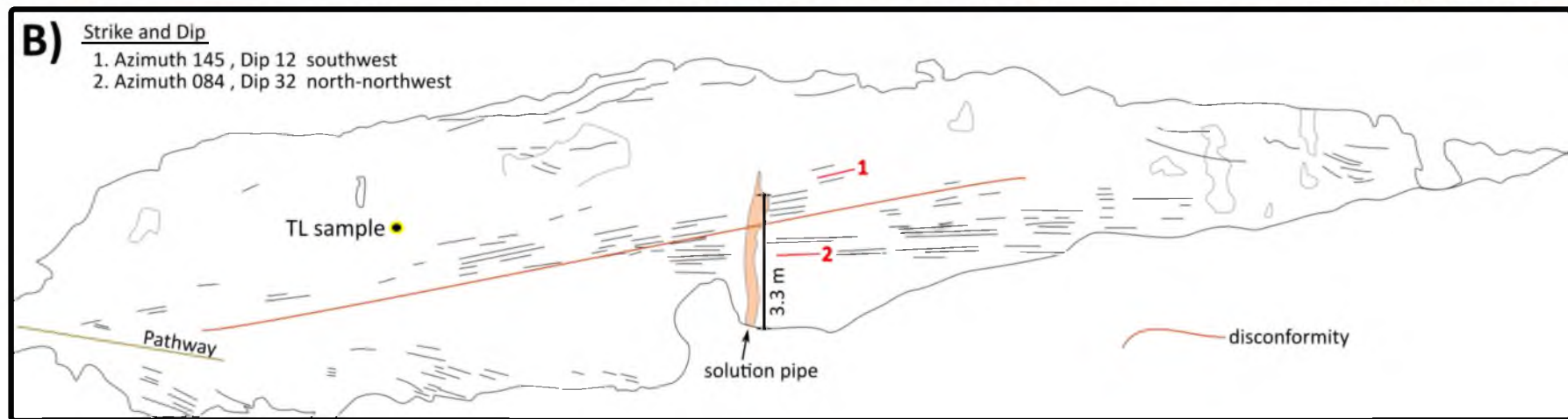


Figure 4.30 *continued*: Photographs are taken in a north-northwest direction. The western end of the beach has suffered extensive alteration by cavernous weathering, solution pipe and rhizolith development. The erosional truncation surface marks a significant change in bedding, strike and dip indicate a change in orientation of the dune from a nearly west east strike to a northeast to southwest strike. TL sample location for this research is indicated.



200

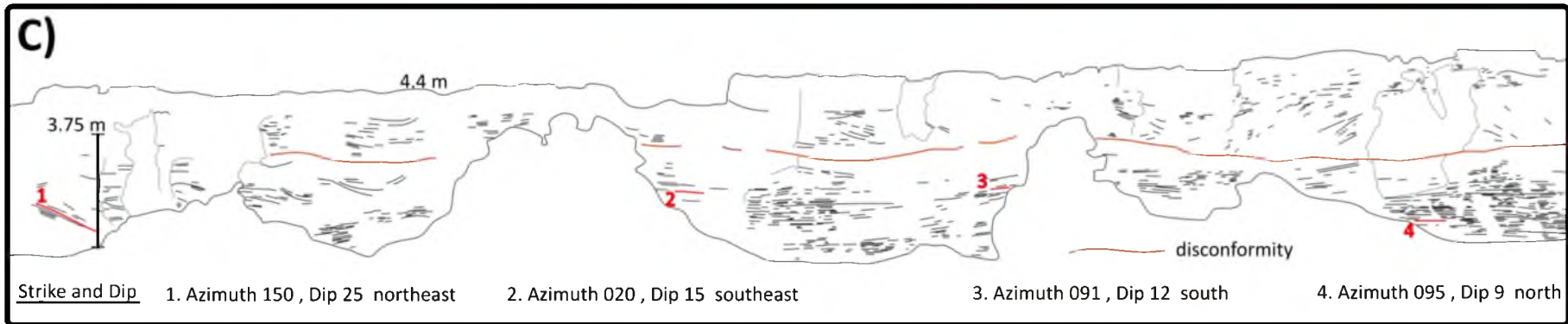


Figure 4.30 *continued*: Photographs are taken in a north-northeast direction. Bedding from both units is well-preserved here except where slumping has occurred. The sequence of troughs in Unit 2 is established in this portion of the beach. The strike and dip directions indicate variable dune trends across Unit 1. The bedding at locations 2, 3 and 4 was relatively fine with some cross-strata as thin as 1 cm. The changing trend of the dune from left to right is 1) northwest to southeast, 2) north-northwest to south-southeast, 3) nearly west-east and 4) nearly west-east. The large change in orientation between locations 1, 2 and 3 may indicate a swale within the aeolianite.

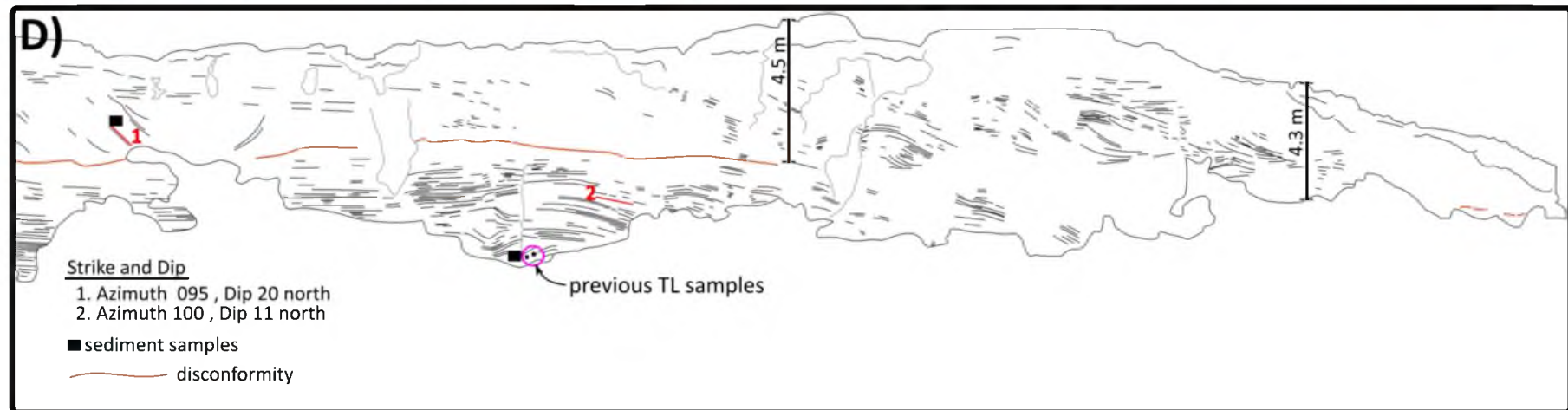


Figure 4.30 *continued*: Photographs are taken in a northwest direction. Unit 1 bedding remains well-preserved at the eastern edge of the beach. Location of previous TL samples are indicated. Sediment sample KB II was taken adjacent to the TL sample holes. Sample KB III was taken from the margin of a trough deposit. Unit 2 showed extensive gullying near the 4.5 m height marker and rhizolith development farther to the east. Unit 1 and 2 strikes are roughly west-east.

eroded away (Figure 4.30b, c, d). It is possible that the trough cross-bedding has been more susceptible to erosion due to the angle of the bedding.

The aeolianite has been previously dated by thermoluminescence. Two samples, taken from adjacent holes located on the eastern cliff at 7 m depth of burial from the top of the cliff and 3 m below the unconformity surface, were dated: one at the University of Wollongong Laboratory (W2347) and the other at the University of Adelaide (AdTL01005). The results were disparate. The University of Wollongong provided an age of 266 ± 34 (Bourman *et al.*, 2000) whereas the University of Adelaide provided an age of 130 ± 15 (Murray-Wallace *et al.*, 2010). AAR whole rock results supported the MIS 5e age (Murray-Wallace *et al.*, 2010). For this thesis a TL sample was taken from the western side of the aeolianite dune ~1.5 m above the erosional truncation surface (Figure 4.30b). Sediment samples, which are described here, were taken from the back of the TL sample site (KB TL), adjacent to the two previous TL samples (KB II), from above the unconformity near the base of trough cross-bedding (KB III) and from the modern beach (KB MOD) (Figure 4.30b, d). The modern beach sample was taken from damp sand to ensure recent deposition.

The Knights Beach modern and TL sediments are nearly identical; both are 100% sand with nearly equivalent quantities of fine, medium, and coarse quartz grains (Table 4.9) and are considered grainstones (Dunham, 1962). Knights Beach II and Knights Beach III contain similar quantities of clay, silt and sand but differ markedly in their sand grain size composition (KB III is coarse sand dominant, whereas KB II is medium); however, both are considered to be packstones due to their silt content (Dunham, 1962). The three Pleistocene samples are regarded as sandy allochemical limestones and the modern sample, with lower carbonate content, is allochemical sandstone (Mount, 1985). The sediments are generally well-sorted and composed predominantly of rounded to sub-rounded grains with clear and vitreous lustre surfaces; although frosted surfaces are common in all but the modern sand. Iron-stained grains fall on the margin of sparse to common. Carbonate grains are abundant in the three Pleistocene sediments and are only common in the modern sample. Carbonate is well preserved in Knights Beach TL, perhaps reflecting the sampling from within the back of the TL sample-hole

Table 4.9: Analytical results of the Knights Beach Bridgewater Formation dune succession. The percentage of sand-sized particles is based on the total sand-size fraction and not the total sediment.

SITE KNIGHTS BEACH				
Field Code	KB TL	KB II	KB III	KB MOD
Calcrete	yes	yes-massive	yes-massive	no
Calcrete thickness	inaccessible	<1 m	inaccessible	-
SEDIMENTS				
Depth of burial (m)	3.00	7.00	3.00	0.40
Munsell Colour	10YR 5/6 yellowish brown	10YR 6/4 light yellowish brown	10YR 6/4 light yellowish brown	10YR 7/3 very pale brown
% CaCO ₃ (250-500 µm)	44	62	62	18
Heavy minerals	very rare	very rare	very rare	spase/common
Particle Size Analysis (Malvern Mastersizer)				
clay	0	1	1	0
silt	0	9	10	0
sand	100	89	89	100
very fine	0	3	4	0
fine	20	17	5	22
medium	61	45	13	66
coarse	19	24	39	12
very coarse	0	0	29	0
QUARTZ (binocular analysis)				
Sorting	moderately	well-sorted	well-sorted	well-sorted
Particle Size	fine-medium	fine-coarse	fine-very coarse	fine-coarse
Roundness	abundantly rounded/sub-rounded; finer grains are abundantly sub-rounded/sub-angular	abundantly sub-rounded/sub-angular; commonly rounded	abundantly rounded/sub-rounded with common angularity	abundantly rounded; very commonly sub-rounded/sub-angular
Surface texture	abundantly clear and lustrous; commonly frosted; sparse/common iron-stained	abundantly clear or translucent, medium grains sparsely frosted; common iron-stain	abundantly clear and lustrous; commonly frosted; sparse/common iron-stain	abundantly lustrous and clear; commonly iron-stained
CARBONATE (binocular analysis)				
	Abundant	Abundant	Abundant	Common
Molluscs	≤ 2 mm; juveniles present	≤1 mm; rounded fragments	≤1 mm; angular fragments	≤1 mm; angular fragments
Foraminifer	abundant	common	very common	very common
Other fauna	very common	common	very common	rare

and removal from the diagenetic processes at the surface of the cliff. Carbonate is also well preserved in the modern sand, exhibiting polished surfaces regardless of evidence of staining. Different degrees of staining are evident in all four samples. Recrystallisation of fauna is common in KB III and the mollusc fragments of KB II tend to have a chalky texture.

The disconformity within Knights Beach indicates two phases of deposition. The well-consolidated nature of Unit 1 and general lack of erosion during the second phase of deposition (except at the western extent of the aeolianite) suggests a significant period of time had lapsed between depositional phases potentially relating the aeolianite to MIS 5e and a later interstadial. MIS 5c would be more likely due to the reported higher sea-level (9 m BPSL) of the interstadial in comparison to MIS 5a (17 m BPSL) ((Belperio and Cann, 1990; Murray-Wallace *et al.*, 2001)).

Knights Beach must also be considered in its relation to other MIS 5e deposits on Fleurieu Peninsula. Both Victor Harbor and Watsons Gap have uplifted since the Last Interglacial as made evident by the level of estuarine deposits, 6 m and 10 m APSL (section 4.3.3.3). Knights Beach, however is actively being eroded by the Southern Ocean suggesting that although the aeolianite is positioned on the generally uplifting Fleurieu Peninsula, it is within the margin of the subsiding Murray Basin.

4.3.5.3 Point McLeay, Narrung Peninsula

Point McLeay is located on the northwestern corner of Narrung Peninsula opposite of Point Sturt, separated by a distance of ~6.5 km (Figure 4.31). The peninsula reaches its maximum elevation of ~45 m at Point McLeay, nearly double the maximum elevation of Sturt Peninsula of ~24 m. The difference in height is equivalent to an elevation loss of 3.8 m per km between Point McLeay and Point Sturt. One explanation for the offset is the presence of subsurface granite beneath Narrung Peninsula (Gatehouse *et al.*, 1991). Drillhole data (DMITRE, 2014) reveal Cambro-Ordovician granite at 142 m depth of burial (Figure 4.31). The granitic basement highs of the Padthaway Ridge have already been suggested as loci for the deposition and formation of beach-barrier deposits (section 2.6).

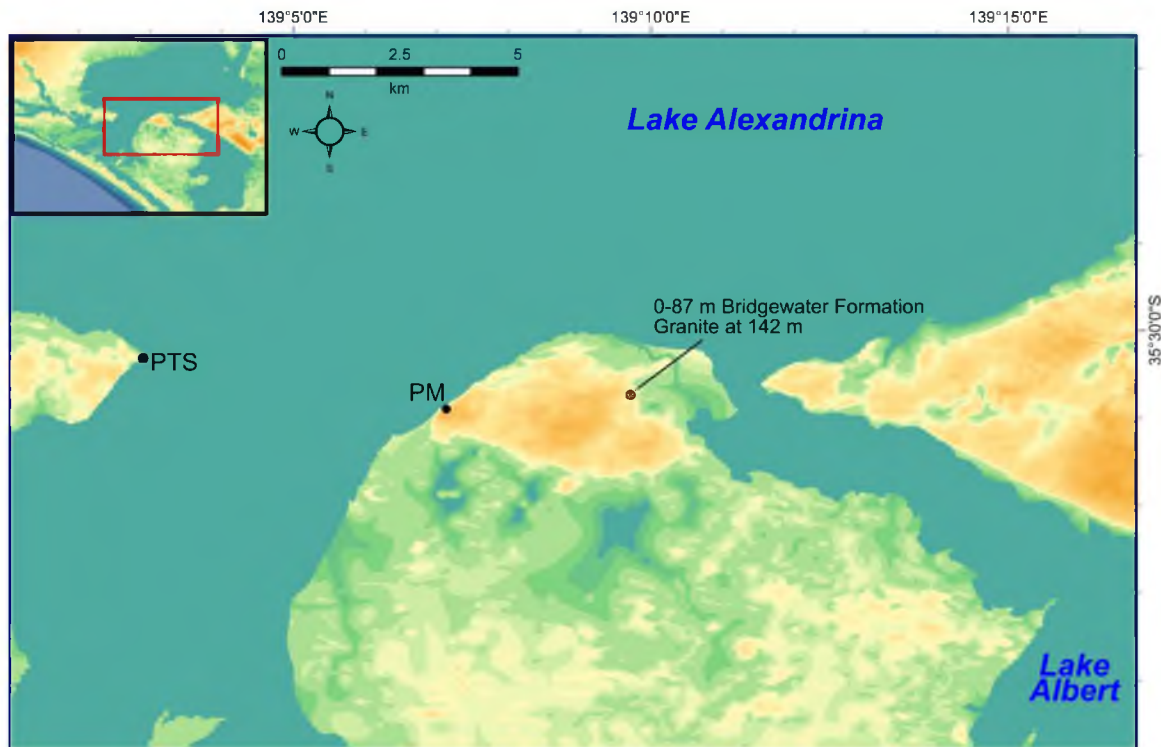


Figure 4.31: The location of Point McLeay on Narrung Peninsula. The change in elevation between Point McLeay (PM) and Point Sturt (PTS) may be due to underlying granite.

Point McLeay forms a steep cliff slope facing Lake Alexandrina as a composite aeolian structure. At least six units can be identified within the slope: two *terra rossa* soils and four aeolianites associated with interglacial sediments. Another unit (<2 m thick) appears to be sandwiched between PM A3 and PM A4 but was not accessible. Stratigraphical boundaries between most units, where not obscured by slope wash, are sharp; PM A2 and PM A3 are separated by a pisolitic lens with diffusive boundaries. A calcrete caps the succession at the crest of the point and a small modern dune is found overlying the calcrete. Due to the steepness of the slope accessibility to the units is limited. Many of the units are only accessible via steep rivulets to the north where erosion has removed most of the sediments above PM G2. From the rivulets the units are accessed by walking across the slope of the cliff. Due to the cliff steepness and inaccessibility the depth of burial of the bottom two units is not known; although, PM G2 is at ~8 m below the surface of the cliff.

The most deeply buried unit identified within the cliff is PM G1, a dark red (2.5R 3/6) *terra rossa* soil. This unit retains no bedding and is made up of moderately sorted

sand (70%) and silt (27%) (Table 4.10). Quartz grains are well-rounded with a vitreous lustre.

PM G1 is overlain by the aeolian PM A1. The contact between the two units has been obscured by slope wash but it is thought to be sharp. The aeolianite is composed of moderately-well indurated very pale brown (10YR 7/4) allochemical sandstone (Mount, 1985) composed entirely of sand-sized particles (Table 4.10). Faint bedding features remain within rivulet exposures indicating dune migration in a general northwards direction. The sands are well sorted and composed predominantly of sub-angular to sub-rounded medium grains with a clear lustre. An OSL sample was taken from within a rivulet where the unit was exposed.

PM A1 is overlain by the second *terra rossa* soil, PM G2. This soil is also dark red (2.5 YR 4.8). It contains a higher silt content (38%) than PM G1. The sand fraction (55%) is moderately-well sorted (Table 4.10). The quartz grains are predominantly sub-rounded to rounded with mixed surface textures, clear vitreous lustre, translucent or frosted. PM G1 and PM G2 have achieved their dark red colour from iron-stained clay cutans which coat the grains.

PM A2 sharply overlies the *terra rossa* PM G2. PM A3 is a very well indurated and massive light brown (7.5YR 6/4) unit 170 cm thick. PM A2 is separated from PM A3 by a diffusive 30 cm thick pink (7.5Y 7/4) pisolith lens (PM A2PL) (Figure 4.32). PM A3 is at most 45 cm thick and displays extensive rhizolith development and is capped by a massive and blocky ≤ 50 cm calcrete. The sediment is well-indurated and reddish yellow (7.5YR 7/6) in colour. PM A2, PM A2PL and PM A3 contain much higher quantities of silt and clay than the other interglacial units and are more similar in their contents to the *terra rossa* soils (Table 4.10). The sand size fraction is composed predominantly of very fine-fine, angular to sub-rounded quartz grains. The grains are either clear or transparent with lustre; frosted grains are only present in PM A2PL and PM A3. Iron-staining is common across all three units. Carbonate is very rare in all three units and composed predominantly of fine, well-rounded mollusc fragments.

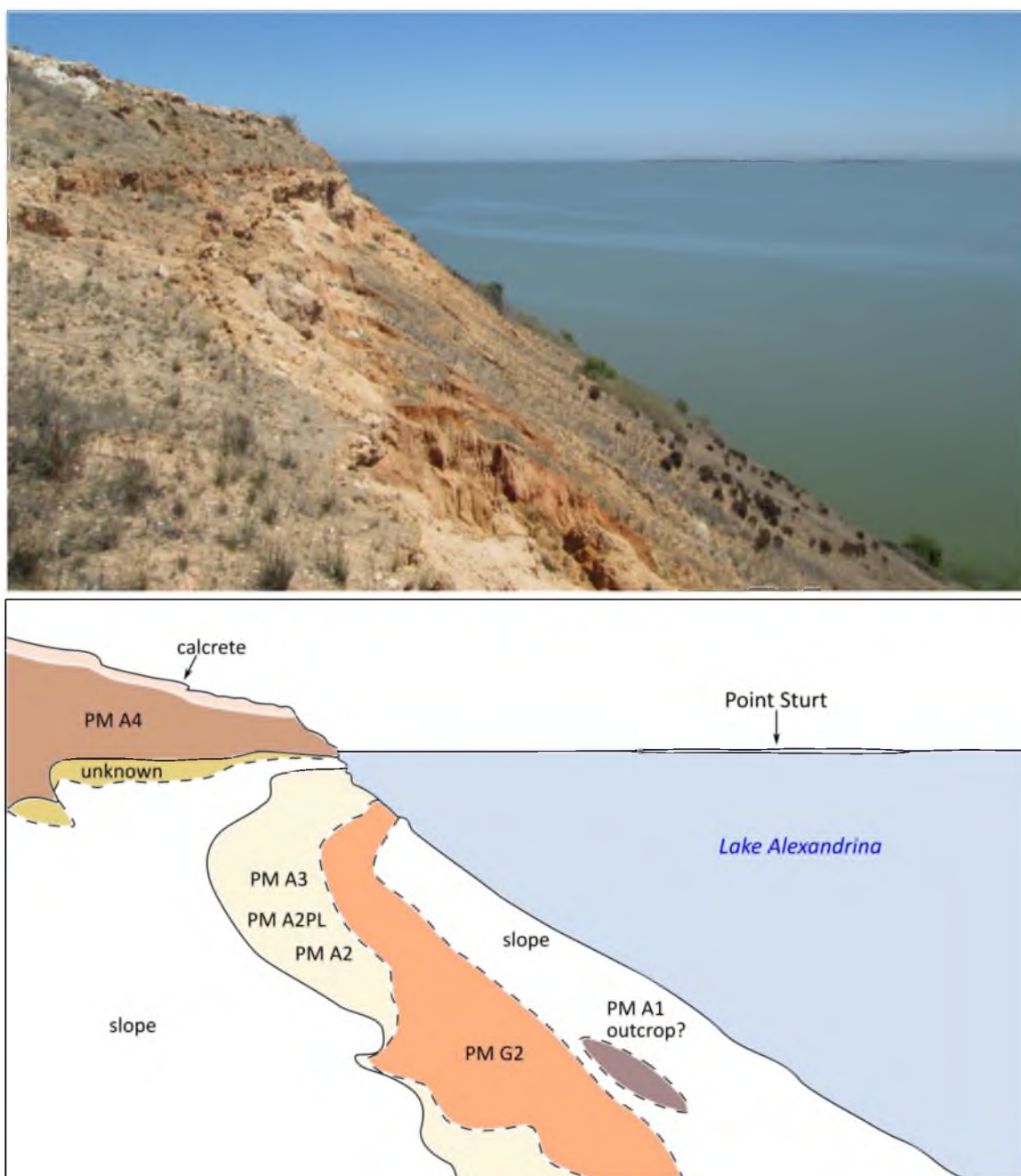


Figure 4.32: Looking across the Point McLeay slope on Narrung Peninsula. The steepness of the slope hindered access to the units preserved there. Point Sturt, visible to the west, is ~6.5 km distant.

4.32 *continued next page*: The succession of PM G2, PM A2, PM A2PL and PM A3. The boundary of PM A2PL with PM A2 and PM A3 is diffuse. The pisolith lens bulges slightly from the cliff in areas. PM A3 is overlain by an inaccessible unit which underlies PM A4. TL samples were collected from PM A3 and PM A2.

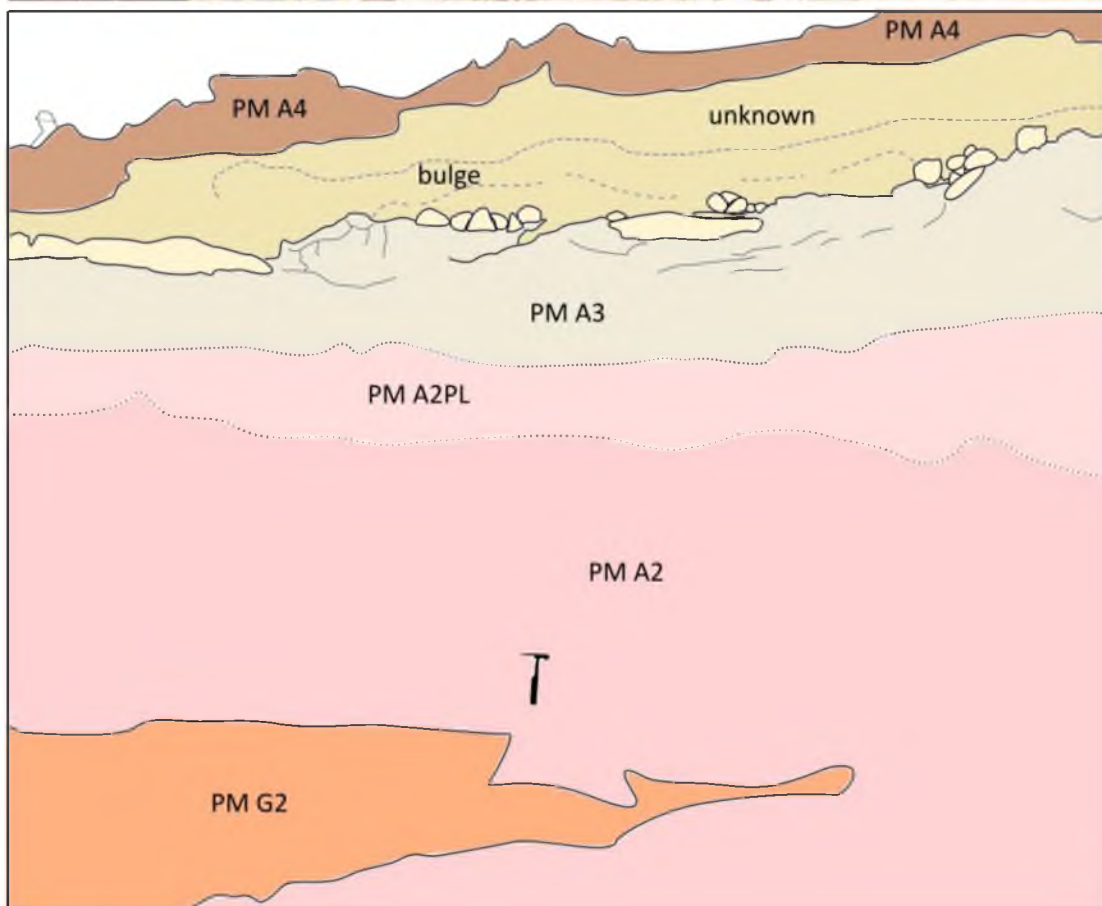


Table 4.10: Analytical results of the Point McLeay dune succession. The percentage of sand-sized particles is based on the total sand-size fraction and not the total sediment.

SITE	POINT MCLEAY							
Field Code	PM G1	PM A1	PM G2	PM A2	PM A2PL	PM A3	PM A4	PM A5R
Calcrete	no	no	no	yes - pisolith lense (PM A2)	yes	yes - blocky/massive	yes	no
Calcrete thickness	-	-	-	-	30 cm	50 cm	unknown	-
SEDIMENTS								
Depth of burial (m)	unknown	unknown	~8	7.1	6.1	5.85	5	0.1
Munsell Colour	2.5R 3/6 dark red	10YR 7/4 very pale brown	2.5YR 4/8 dark red	7.5YR 6/4 light brown	7.5YR 7/4 pink	7.5YR 7/6 reddish yellow	7.5YR 5/6 strong brown	10YR 5/4 yellowish brown
% CaCO ₃ (250-500 µm)	0	10	0	6	10	4	55	12
Heavy minerals	sparse/common	sparse	-	common	common	common	sparse	rare/sparse
Particle Size Analysis (Malvern Mastersizer)								
clay	4	0	7	16	18	6	1	1
silt	27	0	38	44	39	28	6	8
sand	70	100	55	41	43	67	93	91
very fine	2	0	9	39	37	44	12	27
fine	24	25	43	50	40	44	54	59
medium	56	68	42	11	21	13	33	14
coarse	18	7	5	0	1	0	1	0
very coarse	0	0	0	0	0	0	0	0
QUARTZ (binocular analysis)								
Sorting	moderate	well-sorted	moderate-well	poor		moderate	moderate	well-sorted
Particle size	very fine-coarse	fine-medium; cemented granules	very fine-coarse	very fine- medium; cemented granules	very fine-fine; sparse medium	very fine-fine; cemented granules	very fine-coarse	very fine- medium
Roundness	abundantly sub- rounded to well- rounded with increasing angularity with decrease in size	abundantly sub- angular to sub- rounded, commonly rounded	abundantly sub- rounded to rounded	fine grains abundantly angular; medium grains variably angular to rounded	angular to sub- rounded	angular to sub- rounded	decrease in angularity with increase in size; coarse grains abundantly rounded	decrease in angularity with increase in size; medium grains sub-rounded to rounded

Table 4.10 *continued*: Analytical results of the Point McLeay dune succession. The percentage of sand-sized particles is based on the total sand-size fraction and not the total sediment.

Field Code	PM G1	PM A1	PM G2	PM A2	PM A2PL	PM A3	PM A4	PM A5R
Surface texture	abundant lustre, translucent grains very common, milky grains rare; iron-staining very common; clay cutan	abundant lustre and translucent, rarely frosted; minor calcite	variable: clear, vitreous lustre, translucent and frosted grains; iron-staining common at varying degrees	medium grains lustrous, clear or transparent, iron-staining greater among larger grain size; extensive calcite	lustrous clear, translucent or frosty; iron-staining is common	lustrous clear, translucent or frosty; iron-staining is common; extensive calcite	variable among all grain sizes: lustrous, clear, translucent, iron-staining, minor calcite	finer grains abundantly frosted or translucent, larger grains variably frosted or lustrous, clear or translucent
CARBONATE (binocular analysis)	none	rare / sparse	possible very rare and very altered grains	very rare	very rare	very rare	abundant	sparse
Molluscs	-	very fine, well-rounded	-	fine, well-rounded	fine, well-rounded	fine	≤1 mm; one whole gastropod	fine, well-rounded
Foraminifer	-	rare: <i>Elphidium</i>	-	-	1 <i>Discorbus</i>	1 unknown?	rare: <i>Elphidium</i> , <i>Discorbus</i>	-
Other fauna	-	sparse	-	1 bryozoa	1 algae?	small rhizoliths	very common	very rare
X-ray Diffraction								
Quartz	83.5	85.2	85	48	-	70	55.2	73.9
Aragonite	0	0	0.5	0	-	0	2.7	0.8
High Mg Calcite	0	0	0.6	2.1	-	0.8	5.3	1.8
Low Mg Calcite	0	5.8	0	8.1	-	12.6	26.2	11.2
Other CaCO ₃ cements	0	0.1	0.2	26.7	-	0.2	4.3	0
Feldspar Group	13.6	8.6	4.4	8.2	-	10.9	2.4	11.4
Clays	2.8	0.2	8.9	5.6	-	4.1	4	1
*Other	0	0	0.2	0.7	-	1.4	0	0.1
*Other: sodium chloride, pyrite, gypsum								

PM A2 has a relatively high content of dolomite (13.5%) and ankerite (12.9%) (Table 4.10). These minerals are generally an indication of diagenesis within a zone of groundwater discharge and evaporation (O'Driscoll, 1960; von der Borch *et al.*, 1975; von der Borch and Lock, 1979). Their contribution to the aeolian units at Point McLeay suggests a nearby ephemeral lagoon environment.

The top unit within the cliff succession is PM A4. It is separated from PM A3 by an inaccessible unit (Figure 4.32) which appears to share characteristics similar to the interglacial units and is not a *terra rossa* soil. PM A4 is ~1.5 m thick and composed of lightly indurated strong brown (7.5YR 5/6) silty sand (Table 4.10) which retains traces of faint planar bedding. The unit is capped by a massive calcrete of unknown thickness but appears to be <1 m thick. The sediments of PM A4 are well-sorted and have a carbonate content of 55% in the 250-500 μm fraction. Mollusc fragments reach up to 1 mm (including a whole gastropod).

The modern dune which caps the cliff is composed of a loose, yellowish brown (10YR 5/4) sand. This aeolianite is similar in grain size and content to PM A1 and PM A4 (Table 4.10). Using the classification system of Mount (1985) PM A4 is a sandy allochemical limestone and PM A1 and PM A5 are both allochemical sandstones.

PM A4 had been previously sampled by Murray-Wallace *et al.* (2010) for TL analysis and returned an age of 120 ± 15 ka. If the *terra rossa* soils are associated with periods of glacial deposition and the remaining units to successive periods of interglacial deposition, the dune succession within the cliff face from PM A4 down could be interpreted as PM A4 (MIS 5e), the inaccessible unit (MIS 7), PM A3-PM A2 (MIS 9), PM G2 (MIS 10), PM A1 (MIS 11) and PM G1 (MIS 12) with the modern dune capping the cliff. Murray-Wallace *et al.* (2010) reported an additional TL age (470 ± 70 ka, AdTL01007) for a strongly indurated mixed quartz-carbonate sand retrieved from a rivulet exposure and correlated the deposit to MIS 13/15. This unit is PM A1. The large uncertainty of the TL age could allow correlation of the unit to MIS 11.

4.3.6 Inland locations

The aim of this thesis is to describe the Quaternary development of the River Murray Mouth region. Field sites described so far extend back to MIS 7 and potentially

to MIS 10 or MIS 12. To better understand the early development of the region south of the Murray Gorge and the regional relationship to the Bridgewater Formation extending across the Coorong Coastal Plain, investigations were made farther inland to locate and identify early Pleistocene Bridgewater Formation using Maps 2 (Positions of Stranded Beach Ridges and Outcrops of Pre-Pleistocene Hard Rocks) and 4 (Distribution of Major Karst Features in South-east South Australia) of Blackburn *et al.* (1965) as a guide. Google Earth was also used to identify quarries in the region which may contain exposures. Although the presence of the Bridgewater Formation in this area had been previously noted (Sprigg, 1959; Blackburn *et al.*, 1965; Firman, 1973), the successions have not been described in any detail.

Nine field sites are described here (Figure 4.33) and are summarised in Table 4.11. Six of the field sites provide details of the early Pleistocene (West Naracoorte and older) Bridgewater Formation at the northern end of the Coorong Coastal Plain. Also described are two sites (Murray Bridge and Tailem Bend) at the base of the Marmon Jabuk Escarpment which provide insight into earlier alluvial deposition in the region. The Carcuma site is a location where extensive deposits of the siliceous Molineaux Sand were identified. Descriptions begin with deposits identified as Bridgewater Formation, beginning with the most seaward and moving inland. These descriptions are followed by the three additional sites: Carcuma, Tailem Bend and Murray Bridge.

4.3.6.1 Mount Misery

Mount Misery, located 26 km inland from the modern coastline and 4 km northeast of the Lake Albert shoreline, is an allochemical sandstone (Mount, 1985) aeolianite exposed within a road cutting reaching 4 m in height. The field site is located at ~10 m APSL but is situated north of the aeolianite complex apex which reaches over 60 m APSL. A 1-2 m thick calcrete is variably nodular and blocky and has been infilled by soil. The bedding within the aeolianite has been largely obliterated by extensive pedogenesis and the development of rhizoliths and solution pipes along the length of the cutting. Faint traces of bedding remain only at the most northern extent of the exposure (Figure 4.34).

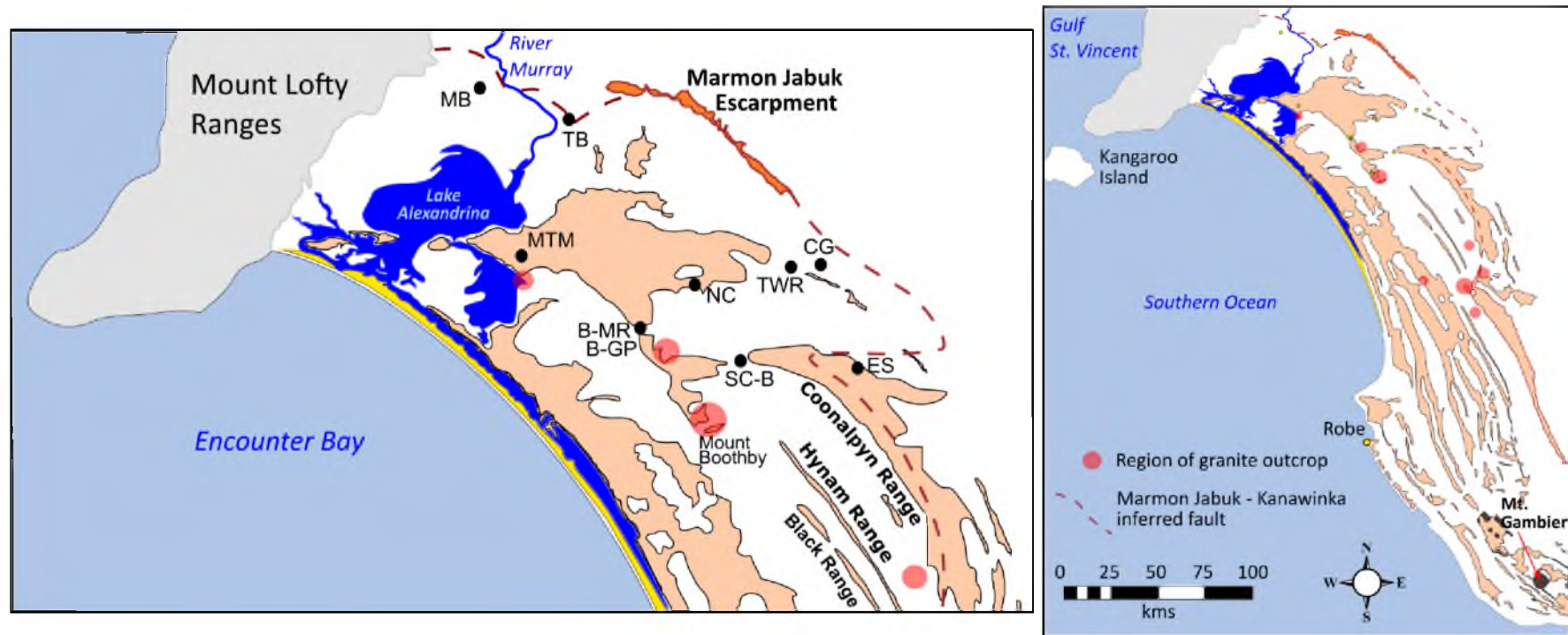


Figure 4.33: The location of the inland sites within the study area and their relationship to the ranges of Bridgewater Formation on the Coorong Coastal Plain. The Mount Monster and Black Ranges are at least equivalent in age to the West Naracoorte Range and the Coonalpyn Range is a composite dune of the East Naracoorte Range and older pre-Naracoorte barriers (Blackburn *et al.*, 1965; Cook *et al.*, 1977; Rogers, 1980; Bowler *et al.*, 2006) (Chapter 2). The intermittent range inland of the Coonalpyn Range is Cannon Ball Hill (Bowler *et al.*, 2006). The granite outcrops of the Padthaway Ridge formed headlands which served as loci for deposition (Rogers, 1980). The range to the north approaching Lake Albert, in which Sprigg (1959) placed the Lake Albert Beach and De Mooy (1959) identified as the Alexandrina coastline, remains nameless and is here referred to as the Murray Lakes Range. Note how the post-Naracoorte dunes, which have only minimal contact with granite, all coalesce and subside towards southeast Lake Albert, whereas the Naracoorte and older dunes are preserved to the north and west of the Padthaway Ridge granites. Abbreviations as follows: MB – Murray Bridge, TB-Taillem Bend, MTM – Mount Misery, B-MR – B-McIntosh Road and Gravel Pit, NC – North Coonalpyn, SC-B – South Coonalpyn, TWR – Tauragut Well Road, CG – Carcuma, ES – Emu Springs.

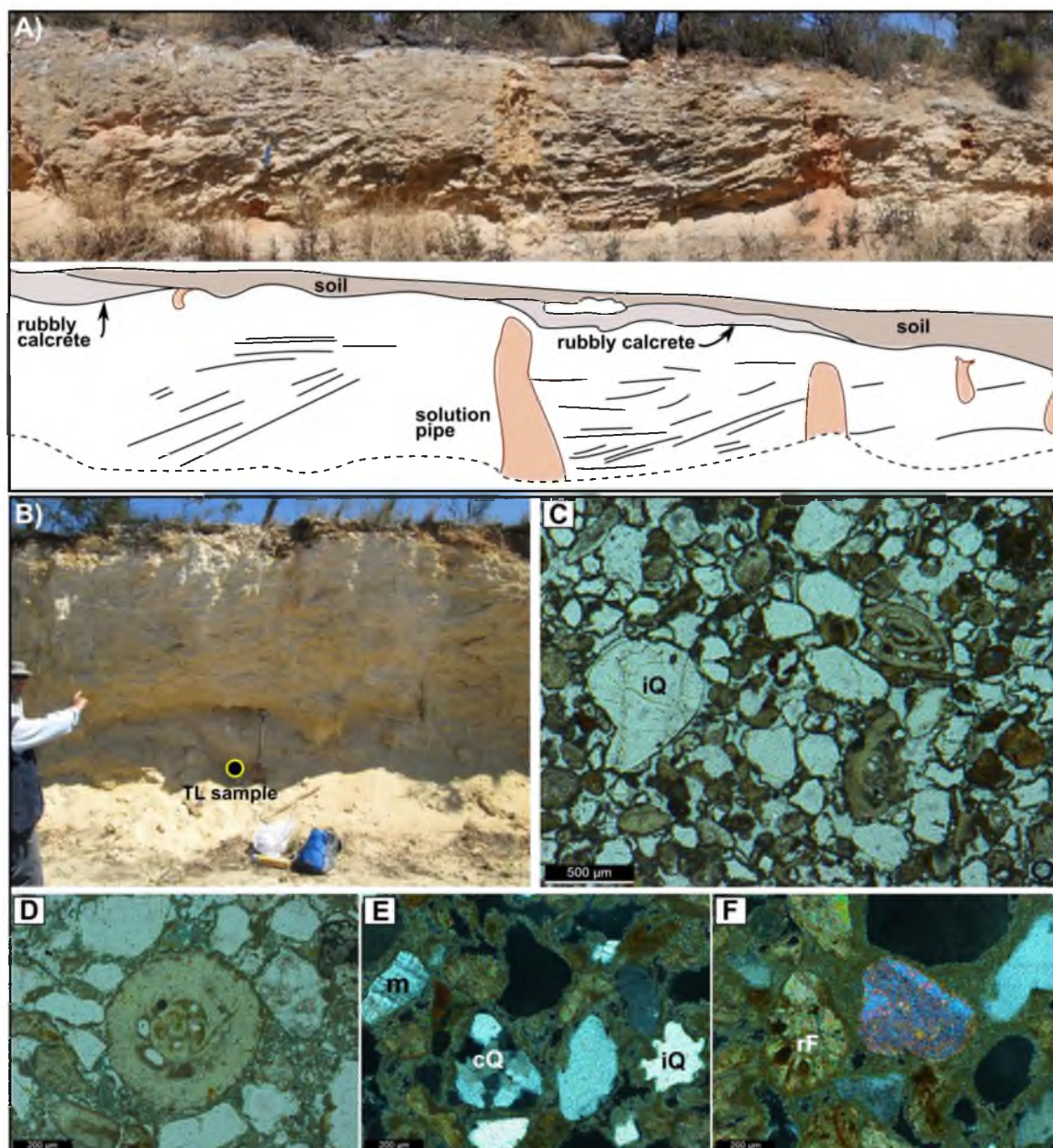


Figure 4.34: Mount Misery. A) Only faint traces of bedding remain at the northern extent of the road cutting where dune exposure is ~2 m high. B) The location of the TL sample from within the dune at ~4 m height. C) The moderately-well sorted sand contains irregularly shaped quartz grains (iQ). Scale 500 μm . D) Peloidal microcrystalline cement surrounding foraminifer. Scale 200 μm . E) Microcline (m), composite quartz (cQ) and irregularly shaped quartz grain (iQ). Scale 200 μm . F) A recrystallised foraminifer (rF) with iron-stained micrite infilling intraskeletal space. Note the low porosity in thin section. Scale 200 μm .

The yellow (10YR 7/6) sand beneath the calcrete is generally well indurated except at the base of the deposit where induration can be superficial. The sand is dominantly fine-medium grained (Table 4.11). The medium to coarse grains are commonly rounded to sub-rounded; however, sphericity is very variable as seen in thin

section (Figure 4.34). Carbonate grains are common. Mollusc fragments are mainly fine (<1 mm) and altered by diagenesis. Foraminifers are recrystallised and most faunal material has a coating of calcite making identification difficult; however, *Discorbis* sp., bryozoan, echinoderm and sponge fragments were identified. An SEM image was taken of a foraminifer likely to be an *Elphidium* sp. (Figure 4.4). In thin section carbonate grains show evidence of algal boring as well as iron-staining and calcite replacement. Broken and abraded foraminifers are present.

Porosity is generally low and remains in intergranular and intraskeletal spaces; however, secondary porosity has developed within skeletal grains that have been replaced by calcite. Grains exhibit meniscus micrite coatings with intergranular space filled by irregular granular microspar. Peloidal microcrystalline cement is found surrounding some grains. The meniscus and granular nature of the cements suggest diagenesis in the meteoric realm, either vadose or phreatic. Peloidal microcrystalline cement found in association with micrite and irregular void filling is indicative of a shallow marine environment or beachrock.

AAR whole rock and TL analyses has already been completed on this dune (Murray-Wallace *et al.*, 2010) but were inconclusive. The TL age, 350 ± 65 ka (AdTL01006), has a large uncertainty and the dune could be correlated with either MIS 9 or 11. An additional TL sample was taken during this thesis to try to resolve the age of the dune.

4.3.6.2 B-McIntosh Road and Gravel Pit

B-McIntosh Road (B-MR) and the Gravel Pit site (B-GP) are set within a northwest to southeast trending arc, which forms an unnamed range referred to within this thesis as the Murray Lakes Range (Figure 4.33). This name was chosen in recognition of the juxtaposition of the northwestern end of the range between Lake Alexandrina and Lake Albert and the designation of Lake Albert Beach (Sprigg, 1959) and the Alexandrina coastline (De Mooy, 1959) within the range. The range is anchored in the south to a granite outcrop (Mt Boothby) (Figure 4.33) associated with the basement feature, the Padthaway Ridge. The range peaks at 170 m APSL ~2.5 km north of B-MR. The two sites

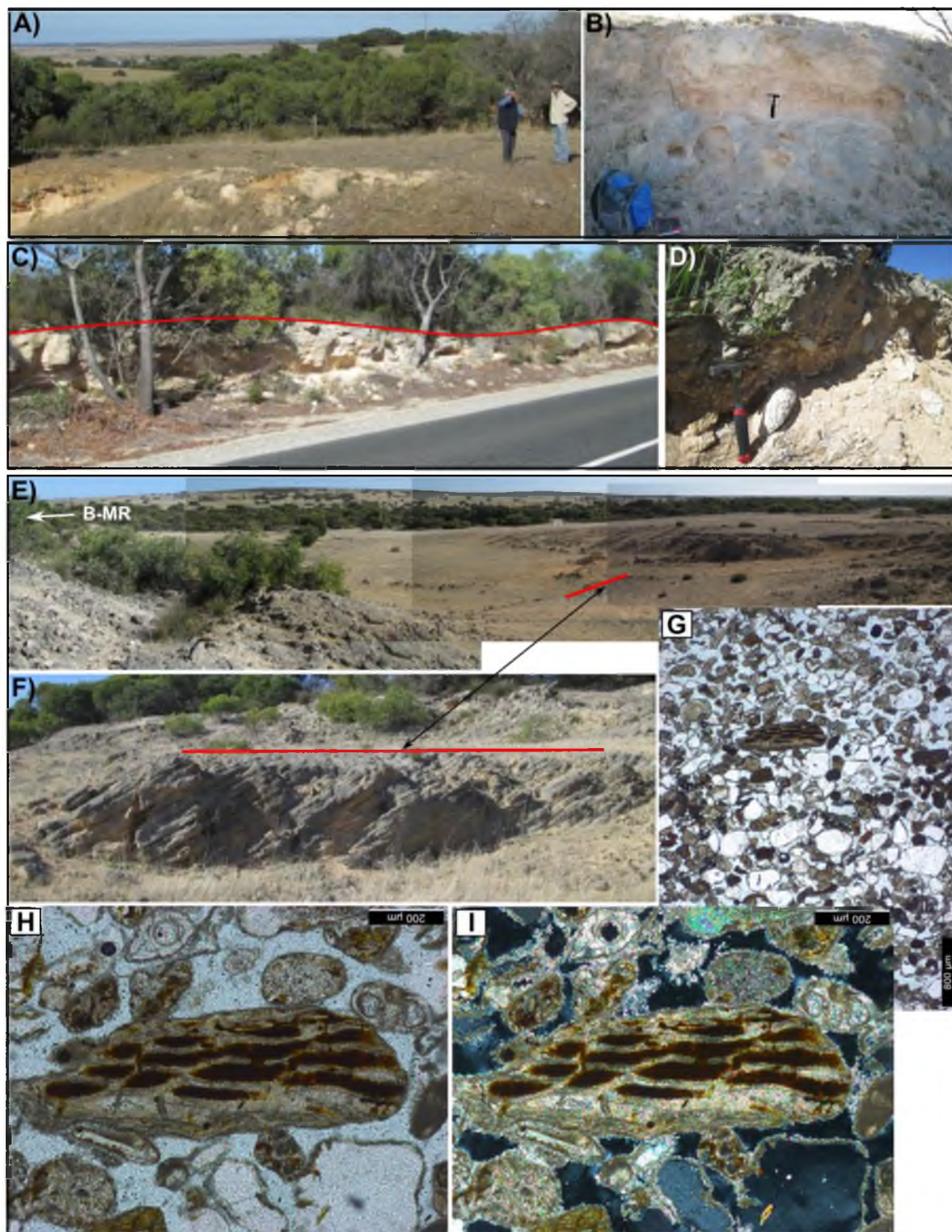


Figure 4.35: B-McIntosh Road and Gravel Pit sites. A-B) McIntosh Road. A) View from above McIntosh dune towards the modern coastline. B) McIntosh exposure. C-D) Aeolianite exposed in road cutting between the two sites. D) The calcrete in places was composed of reworked calcrete gravel and pebbles. E-I) The Gravel Pit. E) View from above the gravel pit bedding (red line) towards the north with the crest of the Murray Lakes Range (~170 m APSL) in the background. F) Preserved bedding within the quarry dipped at 19° towards the east. G) Grains show a consistent orientation and fine lamination. 800 µm. H-I) Plain- and cross-polarised light at 200 µm of bryozoan in G). Note traces of boring on the bryozoan grain. The bryozoans and Foraminifers have been replaced and are variably infilled by iron-stained micrite. Cements are meniscus type but are not isopachus.

are located ~1.3 km apart and 33 km from the modern coastline at ~60 m APSL; the modern Younghusband Peninsula is visible from B-MR (Figure 4.35). At this point the Murray Lakes Range is ~5.5 km in width.

B-MR is the more western of the two sites and consists of a 2.5 m high exposure of very pale brown (10YR 7/4) sand with an overlying massive calcrete (Figure 4.35). The dune crests at a height of ~3 m. The top 2 m of the unit contains extensive rhizolith development and the sand at the base of the rhizoliths is only superficially case hardened. The sand beneath this zone (making up the remaining 1 m) is well indurated. No visible bedding remains in the exposure. A sediment sample was taken from the base. A gravel quarry (B-GP), farther to the east and higher elevation, has exposed some eastward dipping (19°) beds (Figure 4.35). The unit is well consolidated and a sample was taken for thin-section analysis. Between the two sites a road cutting exposes additional aeolianite where faint bedding is observed beneath a massive calcrete (Figure 4.35).

The B-McIntosh Road sand is a poorly-sorted, mainly fine-grained allochemical sandstone (Mount, 1985). The fine quartz grains are angular to sub-angular with a clear vitreous lustre (Table 4.11). Medium and coarse grains are commonly sub-rounded to rounded and are variably frosted or clear with a vitreous lustre. Mollusc fragments as well are fine with abraded surfaces and well-rounded edges (Table 4.11). Foraminifers are rare to sparse and all recrystallised making features difficult to distinguish; there is likely some *Discorbis* sp. present. Similarly, there are likely other fauna types present but diagenesis has made identification difficult.

The sediment at B-GP is a very pale brown (10YR 8/4) well-sorted packstone (Dunham, 1962). Primary porosity is moderate in inter-granular and intra-skeletal spaces. Quartz grains are abundantly fine to medium with mixed sphericity; medium to coarse grains are more commonly sub-angular to sub-rounded. The abundant carbonate fraction is made up of all fauna types. Carbonate grains are abundantly fine to medium in size, generally well-rounded and iron-stained grains are very common. Many of the grains show evidence of algal boring and replacement by calcite. Less common are carbonate grains which have been dissolved to form moulds and are only partially filled

creating secondary porosity. The thin-section shows consistent grain orientation and indications of fine laminae composed of upward fining sequences (Figure 4.35). Most grains have a meniscus micrite cement and subsequent development of dog tooth spar; however, some grains have spar developed directly on the grains substrate.

The sediment at B-GP has a reworked component as indicated by the mix of iron-stained carbonate grains, the general rounding of grain edges and fine to medium grain size. The variety of types of carbonate grain alteration most likely reflects this reworking as well. The meniscus cement, small crystal size of the dog-tooth spar and its scattered development (it is not isopachous) and the amount of remaining pore space indicate a meteoric vadose environment for diagenesis of the sediment.

Although located within 1.5 km of each other, the lithology and skeletal carbonate grains of B-McIntosh Road and the Gravel Pit sites in the field and their petrology suggest different environments of deposition with the former, younger aeolianite located in a high energy environment much nearer to the source of carbonate sediments, the inner shelf.

4.3.6.3 North Coonalpyn

The North Coonalpyn (NC) site is a shallow cutting (60-70 cm) in a 3 m carbonate aeolian dune ~50 km inland from the modern shoreline at approximately 40 m APSL (Figure 4.33). The site is ~18 km northeast of the seaward side of the Murray Lakes Range. The dune retains no visible bedding structures or intact calcrete; although, calcrete gravel and pebbles are on the surface (Figure 4.36). The road cutting is the former Dukes Highway (situated between the modern highway to the east and the railway line to the west) and it is possible that the sediments have been previously disturbed. Two samples were taken, NC1 and NC2, from the base of the dune within the shallow exposure. NC2, reddish yellow (7.5YR 7/6) in colour, was believed to possibly be solution pipe material based on colour. However analysis showed it to be a carbonate dune. Both sediment samples were subject to particle size analysis and binocular microscope analysis (Table 4.11). A thin section was also prepared from NC2.

NC1 is a very pale brown (10YR 7/4) sediment. NC1 and NC2 have similar carbonate contents in the 250-500 μm fraction (30% and 31% respectively) and are

predominantly fine-medium grained allochemical sandstones (Mount, 1985); although, NC2 has a higher silt content (15% versus 9%). NC1 is moderately sorted with abundant rounded to well-rounded medium to coarse quartz grains that have a transparent to frosty appearance and are rarely clear. Fine grains are mainly angular to sub-angular and clear with a vitreous lustre. Carbonate grains are common. Mollusc shell is present as fine to medium, rarely coarse, comminuted and iron-stained fragments with well-rounded edges. Foraminifera are sparse and show varying degrees of preservation with some tests showing abrasion marks. *Discorbis* sp. was positively identified and a SEM image was acquired (Figure 4.4). They are very commonly opaque but also appear orange and red due to iron-staining. Other faunal types are more common than Foraminifers and include bryozoan and echinoderm fragments.



Figure 4.36: The sample locations of NC1 and NC2. Note the same small bush in both photographs.

4.3.6.4 South Coonalpyn

This site (SC-B) is located 47 km inland from the modern shore and on the margin of the Coonalpyn Range (Figure 4.33). It is 21 km to the southeast of the North Coonalpyn site and at least 20 m APSL. A quarry has been cut 8-10 m deep within a massive dune. The dune exposure at the eastern end of the quarry is highly indurated with a vibrant reddish yellow colour (7.5YR 6/6), extensive solution pipe development and only faint traces of original low-angle planar bedding (Figure 4.37). The capping

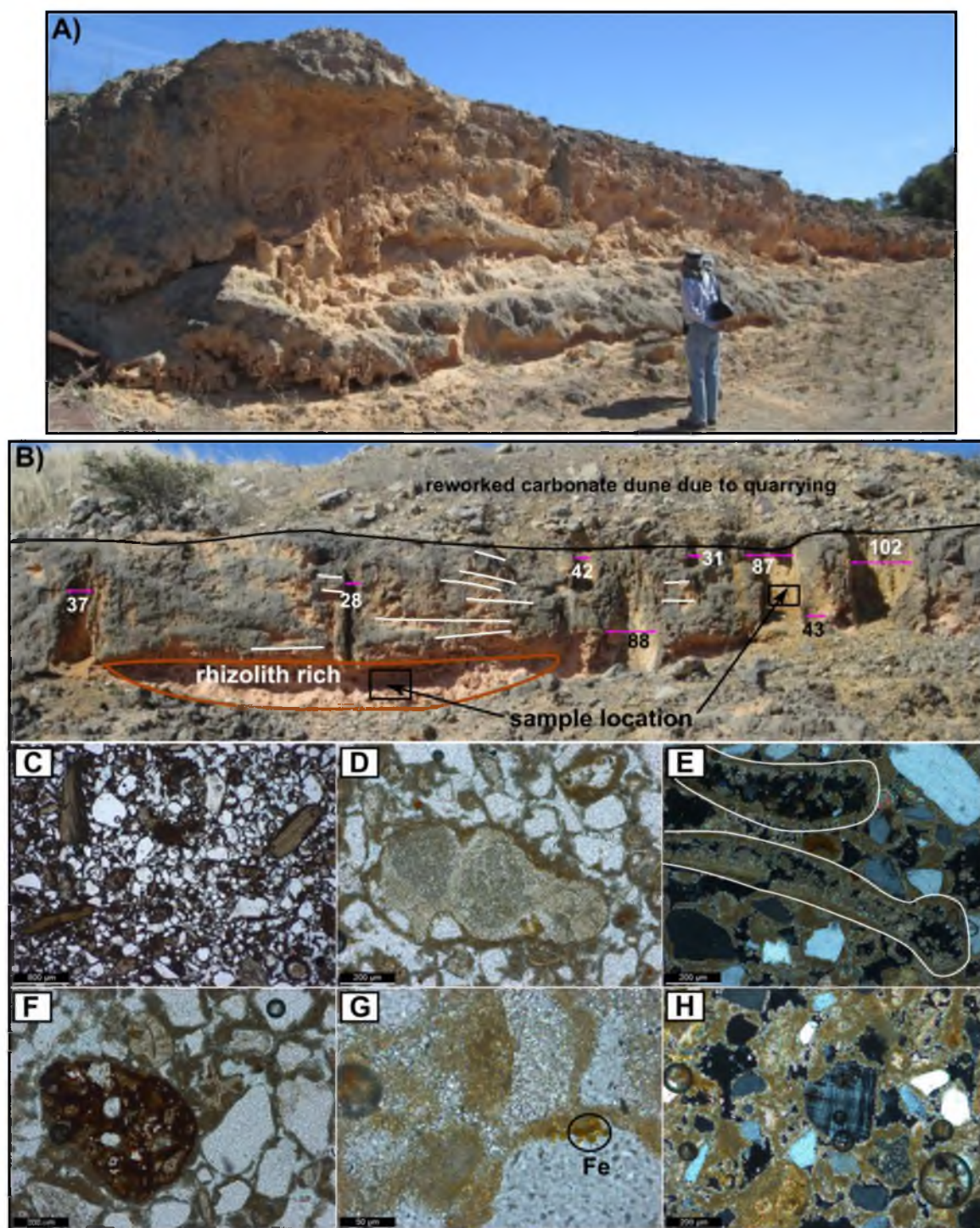


Figure 4.37: South Coonalpyn. A) Western exposure with massive calcrete and extensive rhizolith development. B) Eastern exposure contains well-indurated faint bedding (white) overlying a rhizolith-rich zone. Solution pipes have developed throughout, and their width (pink line) is provided in cm (associated number). C) The sediment is poorly sorted, fine to coarse grained. Scale 800 µm. D) A recrystallised gastropod fragment. Scale 200 µm. E) Cement replaced grains (outlined in white) has produced secondary porosity. Scale 200 µm. F) Intraclast grain. Scale 200 µm. G) Microspar cement and iron-rich cutan. Scale 50 µm. H) Microcline grain off-center. Scale 200 µm.

calcrete here has been either removed or obscured by quarrying activities; however, another exposure at the western end of the quarry exhibits a massive and potentially laminar calcrete. A sediment sample was taken from a rhizolith-rich zone near the base (~3.5 m depth of burial) of the eastern exposure. A second sample was taken from solution pipe infill and will be described in Section 4.3.7.

The SC-B aeolianite is predominantly a sandy (78%) very fine to coarse grained wackestone (Dunham, 1962; Figure 4.37). Quartz grains are mainly sub-angular to sub-rounded. Medium to coarse grains exhibit both angular and rounded grains. Plagioclase, microcline, other feldspars, chert and lithics are identified in thin-section (Figure 4.37). Carbonate grains are abundant; a whole-rock sample of the sand was found to be 57% carbonate. Mollusc fragments can be large, up to 1 mm with well- to moderately-rounded edges. Mollusc appears to be the most abundant type of fauna but Foraminifers, bryozoans, echinoderms and coralline algae are also present (Figure 4.37). Iron-staining of grains is common as well as calcite replaced grains and partially-filled skeletal moulds. Primary inter-granular and intra-skeletal pore space is minimal. Secondary porosity has been generated by the partially-filled skeletal moulds. The cement is mainly granular microspar indicating diagenesis in the meteoric-vadose zone.

4.3.6.5 Emu Springs

Emu Springs (ES) is a shallow (2 m) quarry 69 km inland from the modern shore, 28 km nearly due east of the South Coonalpyn site and within the Coonalpyn Range at nearly 80 m APSL (Figure 4.33). It is located on the western margin of the Big Desert which is composed of vast deposits of Molineaux Sand (Firman, 1973; Chapter 2.5.1). There is no calcrete surface or bedding exposed within the quarry and the sediments are well indurated. The presence of solution pipes is indicated by changes in sediment colour (Figure 4.38) but they may have been obscured by quarry activity. A sediment sample was taken from the base of the quarry at 2 m depth.

The sediment is a pink (7.5YR 8/4) mainly very fine to fine-grained sandy allochemical limestone (Mount, 1985) (Table 4.11). Medium-grained quartz makes up 19% of total sand-sized grains. The finer grains are mainly angular to sub-angular with a clear vitreous lustre. Medium-sized grains are sub-angular to rounded with a clear lustre

to translucent appearance and are commonly iron-stained. Although calcite development is extensive and carbonate grains showed evidence of diagenetic alteration, they are well preserved and retain many of their identifying characteristics as seen in SEM analysis (Figure 4.4). Carbonate of all faunal types is abundant. Mollusc fragments are mostly fine-grained with well-rounded edges. One small gastropod was identified. Foraminifers are sparse and found predominantly within the medium-grain size fraction. Identified species include: *Discorbis* sp., *Elphidium* sp. and *Triloculina*. Other fauna is also well represented in the medium-grain size including bryozoan, echinoderm and calcareous algae fragments.

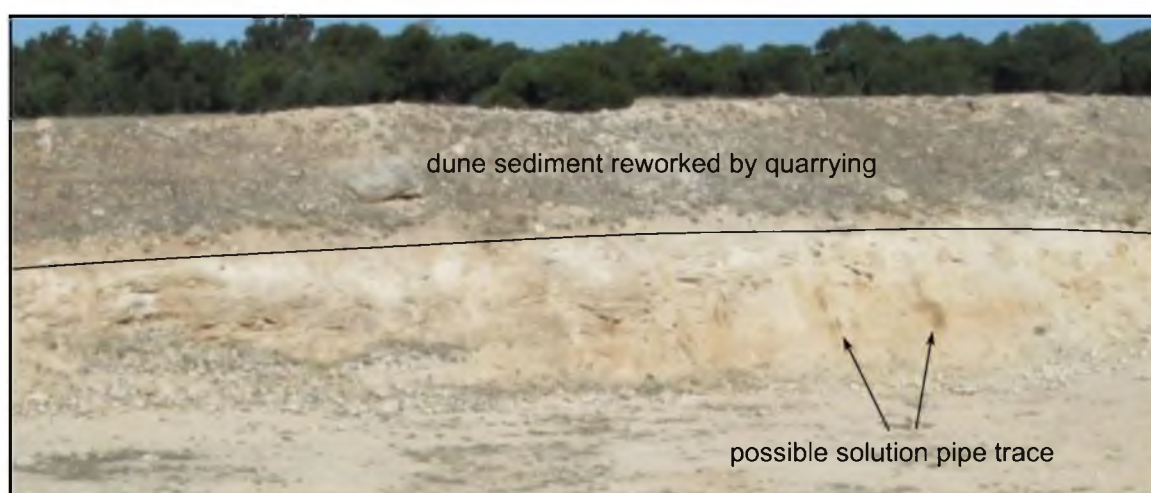


Figure 4.38: The shallow exposure at Emu Springs.

4.3.6.6 Tauragut Well

The Tauragut Well site (TWR) consists of a small outcrop within a field 70 km inland from the modern shore at ~40 m APSL (Figure 4.33). The outcrop is 110 cm high and capped by a thin laminar calcrete (Figure 4.39). The very pale brown (10YR 8/4) poorly sorted sediment is a moderately indurated allochemical sandstone (Mount, 1985). Quartz grain size ranges from very fine to coarse but is predominantly fine-medium (Table 4.11). The fine to very fine fraction is mostly composed of angular to sub-angular grains with a clear vitreous lustre appearance. The medium to coarse grains are commonly sub-rounded to rounded. Medium grains tend have a clear lustre, whereas coarse grains are mainly translucent to frosty. Carbonate grains are sparse. Mollusc



Figure 4.39: The Tauragut Well exposure reaches 1.10 m with a thin laminar calcrete.

sparse and are abraded and broken, mostly pitted, recrystallised and coated with calcite. *Elphidium* sp. and *Discorbis* sp. were tentatively identified. Other fauna is present but also poorly preserved.

4.3.6.7 Carcuma

Carcuma (CG) is located 6.3 km due east of Tauragut Well at 60 m APSL (Figure 4.33). The site is a road cutting through the siliceous Molineaux Sand which form the Big Desert stretching into New South Wales (section 1.5.1; Figure 4.40). The dune reaches a height of ~5 m. Layers have formed within the dune by a post-depositional process which has concentrated iron oxides and small amounts of clay; the layers could reflect original dune bedding and the contribution of fine dust to the aeolianite. The dune contains a weakly developed soil profile which is overlain by reactivated sands (~40 cm thick) and vegetation. Samples were taken from 4 m below the land surface and from within the soil profile at 0.45 m depth of burial.

The well sorted sands are yellow (10YR 7/6) with a minor silt (5%) and clay (1%) component (Table 4.11). Medium to fine grains (47% and 31% respectively) are most abundant with a lesser quantity (19%) of coarse grains and minor (4%) quantity of very fine grains. Fine and very fine grains are mainly sub-angular to sub-rounded, either clear or translucent with a lustre, rarely milky. Larger grains are sub-rounded to rounded. Medium grains exhibit a translucent lustre with milky grains common. Coarse grains are mostly frosted to milky. The soil profile sands are similar to the underlying sands but with traces soil pedogenesis indicated by organic matter, rootlets and brown clay on grains.

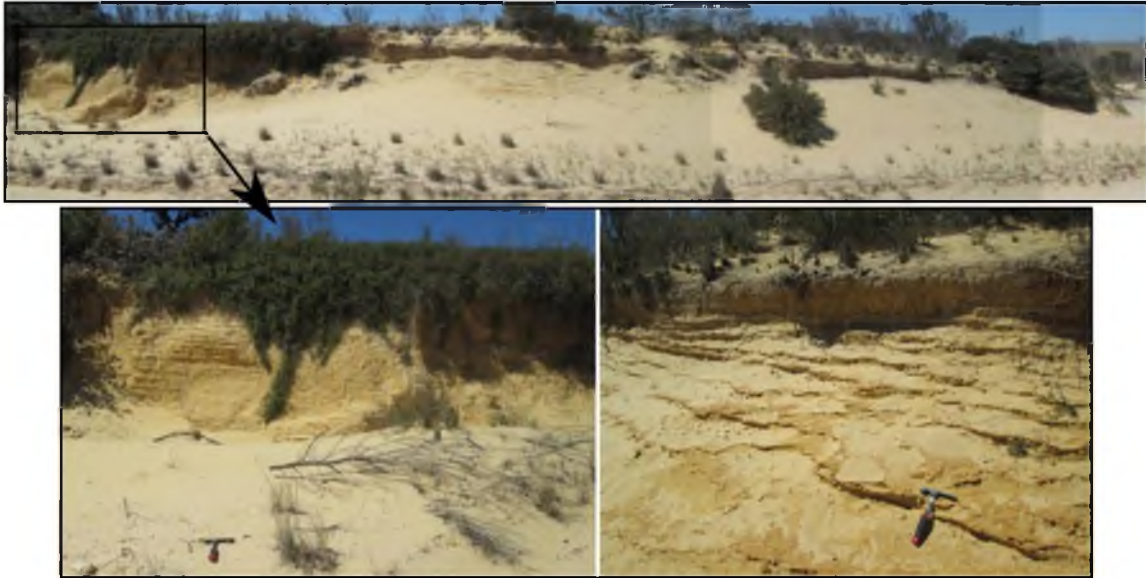


Figure 4.40: A road cutting at Carcuma bisects a dune of Molineaux Sand exposing layers that may reflect the original dune bedding. A weakly developed soil horizon is found at the crest of the dune which is overlain by reactivated sands.

4.3.6.8 Taillem Bend

The Taillem Bend field site (TB) is 59 km inland from the modern shoreline at ~30 m APSL (Figure 4.33). It is 3.1 km east of the River Murray and at the base of the westernmost extent of the Marmon Jabuk Escarpment. A ~7 m deep quarry has exposed a 4 m thick, highly indurated yellowish red (5YR 4/6) sediment which is capped by a blocky and nodular calcrete 2-3 m thick (Figure 4.41). A sample of the red-hued sediment was taken from 4 m depth of burial. The sediment is composed of 47% sand, 32% silt and 21% clay (Table 4.11). There is no carbonate within the sediment. The silt-clay matrix forms gravel and pebble-sized clasts which are easily broken by light pressure. The sand is predominantly fine- to medium-grained with minor components of very fine and very coarse grains. The angularity of the quartz grains decreases as size increases. Finer grains are mainly angular to sub-angular whereas medium-coarse grains are more likely to be sub-rounded to rounded. However, there is the rare angular coarse grain and a sparse amount of sub-angular grains. Medium-coarse grains are iron-stained while fine-very fine grains are rarely discoloured. Grains are mostly translucent with sparse quantities of frosted medium-coarse grains. The particle content of the Taillem

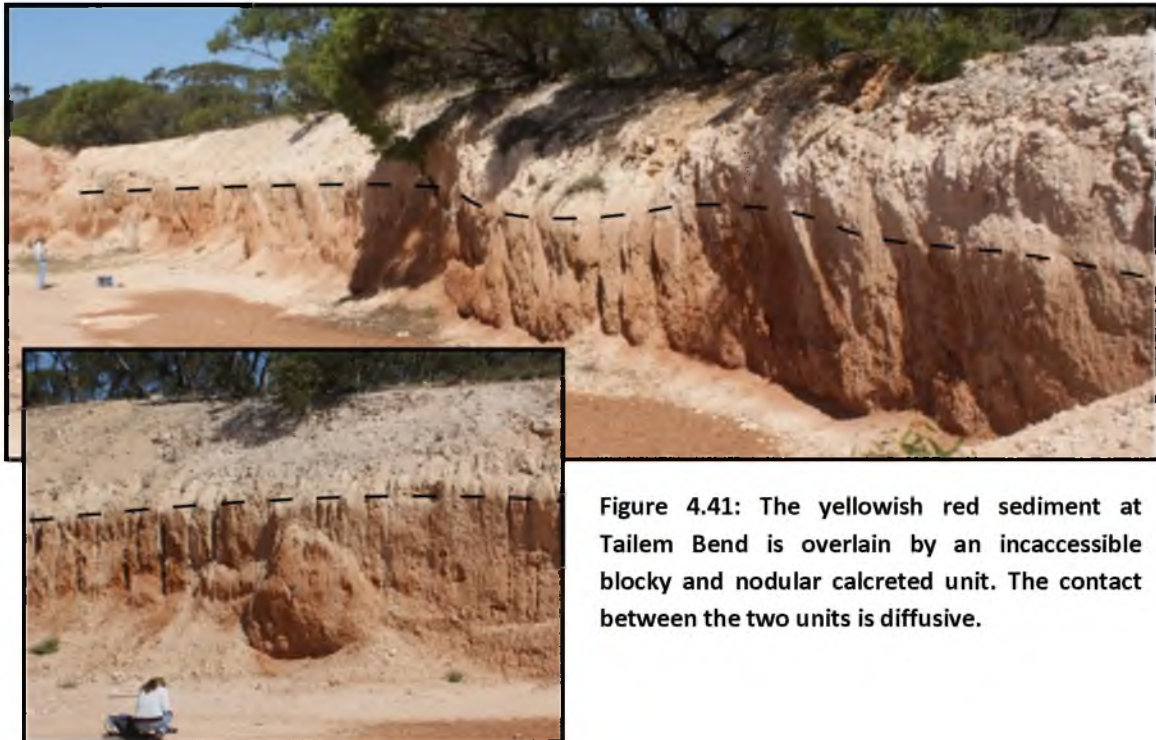


Figure 4.41: The yellowish red sediment at Taillem Bend is overlain by an inaccessible blocky and nodular calcreted unit. The contact between the two units is diffusive.

Bend sediment and the proximity of the site to the Marmon Jabuk Escarpment imply that it is an alluvial deposit. The overlying calcrete would have formed with the movement of carbonate through the profile most likely associated with water evaporation.

4.3.6.9 Murray Bridge

The Murray Bridge site (MB) is located within a distal alluvial fan to the east of the Mount Lofty Ranges (~20 km west) at ~20 m APSL and 4.8 km west of the Murray River (Figure 4.33). The land surface of the immediate region to the north consists of rubbly calcrete. The plain to the south is blanketed by dune ridges, trending northwest to east towards Lake Alexandrina. A quarry exposes the old calcrete profile to a depth of 1.4 m. The calcrete is pale, massive and rubbly, showing evidence of multiple cycles of formation, fracture and reformation (Figure 4.42). The calcrete reaches up to 1 m thick and transitions into rubbly, well-indurated, yellowish-brown (10YR 5/4) sediment containing angular gravel and pebbles (Table 4.11). Lenses of finer grained sediments are overlain by lenses of coarser grained sediments indicating fluctuations in the energy of the depositional environment. There are also large intraclasts (≤ 15 cm) of pink calcrete (Figure 4.42). A sample was taken from near the base.

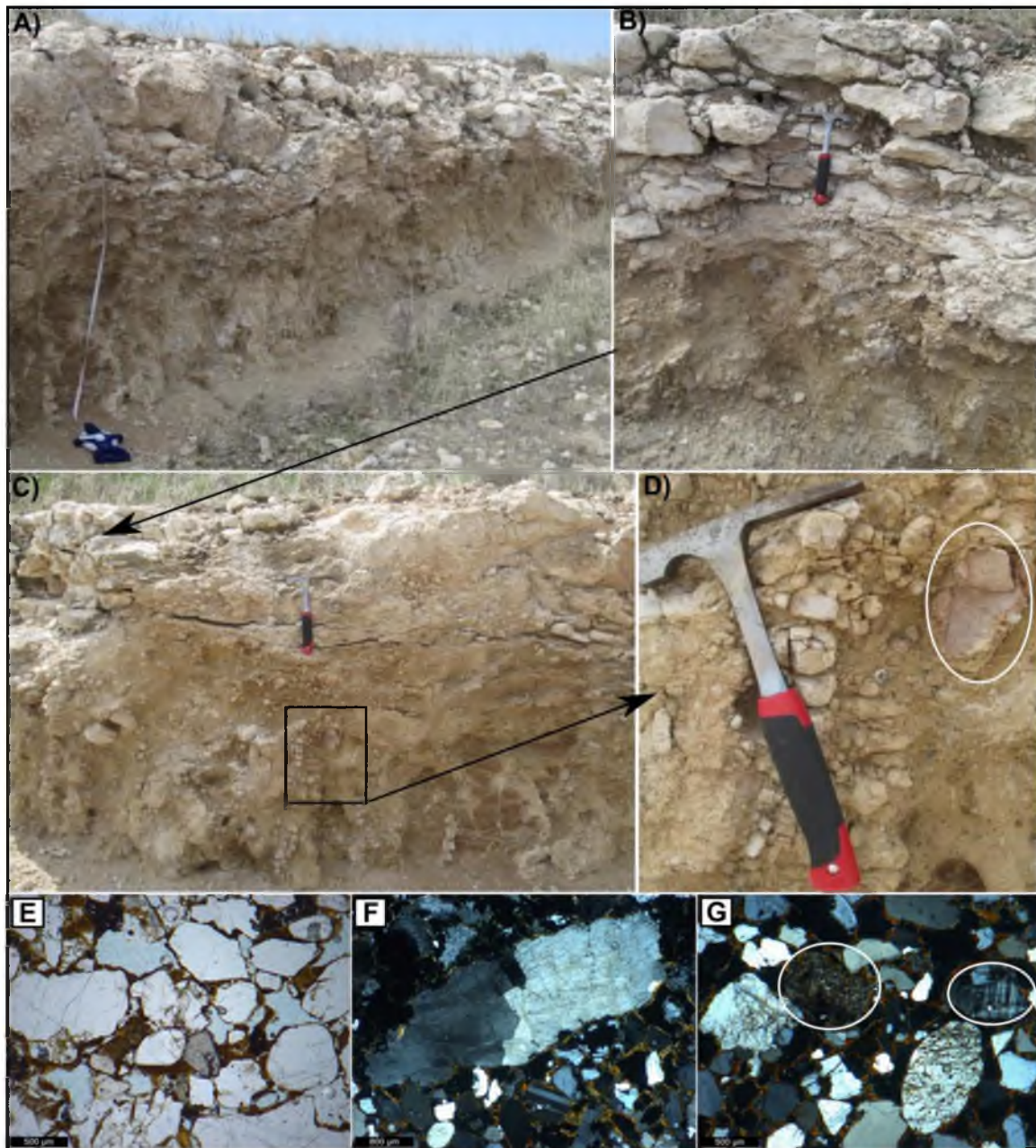


Figure 4.42: The Murray Bridge calcrete is a thick (~1-1.5 m), blocky calcrete with evidence of extensive pedogenesis. A) The calcrete exposed is extensive and well developed. B) Infiltration of the rubbly calcrete by the upper A-component of the soil profile is greater at some locations than others. C) The calcrete is more massive and nodular in other places. D) A close-up of a large calcrete clast. The hammer rests on a fractured rhizolith which were extensive throughout the deposit. E) A plane-polarised view of Murray Bridge grains in a matrix of iron-stained clay cutans. Note the embayment of some grains, indicative of corrosion during diagenesis; also, the evidence of compaction (grains in centre) and fractured quartz grains. Scale 500 μm . F) A large composite quartz grain. The straight crystal boundaries indicate an igneous source. A plagioclase grain is located directly beneath the large grain. Scale 800 μm . G) A lithic fragment (circled left) is surrounded by sutured and fractured quartz grains. Fractured grain to the left may have undergone solution as indicated by the concavo-convex contact with surrounding grains. The grain circled to the right is a composite grain of quartz and microcline. Scale 500 μm .

Thin section analysis of the less pedogenically modified sediments underlying the calcrete show the sediment at Murray Bridge to be an immature feldspathic greywacke (Folk, 1974). It contains weathered, altered, sutured and composite quartz grains, quartz with inclusions, plagioclase, microcline and other feldspars, lithic grains and chert within iron-oxide stained clay cutans (Figure 4.42). Tangential and sutured contacts between grains indicate compaction and reduction of porosity.

The lack of bedding within the unit inhibits identification as either a fluvial or alluvium deposit, however the proximity to the Mount Lofty Ranges indicates it is part of an alluvial fan coming off the ranges. The coarse grains indicate a short transport distance with sediment sourced from the adjacent Mount Lofty Range and underlying adamellite. The adamellite is represented by grains of plagioclase, orthoclase and microcline. The Mount Lofty Ranges are represented by quartzite grains and phyllite (a low grade metamorphic rock). The clay cutans which coat the grains would have developed during pedogenesis and the development of the overlying calcrete. The calcrete appearance indicates multiple cycles of formation, fracture and reformation, suggesting a greater period of time has lapsed since initial deposition.

4.3.6.10 Discussion of inland field sites

The inland sites of the Bridgewater Formation (Mount Misery, B-McIntosh Road and Gravel Pit, North Coonalpyn, South Coonalpyn, Emu Springs and Tauragut Well) are associated with the Murray Lakes Range, the Coonalpyn Range and the Cannon Ball Hill Range (Figure 4.33). The former ranges are linked to the granite outcrops of the Padthaway Ridge which would have formed headlands and loci for deposition through multiple interglacial periods. The Cannon Ball Hill Range, with which Tauragut Well appears to be an extension, has been identified as the 'first' Bridgewater Ridge and tentatively correlated with MIS 43 or 47, near 1.3 to 1.4 Ma (Bowler, 2006). The Coonalpyn Range, in which the South Coonalpyn and Emu Springs sites are found, is a composite range in which Sprigg (1979) identified seven different beaches. The range is considered a northwards extension of the West and East Naracoorte Ranges and earlier ranges (Rogers, 1980; Bowler, 2006) and is, therefore, at its youngest, equivalent to the West Naracoorte Range age of 800 ka (MIS 19; Huntley *et al.*, 1994). This range extends

Table 4.11: Analytical results of the inland site locations. The percentage of sand-sized particles is based on the total sand-size fraction and not the total sediment.

SITE	MOUNT MISERY	B-MCINTOSH ROAD	NORTH COONALPYN	NORTH COONALPYN	SOUTH COONALPYN	EMU SPRINGS	TAURAGUT WELL	CARCUMA	MURRAY BRIDGE	TAILEM BEND
Field Code	MTM	B-MR	NC1	NC2	SC-B	ES	TWR	CG	MB	TB
Calcrete	yes-massive, rhizolitic	yes-massive, rhizolitic	no	no	yes-completely	no	yes-laminar	-	yes-massive, rubbly	yes-nodular
Calcrete thickness	1-2 m	1-2 m	-	-	8-10 m	-	≤5 cm	-	1 m	1-1.5 m
SEDIMENTS										
Depth of burial (m)	3	2.50	0.65	0.60	3	2	1.10	4	1.40	4
Munsell Colour	10YR 7/6 yellow	10YR 7/4 very pale brown	10YR 7/4 very pale brown	7.5YR 7/6 reddish yellow	7.5YR 6/6 reddish yellow	7.5YR 8/4 pink	10YR 8/4 very pale brown	10YR 7/6 yellow	10YR 5/4 yellowish brown	5YR 4/6 yellowish red
% CaCO ₃ (250-500 µm)	28	29	30	31	57 (whole fraction)	50	12	0	6	0
Heavy minerals	sparse/common	sparse	rare	very rare	none identified	very rare	sparse/common	rare	none identified	common
Particle Size Analysis (Malvern Mastersizer)										
clay	2	1	1	1	3	6	3	1	1	21
silt	15	7	9	15	19	22	18	5	16	32
sand	83	92	90	84	78	72	79	94	83	47
very fine	14	14	1	8	20	29	10	4	13	11
fine	47	53	30	22	38	51	38	31	14	35
medium	34	29	54	42	34	19	42	46	22	42
coarse	3	4	15	27	8	0	10	19	18	11
very coarse	1	0	0	1	0	0	0	0	33	0
QUARTZ (binocular analysis)	**thin section								**thin section	minor component
Sorting	moderate-well	poor-moderate	moderate	poor	poor-very poor	poor	poor-very poor	moderate	very poor	poor-very poor
Particle size	fine-medium	fine-coarse	fine-coarse	fine-coarse	very fine-coarse	very fine-medium	very fine-coarse	very fine-very coarse	very fine-very coarse	very fine-coarse

Table 4.11 *continued*: Analytical results of the inland site locations.

Field Code	MTM	B-MR	NC1	NC2	SC-B	ES	TWR	CG	MB	TB
QUARTZ (continued)	**thin section							**thin section		minor component
Roundness	medium-coarse grains abundantly rounded to subrounded and spherical; finer grains exhibit increased angularity	fine-very fine grains abundantly angular to subangular; medium to coarse grains abundantly subrounded to rounded	fine grains abundantly angular/subangular; medium-coarse grains abundantly rounded to well-rounded	very fine to fine grains very angular to subangular; medium to coarse grains abundantly rounded	angularity decreases with size increase	very fine abundantly angular/subangular; coarse grains subangular to rounded; fine grains mixed	fine grains abundantly angular/subangular; medium-coarse grains abundantly subrounded to rounded	typical increase in angularity with decrease in grain size	abundantly subangular/angular; contains gravel and pebbles as well as intraclasts of older calcrete	abundantly fine-medium grains in a red clay/silt matrix; very fine-fine grains angular to subangular; medium-coarse grains rarely angular
Surface texture	clear vitreous lustre to frosted; finer grains minimal frosting	abundant clear vitreous lustre; coarse grains very commonly frosted/milky	fine grains with clear vitreous lustre; medium coarse grains variably transparent, frosted/milky	coarse grains abundantly frosted; very fine, fine grains abundant vitreous lustre		abundant vitreous lustre; medium grains common frosting and Fe-staining	very fine, fine grains abundant vitreous lustre; coarse grains very commonly frosted and/or Fe-stained	fine grains either vitreous lustre or translucent; coarse grains abundantly frosted/milky	abundantly frosted/milky	very fine-fine grains rarely discoloured; medium-coarse grains commonly frosted/milky or Fe-stained
CARBONATE	common	common	common	common/very common	very common	abundant	sparse	none	none	none
Molluscs	<1 mm, abundantly fine	abundantly fine, abraded, well-rounded	abundantly fine, well-rounded	abundantly fine to very fine, recrystallised	<1 mm, well-rounded, abraded, abundantly replaced	abundantly fine, well-rounded, 1 small gastropod	fine-medium grain size, well-rounded and abraded	-	-	-
Foraminifer	sparse, recrystallised	sparse, recrystallised	sparse	sparse/common, recrystallised	replaced	sparse; <i>Discorbis</i> and <i>Elphidium</i>	sparse, pitted, recrystallised, broken	-	-	-
Other fauna	sparse	none identified	common	sparse, recrystallised	replaced	abundant	common	-	-	-

over the Marmon Jabuk – Kanawinka Escarpment which defines the eastern margin of the Coorong Coastal Plain.

Confining the age of the Murray Lakes Range and the sites at North Coonalpyn, Murray Bridge and Tailem Bend is more difficult. The previously reported (Murray-Wallace *et al.*, 2010) TL age for Mount Misery suggests an age of MIS 9 or 11 for a deposit downslope (at ~10 m APSL) from the crest of the range (>60 m APSL). Petrographical analysis suggests that at least for some time during its deposition it was in a sub-aqueous or near-shore environment. This implies that it could have been deposited during the flooding of a back-barrier corridor and that the core of the Murray Lakes Range may be older than the Mount Misery site. The size (height and width) of the Murray Lakes Range within the Coorong Coastal Plain also suggests that there were multiple phases of deposition to produce the range. This is perhaps best reflected by the B-McIntosh Road and Gravel Pit sites, which, although in close proximity, stratigraphy and petrology suggest were deposited in different environments, the former in a lower-energy environment removed from the source of skeletal carbonate grains and the latter in a high-energy environment near to the source. The calcrete exposed in the road cutting between the field sites is most likely positioned stratigraphically between the units as well. It is possible that the calcrete is an extension of the massive calcrete overlying B-McIntosh Road but more investigation is required to confirm this. The road side calcrete also contains a reworked calcrete component further strengthening the argument for multiple phases of deposition.

XRD analysis of the sediment mineralogy of the inland field sites, which can be diagnostic of the degree of diagenesis that has occurred, was inconclusive. Colwell (1978) found that the mineralogy of sediments from ranges across the coastal plain to show a progressive elimination of unstable and metastable carbonate components (aragonite and high-Mg calcite) with increasing age (distance inland). However, the XRD results of the inland sites do not show a consistent trend, perhaps a further reflection of the composite nature of the ranges.

4.3.7 Siliceous Sands

Many of the field sites examined in the course of this research consisted not only of aeolian calcarenites associated with periods of interglacial high sea-level but also siliceous sands which were deposited during periods of low sea-level and increased aridity (Figure 4.43). These sands filtered into the solution pipe cavities within calcretes to become the ubiquitous solution pipe infill. Solution pipe fill is generally a reddish soil, either clay or sand, associated with a surface soil of the same colour (Blackburn *et al.*, 1965).

The *terra rossa* soils identified at Point McLeay formed during breaks in the deposition of Bridgewater Formation and have been related to extensive periods of subaerial exposure (Boutakoff, 1963; Sprigg, 1979; Milnes, 1982; Brooke *et al.*, 2014). It has been proposed by Mee *et al.* (2004), that the soils are composed of sediments derived from the weathering of Palaeozoic Kanmantoo meta-sediments. The soils represent the earliest known deposits to be associated with glacial conditions in the study area. More recent instances are the siliceous sand sheets overlying MIS 5e deposits on Hindmarsh Island and southeast of Lake Albert. The siliceous sands are recognised as part of the Molineaux Sand Formation (Firman, 1973) which is very well represented at the Carcuma field site.

Siliceous sands from throughout the study area were subjected to particle size, XRD and binocular analysis to determine if any trends or similarities existed across the field sites and through time (Table 4.12). The aeolian derived siliceous sands at Myrtlegrove Road (MR) and Carcuma (CG) have already been described (sections 4.3.5 and 4.3.6). Additional siliceous sands were identified (and have previously been mentioned) at The Drain (TD), Sturt Monument (SM), Riverside (RW), Woolshed (WS) and Yarindale (YRQ). Three solution pipe samples were analysed: Chart House (CH), Point Sturt Road (PSR) and South Coonalpyn (SC-B; Table 4.13). These sediments are compared to the *terra rossa* soils and also the alluvium sediments at The Drain and Myrtlegrove Road.

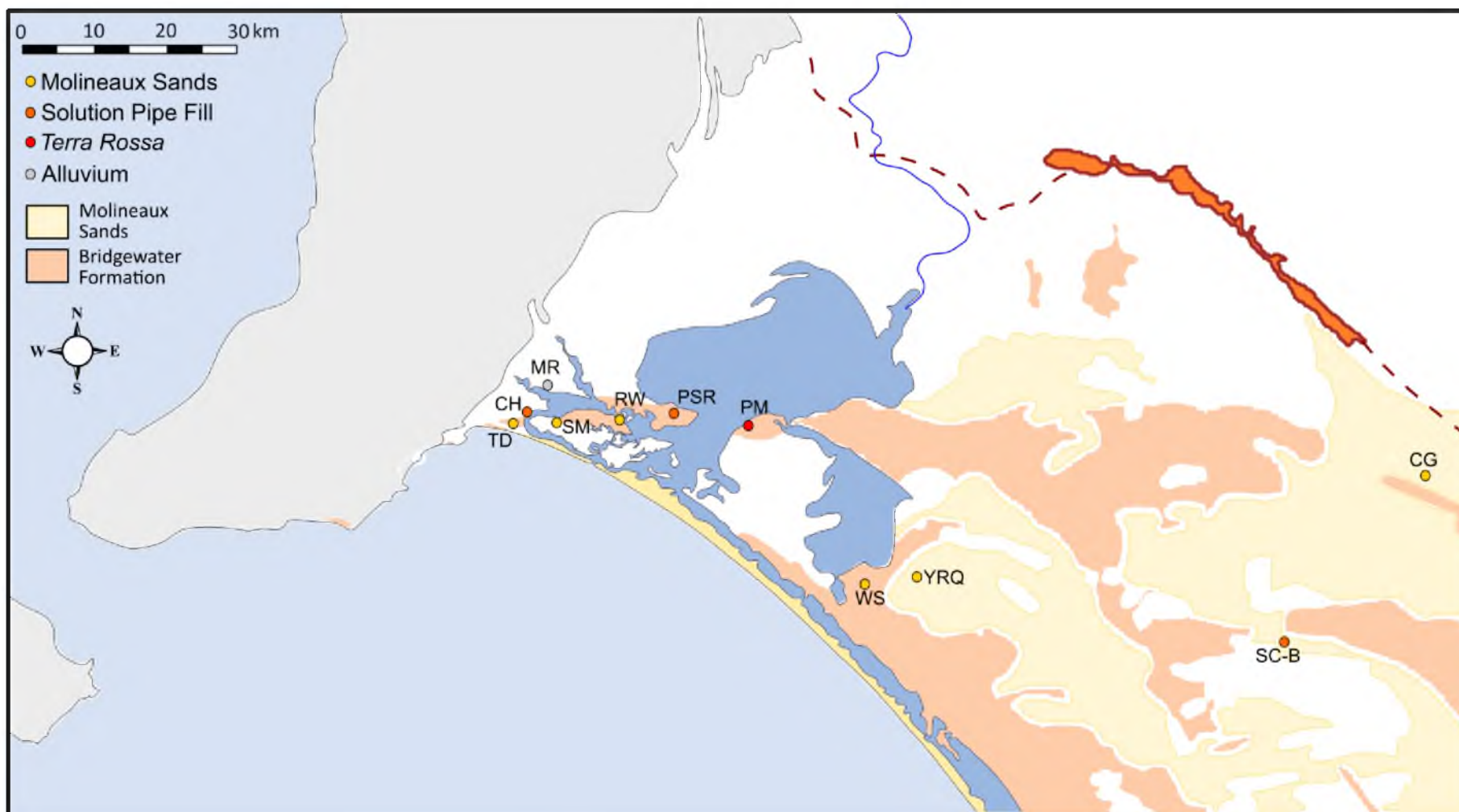


Figure 4.43: Location of Molineaux Sands, *terra rossa* soil, solution pipes and alluvium. Field codes correspond to field sites as follows: Carcuma (CG), South Coonalpyn (SC-B), Yarindale (YRQ), Woolshed (WS), Point McLeay (PM), Point Sturt Road (PSR), Riverside (RW), Sturt Monument (SM), The Drain (TD), Chart House (CH) and Myrtelgrove Road (MR). The Drain and Myrtelgrove Road host both alluvium and Molineaux Sand sediment.

4.3.7.1 Molineaux Sand

The Molineaux Sands not yet described are found at the southeast Lake Albert sites of Yarindale and Woolshed Road, the Hindmarsh Island sites at Sturt Monument and Riverside, and in Goolwa at The Drain field site. All of these sands were located overlying a calcreted surface of MIS 5e interpreted deposits indicating deposition following the Last Interglacial (Figure 4.44). Unlike the dune at Carcuma, none of these sands had traces of lamination that could be interpreted as bedding.

At The Drain site in Goolwa an intervening alluvial sediment (described below) separated the siliceous sand from calcrete. The siliceous sand reached a thickness of over 1 m and deposition appears to have been recent as there was no soil profile developed within the dune but only at the modern surface.

The Sturt Monument sand, located on the western end of Hindmarsh Island (Figure 4.43) is up to 1.5 m thick and overlies a last interglacial aeolianite with laminar and nodular calcrete. The entire exposure is ~2.5 m thick. Approximately 9 km almost due east, the Riverside siliceous sand drapes a section of the northern Hindmarsh shoreline (section 4.3.3.2) at an unknown thickness. The shoreline is composed of two units of Bridgewater Formation, each capped by calcrete. The glacial sand alters the profile of the shoreline where it overlies the younger calcrete.

The calcretes at the Woolshed Road and Yarindale were described in section 4.3.3.1. The Woolshed calcrete is found near the crest of a dune to the southeast of Lake Albert (Figure 4.43). Slightly farther downslope, to the southeast, a dune of siliceous sand is found overlying the Woolshed calcrete. The glacial sands reach a height of ~2.5 m. A change in sand colour within the glacial sands (Table 4.12) indicates two periods of deposition. Sediment samples were taken from both glacial sands. The calcrete at Yarindale is overlain by siliceous sand profile which reaches a maximum depth of 45 cm (Figure 4.44). The sand directly overlying the weakly developed Yarindale calcrete has an orange colour and grades upwards into yellowish brown (10YR 5/6). The stronger colour at the base of the sand likely reflects the accumulation of iron oxides above the more impermeable calcrete. The yellowish brown sand is overlain by pale

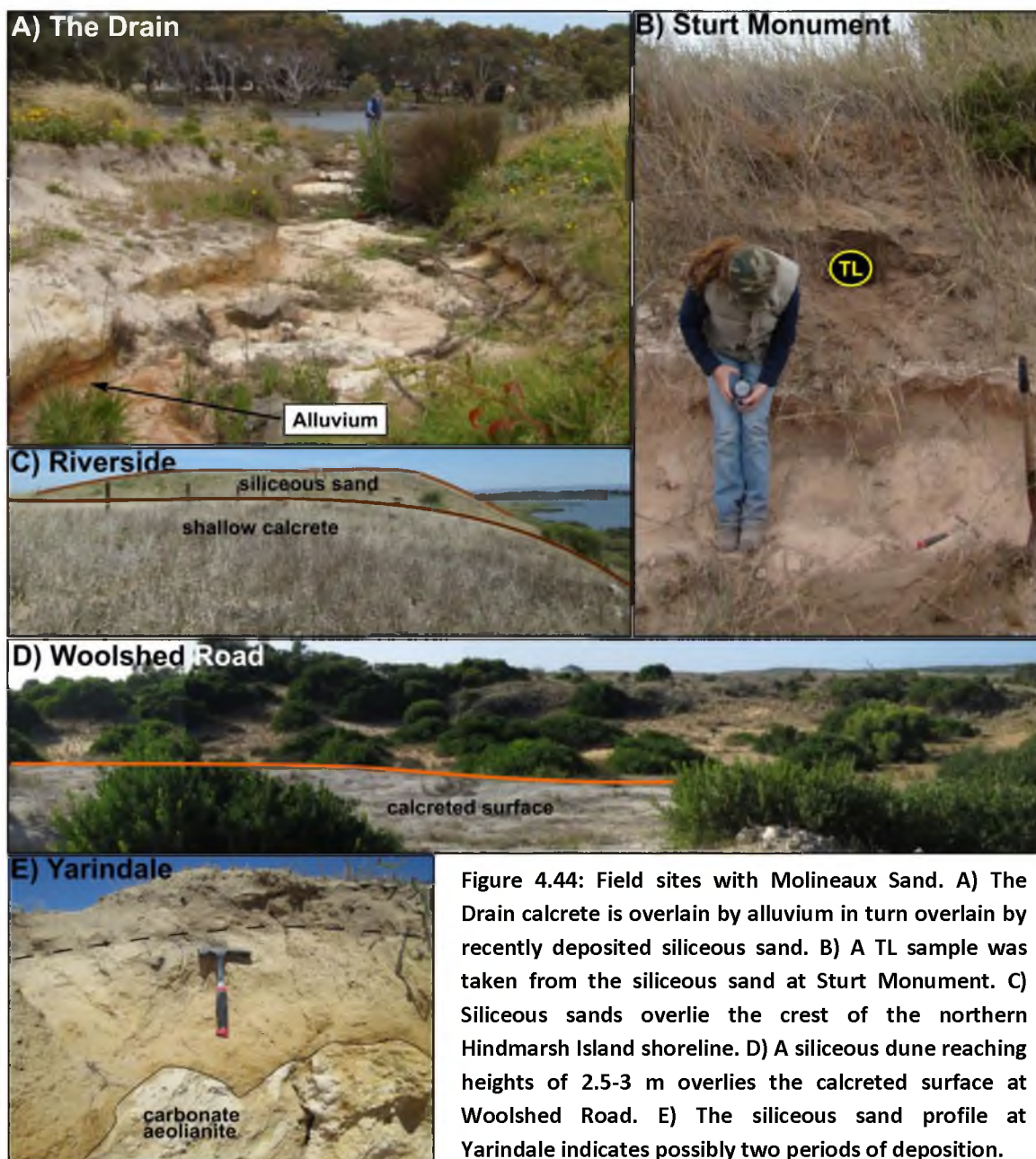


Figure 4.44: Field sites with Molineaux Sand. A) The Drain calcrete is overlain by alluvium in turn overlain by recently deposited siliceous sand. B) A TL sample was taken from the siliceous sand at Sturt Monument. C) Siliceous sands overlie the crest of the northern Hindmarsh Island shoreline. D) A siliceous dune reaching heights of 2.5-3 m overlies the calcreted surface at Woolshed Road. E) The siliceous sand profile at Yarindale indicates possibly two periods of deposition.

brown (10YR 6/3) sand which either reflects pedogenic processes or more recent deposition. Sediment samples were taken from the yellowish brown and the pale brown sand.

The Molineaux Sand identified in this research is similar at all field sites. Although the particle size may vary they are all predominantly composed of sand; mainly fine-medium grained with no very coarse grains and a moderate degree of sorting (Table 4.12). Sediment colour is less consistent. The sediments most similar in colour to the Carcuma (yellow 10YR 7/6) deposit are those at Goolwa and Myrtlegrove Road, which are either very pale brown or yellow. Those most dissimilar are found on Hindmarsh Island

where the sands are a dark yellowish brown (10YR 4/4). The sand at Sturt Monument and Riverside (Hindmarsh Island deposits) is similar in colour to the sediments overlying calcrete on Hindmarsh Island retrieved from auger hole BH:S-R (section 4.3.2). The colours of the Lake Albert sands (Woolshed Road and Yarindale) are in between the pale and dark extremes.

Grain roundness appears to be a reflection of dominant grain size following the inverse relationship of an increase of aeolian grain angularity with a decrease in particle size (Glennie, 1970); sediments with a larger median grain size exhibit a higher degree of rounding than sediments with a predominantly fine-grain fraction (Table 4.12). The grain roundness is consistent between regions and sites where there appears to be more than one period of siliceous sand deposition. The more recent quartz grains at Woolshed Road, Yarindale and Myrtlegrove Road share the same roundness characteristics as the quartz grains of the underlying unit. This is true as well for the two Hindmarsh Island sites, which share similar particle size and roundness characteristics.

Surface texture of quartz grains shows more variability than grain roundness. In general, frosting is very common to abundant reflecting the aeolian origin of the grains. However, at the Woolshed Road and Yarindale sites there is an increase in the quantity of vitreous lustre quartz grains and decrease in the quantity of iron-stained grains within the apparently 'younger' siliceous sand over the 'older' siliceous sand (Table 4.12). Similarly, although the quantity of clear, translucent or frosted grains does not appear to change noticeably between Riverside and Sturt Monument, the latter site shows a much higher quantity of iron-stained grains. This may reflect sampling depth; the Sturt Monument sample was taken at a much greater depth (1 m) than the Riverside sample (0.1 m) and would correlate with the Lake Albert sites where the quantity of iron-stained grains increases with depth. Myrtlegrove Road is an exception where there is no visible difference between the quartz grains of Unit 3 or Unit 2 other than particle size. However, as suggested in section 4.3.5, it is possible that Unit 2 is a reworked deposit of the soft sands of Unit 3 and would, therefore, share many of the same characteristics of Unit 3.

Table 4.12: Analytical results for Molineaux Sand. The percentage of sand-sized particles is based on the total sand-size fraction and not the total sediment.

REGIONS	INLAND	SE LAKE ALBERT				HINDMARSH ISLAND		GOOLWA	MYRTLEGROVE ROAD	
SITE	Carcuma	Yarindale	Yarindale	Woolshed Road	Woolshed Road	Sturt Monument	Riverside	The Drain	Myrtlegrove Road	Myrtlegrove Road
Field Code	CG	YRQ 1	YRQ 2	WR 1	WR 2	SM	RWR	TD2	MR Unit 3	MR Unit 2
SEDIMENTS										
Depth of burial (m)	4	0.45	0.05	2.5	0.04	1.5	0.1	0.5	3.5	0.6
Munsell Colour	10YR 7/6 yellow	10YR 5/6 yellowish brown	10YR 6/3 pale brown	10YR 5/8 yellowish brown	10YR 6/6 brownish yellow	10YR 4/4 dark yellowish brown	10YR 4/4 dark yellowish brown	10YR 7/3 very pale brown	10YR 7/6 yellow	10YR 7/4 very pale brown
% CaCO ₃ (whole)	0	0	0	0	0	0	0	0	0	0
Heavy minerals	rare	sparse	sparse	sparse	sparse	sparse	rare	very rare	very rare	very rare
Particle Size Analysis (Malvern Mastersizer)										
clay	1	2	0	1	0	1	1	0	1	0
silt	5	15	3	7	0	7	5	3	7	2
sand	94	83	97	91	99	92	94	96	92	98
very fine	4	19	19	3	4	10	11	15	21	12
fine	31	58	58	43	42	58	45	36	51	40
medium	46	24	24	49	45	32	40	36	28	40
coarse	19	0	0	5	8	0	4	13	0	8
very coarse	0	0	0	0	0	0	0	0	0	0
QUARTZ (binocular analysis)										
Sorting	moderate	moderate	moderate	moderate	moderate	moderate	well	moderate-well	poor-moderate	poor-moderate
Particle size	very fine-very coarse	very fine-medium	very fine-medium	fine-coarse	fine-coarse	very fine - medium	very fine-medium	very fine - coarse	very fine - medium	very fine - medium

Table 4.12 *continued*: Analytical results for Molineaux Sand.

REGIONS	INLAND	SE LAKE ALBERT		
SITE	Carcuma	Yarindale	Yarindale	Woolshed Road
Roundness	typical increase in angularity with decrease in grain size	abundantly subangular	abundantly subangular	abundantly angular, commonly subrounded
Surface texture	fine grains either clear lustre or translucent; frosting increases with size; coarse grains abundantly frosted or milky	abundantly frosted or translucent; rarely clear with pitted surface; variable Fe-staining from yellow to dark orange	abundantly frosted or translucent; clear with pitted surface common; Fe-staining sparse/ common	abundantly frosted or translucent with Fe-staining abundant
CARBONATE (binocular analysis)				
	none	none	very rare, very fine	very rare, 3 fragments
X-ray Diffraction				
Quartz	91.2	88.2	81	85.9
CaCO ₃ cements	0	0	2.2	1.1
Feldspar Group	8.2	8.9	14.3	10.6
Clays	0.5	2.8	2.7	2.4

	HINDMARSH ISLAND		GOOLWA	MYRTLEGROVE ROAD	
Woolshed Road	Sturt Monument	Riverside	The Drain	Myrtlegrove Road	Myrtlegrove Road
abundantly angular, commonly subrounded	abundantly angular/subangular; very commonly subrounded/rounded	rounded to angular	abundantly angular to subangular; medium grains abundantly subrounded to rounded	abundantly rounded to subrounded, very rarely angular; fine grains commonly angular	abundantly rounded to subrounded, very rarely angular; fine grains commonly angular
abundant translucent with lustre; clear lustre or frosting common; Fe-staining common, light and dark	variably clear, translucent, frosted; abundant Fe-staining with rare calcite coating; all grains pitted with soil traces	very commonly translucent to frosted with rare calcite coatings; Fe-staining rare	abundantly frosted; fine to very fine grains variably frosted and clear; grains have yellowish tint	Variably frosted and translucent, very commonly Fe-stained with rare milky grains	Variably frosted and translucent, very commonly Fe-stained with rare milky grains
none	none	none	none	none	none
89.6	90.8	84.8	92.3	-	92.6
0.1	0	0.5	0	-	0.2
9.3	7.1	14.5	6.2	-	4.5
0.9	1.9	0.2	1.5	-	2.6

Carbonate content in the whole fraction for all of the Molineaux Sand sediment samples is 0%. Very rare, very fine fragments of shell were identified within the lower siliceous sand at Woolshed Road and the upper siliceous sand at Yarindale. Given the size of the fragments, they were most likely transported with the remainder of the aeolian sediments. Perhaps relatedly, these two sands also showed the highest content of CaCO_3 cement in XRD analysis (Table 4.12) at 1.1% and 2.2%, respectively. However, overall XRD results are fairly consistent between sediments except with regards to the percentage of feldspars which showed the greatest variation (Table 4.12) but could reflect natural variation in the sand source.

4.3.7.2 Solution pipes, *terra rossa* and alluvium

Infill sediment of solution pipes was retrieved from solution pipes at the already described sites of Chart House (section 4.3.3.2), Point Sturt Road (section 4.3.4) and South Coonalpyn (section 4.3.6; Figure 4.43). These sediments should be similar to the contemporaneous soil developed at the surface (Blackburn *et al.*, 1965). The contemporaneous soil at all of these sites has been lost to erosion. The sediments are therefore described alongside the *terra rossa* soils at Point McLeay which also developed during hiatuses in the Bridgewater Formation deposition. Alluvial sediments from The Drain and Myrtlegrove sites are also described here. Although they did not necessarily develop during glacial periods, they are very similar in some respects to the solution pipe and *terra rossa* sediments (Table 4.13).

The solution pipe fill, *terra rossa* soil and alluvial sediments are all predominantly moderately sorted; the Chart House solution pipe is the exception and is poorly sorted (Table 4.13). Clay is present in minor quantities in all sediments. Silt constitutes a considerable portion of the sediments and within the South Coonalpyn solution pipe and The Drain alluvium is dominant over the sand-size fraction. However, the sand fraction in all sediments is composed principally of fine-medium grains and very coarse grains are absent.

Like the Molineaux Sand, angularity is in general a reflection of grain size with an increase of roundness correlated to an increase in grain size and surface texture

Table 4.13: Analytical results for solution pipe fill, *terra rossa* and alluvium. The percentage of sand-sized particles is based on the total sand-size fraction and not the total sediment.

	SOLUTION PIPE FILL			TERRA ROSSA		ALLUVIUM	
SITE	Chart House	Point Sturt Road	South Coonaplyn	Point McLeay	Point McLeay	The Drain	Myrtlegrove Road
Field Code	CHR SP	PSR SP	SC-B SP	PM G1	PM G2	TD1	MRU4
SEDIMENTS							
Depth of burial (m)	1	1	2	unknown	~8	0.75	3.5
Munsell Colour	10YR 4/4 dark yellowish brown	10YR 3/4 dark yellowish brown	10YR 5/8 yellowish brown	2.5R 3/6 dark red	2.5YR 4/8 dark red	5YR 4/6 yellowish red	7.5YR 5/6 strong brown
% CaCO ₃ (whole rock)	0	0	6	0	0	0	8
Heavy minerals	sparse	common	common	sparse	-	rare	very rare
Particle Size Analysis (Malvern Mastersizer)							
clay	2	1	8	4	7	8	7
silt	30	22	63	27	38	65	40
sand	68	77	28	70	55	28	53
very fine	11	17	13	2	9	9	11
fine	31	35	48	24	43	39	38
medium	45	35	35	56	42	44	42
coarse	12	13	4	18	5	7	8
very coarse	0	0	0	0	0	0	0
QUARTZ (binocular analysis)			minor			minor	
Sorting	poor	moderate	moderate	moderate	moderate-well	moderate	moderate
Particle size	very fine - coarse	very fine - coarse	fine-medium	very fine-coarse	very fine-coarse	very fine - coarse	very fine - coarse
Roundness	coarse grain rounded to subangular	medium/coarse grains abundantly rounded	rare angular medium grain	abundantly rounded to well-rounded	abundantly sub-rounded to rounded	very commonly rounded grains	abundantly subrounded / rounded to subangular
Surface texture	frosting and Fe-staining very common	abundantly frosted, commonly clear; Fe-staining common to very common	abundant clear vitreous lustre, rare Fe-staining, sparse to common frosting	abundant lustre, translucent very common, milky grains rare; Fe-staining very common	variable: clear, vitreous lustre, translucent and frosted; Fe-staining common but uneven	abundantly frosted; sparse Fe-staining	abundantly frosted; sparse/common Fe-staining
CARBONATE (binocular analysis)							
	none	none	very rare, fine fragments, rust coloured	none	possible very rare and very altered grains	none	calcite nodules, possibly incipient rhizoliths
X-ray Diffraction							
Quartz	96.5	86.3	67.2	83.5	85	80.2	79.7
CaCO ₃ cements	0	0.2	0.7	0	1.3	0.1	4.3
Feldspar Group	0	9.3	13.6	13.6	4.4	7.4	4.1
Clays	3.3	3.9	18.4	2.8	8.9	12.3	11.4

shows the greatest variability (Table 4.13). Quartz grains from the solution pipe fill of the younger Chart House (MIS 5e) and Point Sturt Road (MIS 7) are predominantly frosted and very commonly iron-stained. However, the quartz grains within the South Coonalpyn (Early-Middle Pleistocene) solution pipe fill are mainly clear with a vitreous lustre and rare iron-staining. The PM G2 *terra rossa* soil shows an increased quantity of frosted grains than its older counterpart PM G1, but a slightly decreased degree of iron-staining. The quartz in the two alluvial sediments is similar to the younger solution pipes and is mostly frosted but with a lesser degree of iron-staining.

Carbonate quantities are low (<10%) if present. Possible fragments of carbonate were identified by binocular analysis within the South Coonalpyn solution pipe fill and the PM G2 *terra rossa* soil but were too altered to be conclusive.

XRD analysis is consistent within the sediment types. The South Coonalpyn solution pipe has a much lower quartz content and higher clay content than its younger counterparts. However, this is consistent with particle size analysis and to be expected due to its much greater age than the latter sediments. Blackburn *et al.* (1965) found the older, more inland solution pipes of the Coorong Coastal Plain to generally have a higher clay content than their younger counterparts. The PM G2 *terra rossa* has a higher clay content than the PM G1 *terra rossa*; again consistent with particle size analysis. PM G2 is the younger and is overall composed of finer sediments than PM G1 and most likely reflects slightly different aeolian conditions (either wind strength or distance from source) during deposition. The alluvium at The Drain and Myrtlegrove Road are similar, although Unit 4 of Myrtlegrove Road has a higher CaCO₃ content. Feldspars show the greatest dissimilarity among the sediments and may reflect natural variability.

4.3.7.3 Siliceous sands discussion

Deposits of Molineaux Sand are pervasive throughout the study area. The dunefields of the Big Desert (section 1.5.1) are anchored in the southeast corner of the study area where the Carcuma field site is found. The Molineaux Sand exhibited great similarity across the study area with the largest differences found in sediment colour and surface texture changes between regions. The regional changes are possibly

explained by variations in diagenetic environments as there is no consistent change in sorting, particle size, grain roundness or mineralogy between regions.

The change in sand colour amongst glacial sands at the same field site (e.g. Woolshed Road and Yarindale) was initially thought to possibly reflect two phases of deposition. However, the similarity in grain size distribution and quartz grain roundness suggests that the sands are the same. It is suggested that the change in iron-oxide staining and quartz grain frosting through the profile reflects the effect of ground water flow through the sand. As rainwater infiltrates the sand its downward penetration is hindered by the underlying, more impermeable calcrete surface. Water would then flow downslope across the calcreted surface of the dune and as the water evaporated oxidation and frosting of the quartz grains would occur.

The other siliceous sand deposits within the study area (the solution pipe fill, *terra rossa* soil and alluvium) share comparable characteristics with the Molineaux Sand. They are in general similarly sorted and also exhibit a trend of increasing angularity with a decrease in grain size. The sand size fraction is also alike in the dominance of fine to medium grains with no very coarse grains. However, these deposits have a much higher silt and clay content than the Molineaux Sand and in turn typically have a stronger colour reflecting both pedogenic processes and an accumulation of clays and silt in low-lying areas (the solution pipes and alluvium). The carbonate content within the Myrtlegrove alluvium is likely to be a result of its close association with an adjacent lagoonal deposit (section 4.3.6). The carbonate content within the solution pipe fill at the South Coonalpyn site can be attributed to multiple possibilities. It could have been derived from an aeolian component. The age of the dune implies it may have been leached from the surrounding sediments and is non-indigenous. Quarrying activities may have contaminated the original solution pipe material with carbonate aeolianite. The presence of carbonate could be a laboratory error. However, given the presence of possible fragments of carbonate, it is most likely that carbonate was deposited alongside the solution pipe material.

4.3.8 Quartz grains

An objective of this research was to determine if there were any conspicuous trends of quartz grains within the Bridgewater Formation across depositional environments or the ages of the different successions. The character of the sand grains within the Bridgewater Formation should closely resemble the sediments that serve as principle sedimentary sources (McKee and Ward, 1983). The sources of sediment for the Bridgewater Formation are the Lacepede Shelf, the River Murray and the continental dunefields (equivalent to the Molineaux Sand) that were deposited during periods of lowered sea-level (Chapter 2). The modern River Murray contribution to the coast is restricted due to the majority of the bedload being trapped upstream (James *et al.*, 1992) and the construction of barrages inside the Murray Mouth (Barnett, 1993; Bourman and Barnett, 1995). However, it potentially delivered a greater amount of terrestrial sediment during more pluvial periods of the late Pleistocene, which would have been quickly and widely dispersed by the longshore and tidal currents (Bourman and Murray-Wallace, 1991; James *et al.*, 1992). Sediments from the Lacepede Shelf, Molineaux Sand and other potential siliceous sand sources have been described above (sections 4.3.1 and 4.3.7). By comparing the quartz grains characteristics of the Lacepede Shelf sediment, the siliceous sands and the Bridgewater Formation sediments, conclusions may be made regarding any trends in quartz grains within the carbonate aeolianite and in comparison to their source sediments.

As the previous section has shown, the principle differences between the Molineaux Sands and other siliceous sediments (solution pipe infill, *terra rossa* soil and alluvium) is the presence of a much higher silt and clay content and a stronger colour in the latter over the former. In general the roundness of the quartz grain was related to its size with angularity increasing as grain size decreased. Frosting could also be related to size, with frosted grains more likely to be present among the larger grain sizes. However, there does not appear to be any trend across the study area with regards to the quantity of frosted or translucent or clear grains with a vitreous lustre. As was shown at Woolshed Road and Yarindale sites, the degree of iron-staining and frosting within a profile could be related to diagenetic processes. However, if such a unit was to be

reworked by rising sea-level, the grains would become mixed making any distinction unlikely.

The Lacepede Shelf sediments have a general grain size of fine to medium (like the siliceous sands) with a few exceptions. However, they differ in sorting which varies between poor to very well and are typically angular which may reflect a prevalence of fine over medium grains. The preponderance of angular grains also suggests a nearby source for the sediments and could reflect erosion of granites within Encounter Bay and sediment supplied by water flow off Fleurieu Peninsula where Permian sediments are still encountered (Alley and Bourman, 1984; 1985; Bourman and Alley, 1990; 1995). The supply of coarse and angular grains from Fleurieu Peninsula is made evident by the quartz and lithic pebbles identified at Watsons Gap and Victor Harbor. The surface texture of quartz grains on the Lacepede Shelf is a mix of clear, translucent and frosted grains, although, frosting appears to be a less common feature than amongst the siliceous sands. Iron-staining is a common feature in all the core samples and, alongside the fauna record of mixed relict, stranded and recent carbonate grains, the Lacepede Shelf sediments predominantly appear to be the result of reworked and flooded coastal environments.

Carbonate aeolianites are generally composed of fine to medium, well-sorted and moderately sorted grains reflecting the beaches or nearshore marine environments from which the sands were derived (McKee and Ward, 1983). This is reflected in the Bridgewater Formation sediments of this thesis which are predominantly composed of fine- to medium-grained sand that in nearly every instance (excluding four) contains some quantity of very fine grains (usually <20%; *Appendix 2*). Very coarse grains are common but typically account for less than 10% of grains and are consistent with sediment samples containing large mollusc shell fragments. Coarse grains are present in over half the samples and also appear to be at least partially due to the size of carbonate grains within the sample.

Quartz grains are predominantly sub-rounded with some rounded or sub-angular grains. Sediments identified as containing fine or very fine grains as a principal component are more likely to be identified as having a majority of angular or sub-

angular grains. Quartz grains are mainly clear or translucent with a vitreous lustre. However, frosting can be very common or abundant especially amongst the medium to coarse grain size fraction. There does not appear to be a trend in where frosting occurs as it is found in almost every sediment with no particular preference for depositional environment or age. The presence and degree of iron-staining is equally variable with no relationship to frosting. Iron-staining of quartz grains was also not consistent with iron-staining of carbonate grains which was present in every sample.

The lack of any characteristic features of quartz grains by environment of deposition or age can be attributed to the location of the study area. The River Murray mouth is located in a region of ongoing subsidence exposed to cycles of glacio-eustatic sea-level and climate change. The fluctuation in sea-level and environment produces sedimentary successions that are composed of reworked material from the previous system which was also composed of siliceous dunes and coastal and near-shore marine sedimentary successions. Furthermore, the constant recycling of grains does not allow quartz grains the necessary quantity of time to imprint any characteristics that would indicate environment of deposition. Variability in quartz grains can also be expected because their source is the River Murray and the extensive land area through which it flows. This could also explain the variability in feldspar mineralogy across the study area (*Appendix 3*).

4.3.9 Carbonate Grains

The coarse and very coarse grains of the Bridgewater Formation are, in many instances, attributed to the presences of Foraminifers and mollusc fragments, juvenile disarticulated bivalves, small gastropods and other faunal types including bryozoans, echinoderms, coralline algae and sponge spicules. Iron-stained carbonate grains were present in every sediment sample reflecting both diagenetic processes and the reworking of sediments as sea-level transgressed the Lacepede Shelf after a period of lowered sea-level. Whereas Foraminifers and other faunal fragments almost always exhibited some degree of staining, the presence of staining on mollusc fragments could be variable and can be explained by original skeletal mineralogy (calcite versus aragonite) and skeletal structure affecting resistance to diagenetic processes. Carbonate

grains in general exhibited rounded to well-rounded edges and corners. The rounding of carbonate grains is likely to be a result of beach processes (McKee and Ward, 1983).

A trend of increased content of low-Mg calcite and decreased content of aragonite and high-Mg calcite farther inland is expected as the age of the deposits and diagenesis increases (Colwell, 1978). Mineralogical analysis by XRD shows a faint trend of decreased content of aragonite and high-Mg calcite with age and distance inland (Figure 4.44), i.e. if aragonite and high-Mg calcite were present, they tended towards a comparably decreased content in older, more inland sediments. However, some younger sediments, for example the MIS 5e correlated Chart House aeolianites, contain no traces of aragonite while much older inland sediments still retain minor quantities of aragonite. The trend towards increased content of low-Mg calcite is at some sites, disrupted by the presence of other types of calcium carbonate cement. Sediments were analysed for the presence of siderite, dolomite and ankerite with the latter two accounting for the majority of other carbonate cements. The lack of any distinct trend may reflect the reworking of sediments within the region.

4.3.10 Analysis of drillhole log data within the northern Coorong Coastal Plain

Sedimentological descriptions are available for drillholes across the Coorong Coastal Plain provided by the Government of South Australia (DMITRE, 2014) and made available through the South Australian resources Information Geoserver (SARIG). Review of these data has indicated the extent and depth of the different Quaternary successions in the northern Coorong Coastal Plain. It aids in correlating the northern successions with those in the southeast, and in understanding the development of the Coorong Coastal Plain.

Drillhole stratigraphy provides a brief interpretation of the sedimentary successions encountered within the drillhole but is subject to generalisation and error in labelling. As an example of the former, many of the sediments were labelled as “Undifferentiated Quaternary”. Errors in labelling include the identification of sediments underlying calcretes over 1 m in thickness as Holocene and the identification of units such as Blanchetown Clay and Bungunnia Limestone within the study area but these are

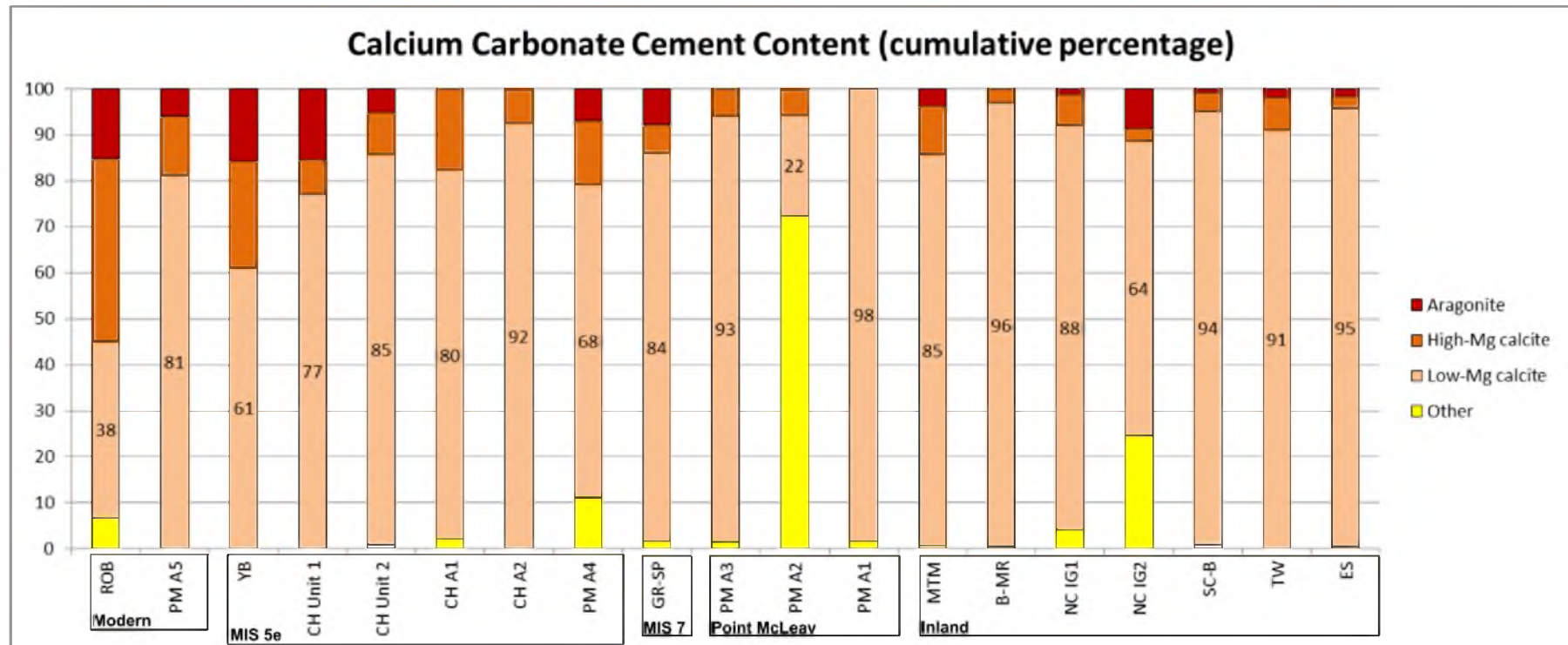


Figure 4.45: Results of XRD mineralogical analysis of Bridgewater Formation sediments from within the study area. A trend of increased low-Mg calcite and decreased aragonite and high-Mg calcite with distance inland and age is not distinct. The percentage of low-Mg calcite per total CaCO_3 content is provided. Complete results of XRD mineralogical analysis are provided in Appendix 3.

misnomers as both Blanchetown Clay and Bungunnia Limestone are lake sediments that were deposited in the more northerly located Lake Bungunnia. However, the provision of major and minor lithologies and sediment descriptions provided alongside stratigraphic unit names usually allowed the interpretation of the correct stratigraphic unit. For example, sediments incorrectly labelled as Blanchetown Clay were most often assigned to deposits within the dolomite plain and are interpreted here as a low-energy marine or estuarine environment.

Drillhole data analysed from the eastern margin of the Mount Lofty Ranges southeast of the Coonalpyn Range encompass the Murray Lakes Range and leeward dolomite plain (Figure 4.33). Drillholes are not as numerous to the southeast and are most abundant within the dolomite plain and around the northeastern margin of Lake Alexandrina. Adequate drillhole data were also found to be lacking in detail on Fleurieu Peninsula and in the Goolwa-Hindmarsh Island region. However, valuable conclusions could still be made for the extent of Quaternary successions on the northern Coorong Coastal Plain. The underlying pre-Cenozoic sediments comprise the Permian Cape Jervis Formation, Early Palaeozoic Kanmantoo Group and undifferentiated igneous and volcanic rocks which, in some instances, are designated as Delamerian. Pre-Quaternary Cenozoic sediments include the Pliocene - ?Pleistocene marine Coomandook Formation, the Paleogene marine Murray Group and Buccleuch Formation and the fluvial-lacustrine Renmark Group (which includes the Early Paleogene Warina Sand and Paleogene-Neogene Olney Formation).

Molineaux Sand was encountered in the majority of drillholes across the northern Coorong Coastal Plain. This is to be expected as the Big Desert, composed of Molineaux Sand, extends east from this region (Firman, 1973; Rogers, 1979; Sprigg, 1952; 1979). The Molineaux Sand is largely absent in drillholes from the dolomite plain and west of the River Murray.

The Bridgewater Formation is found extensively on the seaward side of the Murray Lakes Range and continues to the southeast confirming the presence of Bridgewater Formation both at the surface and at depth. The maximum recorded thickness of Bridgewater Formation seaward of the Murray Lakes Range is -48 m. The

Padthaway Formation was only recorded in one drillhole seaward of the Murray Lakes Range near its southern end but indicates the development of lagoon/lacustrine conditions following the initial deposition of Bridgewater Formation seaward of the Murray Lakes Range. Padthaway Formation is also found in most drillholes between the Coonalpyn Range and the Black and Murray Lakes Ranges. The Padthaway Formation reaches a maximum 14 m thickness in the lee of the Hynam dune.

Drillholes within the Murray Lakes Range and Coonalpyn Range are not abundant but confirm the presence of Bridgewater Formation throughout the Murray Lakes Range and to the west of the Emu Springs field site. Drillholes to the north of the Murray Lakes Range within eastward trending dunes contain a series of sandstones described as either fossiliferous or limey extending to depths of 39 m and could correlate with either the Bridgewater or Padthaway Formation.

The drillholes adjacent to the margin of northeastern Lake Alexandrina record relatively shallow (≤ 8 m) depths of undifferentiated Quaternary sediments below the surface. Most are described as calcrete or soil with sand or clay. The drillholes are located within the Cooke Plains Embayment, which extends northeastwards into the dolomite plain and was inundated by Lake Alexandrina during the early-mid Holocene highstand (de Mooy, 1959; von der Borch and Altman, 1979).

The dolomite plain is an unnamed and not formally defined geological unit designated the “Qpu” dolomite on the Pinnaroo 1:250 000 Geological Sheet (Rogers, 1979). It is suggested that it is an early Pleistocene marginal-marine and lagoonal unit formed in a partially protected, low-energy environment (Brown and Stephenson, 1991). The Quaternary sediments within the dolomite plain are described as undifferentiated Quaternary sediments, usually containing some combination of clay, silt or sand with clay, sometimes as carbonaceous clay, sometimes with calcretes, and extending up to 23.5 m in thickness. Pleistocene lagoonal algal dolomite is also supplied as a stratigraphic unit in some drillholes. The centre of the plain contains deposits of gypsum at the surface extending to 4 m depth. However, the most common stratigraphic unit name is undifferentiated Quaternary calcrete recorded to a maximum depth of 16 m but it is generally represented by fairly even deposits of calcrete 6-10 m thick. The sediments

of the dolomite plain are considered to have been deposited in an environment equivalent to the Padthaway Formation or low-energy marginal marine environment as suggested by Brown and Stephenson (1991).

The margin of the dolomite plain, beneath the Marmon Jabuk Escarpment is characterised by red-brown mottled clay with a minor sand component, overlain by a massive or nodular calcrete up to 4 m thick. This description is very similar to the deposit found at the Tailem Bend field site where a yellowish red (5YR 4/6) sand (47%) is found in a silt-clay matrix beneath a blocky and nodular calcrete of 1 to 1.5 m thickness. The similarities in the deposits and their association with the Marmon Jabuk Escarpment suggest that they are an alluvial deposit composed of grains reworked from the Loxton-Parilla Sands, which are found on the escarpment.

Alluvial plains extend south from the River Murray Gorge and east from the Mount Lofty Ranges to surround Lake Alexandrina to the north, west and south. Bathymetry indicates that the lake reaches a maximum depth of ~9.4 m water depth to the north and east of Narrung Peninsula, approximately in the centre of the lake (Brooks *et al.*, 2009). The Pleistocene-Holocene sedimentary boundary beneath the lake floor is identified in sediments only in the north and northwestern part of the lake and exceeds 5 m depth throughout the southern half of the lake implying the location of the river preceding the Holocene to be in the southern half of the lake (Barnett, 1993).

The depth to the base of Quaternary sediments to the west of the River Murray is difficult to ascertain as many of the sediments are described as undifferentiated Tertiary to Pleistocene deposits. The Quaternary sediments have not been adequately described to determine their origin as alluvial, fluvial or estuarine/marine and a lack of ages inhibits the development of regional relationships between the sediments. Longitudinal dunes of windblown sand, reworked from the adjacent Mount Lofty Ranges and underlying Palaeogene-Neogene estuarine and marine sands, have blanketed much of the area, possibly within the late Pleistocene (Gibson, 2004) and were mapped as Molineaux-Lowan Sand by Brown and Stephenson (1991). Drillhole data indicate that the calcrete extends across the northern alluvial fan to within 4 km of the northernmost tip of Lake Alexandrina. De Mooy (1959) suggested that the region was an extension of

the Mallee country and is Pleistocene in age. The Quaternary sediments beneath the calcrete on the margins of the Mount Lofty Ranges near the Murray Gorge are typically described as clay to fine sand overlying Parilla Sands. An exception ~8.5 km to the southeast of the Murray Bridge field site and ~8 km south of the River Murray records a Quaternary pebble conglomerate at a depth of 18-22 m possibly reflecting a former course of the river.

The 1 m thick calcrete at the Murray Bridge field site, located within the northern alluvial calcreted plain, exhibits evidence of multiple cycles of formation and fracture. This indicates deposition at least within the middle Pleistocene allowing sufficient time for multiple cycles of calcrete development and fracture. The indurated sediments directly beneath the calcrete are not of a clayey nature as described in the drillholes but this may be a reflection of the depth of the exposure at the field site which reaches a height of 1.4 m. The clay sediments in drillholes, although identified as shallowly as 1.2 m beneath the surface, are more commonly encountered at depths greater than 2 m. The sediments within the calcrete profile at Murray Bridge indicate fluctuations in the energy of the depositional environment with angular gravel, pebbles and large intraclasts (≤ 15 cm) of calcrete interlayered with lenses of finer grained sediment (section 4.3.6.9).

Quaternary sediments to the north of Lake Alexandrina are generally less than 20 m thick but to the southeast in the Angas Bremer Plains reach nearly 40 m depth on the downthrown side of the Bremer Fault. The sediments within this alluvial plain are most commonly described as clay but include clay with silt, clay with calcrete and sand with clay.

4.3.11 Conclusions

The subsidence in the region of the Murray Mouth has resulted in the individual beach-barrier-lagoon successions recognised to the southeast on the Coorong Coastal Plain as individual ranges, to coalesce and lose topographic expression within the study area. This research has built upon previous investigations (De Mooy, 1959; Sprigg, 1959; Bourman and Murray-Wallace, 1991; Bourman *et al.*, 2000; Murray-Wallace *et al.*, 2010) to expand the known extent of Pleistocene coastal stratigraphic successions within the

Murray Mouth region and to provide stratigraphical and petrological descriptions. The chapter has also presented descriptions of various siliceous sand deposits within the region including Monlineaux Sands, solution pipes, *terra rossa* soils and alluvium. Binocular, thin section and mineralogical analysis has been used to determine any trends within or between the sedimentary successions described.

The record on southern Hindmarsh Island is of the mid-Holocene sea-level highstand. The relationship of the Holocene sediments to the underlying calcretes and the glacial Molineaux Sand indicates the presence of a Last Glacial Maximum river valley and the limit of the Holocene transgression. The sediments of the auger hole AL-BH2 record the sea-level peak (between 5-8 m depth of burial) and following regression.

The last interglacial shoreline shows localised variation in the sedimentary facies preserved, carbonate content and calcrete development. The Lake Albert deposits have, overall, very low carbonate contents. This could support the presence of a former Murray Mouth at the southern tip of Lake Albert as proposed by De Mooy (1959). The highly fragmented nature of the carbonate grains of the Camp Coorong shell beds and within the Stratland aeolianite and underlying sands are evidence of a high-energy coastline. Drill holes in the region show the Bridgewater Formation to extend to depths greater than 30 m reflecting the accumulation of sediments over multiple interglacial periods.

The Hindmarsh Island and Goolwa area contains intertidal marine, beach, aeolian and estuarine facies and indicate the presence of at least one palaeo-Goolwa Channel and Murray Mouth during the Last Interglacial. Hindmarsh Island is also shown to be composed of MIS 5e and MIS 7 aeolianite which, alongside the MIS 9 inlier reported by Murray-Wallace *et al.* (2010), provides additional support for long-term subsidence in the region and the return of sea-level to a similar location for multiple interglacials. This conclusion is further supported by the presence of the MIS 5c aeolianite at Surfer Beach and calcrete inlier of Sir Richard Peninsula. The aeolianite on which the calcrete has formed is also likely to be MIS 5c given sea level during MIS 5a is believed to have been as much as 17 m below present sea level in the region (Belperio and Cann, 1990; Murray-Wallace *et al.*, 2001).

Deposition of MIS 5e sedimentary successions on Fleurieu Peninsula is controlled by the presence of bedrock valleys, beach orientation, Kangaroo Island, granite headlands and islands within Encounter Bay and Quaternary neotectonics. The greatest accumulation of sediments is found at Waitpinga and Knights Beach, both of which face nearly directly south. Knights Beach, in comparison to other Fleurieu Peninsula sites, has been subject to erosion by the Southern Ocean. A note of interest is the apparent lack of MIS 7 deposits on the peninsula. This may be due to minimal deposition or erosion as indicated by the inclusion of large quartz and lithic sandstone pebbles within the estuarine deposits at Watsons Gap and Victor Harbor. However, it may also reflect a need for additional exploratory research along the peninsula.

The morphostratigraphic and geographic relationship of the previously identified (Murray-Wallace *et al.*, 2010) MIS 7 deposits on Sturt Peninsula and those identified in this research (including northern Hindmarsh Island) indicate Sturt Peninsula, as thus far described, to be composed predominantly of MIS 7. However, the possibility of older inliers is not discounted. The relationship of Sturt Peninsula to the eastward Point McLeay succession depends on identifying the MIS 7 deposit that is likely located there.

The sedimentary successions of southeast Lake Albert, Hindmarsh Island, Goolwa, Fleurieu Peninsula and Sturt Peninsula are all related to the post-Naracoorte Bridgewater Formation preserved across the Coorong Coastal Plain to the southeast. Many of the inland deposits described in this research are correlated to the pre-Naracoorte early Pleistocene barriers. Deposition and preservation of these barriers is related to the Padthaway Ridge granites which served as headlands and loci for deposition during multiple interglacial periods. The Murray Lakes Range, which by extension includes Point McLeay, is a composite range of both early and middle Pleistocene Bridgewater Formation.

The Bridgewater Formation consists of aeolian dune facies composed of calcareous sands with variable content of skeletal material and quartz grains. Subtidal and littoral facies share similar characteristics. The back-barrier lagoon and estuarine sediments are represented by the Padthaway Formation and last interglacial Glanville Formation. Within the study area, the bedding characteristics of the majority of deposits

have been obliterated by bioturbation, diagenetic processes or erosion. Where preserved, the bedding at the majority of sites indicates a northwest or north-northwest direction of dune migration. The Surfer Beach dune bedding indicates migration to the northeast. The orientation of bedding within the succession at Knight Beach, which drapes an Encounter Bay granite, suggests influence by winds from the southwest, south and southeast. The most common form of calcrete capping carbonate sands is massive. The massive calcretes typically contain rhizolith development and in some cases include laminar calcrete on top of or within the profile. Less common are laminar, rubbly, nodular or pisolitic calcretes.

The Bridgewater Formation is consistently of the hue 10YR and coloured very pale brown or light yellowish brown with very few exceptions. The dominant grain size is fine to medium followed by very fine, coarse and very coarse grains. Quartz grains within the Bridgewater Formation show a general increase in angularity with a decrease in grain size; medium grains are usually sub-rounded to rounded. Surface textures with regards to frosting and iron-staining is variable with no consistent trend between age and distance inland. The variable feldspar content within the sediments is likely a reflection of the variable sources of quartz grains which includes the River Murray, the Lacepede Shelf and Fleurieu Peninsula.

The dominant component of the carbonate fraction in every sediment sample is mollusc fragments, except for the Lacepede Shelf sediment sample VC 23 retrieved from margin of the continental shelf. Mollusc fragments reach sizes greater than 2 mm but are generally less than 0.50 mm in diameter. Iron-stained carbonate grains are present in every sediment sample except VC 23. The sediment mineralogy of calcium carbonate cements does not show a distinct trend of decreasing aragonite and high-Mg calcite and increased content of low-Mg calcite with age and distance inland.

Also described within this research is the siliceous Molineaux Sand, solution pipe infill, *terra rossa* soil and alluvium. These sediments (with the exception of Murray Bridge immature feldspathic greywacke) share similar quartz grains characteristics with the content of silt, clay and sediment colour the largest indicator of different depositional environments. Like the Bridgewater Formation the dominant grain size

within the sand fraction of these sediments is fine to medium with the degree of angularity a function of size. The surface texture is variable and, as indicated by the Molineaux Sand at Woolshed Road and Yarindale, can be related to diagenetic processes. The presence of a calcrete capping the alluvial sediment at Tailern Bend suggests a significant period of time for diagenetic processes to occur.

Analysis of the quartz grains from the different sedimentary successions did not identify any significant trend or characteristic that could be related to environment of deposition. The cyclical change in climate and glacio-eustatic sea-level does not allow quartz grains to reside in any one environment for the obligatory time needed to develop identifying characteristics.

Geochronological analyses of the sedimentary successions described in this chapter will be presented in Chapter 6. The geochronological results will assist in confirming the relationships of sedimentary successions described in this chapter. Accordingly, varying results of AAR whole rock analysis (Chapter 6) may potentially be explained by the composition of sediments as described here. Analyses of drillhole logs across the northern coastal plain have provided an indication of the spatial distribution of Quaternary sedimentary successions in the region between the study area and the record of sea-level change recorded between Robe and Naracoorte. This understanding will assist in developing the depositional history of the northern Coorong Coastal Plain and the correlating the sedimentary successions within the study area to their counterparts in the southeast. This discussion occurs in Chapter 7.

Chapter 5

Methodological considerations of Amino Acid Racemisation and its application in dating Pleistocene interglacial sedimentary successions

5.1 Introduction

The primary geochronological method used in this research was amino acid racemisation (AAR) which was applied to interglacial sedimentary successions containing mollusc shell and/or sediments composed of skeletal carbonate grains. This chapter reviews the principle of the method and describes the analytical procedure. This chapter also discusses the complexities encountered in the analyses of the Murray Lakes region. The results of AAR analyses are provided in Chapter 6 where their implications are evaluated alongside the results of other geochronological analyses.

5.2 Amino Acid Racemisation

Amino acids are vital components in living systems. They serve as the building blocks of proteins which form the structural components of organisms and as enzymes which catalyse biochemical reactions (Kvenvolden, 1975). There are twenty amino acids which commonly occur in proteins of organisms (Kvenvolden, 1975). The general enantiomeric amino acid structure is made up of a central asymmetric α -carbon atom, an amino ($-\text{NH}_2$), a carboxyl (COOH), a proton ($-\text{H}$) and a radical $-\text{R}$ group. The $-\text{R}$ group differs for each amino acid (Schroeder and Bada, 1976). There are two possible forms of these amino acids, L- and D-, which are mirror images of each other (Figure 5.1).

Enantiomers share identical chemical and physical properties, the only difference being the direction they rotate plane-polarised light. Glycine is an exception, which lacks asymmetry and is not optically active. An L-amino acid enantiomer rotates plane-polarised light left (*levo*-) and a D-amino acid enantiomer rotates plane-polarised light right (*dextro*-) (Kvenvolden, 1975). Virtually all proteins of living animals and plants consist exclusively of the L- amino acids due to enzymes which stereo-selectively utilise

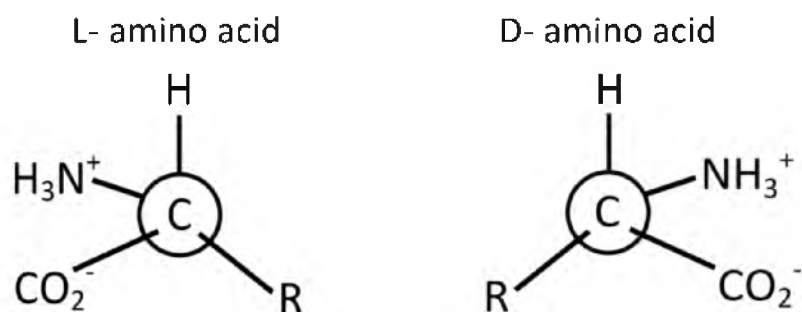
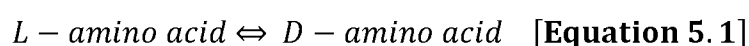


Figure 5.1: Generalised left- and right –handed amino acid enantiomers (Schroeder and Bada, 1976).

only the L- form. Following the cessation of the metabolic reactions that maintain L- and D- disequilibrium (the cessation of protein formation), L-enantiomers are reversibly transformed into D- enantiomers until an equilibrium mixture of both is obtained in a process known as racemisation (Hare and Hoering, 1973; Schroeder and Bada, 1976; Williams and Smith, 1977; Bada and Shou, 1980). Both the natural hydrolysis of proteins and related racemisation of constituent amino acids have been directly related to the time elapsed since the death of an organism (Miller and Hare, 1975), although racemisation in life has been detected in teeth (Helfman and Bada, 1975), eye lenses (Masters *et al.*, 1977) and long lived shells such as *Arctica islandica* (Goodfriend and Weidman, 2001). The general racemisation reaction for amino acids is represented by the following relationship:



Some amino acids have a second carbon atom and are asymmetric. These form diastereoisomers and unlike single carbon amino acids, are not mirror images. The term epimerisation is used for the transformation of diastereoisomers and the product is an allo-amino acid (Hare and Hoering, 1973; Miller and Brigham-Grette, 1989; Mitterer and Kriaušakul, 1989). Among diastereoisomers on Earth, epimerisation occurs about the α -carbon and is not recognised around the β -carbon (Hare, 1969; Miller and Brigham-Grette, 1989). Isoleucine is a common example. L-isoleucine interconverts to D-alloisoleucine with no D-isoleucine or L-alloisoleucine forming. Unlike amino acids with a single carbon centre, where equilibrium is reached at 1, equilibrium for these amino

acids is approximately 1.3 (Hare and Abelson, 1967; Hare and Mitterer, 1968; Miller and Brigham-Grette, 1989; Miller *et al.*, 2000).

Abelson (1954) recognised the abundance of proteins in ancient shell, bone and teeth; for example, the amino acids alanine, glutamic acid and valine were found in a fish bone 360 million years old. Following this, Abelson (1955) first suggested that the rate of degradation of proteins in fossils could provide a dating method. Hare and Mitterer (1966) found a correlation between amino acid racemisation and age when looking at isoleucine and the accumulation alloisoleucine in fossil marine shells. It was recognised that the ratio of D- to L- enantiomers of an amino acid could be used to estimate the amount of time passed since the onset of racemisation (Schroeder and Bada, 1976).

5.2.1 The Rate of Racemisation

Racemisation is, in general, a nonlinear reaction (an exception being ostrich eggshell, see below Kinetic models), beginning at a relatively rapid pace early in diagenesis which then decreases. The initial rapid rate is due to natural hydrolysis (discussed below) of polypeptides and the accumulation of amino acids exhibiting a higher degree of racemisation, and free or short polypeptide-bound amino acids (Wehmiller, 1984). The transition zone between fast and slow rates coincides roughly with the point at which free amino acids reach maximum abundance. The decreased rate of racemisation is controlled by slow hydrolysis, continued racemisation of free amino acids (which racemise more slowly) and some racemisation of bound amino acids (Wehmiller and Hare, 1971; Wehmiller, 1980).

The extent of racemisation in a fossil is determined by the rate at which racemisation has occurred over a given period of time. The integrated rate expression for the racemisation reaction is:

$$\ln \left\{ \frac{1 + D/L}{1 - D/L} \right\} - \ln \left\{ \frac{1 + D/L}{1 - D/L} \right\}_{t=0} = 2 * k * t \quad [\text{Equation 5.2}]$$

where D/L is the amino acid enantiomeric ratio at any particular time, t , and the rate is k (Bada & Shou, 1980). If either time or rate is known, the other can be calculated.

Amino acid racemisation is just one of multiple chemical and biological diagenetic changes that can affect proteins and amino acids. Hydrolysis of the peptide bond is directly related to racemisation. Other diagenetic processes include destruction or alteration by microorganisms, condensation reactions with other molecules, and decomposition reactions characteristic to the particular amino acid (Schroeder and Bada, 1976). Similar racemisation and hydrolysis trends among molluscs and foraminifera define a basic chemical process common to the diagenesis of calcareous organisms. Variables affecting racemisation rates include amino acid, temperature and genus (Wehmiller, 1980; 1982). This section examines the factors that influence the rate of racemisation, the measured extent of racemisation, and therefore, the D/L value.

5.2.1.1 Hydrolysis

During hydrolysis the peptide bonds between amino acids are cleaved with the addition of water, fragmenting proteins into polypeptides and free amino acids (Figure 5.2). The speed of hydrolysis and racemisation is depended upon the stability of the peptide which in turn is largely dependent on which amino acids are forming the bond. For example peptide bonds involving valine and isoleucine are among the most stable, while those with serine and aspartic acid are among the least stable (Hare *et al.*, 1975). The position of amino acids further determines the rate at which racemisation occurs. Amino acids in the terminal position of a peptide sequence racemise more quickly than those in an internal position. Cleavage of the racemised terminal amino acids creates a population of largely racemic free amino acids where racemisation proceeds at a slower rate. The upper limit to the use of AAR as a dating technique is reached when the ratio of D- and L- amino acids is not statistically resolvable from equilibrium (Hare and Abelson, 1967; Williams and Smith, 1977; Kriausakul and Mitterer, 1978; Mitterer and Kriausakul, 1989). This upper limit is spatially variable (geographically) due to contrasting diagenetic temperatures (discussed below).

The initial rate of racemisation proceeds relatively rapidly because high molecular weight polypeptides are broken down quickly into smaller fragments by hydrolysis (Hare and Mitterer, 1966; Miller and Hare, 1980; Walton, 1998). Hydrolysis is most rapid in the first 30-40 ka from the onset of racemisation. This is evident in a rapid

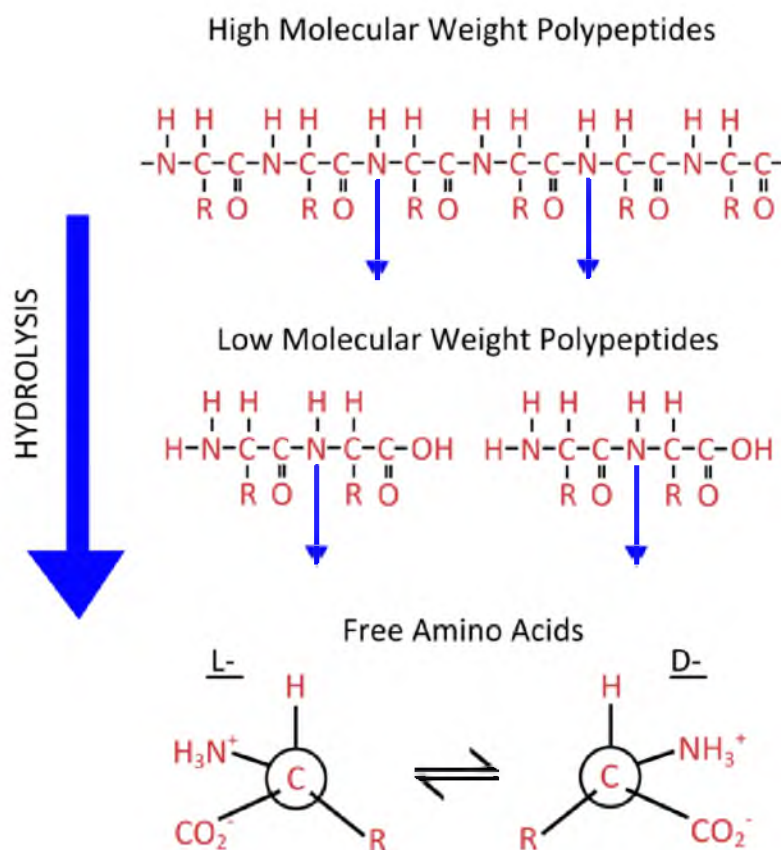


Figure 5.2: The breakdown of polypeptide chains to free amino acids by hydrolysis (modified from Wehmiller, 1980).

decline of total amino acid (bound + free) abundance with a simultaneous rapid rise in free amino acid abundance (Wehmiller, 1980). Racemisation (as seen for the total hydrolysable amino acids) slows with the accumulation of short polypeptide-bound amino acids, free amino acids, and a slower rate of hydrolysis producing a nonlinear racemisation curve when time is plotted in a linear format (Figure 5.3). Hydrolysis slows either because of a lack of available water or because the remaining 'bound' proteins are more resistant to hydrolysis (Hoering, 1980; Walton, 1998; Miller *et al.*, 2000; Penkman *et al.*, 2008; Demarchi *et al.*, 2013b). The transition zone between the two rates is roughly equivalent to the maximum accumulation of free amino acids (Wehmiller and Hare, 1971; Wehmiller, 1980).

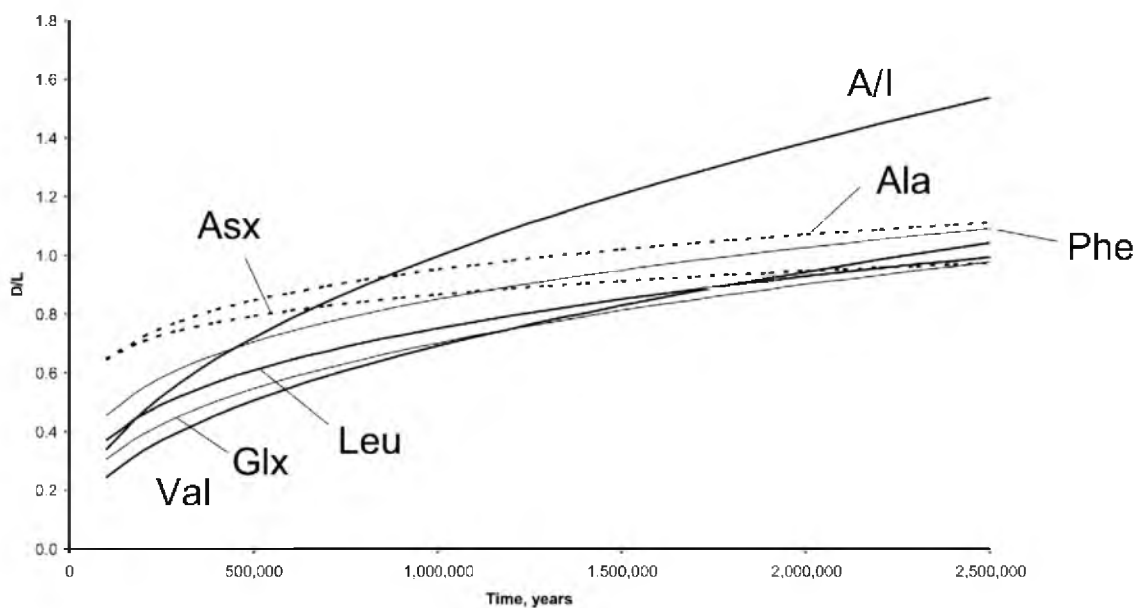


Figure 5.3: Summary of intragenetic racemisation rates for multiple amino acids in the marine mollusc *Mercenaria* from the North Carolina coastal plain (Wehmiller *et al.*, 2010; 2011; 2012) illustrating fast and slow rates of racemisation and different apparent rates per amino acid. Regressions were derived using sample ages derived from Sr-isotope calibration (Wehmiller *et al.*, 2011, 2012).

5.2.1.2 Temperature

Racemisation, as a chemical reaction, is sensitive to temperature. Amino acid D/L values increase with temperature in mollusc shell, foraminifera and bone (Hare and Mitterer, 1966; Hare and Abelson, 1967; Wehmiller and Hare, 1971; Bada and Helfman, 1975; Miller and Hare, 1975; Lajoie *et al.*, 1980; Murray-Wallace and Kimber, 1987). At lower temperatures racemisation proceeds at a slower pace and a greater age range is possible, while at higher temperatures racemisation proceeds at a faster pace and results in a smaller age range (in regards to reaching a racemic state of D/L value). In shell the racemisation rate increases approximately 18% per 1°C rise in temperature (Wehmiller, 1982).

Latitudinal variations in temperature are evident in the D/L values of samples of the same age (Lajoie *et al.*, 1980; Wehmiller, 1982; 1984; 2012). Racemisation in high latitude regions with temperatures of -20 to -10°C may take 5 Ma to reach equilibrium whereas in tropical regions equilibrium can be reached in as little as 150 ka (Murray-Wallace, 2000). In an early application Kennedy *et al.* (1982) used the latitudinal variation of D/L values in conjunction with faunal evidence to refine aminostratigraphic

age estimates of Quaternary marine terraces on the Pacific coast of the United States and to correlate the terraces with worldwide climatic and sea-level events.

The integrated kinetic effect of all temperatures to which a sample of a certain age has been exposed is known as the effective Quaternary temperature (EQT) or effective diagenetic temperature (EDT) (Wehmiller, 1982; Wehmiller and Miller, 2000). Samples collected from a region of equal present temperatures are assumed to have experienced the same EQT over their diagenetic history (Wehmiller and Miller, 2000) because it is assumed closely-spaced localities have experienced the same temperature histories. In a similar manner, present temperature differences between widely spaced localities are assumed to represent a reasonable estimate of past differences in temperatures (Wehmiller, 1982). The former assumptions are necessary because temperature histories are rarely known to any great accuracy. Differences in D/L values within closely-spaced localities are interpreted as relative age differences. If it is assumed that latitudinal gradients of temperature have not changed significantly over time, multiple independent calibrations in conjunction with D/L values for samples of the same age over a broad temperature range and gradients of effective temperature allow the establishment of latitudinal trends called isochrons (Wehmiller, 1982; 1984; 2012) (Figure 5.4).

Miller and Brigham-Grette (1998) showed the EQT to be nearly equivalent to the current mean annual temperature (CMAT) at depth greater than 1 m due to the decreasing influence of annual temperature variation with depth. Later work by Wehmiller *et al.* (2000) showed that the effective ground temperature can be greater than the long-term mean air temperature up to depths of 4 m and that the difference between effective ground temperatures and mean air temperatures increases with latitude. These results have implications for sampling strategies (Wehmiller *et al.*, 2000). It is best to sample from depths >2 m, although >1 m is acceptable. An effort should be made to sample from sites with similar modern air temperatures but potentially different ground temperature histories so that AAR data can be analysed in the context of the potential differences. The temperature history must also be considered when

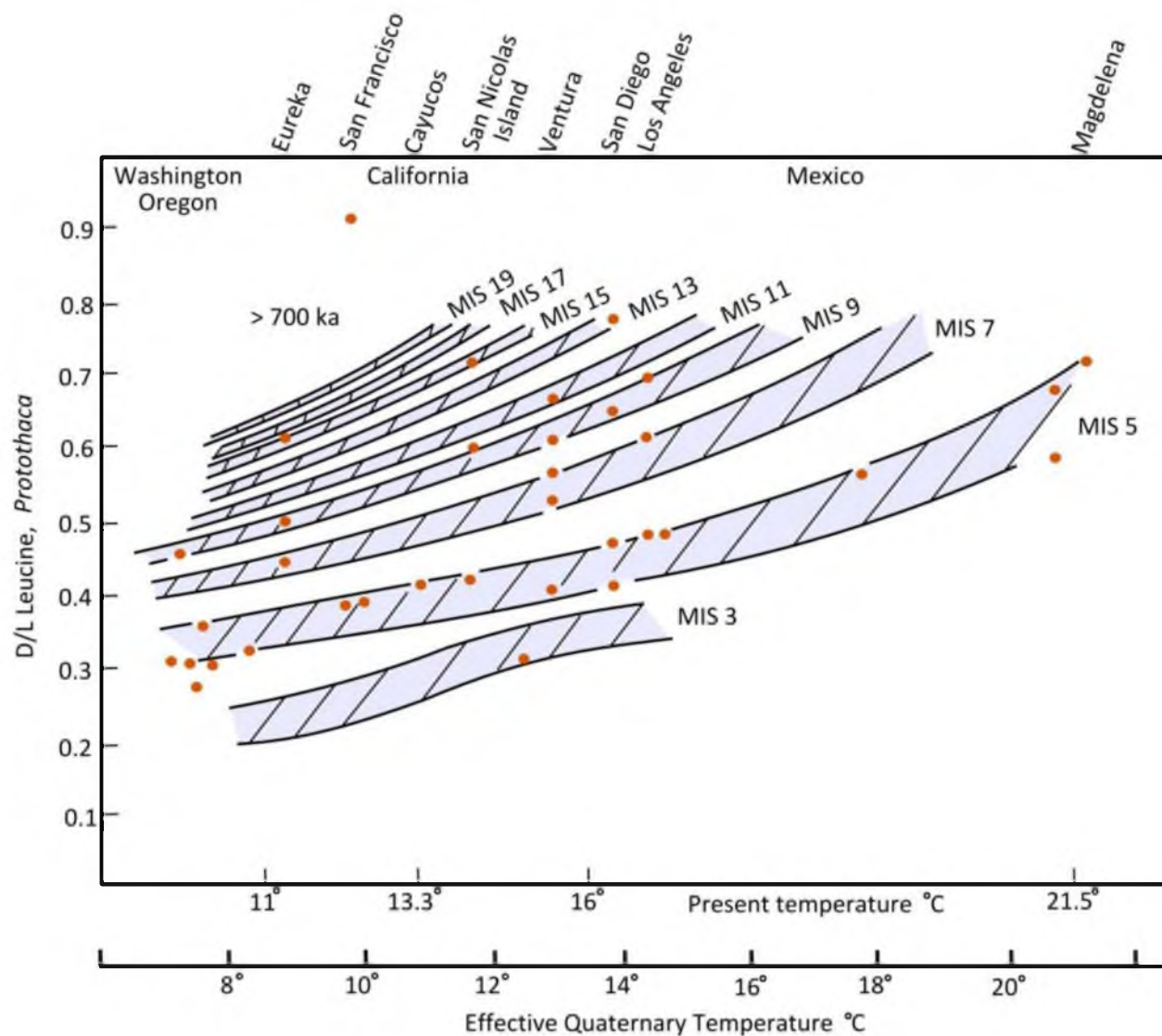


Figure 5.4: Aminostratigraphy and kinetic model interpretation of Pacific coast (USA, Mexico) enantiomeric ratio data illustrating the latitudinal trends in D/L values due to latitudinal gradient of effective temperature (Wehmiller, 1982). Isochrons represent ice-volume minima stages within the Marine Isotope record (modified from Wehmiller 1982).

comparing AAR data from shallowly buried samples versus more deeply buried samples. For example, in a study of Holocene mollusc shell retrieved from the same locality but at varying depth of burial, Murray-Wallace *et al.* (1988) found two surface samples to show a large variation in their individually derived palaeo-temperatures. Furthermore, both samples indicated higher diagenetic temperatures than samples retrieved from greater than 1 m burial depth. The palaeo-temperatures derived from the buried shell closely agreed with contemporary mean annual temperature.

5.2.1.3 Genus-effect

The genus-effect is another important consideration in the application of amino acid racemisation. Different apparent rates of racemisation are not detectable among species of the same genus but are detectable among genera in different families and at higher taxonomic levels (Lajoie *et al.*, 1980). This is related to differing initial rates of hydrolysis between genera as determined by their composition; the inherent nature of the proteins, peptides and the proportion of hydrolysis-resistant peptide bonds within a genus; i.e. the stability of peptide linkages (Lajoie *et al.*, 1980; Wehmiller, 1980). Long-chain polypeptides containing amino acids more resistant to hydrolysis will slow the overall apparent rate of racemisation. However, the order of apparent rates of racemisation (using relative D/L values) among five amino acids is the same in different genera: proline \geq phenylalanine \geq leucine > Glutamic acid > valine (Lajoie *et al.*, 1980).

5.2.1.4 Environmental Factors

Environmental factors (pH, ionic strength and diffusion effects, surfaces, metallic cations, the concentration of water) and contamination, leaching and decomposition have all been identified as having various influences over AAR (Hare and Mitterer, 1968; Hare, Miller and Tuross, 1975; Smith *et al.*, 1978). The impact of environmental factors on diagenesis can be considered minimal because even though experimental studies have shown marked differences in the rates of hydrolysis, racemisation, amino acid decomposition and loss of organic fraction, the observed rates of racemisation in fossils display little variation between amino acid, genera or biomineral type (Collins and Riley, 2000). For example, although pH was found to be a significant factor in the stability of some amino acids in laboratory heating experiments (Hare and Mitterer, 1968), racemisation rates are effectively independent of pH in the natural environment (pH

value ranges from 6-9) at temperatures between -2 and 28°C (Bada and Shou, 1980). Furthermore, bivalve and gastropod shell matrices are highly effective at excluding most environmental influences, approximating a closed system able to retain indigenous free amino acids and peptide chains while preventing contamination by secondary amino acids in a sedimentary environment for at least 10^5 years (Miller and Hare, 1980).

In well-preserved fossils the intracrystalline fraction of a shell effectively isolates the sample from the influence of external rate factors including allochthonous organic matter, microbial reworking and contamination, and leaching (Sykes *et al.*, 1995; Penkman *et al.*, 2008). This 'protection' decreases with the preservation state of the fossil. Samples analysed using only amino acids within the intracrystalline matrix exhibit the same rates of hydrolysis and racemisation and the same taxonomic differences as samples analysed using both intra- and inter-crystalline fractions, albeit with improved precision.

Sykes *et al.* (1995) suggested that despite the potential problems contamination of the intercrystalline fraction by allochthonous peptides and amino acids may present, the success of amino acid stratigraphy under most diagenetic regimes implies the exchange of amino acids between fossils and the environment either does not occur or does not significantly affect amino acid D/L values in molluscs. Furthermore, as the shell matrix decays the movement of amino acids is more likely to be out of the shell and into the surrounding sediments than the reverse. Excess water, present as soil moisture or percolating groundwater, allows leaching and loss of indigenous amino acids (Rutter and Blackwell, 1995). Intercrystalline protein progressively leached from fossil shells with a preferential loss of racemic free amino acids results in a decrease in D/L for the total hydrolysable amino acid fraction of the whole shell and an increasing importance with age of the proportion of amino acids within the intracrystalline fraction (Penkman *et al.*, 2008). Therefore, although the bio-matrix of calcareous organisms is very good at preserving the amino acids within the intracrystalline fraction it is still important to choose samples as well preserved as possible. Robust shells are preferable whose visual characteristics of lustre, porosity and texture are most similar to modern equivalents (Wehmiller and Miller, 2000). More variation in D/L values can be expected from shells that are abraded, weathered, chalky, fragmented or worn.

5.2.1.5 Kinetic Models

Three model types developed to represent the kinetics of racemisation are reviewed here: linear, non-linear, and parabolic. The extended linear model (Hare and Mitterer, 1966; 1968) can be effective at describing the relationship between D/L and t (time) for the initial rapid rate of racemisation (Clarke and Murray-Wallace, 2006). However, it is relatively restrictive and is less favoured for samples beyond the age of the Holocene (Wehmiller and Hare, 1971; Kriausakul and Mitterer, 1978; Wehmiller, 1980a; 1980b), although Kvenvolden *et al.* (1981) argued that the linear method was favourable where leucine D/L ratios were less than 0.5 due to its relative simplicity. An exception would be in the analysis of eggshell. Miller *et al.* (2000) in a number of heating experiments using eggshell of the extant emu *Dromaius novaehollandiae* and the extinct ostrich-sized *Genyornis newtoni*, showed that an initial period of a non-linear rate in the epimerisation of isoleucine was rather insignificant at ambient temperature (less than a decade) and was followed by a linear relationship which continued to an alle/Ile value of approximately 1.0. Within the context of Arrhenius parameters the nonlinear interval has an inconsequential impact on quantitative geochronology or palaeothermometry.

The non-linear kinetic model is based upon first order reversible kinetics and relies heavily on identification of the transition zone where the rates of racemisation change from an initial rapid rate to a slower rate. The rates are represented by linear segments with decreasing rate constants (Wehmiller, 1980). Ideally for this model radiometric calibration data would be available for samples both young and old (from either side of the transition zone) and an Effective Quaternary Temperature (EQT) would be discernible (for estimation of maximum temperature variation) to allow minimisation of uncertainties (Wehmiller, 1982).

The parabolic model is derived from simple curve-fitting routines applied to data from laboratory experiments and natural geologic settings. It generates a linear relationship between the square root of age of samples and D/L values (Mitterer and Kriausakul, 1989; Wehmiller and Miller, 2000). However, for D/L values >0.8, the ability of the parabolic approach to reliably discriminate ages significantly decreases (Murray-Wallace and Kimber, 1993).

Kinetic models require both Holocene and Pleistocene calibration samples and palaeoclimatic information with which to estimate EQT. The choice of kinetic model is dependent upon comparison with the available independent control and the temperature dependence of racemisation within the chosen samples as well as the age of the samples (Wehmiller, 1984; Wehmiller and Miller, 2000; Clarke and Murray-Wallace, 2006). All models work best when calibrated with multiple independent ages.

5.2.2 Applications of AAR

The results of AAR are applied for use in Quaternary research in the resolution of mixed-age populations, aminostratigraphy, numeric and relative ages, and in aid of radiocarbon dating by performing as an 'age-screening' tool before radiocarbon analysis (Miller and Hare, 1980). Palaeothermometry is another application in which the thermal term is determined with the D/L value from a sample of known age. This is possible due to the relationship between burial temperature and the extent of racemisation (Miller and Brigham-Grette, 1989). Palaeothermometry is not used in this work and will not be discussed further. However, the other uses of AAR are considered in further depth below.

5.2.2.1 Resolution of mixed-age populations

One of the most direct applications of D/L values is the resolution of mixed-aged populations and determination as to whether the death assemblage represents a biocenose or thanatocenose fossil population (Murray-Wallace and Belperio, 1994; Wehmiller *et al.*, 1995; Murray-Wallace *et al.*, 1996) where shells or carbonate sediments are beyond the age-range of radiocarbon analysis and capabilities of isotopic dating. In a locality where reworking may have occurred, analysis of sufficient samples to demonstrate a bimodal distribution or an apparent clustering of ratios, allows the identification of two or more populations of significantly different ages (Miller and Hare, 1980; Miller and Brigham-Grette, 1989). Among monogeneric populations where similar kinetic pathways are to be expected within species, significant deviations are indicators of reworking or chemical contamination (Lajoie *et al.*, 1980). The preference for robust shell in AAR analysis (which is more likely to survive the mixing process) reiterates the need for careful sample collection of multiple samples from a stratigraphic unit

(Wehmiller, 2013). Any conclusions regarding outliers should be based on multiple analyses and good stratigraphic control.

5.2.2.2 Aminostratigraphy

The term aminostratigraphy was introduced by Miller and Hare (1980) to describe the application of amino acid results from deposits within a region having a similar climatic regime to develop stratigraphic correlation and a regional chronology. D/L values from localities within the same region having similar or identical current mean annual temperatures (CMAT) and thereby inferred similar effective diagenetic temperatures can be used to determine a relative age sequence (Wehmiller, 1982; Hearty *et al.*, 1992; Hearty, 1998; Wehmiller and Miller, 2000). Chronostratigraphic units representing discrete time intervals identifiable by the clustering of similar D/L values are known as 'aminozones' (Murray-Wallace and Kimber, 1987), the identification of which can be further supported by litho-, bio- and morphostratigraphical evidence and calibration by other geochronological methods (Hearty, 1998; Murray-Wallace, 2000). An example of how multiple chronostratigraphic units can be discerned with the combined use of lithostratigraphy and the identification of aminozones through the use of AAR is provided in Figure 5.5.

Isochrons of D/L values across latitudes can be used for aminostratigraphic comparisons and correlations. The latitudinal temperature gradient is reflected in corresponding D/L values of the same age because of the role temperature has in the rate of racemisation (Wehmiller, 1984). Relative age resolution successful to at least the scale of interglacial intervals has proven to be successful across twenty degrees of mid-latitude (and temperatures) on the Pacific and Atlantic coasts of North America (Wehmiller, 2013) and across southern Australia from Western Australia to Tasmania (Murray-Wallace, 2000) (Figure 5.6). Isochrons developed with data from taxa of the same family can be used as a working model for the interpretation of AAR results for the same taxa from other sites within the same range of effective temperatures. The trend of D/L values for fossils of the same genus and common age should be exponential along the linear trend of changing temperature (Murray-Wallace, 2000; Wehmiller, 2013a; Murray-Wallace and Woodroffe, 2014).

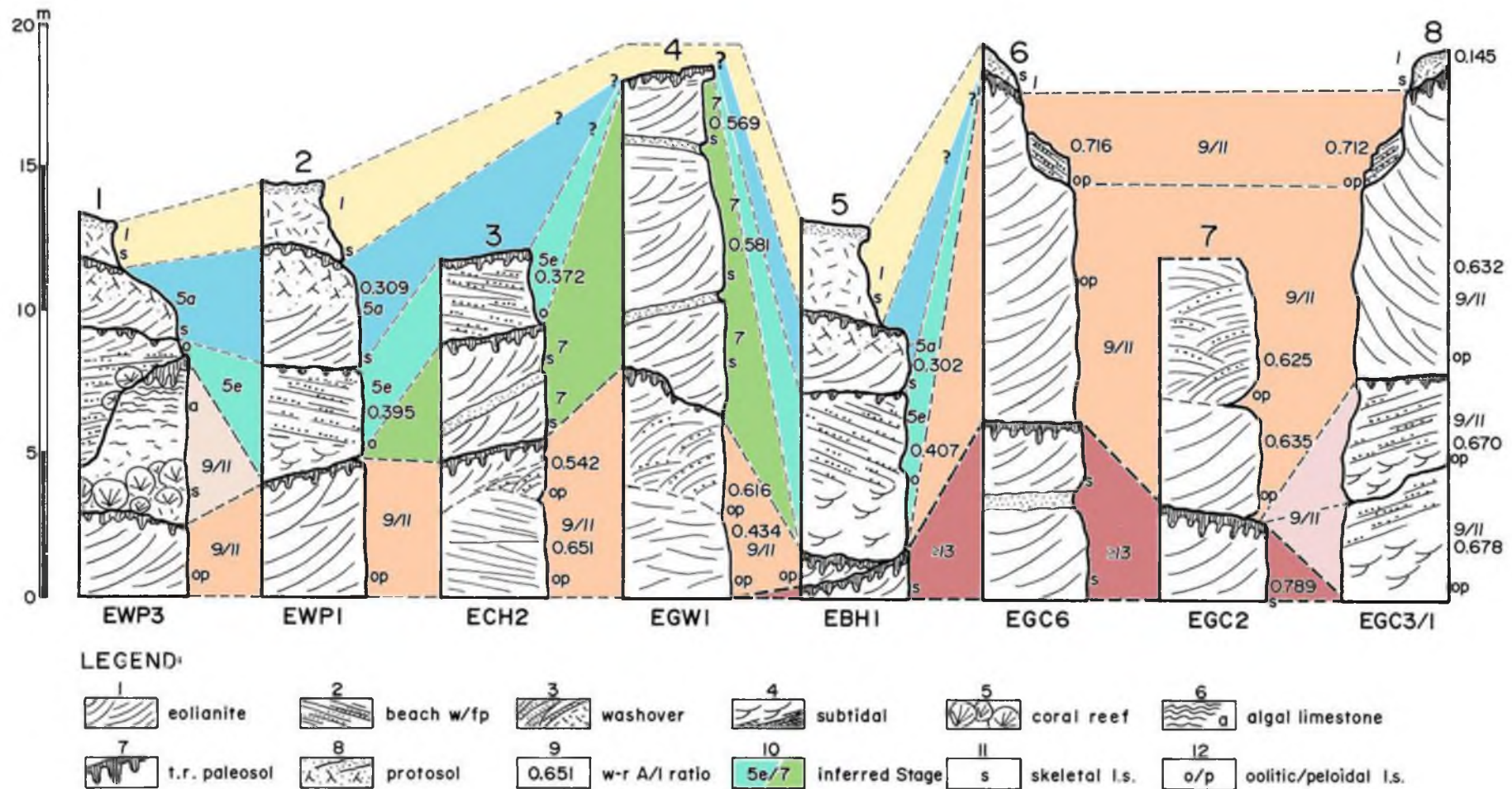


Figure 5.5: Stratigraphy and correlation of eight sections in north Eleuthera, Bahamas demonstrates the combined use of lithostratigraphy and aminozones. Whole-rock alioisoleucine/isoleucine values, limestone composition (skeletal, oolitic, peloidal, and algal) and inferred correlation with Marine Isotope Stages (MIS) are provided for the sections (from Hearty, 1998).

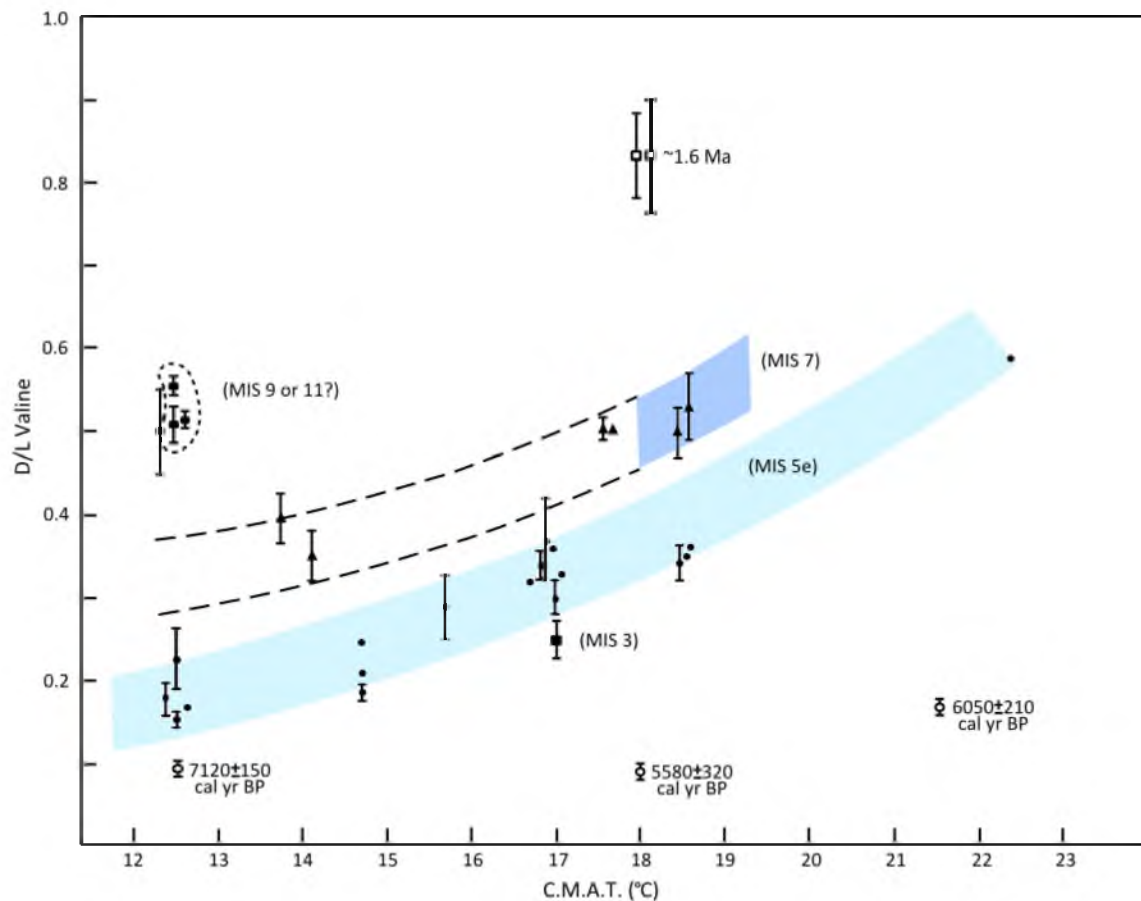


Figure 5.6: Plot of the exponential change in D/L valine data against the linear current mean annual temperature for Quaternary marine molluscs from interglacial and interstadial highstand deposits from southern Australia (Western Australia, South Australia, Victoria, and Tasmania). The exponential effect of temperature on diagenetic racemisation is evident in the plot of data for the last interglacial Marine Isotope Stage 5e deposits (Murray-Wallace and Woodroffe, 2014). Open circles represent results for radiocarbon-dated Holocene fossil molluscs (modified from Murray-Wallace, 2000).

5.2.2.3 Whole-rock analysis

Sedimentary successions with a bioclastic component which are not suitable for dating by other geochronological methods due to a lack of necessary components (i.e. quartz sand for TL or OSL, corals for U-series) can be analysed by AAR as 'whole-rock' sediment (Hearty *et al.*, 1992; Murray-Wallace *et al.*, 2001; 2010). AAR analysis of whole-rock sediment containing carbonate grains (generally comminuted shell and foraminifera) of contrasting mass and age provides average D/L values representing an integrated average of all the biominerals within that sample dependent upon the concentration and sample mass of the different skeletal carbonate grains. Although

some grains are likely to be from an older re-worked source, the majority of grains are expected to be of a common age representing, for example, a single isotopic stage.

The measured extent of racemisation is influenced by the degree of diagenesis and weathering of sediments, sediment reworking, the genus-effect on individual grains and their thermal history (Murray-Wallace *et al.*, 2001; 2010). Whole-rock samples will predate *in situ* marine shell (provided it is not reworked from an older source). This is attributed to the possible long residence time for bioclasts within a high wave energy environment and sediment recycling from older barriers. The age of a sedimentary successions derived from whole-rock analysis, depending on the nature of the sedimentary environments, can predate ages derived from the geochronological methods of thermoluminescence (TL) and optically stimulated luminescence (OSL) because AAR ages the cessation of protein formation (commonly equated with death) while the latter date the time of deposition (Murray-Wallace *et al.*, 2010). This is statistically accounted for by subtracting the whole-rock time zero (or residence time) of sediment (as determined by AAR measurement of modern beach samples) from the D/L values of the Pleistocene sedimentary successions prior to calibration of AAR numerical ages.

5.2.2.4 Numerical age

The numerical age of shell is commonly determined with the use of an independently calibrated sample usually by means of radiometric dating with radiocarbon (^{14}C) or uranium/thorium on associated corals (Hare *et al.*, 1997). D/L values from any locality that has been independently calibrated and for which a rate constant has been determined, can be used to derive numerical ages using a kinetic model of diagenetic racemisation and an accurate integrated thermal history of the site (Wehmiller, 1984; Miller and Brigham-Grette, 1989). Ideally multiple samples of numerical age spanning from the Holocene and through the Pleistocene will be available allowing the development of a robust curve of D/L versus time. Unfortunately, this is seldom the case due to the fragmentary nature of most terrestrial and coastal Quaternary sedimentary records (Wehmiller, 2013). When suitable samples are lacking it then becomes necessary to choose the appropriate kinetic model based upon the anticipated age of the samples (see kinetic model discussion above). The EQT can then

be incorporated into a kinetic equation along with a series of D/L values to solve for the age of each sample analysed (Hare *et al.*, 1997). Due to the reliance of the age model on racemisation kinetics and accurate thermal history, a new model must be developed for each taxon and field setting because of the genus effect and changes to EQT, respectively.

5.2.3 AAR analytical methods

This section describes the methods used in the amino acid racemisation analysis in this thesis. Firstly, the terms 'sample' and 'sub-sample' (Figure 5.7) are defined:

- *Field sample*: the total amount of shell or whole-rock retrieved from a field site representing a single bed. Field sites can be represented by multiple field samples.
- *Laboratory sample*: Either the entirety or portion of a shell taken from a stratigraphic unit for AAR analysis; or a portion of whole-rock sediment taken from a whole-rock field sample representing a single stratigraphic unit for AAR analysis.
- *Sub-sample*: Samples, in preparation for AAR analysis were commonly sub-sampled so that only a fraction of the shell or whole-rock sediment was used for analysis. Multiple sub-samples could be taken from one sample to check for reproducibility and integrity of the results.

Each laboratory sample was given a unique laboratory ID, a University of Wollongong, Australia (UWGA) number. Sub-samples of a laboratory sample were assigned the same UWGA number with an additional identifier (Figure 5.7). This was to limit the number of UWGA numbers generated and decrease the possibility of confusion. Sub-samples from shell could represent a portion of the shell or the entire sample depending on size (i.e. smaller samples generally weighing less than 100 mg). Foraminifera were always run whole as the specimens are too small for subsampling.

FIELD CODE / SITE	12.24.2 CF / Cheese Factory, Hindmarsh Island				
STRATIGRAPHIC UNITS	Calcrete	Aeolian Sand	Muddy Sand	Shelly Sand	
FIELD SAMPLES	calcrete	whole rock	whole rock	whole rock	shell
LABORATORY SAMPLES	No Lab Sample	UWGA 10164	UWGA 10153	UWGA 9927	UWGA 9773
SUB-SAMPLES		10164.1 10164.2 10164.3 10164.4 10164.5	10153.1 10153.2 10153.3 10153.4 10153.5	9927.1 9927.2 9927.3 9927.4 9927.5	9773.1 9773.2 9773.3 9773.4 9773.5
					Each sub-sample represents a portion of, or an entire shell sample (i.e. part of a valve, an entire gastropod etc.). Five valves of <i>S. trigonella</i> are represented by UWGA 9773. <ul style="list-style-type: none"> <i>Spisula (Notospisula) trigonella</i> <i>Tellina (Macomona) deltoides</i> <i>Eumarcia fumigata</i>

Figure 5.7: An example of the sampling and sub-sampling method used in this research.

5.2.3.1 Sample selection

Field sample selection is critical in AAR to control the variables which can affect AAR results on a “micro” scale: age mixing, diagenetic alteration of analysed samples, local variations in thermal history, and taxonomic differences in inter- and intrageneric rates (Wehmiller, 2013). Factors influencing the rate of racemisation: temperature, genus-effect and environmental influences, have implications for the selection of samples to be used in AAR analysis, although in whole-rock analysis it is generally not possible to control any genus effect on racemisation.

Depth of burial is important with regards to the diagenetic temperature. A field sample may be exposed to alternating periods of burial and exhumation, altering temperature and the rate of racemisation (Walton, 1998). It is recommended to sample at depth where the field sample has been exposed to a temperature amplitude less than 6°C, preferably 2 m or more (Miller and Hare, 1980; Miller and Brigham-Grette, 1989; Wehmiller *et al.*, 2000). However, 0.5-1 m depth of burial may be acceptable. Anything buried at 30 cm or less for a significant portion of its post-depositional history should be avoided. It should be noted that surface exposures (i.e. road cuttings, stream banks) aged a few decades and even centuries, although possibly exposed to large variation in temperature, can still provide suitable samples as the racemisation rates have not been too altered due to the short term affect it would have on the EQT of a fossil deposited during MIS 5e or earlier.

It is rare for the same genus to be found across all localities of interest in a regional study and commonly multiple genera are needed for larger-scale AAR based research projects (Wehmiller, 1982; 1984; Wehmiller and Miller, 2000). Genera which are intergenerically and geochemically consistent as well as consistent in their stratigraphic relationships can be used for aminostratigraphic applications in regions with little other age information. The use of multiple genera provides the opportunity to test the internal consistency of D/L data from a given site. Because D/L intershell variation exists even within monogeneric samples it is recommended to test at least three *in situ* samples from the same anatomical part of the shell (e.g. hinge region) retrieved from the same stratigraphic unit and if possible paired and in life position or at least visually well preserved (Miller and Hare, 1980; Miller and Brigham-Grette, 1989).

The group mean should be used to characterise the deposit. Significant deviation from the relative kinetics within genera can indicate geologic reworking or chemical contamination (Lajoie *et al.*, 1980). In order to avoid chemical contamination or leaching of indigenous proteins and amino acids, shell material showing obvious signs of poor preservation or contamination should be avoided.

From the field samples containing mollusc shell, twenty different bivalve species and ten gastropod species were identified (see 4.2.1). Four bivalve species were used in AAR analysis: *Spisula* (*Notospisula*) *trigonella*, *Paphies* (*Amesmodesma*) *elongata*, *Macra rufescens* and *Donax deltoides*. Three gastropods were used in AAR analysis: *Hydrococcus brazieri*, *Coxiella striata* and the opercula of *Turbo* sp. These species were selected due to their presence across multiple sites and depositional environments. In some cases two or more of the species were found at one site allowing cross-comparison of D/L values and an indication of reworking. Wherever possible at least four samples of the same species from each field sample were analysed. Shell samples were chosen based on their taphonomic grade based on whether or not the shell is articulated (if bivalve) and the condition of individual valves (i.e. whole or fragmented, level of corrosion and level of preservation of distinguishing features) (section 4.2.1).

Whole-rock, as a sample of sediment, could not be subjected to a grading scheme. The level of induration of the sediments was noted in the field, as this is an indicator of the degree of diagenesis and potentially the age of the sediment. Foraminifera for AAR analysis were picked from whole-rock samples. The quality of foraminifera and the ability to identify individuals (tests) to a species level was, to a certain degree, dependent upon the induration and calcite cement content of the whole-rock sample. Identification was hampered by whole-rock containing calcite cement which coats the test obscuring distinguishing physical features. Identification was also complicated by recrystallization of the test, staining by iron or manganese oxides and reworking which could abrade distinguishing characteristics. In many cases identification was made at the genus level by either the shape of the test or surface ornamentation. A study of Holocene sediments at the Murray Mouth (Cann *et al.*, 2000) found that *Ammonia beccarii* and *Elphidium articulatum* characterise the estuary and Coorong Lagoon, while the inner-shelf marine environment was dominated by *Discorbis*

dimidiatus, *E. crispum*, *E. macelliforme* and other cibicidid species. The two most commonly identified genera were *Discorbis* sp. and *Elphidium* sp. The most robust tests of the two genera were preferentially chosen for analyses from whole-rock.

5.2.3.2 Sample preparation

Sample preparation and hydrolysis of mollusc shell, whole-rock and foraminifera followed the method established by Kaufman and Manly (1998), Hearty and Kaufman (2000), and Hearty *et al.* (2004). A summary of the method is provided here.

The majority of shell used for AAR analysis was of taphonomic grade '3', whole valve with minimal-moderate corrosion maintaining at least some distinguishing features; or '6', articulated, both valves whole with minimal-moderate corrosion maintaining at least some distinguishing features. Grade '6' shells were analysed using only one valve. At some sites, due to the paucity of samples available, shell of lesser grade was used. Shell chosen for analysis was commonly subsampled. Where possible the subsample of a bivalve was taken from the umbo and hinge region of the shell (Figure 5.8) to reduce intra-shell variability in D/L values. In some cases, if the shell sample was small (less than 100 mg), the entire shell was used in analysis; this was always the case with the small gastropod species *Coxiella striata* and *Hydrococcus brazieri*. Gastropod *Turbo* sp. opercula were subsampled from the margin. Before subsampling sediment, cements, other adhering impurities, or diagenetically altered surfaces were removed by use of a dentist drill.

Whole-rock preparation began with isolating the 250-500 µm sediment particle fraction which was used in analysis. This process included multiple cycles of gentle grinding of the sample with mortar and pestle and sieving. Grinding helped to disaggregate the sample and remove cements. The fraction less than 250 µm is composed of cements and small fragments of comminuted shell that likely represents an older reworked component (Murray-Wallace *et al.*, 2010). Additionally, due to the small grain size, it is very difficult to pretreat (i.e. remove contaminants) and was not considered suitable for determining a representative D/L value of the deposit. It was

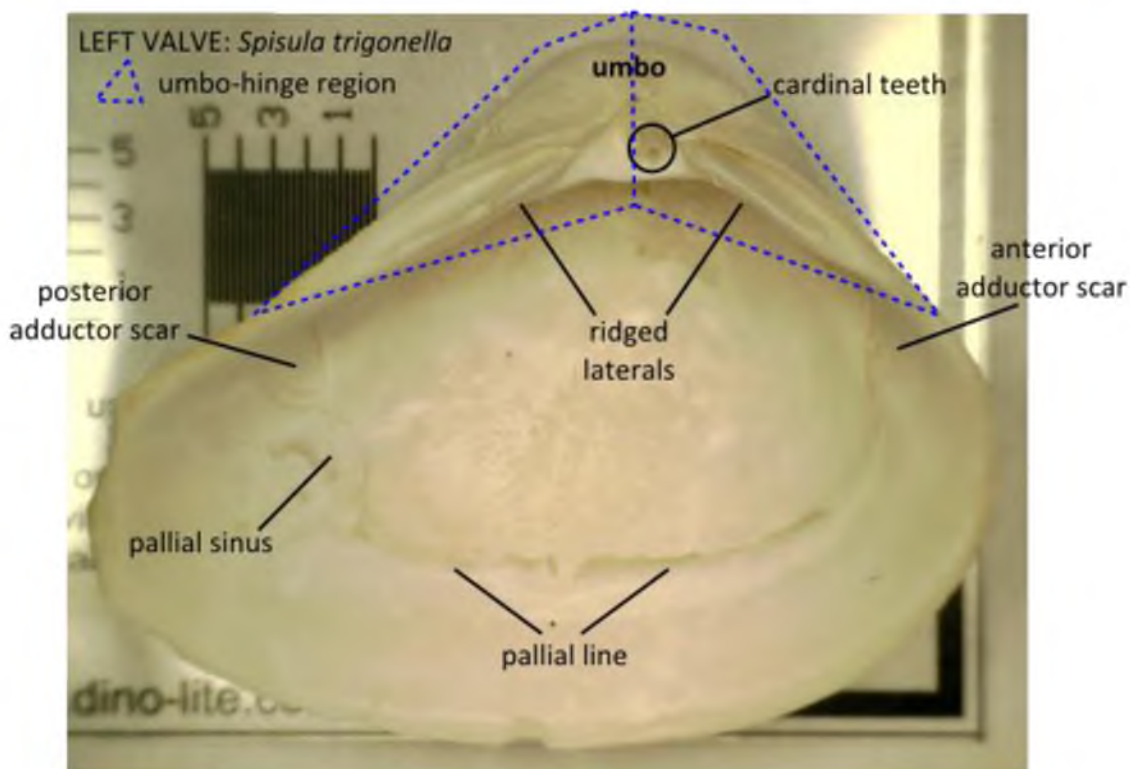


Figure 5.8: Internal features of the bivalve *Spisula trigonella*. Each valve has two umbo-hinge regions; only one was taken as a sub-sample. The large scale bars are in mm units.

necessary to determine the percentage calcium carbonate in the whole-rock sample which also contained (other than carbonate) varying quantities of quartz grains, feldspar and heavy minerals. The percentage of calcium carbonate was determined by hydrochloric acid (HCl) digestion and then applied to mass based calculations used to determine etch and hydrolysis volumes. Carbonate percentages for aeolianites, subtidal beach deposits, and subtidal-intertidal lagoon and channel deposits in the study area ranged from 4% to 84% in the 250-500 μm fraction.

Shell, whole-rock and foraminifer sub-samples were put into a test tube, submerged under distilled water and cleaned in a sonic bath for 10 minutes and then rinsed using distilled water. After drying and weighing, the shell and whole-rock samples were subjected to a 2 M HCl stoichiometric etch removing 33% of the outer shell and reducing the likelihood of contamination by altered carbonate. The stoichiometric etch was omitted in preparing foraminifera; due to their small size they did not register a mass on the laboratory balance. The samples were washed again before being submerged in an oxidising agent, either 3% hydrogen peroxide (H_2O_2) for 2 hours or 12.5% sodium hypochlorite (NaClO) for 24 hours to remove non-indigenous organic

material. Both H_2O_2 and NaClO have been shown to be effective at removing organic material from the intercrystalline matrix of shell (Love and Woronow, 1991; Gaffey and Bronnimann, 1993, Sykes *et al.*, 1995), although the types of organic material removed has been shown to be dependent on the treatment used (Love and Woronow, 1991) with NaClO shown to be more effective at removing “all types” of organic material (Gaffey and Bronnimann, 1993). To test the effectiveness of NaClO , shell samples of the bivalve *Spisula trigonella* (taphonomic Grade 3) from six different late Pleistocene sites totalling twenty-two samples were prepared with both NaClO and H_2O_2 . The umbo/hinge area of each valve was split into two parts; one half underwent NaClO preparation, the other half H_2O_2 preparation, in order to gauge the difference in results between the two treatments. H_2O_2 samples were then rinsed with Millipore water and dried while NaClO samples were rinsed with 100% methanol and then Millipore water. Results are presented at the end of this section. All shell, whole-rock, and foraminifer samples were dried prior to hydrolysis.

After drying, samples were weighed again, put into reaction vials and the shell carbonate was dissolved using a stoichiometric volume of 8 M HCl to produce a 7 M HCl solution containing shell proteins and free amino acids (FAAs). FAAs were in some instances subsampled (generally at 50 μL). The 50 μL sample size is a sufficient sample mass to ensure the development of Gaussian peaks during a RP-HPLC (reversed phase – high performance liquid chromatography) run. Again due to their small size, foraminifera could not be weighed to determine a stoichiometric volume of HCl and were dissolved using 5 μL of high purity 6 M HCl. FAAs could not be taken from foraminifera due to the low sample mass. The vials were flushed with N_2 and sealed to prevent oxidation during hydrolysis before being placed in an oven at 110°C for 22 hours for solution hydrolysis. After hydrolysis the samples were subsampled, generally at 50 μL . The measure of whole-rock sub-samples for both FAA and total hydrolysable amino acids (THAA) was dependent upon the carbonate percentage of the sample. If a whole-rock sample was less than 50% calcium carbonate the sub-sample volume was doubled to 100 μL and in some instances where total carbonate was less than 25% of the sample volume, the sub-sample volume was increased to 150 μL . Prior to THAA subsampling, whole-rock samples were filtered to remove any undissolved solids which may have blocked a component of

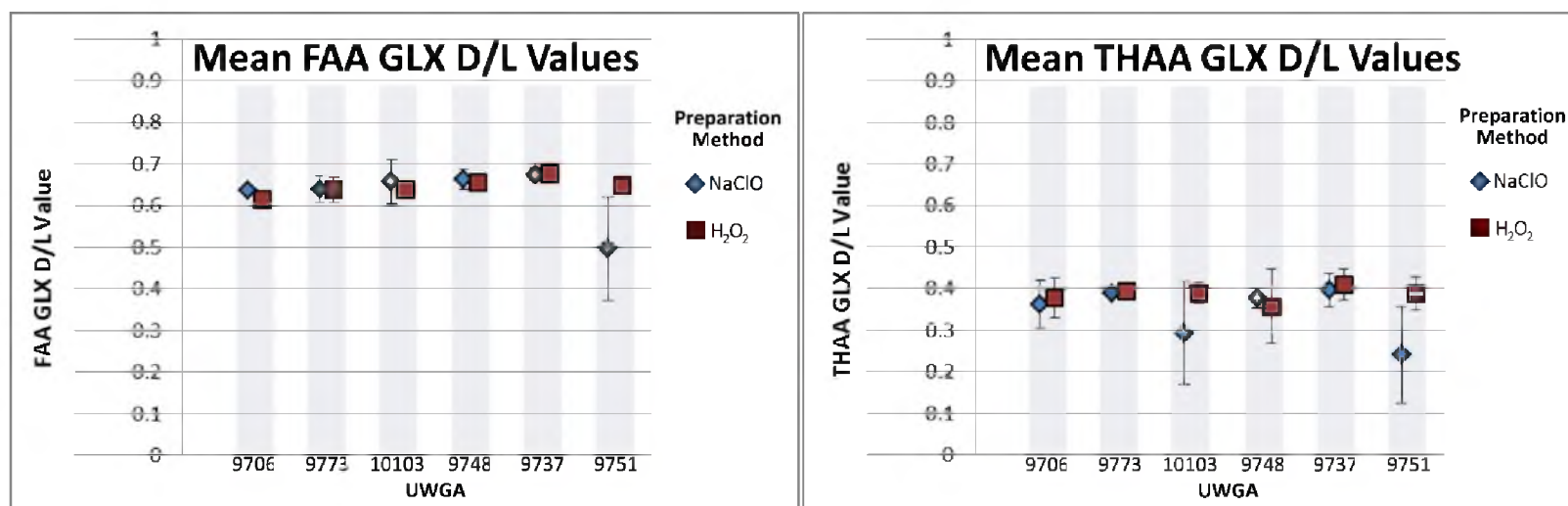
the RP-HPLC Autosampler. FAA and THAA subsamples, placed in chromatography vials, were desiccated and then rehydrated with a solution of 0.01 M HCl + 0.77 mM sodium azide + 0.01 mM L-Homoarginine (an internal standard to calculate sample yield if necessary) and mixed on a vortex-mixer. The rehydrated solution was then ready for analysis in the RP-HPLC.

Analysis of mean glutamic acid (GLX) D/L values from shell prepared using both NaClO and H₂O₂ oxidising agents shows NaClO to produce more consistent FAA and THAA D/L values (Table 5.1 and Figure 5.9), especially THAA D/L values. The relatively low covariance amongst FAA D/L values from almost all field sites, regardless of the preparation method, suggests that little or no leaching had occurred. H₂O₂ prepared FAA D/L values from the Victor Harbor field site are the exception with the corresponding H₂O₂ prepared THAA D/L values also showing high variability. Although all shell valves chosen for this analysis were of taphonomic Grade 3, shell from field sites Victor Harbor and Myrtlegrove Road lagoon (showing the second highest variability in H₂O₂ prepared FAA and THAA D/L values) were both stained by algae. The increased variability of H₂O₂ prepared THAA D/L values (judged by covariance) supports the conclusion of Gaffey and Bronnimann (1993) that NaClO is more effective at removing organic material than H₂O₂. Depth of burial has had no apparent effect on the rate of racemisation in these samples or the integrity of the shell in retaining amino acids, but there are too few samples to make any absolute conclusions regarding these factors. NaClO is shown to generate more consistent D/L values; however, all D/L values, regardless of oxidising agent employed, are within one σ standard deviation. In the interest of time, oxidation by H₂O₂ (2 hours) versus NaClO (24 hrs) serves as a much quicker and still suitable method for removing organic material except for possibly in the case of algal staining. This exercise also confirms the necessity of good field sample selection to minimise the variability of AAR results.

Table 5.1: THAA and FAA GLX D/L values for shell prepared using either H₂O₂ or NaClO as an oxidising agent. The number of samples varies between FAA and THAA due to a broken vial following hydrolysis and bad results off the RP-HPLC.

Field Code	Depth of Burial	Lab Number (UWGA)	Number of Samples	FAA GLX D/Lvalue \pm 1 σ (H ₂ O ₂) ^a [CV] ^b	FAA GLX D/L value \pm 1 σ (NaClO) ^a [CV] ^b	Number of Samples	THAA GLX D/Lvalue \pm 1 σ (H ₂ O ₂) ^a [CV] ^b	THAA GLX D/L value \pm 1 σ (NaClO) ^a [CV] ^b
BR	surface	9706	1	0.636	0.615	2	0.362 \pm 0.057 [16]	0.376 \pm 0.048 [13]
CF-Sh	2.2 m	9773	4	0.658 \pm 0.033 [5]	0.640 \pm 0.030 [5]	3	0.389 \pm 0.012 [3]	0.393 \pm 0.009 [2]
MR L	< 0.30 m	10103	4	0.639 \pm 0.054 [9]	0.638 \pm 0.018 [3]	3	0.293 \pm 0.123 [42]	0.389 \pm 0.025 [6]
CSP-1	1.85 m	9748	3	0.663 \pm 0.023 [4]	0.655 \pm 0.010 [2]	4	0.377 \pm 0.025 [7]	0.357 \pm 0.090 [25]
CSM-D	reworked	9737	4	0.674 \pm 0.015 [2]	0.675 \pm 0.011 [2]	4	0.397 \pm 0.040 [10]	0.409 \pm 0.038 [9]
VHR	reworked	9751	4	0.496 \pm 0.123 [25]	0.646 \pm 0.019 [3]	4	0.240 \pm 0.116 [49]	0.388 \pm 0.041 [11]
^a oxidising agent used in sample preparation								
^b covariance of mean D/L value rounded to the nearest whole number								

Figure 5.9: Charts illustrating the mean trends in free amino acids (FAA) and total hydrolysable (THAA) D/L values dependent upon the oxidising agent used in preparation of shell for hydrolysis.



5.2.3.3 Data screening and rejection criteria

AAR data were analysed to identify and reject outliers while still maintaining the integrity of the sample group (Kosnik and Kaufman, 2008). D/L values were expected to vary between and within samples due to age-population distribution, genus effect, taphonomic affects, and individual diagenetic histories so it was important to establish a data screening approach that would allow for these differences. Variation in D/L values from the same deposit can be accounted for in analytical and sampling uncertainty (Murray-Wallace and Kimber, 1987), the latter of which can be minimised by rigorous sample selection (see above discussion). The RP-HPLC D/L values from this study were evaluated on the basis of the following several rejection criteria.

Amino acid abundance

The RP-HPLC produces a chromatograph trace where the fluorescence signals derived from amino acids are displayed as peaks above a baseline (Figure 5.10). An amino acid D/L value is the ratio of two adjacent peaks. The baseline represents the threshold 'noise' level, which is automatically defined by the RP-HPLC software but can be manually adjusted for each peak if necessary (e.g. inappropriately assigned integration and removal of rider peaks). The strength of the fluorescence signal, and therefore size of the peak, is related to amino acid concentration. A qualitative approach to the estimation of amino acid abundances is made, based upon an internal standard L-homoarginine (L-hArg) that is added to samples during preparation. The area of the internal standard peak serves as an indicator to the concentration of residual amino acids within the fossil. Small peaks are subject to large errors because the baseline noise may affect the beginning and end of peak integration for the peaks. Low peaks and/or background issues (e.g. uneven baseline, rider peaks or the presence of normally absent peaks) are generally associated with low concentrations of amino acids due to strong leaching or decomposition and generate large uncertainties. If the peaks were too low, generally below 20-30 fluorescence units (LU), or obscured by background noise, the sample was rejected.

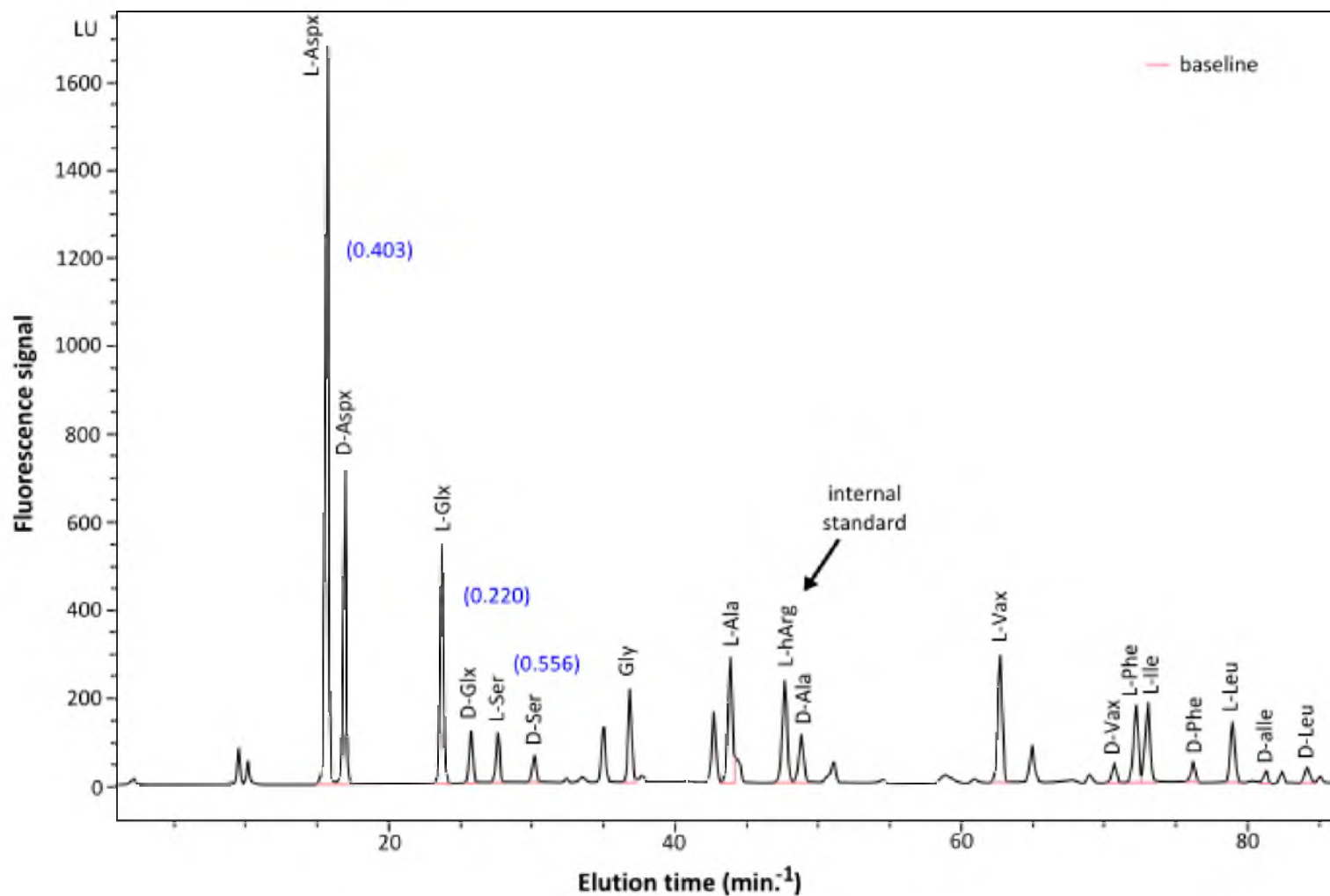


Figure 5.10: A chromatograph trace from the interlaboratory comparison (ILC) standard A, a homogenous powder of Pleistocene mollusc samples used as a comparative standard (Wehmiller, 1984; 2013). The fluorescence signal is a measure of lumens. D/L values for aspartic, glutamic and serine are provided.

Serine abundance

The amino acid serine (Ser) is one of the least stable amino acids and decomposes quickly, undergoing extensive racemisation much earlier than other amino acids (Williams and Smith, 1977). The estimated half-life for the chemical decomposition of serine in skeletal material at $\sim 0^{\circ}\text{C}$ is $\sim 10^6$ years, compared to $\sim 10^7$ for aspartic acid and phenylalanine, $\sim 10^8$ for leucine, and $>10^8$ for glutamic acid, alanine, isoleucine and valine (Schroeder and Bada, 1976). Low D/L values for serine in Pleistocene fossils indicates contamination by modern amino acids. What constitutes 'low' depends on the anticipated age of the sample and this was judged by the height of Ser fluorescence peaks compared with other amino acids. A D/L value of ≤ 0.100 in samples older than the Holocene was interpreted as evidence of contamination and the sample was rejected.

Amino acid covariance

Aminostratigraphic studies typically aim to resolve the central tendency of a collection of shells to assign a single best age (Kosnik and Kaufman, 2008). Ideally, amino acids within a single shell or foraminifer (and to a limited extent, within a whole-rock sub-sample) will exhibit an equally covariant concentration and extent of racemisation through time. The D/L values of Aspartic acid (ASX) and Glutamic acid (GLX) were used to test the internal consistency of results. Individual results that fell outside the trend of the data (2σ outside group mean) were flagged for further analysis or rejection. ASX was chosen because it was the most abundant amino acid found in all types (mollusc shell, whole-rock, foraminifera) of analyses. GLX was chosen because has been shown to exhibit a stable kinetic behaviour (Lachlan, 2011) whereas ASX can be subject to loss of concentration over time and kinetic reversal (Kimber *et al.*, 1986).

Analytical uncertainty

Analytical uncertainty generally accounts for less than 5% of the variation reported for D/L values and can be decreased by repeated injection (Murray-Wallace and Kimber, 1987). The analytical uncertainty associated with instrument reproducibility and laboratory error can be determined with repeat injections of the same sample; in this case, inter-laboratory comparison standards (ILCs). ILC-A, ILC-B, and ILC-C are three

homogeneous powdered Pleistocene mollusc samples with varying extent of racemisation that were used as comparative standards in an inter-laboratory comparison (Wehmiller, 1984) and continued to be used as a “within-laboratory” reference (Wehmiller, 2013). The ILCs were analysed at various times during this research to determine the analytical uncertainty due to instrument reproducibility and laboratory uncertainty (Figure 5.11) and to evaluate the comparability of all samples through the course of the project. The analyses were also compared with the original series of Wehmiller (1984) and Kaufman and Manley (1998) (Table 5.2). The results are in accordance within 1σ except for serine which is higher in all cases and is most likely due to diagenetic breakdown reactions which can produce serine (Williams and Smith, 1977).

Glutamic acid (GLX) and valine (VAL) were chosen for geochronological analysis in this research following the reasoning of Lachlan (2011); although aspartic acid was consistently present in the highest concentration, the amino acid (as mentioned above)

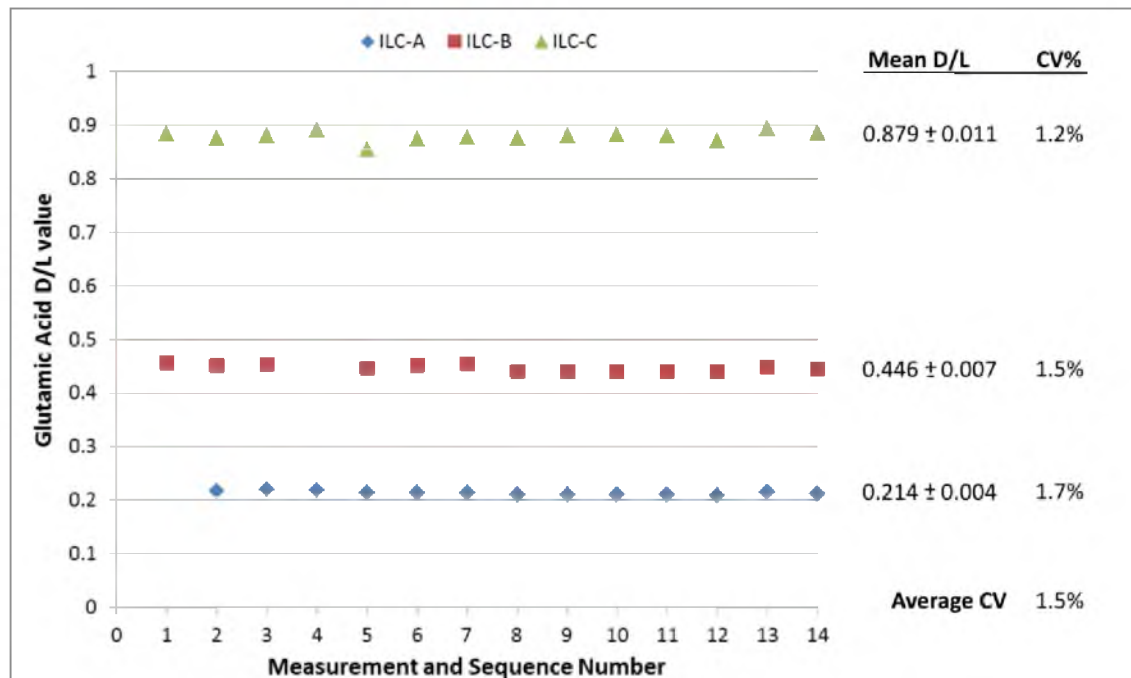


Figure 5.11: The analytical precision for glutamic acid was determined by repeat measurement of inter-laboratory comparison standards (ILC-A, B, and C) (Wehmiller, 1984) throughout AAR analysis (May 2012 to October 2014). Sequences with multiple measurements (indicated in parenthesis) correspond to multiple injections from a single vial. The mean D/L values were determined using every measurement; covariance percentages (CV%) are provided.

Amino	Wehmiller, 1984 ^a			Kaufman and Manley, 1998 ^b			This study ^b		
Acid*	ILC-A	ILC-B	ILC-C	ILC-A	ILC-B	ILC-C	ILC-A	ILC-B	ILC-C
ASX	0.378 ± 0.028	0.705 ± 0.028	0.894 ± 0.079	0.393 ± 0.006	0.684 ± 0.011	0.824 ± 0.028	0.407 ± 0.009	0.720 ± 0.015	0.894 ± 0.021
GLX	0.203 ± 0.011	0.432 ± 0.017	0.849 ± 0.035	0.205 ± 0.009	0.424 ± 0.009	0.849 ± 0.010	0.214 ± 0.004	0.446 ± 0.007	0.879 ± 0.012
SER	-	-	-	0.430 ± 0.046	0.308 ± 0.018	0.208 ± 0.019	0.588 ± 0.030	0.623 ± 0.039	0.526 ± 0.149
alle/Ile	0.364 ± 0.017	0.725 ± 0.034	0.946 ± 0.029	0.397 ± 0.024	0.766 ± 0.018	1.019 ± 0.019	0.401 ± 0.078	0.781 ± 0.092	1.031 ± 0.104
VAL	0.159 ± 0.030	0.449 ± 0.068	0.868 ± 0.084	0.164 ± 0.017	0.425 ± 0.012	0.906 ± 0.034	0.150 ± 0.010	0.418 ± 0.029	0.914 ± 0.065
PHE	0.239 ± 0.020	0.583 ± 0.059	0.873 ± 0.089	0.256 ± 0.014	0.601 ± 0.021	0.923 ± 0.069	0.266 ± 0.012	0.634 ± 0.029	1.036 ± 0.191
A/I	0.212 ± 0.036	0.540 ± 0.081	1.215 ± 0.015	0.176 ± 0.018	0.509 ± 0.062	1.124 ± 0.066	0.144 ± 0.016	0.487 ± 0.045	1.070 ± 0.103
LEU	0.196 ± 0.021	0.497 ± 0.049	0.833 ± 0.043	-	-	-	0.249 ± 0.053	0.602 ± 0.105	1.071 ± 0.249
* Abbreviations are as follows: ASX = aspartic acid, GLX = glutami acid, SER = serine, ALA = alanine, VAL = valine, PHE = phenylalanine, alle/Ile =									
alloisoleucine/isoleucine, LEU = leucine.									
^a Analysis of powdered marine shell using GC									
^b Analysis of powdered marine shell using RP-HPLC									

could show significant loss over time and is subject to kinetic reversal (Kimber *et al.*, 1986). GLX and VAL both exhibit relatively stable concentrations and kinetic behaviour over time (Kimber and Griffin, 1987), although VAL results have typically larger uncertainties (Table 5.2; Lachlan, 2011). Amino acids with slower rates of racemisation (e.g. leucine (LEU) or isoleucine (Ile/Ile)) were typically present in low concentrations (Figure 5.10) with difficulties in integration due to baseline noise and were subject to very high uncertainties (Table 5.2).

5.3 Complexities of the River Murray Mouth Region

Amino acid racemisation was the preferred method of analysis for interglacial sediments in this research due its suitability in analysing shell and aeolian whole-rock sediments with a high bioclastic carbonate component (Hearty *et al.*, 1992; 2000; Murray-Wallace *et al.*, 2001; 2010). Additionally, to the southeast but still within the Coorong Coastal Plain, the potential dating capability of the method has been shown to range between 100 ka and to at least 1.2 million years (Murray-Wallace *et al.*, 2001). AAR was also chosen due to a lack of coral for U-series dating. However, the generally low carbonate content (Chapter 4) of the sedimentary succession sampled within the study area and the apparent reworking that has occurred has had implications for the results of AAR whole-rock sediment and foraminiferal analysis within this research. These are discussed here with the results of AAR analyses presented and discussed in Chapter 6.

5.3.1 Low calcium carbonate content

The sedimentary successions within the Murray Mouth and Lakes region are directly comparable to the coastal barrier complexes located on the Coorong Coastal Plain to the southeast and in a depositional and lithological sense to coastal carbonate aeolianites located globally. Abegg *et al.* (2001) emphasized that the term carbonate aeolianite should be used only for all aeolian rocks with greater than 50% carbonate *grains* [added stress] and that cement was not to be considered in the definition. Many of the sedimentary successions sampled in this research are mixed carbonate and siliciclastic sediments with less than 50% carbonate (some <10%), which is why the

Mount classification scheme for mixed siliciclastic and carbonate sediments was used in this thesis (section 4.2.4).

Kindler and Hearty (1996) found in analysis of the carbonate petrography of Pleistocene carbonate aeolianites in the Bahamas, that coeval stratigraphic units have comparable petrographic composition. In comparison, the carbonate content of the study area coastal barriers varies greatly from their counterparts to the southeast. For example, back-barrier washover facies of the MIS 5e Woakwine Range consists of 81% CaCO_3 (Murray-Wallace *et al.*, 2001) and the MIS 5e MacDonnell Range near Mount Gambier contains 96% CaCO_3 (Blakemore *et al.*, 2015), whereas in the study area, MIS 5e aeolianites within Goolwa-Hindmarsh Island are typically composed of 18-21% CaCO_3 but can reach up to 54% CaCO_3 and do not exceed 29% southeast of Lake Albert (section 4.3.3.2). The low calcium carbonate content within the Murray Lakes region is attributed to the presence of the River Murray, the offshore quartz-rich zone on the Lacepede shelf and the incorporation of siliceous Molineaux Sand during sea-level transgressions (section 4.3.8).

The low calcium carbonate content of the sedimentary successions within the study area was found to affect AAR analysis. Most directly this had an impact on the abundance of amino acids present and would result in chromatograph traces with peaks below 20-30 fluorescence units (LU) or obscured by background noise and the sample would be rejected. Pleistocene whole-rock samples containing less than 20% calcium carbonate were found to be unsuitable for AAR whole-rock analysis. Holocene whole-rock samples were in general successful if the sub-sample volume was increased prior to desiccation and analysis by the RP-HPLC. The success of the Holocene whole-rock sediment is accredited to the overall comparative youth and integrity of the constituent amino acids compared to the Pleistocene whole-rock samples.

5.3.2 Carbonate grain origin

Another factor found to have had an influence on the D/L values of whole-rock sediments and foraminifers is the potential for reworking of the skeletal carbonate grains. Carbonate aeolianites typically develop on the coastal margins of extensive carbonate provinces where they form elongate, shore-parallel bodies deposited as

transverse ridges, generally coalescing and in places stacked (Brooke, 2001). The extent of stacking is not only a function of uplift and the width and gradient of the off-shore shelf, but also a function of ongoing sediment availability either via new sources or the recycling of sediments from previous barriers (Bateman *et al.*, 2011). The effect of a subtle rate of uplift is seen on to the southeast of the study area where the coastal barriers on the Coorong Coastal Plain have formed and been preserved ~10 km apart; although it should be noted that it takes at least two full glacial cycles to spatially remove former successions from the influence of younger shorelines resulting in composite structures (Murray-Wallace *et al.*, 2001). The Wilderness Embayment of South Africa has a similar physical landscape and sediment supply as the southeastern Coorong Coastal Plain but has a more stable tectonic setting resulting in a combination of erosion, resedimentation and stacking during highstands (Bateman *et al.*, 2011) similar to the study area (Chapter 4).

The Murray Mouth region is also unique in that it is not located near to active carbonate sedimentation, i.e. recent carbonate sedimentation on the Lacepede Shelf is restricted to the deep neritic zone near the continental margin (~190 km southwest) and adjacent to Kangaroo Island (>70 km southwest) with the carbonate grains adjacent to Fleurieu Peninsula and the Murray Mouth region consisting predominantly of relict grains deposited mid-shelf during MIS 3 and 4 (James and Bone, 2011; section 3.5.1). The erosion and reworking of older coastal barriers, including those deposited mid-Lacepede shelf during interstadial periods, with sea-level transgression and the paucity of recent carbonate grains supplied by the outer shelf implies that whole-rock sediments in the study area are going to contain a large quantity of reworked grains, potentially spanning multiple interstadial and interglacial periods. This has implications for the development of aminozones which is dependent on chronostratigraphic units representing a discrete time interval being identifiable by the clustering of similar D/L values (Murray-Wallace and Kimber, 1987). The lack of Pleistocene shell deposits older in age than MIS 5e also makes the constraint of aminozones difficult. The continued degradation of amino acids with increasing age will have an adverse effect on the D/L values and therefore the integrity of AAR whole-rock results, especially with increasing age of the barrier succession. Within this research, AAR whole-rock analysis was

successful only to an age of MIS 7 (Chapter 6), but this is attributed to the low CaCO_3 content of sedimentary successions in the region, the high quantity of reworked grains within the sediments and the relative lack of older, suitable sedimentary succession for AAR analysis.

Two other factors could be contributing to the variability of whole-rock and foraminiferal D/L values, genus effect and leaching. Genus effect, as reviewed above (section 5.2.1) reflects the different rates of racemisation exhibited by mollusc and foraminifers from different genera. The compositional variations of sedimentary successions due to environmental preferences by the constituent genera could influence D/L values. The study area, as a zone of minimal uplift and also subsidence (section 2.5.3), consists of low-lying topography in close proximity to the water table and fluvial channels subject to periodic inundation by meteoric or marine water. Excess water allows the leaching of low molecular weight peptides, amino acids and other degradation products of racemisation resulting in lowered D/L values (Rutter and Blackwell, 1995). The chemistry of pore water also influences the rate of diagenesis in the carbonate grains. Freshwater leads to much higher rates of dissolution than shallow marine water, James and Choquette, 1984; Flügel, 2010 making the grains more susceptible to leaching.

5.4 Summary

AAR is a useful geochronological tool for stratigraphic correlation and determining relative ages within regions with similar climatic regimes. Where other dating methods are not suitable, the identification of aminozones, clusters of similar D/L values identifying discrete time intervals, bolster stratigraphic interpretations. However, the determination of a numerical age from D/L values is only possible if calibration is possible, usually by either radiocarbon or uranium/thorium analysis. Unfortunately the only calibration available within the study area is radiocarbon analysis with, as yet, no calibration material available for Pleistocene deposits.

Luminescence methods, TL and OSL, can be used to determine the age of sedimentary successions and support AAR analysis but will always postdate AAR D/L

values because they measure time elapsed since mineral grains were last heated or exposed to daylight (deposition) as opposed to the cessation of protein formation (organism death). The degree to which the two results differ depends on the residence time of the carbonate grains prior to redistribution and final deposition. The conclusions of this work depend heavily on the integrity of the AAR samples selected and the AAR analysis performed. In that regard, the selection of shell and foraminifer samples for analysis was rigorous and whole-rock sediment samples were subjected to multiple analyses including double injections, which served as a check on individual results. All results were subjected to multiple rejection criteria in order to determine the most representative D/L value for a deposit, to identify reworked material and to exclude any contaminated or leached material.

The Murray Mouth region, as a location for coastal carbonate aeolianite, is unique in that many of the sedimentary successions within the study area are, based upon their percentage of total carbonate grain content, not considered carbonate aeolianite. They also differ substantially in carbonate grain content from their southeastern equivalents on the Coorong Coastal Plain. AAR analysis was found to be unsuitable for Pleistocene sedimentary successions composed of less than 20% CaCO_3 . The tectonic setting in which the study area is located, distance from zones of active carbonate sedimentation and the contribution of relict carbonate grains from the Lacepede Shelf and reworked coastal sedimentary successions has resulted in a large component of reworked grains which is reflected in whole-rock and foraminiferal AAR results and made the constraint of aminozones within the study area problematic. The results of AAR analyses are presented in the following Chapter.

Chapter 6

Geochronological Analysis of the Quaternary sedimentary successions within the River Murray Lakes Region, southern Australia

6.1 Introduction

The amino acid racemisation (AAR) analysis in this research was constrained by thermoluminescence, optically stimulated luminescence and radiocarbon analyses. The luminescence techniques were applied to sedimentary successions with a lack of carbonate grains for AAR analysis, in an attempt to clarify the results of earlier analyses or to provide additional support to AAR and morphostratigraphic interpretation. The radiocarbon analyses allowed calibration of the AAR results of Holocene *Spisula trigonella* analyses and helped to develop a model of the Holocene shoreline development. This chapter begins with a brief review of the principles of the luminescence dating techniques used in this research and radiocarbon analysis. The results of geochronological analyses are then provided in a time sequential manner beginning with the Holocene, including modern beach and channel deposits, before progressing back in time and generally in a landward direction.

6.2 Luminescence techniques

Luminescence dating techniques measure the time elapsed since mineral grains (usually quartz and/or K-feldspar) were last exposed to sunlight or heated to a few hundred degrees Celsius (Aitken, 1985; 1998; Huntley *et al.*, 1985; Preusser *et al.*, 2008). The mineral grains when removed from light or heat (by burial) begin to accumulate electrons in 'electron traps'. Luminescence techniques measure the release of photons produced by the ionisation of atoms within the crystal lattice of a mineral as a consequence of either thermal (TL) or optical (OSL) stimulation (Aitken 1985; 1998; Wintle 1997; Roberts *et al.* 1999; Murray & Wintle 2000; Spooner & Questiaux 2000; Jacobs & Roberts 2007; Jankowski *et al.* 2014).

The ionisation process is driven by naturally occurring radionuclides (^{235}U , ^{238}U , ^{232}Th and ^{40}K) located within the surrounding sediments. The radioactive decay of these elements (and their radioactive daughters, with the exception of ^{40}K) produces alpha, beta and gamma radiation. A contribution to the total ionising radiation is also derived from cosmic rays from outer space (Prescott & Hutton, 1994). The total amount of radiation absorbed each year is known as the dose rate (Preusser *et al.*, 2008). When the mineral grains are re-exposed to light or heat the accumulated electrons are released, with some released as visible light (Aitken, 1985; 1998; Huntley *et al.*, 1985). The longer the period of time since electrons were last released, the more radiation absorbed and subsequently released (Wintle & Huntley, 1982; Shepherd & Price, 1990; Preusser *et al.*, 2008). If the ionising radiation flux, i.e. the dose rate, is known, then the luminescence age (a) of the sample can be determined by dividing the amount of radiation energy absorbed (termed the Palaeodose or Equivalent dose and measured in Gray where $1 \text{ Gy} = 1 \text{ J kg}^{-1}$) by the dose rate (measured in Gy a^{-1}) using the following equation:

$$\text{Luminescence age } (a) = \frac{\text{Palaeodose (Gy)}}{\text{Dose rate (Gy a}^{-1}\text{)}} \quad [\text{Equation 6. 1}]$$

The equation assumes the luminescence response to the dose is linear over time and that all accumulated electrons are released leaving the electron traps empty or ‘bleached’ (this is not always the case and can result in age overestimates) (Wintle & Huntley, 1982; Preusser *et al.*, 2008). However, due to the finite number of electron traps in each mineral grain and because the relationship between the radiation dose rate and electron accumulation is not linear, the signal grows asymptotically towards a maximum saturated level (Duller, 2004). The luminescence dating technique is therefore constrained by the point at which the electron traps are filled; i.e. grains subject to a high radiation level will reach saturation before those receiving less radiation and therefore the maximum luminescence age for the former will be much smaller than the latter (Shepherd & Price, 1990).

The upper age range of quartz OSL analysis is typically around 100 ka to 200 ka due to saturation but the age range varies by site and is directly a function of dose rate (Duller, 2004; Walker, 2005; Liritzis *et al.*, 2013). TL analysis has been pushed past the

400 ka limit (Aitken, 1998) and was applied across the Coorong Coastal Plain to the mixed quartz-skeletal carbonate sediments to an age up to 800 ka (Huntley *et al.*, 1993; 1994). The exceptionally long record in southern Australia is attributed to a consistently low dose rate between $0.380 \pm .03$ Gy/ka and $0.650 \pm .03$ Gy/ka (Huntley *et al.*, 1993; 1994).

For all the luminescence ages presented in this thesis, quartz grains were used to measure the amount of radiation energy absorbed over the period of burial. Firstly, quartz is much more abundant in the sediments of this region than feldspar. Secondly, although a disadvantage of using quartz is that the saturation dose is usually one order of magnitude lower than that of feldspar, decreasing its potential dating range (Preusser *et al.*, 2008), the luminescence properties of quartz do not appear to suffer from the phenomenon of anomalous fading like some feldspar which produces age underestimates (Duller, 2004; Preusser *et al.*, 2008).

6.2.1 Luminescence methods used in this research

There is a variety of methods used in luminescence dating (Preusser *et al.*, 2008). Thermoluminescence (TL) and optically stimulated luminescence (OSL) were used in this research for reasons explained below. Both methods use the same luminescence age equation (Equation 6.1). The principle difference between the two methods is the way in which they stimulate the trapped electrons in order to measure the subsequent luminescence signal. As the name suggests, TL uses heat stimulation that ramps the sample temperature from room temperature to $\sim 450^{\circ}\text{C}$, whereas OSL uses visible light (Duller, 2004).

The application of luminescence dating to aeolian sands, such as in this research, has been used on a variety of dryland depositional environments around the world (Preusser *et al.*, 2008). Currently OSL is the preferred method for dating Quaternary sediments (Duller, 2004; Preusser *et al.*, 2008). The OSL signal is more sensitive to light exposure and therefore, resets to zero much more quickly and more completely than the TL signal when also exposed to sunlight. This means that when using OSL the sediments require less exposure time before deposition to be fully bleached and younger samples can be dated (Duller, 2004). The use of OSL dating in this research was

limited by laboratory availability with only one sample dated using this method. The remaining samples were dated using the TL method; although OSL is preferred, TL was found to be acceptable because:

- the composite grains of aeolian sediments deposited in dunes (e.g. the Bridgewater Formation) are most likely to have been sufficiently bleached during the transport process (Shepherd & Price, 1990; Bryant *et al.*, 1994; Price *et al.*, 2001; Frechen *et al.*, 2001);
- numerous deposits within and adjacent to the study region have been successfully dated using the TL method (Huntley *et al.*, 1993a; 1994; Huntley & Prescott, 2001; Murray-Wallace *et al.*, 2010); and
- the subsequent use of the TL method (using the same analytical protocols) in this research will allow a direct comparison of results.

The sampling methodology for both OSL and TL samples is the same. In total, eight luminescence samples were taken from the face of fresh exposures, preferably from units that were easily accessible and homogenous (i.e. lacking pedogenic features and at least 30 cm from the stratigraphic boundary to minimise sampling of reworked and potentially partially bleached sediments). Samples were collected using either a steal or PVC pipe depending on the induration of the sediments. The pipe was 'hammered' into the face of the exposure to a depth of at least 10 cm and up to 30 cm. The ends were packed with plastic prior to sealing to minimise sediment mixing within the sample. The samples were sealed to prevent light exposure and to preserve prevailing moisture content which is factored into the determination of the radiation dose. One TL sample taken from Point McLeay (PM A2) was too strongly consolidated for 'pipe' sampling so a block of sediment was removed from the exposure face and then wrapped in dark plastic and cardboard. The heat-sensitive fractions of quartz grains within the samples were prepared and TL-dated by David Price at the University of Wollongong following the methods of Shepherd and Price (1990) and Price *et al.* (2001). The light-sensitive fractions of quartz grains within the sample were prepared and OSL-dated by Terry Lachlan at the University of Wollongong following the methods of Aitken (1998) and

Jacobs (2010). A summary of the luminescence results from this research is provided in Table 6.1. The results will be individually discussed in section 6.4 below.

Table 6.1: Luminescence ages and analytical results from within the study area. TL results are at top with the OSL result at bottom. The results are discussed in their morphostratigraphic context below.

Field Site (Sample ID)	Laboratory Code	Depth of Burial (m)	Equivalent Dose (GY)	Radiation dose (GY/ka)	TL age (ka)	Marine $\delta^{18}\text{O}$ Stage
Sturt Monument (SM TL)	W4781	1	13.6 ± 1.6	$1.325 \pm .027$	10.2 ± 1.1	2
Knights Beach (KB TL)	W4780	3	202 ± 24	$1.052 \pm .027$	192 ± 23	7
Griffin Road (GR-SP TL)	W4782	1.5	202 ± 20	$0.965 \pm .027$	209 ± 21	7
Myrtlegrove Road (MR U4TL)	W4779	3.5	394 ± 41	$1.740 \pm .031$	227 ± 24	7
Point McLeay (PM A3TL)	W4785	*5.85	$\geq 201 \pm 7$	$2.169 \pm .031$	$\geq 92.4 \pm 3.5$	minimum age
Point McLeay (PM A2TL)	W4786	*6.5	$\geq 201 \pm 8$	$2.413 \pm .033$	$\geq 83.1 \pm 3.7$	minimum age
Mount Misery (MTM TL)	W4787	4	$\geq 267 \pm 33$	$0.729 \pm .026$	$\geq 366 \pm 47$	minimum age
Sample Location (ID)	Laboratory Code	Depth of Burial (m)	Equivalent Dose (GY)	Radiation dose (GY/ka)	OSL age (ka)	MIS Stage
Point McLeay (PM A1OSL)	UOW-1296	*11	216 ± 10	$0.512 \pm .053$	421 ± 48	11
*depths are best estimates due to the steepness of the cliff and accessibility of the units						

6.3 Radiocarbon analysis

Radiocarbon (^{14}C) atoms are formed in the upper atmosphere through the interaction of cosmic radiation and nitrogen. ^{14}C combines with oxygen to produce radioactive carbon dioxide ($^{14}\text{CO}_2$) which is uniformly mixed throughout the atmosphere to become part of the global carbon cycle. Radiocarbon is incorporated into the biosphere primarily through plant photosynthesis and the ingestion of plant tissues by animals and absorbed into oceans as dissolved carbonate (Terasmae, 1984; Trumbore, 2000; Walker, 2005) where it is available to plankton, corals, molluscs and fish (Gupta & Polach, 1985). Once an organism dies it is isolated from the global system, ^{14}C input ceases and ^{14}C content begins to decrease with radioactive decay through the emission of beta particles (Terasmae, 1984; Walker, 2005).

The upper limit of radiocarbon dating capabilities is limited by the decay rate of ^{14}C (Walker, 2005). Measurement is only possible for eight half-lives or an upper age limit of ~45 000 years. There are two ^{14}C half-life values: 5568 years (the Libby half-life) and a more accurate value of 5730 years. The Libby half-life is conventionally used for dating applications because numerous dates had been published based on that value before determination of the latter, more accurately defined value (Arnold, 1995). With the half-life of radiocarbon known, an age can be inferred for the death of an organism by measuring the decrease in the ^{14}C content (residual radiocarbon content) of the fossil material and comparing it to modern radiocarbon in standard material (Terasmae, 1984; Gupta & Polack, 1985; Trumbore, 2000; Walker, 2005).

6.3.1 AAR numerical age determination

Numerical ages of Holocene shell were determined to gauge the amount of reworking occurring on the Goolwa Channel and the Coorong shoreline and to determine if any conclusions could be made about the timing and/or rate of deposition of the Hindmarsh Island. One disarticulated valve of the estuarine bivalve *Spisula trigonella* retrieved from Annie Lucas auger hole 2 (section 4.3.2) was chosen for radiocarbon analysis. One half of the shell was used for AAR analysis (sample UWGA 10163.3), the other half was sent to the University of Waikato Radiocarbon Dating Laboratory for analysis. Due to the small sample mass, radiocarbon measurement was determined using Accelerator Mass Spectrometry (AMS).

Numerical ages for *S. trigonella* AAR mollusc shell samples were derived from the extent of aspartic acid (ASX) racemisation within *S. trigonella* shell using the apparent parabolic kinetic model (Mitterer and Kriausakul, 1989; Sloss *et al.*, 2004; Lachlan, 2011). This age model uses the equation:

$$t = \left[\frac{(D/L)_s - (D/L)_{t_0}}{Mc} \right]^2 \quad \text{[Equation 6.2]}$$

where t is the calculated age, $(D/L)_s$ is the extent of racemisation from a specimen of unknown age, $(D/L)_{t_0}$ is the time = 0 (the D/L ratio for a modern sample of the same species as $(D/L)_s$), and Mc is the slope of the regression line, defined as:

$$\left[= \frac{D/L_{cal}}{t^{1/2}} \right] \quad [\text{Equation 6.3}]$$

where D/L_{cal} is the extent of racemisation in a fossil of known age and $t^{1/2}$ is the square root of fossil age.

The fossil of known age is the *S. trigonella* shell used for radiocarbon analysis. The y intercept is the D/L_{t_0} value which is preferably derived from a live-collected shell and should show some degree of racemisation related to hydrolysis induced racemisation. Live *S. trigonella* was not found for collection during this thesis so the D/L_{t_0} value for aspartic acid derived by Sloss *et al.* (2004) was used. The D/L values in their work were measured using gas chromatography (GC) and not the reverse phase (RP) method adopted in this thesis. However, ASX and GLX D/L values derived by GC and RP are usually within 5% of each other (Wehmiller, 2013).

The linear regression of the calibrated data is plotted in Figure 6.1. The ASX ages have an uncertainty of 15% derived from the square root of the sum of the squares of all

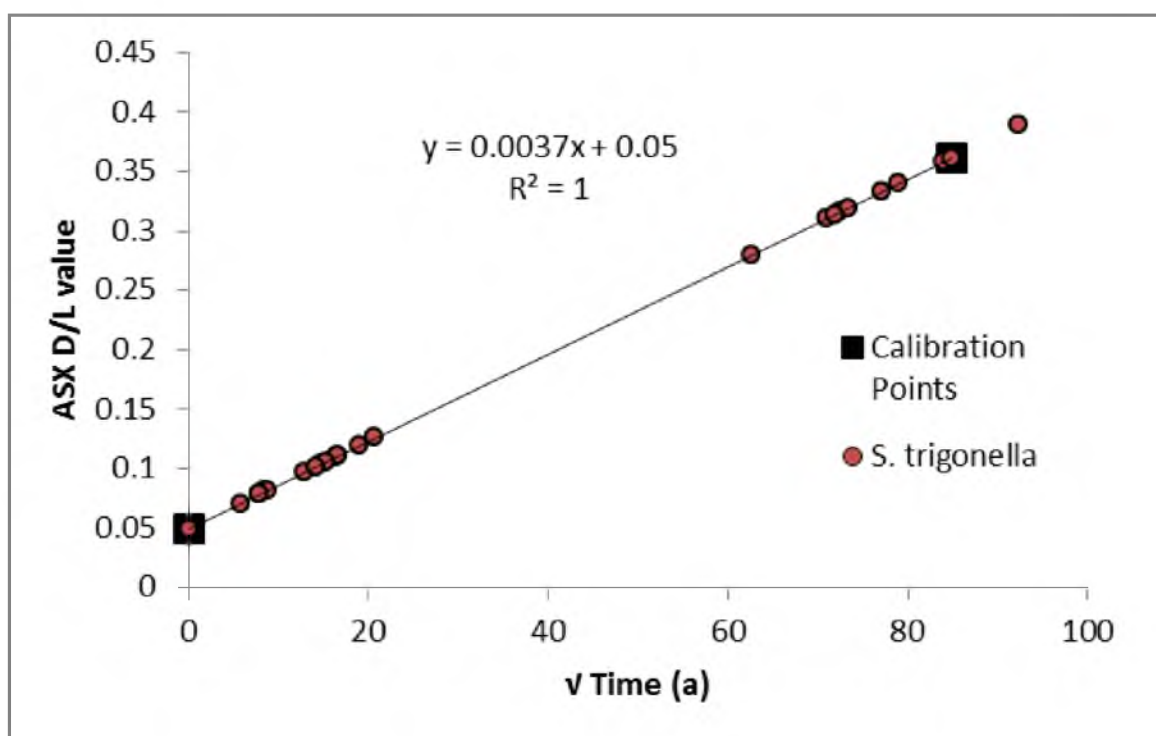


Figure 6.1: Calibration plot of ASX D/L values vs. $\sqrt{\text{Time (a)}}$ for *S. trigonella* shell. The calibration points correspond to D/L_{t_0} value (0.050, 0) and D/L_{cal} value (0.362, 85). $R^2 = 1$ because only two data points were used in the regression.

uncertainty terms: machine uncertainty (1.5%, Figure 5.11), uncertainty on the calibrated radiocarbon date of 7220 ± 170 cal. yr BP (2.4%), and diagenetic temperature variation of 1°C (15%, Belperio *et al.*, 1995). The numerical age results are presented below in section 6.4.1.

6.4 Results of geochronological analyses in this research

The results of this research are presented in a time-transgressive manner beginning with the Holocene and moving back further in time and generally landward. Foraminifers from modern, late, middle and likely early Pleistocene (Chapter 4) sedimentary successions were analysed. AAR whole-rock samples were analysed from modern, late and middle Pleistocene sedimentary successions. Mollusc shell was only available from late Pleistocene (MIS 5e) and Holocene sedimentary successions. The luminescence samples were taken from sedimentary successions anticipated to be middle Pleistocene or glacial in origin. The radiocarbon analysis of shell from the Hindmarsh Island Holocene sand flat was used to calibrate the AAR results of Holocene *Spisula trigonella* and constrain the deposition of the early Holocene shoreline across southern Hindmarsh and Mundoo Islands. Calibration material for the Pleistocene successions was not identified in this research and D/L values are used to identify aminozones (Murray-Wallace and Kimber, 1987; Section 5.2.2.2).

The sedimentary successions at some field sites (Knights Beach, Surfers Beach, Traegers Quarry, the last interglacial recurved spit on Hindmarsh Island, Clayton Water Tower and Sturt Peninsula, Mount Misery) had been previously analysed by AAR analysis and, in some cases, by thermoluminescence as well (Murray-Wallace *et al.*, 2010). These sites were revisited to measure the integrity of AAR analysis between research and to account for variability in results that may arise from instrument reproducibility and laboratory error. Additionally, high uncertainty associated with TL ages at Knights Beach and Mount Misery with conflicting or poor AAR results recommended further analyses. The results of this research are presented within the discussion below.

6.4.1 The Holocene

The Holocene shoreline is divisible into two parts: the modern shoreline and the early Holocene coastline when the shoreline reached ~2 km further inland prior to the

complete development of Sir Richard and Younghusband Peninsulas (Bourman *et al.*, 2000). Here, reference to the modern shoreline includes the modern coastline as well as the shorelines of the Goolwa Channel and the Coorong and any field samples retrieved from it are considered 'modern'. The locations of field sites discussed in this section are shown in Figure 6.2. The early Holocene sites are found across the southern portion of Hindmarsh and Mundoo Islands, not including the Murray Mouth (MM) and Goolwa Channel (GC) sites which are modern. This discussion also includes the modern aeolian deposit found on the crest of Point McLeay, nearly 16 km from the modern shoreline and 22 km from the River Murray mouth (Figure 6.2). The segregation of the early Holocene and modern shorelines is most apparent in the mollusc shell results and they are presented before the results of modern whole-rock and foraminifer analyses. Establishing the potential residence time of sediments and the quantity of reworked skeletal grains within the Holocene beach and channel depositional environments serves as an important indicator to the interpretation of the older Pleistocene sedimentary successions and as such, these factors are discussed thoroughly.

6.4.1.1 Holocene shell results

Modern shells were collected and analysed from Goolwa Beach (MGB), the Goolwa Channel (GC), and the shoreline of the Coorong (CC-sh) southeast of Lake Albert (Figure 6.2). Holocene shells were collected and analysed from Richard Owens Beach (ROB), Annie Lucas auger holes (AL-BH1 and AL-BH2), the Holocene sand flat (HSF) and the Mundoo Island dredge site (MI-D). The D/L values reflect the division of modern and Holocene shorelines (Table 6.2). The radiocarbon age for the *S. trigonella* valve retrieved from the Hindmarsh Island sand flat at 9 m depth of burial (Annie Lucas auger hole 2) provided a calibrated radiocarbon age of 7220 ± 170 yr BP (Wk-39539). This is only slightly younger than the Holocene transgressive peak between 8000 and 7500 cal. yr BP proposed for Australia (Belperio *et al.*, 2002; Lewis *et al.*, 2013). The numerical ages determined for *S. trigonella* are presented in Table 6.3 and Figure 6.3.

Holocene shell was not expected to be retrieved from the Mundoo Island dredge site which was composed predominantly of littoral zone species (see Table 4.2) in a moderately cemented shell coquina. AAR analysis of *Paphies elongata* returned D/L

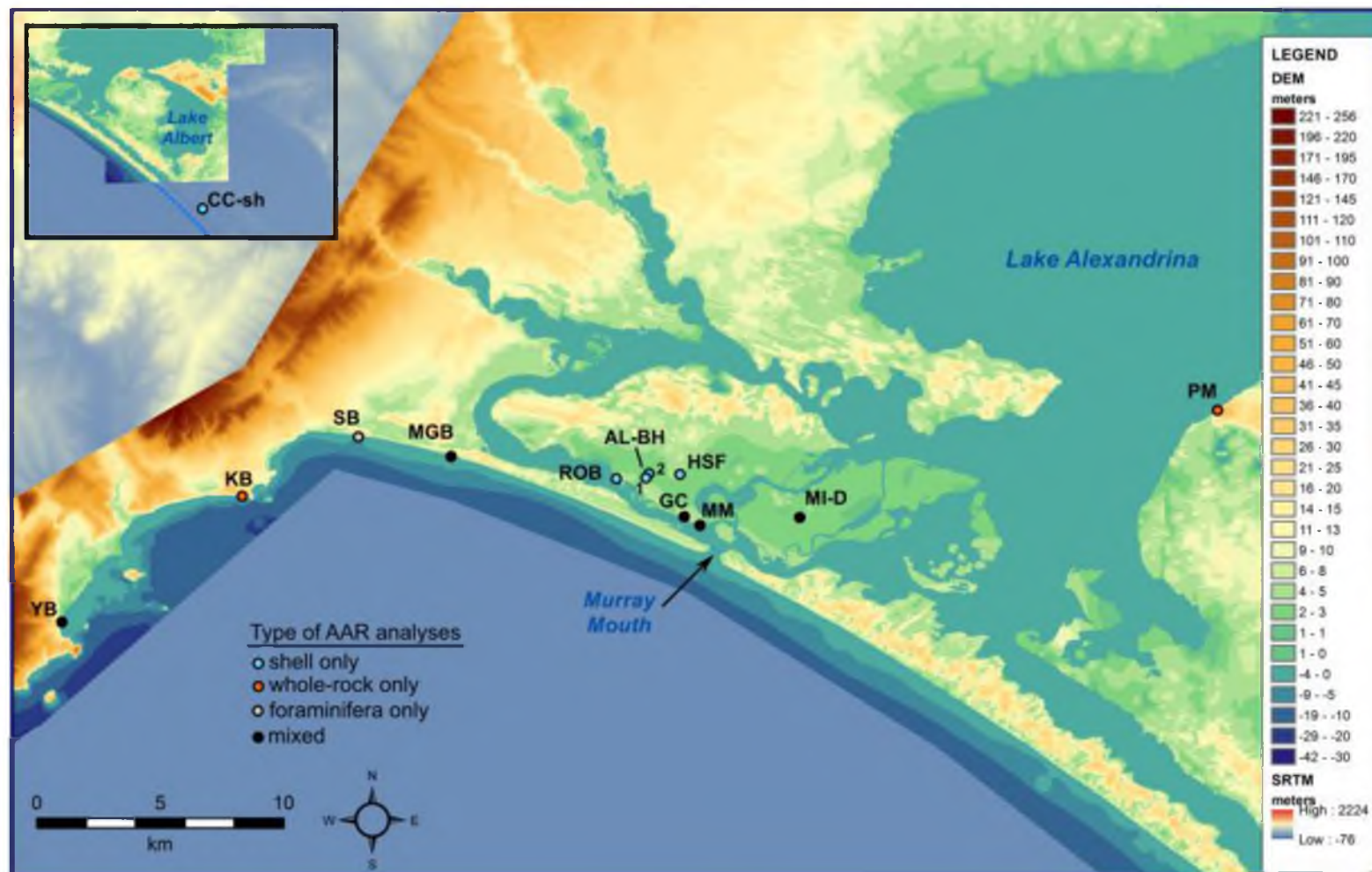


Figure 6.2: Holocene shell and whole-rock samples were retrieved from the modern beaches: Yilki Beach (YB), Knights Beach (KB), Surfer Beach (SB), Goolwa Beach (MGB), the Goolwa Channel (GC), Murray Mouth (MM) and the Coorong shoreline (CC-sh, inset). Holocene shell and sediment was retrieved from Richard Owens Beach (ROB), the Annie Lucas auger holes (AL-BH1 and AL-BH2), the Holocene sand flat (HSF) and the Mundoo Island dredge (MI-D). A sample of the modern aeolianite was also taken from Point McLeay (PM). The radiocarbon sample was retrieved from Annie Lucas auger hole 2.

Table 6.2: Results of AAR analysis of modern (shaded grey) and Holocene shell samples. Note the change in D/L values between the modern and Holocene samples which reflects the initial fast rate of racemisation. The D/L values of the small estuarine gastropod *Hydrococcus brazieri* retrieved from the Holocene sand flat are particularly high and may reflect reworking.

Field Site	Species	UWGA (AAR laboratory code)	n replicates	Amino acid D/L value $\pm 1 \sigma$		
				ASX	GLX	VAL
Goolwa Beach	<i>Macra rufescens</i>	9976	3	0.150 \pm 0.028	0.047 \pm 0.011	0.022 \pm 0.019
	<i>Donax deltoidalis</i>	9975	3	0.062 \pm 0.006	0.033 \pm 0.005	0.012 \pm 0.001
Goolwa Channel	<i>Spisula trigonella</i>	9989	4	0.076 \pm 0.005	0.042 \pm 0.003	0.018 \pm 0.002
Coorong Beach	<i>Spisula trigonella</i>	9988, 9990	11	0.107 \pm 0.013	0.057 \pm 0.013	0.025 \pm 0.009
	<i>Hydrococcus brazieri</i>	10134	6	0.104 \pm 0.024	0.082 \pm 0.024	0.031 \pm 0.026
Richard Owens Beach	<i>Macra rufescens</i>	9750	2	0.262 \pm 0.008	0.146 \pm 0.023	0.089 \pm 0.022
Annie Lucas auger hole 1 (1.5 m depth)	<i>Coxiella striata</i>	10131	3	0.383 \pm 0.013	0.130 \pm 0.010	0.085 \pm 0.026
Annie Lucas auger hole 2 (5 m depth)	<i>Spisula trigonella</i>	10161	2	0.365 \pm 0.027	0.103 \pm 0.005	0.050 \pm 0.001
8 m depth	<i>Spisula trigonella</i>	10162	3	0.321 \pm 0.011	0.101 \pm 0.013	0.052 \pm 0.007
9 m depth	<i>Spisula trigonella</i>	10163	3	0.345 \pm 0.023	0.108 \pm 0.006	0.058 \pm 0.006
5 m depth	<i>Coxiella striata</i>	10175	4	0.403 \pm 0.023	0.125 \pm 0.009	0.073 \pm 0.006
8 m depth	<i>Coxiella striata</i>	10177	5	0.414 \pm 0.036	0.133 \pm 0.008	0.084 \pm 0.011
9 m depth	<i>Coxiella striata</i>	10179	2	0.421 \pm 0.031	0.127 \pm 0.018	0.085 \pm 0.035
Holocene sand flat	<i>Hydrococcus brazieri</i>	10135, 10136	3	0.557 \pm 0.043	0.204 \pm 0.004	0.162 \pm 0.013
Mundoo Island dredge	<i>Spisula trigonella</i>	9985	2	0.298 \pm 0.025	0.105 \pm 0.026	0.057 \pm 0.026
	<i>Coxiella striata</i>	10132	5	0.419 \pm 0.053	0.140 \pm 0.021	0.098 \pm 0.019
	<i>Hydrococcus brazieri</i>	10137	5	0.412 \pm 0.037	0.139 \pm 0.013	0.099 \pm 0.033

Table 6.3: Numerical age calibration results.

Field Site	UWGA	ASX D/L (<i>n</i>)	Age (a)
Goolwa Channel			
	9989.1	0.081 (2)	71 ± 11
	9989.2	0.082 (2)	76 ± 11
	9989.4	0.079 (1)	60 ± 9
	9989.5	0.071 (2)	33 ± 5
Coorong Beach			
	9988.2	0.111 (1)	276 ± 41
	9988.3	0.110 (1)	267 ± 40
	9988.4	0.097 (1)	164 ± 25
	9988.5	0.111 (1)	276 ± 41
	9990.1	0.120 (1)	363 ± 55
	9990.2	0.104 (1)	216 ± 32
	9990.3	0.126 (1)	428 ± 64
	9990.4	0.106 (1)	233 ± 35
	9990.5	0.102 (2)	201 ± 30
	9990.6	0.079 (1)	62 ± 9
AL BH2 (5m)			
	10161.1	0.389 (3)	8540 ± 1281
	10161.2	0.340 (3)	6238 ± 936
AL BH2 (8m)			
	10162.1	0.333 (3)	5954 ± 893
	10162.2	0.311 (3)	5040 ± 756
	10162.3	0.320 (3)	5394 ± 809
AL BH2 (9m)			
	10163.1	0.314 (3)	5169 ± 775
	10163.2	0.358 (3)	7036 ± 1055
	10163.3	0.362 (3)	7220 ± 1083
Mundoo Island			
	9985.1	0.316 (1)	5248 ± 787
	9985.2	0.280 (1)	3924 ± 589

(*n*) = number of replicates

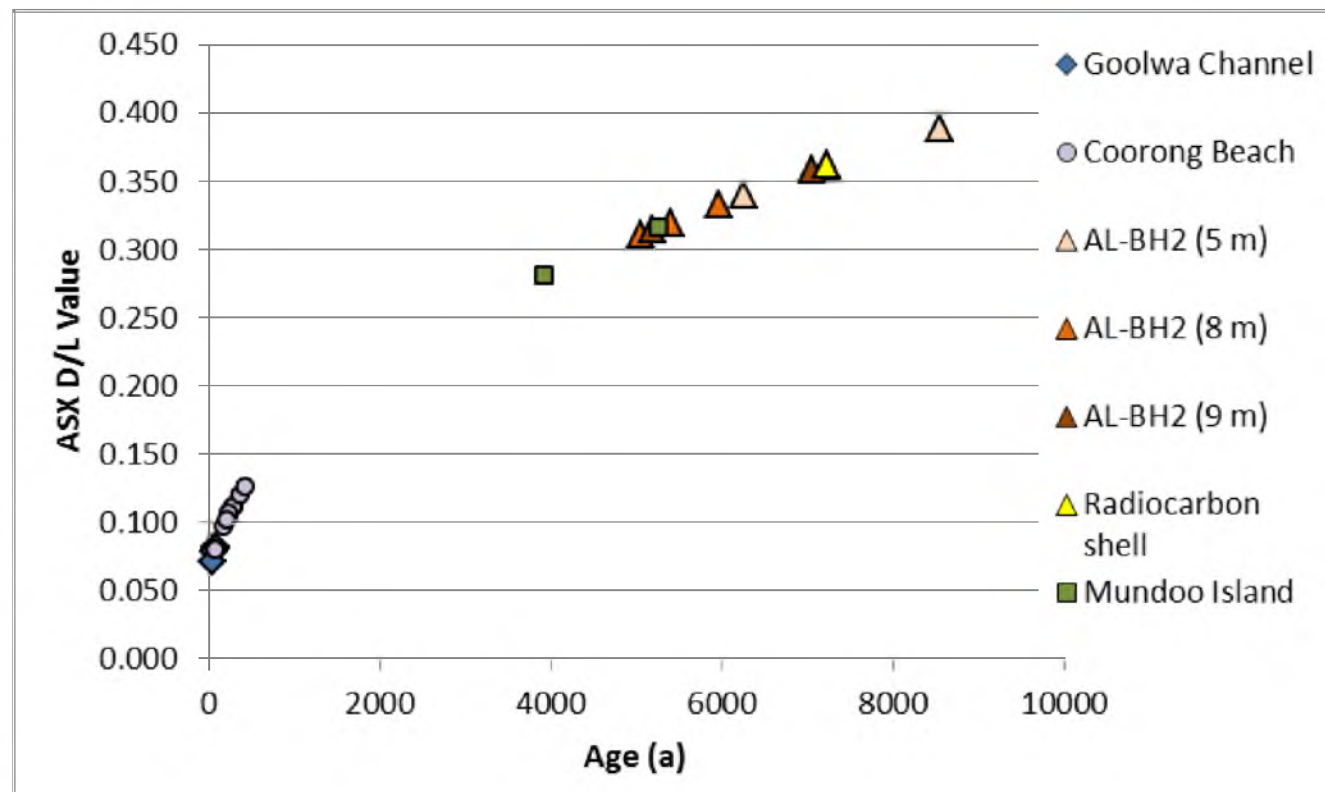


Figure 6.3: Scatter plot of aspartic acid (ASX) D/L values vs. age. The Goolwa Channel, as the main discharge channel for the River Murray, is less likely to accumulate shell on its shoreline explaining the generally lower D/L values compared with the Coorong Beach. Half of the shell used for radiocarbon analysis (retrieved from AL-BH2 9 m) was analysed by AAR with the results from the corresponding shell highlighted in Table 6.2

values typical of a last interglacial deposit (see following section). The presence of early Holocene estuarine bivalve *S. trigonella* and estuarine gastropods *Coxiella striata* and *Hydrococcus brazieri* indicate the development of estuarine conditions as Sir Richard and Younghusband Peninsula formed and suggests the early Holocene estuary was in a more northerly location or greater extent than present. Overall the AAR shell results and numerical ages suggest a significant amount of reworked sediment and shell was deposited in the Holocene sand flat prior to the onset of more restricted settings associated with sea level fall. This is most evident in the spread of D/L values and ages of *S. trigonella* retrieved from Annie Lucas auger hole 2.

6.4.1.2 Modern whole-rock results

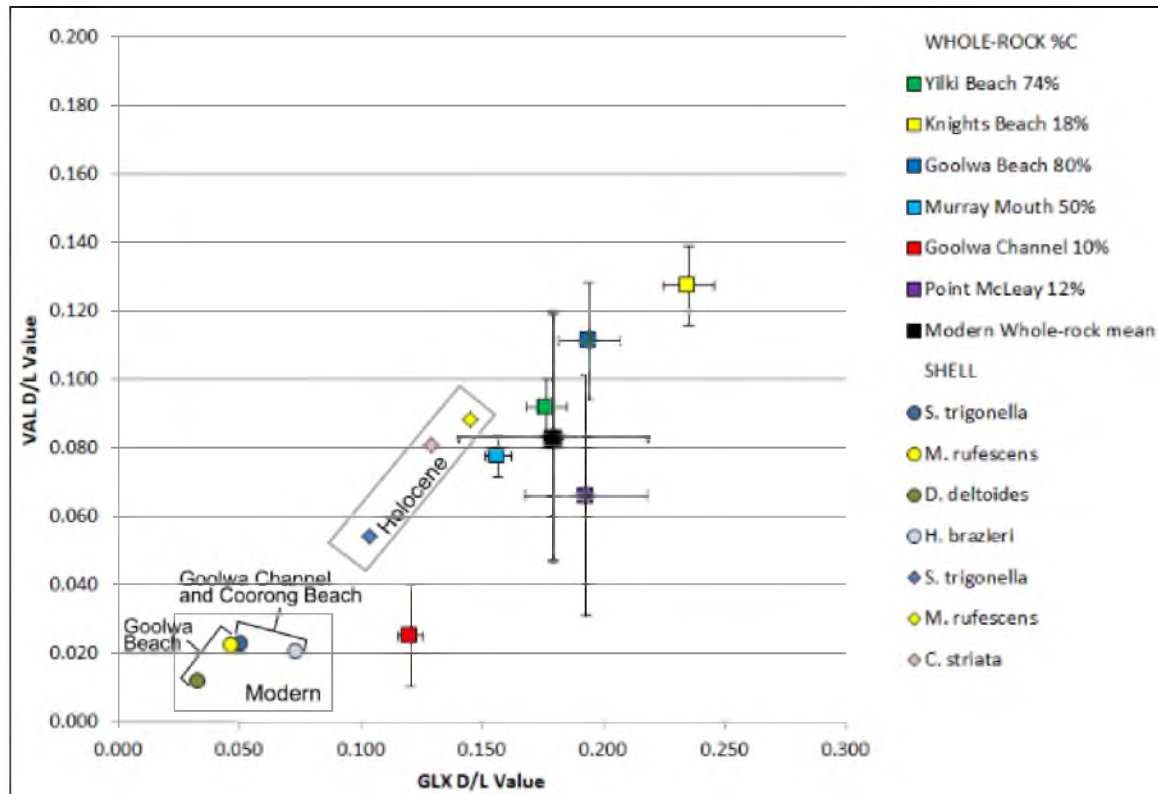
As discussed in Chapter 5 (section 5.3) reworking is expected to be intensive in the Murray Mouth region due to the supposition of interglacial sedimentary successions and is reflected in both the whole-rock samples (Table 6.4) and foraminiferal D/L values (Table 6.5, following section). The D/L values of the modern beach sediments indicate the residence time of skeletal grains before transport landward into dune systems by comparison with modern and Holocene shell results (Figure 6.4). The quantity of relict and modern grains within sediments is assessed by the analysis of individual foraminifers with results presented below.

The D/L values derived from analysis of the whole-rock samples from the modern beaches and channels were variable reflecting not only potential residence time but also sediment source (Table 6.4, Figure 6.4). Modern Knights Beach on Fleurieu Peninsula exhibits the highest degree of racemisation (Figure 6.2). The beach is expected to contain a high quantity of reworked skeletal grains because it is situated within an eroding aeolianite succession of middle to late Pleistocene age with carbonate percentages two to four times the modern beach (section 4.3.5) and it is located onshore of a zone of relict carbonate grains (section 3.5.1), a source of sediment during sea-level transgressions. In contrast, the modern Yilki Beach, also on Fleurieu Peninsula, less than 8 km southwest of Knights Beach, returned D/L values somewhat lower than expected given the beach has formed on a shore platform of sheared last interglacial carbonate aeolianite. However, analysis of the last interglacial sediments (section

Table 6.4: Results of whole-rock analysis from the modern shoreline of the River Murray Mouth region and Point McLeay aeolianite. D/L values are provided for both total hydrolysable amino acid (THAA, in grey) and free amino acids (FAA).

Field Site	% Carbonate	UWGA (AAR laboratory code)	<i>n</i> replicates	Amino acid D/L value $\pm 1 \sigma$		
				ASX	GLX	VAL
Yilki Beach	74	10150	5	0.299 \pm 0.007	0.177 \pm 0.008	0.092 \pm 0.008
FAA			3	0.701 \pm 0.005	0.434 \pm 0.013	0.413 \pm 0.004
Knights Beach	18	10151	5	0.355 \pm 0.009	0.235 \pm 0.011	0.127 \pm 0.012
FAA			5	0.771 \pm 0.007	0.544 \pm 0.010	0.545 \pm 0.026
Goolwa Beach	80	9966	5	0.314 \pm 0.012	0.194 \pm 0.021	0.111 \pm 0.017
FAA			3	0.722 \pm 0.007	0.505 \pm 0.021	0.542 \pm 0.061
Murray Mouth	50	10149	5	0.265 \pm 0.011	0.156 \pm 0.027	0.078 \pm 0.006
FAA			5	0.736 \pm 0.005	0.449 \pm 0.029	0.494 \pm 0.031
Goolwa Channel	10	9967	5	0.151 \pm 0.028	0.120 \pm 0.005	0.025 \pm 0.015
FAA			3	0.740 \pm 0.012	0.362 \pm 0.026	0.524 \pm 0.024
Point McLeay A5	12	10170	5	0.284 \pm 0.025	0.193 \pm 0.025	0.066 \pm 0.035
FAA			4	0.749 \pm 0.022	0.597 \pm 0.101	0.615 \pm 0.028
AVERAGE OF MODERN WHOLE-ROCK SAMPLES				0.278 \pm 0.069	0.179 \pm 0.039	0.083 \pm 0.036
FAA				0.737 \pm 0.024	0.482 \pm 0.084	0.522 \pm 0.067

Figure 6.4: Scatter plot of mean valine acid (VAL) vs. glutamic acid (GLX) D/L values for ‘modern’ whole-rock with uncertainty terms reflecting 1 σ . Mean D/L values for modern and early Holocene shell have been provided for comparison; relationships are discussed in text.



4.3.3.3) show them to have a much lower carbonate content than the modern beach and the older, well-indurated platform sediments may be contributing only a minor quantity of carbonate grains to the modern beach.

The lowest degree of racemisation (and carbonate content) is found at Goolwa Channel (Table 6.4, Figure 6.4) on the shoreline of the main discharge channel for the River Murray suggesting a shorter residence time for the channel sediments than beach sediments and a minimal amount of input from the erosion of upstream sedimentary successions. Interestingly, the Murray Mouth D/L values are much higher. The Murray Mouth sediments are sourced from the River Murray, the Coorong and the Southern Ocean which provide a mixture of both modern and reworked material. The D/L values at Goolwa Beach indicate that the majority of reworked material is provided to the Murray Mouth via the Southern Ocean.

The high uncertainty of the modern aeolianite draping Point McLeay is likely due to its location within the landscape at ~45 m elevation on Narrung Peninsula (Figure 6.2). Carbonate content within the aeolianite was low (12%) and the grains were fine and well-rounded (an indication of the distance travelled) and would have been sourced from a variety of deposits to the south, east and west.

Comparison of shell D/L values to whole-rock values generally shows the latter to exceed the former. This is anticipated as the majority of skeletal carbonate grains within whole-rock samples are expected to pre-date *in situ* modern shell and foraminifer skeletal grains given the reworking potential of the region (section 5.2.2 and 5.3). The Goolwa Channel whole-rock and extent of shell racemisation from within the Goolwa Channel and Coorong shorelines is similar, although this again most likely reflects shorter residence time of sediments and shell on the Goolwa Channel.

There are two possibilities for the similarity in the rate of racemisation between the early Holocene *Coxiella striata* and *Macra rufescens* (retrieved from Annie Lucas auger hole 1 and beachrock at Richard Owens Beach) and whole-rock values. The first possibility is that the whole-rock contains fragments of contemporaneous shell that had not been segregated from the system as had the deposits on southern Hindmarsh Island. The second possibility is that the shell racemisation values reflect genus and depth of

burial effects. The early Holocene *C. striata* shell has consistently higher rates of racemisation than its counterparts (with exception of *Hydrococcus brazieri*) (Table 6.2). These results suggest that the small gastropods may experience higher early rates of racemisation than bivalves. The *M. rufescens* shell, retrieved from beachrock on the surface of southern shoreline of Hindmarsh Island, may have been subject to increased rates of racemisation due to its lack of burial.

6.4.1.3 Modern foraminifers results

Foraminifera hand-picked from the modern sediments of Yilki Beach, Surfer Beach, the Murray Mouth and the Goolwa Channel (Figure 6.2) were analysed to assess the quantity of Holocene and reworked skeletal grains within the sediments at different locations along the modern coastline (Figure 6.5). The distinction between Holocene and modern D/L values for foraminifers has not been made as it has been for mollusc shell (see above), therefore the mean D/L values for *Discorbis* and *Elphidium* tests (Table 6.4) is regarded as reflecting both modern and Holocene values.

Holocene foraminifer tests were distinguished from older, reworked tests by the relative extent of valine (VAL) to glutamic acid (GLX). Pyrolysis experiments (Lachlan, 2011) of the bivalve *Katelysia scalarina*, whole-rock sediments and the foraminifers *Discorbis dimidiatus* and *Elphidium crispum* show GLX to have a more rapid initial rate of racemisation than VAL, followed later by a similar rate and in late diagenesis a slightly decreased rate in comparison to VAL; middle to early Pleistocene VAL D/L values are generally higher than GLX. Furthermore, Lachlan (2011) found that the forward rate of racemisation for GLX was essentially the same within both foraminifer species (i.e. there is no genus effect between the two) and proceeded at a slower rate than within *K. scalarina* or whole-rock. However, it should be noted that the results of a later pyrolysis experiment (Blakemore, 2014) supported the latter conclusion but found the forward rate of glutamic acid to be faster within *D. dimidiatus* than *E. crispum*. Based on the observations of Lachlan (2011), the extent of VAL racemisation in modern foraminifer samples should not exceed that of GLX and has been supported in this research by both modern shell (Tables 6.2) and whole-rock results (Table 6.4). Analysis of modern foraminifer results shows that this is predominantly true with very few exceptions to a.

Figure 6.5: Graphs of glutamic acid (GLX) and valine (VAL) D/L values for individual *Discorbis* and *Elphidium* foraminifers retrieved from modern shoreline sediments alongside mean whole-rock values with 1 σ uncertainty terms. Foraminifers with VAL D/L values not exceeding 0.200 were accepted as Holocene. Note the extent of racemisation of the reworked tests (circled in orange) within Surfer Beach, Murray Mouth and Goolwa Channel sediments reflecting contributions by older interglacial sedimentary successions.

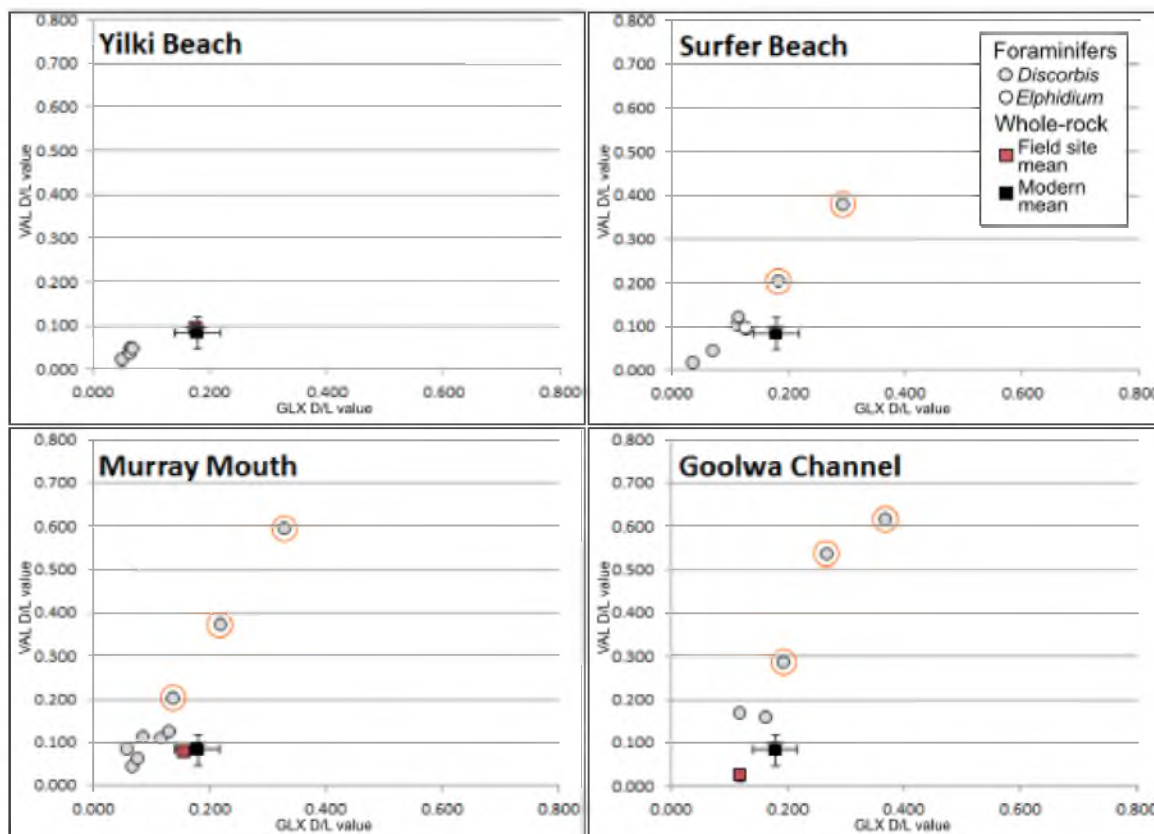


Table 6.5: Average of foraminifer results accepted as Holocene from the modern shoreline within the River Murray Mouth region. GLX and VAL D/L values should not exceed their whole-rock counterparts (Murray-Wallace *et al.*, 2001; 2010; Lachlan, 2011). GLX is below the modern whole-rock mean of 0.179 ± 0.039 . VAL exceeds the whole-rock mean of 0.083 ± 0.036 , although the results are comparable within 1 σ . VAL has been shown to typically be more variable than GLX (Table 5.2, section 5.2.3) and the foraminifer results here are skewed by high but accepted VAL D/L values at the Goolwa Channel site.

Field Site	Foraminifer genus	UWGA (AAR laboratory code)	n replicates	Amino acid D/L value $\pm 1 \sigma$		
				ASX	GLX	VAL
Surfer Beach	<i>Elphidium</i>	10185	7	0.186 ± 0.060	0.093 ± 0.037	0.074 ± 0.043
	<i>Discorbis</i>	10186	1	0.250	0.126	0.096
Yilki Beach	<i>Discorbis</i>	10184	5	0.163 ± 0.168	0.063 ± 0.006	0.037 ± 0.010
Murray Mouth	<i>Discorbis</i>	10183	9	0.250 ± 0.064	0.090 ± 0.029	0.089 ± 0.032
Goolwa Channel	<i>Discorbis</i>	10182	5	0.291 ± 0.093	0.141 ± 0.032	0.164 ± 0.008
AVERAGE OF ALL FORAMINIFER SAMPLES			20	0.228 ± 0.052	0.103 ± 0.031	0.092 ± 0.046

Holocene sedimentary unit with a VAL D/L value greater than 0.200 was regarded as reworked from the erosion of offshore interstadial sedimentary successions or locally derived from earlier Pleistocene successions during sea-level transgression

Yilki Beach is the only sediment which does not contain reworked foraminifera (Figure 6.5) and supports the conclusion that the underlying indurated shore platform of last interglacial aeolianite is only providing a minor contribution to the carbonate content of the modern beach. Although, it may also reflect sampling bias as tests were chosen for analysis based on their robust appearance. However, this seems less likely as the presence of reworked tests is made apparent by D/L values in all other deposits. The Yilki result is also very uniform in comparison to other accepted D/L values (Figure 6.5) and may represent only modern tests without earlier Holocene tests. In contrast, Surfers Beach is backed by a cliffed coastline formed of a high carbonate content (72%) MIS 5c aeolianite (Bourman *et al.*, 2000; Murray-Wallace *et al.*, 2010), which has likely been a source for at least some of the reworked tests there.

The large amount of reworked tests within the Goolwa Channel whole-rock sediment is contrary to expected given the degree of racemisation indicated by the whole-rock D/L values. However, the foraminifer results at the site may be biased as *Discorbis* sp. was selected for analysis because *Ammonia beccarii* (a species typical of the Coorong and estuary) have very delicate tests that are rarely found in whole-rock samples. *Discorbis* tests are more durable than *A. beccarii* tests and are more likely to be present in the Goolwa Channel and other deposits as reworked grains eroded from older aeolianites through which the River Murray flows. As indicated by the whole-rock samples, the Murray Mouth is expected to contain a mix of modern and reworked skeletal grains derived from the river, the Coorong and the Southern Ocean.

6.4.1.4 Summary

The modern and Holocene shell results exhibit the fast rates expected during the initial stages of racemisation which are recognised as two separate aminozones and the earlier Holocene shoreline and the modern shoreline. The shell results support the interpretation of the sedimentary record that before the full development of the Sir Richard and Younghusband Peninsulas the early Holocene shoreline at the peak of the

post-glacial marine transgression extended further inland than present (section 4.3.2). As sea level stabilised, the peninsulas developed and the Murray Mouth shifted position, the sand flat was cut off from flood tidal sedimentation and island expansion ceased.

The length of residence time is a reflection of the environment of deposition and also the position of the deposit in the modern fluvial and aeolian environment. For example, although the mollusc shells within the early Holocene sand flat on southern Hindmarsh Island were deposited within a more open, higher energy environment, they have since been segregated from the modern aeolian and fluvial environment as reflected by the age of the *S. trigonella* shell found there. In contrast, the Goolwa Channel whole-rock and shell results reflect the high energy environment of the main discharge channel of the River Murray with little accumulation of carbonate grains older than 'modern' and a whole-rock D/L value only slightly higher than *in situ* shell. The range in whole-rock D/L values also illustrates the influence of sediment source. The whole-rock sediment and foraminifer results indicate that the majority of reworked material is being delivered to modern coastline via the Southern Ocean with the modern River Murray contributing only a minimal quantity of reworked grains although additional sampling of the Goolwa Channel sediments is needed to confirm this.

6.4.2 Siliceous sand deposition

The Sturt Monument siliceous dune is a deposit of Molineaux Sand located west of central Hindmarsh Island (Figure 4.7), north of the extent of the post-glacial marine transgression (section 4.3.2), overlying a fine-grained aeolianite with a variably rubbly and laminar calcrete of ≤ 50 cm thickness. TL ages for other siliceous dunes in the study area place have provided ages within Last Glacial Maximum, between 16-18 ka (Bourman *et al.*, 2000). The siliceous sands at Sturt Monument were sampled for TL analysis providing an age of 10.2 ± 1.1 ka (W4781) at the margin of the Pleistocene-Holocene boundary. This age is consistent with other evidence - the slight reorientation of the Molineaux Sands dunes from the dominant eastward trend (section 2.5.1) and OSL ages to the southeast (Fitzsimmons and Barrows, 2012; section 2.5.1) - that the siliceous dunes, although most active within a glacial period, can be subject to reworking and renewed mobility outside of glacial periods. The dune is currently stabilised by vegetation, however, the land owner reported that another portion of this dune had

been active within his memory (Nick Grundy, person communication, 21 November 2013) attesting to the continued movement of Molineaux Sand within the Holocene.

6.4.3 The last interglacial

Mollusc shell, whole-rock samples and foraminifers retrieved from sedimentary successions interpreted to be related to the MIS 5e or MIS 5c shorelines (Chapter 4) were analysed by the AAR method in this research. The Pleistocene shell record is limited to the MIS 5e shoreline due to the subsidence in the region and relatively lower sea levels within the Pleistocene (section 2.5.3). As reviewed in section 5.2.1, depth of burial affects the effective Quaternary temperature (EQT) to which a sample is exposed and therefore, the rate of racemisation (Wehmiller, 1982; Miller and Brigham-Grette, 1998). To gauge the impact of burial depth on the rate of racemisation, the mean

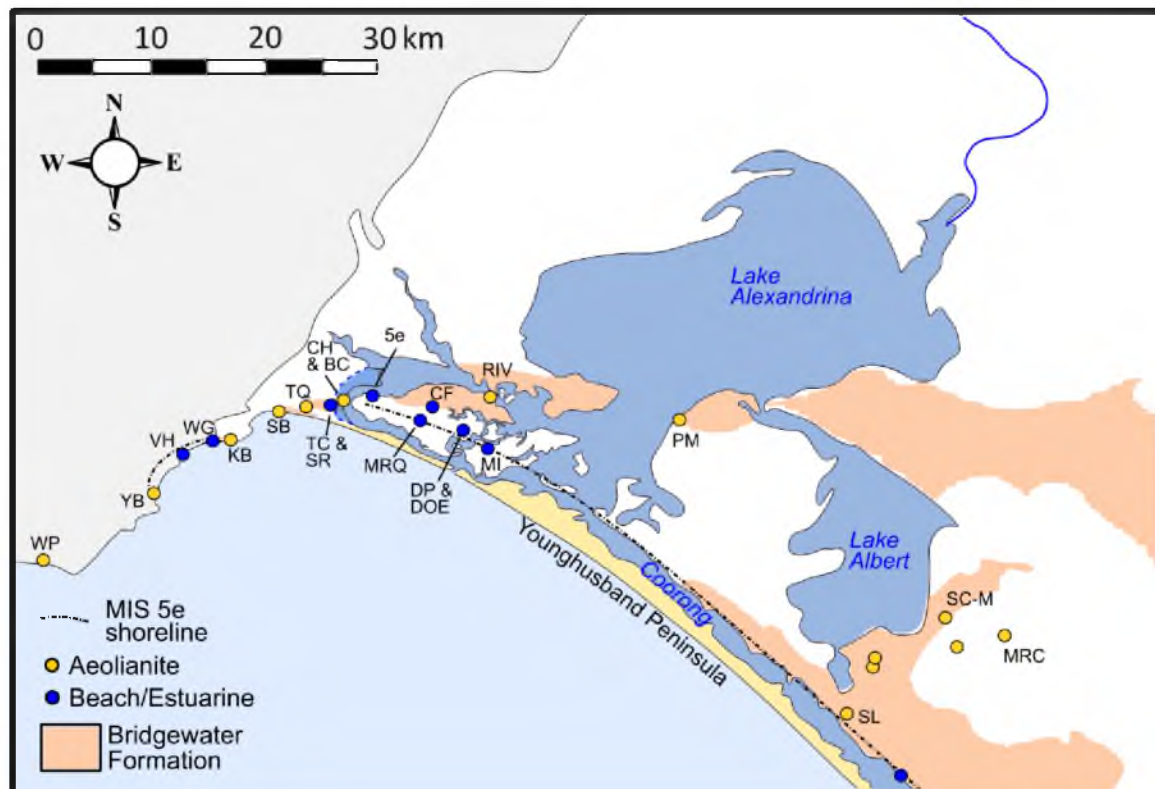


Figure 6.6: The results of analyses from the last interglacial shoreline (*sensu lato*) are presented with regard to their geographic relationships, from east to west, southeast Lake Albert, Hindmarsh Island, Goolwa and Fleurieu Peninsula. For clarity, not all field sites are indicated or labelled in the figure. Field sites labelled as abbreviated are: WP – Waitpinga, YB – Yilki Beach, VH – Victor Harbor, WG – Watsons Gap, KB – Knights Beach, SB – Surfer Beach, TQ – Traegers Quarry, TC & SR – Tennis Court and Stratco Railway, CH & BC – Chart House and Goolwa Bridge Calcrete, 5e – MIS 5e estuarine facies (as determined by AAR and TL analyses, Murray-Wallace *et al.*, 2010), MRQ – McLeay Road Quarry, CF – Cheese Factory, DP & DoE – Denver Property and Department of Environment, RIV – Riverside Calcrete, MI – Mundoo Island dredge, PM – Point McLeay, SL – Stratland, SC-M – Stockcrete and MRC – McIntosh Road.

glutamic acid (GLX) D/L values for the most prevalent shell analysed by AAR, *Spisula trigonella*, were compared. The results of this assessment are presented before other geochronological analyses. Results are presented by their geographic relationships as they were in Chapter 4 (Figure 6.6) to clarify the effects of physical landscape setting.

6.4.3.1 Depth of Burial

The GLX D/L values for *S. trigonella* shell from last interglacial (MIS 5e) deposits fall largely within a range from 0.350 – 0.400 (Figure 6.7). Shallowly buried shell (0 - 0.30 m) shows the most variation providing both the highest D/L values and two of the three lowest D/L values. The third low D/L value is from the reworked site shell (indicated by 'RW' on the x-axis), which, based on the geographic relationship with nearby field sites, was shallowly buried, <1 m. The two sites showing the highest degree of racemisation are sites where the shell was retrieved from excavated wetland shorelines and it would

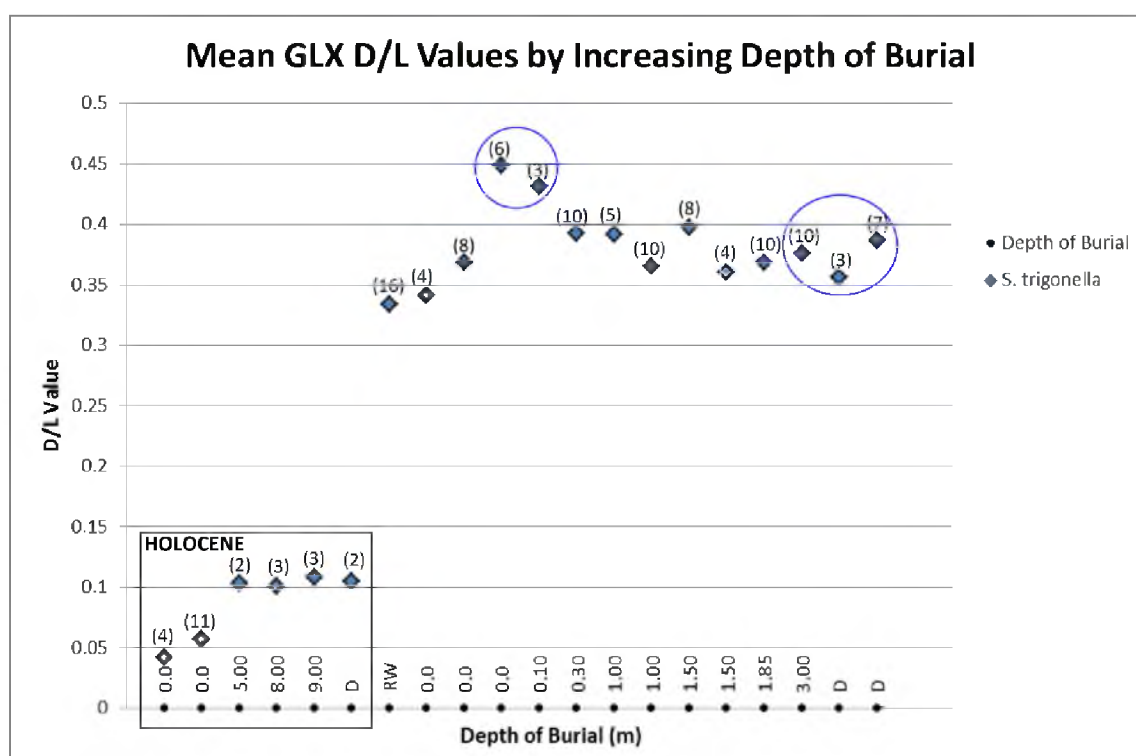


Figure 6.7: MIS 5e mean GLX D/L values for the bivalve *S. trigonella* with increasing depth of burial with Holocene shell retrieved from the modern shoreline for comparison. The 'D' designation on the x-axis for depth of burial indicates the shell was retrieved from dredged material that would have been submerged at an unknown depth until recently. 'RW' indicates a site subjected to reworking in the creation of an artificial wetland. Blue circles surround MIS 5e mean D/L values derived from sites where the shell was retrieved from a dredged site or was located at or near the water table and subject to inundation. The number in parentheses indicates the number of shells analysed.

be expected that the exposure to excess water would promote leaching and loss of indigenous amino acids resulting in a decreased D/L value (Rutter and Blackwell, 1995; Penkman *et al.*, 2008). However, as the wetlands are man-made, the absence of apparent leaching may reflect a lack of necessary time to produce a leaching effect. The results seem to suggest that while shallow burial has the potential to increase the rate of racemisation it may also increase the variability in results.

6.4.3.2 MIS 5e shell record

Sea level during MIS 5e of ~2 m APSL has been reported for Australia (Belperio *et al.*, 1995), which, although lower than the global estimate of at least 6 m APSL (Hearty *et al.*, 2007), is still higher than present levels and helps to explain the preservation of MIS 5e deposits within the study area even with ongoing subsidence. Beach and estuarine/lagoon facies of the MIS 5e coastline were identified on Fleurieu Peninsula and in the Goolwa/Hindmarsh Island regions (Figure 6.6) and help to constrain the location of shoreline during the Last Interglacial (section 4.3.3).

The Pleistocene age of the shell means that the rate of racemisation passed the transition zone of the non-linear racemisation curve (section 5.2.1) and is now proceeding at a slow rate. Variation in D/L values represent chemical and biological diagenetic changes as well as sample selection and laboratory uncertainty and therefore, the resolution of age such as was demonstrated between the modern and early Holocene shell is not possible. However, the clustering of D/L values makes possible resolution to the scale of the interglacial interval (Figure 6.8 inset). The mean glutamic acid (GLX) D/L values for all shell species analysed are consistently between 0.300-0.500, with one exception for *Turbo* sp. opercula at the Tennis Court Field Site (Figure 6.8). This reflects a genus effect as *Turbo* sp. opercula show the highest degree of racemisation among all shell analysed (Figure 6.8). A summary of results by field site is provided in Table 6.6.

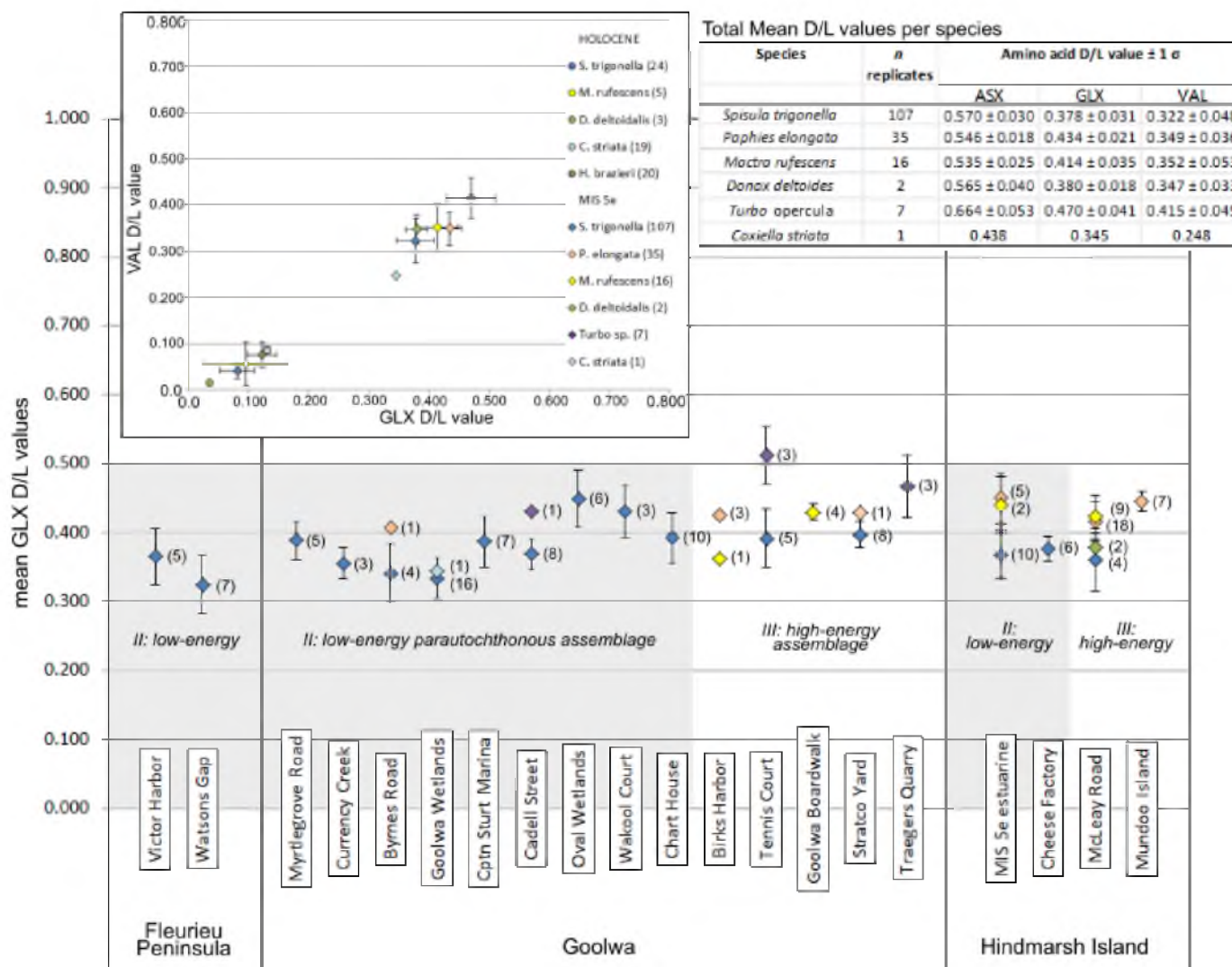


Figure 6.8: Mean glutamic acid (GLX) D/L values with 1σ for mollusc species analysed per site (sections 4.3.3.2 and 4.3.3.3). The fossil assemblages (section 4.2.1) are labelled and indicated by a presence/lack of shading. Uncertainties in GLX D/L values represent diagenetic factors, sampling and laboratory uncertainty. Numbers in parentheses indicates the number of shells analysed but not the number of sub-sample injections which varied between 1 and 3. Variation in the extent of racemisation between different mollusc species is a reflection of the genus-effect (inset). The inset is a scatter plot of mean valine (VAL) and mean GLX D/L values derived from AAR analysis of mollusc shell with 1σ uncertainties. Means derived from last interglacial shell overlaps at 1σ uncertainties (note: *C. striata* represents only one analysis). The large deviation shown by Holocene *M. rufescens* is related to the age of the shells run for analysis, both modern and early Holocene, and reflects the early fast rates of racemisation. The number of shell analysed is indicated by number in parenthesis in legend.

Table 6.6: Summary of mollusc shell analysis from MIS 5e field sites in the River Murray Mouth region.

Field Site	Species	UWGA (UOW AAR laboratory code)	n replicates	Amino acid D/L value $\pm 1 \sigma$		
				ASX	GLX	VAL
FLEURIEU PENINSULA						
<u>Model II low-energy parautochthonous assemblage</u>						
Victor Harbor	<i>Spisula trigonella</i>	9751, 9752	5	0.529 \pm 0.027	0.365 \pm 0.041	0.303 \pm 0.049
Watsons Gap	<i>Spisula trigonella</i>	9753	7	0.504 \pm 0.045	0.331 \pm 0.043	0.259 \pm 0.050
GOOLWA						
<u>Model II low-energy parautochthonous assemblage</u>						
Myrtlegrove Road	<i>Spisula trigonella</i>	10103	5	0.592 \pm 0.015	0.389 \pm 0.028	0.326 \pm 0.030
Currency Creek dredge	<i>Spisula trigonella</i>	9738	3	0.547 \pm 0.014	0.356 \pm 0.023	0.313 \pm 0.031
Byrnes Road	<i>Spisula trigonella</i>	9706	4	0.546 \pm 0.025	0.341 \pm 0.042	0.275 \pm 0.028
	<i>Paphies elongata</i>	9706	1	0.537	0.407	0.295
Goolwa Wetlands	<i>Spisula trigonella</i>	9703, 9704, 9705	16	0.559 \pm 0.029	0.334 \pm 0.030	0.285 \pm 0.032
	<i>Coxiella striata</i>	10133	1	0.438	0.345	0.248
Captain Sturt Marina dredge	<i>Spisula trigonella</i>	9737	7	0.594 \pm 0.030	0.387 \pm 0.037	0.314 \pm 0.059
Cadell Street	<i>Spisula trigonella</i>	9707	8	0.579 \pm 0.027	0.369 \pm 0.023	0.249 \pm 0.030
	<i>Turbo opercula</i>	10160	1	0.607 \pm 0.007	0.431 \pm 0.001	0.365 \pm 0.009
Oval Wetlands	<i>Spisula trigonella</i>	10106	6	0.595 \pm 0.022	0.449 \pm 0.041	0.443 \pm 0.045
Wakool Court	<i>Spisula trigonella</i>	10104	3	0.626 \pm 0.015	0.431 \pm 0.038	0.391 \pm 0.057
Chart House	<i>Spisula trigonella</i>	9754, 10107	10	0.594 \pm 0.035	0.393 \pm 0.037	0.346 \pm 0.050
<u>Model III high-energy assemblage</u>						
Birks Harbour Dredge	<i>Mactra rufescens</i>	9739	1	0.510	0.362	0.285
	<i>Paphies elongata</i>	9739	3	0.555 \pm 0.039	0.426 \pm 0.006	0.343 \pm 0.015
Tennis Court	<i>Spisula trigonella</i>	9716, 9717	5	0.560 \pm 0.040	0.374 \pm 0.042	0.336 \pm 0.039
	<i>Turbo opercula</i>	10158	3	0.710 \pm 0.022	0.512 \pm 0.034	0.451 \pm 0.022
Goolwa Boardwalk	<i>Mactra rufescens</i>	9987	4	0.563 \pm 0.007	0.430 \pm 0.012	0.339 \pm 0.014
Stratco Yard	<i>Spisula trigonella</i>	9719, 10108	8	0.586 \pm 0.021	0.397 \pm 0.019	0.341 \pm 0.036
	<i>Paphies elongata</i>	9718	1	0.544	0.439	0.365
Traegers Quarry	<i>Turbo opercula</i>	9771	3	0.674 \pm 0.027	0.468 \pm 0.045	0.430 \pm 0.045
HINDMARSH ISLAND						
<u>Model II low-energy parautochthonous assemblage</u>						
MIS 5e estuarine	<i>Spisula trigonella</i>	9748, 9749	10	0.577 \pm 0.018	0.368 \pm 0.035	0.293 \pm 0.056
	<i>Paphies elongata</i>	9748, 9749	5	0.528 \pm 0.029	0.450 \pm 0.037	0.374 \pm 0.065
	<i>Mactra rufescens</i>	9748, 9749	2	0.518 \pm 0.045	0.440 \pm 0.041	0.408 \pm 0.036
Cheese Factory	<i>Spisula trigonella</i>	9772, 9773	6	0.556 \pm 0.016	0.376 \pm 0.018	0.317 \pm 0.027
<u>Model III high-energy assemblage</u>						
McLeay Road Quarry	<i>Spisula trigonella</i>	10109, 10110	4	0.590 \pm 0.046	0.360 \pm 0.045	0.347 \pm 0.053
	<i>Paphies elongata</i>	9977, 9980, 9981, 9983	18	0.551 \pm 0.023	0.416 \pm 0.029	0.353 \pm 0.026
	<i>Mactra rufescens</i>	9979, 9982, 9984	9	0.548 \pm 0.029	0.423 \pm 0.032	0.377 \pm 0.045
	<i>Donax deltoidalis</i>	9978	2	0.565 \pm 0.040	0.380 \pm 0.018	0.347 \pm 0.033
Mundoo Island dredge	<i>Paphies elongata</i>	9986	7	0.576 \pm 0.026	0.445 \pm 0.014	0.325 \pm 0.038

6.4.3.3 Late Pleistocene whole-rock and foraminifer

The mean GLX D/L value for Late Pleistocene whole-rock sample and foraminifer results are presented for each field site in Figure 6.9 and Tables 6.7 and 6.8. A regional variation based on physical landscape setting is apparent in whole-rock sample means and individual foraminifer analyses. The inability of AAR to distinguish beyond the scale of interglacial intervals (section 5.2.2) is made apparent by the whole-rock results from Surfers Beach. Although, TL analysis has implied MIS 5c deposition of Surfers Beach with an age of 105 ± 5 ka (W-2348; Murray-Wallace *et al.*, 2010), the D/L whole-rock value is comparable to and higher than many interpreted MIS 5e whole-rock results (Figure 6.9) indicating the potential range of D/L values within MIS 5 (*sensu lato*). Variability in D/L values has the potential to be high in the Murray Mouth region due to the capacity for reworking.

Southeast Lake Albert

The whole-rock samples from southeast Lake Albert are the most consistent within the study area with the lowest degree of uncertainty in the mean whole-rock value. This is expected to be due to the location of the region outside of the zone of subsidence as indicated by the preservation of last interglacial prograding beach facies along the eastern shoreline of the Coorong (Murray-Wallace *et al.*, 1996; 2010; section 4.3.3.1) and therefore slightly removed from the effects of extensive erosion and reworking which occur in the more immediate vicinity of the Murray Mouth during sea level transgressions and highstands. In this regard the, these sediments are likely to contain a smaller proportion of reworked skeletal grains than those to the north. Furthermore, the calcium carbonate content of the Lake Albert whole-rock sediment is generally low (Table 6.9, section 4.3.3.1). This could be due to the position of the region onshore of the quartz-dominated zone of the Lacepede Shelf where minimal active carbonate sedimentation occurs (section 3.5.1). It is additionally interesting that MIS 5 aeolianite extends as much as 15 km inland (McIntosh Road field site) from the MIS 5e shoreline when the beach barriers of the Coorong Coastal Plain typically do not exceed 5 km in width (Schwebel, 1984).

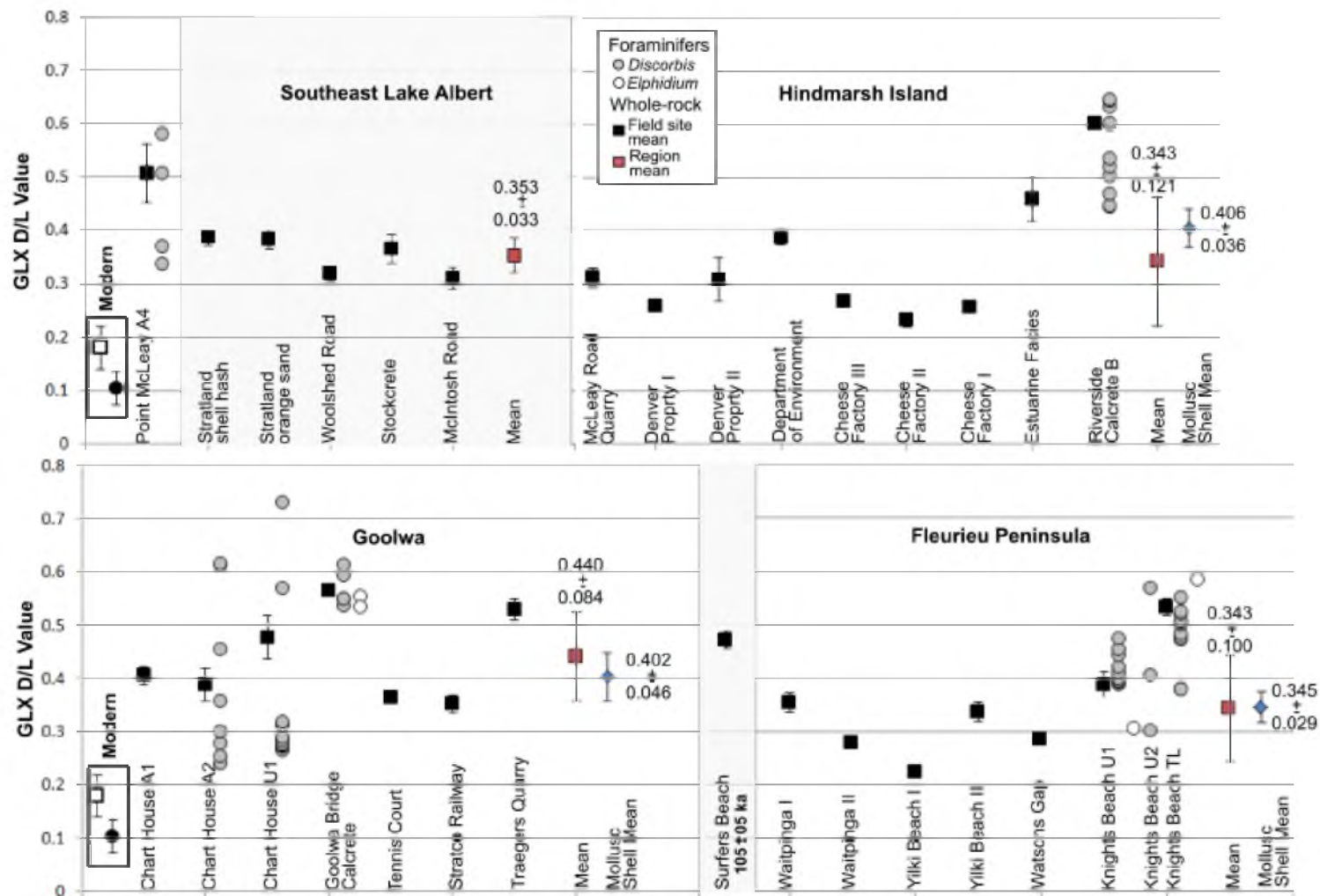


Figure 6.9: Results of whole-rock sample (with 1 σ uncertainty terms) and individual foraminifer analyses per site and grouped by region. Regional variability is apparent in both whole-rock mean and individual foraminifer analyses. The latter makes difficult the identification of contemporaneous foraminifers and reworked foraminifers. The potential causes for the variability in results are discussed in test.

Table 6.7: Summary of whole-rock sample analyses from MIS 5c (Surfer Beach) and MIS 5e field sites in the River Murray Mouth region. Those field sites likely to have been subject to periodic inundation are indicated in blue. Table continues on following page.

Field Site	% Carbonate	Depth of burial (m)	UWGA (UOW AAR laboratory)	n replicates	Amino acid D/L value $\pm 1 \sigma$		
					ASP	GLX	VAL
MIS 5c							
Surfers Beach	28	7	9778	4	0.591 \pm 0.012	0.472 \pm 0.016	0.420 \pm 0.020
FAA				3	0.800 \pm 0.008	0.732 \pm 0.008	0.703 \pm 0.005
SOUTHEAST LAKE ALBERT							
Stratland top hash	12	1	10171	5	0.556 \pm 0.007	0.388 \pm 0.016	0.289 \pm 0.027
FAA				1	0.761	0.582	-
Stratland orange sand	29	6.1	10181	5	0.517 \pm 0.010	0.383 \pm 0.017	0.379 \pm 0.040
FAA				5	0.798 \pm 0.007	0.629 \pm 0.016	0.584 \pm 0.047
Woolshed Road	22	0.9	10172	5	0.425 \pm 0.016	0.319 \pm 0.014	0.191 \pm 0.017
FAA				5	0.783 \pm 0.005	0.642 \pm 0.017	0.611 \pm 0.598
Stockcrete	8	1.1	10173	5	0.475 \pm 0.013	0.366 \pm 0.027	0.282 \pm 0.014
FAA				5	0.673 \pm 0.009	0.519 \pm 0.027	0.365 \pm 0.028
McIntosh Road	8	1	10174	5	0.352 \pm 0.005	0.310 \pm 0.019	0.124 \pm 0.009
FAA				5	0.671 \pm 0.004	0.471 \pm 0.008	0.364 \pm 0.014
AVERAGE OF REGION WHOLE-ROCK SAMPLES					0.465 \pm 0.071	0.353 \pm 0.033	0.253 \pm 0.088
FAA					0.737 \pm 0.055	0.569 \pm 0.065	0.481 \pm 0.117
HINDMARSH ISLAND							
McLeay Road Quarry	60	1	10127	5	0.470 \pm 0.013	0.312 \pm 0.017	0.235 \pm 0.025
FAA				5	0.796 \pm 0.003	0.679 \pm 0.089	0.699 \pm 0.027
Denver Property I	60	0.6	10141	4	0.378 \pm 0.007	0.260 \pm 0.009	0.098 \pm 0.008
FAA				4	0.752 \pm 0.007	0.486 \pm 0.019	0.616 \pm 0.022
Denver Property II	59	1	10121	5	0.389 \pm 0.045	0.309 \pm 0.041	0.194 \pm 0.038
FAA				5	0.790 \pm 0.004	0.716 \pm 0.073	0.710 \pm 0.028
Denver DoE	76	0.9	10120	5	0.543 \pm 0.007	0.388 \pm 0.014	0.309 \pm 0.012
FAA				5	0.793 \pm 0.016	0.703 \pm 0.034	0.712 \pm 0.035
Cheese Factory III	52	0.75	10164	5	0.430 \pm 0.006	0.267 \pm 0.007	0.142 \pm 0.020
FAA				5	0.660 \pm 0.010	0.402 \pm 0.017	0.418 \pm 0.034
Cheese Factory II	36	1.2	10153	5	0.340 \pm 0.010	0.232 \pm 0.012	0.080 \pm 0.006
FAA				5	0.652 \pm 0.007	0.372 \pm 0.006	0.370 \pm 0.033
Cheese Factory Unit I	30	2	9927	5	0.454 \pm 0.017	0.258 \pm 0.010	0.152 \pm 0.019
FAA				5	0.675 \pm 0.022	0.349 \pm 0.012	0.380 \pm 0.051
MIS 5e estuarine facies	13	2-2.5	10142	5	0.574 \pm 0.036	0.460 \pm 0.042	0.345 \pm 0.039
FAA				5	0.825 \pm 0.010	0.622 \pm 0.017	0.720 \pm 0.016
Riverside Calcrete B	54	1	10167	5	0.669 \pm 0.006	0.602 \pm 0.011	0.553 \pm 0.014
FAA				5	0.847 \pm 0.004	0.781 \pm 0.033	0.807 \pm 0.014
AVERAGE OF REGION WHOLE-ROCK SAMPLES					0.472 \pm 0.106	0.343 \pm 0.121	0.234 \pm 0.149
FAA					0.754 \pm 0.074	0.568 \pm 0.166	0.604 \pm 0.168

Table 6.7 continued: Summary of whole-rock sample analyses from MIS 5e field sites in the River Murray Mouth region. Those field sites likely to have been subject to periodic inundation are indicated in blue.

Field Site	% Carbonate	Depth of burial (m)	UWGA (UOW AAR laboratory)	n replicates	Amino acid D/L value ± 1 σ		
					ASP	GLX	VAL
GOOLWA							
Chart House A1	21	1.5	9929	6	0.539 ± 0.017	0.405 ± 0.017	0.227 ± 0.037
FAA				6	0.736 ± 0.053	0.556 ± 0.062	0.560 ± 0.103
Chart House A2	21	1.5	10146	5	0.511 ± 0.026	0.388 ± 0.031	0.270 ± 0.080
FAA				8	0.765 ± 0.011	0.504 ± 0.057	0.430 ± 0.183
Chart House Unit 1	34	1.2	10165	5	0.559 ± 0.017	0.477 ± 0.040	0.390 ± 0.035
FAA				5	0.767 ± 0.005	0.660 ± 0.016	0.720 ± 0.033
Bridge Calcrete	18	1.5	10125	1	0.643 ± 0.002	0.565 ± 0.001	0.488 ± 0.023
FAA				7	0.837 ± 0.006	0.696 ± 0.048	0.820 ± 0.012
Tennis Court	31	1	9957	5	0.495 ± 0.009	0.364 ± 0.008	0.173 ± 0.022
FAA				5	0.813 ± 0.010	0.645 ± 0.036	0.600 ± 0.051
Stratco Yard (Railway)	24	0.75	9928	5	0.349 ± 0.020	0.352 ± 0.017	0.115 ± 0.015
FAA				10	0.792 ± 0.009	0.553 ± 0.020	0.633 ± 0.058
Traegers Quarry	17	2	9930	6	0.640 ± 0.010	0.530 ± 0.020	0.445 ± 0.022
FAA				6	0.829 ± 0.008	0.685 ± 0.043	0.744 ± 0.010
AVERAGE OF REGION WHOLE-ROCK SAMPLES					0.534 ± 0.100	0.440 ± 0.084	0.301 ± 0.142
FAA					0.791 ± 0.037	0.614 ± 0.075	0.644 ± 0.130
FLEURIEU PENINSULA							
Waitpinga I	62	3.5	10128	5	0.434 ± 0.027	0.354 ± 0.018	0.181 ± 0.026
FAA				5	0.840 ± 0.021	0.915 ± 0.229	0.780 ± 0.113
Waitpinga II	70	1.55	10169	5	0.339 ± 0.020	0.279 ± 0.011	0.071 ± 0.015
FAA				5	0.724 ± 0.018	0.673 ± 0.048	0.527 ± 0.048
Yilki I	50	intertidal	9934	3	0.405 ± 0.006	0.224 ± 0.006	0.132 ± 0.010
FAA				3	0.700 ± 0.013	0.514 ± 0.015	0.484 ± 0.053
Yilki II	45	intertidal	9935	4	0.504 ± 0.015	0.337 ± 0.018	0.246 ± 0.021
FAA				4	0.750 ± 0.013	0.548 ± 0.019	0.583 ± 0.028
Watsons Gap	12	1	10166	5	0.356 ± 0.009	0.286 ± 0.009	0.118 ± 0.013
FAA				5	0.786 ± 0.017	0.619 ± 0.016	0.649 ± 0.018
Knights Beach Unit 1	62	7	10139	6	0.494 ± 0.023	0.387 ± 0.024	0.271 ± 0.027
FAA				4	0.834 ± 0.003	0.680 ± 0.039	0.859 ± 0.030
Knights Beach TL	44	3	10152	5	0.617 ± 0.012	0.533 ± 0.016	0.462 ± 0.036
FAA				5	0.843 ± 0.006	0.695 ± 0.014	0.739 ± 0.020
AVERAGE OF REGION WHOLE-ROCK SAMPLES					0.450 ± 0.097	0.343 ± 0.100	0.212 ± 0.131
FAA					0.782 ± 0.059	0.663 ± 0.131	0.660 ± 0.138
NARRUNG PENINSULA							
Point McLeay A4	55	5	10114	5	0.563 ± 0.050	0.508 ± 0.055	0.418 ± 0.062
FAA				5	0.818 ± 0.004	0.809 ± 0.026	0.829 ± 0.013

Table 6.8: Summary of individual foraminifer analyses from MIS 5e field sites in the River Murray Mouth region. Results are inclusive of all foraminifers with no distinction of possibly reworked tests.

Field Site		Species	UWGA (AAR laboratory code)	<i>n</i> replicates	Amino acid D/L value ± 1 σ		
					ASP	GLX	VAL
HINDMARSH ISLAND							
	Riverside Calcrete B	<i>Discorbus</i>	10197	11	0.718 ± 0.059	0.551 ± 0.079	0.706 ± 0.112
GOOLWA							
	Chart House A2	<i>Discorbus</i>	10188	8	0.578 ± 0.117	0.389 ± 0.154	0.493 ± 0.188
	Chart House UI	<i>Discorbus</i>	10187	10	0.624 ± 0.084	0.358 ± 0.159	0.540 ± 0.318
	Bridge Calcrete	<i>Discorbus</i>	10189	5	0.755 ± 0.023	0.568 ± 0.033	0.700 ± 0.102
		<i>Elphidium</i>	10190	2	0.771 ± 0.001	0.544 ± 0.013	0.509 ± 0.009
FLEURIEU PENINSULA							
	Knights TL	<i>Discorbus</i>	10194	11	0.649 ± 0.068	0.481 ± 0.056	0.601 ± 0.099
		<i>Elphidium</i>	10195	1	0.758	0.585	0.661
	Knights Beach U2	<i>Discorbus</i>	10193	3	0.524 ± 0.093	0.425 ± 0.134	0.463 ± 0.142
	Knights Beach UI	<i>Discorbus</i>	10191	9	0.590 ± 0.034	0.315 ± 0.060	0.465 ± 0.105
		<i>Elphidium</i>	10192	1	0.416	0.306	0.226
POINT MCLEAY							
	Point McLeay A4	<i>Discorbus</i>	10607	4	0.660 ± 0.093	0.449 ± 0.116	0.643 ± 0.254

Hindmarsh Island

The Hindmarsh Island results show the greatest variability as indicated by the uncertainty associated with the whole-rock mean for the region (Figure 6.9, Table 6.7). This however, is partially skewed by the Riverside Calcrete B result which is comparable to MIS 7 results (see middle Pleistocene discussion below). The Riverside Calcrete B is opposite the Goolwa Channel from the MIS 7 aeolianite at Clayton Water Tower and overlies the MIS 7 aeolianite on northern Hindmarsh Island (section 4.3.3.2). The high whole-rock result and the foraminifers indicate the sediments of Riverside Calcrete B contain a large component of reworked MIS 7 sediment.

All field sites on Hindmarsh Island for which whole-rock results are presented, except for the estuarine facies and Riverside Calcrete B, are located in close proximity to fluvial channels or subject to periodic inundation due to either low-lying topography or relationship to the water table and are more likely to have been subject to the adverse effects of exposure to excess water (see above depth of burial discussion) possibly explaining some of the variability. Furthermore, other than the Riverside Calcrete B and the Cheese Factory III unit (a thin 65 cm thick aeolian sand) the sites on Hindmarsh Island are interpreted as beach or estuarine/lagoon facies and initially deposited subaqueously or in a near marine environment. The robust results of shell analysis from

Hindmarsh Island (Figure 6.8, Table 6.6) support the conclusion of (Miller and Hare, 1980) that the mollusc shell matrix is effective at excluding most environmental influences (section 5.2.1). The low GLX D/L values of the whole-rock samples reflect the poorly preserved nature of the shell fragments within which makes them more susceptible to the effects of leaching.

Sediments beneath the Denver Property calcrete had been previously analysed and assigned a TL age of 85 ± 7.1 ka (W-2258) indicating deposition during substage 5a. However, sea level during MIS 5a was as much as 17 m below present level in the region (Belperio and Cann, 1990; Murray-Wallace *et al.*, 2001) and the abundant fossiliferous content of the sediments and the minimal rounding of carbonate grains (section 4.3.3.2) indicate an environment of deposition adjacent to a carbonate source with minimal transport. Although sea level during MIS 5c was much higher (~ 9 m below present level) in the region than MIS 5a (Belperio and Cann, 1990; Murray-Wallace *et al.*, 2001) and aeolian evidence persists in the landscape at Surfers Beach and in the calcrete inlier to the modern Sir Richard Peninsula seaward of the MIS 5e shoreline (section 4.3.3.2), sea-level was likely still too far to the south to provide the carbonate grains seen in the Denver Property sediments. In this thesis it has been shown that last interglacial (MIS 5e) intertidal shell beds extend across Mundoo and Hindmarsh Islands directly to the south of the Denver Property (sections 4.3.3.2 and above) signifying that during MIS 5e they were positioned near to the inner continental shelf source of carbonate. Additionally, the whole-rock results from the Department of Environment (~ 600 m to the west) were consistent with deposition during MIS 5e (Table 6.7) indicating the samples from the Denver Property calcrete on the shoreline of the Mundoo Channel and bisected by a smaller tributary would have been subject to the effects of water inundation and leaching.

The Watsons Gap aeolianite drapes a reworked lagoon and beach deposit. The contact between the aeolianite and underlying fossiliferous sediment is obscured by vegetation and free-flowing sands. The potential exists that the sand was deposited during MIS 5c alongside the aforementioned Surfer Beach aeolianite and Sir Richard calcrete inlier. Collection of an adequate whole-rock sample for AAR analysis from beneath the Sir Richard calcrete inlier for comparison was not possible. The whole-rock

results from Surfers Beach exhibit a high extent of racemisation (Table 5.11, Figure 5.22), above the MIS 5e mean, indicating a significant quantity of reworked material. The whole-rock D/L values for the entire study area exhibit high variability (Table 5.11) and suggest that a comparison of D/L values between geographic locations in order to determine relationship may not be adequate, especially if one site is regarded as containing a significant quantity of reworked material.

Goolwa

The Goolwa region has the highest mean D/L value of all four regions (Figure 6.9, Table 6.7). This is interesting because Goolwa is interpreted to be the location of a last interglacial palaeo-Goolwa Channel and River Murray Mouth (section 4.3.3.2). When considering the modern example, the modern Goolwa Channel exhibited the lowest extent of racemisation and the Murray Mouth exhibited a much higher extent of racemisation (section 6.4.1) implying that the Goolwa sedimentary successions are more representative of the river mouth. The modern example also shows the beach deposits, in general, to have higher extents of racemisation than the river channel and mouth sediments and may explain the higher rates of racemisation exhibited by Traegers Quarry and the Goolwa Bridge Calcrete. The foraminifer of Goolwa Bridge Calcrete are also indicative an older, reworked component.

The high uncertainty associated with the Chart House A2 and Chart House U1 foraminifer results is reflective of reworked foraminifers. However, the clusters of foraminifers at Chart House A2 and Chart House U1 have mean GLX D/L values of 0.268 ± 0.026 and 0.285 ± 0.019 respectively and, following the modern example (section 6.4.1), would most accurately represent MIS 5e foraminifers. These values are lower than their shell counterparts but in pyrolysis experiments both Lachlan (2011) and Blakemore (2014) found GLX racemisation to proceed at a slower rate than the mollusc shell *K. scalarina* and these values from the natural environment seem to confirm their conclusions.

Fleurieu Peninsula

Most of the variability exhibited by the whole-rock results on Fleurieu Peninsula (Figure 6.9, Table 6.7) can be explained. Both of the Yilki Beach shore platform sediments interpreted to formed from a MIS 5e aeolianite, were retrieved from the intertidal zone and Yilki Beach I is likely to be exhibiting either the effects of leaching or contamination from younger, non-indigenous amino acids. The Waitpinga II aeolianite set 1.4 km back within a bedrock valley, had been analysed using AAR whole-rock by Murray-Wallace *et al.* (2010) and returned a lower than expected valine D/L value and was retested in this thesis. The additional low value for the Waitpinga II aeolianite confirms the degradation of lower molecular weight peptides and amino acids *in situ*. This result and the extensive pedogenesis of the aeolianite suggest that it is potentially older than MIS 5. The Watsons Gap aeolianite overlies a MIS 5e lagoon deposit as indicated by AAR shell analyses (Figure 6.8, Table 6.6) and may have been deposited during the sea-level regression following MIS 5e or during the highstand at MIS 5c.

The variability at Knights Beach is more complicated. The stratigraphic interpretation at Knights Beach (section 4.3.5) implies that Knights Beach U1 is separated from the overlying Knights Beach TL and Knights Beach U2 by a disconformity related to a hiatus in deposition but that deposition occurred during the same interglacial period. However the overlying Knights Beach TL whole-rock sample and foraminifers exhibit a higher extent of racemisation (similar to MIS 7, see below) than the underlying Knights Beach U1. Whole-rock analyses of Knights Beach U2 were unsuccessful and the foraminifers show a large range. The Knights Beach U1 foraminifer also show much higher extents of racemisation than those at the Chart House site which are likely to be representative of MIS 5e, but could be reflective of reworking like the Riverside Calcrete B field site foraminifers. Due to the subsidence that is occurring at Knights Beach, evident by the current erosion of the aeolian succession by the Southern Ocean, the succession was interpreted to have been deposited during MIS 5. However, the results of two earlier TL samples taken adjacent to each other from Knights Beach U1 were conflicting with one age (266 ± 34 ka, W2347; Bourman *et al.*, 2000) analysed at the University of Wollongong indicating deposition during MIS 7 and the other age (130 ± 15 ka, AdTL01005; Murray-Wallace *et al.*, 2010) analysed at the University of Adelaide

indicating deposition during MIS 5e. The disparate ages could be a result of uncertainties in cosmic and laboratories measurements (David Price, personal communication 07 June, 2015). An additional sample taken for this research from Knights Beach TL and analysed at the University of Wollongong provides an age of 192 ± 23 ka (W4780) supporting the premise of MIS 7 deposition. Although this age is younger than the previously reported age, they do overlap at 2σ and are within 17 ka at 1σ .

Point McLeay

The MIS 5e Point McLeay PM A4 unit has been assigned a TL age of 120 ± 15 ka (W-2693; Murray-Wallace *et al.*, 2010). Whole-rock sample analyses in this research returned GLX D/L values strongly indicative of MIS 5e deposition. The relatively high uncertainty of the GLX D/L values of both the whole-rock sample and foraminifers within the unit in comparison to the other field sites is, like the modern PM A5, due to the position of the Point McLeay within the landscape and reflective of sediment sources from a variety of directions.

6.4.3.4 Summary

All mollusc species analysed in this research were of different genera. The genus effect is most clearly demonstrated by the mean D/L values of all *Spisula trigonella* and *Turbo* opercula analysed with other mollusc species falling between the two (Figure 6.8; the single *Coxiella striata* shell is not considered here). The covariance among MIS 5e mollusc shell results is small, ranging from 5-8%.

The mollusc shell results are highly uniform and identify the MIS 5e shoreline with a clear distinction between the Holocene and older shell. The mollusc shell AAR results confirm the presumed location and extent of the MIS 5e coastline based on morphostratigraphy and geographic relationships and confirm that the last interglacial Goolwa channel was for some time located farther to the west than the last glacial maximum and modern channel.

The whole-rock sample and foraminifer analysis show a regional variation that, like the modern shoreline, is reflective of the depositional environment. The southeast Lake Albert region is removed from the subsidence and intensive erosion exhibited closer to the Murray Mouth and has the lowest variability between whole-rock sample

results and is therefore most representative of MIS 5e aeolian deposition in the region. The comparatively low whole-rock D/L values at some of the Hindmarsh Island field sites most likely reflects a low-lying position in the landscape and proximity to water which can have a detrimental effect to the integrity of whole-rock. The foraminifer clusters within the Chart House units are most representative of MIS 5e following the modern example that the channel, as a high-energy environment, has a very short residence time. They also support the conclusion, as determined by the results of pyrolysis experiments (Lachlan, 2011; Blakemore, 2014), that the forward rate of glutamic acid racemisation proceeds at a slower rate in foraminifer than shell. The GLX D/L values of the MIS 5e aeolianites Goolwa Bridge and Traegers Quarry are comparable to the MIS 7 whole-rock sample mean and reflects the reworking of the MIS 7 barrier during the MIS 5e highstand. Most of the variability on Fleurieu Peninsula is explained by the diagenetic environment following deposition. Knights Beach however, remains perplexing. The foraminifer analysed at Knights Beach indicate that the aeolianite succession is of MIS 7 origin consistent with two of the three luminescence ages reported from there. This conclusion however, raises questions regarding as to why Knights Beach is the only location on Fleurieu Peninsula where MIS 7 deposits have so far been found and why is there a lack of the MIS 5e record there.

6.4.4 Middle to early Pleistocene

Analysis of middle Pleistocene sedimentary successions was inhibited by their lack of outcrop, a result of the ongoing subsidence of the region. The location of the MIS 7 barrier complex on Sturt Peninsula was confirmed using AAR and TL analyses by Murray-Wallace *et al.* (2010). Additional middle Pleistocene aeolianites were identified at Point McLeay and Mount Misery with inconclusive analyses. This research identified additional field sites interpreted to extend the record of MIS 7 deposition, the Point McLeay succession, revisited Mount Misery and identified additional Bridgewater Formation sedimentary successions farther inland (Chapter 4) (Figure 6.10). Whole-rock sample analyses were only successful for interpreted MIS 7 sedimentary successions (Table 6.9). Analysis of the interpreted MIS 9 units within the Point McLeay sedimentary

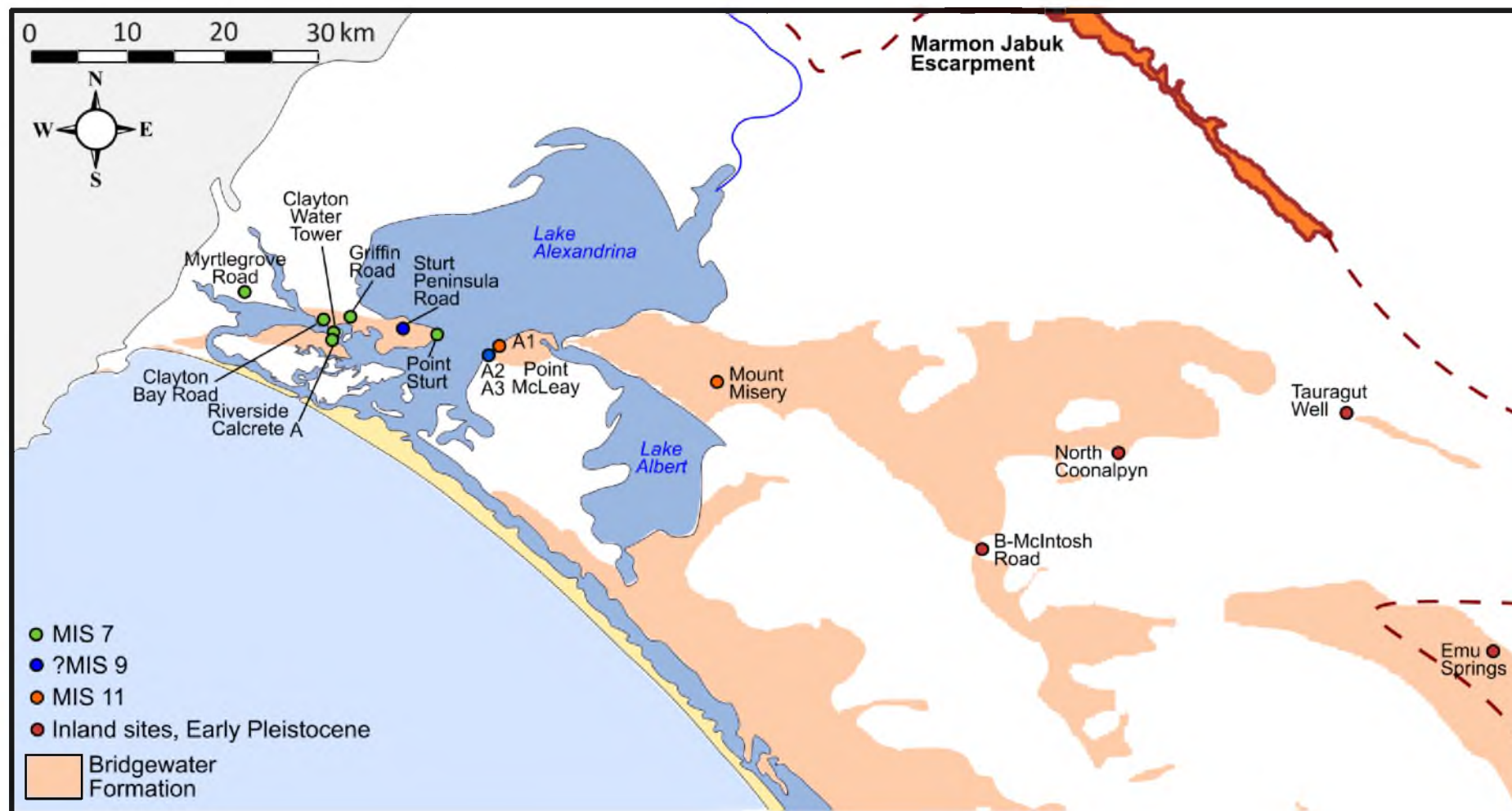


Figure 6.10: Location of middle to early Pleistocene sedimentary successions and field sites. Whole-rock sample analyses were only successful to MIS 7. Individual foraminifers were successfully analysed from the inland field sites B-McIntosh Road, North Coonalpyn and Emu Springs. Results are discussed in text.

Table 6.9: Summary of whole-rock sample analyses for MIS 7 aeolianite on northern Hindmarsh Island and Sturt Peninsula.

Field Site		% Carbonate	Depth of burial (m)	UWGA (AAR laboratory code)	<i>n</i> replicates	Amino acid D/L value ± 1 σ		
						ASP	GLX	VAL
HINDMARSH ISLAND								
	Riverside Calcrete A (East)	64	1	10124	5	0.615 ± 0.012	0.531 ± 0.024	0.493 ± 0.020
	FAA				5	0.825 ± 0.005	0.806 ± 0.085	0.829 ± 0.028
STURT PENINSULA								
	Clayton Bay Road	42	1.5	10123	5	0.657 ± 0.011	0.593 ± 0.017	0.601 ± 0.018
	FAA				5	0.813 ± 0.005	0.723 ± 0.029	0.883 ± 0.025
	Clayton Water Tower I	52	11	9905	5	0.701 ± 0.010	0.645 ± 0.012	0.668 ± 0.056
	FAA				5	0.847 ± 0.013	0.706 ± 0.009	0.847 ± 0.055
	Griffin Road	44	2	10122	5	0.644 ± 0.007	0.614 ± 0.010	0.603 ± 0.037
	FAA				5	0.795 ± 0.004	0.739 ± 0.080	0.852 ± 0.041
	Point Sturt	28	6.5	9907	5	0.694 ± 0.009	0.662 ± 0.018	0.760 ± 0.137
	FAA				1	0.858	0.763	0.928
AVERAGE OF ALL WHOLE-ROCK SAMPLES						0.662± 0.036	0.609 ± 0.051	0.625 ± 0.098
	FAA					0.828 ± 0.025	0.747 ± 0.039	0.868 ± 0.039

Table 6.10: Summary of individual foraminifer analyses for MIS 7 aeolianite on northern Hindmarsh Island and Sturt Peninsula, Point McLeay and more inland field sites. The Clayton Bay Road and Griffin Road means do not include the foraminifer deemed to have suffered a loss of indigenous amino acids; see text for discussion and Figure 6.11.

Field Site		Species	UWGA (AAR laboratory code)	<i>n</i> replicates	Amino acid D/L value ± 1 σ		
					ASP	GLX	VAL
HINDMARSH ISLAND							
	Riverside Calcrete A (E)	<i>Discorbus</i>	10196	17	0.676 ± 0.082	0.508 ± 0.082	0.696 ± 0.156
STURT PENINSULA							
	Clayton Bay Road	<i>Discorbus</i>	10198	3	0.626 ± 0.058	0.373 ± 0.039	0.578 ± 0.160
		<i>Elphidium</i>	10199	4	0.764 ± 0.031	0.630 ± 0.040	0.706 ± 0.075
	Clayton Water Tower I	<i>Discorbus</i>	10600	14	0.745 ± 0.073	0.583 ± 0.071	0.782 ± 0.113
	Griffin Road	<i>Discorbus</i>	10603	3	0.617 ± 0.023	0.364 ± 0.043	0.540 ± 0.023
	Sturt Peninsula Road	<i>Discorbus</i>	10602	5	0.690 ± 0.121	0.488 ± 0.259	0.629 ± 0.322
	Point Sturt	<i>Discorbus</i>	10601	5	0.619 ± 0.034	0.392 ± 0.044	0.589 ± 0.102
POINT MCLEAY							
	Point McLeay A1	Unknown	10608	1	0.782	0.652	0.788
INLAND DEPOSITS							
	B-McIntosh Road	<i>Discorbus</i>	10611	1	0.907	0.919	1.053
	North Coonalpyn	<i>Discorbus</i>	10612	2	0.891 ± 0.033	0.841 ± 0.030	0.977 ± 0.006
	Emu Springs	<i>Discorbus</i>	10613	2	0.876 ± 0.057	0.808 ± 0.013	1.239 ± 0.371

Figure 6.11: Summary of analytical results of middle to early Pleistocene sedimentary successions with the average GLX D/L values for modern and MIS 5 (*sensu lato*) whole-rock (white square), shell (blue diamond) and foraminifers (black circle) provided for comparison. The MIS 5 foraminifer mean is based upon the two clusters of foraminifers at the Chart House field site (see above). Also provided are the TL ages of Griffin Road (this thesis), Clayton Water Tower and Point Sturt (Murray-Wallace *et al.*, 2010) and the OSL age of Point McLeay (this thesis). The whole-rock sample results compare well and with the TL ages support the conclusion of Chapter 4 that Sturt Peninsula is composed predominantly of MIS 7 aeolianite which extends seaward onto northern Hindmarsh Island. *Discorbis* foraminifers exhibit a loss or degradation of amino acids resulting in GLX D/L values within the 1 σ uncertainty of the Chart House foraminifer clusters (circled in red). These foraminifers were not included in the field site summary, Table 6.10. The foraminiferal results for Point McLeay A1 and more inland sites are discussed in text.

succession (PM A3 and PM A2) and Mount Misery by thermoluminescence returned minimum ages (Table 6.1). The results of whole-rock sample, individual foraminifer and thermoluminescence analyses of MIS 7 sedimentary successions are presented before the results of older sedimentary successions. The results of foraminifer analyses from all middle to early Pleistocene field sites are presented in Table 6.10 for comparison.

6.4.4.1 MIS 7

The whole-rock sample results from Sturt Peninsula are in good agreement and are further supported by the results of TL analyses (Table, 6.8, Figure 6.11). The Point Sturt and Clayton Water Tower successions had been previously analysed by Murray-Wallace *et al.* (2010) to respective ages of 230 ± 50 ka (W-2345) and 215 ± 35 ka (W-2346). The age of Griffin Road, positioned on Sturt Peninsula between the former two sites, at 209 ± 21 ka (W4782) further supports the interpretation of the peninsula as a predominantly MIS 7 barrier. Foraminifer analyses from these sedimentary successions were inconsistent. The foraminifers from Riverside Calcrete A and Clayton Water Tower are robust and similar to those GLX D/L values (>0.400) from Goolwa Bridge Calcrete, Riverside Calcrete B and Knights Beach which were considered reworked or indicative of MIS 7 (section 6.4.3.3). The D/L values of the remaining foraminifers from MIS 7 successions are lower than expected, with some comparable to the MIS 5e Chart House foraminifer clusters. It is unlikely that these aeolianites pre-date MIS 7 given their morphostratigraphy and relationship to other sedimentary successions in the surrounding landscape (section 4.3.4). All of the chromatography results from these foraminifers indicate low concentrations of amino acids with most peaks falling below 100 lumens. This indicates a degradation of the low molecular peptides and amino acids. Interestingly, the *Elphidium* sp. analysed at Clayton Road are robust and indicates that the genus may exhibit better preservation potential than *Discorbis*.

An additional MIS 7 deposit identified in this research is the siliceous sand at Myrtlegrove Road on the margin of Currency Creek, seaward of Sturt Peninsula. The lithology of the sand suggests it is equivalent to the alluvial Pooraka Formation (section 3.7.7 and 4.3.5). Analysis by TL provided an age of 227 ± 24 ka (W4779) correlating it to the Sturt Peninsula aeolianites and indicating terrestrial sediments were being supplied to the coastline during MIS 7. This age predates the MIS 5e estuarine deposit located

immediately to the north (Table 6.6) and the oldest recognised age (Last Interglacial) for the Pooraka Formation (Bourman *et al.*, 1997; 2010).

Global estimates of sea level for MIS 7 range from 2.5 m APSL (Hearty *et al.*, 1992) to as much as 6 m BPSL (Schellmann and Radtke, 2004). The Gambier Coastal Plain record provides the lowest estimate for MIS 7 sea-level, 9 ± 2 m BPSL (Blakemore *et al.*, 2015) which is significantly lower than the Coorong Coastal Plain record, which suggests a level similar to present (Murray-Wallace, 2002). If sea level was as low as suggested by Blakemore *et al.* (2015) then it is expected that the MIS 7 succession in the Murray Mouth region, a region of perceived ongoing subsidence, would have been overcome by the last interglacial highstand. The preservation of MIS 7 aeolianite across Sturt Peninsula is supportive of higher estimates of sea level for the interglacial; although, the inundation of the MIS 7 alluvial deposit by the MIS 5e lagoon, as indicated by the depositional record at Myrtlegrove Road, and the stratigraphic record at Riverside does support a lower than MIS 5e sea level during MIS 7. The variable MIS 7 sea-level record across the Coorong Coastal Plain reflects the influence of neotectonics in the preservation of sedimentary successions and the difficulty in identifying terrestrial indicators of past global sea-level free from post-depositional influence.

6.4.4.2 Inland sedimentary successions

Foraminifera were picked from the whole-rock sediment of six sedimentary successions of middle to early Pleistocene age: Point McLeay unit PM A1, Mount Misery, B-McIntosh Road, North Coonalpyn, Emu Springs and Tauragut Well (Figure 6.10). Of one hundred and thirteen tests chosen for analysis, only six produced D/L values that were considered acceptable (Figure 6.11). The majority of foraminifera were rejected for contamination by non-indigenous amino acids, either due to recrystallisation or the degradation of amino acids due to age. The accepted D/L results from Point McLeay PM A1, B-McIntosh Road, North Coonalpyn and Emu Springs are nearing complete racemisation (Figure 6.11), testifying to the greater age of the inland deposits.

The PM A1 aeolianite had previously been analysed by TL (Murray-Wallace *et al.*, 2010) and returned an age of 470 ± 70 ka (AdTL01007). Due to the large uncertainty which could correlate the aeolianite to MIS 11 (367-440 ka), MIS 13 (472-502 ka) or MIS

15 (542-592 ka), an OSL sample was taken in this research. The OSL result of 421 ± 48 ka (UOW-1296) indicates deposition of the dune during MIS 11. This age is well beyond the typical OSL age range of 100 ka to 200 ka (section 6.2) and is likely a reflection of the low dose rate (0.512 ± 0.053 , Table 6.1). Although the uncertainty could correlate the dune to MIS 10 or MIS 12, this is considered unlikely. The inclusion of skeletal carbonate grains and foraminifer, although not recognisable to a genus level, indicates deposition during a sea-level highstand. Furthermore, PM A1 is positioned between two units of *terra rossa* soil which are more typical of glacial period deposition (section 3.6.2 and 4.3.5). The single result of AAR foraminiferal analysis cannot be confirmed as representative of MIS 11 without additional successful analysis. However, the GLX D/L value of 0.652 is comparable to the MIS 7 whole-rock analyses and foraminifers from Riverside Calcrete A and Clayton Water Tower (Figure 6.11) suggesting the foraminifer is not be representative of the much older interglacial.

TL samples were taken from units PM A2 and PM A3, overlying PM A1 and separated from the older unit by *terra rossa* soil. The stratigraphic position of the two units beneath the last interglacial PM A4 and PM A1 (section 4.3.5) suggest deposition during MIS 7 or MIS 9. The TL ages for PM A2 ($\geq 83.1 \pm 3.7$ ka, W4786) and PM A3 ($\geq 92.4 \pm 3.5$ ka, W4785) represent minimum ages only, the grains having been saturated due to high radiation ($2.413 \pm .033$ and $2.169 \pm .031$ respectively, Table 6.1). The annual radiation dose in the study area is variable (between $0.512 \pm .053$ Gy/ka and $2.413 \pm .033$ Gy/ka) and much higher than the palaeodose across the Coorong Coastal Plain to the southeast, which ranges between $0.380 \pm .03$ Gy/ka and $0.650 \pm .03$ Gy/ka (Huntley *et al.*, 1993; 1994). Of additional interest, the minimum ages are inverted with the apparently older sample (PM A2) due to stratigraphic position, having a younger minimum age than the above sample (PM A3).

The Mount Misery site is another aeolianite that had been dated using the TL method previously (Murray-Wallace *et al.*, 2010) yielding an age of 350 ± 65 ka (AdTL01006), suggesting a correlation with either MIS 9 (297-347) or MIS 11 (367-440 ka). The minimum age TL result from this research of $\geq 366 \pm 47$ (W4787) indicates deposition occurred within or before MIS 11 with potential for contemporary deposition to PM A1. The relatively low dose rate at Mount Misery ($0.729 \pm .026$, Table 6.1)

returning a minimum age implies that the age of the succession is near the limit of TL ability.

Mount Misery is unique compared to other TL samples from this research in that its quartz displays different TL energy characteristics (Figure 6.12) (David Price, personal communication 29 August 2014). The different TL spectra characteristics exhibited by quartz grains when heated reflect different impurities at different concentrations within the grains and indicate different conditions under which the grains were formed; i.e. the sediment has a different origin or has undergone different environmental processes (Price, 1994).

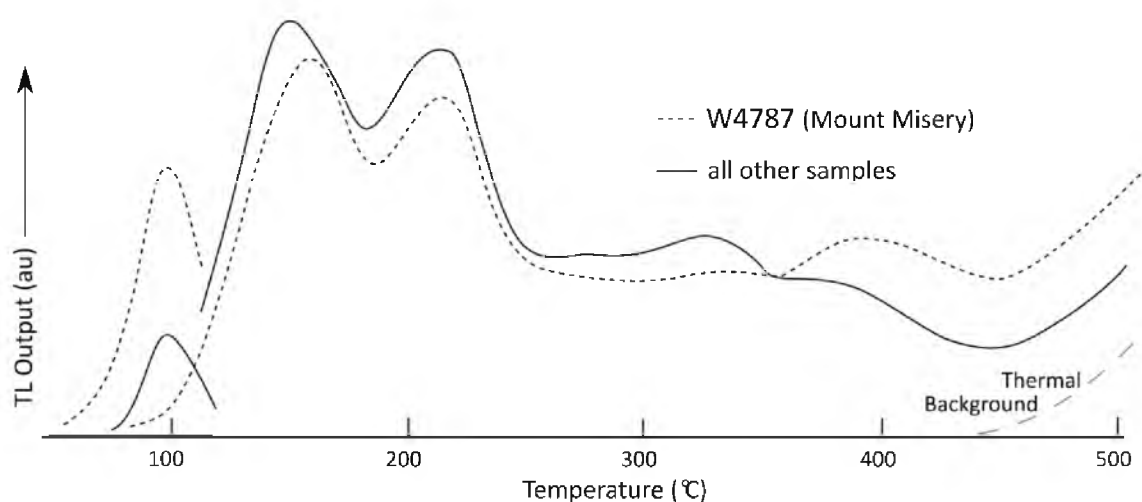


Figure 6.12: Second glow TL glowcurves following 20.07 Gy irradiation demonstrating the different TL energy characteristics of quartz grains from Mount Misery in comparison to quartz from all other TL samples in this thesis.

6.4.4.3 Summary

The MIS 7 age of the sedimentary succession forming Sturt Peninsula, which extends southward onto northern Hindmarsh Island, is indicated by morphostratigraphy and supported by TL analyses in previous research (Murray-Wallace *et al.*, 2010) and this thesis. Whole-rock D/L values are consistently greater than the whole-rock mean for MIS 5 (*sensu lato*) also indicating MIS 7 deposition. Foraminifer results from Clayton Water Tower (Sturt Peninsula) and Riverside Calcrete A (northern Hindmarsh Island) are similarly robust and greater than the foraminifer mean for MIS 5. The inconsistency in foraminifer results from the other MIS 7 locations (Clayton Bay Road, Griffin Road and

Point Sturt) is attributed to low concentrations of amino acids due to the degradation and diffusive loss of amino acids and low molecular peptides. The results of individual foraminiferal analyses indicate that *Elphidium* sp. may have better preservation potential than *Discorbis* sp. but further analyses will be required to confirm this.

Analysis of PM A1 by the OSL method indicates deposition of the unit within MIS 11. Additional analysis is recommended to confirm the validity of this result but it does fit well within earlier TL analysis and the interpreted stratigraphy of sedimentary succession at Point McLeay. Additional geochronological analysis is needed throughout the Point McLeay succession to further constrain the record of interglacial and glacial deposition preserved there but is hampered by the steep slope of the cliff.

The GLX D/L values of individual foraminifers from inland field sites indicate a greater age for the sedimentary successions and support the potential early Pleistocene age as proposed in Chapter 4 (section 4.3.6). Determining the age of the exposures will require geochronological methods with a greater age range than was applied in this thesis. The Mount Misery aeolianite is the most seaward of the inland deposits and the geochronological analysis applied there serves as a sort of litmus test to its applicability to the more inland (and older) deposits. The Mount Misery aeolianite has been analysed by means of TL and AAR analysis of whole-rock and foraminifera. AAR whole-rock analysis within the study area appears to be applicable only to MIS 7 and was unsuccessful in older successions due to apparent leaching and degradation of indigenous amino acids and contamination. The analysis of foraminifera at Mount Misery was unsuccessful and it was determined that the samples were too altered by diagenetic processes as they appeared recrystallised under binocular microscope and nearly all samples showed evidence of nonindigenous contamination. The near racemic results for the more inland field sites indicate greater ages for these successions than those more seaward but do not allow further refinement of the depositional record. The TL results at Mount Misery indicate deposition during MIS 11 but the lack of confidence around the age implies that the dune is at the upper limit of TL analysis for the region. The MIS 11 aeolianite at Point McLeay, dated by OSL (this research), is near saturation and the upper limit for that technique as well. These results indicate that application of

TL and OSL to the older inland dunes would also be unsuccessful and would require a different form of geochronological analysis.

6.4.5 Conclusions

Comparison of all AAR analyses shows a strong correlation amongst shell and whole-rock results with clear and distinctive clusters (Figure 6.11). AAR analysis of mollusc shell is more consistent in the region than either whole-rock or foraminifer analyses showing minimal variability with interglacial periods clearly recognisable. However, due to the subsidence in the region, the mollusc shell record has not been extended beyond MIS 5e. Also, the range in results of whole-rock and individual foraminifer analyses is a reflection of the high potential for reworking within the region and, in low-lying areas, leaching. The ongoing subsidence and return of sea-level highstands with successive interglacials to within 6 m of current level (Belperio and Cann, 1990; Murray-Wallace *et al.*, 2001) has promoted the stacking of sedimentary successions of antecedent interglacial and intervening glacial periods and the reworking of sediments from older deposits. The extensive reworking in the region indicates the palimpsest nature of the sediments there.

The last interglacial shoreline (*sensu stricto*) is the most visible of Pleistocene shorelines within the study area due the high sea level during the interglacial and insufficient time for subsidence and reworking to occur. The preservation of the MIS 7 barrier on Sturt Peninsula is in support of higher estimates of sea-level for the interglacial. The relative lack of other middle Pleistocene sedimentary successions (except at Point McLeay) implies that the gentle subsidence in the region requires two interglacial periods for a barrier complex to diminish in the landscape (provided it is not removed by erosion), similar to the required two interglacial periods for a barrier complex on the southeast Coorong Coastal Plain to uplift above the influence of younger shorelines (Murray-Wallace *et al.*, 2001).

A TL age at Myrtlegrove Road confirms deposition of an alluvial fan during MIS 7. The D/L values of the lagoonal deposit north of the siliceous sand indicate the low-lying region behind the dune was inundated during the Last Interglacial. This is likely given that the last interglacial period is expected to have been wetter than present

(Nanson *et al.*, 1992; Bourman *et al.*, 1997; 2010; Fujioka and Chappell, 2010; Cohen *et al.*, 2011) and, as indicated by this research (section 5.8.4), the Goolwa Channel was farther to the west and the River Murray Mouth would have been located nearer to the Myrtlegrove Road field site. The inundation of the MIS 7 alluvial fan by the later MIS 5e lagoon deposit indicates a change in base level between the two interglacials, supporting the higher sea-level record of MIS 5e.

Age determination for the units within sedimentary succession at Point McLeay and the more inland field sites is currently largely dependent upon lithology, stratigraphic interpretation and the near racemic results of individual foraminifer analyses. This indicates that these sedimentary successions there are potentially beyond the capabilities of the AAR method and other geochronological analytical methods applied in this research limiting age-determination (within this research) to morphostratigraphic and geographic interpretation.

The results of geochronological analyses reported in this chapter are discussed in the context of previous research related to deposition of the Bridgewater Formation on the Coorong Coastal Plain and Kangaroo Island in the following chapter. The discussion explores the geomorphological evolution of the River Murray terminus region throughout the cyclic changes of eustatic sea-level and climate change of the Quaternary. It will also consider the development of the River Murray mouth and lakes in a landscape shaped by subtle yet ongoing neotectonics.

Chapter 7

Quaternary landscape development of the River Murray terminus, Southern Australia and correlation with the sea-level record of the Coorong Coastal Plain

7.1 Introduction

This chapter builds upon the content of previous chapters to discuss the Quaternary geomorphological development of the River Murray terminus. The depositional history within the region is complex as it is affected by ongoing Quaternary neotectonism, the presence of the River Murray and the environmental changes associated with eustatic sea-level fluctuations and climatic changes. Correlating the successions of Bridgewater Formation within the study area with those across the Coorong Coastal Plain to the southeast assists in developing understanding of the Quaternary landscape evolution across the entire length of the coastal plain, which spans more than 300 km in length and 90 km in width. Between Robe and Naracoorte, where the coastal plain reaches its greatest width, the beach-barrier successions of Bridgewater Formation are preserved as composite range structures, generally formed over two interglacial periods, separated by associated back-barrier lagoon and/or lacustrine deposits which have been used to develop one of the longest terrestrial records of Quaternary sea-level highstands (Huntley *et al.*, 1993; 1994; Murray-Wallace *et al.*, 2001). The distribution and preservation of the Bridgewater Formation across the Coorong Coastal Plain indicates that regional neotectonics have played a large role in the development of the region with the barriers ranges coalescing and losing expression in the northern coastal plain, where the course and position of the palaeo-River Murray and coastal lakes have also been affected.

The chapter begins with the correlation of Pleistocene Bridgewater Formation in the northern coastal plain with the record of the Bridgewater Formation between Robe and Bordertown, approximately 160 km to the southeast. This discussion is followed by a review of and association with global sea-level highstands throughout the Pleistocene using the oxygen isotope scheme of Lisiecki and Raymo (2005) and the EPICA Dome C ice core record (Masson-Delmotte *et al.*, 2010). The deposition and distribution of the glacial period aeolian Molineaux Sand is discussed followed by the development of the River Murray. This chapter finishes with a list of major conclusions from this research and ideas for future research.

7.2 Correlating the Bridgewater Formation successions within the Murray Lakes region with the Robe-Naracoorte record

Correlation of the sedimentary successions of the Bridgewater Formation at the northern end of the Coorong Coastal Plain with their southeastern counterparts has been hindered by the glacial Molineaux Sand, which blankets the regional landscape obscuring the interglacial record, and the apparent ongoing subsidence within the Murray Lakes Region. However, when considering the northern Coorong Coastal Plain the arcuate shape and size of the Murray Lakes Range and the Coonalpyn Range are distinct features within the landscape (Figure 7.1). These barrier dune ranges are associated with the Padthaway Ridge, a horst-like structure of Late Cambrian-Ordovician granitoids forming the diffuse boundary between the Murray Basin and the Gambier Basin. The Padthaway Ridge has repeatedly, since the Palaeocene, served as a laterally extensive high and natural breakwater or archipelago during marine incursions into the Murray Basin, as well as loci for sediment deposition (section 2.3). The Coonalpyn and Murray Lakes Ranges remain preserved within the landscape, whereas the dunes to the south and west coalesce and lose topographic expression as they approach the Murray Lakes region. These dunes are traced to the southeast where Bridgewater Formation was deposited across the Coorong Coastal Plain between Robe and Naracoorte from MIS 17 and later (Huntley *et al.*, 1993; 1994; Murray-Wallace *et al.*, 2001), i.e. those dunes deposited after the West Naracoorte Range.

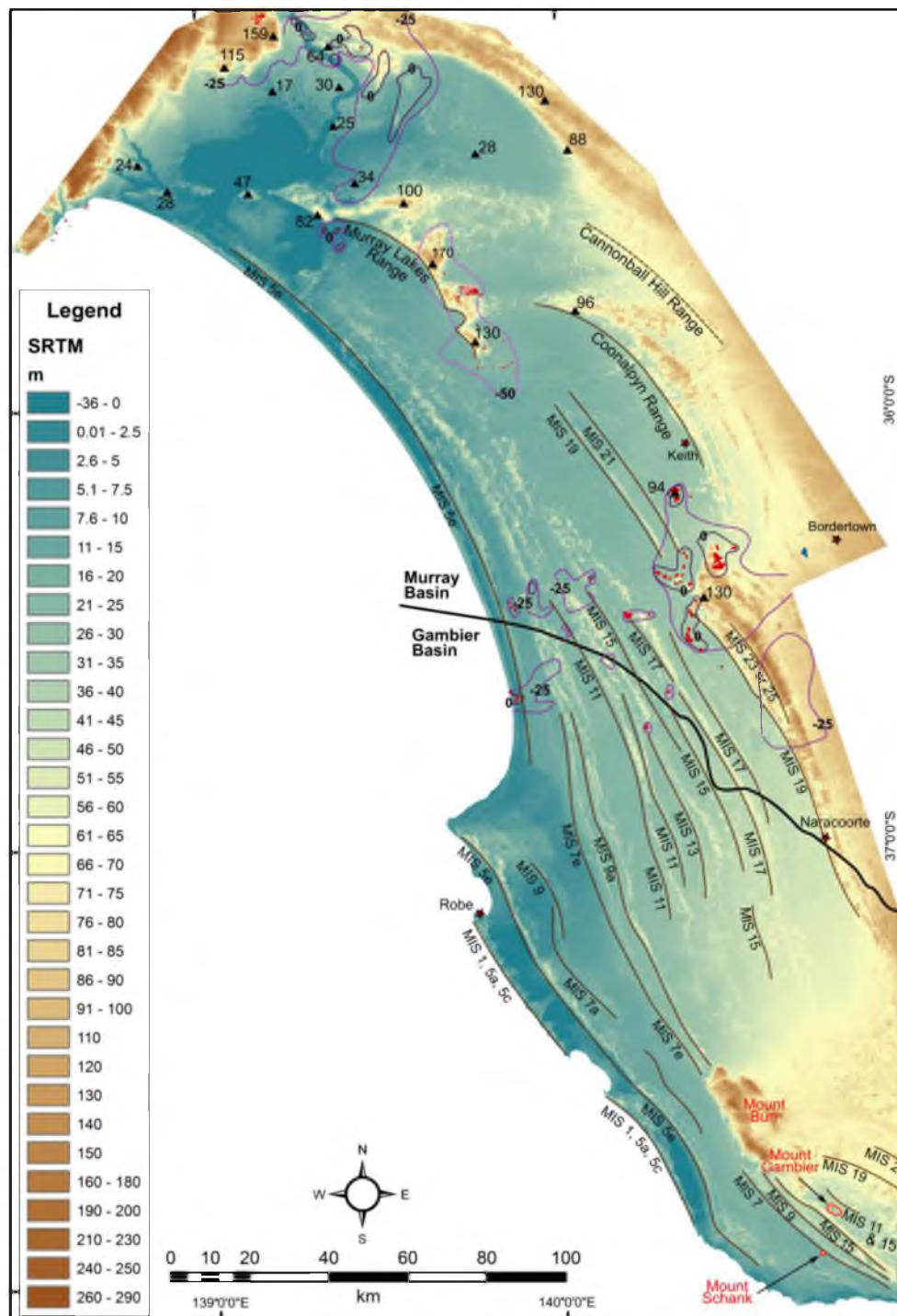


Figure 7.1: SRTM image of the Coorong Coastal Plain in which the distinct coastal landform features of the Bridgewater Formation are visible. Note that not all the barriers are present in a single line of transect reflecting the subtle differential rates of uplift along and across the coastal plain as recognised by Hossfeld (1959). The Middle to Late Pleistocene record is preserved as distinct ranges between Naracoorte and Robe. Early Pleistocene Bridgewater Formation has been identified at Naracoorte and between Bordertown and Keith. Late Cambrian-Ordovician granitoids (red = at surface) form the Padthaway Ridge (purple = depth to pre-Cenozoic successions), a diffuse boundary between the Murray Basin and the Gambier Basin, extending northwards to the Mount Lofty-Flinders Ranges. The Padthaway Ridge has been a locus for sediment deposition throughout the Cenozoic. Spot heights (triangles) in metres are from the 1:250,000 Baker (Thompson and Horwitz, 1962), Pinnaroo (Rogers, 1979) and Naracoorte (Rochow, 1969) geological sheets.

An understanding of the northern Coorong Coastal Plain development is not possible without the consideration of the neotectonics that have influenced deposition of the Bridgewater Formation throughout the Quaternary (Chapter 2) and is briefly revisited here. Uplift along the southern margin of Australia is related to continental tilt (section 2.3.4) and the more localised epeirogenic uplift associated with Quaternary volcanism in the Mount Burr-Mount Gambier region resulting in broad regional doming (Sprigg, 1952, Cook *et al.*, 1977; Murray-Wallace *et al.*, 1998; section 2.5.3). Rates of uplift across the coastal plain are dependent upon the proximity to the centre of volcanism and decrease northwards (Murray-Wallace *et al.*, 1998). As an illustrative example, the back-barrier lagoon facies associated with the Woakwine Range decreases from a maximum height of 18 m APSL at its southern extremity, to 8 m APSL at Robe, 3 m APSL at Salt Creek, 1 m APSL at Hindmarsh Island (Murray-Wallace *et al.*, 1998) and less than 1 m at Goolwa (section 4.3.3.2). Uplift has also occurred normal to the shoreline allowing the preservation of sea-level highstands in transect across the coastal plain from Robe to Naracoorte (Belperio and Cann, 1990; Murray-Wallace *et al.*, 1998). Regional uplift associated with volcanism before the deposition of the West Naracoorte Range on the Coorong Coastal Plain is made evident by the recurved palaeo-shoreline around the Mount Burr volcanic province and the erosive modification of the volcanic group by Pleistocene high sea levels (Murray-Wallace *et al.*, 1998; Blakemore *et al.*, 2015).

Subsidence at the Murray Mouth has been occurring since the Last Interglacial at a rate of 0.02 mm yr^{-1} with downtilting towards the region occurring from the southeast coastal plain and also from the western Fleurieu Peninsula (Bourman *et al.*, 2000). Transpressional deformation, which is driving the uplift of the Mount Lofty-Flinders Ranges, is also causing downwarping and the depression in which the River Murray and Lakes Alexandrina and Albert occur (Sprigg, 1952; James *et al.*, 1992; Jayawardena, 2013). Subsequent sediment loading is also likely to be causing additional subsidence. Given that the uplift of the Mount Lofty Ranges was initiated before the commencement of the Quaternary (section 2.3.4) and that doming to the southeast had occurred prior to the deposition of the West Naracoorte Range (MIS 19), it could be expected that

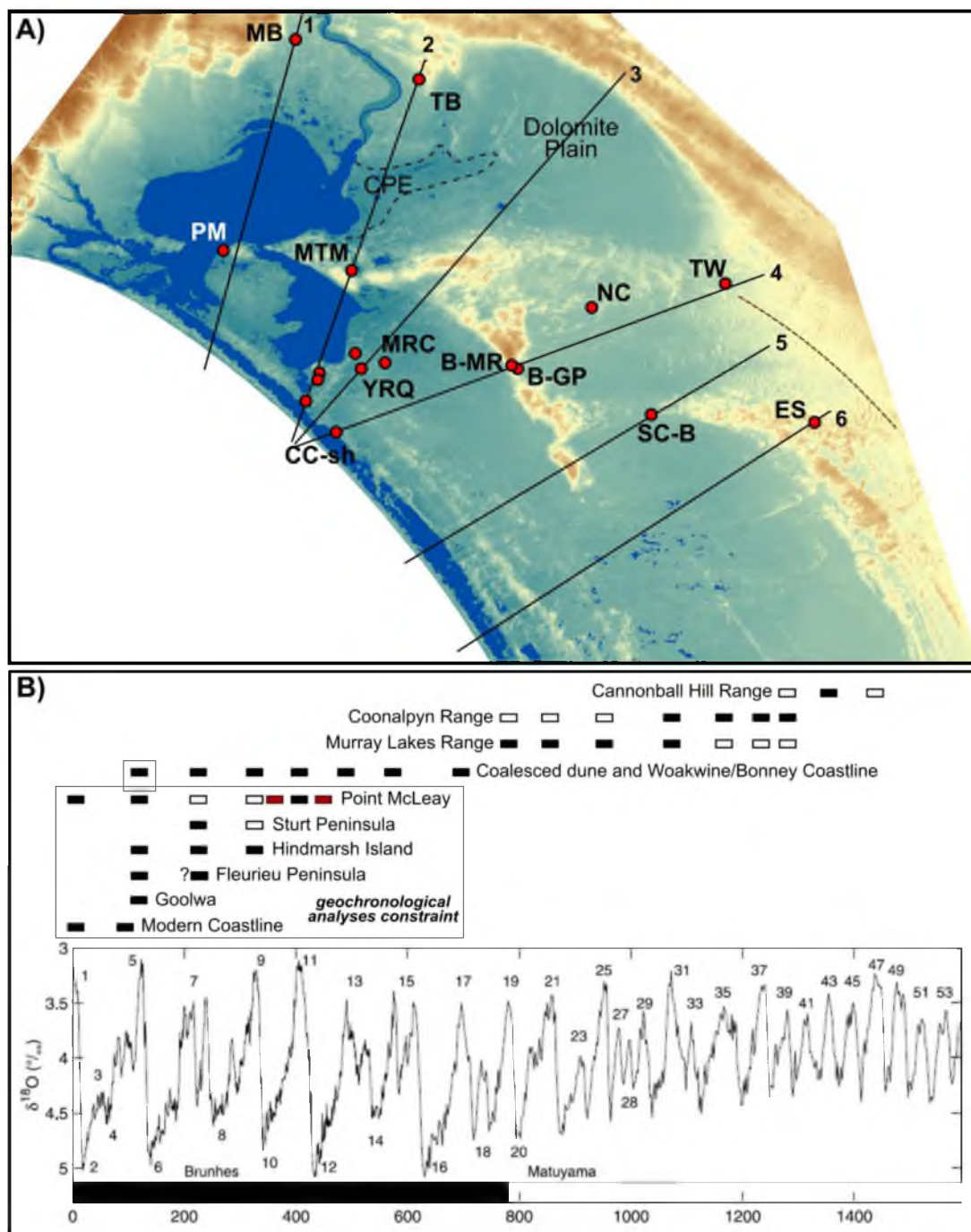


Figure 7.2: A) closer view of the northern Coorong Coastal Plain and features. The location of topographic transects (Figure 7.3) derived from SRTM data is provided. Field sites discussed in text or indicated in Figure 7.3 are labelled. CPE = Cooke Plains Embayment. B) The correlation of coastal barrier ranges in the northern coastal plain to the oxygen isotope record developed by Lisiecki and Raymo (2005) and discussed in text. The age of the barrier features within the more immediate region surrounding the Murray Mouth have been constrained by geochronological analyses (amino acid racemisation and luminescence methods) by Murray-Wallace *et al.* (2010) and in this research. The presence of MIS 7 aeolianite on Fleurieu Peninsula is questionable. The interstadial within the modern coastline refers to Surfer Beach and the calcrete inlier to Sir Richard Peninsula (this research) and likely to Younghusband Peninsula. The correlation of the older more inland regions and coalesced dunes is based upon geographic, morphostratigraphical and chronostratigraphical methods. Black squares indicate a strong correlation and white square a more tenuous association.

downwarping in the Murray Mouth region and the differential uplift along the length of the coastal plain began before the initiation of MIS 19 at 790 ka.

In this section, Bridgewater Formation successions of the northern Coorong Coastal Plain are correlated to the Robe-Naracoorte record and the record of early Pleistocene Bridgewater Formation between Naracoorte and Bordertown (Figure 7.2) using geographic, morphostratigraphical and chronostratigraphical correlation, building upon the conclusions of previous research and contributing new insights into the development of the northern Coorong Coastal Plain. A series of transects (Figure 7.3) across the northern coastal plain were derived using SRTM data (Commonwealth of Australia, Geoscience Australia; 2009) to assist in the establishment of relationships between the sedimentary successions in the north and the south, which has been hindered by the changing geomorphological expression of the barrier dunes in the landscape. Between Robe and Naracoorte, the well-preserved coastal barriers typically crest 20-30 m above the coastal plain, reach between 1 and 3.5 km in cross-sectional width and are, on average, spaced 10 km apart (Murray-Wallace, 2002). However, as will be shown, in the northern coastal plain the middle Pleistocene barriers coalesce and lose topographic expression to produce a gently undulating landscape, whereas the early Pleistocene barriers far exceed the height and width dimensions of their younger counterparts to the south. The transects help to expose subtleties within the landscape that had not been previously identified. The connection of the sedimentary records across the coastal plain facilitates synthesis of interglacial deposition within the Murray Lakes region. It is stressed that this section discusses development of the northern Coorong Coastal Plain specifically within the context of the coastal plain and the rates of uplift and sea-level change observed there. The discussion of northern Coorong Coastal Plain development in the context of global eustatic sea-level change occurs in the following section.

7.2.1 Early Pleistocene Bridgewater Formation and associated deposits

Early Pleistocene Bridgewater Formation to the southeast of the study area includes the East Naracoorte Range (Figure 7.1) located north of the Kanawinka Escarpment and those ranges found farther to the east. The age of the East Naracoorte Range has been determined by palaeomagnetism (Idnurm and Cook, 1980) and, as with

the more eastern ranges, correlation with oxygen isotope record (Belperio and Cann, 1990; Murray-Wallace *et al.*, 2001; Bowler *et al.*, 2006).

The most evident characteristic of the early Pleistocene ranges is their varying orientation along the length of the Coorong Coastal Plain compared with the middle Pleistocene and younger ranges (Figure 7.1). The change in orientation has been associated (Bowler *et al.*, 2006) with differential uplift along the Padthaway High (note: not the Padthaway Ridge) and Pinnaroo Block in the formation of the Marmon Jabuk-Kanawinka Escarpment, which marked the limit of a late Pliocene-early Pleistocene marine incursion (Chapter 2). Continued differential uplift of these features since then would have contributed to the varying rates of uplift across the coastal plain and the changing orientations of the shoreline.

The Coonalpyn and the Murray Lakes Ranges form two large arcuate shorelines in the middle to northern coastal plain. The size of the ranges in comparison to their younger counterparts across the Robe to Naracoorte transect suggests that they are composite features composed of multiple barrier structures formed over multiple interglacial periods. The ranges exceed 10 km in width, reaching heights in excess of 75 m above the surrounding coastal plain (Figure 7.3 Transect 6). The height of the early Pleistocene ranges may be attributed to their position north of the Marmon Jabuk-Kanawinka lineament and the Padthaway Ridge but is also suggestive of a larger supply of sediment available during coastal barrier formation and/or multiple phases of deposition. The differential rates of uplift, which have affected the middle to late Pleistocene Bridgewater Formation, appear to have been in effect during the early Pleistocene as the composite nature of the ranges becomes more evident in a southerly direction where individual strandlines become more discernible (Figure 7.1).

The lack of geochronological constraints (this study only utilised amino acid racemisation analysis of individual foraminifers returning near racemic D/L values) on the inland field sites of the northern coastal plain require considerations regarding the timing of deposition and correlation to the sedimentary successions on the Coorong Coastal Plain to the southeast to be based upon geographic and morphostratigraphic relationships.

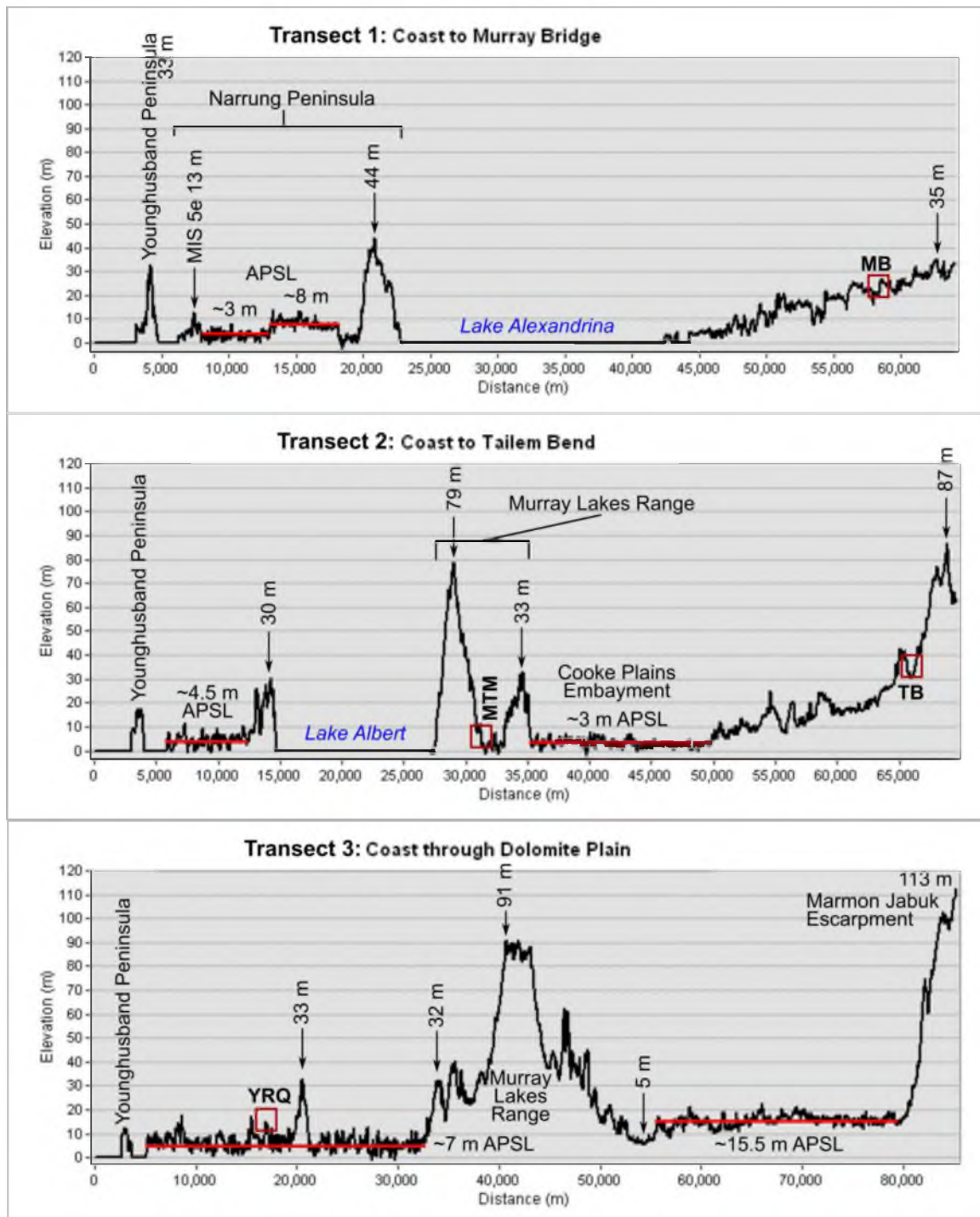


Figure 7.3: Topographic transects of the northern Coorong Coastal Plain derived from SRTM data from north to south numbered 1 through 6 (Figure 7.2). The transects highlight and expose features in the landscape not highly visible on the SRTM. Red boxes indicate the approximate position of a field site in transect. Note the y-axis extends to the same elevation on all transects but the x-axis differs with each transect. The heights provided are as height above '0' or sea-level and not height

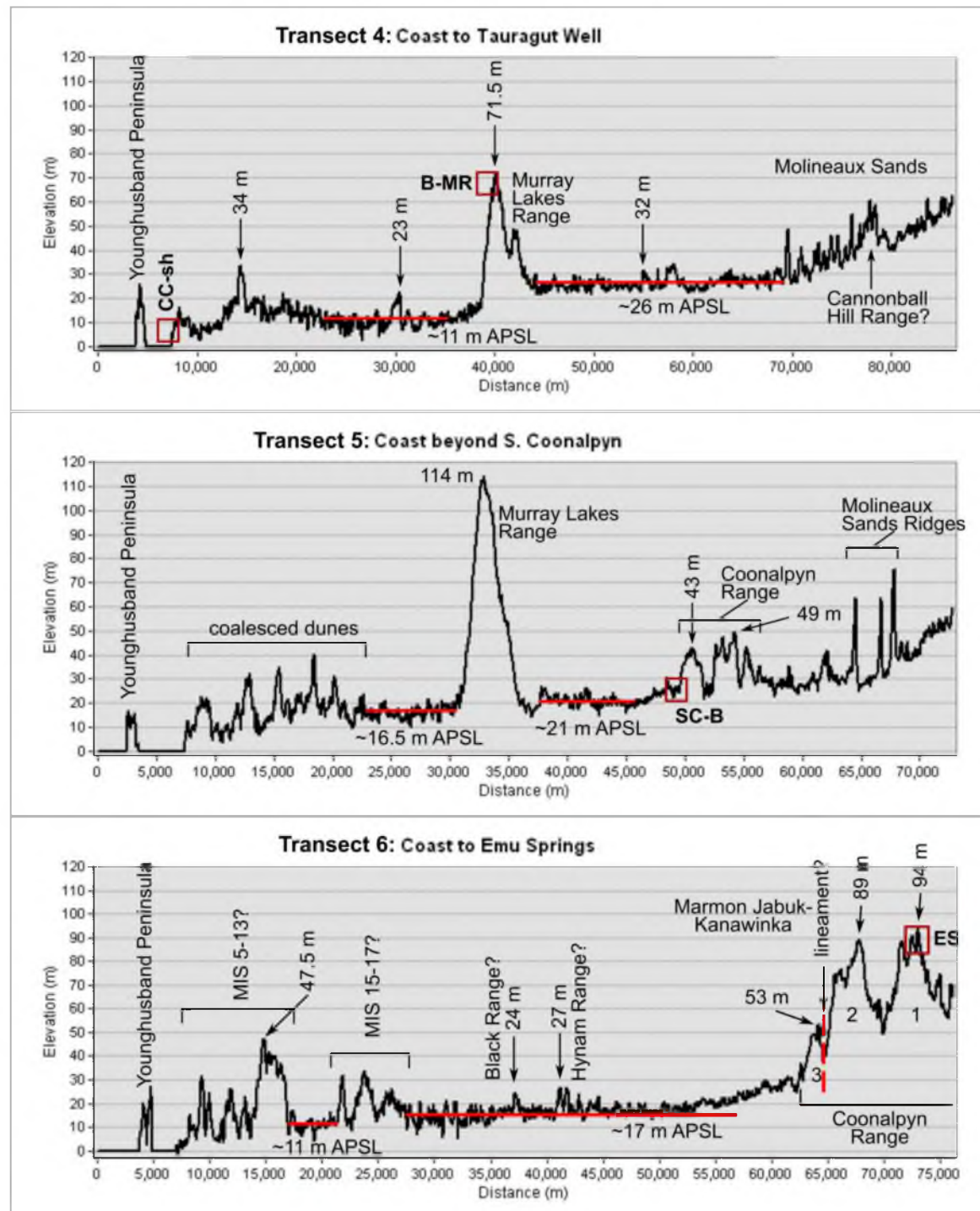


Figure 7.3 *continued*: above the coastal plain. The coastal plain to the east of the Murray Lakes Range reaches an elevation up to 15 m higher than the coastal plain seaward of the Murray Lakes Range (Transect 4) likely reflecting a more shallow depth to pre-Cenozoic successions (Figure 7.1). The progressive coalescing of the middle Pleistocene barriers is visible in Transects 6-4. The 33 m high in Transect 3 is directly to the west of the McIntosh Road (MRC) field site.

7.2.1.1 Cannonball Hill Range

The Cannonball Hill Range (Bowler *et al.*, 2006) was first identified as the earliest facies of the Bridgewater Formation and correlated to MIS 43 or 47 near 1.3 – 1.4 million years ago based on the previous correlation of the East Naracoorte Range to MIS 25 by Murray-Wallace *et al.* (2001) (Figure 7.2). Blakemore *et al.* (2015) have since correlated the East Naracoorte Range to deposition of the Dismal Range to the southeast and MIS 23 implying a possibly slightly younger age for the Cannonball Hill Range of MIS 39 or 43 (1.27 – 1.35 Ma; Lisiecki and Raymo, 2005).

The exposure identified in this thesis at Tauragut Well geographically conforms to the Cannonball Hill Range and also lies within the region at the base of the Marmon Jabuk Escarpment that Rogers (1979; 1980) identified as the earliest Bridgewater Formation underlying Molineaux Sand. The field site occurs at ~40 m APSL as a shallow outcrop, reaches 110 cm in height, is capped by a thin laminar calcrete and lacks the vibrant colour exhibited by some of the other inland deposits of Bridgewater Formation (e.g. North Coonalpyn, South Coonalpyn and Emu Springs) (section 4.3.6). Calcrete development however, is locally variable depending on underlying lithology and landform (Milnes, 1982), while the lack of diagenetic indicators such as colour and hardness characteristic of mature calcretes could be due to the low carbonate content (12%) of the sediment.

The Cannonball Hill Range described by Bowler *et al.* (2006) is east of the Kanawinka Escarpment located near Bordertown (Figure 7.1) and is at least 80 m APSL based on the elevation of lagoonal sediments landward of the East Naracoorte Range (Murray-Wallace *et al.*, 2001), a much higher elevation than Tauragut Well. However, Transect 4 (Figure 7.3) indicates a possible barrier dune feature in the vicinity of the field site. Under the assumption that deposition of the Cannonball Hill Range crossed the lineament of the Marmon Jabuk-Kanawinka Escarpment, and given the more northerly location of the Tauragut Well field site compared with the Cannonball Hill site as indicated by Bowler *et al.* (2006), then the former site could have been subjected to the differential rates of uplift that occur across the coastal plain. Assuming that Tauragut Well is equivalent to the Cannonball Hill Range, this would imply subsidence (as a reflection of the different rates of uplift along the length of the coastal plain) of the

coastal plain at Tauragut Well in excess of 40 m since deposition of the coastal barrier ridge at ~ 1.27 Ma; >0.031 mm/yr⁻¹.

If the Cannonball Hill Range had been deposited across the Marmon Jabuk-Kanawinka lineament at 1.27 – 1.35 Ma, it implies that displacement of the Kanawinka Fault at 2.2 Ma (Singleton *et al.*, 1976) was not continuous along the length of the lineament or that the height of displacement was insufficient to affect the deposition and orientation of the barrier. Although, the correlation of Tauragut Well to the Cannonball Hill Range is tentative, it indicates that the northern Coorong Coastal Plain also retains a record of the earliest deposition of the Bridgewater Formation.

7.2.1.2 Coonalpyn Range

Bowler *et al.* (2006) identified up to six additional coastal barrier ridge systems between Cannonball Hill and the East Naracoorte Range, which make up the southern extent of the Coonalpyn Range between Keith and Bordertown and correlated them to interglacial high sea levels at MIS 31, 35, 37 and 39. Sprigg (1952) identified multiple units of Bridgewater Formation within the West Naracoorte Range and it was suggested by Cook *et al.* (1977), after the identification of intervening palaeosols, that the units separated into four discrete ridges within the Coonalpyn Range. However, it has been shown that the West Naracoorte Range is of normal polarity while the East Naracoorte Range and those farther to the east are of reversed polarity (Idnurm and Cook, 1980). Furthermore, the West Naracoorte Range is located at the base of the Kanawinka Escarpment, while the older ranges are found on the higher relief surface to the east (Sprigg, 1952; Bowler *et al.*, 2006) confirming movement along the escarpment before the earliest deposition of the West Naracoorte Range. This evidence suggests that the West Naracoorte Range cannot be correlated with the ridge systems south of the Coonalpyn Range.

Transect 6, which crosses the Coonalpyn Range from west to east, indicates the presence of up to three distinct barrier features within the northern end of the range (Figure 7.3). The height of the crests of the two more easterly barrier ranges above the seaward coastal plain (72 - 77 m) suggests that these features are located to the east of the Marmon Jabuk-Kanawinka lineament and correspond with the ridge systems

between Cannonball Hill and the East Naracoorte Range. The third barrier range crests at a significantly lower height above sea level than the former two ranges (~36 m above the coastal plain) and is likely to lie west of the lineament. The former two ranges each exceed 5 km in width suggesting that they are composite features. In contrast, many of the ranges on the Coorong Coastal Plain are composite features reflecting deposition over two interglacial periods yet do not exceed 3.5 km in width (Murray-Wallace, 2002). The westernmost and smallest range within the Coonalpyn Range complex, at over 2 km in width, is also potentially a composite feature. The Emu Springs field site identified in this thesis is located within the crest of the most easterly dune. The lithology of the sediments at Emu Springs indicates aeolian deposition near the source of carbonate grains (the inner shelf) (section 4.3.6.5) and therefore deposition before development of the range immediately to the west.

Assuming that the topographically high dunes within the Coonalpyn Range are a composite of pre-Naracoorte barriers and post-Cannonball Hill Range, the deposition of the Emu Springs Range corresponds to MIS 35 and/or 37 (assuming the latest deposition for the Cannonball Hill Range at MIS 39) with deposition of the second barrier in the transect deposited during MIS 31 and/or MIS 35. The third barrier in the transect may have been deposited, like the West Naracoorte Range, at the base of the lineament following movement and implies correlation to the more southern range.

Transect 5 shows the northern margin of the Coonalpyn Range to be at a much lower elevation than to the south, cresting at 28 m above the coastal plain, which is on average ~21 m APSL (Figure 7.3), with similar implications for rates of uplift along the length of the coastal plain as with the change in elevation of the Cannonball Hill Range between Bordertown and the Tauragut Well field site. The South Coonalpyn field site is located at the base of the northwestern tip of the Coonalpyn Range at 20-30 m APSL and exhibits diagenetic characteristics of a mature calcrete (diagenetic grade IV of V) (Hearty and O'Leary, 2008; section 4.3.6.4). The lithologies of the sediment, particularly the content of coarse quartz grains and large mollusc fragments (≤ 1 mm), are characteristic of a stranded beach ridge.

The coalescing of the discrete ridges between Keith and Bordertown to form the composite Coonalpyn Range further substantiates the notion of differential uplift across the coastal plain within the early Pleistocene. It also brings into question the location and expression of the Marmon Jabuk-Kanawinka lineament within the Coonalpyn Range through which it most likely passes.

7.2.1.3 Murray Lakes Range

The correlation of the Murray Lakes Range southeast of Lake Alexandrina is more complicated as it has a less visibly direct relationship with the dunes to the southeast, occupying a position on the coastal plain detached from the other ranges. The Murray Lakes Range reaches 170 m APSL and exceeds 6 km in width north of the B-McIntosh Road and Gravel Pit field sites (Figure 7.1, Figure 7.2). Transect 3 crosses the range further to the north where the range is less consolidated and reaches 20 km in width and over 90 m APSL (Figure 7.3). The size of the range indicates multiple phases of deposition. The arcuate shape of the Coonalpyn Range in plan, and the trend of the northern margin of the range towards the Murray Lakes Range in the vicinity of Ordovician granites (Figure 7.1) suggest that the northern Coonalpyn Range joined to the southern Murray Lakes Range, implying the same age for the ranges.

Two ranges, the Black Range and Hynam Range, extend northwards from the Naracoorte Ranges towards the southern margin of the Murray Lakes Range (Figure 7.1). These ranges are subtle features in the landscape and have not been described in any detail by previous authors. The ranges lose expression in the SRTM but Transect 6 indicates that these ranges extend farther north across the coastal plain and are likely joined to the granite outcropping in the southern Murray Lakes Range (Figure 7.3). Belperio and Cann (1990) correlated deposition of the Black and Hynam Ranges to the composite West Naracoorte Range and assigned preliminary ages by matching the barriers to the marine oxygen isotope record in association with known palaeomagnetic and geochronological (thermoluminescence) age constraints. The Hynam Range is referred to as the Mt Monster Range by Belperio and Cann (1990) but this thesis uses the earlier designation by de Mooy (1959). The Black Range was assigned to MIS 19. The Hynam Range was correlated to MIS 21. The subtlety of these ranges in the landscape

suggests that they were deposited during highstands of short duration or much lower sediment supply.

The Murray Lakes Range reaches a height of ~72 m APSL near the B-McIntosh Road (B-MR) and Gravel Pit (B-GP) field sites and crests to the north at 170 m APSL (Figure 7.3 Transect 4). The field sites are separated by a distance of less than 1.5 km, while a massive calcrete exposed in the intervening road cutting appears to be positioned stratigraphically between the B-McIntosh Road field site and the topographically higher gravel quarry site (section 4.3.6.2). The B-McIntosh Road field site is predominantly fine-grained with a minor fine-grained carbonate component indicating aeolian deposition some distance away from the marine source of carbonate. Blackburn *et al.* (1965) found that coarser sands on the coastal plain tend to be associated with the stranded beach ridges with finer sands occurring on the inter-ridge plains. Given the height of the sediments at B-McIntosh Road above the coastal plain, it is unlikely that the sediments were deposited as a back-barrier deposit, however, they could have been deposited on the lee-side (landward) of the coastal barrier dune. In contrast, the sediment from the overlying dune within the gravel quarry contains >50% rounded carbonate grains, fine-medium in size, composed of all faunal types with a reworked component and was likely deposited under higher energy conditions nearer to the coastline and inner shelf than the underlying B-McIntosh Road sediment (section 4.3.6.2). The distinct depositional environments of the two sites and intervening calcrete confirm the deposition of the Murray Lakes Range over a period of at least two interglacials and imply different palaeo-sea-level heights.

The transects show that the low-lying region landward of the Murray Lakes Range rises to an elevation of ~26 m APSL to the south of the dunes trending eastward from the range before dropping to ~15.5 m APSL at the dolomite plain to the north (Figure 7.3 Transects 3-5), indicating the presence of a topographic high landward of the Murray Lakes Range and a link to the eastern Coonalpyn Range. This is likely given the shallow depth of the Padthaway Ridge below the southern half of the Murray Lakes Range (Figure 7.1). The link between the two ranges indicates that the southern Murray Lakes Range was a locus for sediment deposition during the early Pleistocene.

The different rates of uplift along the northern to southern length of the Coorong Coastal Plain could explain the greater elevation above the surrounding plain exhibited by southern half of the range compared with the north, in a similar manner to the expression of the tilted last interglacial Woakwine and associated facies along the length of the coastal plain driven by uplift. Different rates of uplift at the northern end of the coastal plain also imply that development of the range could have proceeded in a sequentially northwards manner as the landscape eventually rose above the height of marine/estuarine inundation during periods of high sea-level. However it is difficult to quantify the rates of uplift, which would require geochronological constraint of the individual barriers within the Murray Lakes Range and the identification of lagoonal or intertidal facies, which could constrain sea level and allow comparison with southeastern coastal plain correlatives.

The coalescing of the MIS 17 and younger ranges of the Coorong Coastal Plain to the seaward side of the Murray Lakes Range, as indicated in the SRTM and transects, implies that sea level following MIS 19 did not extend to the base of the range and there was minimal direct contribution by the MIS 17 and younger shorelines to the range. It follows then, that the Murray Lakes Range is composed predominantly of Bridgewater Formation deposited during interglacials of MIS 19 and greater age. However, the presence of the potentially middle Pleistocene (\geq MIS 11) Mount Misery field site (MTM) (section 6.6.6) suggests continued contribution to the northern end of the range throughout the Pleistocene. The Mount Misery aeolianite is located at ~10 m APSL (only 7 m above the Cooke Plains Embayment, (Figure 7.3 Transect 2) and the intergranular cements as seen in thin-section provide evidence of carbonate grain diagenesis in a meteoric phreatic environment (section 4.3.6.1), implying a lagoon or lacustrine environment east of the Murray Lakes Range at some point during the middle Pleistocene.

Rogers (1979) mapped the dunes trending eastwards from the northern Murray Lakes Range as Bridgewater Formation. Drill logs within this region describe a series of sandstones as fossiliferous or limey extending to depths up to 39 m which could correlate with either Bridgewater Formation or Padthaway Formation (section 4.3.10). The North Coonalpyn (NC) field site is located within the southern margin of the dunes

and indicates aeolian Bridgewater Formation. Padthaway Formation is identified in drillholes in the intervening space between the North Coonalpyn and South Coonalpyn field sites (section 4.3.10). At present it is not possible to say whether deposition on the dolomite plain to the north was at any point physically connected to the deposition of Padthaway Formation farther to the southeast.

7.2.1.4 Padthaway Formation and Quaternary dolomite plain

The lacustrine sediments of Padthaway Formation were deposited during interglacial sea-level highstands within in the inter-dune corridors separating the coastal barrier ranges of Bridgewater Formation on the Coorong Coastal Plain. Although the sediments are not necessarily coeval with the barrier immediately seaward of their position and could accumulate over multiple interglacial periods, they generally follow the trend of the Bridgewater Formation and increase in age landward. The recognition of Padthaway Formation in the northern Coorong Coastal Plain has been made possible in this thesis by analysis of drillhole sedimentary logs as provided by the Government of South Australia Department for Manufacturing, Innovation, Trade, Resources and Energy (DMITRE, 2014) (section 4.3.10). Analyses of drillholes sedimentary logs across the northern Coorong Coastal Plain indicate deposits of the Padthaway Formation within the low-lying regions seaward of the Coonalpyn Range and landward of the Murray Lakes Range, with probable deposition seaward of the latter range as well. The dolomite plain, an unnamed and not formally defined geological unit designated the “Qpu” dolomite on the Pinnaroo 1:250 000 Geological Sheet (Rogers, 1979), is suggested to be an early Pleistocene marginal-marine and lagoonal unit formed in a partially protected, low-energy environment, genetically related to the Padthaway Formation but lithologically and stratigraphically distinct (Rogers, 1980; Brown and Stephenson, 1991; sections 2.3.5 and 3.7.5).

The coastal plain to the west of the Coonalpyn Range is relatively level at ~17 m APSL (Figure 7.3 Transect 6). Padthaway Formation has been identified between the Coonalpyn Range and the seaward Black and Hynam Ranges (Figure 7.1), indicating that a protective estuarine environment was provided by the latter two ranges and initial deposition of Padthaway Formation could have commenced before or during MIS 21. Given the flatness of the coastal plain and relatively low height above sea-level, it is

highly likely that the region was inundated during multiple interglacial periods. The Padthaway Formation reaches a maximum thickness of 14 m east of the Hynam Range and varies in thickness between 12-14 m to the east of the southern Murray Lakes Range which is comparable to the reported 13 m maximum thickness of the unit immediately west of Naracoorte (Cook *et al.*, 1977).

The un-named Quaternary dolomite plain (Figure 7.2) is found north of the Murray Lakes Range, occupying a relatively flat plain (~15.5 m APSL, Figure 7.3 Transect 3) extending to the Marmon Jabuk Escarpment. The dolomite has been shown to inter-finger with colluvial fans adjacent to the escarpment. It post-dates the initial deposition of Bridgewater Formation on the plain as it is separated from the southern margin of the Marmon Jabuk Escarpment by a wedge of lower Bridgewater Formation (Rogers, 1979; 1980) in which the Tauragut Well field site is found and potentially correlates to the deposition of Cannonball Hill Range (1.27 – 1.35 Ma) (see above). Brown and Stephenson (1991) suggested that the dolomite plain was formed in a low-energy marginal marine environment partially protected by the shallowly buried Cambrian Kanmantoo Group meta-sediments to the west during a minor marine transgression (Figure 7.1). These authors based this interpretation on stratigraphic relationships and tentatively placed the latest possible initiation of deposition on the plain as equivalent to the East Naracoorte Range, MIS 23 or 25 (917 ka or 936 ka; Lisiecki and Raymo, 2005). Lachlan (2011) found evidence on Kangaroo Island, west of Fleurieu Peninsula, of sea-level reaching a highstand of 2-4 m APSL between 1.0 ± 0.2 Ma and 1.2 ± 0.3 Ma (AAR numerical ages), which would correspond well to the suggested age of Brown and Stephenson (1991) and deposition following formation of the Cannonball Hill Range.

Initial deposition within the dolomite plain would have been dependent upon when protection to the region from the open ocean developed. The Murray Lakes Range was well developed by MIS 17 when the Bridgewater Formation began deposition seaward of the range. The arcuate trend of the Coonalpyn Range towards the granites within the southern Murray Lakes Range also suggests that deposition of the latter range coincided with the early Pleistocene deposition of the former range. Therefore, the protective conditions allowing deposition of lagoon/lacustrine sediments landward of the Murray Lakes Range were in place during the early Pleistocene. However, under

the presumption of Brown and Stephenson (1991) that adequate protection was provided to the west by the shallowly buried Cambrian sediments, the Padthaway Ridge underlying the Murray Lakes Range may have been sufficient to create the low-energy environment necessary for development of the dolomite plain before development of the Murray Lakes Range, strengthening the case for early Pleistocene deposition of the dolomite plain correlative to the early Coonalpyn Range.

The majority of the dolomite plain is ≤ 20 m APSL, averaging ~ 15.5 m APSL across the centre of the plain (Figure 7.2 Transects 3). The early Holocene flooding of the Cooke Plains Embayment over 20 km north-eastwards from Lake Alexandrina (de Mooy, 1959; von der Borch and Altman, 1979) towards the dolomite plain suggests multiple phases of estuarine deposition within the region throughout the Pleistocene. Emergence of the plain above inundation levels can be attributed to ongoing slow rates of uplift in the area.

7.2.1.5 Alluvial fans

The inferred early Pleistocene deposition of the dolomite plain and Padthaway Formation coincided with the demise of Lake Bungunnia, which began at 1.5-1.4 Ma (McLaren *et al.*, 2009; McLaren and Wallace, 2010; section 2.3.3) and the development of the modern River Murray system in South Australia. Relict streams within the Marmon Jabuk Scarp indicate fluvial delivery to the dolomite plain soon after the early Pleistocene high sea-level, which has been attributed to the creation of the scarp and deposition of the marine Coomandook Formation, which underlies the Bridgewater Formation and associated sedimentary successions (Hossfeld, 1950; Belperio and Bluck, 1990). Palaeo-valleys were also identified within the Coonalpyn Range during this research southwest of the Emu Springs field site. The palaeo-valleys have been infilled and are overlain by glacial period dunes of unconsolidated aeolian quartz sand identified as the Molineaux Sand. The relict streams and palaeovalleys reflect more humid climatic conditions within the early Pleistocene than today (Martin, 2006).

Wetter conditions at the beginning of the Quaternary would be at least partially responsible for the alluvial deposits seen at the base of the Marmon Jabuk Escarpment and surrounding Lake Alexandrina to the north and west (section 4.3.10). The alluvium

found at the base of the Marmon Jabuk Escarpment in drillholes and at the Taillem Bend field site is likely to have been derived from the Loxton-Parilla Sands, which cap the escarpment (section 4.3.6.8). The alluvial sediment, which contains no carbonate, is capped by a thick (2-3 m) nodular calcrete. Calcrete development was most likely formed by the migration of carbonate up profile and was driven by water evaporation. The thickness of the calcrete profile indicates a substantial period of time for calcrete development.

The alluvial fan north of Lake Alexandrina, extending south from the River Murray Gorge towards the lake, is capped by a thick calcrete (≥ 1.2 m) (section 4.3.10). The calcrete is overlain by possible late Pleistocene age longitudinal dunes of windblown sand reworked from the adjacent Mount Lofty Ranges and underlying Palaeogene-Neogene estuarine and marine sands (Gibson, 2004). An exposure within the calcrete at the Murray Bridge field site (section 4.3.6.9) indicates that the calcrete has been subjected to multiple cycles of formation, fracture and reformation with initial deposition at least within the middle Pleistocene. The coarse-grained sediment at Murray Bridge has been sourced from the nearby adjacent Mount Lofty Ranges and underlying adamellite, indicating a short transport distance. Large calcrete clasts indicate the reworking of an older deposit. De Mooy (1959) suggested that this region was an extension of the Pleistocene Mallee country to the northeast and traced its extent westward below the Holocene St Kilda Formation and modern sea-level. This thesis has not investigated the validity of the relationship to the Mallee country, but the calcrete does extend southward towards Lake Alexandrina.

The calcretes studied at Taillem Bend and Murray Bridge indicate a substantial age for the calcretes and the underlying successions with deposition pre-dating the Late Pleistocene. The sedimentation patterns of the alluvial plain throughout the Pleistocene would have been dependent upon the location and nature of the coastline, the occurrence of pluvial events and the sediment delivery from the eastern slopes of the Mount Lofty Ranges. The overall trend throughout the Quaternary has been one of decreasing precipitation (Nanson *et al.*, 1992; Fujioka and Chappell, 2010; Cohen *et al.*, 2011) and although the modern climatic pattern had been established at the beginning of the Quaternary, Australia was still considerably wetter than today (Martin, 2006;

section 2.4.4). The location of the alluvial fan adjacent to the uplifting Mount Lofty Ranges and within a zone of subsidence and potential downwarping also indicates that the immediate neotectonics would have affected sedimentation patterns.

7.2.2 Middle through late Pleistocene Bridgewater Formation

In this thesis, the depositional record of the middle to late Pleistocene Bridgewater Formation within the study area has been constrained by geochronological analyses, the majority of which have been analysed using amino acid racemisation (AAR) (Chapter 6). Due to the ongoing subsidence, mollusc shell for analysis was only found in association with MIS 5e and younger successions. The analysis of bioclastic carbonate sand via whole-rock analysis was found to be successful to MIS 7 but could be compromised by leaching which appears to be extensive throughout the study area (section 6.8.7). Analysis of foraminifers supported the mollusc shell and whole-rock analyses and indicated the presence of significant quantities of reworked grains, in some cases from multiple preceding interglacials. Luminescence ages helped to provide geochronological restraint, most especially in sedimentary successions that were not suitable for AAR analysis either due to a lack of carbonate or the unsuitability of carbonate grains following diagenetic alteration.

Middle to late Pleistocene Bridgewater Formation and associated deposits have been identified via morphostratigraphy and confirmed using geochronological analyses at Point McLeay, Sturt Peninsula, sub-parallel to the modern shoreline from Lake Albert north to the Mount Lofty Ranges and on Fleurieu Peninsula (Murray-Wallace *et al.*, 2010; this research) (Figure 7.4). The sedimentary successions are divisible into the last interglacial shoreline, the pentultimate interglacial shoreline and the stacked succession at Point McLeay. The following discussion, which relates these features to the sedimentary succession and Quaternary sea-level highstand record of the Bridgewater Formation between Robe and Naracoorte, begins with Point McLeay and proceeds forward through time.

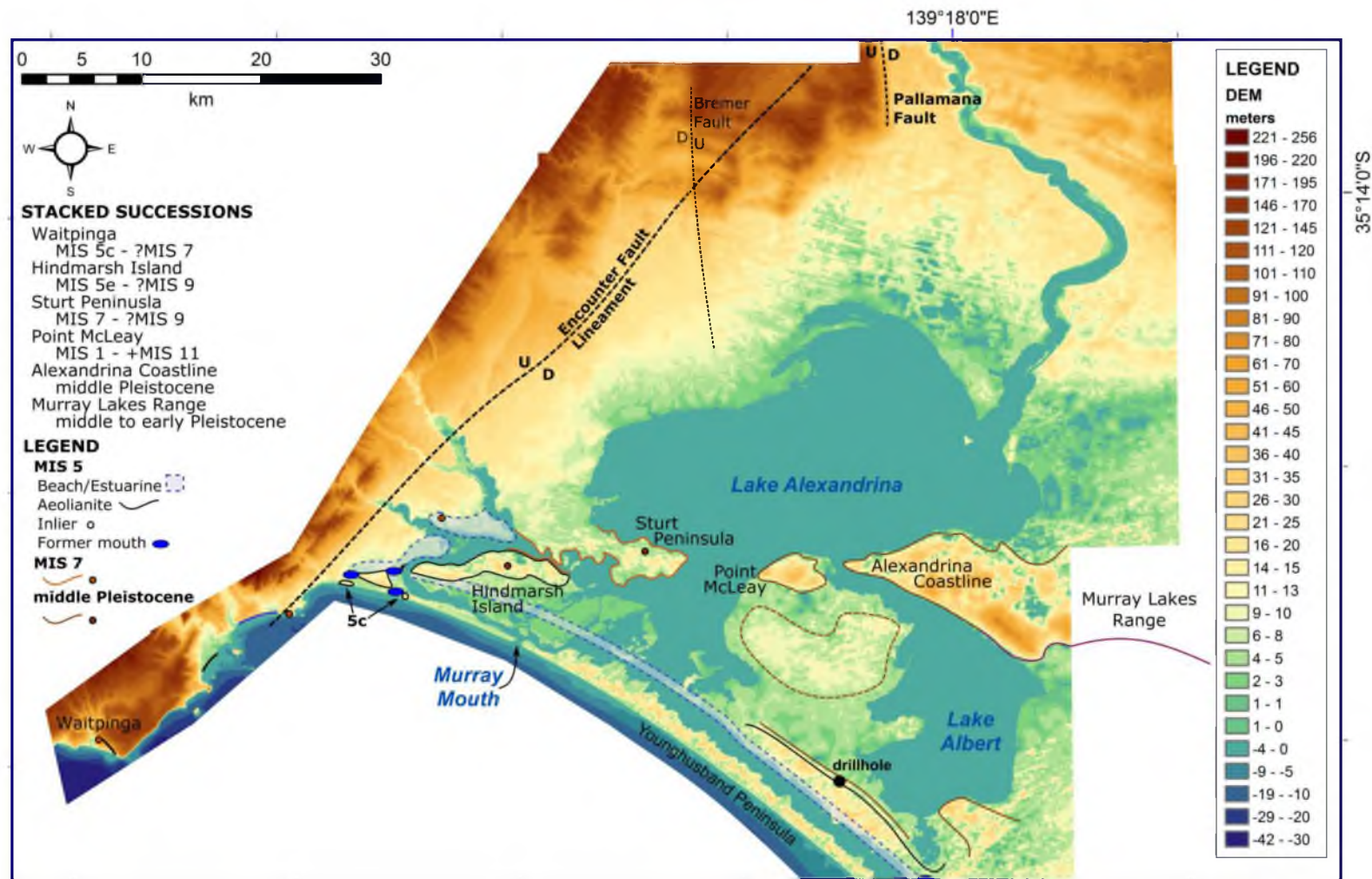


Figure 7.4: The extent of Middle to Late Pleistocene Bridgewater Formation and associated deposits within the Murray Lakes region. The Alexandrina Coastline forms the northernmost extension of the Murray Lakes Range which is a potentially emergent feature consisting of both Middle and Early Pleistocene successions. Uplift of the Mount Lofty Ranges has occurred along the Encounter Fault/lineament and Pallamana Fault throughout the Quaternary.

7.2.2.1 Point McLeay

Point McLeay is a distinct feature at the northern tip of the Narrung Peninsula, the orientation of which suggests a genetic relationship to the northern margin of the Murray Lakes Range and Alexandrina coastline north of Lake Albert (Figure 7.4). The ~45 m high aeolian succession is less than 16 km from the modern coastline and contains a record of at least six phases of deposition. The northern part of Narrung Peninsula has been shown to be underlain by Cambrian-Ordovician granite found at a depth of 142 m (section 4.3.5.3). To the south the remainder of the peninsula is comparatively low-lying, but a band of relatively higher topography (at ~10 m APSL), in accordance with the MIS 7 shoreline to the west on Sturt Peninsula, is distinctive across the middle of the peninsula and may indicate the accumulation of Bridgewater Formation (Figure 7.3 Transect 1). Drillhole data is absent within the 10 m topographic high but a drillhole to the southeast on the southern margin of Narrung Peninsula records Bridgewater Formation to a depth of 58 m (Figure 7.4). Directly to the north of Narrung Peninsula is Lake Alexandrina. Bathymetry indicates that the lake reaches a maximum depth of ~9.4 m north and northeast of Narrung Peninsula, approximately in the centre of the lake (Brooks *et al.*, 2009). The boundary of Pleistocene-Holocene sediments beneath the lake floor is identified in sediments only in the north and northwestern part of the lake and exceeds 5 m depth throughout the southern half of the lake implying that the location of the river preceding the Holocene was in the southern half of the lake (Barnett, 1993).

The oldest unit identified during this research within the sedimentary succession at Point McLeay was a *terra rossa* soil (Unit PM G1). The base of unit PM G1 was not identified due to the steepness of the cliff but as the unit is approximately midway down the face of the cliff exposure (~20 m) it is very likely that additional units are preserved beneath.

The deposition of PM A1, which overlies PM G1, has been correlated with MIS 11 (421 ± 48 ka; UOW-1296) based upon an optically stimulated luminescence (OSL) age (section 6.6.5). The deposition of the sedimentary succession at Point McLeay has been partially constrained by last interglacial aeolianite PM A4, which forms the crest of the point and the OSL age of PM A1. The intervening units based on stratigraphy could be correlated to MIS 10 (PM G2), MIS 9 (PM A3-PM A2) and MIS 7 (the inaccessible unit)

(section 4.3.5.3). However, without confirming interglacial deposition for the inaccessible unit, this cannot be confirmed. Of the units for which the bounding surfaces were identified (all but the PM G2, PM A1 and PM G2), none reach 2 m in thickness indicating slow rates of sediment accumulation. As a topographic high in the landscape, Point McLeay is more susceptible to aeolian erosion.

The MIS 11 age of PM A1 places deposition concurrent with the East Avenue (414 ± 29 ka, TL age; Huntley *et al.*, 1993) and Ardune Ranges to the southeast. Sea level during MIS 11 has been placed at 3 m BPSL in the Robe to Naracoorte record (Belperio and Cann, 1990; Murray-Wallace *et al.*, 2001), although Blakemore *et al.* (2015) calculated palaeo-sea-level for MIS 11 at Mount Gambier to be $+2 \pm 2$ m. The Ardune Range is a minor range with a simple dune structure, not exceeding 1.6 km in width, found directly landward of the East Avenue Range (Sprigg, 1952) (Figures 7.1) possibly deposited during a hiatus within sea-level regression. The East Avenue Range is a major complex dune range, containing up to 8 beach ridges (Sprigg, 1952), is up to 3 km wide and at most 20 m above the level of the adjacent coastal plain (Murray-Wallace *et al.*, 2001) and was emplaced during a particularly long interglacial (section 7.3.2.1). The seaward margin of the dune is found nearly 50 km inland from Robe but can be traced to the northwest within 17 km of the modern coastline before coalescing with younger ranges. The very fine and well-rounded character of the carbonate grains within PM A1 at Point McLeay and overall low quantity of carbonate suggests that the dune was not deposited near to the inner shelf carbonate source.

The identification of an MIS 9 inlier on Hindmarsh Island (Murray-Wallace *et al.*, 2010) and the MIS 7 composition of Sturt Peninsula with deposits extending onto Hindmarsh Island (Murray-Wallace *et al.*, 2010; this research) indicate that the coastline during these interglacials was seaward of Point McLeay. This, alongside the relatively thin nature of the interglacial units (<2 m) support the conclusion that at the time of deposition Point McLeay was not near to the coastline and was present within the landscape as a topographic high, similar to modern deposition on the point. The sea-level record for MIS 7 and MIS 5 on the Coorong Coastal Plain are reviewed in the following two sub-sections. However, the MIS 9 record is reviewed here.

The Robe-Naracoorte record indicates that sea level during MIS 9 was at 1 m BPSL during the MIS 9c substage and is represented by the West Avenue (342 ± 32 ka, TL age; Huntley *et al.*, 1993) and East Dairy Ranges (Figure 7.2) (Belperio and Cann, 1990; Murray-Wallace *et al.*, 2001). Blakemore *et al.* (2015) reported a higher sea level for MIS 9 of 4 ± 1 m APSL based upon lagoonal facies associated with the MIS 9 correlated Caveton Range (334 ± 83 ka, AAR numeric age). The East Dairy Range, ~20 km inland from the modern coastline, is a poorly preserved range that has been modified and reworked by subsequent high sea levels (Sprigg, 1952). The West Avenue Range is 1-1.5 km wide cresting at an average of 20 m above the surrounding coastal plain (Murray-Wallace *et al.*, 2001) and located ~38 km inland from the modern coastline at Robe. The range comes within 20 km of the coastline before coalescing with the seaward Reedy Creek Range ~40 km to the north (Figure 7.1).

The potential MIS 9 correlatives at Point McLeay, PM A2-PM A3 units, are significantly different in their lithologies to typical Bridgewater Formation being composed predominantly of very fine-grained quartz grains and containing large quantities of silt (28-44%) (section 4.3.5.3). Furthermore, PM A2 contains dolomite (13.5%) and ankerite (12.9%), minerals typically associated with deposition in a shallow ephemeral lake. However, the height of these units above Lake Alexandrina (>25 m) makes it unlikely they were deposited in an ephemeral lake environment. Instead it is suggested that the minerals were derived from a nearby ephemeral lake source and delivered via aeolian deposition. The dominant southwesterly wind patterns of interglacial periods (section 2.5) suggest that the sediment source was located in a seaward direction to Point McLeay. The two calcrete horizons (the laminar capping PM A3 and the nodular calcrete PM A2PL) and extensive pedogenesis of the entire sequence could potentially represent two phases of deposition corresponding with the two phases of deposition as recorded in the southeast. However, the transition between PM A2PL and PM A3 is not sharp and the entire profile is similar to a common variation of calcrete soil profiles (Esteban and Klappa, 1983). The development of calcrete within the soil profile helps to constrain deposition of the unit to within an interglacial period. Calcrete formation is controlled by climate, requiring a semi-arid environment with minimal leaching, adequate soil moisture and rates of evaporation (section 3.6.2.1); climatic conditions

typical of southern Australia during interglacial periods. The increased aridity of glacial periods, reduced vegetation and landscape instability are not conducive to calcrete development (Candy and Black, 2009).

The sedimentary succession at Point McLeay differs from the remainder of the middle to late Pleistocene successions near the Murray Mouth in its long record and height in the landscape. This is perhaps most evident when comparing the Point McLeay sedimentary record with that preserved at Point Sturt 5.5 km to the west, the easternmost point of Sturt Peninsula. Point McLeay reaches a maximum height of over 40 m APSL whereas Point Sturt reaches ~24 m APSL and in contrast to Point McLeay, the cliffs of Point Sturt indicate only one sequence of deposition (in excess of 24 m) which has been correlated to MIS 7 (although an older inlier is possible, section 7.2.2.2). The units within Point McLeay, which could possibly be related to MIS 7, are located at heights estimated to be greater than 30 m above present water level at Lake Alexandrina and do not exceed 2 m in thickness implying a change in thickness between the MIS 7 succession in the two coastal cliffs of at least 22 m and vertical variation in the base of MIS 7 deposition in excess of 30 m. The different records in the two points further support the notion that Point McLeay has been a topographic high since at least the middle Pleistocene.

There are two possible explanations for the presence of Point McLeay as a topographic high within the Murray Lakes region. The first is, following the above discussion regarding the Murray Lakes Range, that Point McLeay is slowly uplifting. However, the point appears to be located on the margin of subsidence in the region as evidenced by the location of last interglacial shelly beach facies at 1-3.5 m water depth beneath the barrages within the Murray Mouth and the exposure of equivalent facies at 0.25 m APSL on southern Narrung Peninsula. If Point McLeay is within the margin of subsidence, then its elevation above the remainder of Narrung Peninsula may be related to the underlying granite possibly slowing the rate of subsidence. A second alternative is that a fault running between Point Sturt and Point McLeay explains the sharp contrast in the height and record of the two localities. The Bremer Fault, which extends southward out of the Mount Lofty Ranges in the direction of Point McLeay (Figure 7.4), has already been shown to offset the Cenozoic sequence by up to 80 m (Gibson, 2004). The

presence of a fault between Point Sturt and Point McLeay could have further implications for the position of the River Murray and its mouth throughout the Quaternary. However, movement along the Bremer Fault within the Quaternary has not been recorded and the fault does not explain why only Point McLeay persists as a topographic high and not all of Narrung Peninsula. Furthermore, uplift and reverse faulting on the eastern side of the ranges within the Quaternary has typically produced east-facing scarps (e.g. Encounter and Pallamana Faults) (Bourman and Lindsay, 1989; Gibson, 2004), which would imply a downward movement of Point McLeay.

7.2.2.2 Penultimate Interglacial coastline

Morphostratigraphy and geochronological analyses have allowed the identification of MIS 7 aeolian Bridgewater Formation across Sturt Peninsula, northern Hindmarsh Island and on Fleurieu Peninsula with contemporaneous deposition of alluvium north of Currency Creek. Sea level during MIS 7e (240-230 ka) as determined by the Robe-Naracoorte record, was similar to the current sea level and 6 m below present level during MIS 7a (201-193 ka) with no record of MIS 7c (220 ka) (Belperio and Cann, 1990; Murray-Wallace *et al.*, 2001; Murray-Wallace and Woodroffe, 2014). The Mount Gambier record indicates sea-level as much as 9 ± 2 m BPSL during MIS 7 (Blakemore *et al.*, 2015). Dual sea-level highstands imply a potential record for both substages within the Murray Lakes region. The difference in sea level between the two MIS 7 substages is ~6 m, based upon the sea-level estimates of Belperio and Cann (1990) and Murray-Wallace *et al.* (2001).

The Reedy Creek Range (258 ± 25 ka, TL age) and an inlier to the southernmost MIS 5e Woakwine Range have been correlated to MIS 7e (Figure 7.1) (Huntley *et al.*, 1993; Murray-Wallace *et al.*, 1999; 2001). The range is well preserved and laterally extensive and although it crests at only 15 m APSL, reaches 3 km in width and indicates a sustained period of high sea-level (Sprigg, 1952; Murray-Wallace *et al.*, 2001). The seaward margin of the Reedy Creek Range is ~34 km inland from Robe. Sea level during deposition would have surpassed the MIS 9 East Dairy Range located to the west and reached the MIS 9a West Avenue Range in the north (Figure 7.1). The Reedy Creek aeolianite is yellow (10 YR 7/6) in colour and contains 55% CaCO_3 (Murray-Wallace *et al.*, 2001). The West Dairy Range is much smaller than the Reedy Creek Range but is well

preserved and merges with the East Dairy Range ~23 km northwest of Robe (Figure 7.1). The coastal plain surrounding the Dairy Ranges was inundated by the last interglacial lagoon, which formed landward of the Woakwine Range and helped to constrain deposition of the range to MIS 7 (Sprigg, 1952; Ludbrook, 1984; Belperio *et al.*, 1995).

The MIS 7 sedimentary succession on Sturt Peninsula and extending onto northern Hindmarsh Island has been inferred by morphostratigraphy and confirmed by thermoluminescence (TL) and AAR whole-rock and foraminifer analyses (Chapters 4 and 6). This implies the succession was breached by the River Murray following deposition and is discussed below (section 7.5). AAR analysis also suggests the presence of an MIS 7 aeolian inlier located within the Goolwa area (Chapter 6). Intertidal mollusc shell deposits, associated with either marine or estuarine conditions during MIS 7, with which the height of sea level in the Murray Mouth region or breadth of the MIS 7 aeolianite could be constrained, were not identified in this research. If subsidence in the Murray Mouth region has been ongoing throughout the Quaternary (section 7.2), assuming the same rate of subsidence (0.02 mm yr^{-1}) as the last interglacial shoreline (Bourman *et al.*, 2000), MIS 7e shell beds would be expected at 4.6 m below present sea-level and MIS 7a shell beds at 9.86 m depth if the initiation of subsidence is placed at the close of MIS 7e (230 ka) and MIS 7a (193 ka). The TL ages from Sturt Peninsula could be, at 1σ uncertainty, correlated with either MIS 7e or MIS 7a deposition. The peninsula reaches up to 24 m APSL and reaches a width of ~4.5 km at its widest point, exceeding the Reedy Creek Range in both height and width measurements and suggesting a composite structure. The size of the range also suggests that the river Murray was providing a large quantity of sediment that was incorporated into the peninsula dunes.

A complex structure within Sturt Peninsula would be expected considering the evidence of ongoing subsidence. Stacking of successive units of Bridgewater Formation within the study area has already been demonstrated at Point McLeay in this research, and Hindmarsh Island is now known to contain MIS 5e, MIS 7 and a likely MIS 9 aeolianite (Bourman *et al.*, 2000; Murray-Wallace *et al.*, 2010; this research). This compares well to the barrier shorelines successions within the Robe-Naracoorte and Mount Gambier regions, which have also been shown to be composite structures (Murray-Wallace *et al.*, 1999; Murray-Wallace, 2002; Blakemore *et al.*, 2015).

The Sturt Peninsula Road aeolianite on Sturt Peninsula is unique to the other aeolianites identified on the peninsula in its extensive depth of pedogenic development, extremely low carbonate content and high content of silt (section 4.3.4) suggesting a different environment of deposition to the other MIS 7 aeolianites on Sturt Peninsula. The features of the Point Sturt Road aeolianite are similar in character to anticipated MIS 9 units on Point McLeay (PM A2-PM A3) and could represent a contemporaneous deposit. The MIS 7e shoreline to the southeast has already been shown to have overtaken the MIS 9 East Dairy Range and to overlap the MIS 9a East Avenue Range, lending further support to the notion that MIS 7 deposition may have superseded MIS 9 deposition within the study area.

The presence of a MIS 7 aeolianite at Knights Beach on Fleurieu Peninsula is questionable given its location on a subsiding coastline and on the downthrown side of the Encounter Fault. The seafloor sediments offshore of Fleurieu Peninsula are composed of relict-rich skeletal carbonate sand and gravel and mollusc-rich relict sand (James and Bone, 2011) and, as the sediment source for Knights Beach, may be responsible for the apparently older than MIS 5e AAR results from whole-rock analyses. This would explain why the whole-rock results from the well-preserved carbonate grains retrieved from Knights Beach TL fell between the MIS 5e and MIS 7 whole-rock means. However, the disparity in the TL results remains unexplained. The conflicting regional stratigraphic interpretation, AAR and TL results require additional research at this locality.

The alluvial sediment found at Myrtlegrove Road is considered an equivalent to the Pooraka Formation, which is described as having a reddish-brown colour with weakly developed calcareous pedogenic horizons and variable lithology, including clayey sand (Williams, 1969; Bourman *et al.*, 1997; 2010). The TL age for the sedimentary succession of 227 ± 24 ka extends the earliest deposition of Pooraka Formation beyond previous ages within the last interglacial (Bourman *et al.*, 1997; 2010) and confirms the presence of MIS 7 alluvium expected to be present flanking the Mount Lofty-Flinders Ranges (Bourman *et al.*, 2010). Bourman *et al.* (2010) argued for the likelihood of MIS 7 Pooraka Formation following the proposal of Nanson *et al.* (1992) of Australian Pluvial Stages 5 and 7 (equivalent to corresponding interglacials) during which the widespread

deposition of alluvium is considered a proxy for periods of greater rainfall and runoff than at present. The later inundation of the alluvial deposit by the MIS 5e estuary reflects a change in base level between the two interglacials as a consequence of either the higher sea-level reported for the Last Interglacial on the Coorong Coastal Plain (2 m APSL, Belperio and Cann, 1990) or ongoing subsidence at the Murray Mouth or a combination of both factors. If the Quaternary alluvium extends below modern sea-level as suggested by de Mooy (1959) and Gibson (2004), then it was either deposited at times of lower sea-level or it supports the notion of downwarping in the region. The association of alluvium with the Holocene, MIS 3, the Last Interglacial (Ward, 1966; Bourman *et al.*, 2010) and now the Penultimate Interglacial strongly implies alluvium is deposited during interglacial periods. However, this is not to imply that alluvial deposition is relegated only to interglacial as it likely continues within the glacial periods explaining why Quaternary alluvium extends beneath modern sea level.

7.2.2.3 Last Interglacial coastline

This thesis has investigated the presence of a suspected last interglacial recurved spit and Murray Mouth southeast of Lake Albert (de Mooy, 1959) and extended the record of the Bridgewater and Glanville Formations sedimentary successions on Hindmarsh Island, Goolwa, Sir Richard Peninsula and the Fleurieu Peninsula through morphostratigraphic correlation and geochronological analyses based on AAR (Chapters 4 and 6).

The Robe to Naracoorte record contains sedimentary successions, which have been correlated with the MIS 5e highstand (123 ka, 2 m APSL) and highstands at MIS 5c (105 ka, 9 to 20 m BPSL) and MIS 5a (84 ka, 19 to 33 m BPSL) (Belperio and Cann, 1990; Lambeck and Chappell, 2001; Murray-Wallace *et al.*, 2001; Cann and Murray-Wallace, 2012). The MIS 5e Woakwine Range occurs up to 10 km inland from the modern coastline at Robe, contains an MIS 7 inlier (Murray-Wallace *et al.*, 1999), rises up to 30 m above the coastal plain and ranges in width between 1 and 2 km (Murray-Wallace *et al.*, 2001). The Woakwine Range can be traced along the length of the coastal plain (Figure 7.1), forming the landward margin of the Coorong, to the Murray Mouth region where it has been recognised as the Bonney Coastline (de Mooy, 1959).

The Robe Range is a composite structure composed of modern (Robe I) aeolianite draping the older, late Pleistocene MIS 5a (Robe II) and MIS 5c (Robe III) sedimentary successions (Schwebel, 1984; Murray-Wallace *et al.*, 2001), including subaqueously-deposited MIS 5c coastal strata that further constrain minimum sea-level at the time to -14 m (Blakemore *et al.*, 2014). The Robe Range southeast of Robe forms prominent coastal cliffs with the seaward toe of the dunes extending below modern sea level. It has been proposed that the MIS 5c component of the Robe Range extends northward through the modern Coorong Lagoon as a series of islands exhibiting a linear trend (Cann and Murray-Wallace, 2012). The presence of MIS 5c Bridgewater Formation within the study area has been suggested by a TL age of 105 ± 5 ka (W-2348) for aeolianite at Surfers Beach west of Goolwa (Murray-Wallace *et al.*, 2010).

MIS 5e

The last interglacial record within the study area is the best preserved of any Pleistocene interglacial. The preservation of beach, aeolian dune and estuarine/lagoon sedimentary successions within the Murray Mouth region has been dependent upon the degree of lithification and calcrete development within the sedimentary successions (section 3.8) and their position in the landscape. The record on Fleurieu Peninsula is confined to bedrock valleys with deposition and preservation influenced by the valley orientation and by migration of the contained rivers (section 4.3.3.3). For example, the Waitpinga Valley has been completely infilled by MIS 5e and potentially older aeolianite due to its southerly exposure and the apparent entrenchment and low discharge of Waitpinga Creek (Figure 7.4). In contrast, the Hindmarsh and Inman River valleys, where valley infill is minimal, have a more eastward orientation and are provided protection by Rosetta Head and nearshore granite islands. The rivers are also larger and meander within the valley confines. The latter valleys are host to reworked aeolian, lagoon and beach deposits; the preservation of the latter has been partly due to the uplift occurring along Fleurieu Peninsula. Last Interglacial, as indicated by the presence of *Anadara trapezia*, mollusc shells occur 1.6 km up Hindmarsh River Valley, interfingering with Pooraka Formation alluvium at 6 m APSL (Bourman *et al.*, 1997).

Preservation of the last interglacial sedimentary successions on the Coorong Coastal Plain within the study area has been affected by subsidence, the River Murray

and the extent inland of the Holocene sea-level peak. The slow-rate of subsidence within the Murray Mouth region and a higher sea-level (up to 2 m APSL) during the last interglacial means that much of the MIS 5e sedimentary successions remained above the Holocene sea-level peak, which reached the present eastern shoreline of the Coorong Lagoon (Bourman *et al.*, 2000; Murray-Wallace *et al.*, 2010). Erosion of the MIS 5e record is most closely related to the River Murray. MIS 5e aeolianite is absent from the easternmost margin of Hindmarsh Island eastwards to Mark Point, a length of nearly 17 km. Erosion and reworking of the sediments most likely occurred during the sea-level rise following stadials and the Last Glacial Maximum as the river adjusted to the changing base levels. The extent of eroded sediment is also directly south of the gap between Point Sturt and Point McLeay, a location directly subject to the erosion by the River Murray and the Southern Ocean before the development of the Sir Richard and Younghusband Peninsulas.

MIS 5e beach, aeolian dune and estuarine/lagoon facies have been identified across northern Hindmarsh Island and extending west across the Goolwa Channel (sections 4.3.3 and 5.8) (Figure 7.4). The width of the aeolian succession is less than 2 km and compares well to the Woakwine Range to the southeast. Shell beds related to the MIS 5e shoreline were the only mollusc shells of Pleistocene age to be identified in this research. No shell beds reflecting a life assemblage were identified in this research; shell beds were either a low-energy parautochthonous fossil assemblage or a high-energy fossil assemblage (Kidwell *et al.*, 1986; section 4.2.1). High-energy fossil assemblages with mixed species indicative of both exposed marine and estuarine environments were found within the Goolwa area in association a narrow (<300 m) remnant of the last interglacial recurved spit distal margin on the western shoreline of the Goolwa Channel indicating the location for the MIS 5e Murray Mouth. The remaining landward shell beds are, with one exception, composed of a low-energy parautochthonous fossil assemblages composed of species indicative of an estuarine environment typical of the modern Coorong. The exception was a fossil assemblage removed by a dredge of the Goolwa Channel at unknown depth and likely reflects an earlier position of the Murray Mouth prior to the development of the recurved spit at the western margin of Hindmarsh Island.

The dynamic environment of the Murray Mouth during MIS 5e is indicated by lagoon facies with a shell deposit seaward of the last interglacial aeolianite on Hindmarsh Island (section 4.3.3.2) and the isolation of MIS 5e aeolianite west of Goolwa and in a position seaward of the recurved spit on Hindmarsh Island. Both features suggest the landward migration of the last interglacial barrier. The aeolianite west of Goolwa, which contains rocky shoreline facies on its seaward margin (Murray-Wallace *et al.*, 2010), is surrounded by low-lying topography, which includes the palaeo-Goolwa Channel to the east and potential former Murray Mouths to the south and west. The preservation of the Hindmarsh Island lagoon facies, palaeo-channel and mouth facies imply protection is provided to these depositional settings by aeolianite structures in a seaward location, which have been largely removed by erosion. The seaward margin of the west Goolwa aeolianite is less than 1 km from the modern coastline whereas the seaward margin of the recurved spit is more than 2 km from the modern coastline suggesting an adjustment of the coastline since the MIS 5e highstand, probably related to tectonic subsidence in the area as suggested by Bourman *et al.*, (2000).

An alternative location for the MIS 5e Murray Mouth was proposed by de Mooy (1959) at the southeastern margin of Lake Albert. The location for the proposed mouth is well indicated by the DEM produced for this research (Figure 7.4) and the topography immediately to the east is low-lying, averaging less than 5 m (Figure 7.3 Transect 2). Although the lithology of the Stratland aeolianite located on the eastern margin of the proposed mouth is indicative of a high-energy nearshore environment (section 4.3.3.1), further investigation is required to confirm the presence of a former mouth.

The cross-sectional width normal to the modern coastline of Bridgewater Formation deposits at the surface (>15 km) and depth below the surface (≤ 48 m, section 4.3.10) to the southeast of Lake Albert far exceeds the dimensions of any other Pleistocene individual range, which generally do not exceed 3.5 km (Murray-Wallace, 2002), suggesting that the region is composed of multiple successions of Bridgewater Formation. However, whole-rock sample analyses by amino acid racemisation support the MIS 5 deposition of aeolianite 15 km inland of the MIS 5e shoreline (section 6.4.3.3) and it is interesting to note that this north-east trend of aeolianite is almost directly seaward of the east-north-east trend of aeolianite landward of the Murray Lakes Range

(Figures 7.1 and 7.2), implying a long term influence of interglacial wind patterns on the deposition of Bridgewater Formation on this part of the Coorong Coastal Plain. The more eastward trend of the older aeolianite associated with the Murray Lakes Range may reflect overprinting by glacial wind patterns which have shaped the east-west trending Molineaux Sand.

The width of the MIS 5e barrier extending north to south from Lake Albert along southern Narrung Peninsula is also consistently 2 km in width or slightly greater and includes the location where a drillhole records Bridgewater Formation to a depth of 58 m (section 7.2.2.1). These features indicate that coalesced dunes continue at depth beneath southern Narrung Peninsula and the modern Coorong and beach-barrier system. The coalescing ranges of MIS 17 and younger are directed specifically to this region as visible on SRTM (Figure 7.1) and as indicated by the transects (Figure 7.3). While not entirely discounting the hypothesis of a former Murray Mouth south of Lake Albert de Mooy (1959), it does bring into question the proposed development of the coastline there through a series of recurved spits, but it does not discount the development of the coastline through island establishment on offshore bars and expansion to eventually produce one continuous shoreline (Hesp, 1984; Harvey, 2006; Chapter 3). This former model would allow for the low-lying region to the south of Lake Albert identified as a former Murray Mouth by de Mooy (1959) to be recognised as one of many river mouths that were present during the development of the coastline.

The generally low carbonate content (over half the field sites are composed of less than 15% CaCO_3) within the Bridgewater Formation sedimentary successions found southeast of Lake Albert, suggest that an alternative method of geochronological analysis (e.g. TL or OSL) to AAR may be required to determine the period of deposition for the successions there. The high content of siliceous sediment can be attributed to the possible presence of a palaeo-River Murray channel and the predominance of quartz sand (>50%) on the Lacepede Shelf offshore of the region, which would provide sediment for the development of the interglacial beach barriers with each interglacial sea-level transgression (section 4.3.3.1).

MIS 5c

A calcrete inlier at the proximal end of Sir Richard Peninsula has been identified in this research (section 4.3.3.2). The inlier has been attributed to MIS 5c due to its geographic position, its morphostratigraphic relationship to the aeolianite at Surfers Beach and its position seaward of the MIS 5e sedimentary successions in the Goolwa area, but further analyses for confirmation is required. The lack of aeolianite between Surfer Beach and the proximal end of the Sir Richard Peninsula (Figure 7.4) most likely reflects erosion due to the adjustment of coastal orientation from the tectonic subsidence discussed above and the early Holocene high sea level. The lack of aeolianite may also be due to river erosion. The position of the Murray Mouth during MIS 5c is unknown. De Mooy (1959) suggested a location to the south of the MIS 5e aeolianite west of Goolwa, but a low-lying region between Sir Richard Peninsula and the MIS 5e aeolianite west of Goolwa may be more accurate (Figure 7.4).

7.2.3 Holocene

The Holocene record on Hindmarsh Island provides an analogue for the impacts of sea-level transgression on antecedent shorelines during previous interglacials. Holocene sediments reach their greatest depth across southern Hindmarsh Island reflecting both the erosive nature of the glacial River Murray and the extent of early Holocene sea level, which reached up to 2 km inland from the present coastline (sections 3.3.1 and 4.3.2). Auger hole analysis indicates more intensive erosion, most likely related to the development of a river valley formed during the lowered base levels following the Last Interglacial, has prevented formation of or removed late Pleistocene calcrete and underlying sediments from southern Hindmarsh Island.

As discussed above, changing base levels following the last interglacial highstand and the early Holocene transgression facilitated substantial erosion of the MIS 5e and 5c barriers. The river and high sea level would also have reworked and incorporated the unconsolidated Molineaux Sand deposited during the intervening glacial period (MIS 2) (see below discussion, section 7.5). The inland limit of the post-glacial marine transgression is reflected in the current distribution of the glacial Molineaux Sand, which rests on calcreted surfaces (section 4.3.2). Southern Hindmarsh Island developed as an extensive sand flat in the period following the post-glacial marine transgression as

indicated by the fossil assemblage but was eventually segregated from sediment supply with the development of more restrictive conditions coinciding with growth of Sir Richard and Younghusband Peninsulas and migration of the Murray Mouth (sections 4.3.2 and 6.4.1).

The erosion and reworking that has occurred in the Murray Mouth region since the last interglacial has implications for the preservation of sedimentary successions overcome by subsequent transgressions during higher sustained sea levels. The extent of erosion that occurs during a sea-level transgression is a function of ongoing sediment availability (Bateman *et al.*, 2011). If the quantity of freely available sediment is low, then erosion of antecedent structures will be more intensive. The apparent extensive recycling of sediment, as indicated by the comparison of quartz grains from the Lacepede Shelf sediment samples and field samples of the Bridgewater Formation, the Molineaux Sand and other siliceous sands (section 4.3.7) and the results of amino acid racemisation foraminifer analysis (Chapter 6), suggest that sediment supply to the region is low, supporting the identification of the Murray Mouth region as a failed delta (Murray-Wallace *et al.*, 2010). Therefore, it can be expected that when interglacials with sea-levels higher than that which the previous interglacial returned to, or superseded the older sedimentary successions, extensive erosion and reworking occurred. Hence it can also be expected that the preservation of middle Pleistocene sedimentary successions in the zone of subsidence (i.e. the Murray Mouth region) is minimal. Furthermore, as subsidence proceeds through time, successions that were perhaps initially above the height of the transgressing shoreline will eventually become subject to marine reworking providing that the successions evade river erosion.

7.2.4 Summary

The above discussion demonstrates that the deposition of Bridgewater Formation occurring on the northern Coorong Coastal Plain has been influenced by the Padthaway Ridge since the early Pleistocene, with initial deposition likely to be contemporaneous with the earliest known Bridgewater Formation, the Cannonball Hill Range. The Coonalpyn and Murray Lakes ranges were developed within the early Pleistocene along with the associated Padthaway Formation. The slower rates of uplift towards the Murray Lakes suggest that the northern Murray Lakes Range accreted in a

northwards direction as the landscape emerged above the height of sea-level highstands. Slow rates of uplift to the north of the Padthaway Ridge have helped to preserve the record of an early Pleistocene low-energy marine environment recognised as the dolomite plain. The low-lying region to the north of the Murray Lakes Range is likely to have been inundated numerous times throughout the Pleistocene in association with interglacial sea-level highstands.

Deposition of the Cannonball Hill, Coonalpyn and Murray Lakes ranges during the early Pleistocene places them beyond the range of most current geochronological methods. To date, no shell beds, which may assist in constraining the timing of deposition or contemporaneous sea level have been identified in association with these ranges. The ages of the ranges and their apparent constituents have been determined by correlation with the marine isotope record using geographic relationships within the landscape and morphostratigraphic interpretations to identify and relate the sedimentary successions (Belperio and Cann, 1990; Bowler *et al.*, 2006; this research).

The middle to late Pleistocene sea level record in the study area exists in a very narrow zone that was altered with each returning interglacial. The Robe-Naracoorte record in which thirteen highstand successions are recognised, spans 90 km with dunes on average spaced 10 km apart and typically reaching heights up to 30 m above the coastal plain (Murray-Wallace *et al.*, 2001). In contrast, the width of the coastal record within the study area (including the modern shoreline and Coorong) is less than 19 km southeast of Lake Albert where the average height of the coastal plain is 7 m APSL (Figure 7.3 Transect 3). Also, within the Murray Mouth, 14 km separates the northern margin of Sturt Peninsula from the modern mouth where only the modern, MIS 5e and MIS 7 sedimentary successions have been identified at surface. The longest record of Pleistocene deposition is found within the stacked sedimentary succession at Point McLeay. The sedimentary successions within the study area also differ from their southeastern counterparts in their high content of quartz, which is attributed to the offshore zone being composed of more 50% quartz grains (and far from the zone of modern carbonate production), the presence of the River Murray throughout most of the Quaternary, the deposition of Monlineaux Sands (see below discussion) and the reworking of sediments during each interglacial period.

The middle Pleistocene record within the study area has been affected by ongoing subsidence and downwarping adjacent to the Mount Lofty Ranges and by river erosion, changing base levels, sea-level transgressions and highstands. The most well-preserved middle Pleistocene succession is that of the aeolianite of MIS 7, which forms Sturt Peninsula and extends seaward onto Hindmarsh Island. This does not support the notion of sea level as much as 9 m BPSL during MIS 7 as reported by Blakemore *et al* (2015). However, the sea-level record for MIS 7 is conflicted globally and reviewed below (section 7.3.2.3). The late Pleistocene record of the last interglacial highstand (*sensu stricto*) is the best preserved of the beach-barrier-lagoon shoreline systems, other than the modern example. It is also the only Pleistocene barrier system with associated Pleistocene shell beds, which assist in constraining sea level.

7.3 Comparison with global interglacial sea-level records

As reviewed in Chapter 2, biological, geomorphological and geological proxies can all be used to determine Quaternary palaeo-sea level. The most complete records, however, are derived from deep sea and ice sheet cores that can be dated using orbital tuning to Milankovitch cycles. These records have allowed the recognition of interglacial and glacial extremes. The establishment of marine isotope stages and more minor fluctuations in sea level identified as interstadial and stadials has been made possible by the deep-sea cores. While the record of sea-level change inferred from deep-sea cores may exhibit a contrasting magnitude of sea-level change reflecting local variation, there is consistent agreement on the broad timing of glacial to interglacial transitions (Shackleton and Opdyke, 1973; Lisiecki and Raymo, 2005; Siddall *et al.*, 2004; 2007; Masson-Delmotte *et al.*, 2010; Murray-Wallace and Woodroffe, 2014). The less complete records provided by biological, geomorphological and geological proxies might then be compared with the marine and ice core records to check for consistency and accuracy.

The deposition and accumulation of carbonate aeolianite as coastal dune successions is driven by eustatic sea-level change, the development of an extensive carbonate province with beaches as the carbonate sediment source (McKee and Ward, 1983; Abegg *et al.*, 2001; Brooke, 2001). Quaternary carbonate aeolianites have been

associated with interglacial highstands around the world (McKee and Ward, 1983; Brooke, 2001), and recently Brooke *et al.* (2014) has confirmed the development of coastal aeolianites outside of interglacial peaks on continental shelves with gentle gradients under a wide range of climatic conditions and sea levels. The following sections compare the record of global sea-level change with the carbonate aeolianite record provided in the Murray Lakes region of the Coorong Coastal Plain.

7.3.1 Early Pleistocene

The development of the interglacial record on the northern Coorong Coastal Plain begins with initial deposition of Bridgewater Formation, which is potentially equivalent to the Cannonball Hill Range, the earliest known example of Bridgewater Formation. The apparent ages of the early Pleistocene (MIS 43-MIS 31) Cannonball Hill and Coonalpyn Ranges and the inclusion of Early Pleistocene (MIS 21+) dunes within the composite Murray Lakes Range places deposition immediately before and during the middle Pleistocene Transition (MPT), 1.25-0.70 Ma, a period within the Quaternary in which eustatic sea-level fluctuations switched from lower-amplitude, higher-frequency 41-ka glacial cycles to higher-amplitude, lower-frequency 100-ka glacial cycles (Ruddiman *et al.*, 1986; Maslin *et al.*, 2001; Head and Gibbard, 2005; Lisiecki and Raymo, 2005; Clark *et al.*, 2006). Maximum glaciations (characterised by ~50 m ice-equivalent sea-level lowering) were not established until the end of the MPT (700 ka) when the 100-ka cycle of higher-amplitude fluctuation in eustatic sea-level change was fully established (Clark *et al.*, 2006). As a result of the 41-ka cycle of sea-level change, the differential rates of uplift across the Coorong Coastal Plain would have had less time to affect the spacing of the Early Pleistocene dune ranges resulting in more closely spaced ranges. Differential uplift occurring during the MPT is recognised by the more broadly spaced dunes in the southern Coonalpyn Range coalescing towards the north. The slower rates of uplift in the northern Coorong Coastal Plain would explain why the Murray Lakes Range, which is composed of at least two phases of dune deposition and likely many more, appears as one very large range.

Early Pleistocene coastal landforms are lacking in the global sedimentary record with few coastal deposits to provide evidence of sea-level change (Murray-Wallace and Woodroffe, 2014). Furthermore, they are beyond the range of most geochronological

methods, requiring the application of the marine isotope record and other indirect evidence to determine the age of successions and the height of early Pleistocene sea levels. The strength of the MPT interglacials does not appear to have exceeded those following the transition (Raymo, 1992; Lisiecki and Raymo, 2005) and implies similar sea-level heights when the early Pleistocene Bridgewater Formation was deposited. No shell beds of marine or estuarine origin with which palaeo-sea level can be determined has yet been found in association with the early ranges but sea-level during deposition of the East Naracoorte Range has been placed at <3 m (Murray-Wallace, 2002). Murray-Wallace and Woodroffe (2014) have suggested that the shorter duration of interglacial periods during the 41-ka dominated cycle would likely have resulted in shorter highstand events of only a few thousand years duration, and therefore would not leave as prominent a record on the coastal landscape. This would potentially be reflected in the Bridgewater Formation by ranges of narrower width and less height above the surrounding plain due to less time being available for the accumulation of sediments. However, no consistent measurements of the early Pleistocene ranges have been made to draw other than broad comparisons with their younger counterparts deposited during the middle to late Pleistocene. Furthermore, the Coonalpyn and Murray Lakes ranges are compound structures, composed of multiple stages of deposition but of unknown number and would therefore be unsuitable for direct comparison. Additional research is needed to determine both the number interglacial periods of deposition within each range and their sizes and extents.

7.3.2 Middle and late Pleistocene

The record of global sea-level change is well-established for the middle through late Pleistocene from marine (Siddall *et al.*, 2004; Lisiecki and Raymo, 2005) and ice cores (Jouzel *et al.*, 2007; Masson-Delmotte *et al.*, 2010) and also includes coastal sedimentary records provided by coral reefs (Hearty *et al.*, 1992; Pirrazoli *et al.*, 1993; Chappell *et al.*, 1996; Hearty, 1998; Vézina *et al.*, 1999; Yokoyama, *et al.*, 2001) and carbonate aeolianites (Schellmann and Radtke, 2004; Hearty and O’Leary, 2008; Bateman *et al.*, 2011; Muhs *et al.*, 2012). As reviewed in Chapter 2, the middle to late Pleistocene record of sea-level change for the southeast Coorong Coastal Plain has been well-constrained through amino acid racemisation and thermoluminescence analyses of

aeolian dune, beach and/or lagoon facies from Robe to Nararcoorte (Huntley *et al.*, 1993; 1994; Belperio and Cann, 1990; Murray-Wallace *et al.*, 2001; Murray-Wallace, 2002). Additional work within the Mount Gambier region has extended the record there and shown discrepancies with that of the Robe-Naracoorte record (Blakemore, 2014; Blakemore *et al.*, 2015), illustrating the potential for localised variability, which had been appreciated by Hossfeld (1950) but lacked geochronological evidence.

The middle Pleistocene record within the study area is comprised predominantly of the MIS 7 sedimentary succession on Sturt Peninsula, which extends southward onto Hindmarsh Island. The lack of middle Pleistocene shell beds identified within the study area limits the conclusions that can be made regarding sea level within the region. Inferences must therefore be made based upon the dune record preserved. In contrast the record for the last interglacial (*sensu stricto*) is well preserved and traceable along the length of the Coorong Coastal Plain and eastern shoreline of the modern Coorong. The following section will review the global sea-level record for the middle Pleistocene MIS 11 through MIS 7 as well as the late Pleistocene MIS 5 (*sensu lato*) and discuss the implications of the sea-level record for the study area.

7.3.2.1 Marine Isotope Stage 11

Records developed from marine and ice cores have supported MIS 11 as a particularly strong and warmer interglacial with a particularly long duration indicated by the EPICA Dome C ice core of 32.6 ka from 424.6-392.0 ka (Raymo, 1992; Jouzel *et al.*, 2007; Masson-Delmotte *et al.*, 2010), which has led to comparisons with the current Holocene interglacial (Cronin, 2010; Rohling *et al.*, 2010). The length of the interglacial peak has been associated with orbital forcing and the span of MIS 11 across two precession cycles (Raymo and Mitrovica, 2012).

An estimate of a particularly high sea level during MIS 11 of 20 ± 3 m APSL was derived from cave flowstone bounding reworked limestone on the tectonically stable coastlines of Bermuda and the Bahamas and attributed to a 20% decrease in polar ice during the stage (Hearty *et al.*, 1999). Although, Raymo and Mitrovica (2012) supported the notion of polar ice sheet collapse during MIS 11, the highstand was adjusted to 6-13 m APSL to account for post-glacial crustal subsidence. Conservative estimates from

Curaçao, Leeward Antilles Islands place maximum sea level between 8.4-10 m APSL (Muhs *et al.*, 2012). These values differ substantially however, from the Robe-Naracoorte record of 2 m APSL (Belperio and Cann, 1990; Murray-Wallace *et al.*, 2002) and the Mount Gambier region estimate of 2 ± 2 m APSL (Blakemore *et al.*, 2015). Depending upon the uplift rate used, the Barbados coral reef terraces indicate sea level at -1, 5 or 18 m APSL (Schellmann and Radtke, 2004) and do little to clarify the sea-level record.

Although MIS11 is expected to have been a particularly long interglacial, there is little stratigraphical evidence remaining for this high sea level globally or within the study area and this may be due to the low preservation potential of the coastal sedimentary successions (Murray-Wallace and Woodroffe, 2014) especially in subsiding regions where sea-level returns to similar levels with successive interglacials (Bateman *et al.*, 2014; this research). The MIS 11 interglacial is represented in the study area by the PM A1 aeolianite within the stacked succession at Point McLeay, which at the time of deposition was most likely a topographic high, given the height of the unit above present sea level, ~25 m, and the relative thinness of the unit, <9 m (section 7.2.2). However, given the apparently different rates of subsidence between Point McLeay and the surrounding Murray Lakes region, it is possible that the succession was much nearer to the contemporaneous sea-level than appears today, especially considering the potential height of sea-level.

7.3.2.2 Marine Isotope Stage 9

Sea level during MIS 9 is estimated to have been within 4 m of present day level (Hearty and Kindler, 1995; Vézina *et al.*, 1999) and therefore very few coastal landform records of MIS 9 persist in the landscape as later highstands have overcome and/or eroded and reworked the earlier features (Murray-Wallace and Woodroffe, 2014). Based on analysis of the EPICA Dome C ice core, the interglacial is estimated to have had a duration of ~18.8 ka, commencing at 335.6 ka and ending at 316.8 ka (Masson-Delmotte *et al.*, 2010), with an MIS 9c sea-level peak indicated by coral on Henderson Island between 324 ± 3 ka and 318 ± 3 ka and potential for a later secondary peak near 306 ± 4 ka (Stirling *et al.*, 2001). The Robe-Naracoorte record indicates sea-level during MIS 9 at 1 m BPSL based upon back-barrier lagoon facies (Murray-Wallace, 2002), whereas

lagoon facies in the Mount Gambier region indicate sea-level at 4 ± 1 m APSL although the uncertainty on the age is large (Blakemore *et al.*, 2015). The estimates from the southern Coorong Coastal Plain are uplift-corrected and the discrepancies may be due to variations in the long-term rates of uplift between the two regions. Both sea-level estimates are in broad agreement with the global record in terms of order of magnitude as it has thus far been established.

The MIS 9 record within the Murray Mouth region is, unfortunately, negligible and based on conjecture of stratigraphic relationships. However, the potential MIS 9 aeolian succession at Point McLeay could represent early deposition within MIS 9c followed by extensive pedogenesis during the remainder of the interglacial.

7.3.2.3 Penultimate Interglacial coastline, MIS 7

The Penultimate Interglacial is one of the weakest interglacials during the past 400 ka with a duration of 12 ka between 245.6 ka and 233.6 ka as indicated by the EPICA Dome C ice core (Jouzel *et al.*, 2007; Masson-Delmotte *et al.*, 2010). Marine oxygen isotope records indicate up to three sea-level peaks, MIS 7e, 7c and 7a, separated by episodes of substantially lower sea level (Lisiecki and Raymo, 2005; Siddall *et al.*, 2007). The timing of the two later substages has been constrained by speleothem evidence: MIS 7c (217.2 ± 1.9 to 206.0 ± 1.9) and MIS 7a (201.5 ± 1.7 to 189.7 ± 1.5) (Dutton *et al.*, 2009). The speleothem record of the Argentarola Cave in Italy is one of the few terrestrial records to show evidence of all three highstands and provides an estimate for MIS 7c sea-level near 18 m BPSL and greater than that height for MIS 7e and MIS 7a (Dutton *et al.*, 2009). Estimates for MIS 7a from Barbados range from -20 m to -10 m depending upon the rate of uplift applied. The Sumba Island record indicates MIS 7a sea level corresponding to -6 m but with large uncertainty of 10 m (Pirazzoli *et al.*, 1991). This is, however, comparable with the sea-level estimate for MIS 7a from the Robe-Naracoorte record of -6 m (Murray-Wallace, 2002). Other records refer to the MIS 7 highstand and correspond to MIS 7c and 7a (Siddall *et al.*, 2007) and suggest a sea level somewhat near present day: 2.5 m APSL (Hearty *et al.*, 1992), -2.5 to +1.0 m (Vézina *et al.*, 1999), -3.3 to +2.3 m (Muhs *et al.*, 2012), between -5 m and 0 m (Hearty and Kindler, 1995) and equivalent to the present as indicated by the Robe-Naracoorte record (Murray-Wallace, 2002). The Barbados record, even accounting for possible rates of

uplift, indicates sea level during MIS 7e between -6 m and 4 m (Schellmann and Radtke, 2004). The Mount Gambier Coastal Plain record provides the lowest estimate for MIS 7e sea-level, 9 ± 2 m BPSL (Blakemore *et al.*, 2015).

The MIS 7 sedimentary succession is the best preserved of the middle Pleistocene records within the study area. There has been less time available for subsidence, erosion and reworking by the river and subsequent sea-level transgressions, explaining why the record persists when the MIS 11 record, which was potentially deposited during a period of higher sea-level, does not. The relatively similar estimates of sea-level for MIS 9c and MIS 7e (both are within 5 m of present level) accounts for the lack of MIS 9c record as MIS 7e sea-level returned to a similar height. This notion is supported by the breadth of the MIS 7 succession across Sturt Peninsula and two potential MIS 9 inliers, one on Hindmarsh Island (Murray-Wallace *et al.*, 2010) and the other at Sturt Peninsula (section 7.2.2). However, if the similar sea-level heights between MIS 9c and MIS 7e led to removal or burial of the former interglacial sedimentary successions from the study area, then it is expected that MIS 5e, which attained a greater sea-level maxima than MIS 7, would have removed or buried the MIS 7 sedimentary succession. This is not the case and implies either different rates of subsidence between interglacials, a higher sea-level maximum during MIS 7 or a lower sea-level maximum during MIS 5e. However, the similarity in sea level between MIS 7e and MIS 7a (within 6 m) as indicated by the Robe to Naracoorte record implies that a greater accumulation of barrier sediments could have accumulated during MIS 7 (*sensu lato*). Furthermore, the inundation of the MIS 7 alluvial Pooraka Formation at Myrtlegrove Road by the MIS 5e lagoon (sections 4.3.5 and 6.4) indicate a lower base level during MIS 7 than MIS 5e.

7.3.2.4 Last Interglacial coastline, MIS 5

The last interglacial record is composed of three substages, MIS 5e, 5c and 5a with the record of the MIS 5e shoreline within the study area and Australia having been well established (Belperio *et al.*, 1995; Bourman *et al.*, 2000; Murray-Wallace, 2002; Murray-Wallace and Belperio, 1991; Murray-Wallace *et al.*, 2010). The last interglacial has been subject to considerable study, interpretation and disagreement due perhaps to the complexity and size of the record (Siddall *et al.*, 2006; Murray-Wallace and

Woodroffe, 2014). Also, an assumption by many of a 6 ± 4 m high sea-level during the last interglacial based upon the work of Veeh (1966) who found late Pleistocene fossil coral occurring consistently between 2 and 9 m APSL in locations the Pacific and Indian Oceans remote from plate boundaries may have complicated the issue (Schellmann and Radtke, 2004; Murray-Wallace and Woodroffe, 2014). Global variability is also attributable to glacio-hydro-isostatic effects before, during and after an interglacial highstand (Lambeck *et al.*, 2012).

In an attempt to clarify the last interglacial (MIS 5e) sea-level record, Hearty *et al.* (2007) reviewed the field evidence and geochronologically analysed coastal sedimentary successions from fifteen different well-studied and tectonically stable global localities within the Mediterranean, Bermuda, Bahamas, Barbados, Hawaii and Western Australia and concluded sea-level remained relatively stable at 2.5 ± 1 m APSL for the early half of MIS 5e (~132-125 ka), was followed by a brief, minor regression, then a rise to 3 m to 4 m APSL and the period ended with a sea-level high between 6 m and 9 m APSL (ca 120-118 ka). Subsequent U-series dating of fossil corals in the Bahamas by Thompson *et al.* (2011) supported the rise-fall-peak of sea-level indicated by Hearty *et al.* (2007): 4 m APSL at 123 ka, an intervening period of 0 m, and 6 m APSL at 119.2 ka. The EPICA Dome C ice core record also places MIS 5e from 132-115 ka (Masson-Delmotte, 2010). A review and screen of U-series dating from Bermuda, the Bahamas, Hawaii and Australia (Muhs, 2002) found reliable ages for MIS 5e to fall between 128 and 116 ka, all indicating sea-level was at least as high as present. Kopp *et al.* (2009) statistically modelled the probability of last interglacial sea-level and determined with 95% confidence level that global sea level peaked at 6.6 m APSL, however, their modelling is based upon the assumptions that deglaciation leading up to MIS 5e began at 135 ka and a sea-level highstand at 127 ka.

Following the last interglacial highstand of MIS 5e, two subsequent highstands occurred at ~105 ka (MIS 5c) and ~85 ka (MIS 5a) as determined by electron spin resonance dating of coral reef terraces at Barbados (Schellmann *et al.*, 2004). Sea-level during MIS 5c fluctuated between -13 ± 2 m and -25 ± 2 m during MIS 5c and between -19 ± 2 m and 21 ± 2 m during MIS 5a according to the record there. Low sea-levels are supported by coral reef terraces on Huon Peninsula (Chappell *et al.*, 1996) and the

oxygen-isotope record of marine cores (Chappell and Shackleton, 1986; Lisiecki and Raymo, 2005); the Red Sea record indicates sea level as low as 17 m BPSL (Rohling *et al.*, 2004). The Robe Range supports the notion of much lower sea-level during the two later substages with MIS 5c at 9 m BPSL and MIS 5a at 17 m BPSL (Belperio and Cann, 1990; Murray-Wallace *et al.*, 2001).

The last interglacial (MIS 5e) palaeo-sea-level around Australia is consistently recorded at 2 m APSL with regional differences attributed neotectonic deformation (Murray-Wallace and Belperio, 1991; Belperio *et al.*, 1995). The 2 m highstand is lower than the sea-level peak near 6 m APSL indicated elsewhere and may explain why the MIS 7 sedimentary succession in the Murray Mouth was not overcome during the MIS 5e highstand.

7.4 Molineaux Sand deposition

The Molineaux Sand is extensive within the study area and trend east across the Marmon Jabuk-Kanawinka lineament to form the Big Desert. Various sources have been suggested for the sands including the underlying Parilla Sand, the Bridgewater Formation and the thalassostatic terraces of the River Murray (section 2.5.1). The accumulation of Molineaux Sand in the northern Coorong Coastal Plain may reflect the ongoing uplift to the southeast, as desert dunes tend to accumulate in low-lying areas (Glennie, 1970).

The initial deposition of the glacial Molineaux Sand on the northern Coorong Coastal Plain has not been determined; although the development of the arid climatic conditions necessary for dunefield expansion would have taken place in the middle Pleistocene (Hesse, 2010). In comparison, the infill of solution pipes and *terra rossa* soils are remaining traces of soil development during hiatuses in the deposition of the Bridgewater Formation (sections 3.6.2 and 4.3.7) and while the *terra rossa* record is found only at Point McLeay, solution pipe infill is identified within all stages of the Pleistocene Bridgewater Formation (Chapter 4). The Molineaux Sand within the study area, however, is only identified superseding last interglacial sedimentary successions. Deposition of the Molineaux Sand downwind of the East Naracoorte Range has taken

place more or less continuously over the last 200 ka and it has been suggested that deposition is constrained by available sediment supply driven by climate and the weathering and erosion of the range (Fitzsimmons and Barrows (2012).

Similar to the Coorong Coastal Plain, the Perth Basin of Western Australia contains a record of interglacial calcareous coastal aeolianite dune ridges, which are bordered by glacial period yellow siliceous quartz sand of mainly middle Pleistocene age (Playford *et al*, 1975; Semeniuk and Glassford, 1988; Hearty and O’Leary, 2008). The coastal aeolianites interfinger with the siliceous sands, the extent of which is driven by the height of marine transgression and aeolian processes which drive parabolic dunes of coastal limestone inland (Semeniuk and Glassford, 1988). During glacial periods the aeolian sands would intrude onto the exposed continental shelf to be later incorporated into the coastal dunes with sea-level transgression (Searle and Semeniuk, 1987; Semeniuk and Glassford, 1988). In the Perth Basin, the alternating episodes of desert aeolian and coastal aeolian limestone (Tamala Limestone) deposition have produced a series of limestone lenses within siliceous sands inland of the main limestone ridges.

The cycle of desert siliceous dune and calcareous coastal dune deposition driven by climate and sea-level change in the Perth Basin is the same process as occurring on the northern Coorong Coastal Plain. During glacial periods, desert dunefields composed of Molineaux Sand develop on the Lacepede Shelf south of the Murray Lakes region and are incorporated into coastal sediments with sea-level transgression during interglacial periods explaining the lack of Molineaux Sand within the Bridgewater Formation. For example, the limit of Molineaux Sand on Hindmarsh Island is roughly concordant with the mid-Holocene sea level peak (section 4.3.2). The incorporation of the siliceous sands contributes to the high content of quartz grains within the Bridgewater Formation in the Murray Lakes region and the erosion of the Bridgewater Formation by the river with subsequent delivery to the continental shelf during lowstands provides sediments for the development of the terrestrial dunefields. However, without being able to constrain the initial deposition of the Molineaux Sand it is not possible to make any conclusion on when the cycle of sediment reworking began, although it likely to have been in operation on some scale throughout the Pleistocene following the establishment of climate and sea-level oscillation characteristic of the Quaternary.

The record of limestone lenses within the Perth Basin siliceous sands formed through the inland encroachment of parabolic dunes (Semeniuk and Glassford, 1988) appears to not occur within the Murray Lakes region, possibly due to the presence of the Coorong. As the dunes of the modern Younghusband and Sir Richard Peninsula move landward, they spill into the Coorong and become incorporated into the lagoonal environment. Furthermore, the semi-arid climate of southeastern Australia promotes early meteoric cementation and vegetation, which increases the stability of the dunes (Abegg *et al.*, 2001). However, the record at Point McLeay provides evidence that quantities of the Bridgewater Formation can be transported inland through aeolian processes. There is also the potential that because much of the Quaternary record within the study area is beneath the surface, the Molineaux Sand has not been recognised when encountered in drill holes.

The record of Molineaux Sand deposition is unlikely to extend beyond the last interglacial due to the high reworking potential of the dunes. The Molineaux Sand, unlike the glacial aeolian Woorinen Formation within the Murray Basin, lacks carbonate and clay minerals that encourage soil development and dune stability (Lawrence, 1966; 1980; Bowler, 1976) and this is reflected in the modern asymmetric dunes of Molineaux Sand (Lawrence, 1980). The low stability and lack of consolidation of the Molineaux Sand makes it more susceptible to reworking by changing wind patterns and sea-level transgressions. Luminescence analysis of the dunes would therefore reflect the most recent period of reworking and not necessarily when the dunefield was first established.

7.5 River Murray

Development of the modern River Murray, in the sense of a river recognisable in the present regional landscape, coincides with the desiccation of Lake Bungunnia, which transgresses the Brunhes-Matuyama Boundary (sections 2.3.5 and 2.5.2). The incision of the Murray Gorge and entrainment of the river there signifies that since its development the River Murray has been flowing south from Murray Bridge (Twidale *et al.*, 1978; Harvey *et al.*, 2001; Gingele *et al.*, 2004). The preservation of the Murray Lakes Range and the dolomite plain indicates that river discharge has always been to the west of these features since their deposition and palaeo-channels on the Lacedpede Shelf show

that the river flowed south from Lakes Alexandrina and Albert since at least within the middle Pleistocene (Hill *et al.*, 2009). This indicates that dominant longshore drift along the coastline during sea-level highstands of the middle Pleistocene has been to northwest, as it was during the late Pleistocene and is currently (section 3.3), and similarly, prevented migration of the river mouth to the southeast. The modern Younghusband Peninsula is highest and widest near the Murray Mouth, as is the last interglacial shoreline of Hindmarsh Island. The northwest longshore drift explains the size of the MIS 7 barrier succession on Sturt Peninsula and also helps to explain the accumulation of sediment at Point McLeay and northward development of the Murray Lakes Range.

The increasing development of aridity throughout the Quaternary in Australia has been marked by a trend of decreasing precipitation (section 2.4.4) implying greater discharge from the River Murray with each previous interglacial through the Pleistocene and the potential for larger and/or multiple river mouths. Migration of the modern Murray Mouth has been shown to be highly variable with major directional shifts (Harvey, 1996). Potential mouth migration of 6 km over the past 3000 years (Bourman and Murray-Wallace, 1991) has implications for the preservation of Quaternary sedimentary successions within the Murray Lakes region. The erosion of 17 km of last interglacial Bridgewater Formation from the northeastern margin of Hindmarsh Island southeast to Mark Point is indicative of the erosive capability of the river (section 4.3.3.3). This erosion would have occurred following the last glacial maximum as base level rose and the river exceeded the heights of entrenchment in the Goolwa Channel.

The increased wetness of southern Australia during the early Holocene (Bowler *et al.*, 1976; Cohen and Nanson, 2007; Quigley *et al.*, 2010) and lack of protection afforded by the not-yet-developed Sir Richard and Younghusband Peninsulas exposed the last interglacial barrier to the erosive forces of the river from the north and one of the world's highest wave energy coastlines to the south. At the time the Murray Mouth was much larger with multiple outlets to Encounter Bay expected as the peninsulas were forming. The erosion and reworking of such a length of the MIS 5e barrier implies a similar fate for much of the MIS 5c barrier that remained in the region and would help to explain why only two instances of the MIS 5c barrier have yet been found within the

study area (e.g. Surfer Beach and the Sir Richard Peninsula inlier), although unidentified remnants may reside within Younghusband Peninsula. A similar fate would have befallen previous deposits of the Bridgewater Formation as sea level has repeatedly returned in southern Australia to within ± 6 m of present during each interglacial highstand since the initiation of the middle Pleistocene (Belperio and Cann, 1990; Murray-Wallace *et al.*, 2001; Murray-Wallace, 2002). This could help to explain the broad west-east shape of Lake Alexandrina and possibly the channel connecting the lake to the eastern Lake Albert, which could have formed and been maintained with various phases of river migration throughout the Pleistocene.

The preservation of the coalesced dunes southeast of Lake Albert and the topographic high on the middle of Narrung Peninsula suggests some level of protection from river erosion has been provided to these areas by Point McLeay. It also suggests that the river is not present in the landscape southeast of Lake Albert during glacial lowstands as the change in base level with sea-level transgression would promote erosion that has not occurred in the region. The preservation of Sturt Peninsula indicates that the River Murray has flown east of Point Sturt since MIS 7 deposition. The establishment of the Goolwa Channel across northern Hindmarsh Island through MIS 7 Bridgewater Formation and calcrete implies that during MIS 7 the River Murray was located in a more easterly location and that the development of the Goolwa Channel occurred during MIS 5e.

7.6 Conclusions

This thesis has examined the Quaternary geomorphological evolution of the River Murray Lakes region in South Australia through the record of interglacial highstand sedimentary successions, most recognisably the Bridgewater Formation. The presence of the River Murray, the largest exoreic river in Australia, and the neotectonics of the region as reflected in ongoing subsidence, have influenced depositional patterns and preservation of the sedimentary successions. Numerous sedimentary successions associated with both interglacial and glacial periods of deposition have been investigated by morphostratigraphic, petrographic and geochronological analyses in the form of amino acid racemisation, thermoluminescence, optically stimulated

luminescence and radiocarbon, to determine their geographic relationships, lithological similarities and ages. A review of drillhole data within the region has helped to determine the extent of Bridgewater Formation within the Murray Lakes region. These examinations have led to the following conclusions:

1. The distribution and preservation of the Pleistocene Bridgewater Formation within the Murray Lakes Region has been influenced by the presence of the Padthaway Ridge, differential rates of uplift experienced across and along the Coorong Coastal Plain and a dominant northwest direction of longshore drift. Similarly, the distribution of Bridgewater Formation on Fleurieu Peninsula has been influenced by coastline orientation with the preservation of deposits driven by variable rates of uplift.
2. The Quaternary record of interglacial highstands within the northern Coorong Coastal Plain retains early Pleistocene sedimentary successions of the Bridgewater Formation, likely including the earliest deposition of the Bridgewater Formation and the Padthaway Formation. Due to these sedimentary successions being beyond the dating capabilities of the geochronological methods used in this research, the Coonalpyn and Murray Lakes Ranges were correlated with the marine isotope record based on geographic and morphostratigraphic interpretations. Amino acid racemisation analyses of single foraminifers were able to substantiate the apparent age of the successions.
3. The middle Pleistocene Bridgewater Formation to the southeast of Lake Albert is more extensive than previously realised but has lost all topographic expression, whereas it is most likely that much of the Bridgewater Formation within the immediate region of the Murray Mouth has been eroded and reworked by the River Murray and successive interglacial highstands due to the palimpsest nature of sediments in the region.
4. The identification of a previously unrecognised MIS 7 component of the alluvial Pooraka Formation extends the record of the sedimentary succession farther into the Pleistocene and also supports the notion that sea level during the controversial MIS 7 was lower than MIS 5e sea level.

5. It may not be possible to constrain the initial deposition of the Molineaux Sand within the Murray Lakes region due to the unconsolidated nature of the succession and sediment recycling. Molineaux Sand deposited on the exposed continental shelf during glacial periods or within the range of sea-level transgression is reworked and incorporated into the interglacial coastal sedimentary successions. The erosion of the coastal sedimentary successions and delivery of sediments to the continental shelf via the River Murray during sea-level lowstands to be redistributed as terrestrial dunefields completes the cycle.
6. The recycling of sediments between interglacial coastal sedimentary successions and glacial siliceous dunes is supported by quartz grain analysis (Chapter 4) of Bridgewater Formation, Molineaux Sand, *terra rossa*, solution pipe and alluvial sediments which did not identify any significant trend or characteristic which could be related to environment. This indicates sediments do reside in any one environment for the obligatory time needed to develop identifying characteristics.
7. Amino acid racemisation (AAR) of mollusc shell, calcareous aeolianite sediments and foraminifer tests has been proven to be successful for stratigraphic correlation in the Murray Lakes region. The lack of mollusc shell older than MIS 5e necessitated the analysis of older sedimentary succession through whole-rock and single foraminifer test analyses. Analysis of the calcareous sediments was hampered by low carbonate content, which was found to be critical below 20%, extensive leaching of the sediments within the study area and was unsuccessful on sediments older than MIS 7. Individual foraminifer analysis was more successful from sedimentary successions with low carbonate content and beyond the age of MIS 7 which provided near racemic D/L values for inland sedimentary successions within the Murray Lakes and Coonalpyn Ranges attesting to their greater age. Results were more robust from *Elphidium* sp. than *Discorbis* sp. and indicate the former genus should be preferred for future analyses.
8. Geochronological analysis by thermoluminescence method was not as successful in the Murray Lake region as it has been to the southeast and this can be attributed to more variable dose rates which limit the age range of the methods. However, the successful analysis of the MIS 11 aeolianite at Point McLeay by

optically stimulated luminescence indicates the analytical method can be applied in the region beyond its typical range of 100 ka to 200 ka.

7.7 Further Research

The Murray Lakes region is a captivating and enigmatic landscape and as is usually the case, answers lead to more questions. Further research projects suggested could include:

- Additional field investigations of the early Pleistocene coastal ranges to further define their extents, relationships and compositions. This includes the Black and Hynam Ranges, which can relate and further constrain deposition between and within the West Woakwine and Murray Lakes Range. Field investigations should also be supported by additional sedimentological, petrological and geochronological analyses. This work would help to understand the long-term development of the coastal plain, the differential uplift rates along the coastal plain, localised variations in sea level and contribute to the global sea-level record.
- Stratigraphic analysis and sampling of drillhole cores kept in storage by the Government of South Australia. Analysis of the cores will assist in clarifying the stratigraphy of the region including depth to the base of Quaternary sediments and the identification of Bridgewater Formation sequences interposed with beach sediments, Padthaway Formation and potentially Molineaux Sand. Mollusc shell and foraminifer retrieved from cores could be analysed for indications of depositional environment and by amino acid racemisation for timing of deposition. Shells and tests could also be used to determine palaeo-sea levels and define the different rates of uplift throughout the Coorong Coastal Plain.
- Similar investigations should continue at Point McLeay sedimentary succession, which contains the longest record of interglacial and glacial deposition. Approximately half (the bottom ~20 m) of Point McLeay has not yet been investigated and other locations on the slope may be more suited for geochronological analyses.

- The uplift of Fleurieu Peninsula indicates that sedimentary successions related to sea-level highstands earlier than MIS 5e are potentially located within the landscape and require further field investigations. Furthermore, the age and depositional record at Knights Beach needs further clarification.
- Refine the age and deposition of the middle Pleistocene alluvium at Murray Bridge and Tailem Bend, which could have implication for climatic conditions within the Pleistocene.

References

- Abelson, P.H. (1954). Organic constituents of fossils. *Carnegie Institution of Washington*, **53**, 97-101.
- Abelson, P.H. (1955). Organic constituents of fossils. *Carnegie Institution of Washington*, **54**, 107-109.
- Adams, A.E. and MacKenzie, W.S. (1998). *A Colour Atlas of Carbonate Sediments and Rocks Under the Microscope*. Manson Publishing Ltd., London, 180 pgs.
- Adams, A.E., MacKenzie, W.S., Guilford, C. (1984). *Atlas of Sedimentary Rocks Under the Microscope*. Longman, Harlow, 104 pgs.
- Aitken, M.J. (1985). *Thermoluminescence Dating*. Academic Press, London, 359 pgs.
- Aitken, M.J. (1998). *An Introduction to Optical Dating*. Oxford University Press, Oxford, 267 pgs.
- Alley, R.B. (1998). Icing the North Atlantic. *Nature*, **392**, 335-337.
- Alley, N.F. and Bourman, R.P. (1984). Sedimentology and origin of Late Palaeozoic glacigene deposits at Cape Jervis, South Australia. *Transactions Royal Society of South Australia*, **108**, 63-75.
- Alley, N.F. and Bourman, R.P. (1995): Troubridge Basin, Chapter 8, Late Palaeozoic. In, Drexel, J. F. and Preiss, W.V. [Eds.] *The Geology of South Australia. Vol. 2, The Phanerozoic*. Geological Survey of South Australia, Bulletin 54, pp 65-70.
- Alley, N.F., Bourman, R.P., Milnes, A.R. (2013). Late Palaeozoic Troubridge Basin sediments on Kangaroo Island, South Australia. *MESA Journal*, **70** (3), 24-43.
- Alley, R.B., Shuman, C.A., Meese, D.A., Gow, A.J., Taylor, K.C., Cuffey, K.M., Fitzpatrick, J.J., Grootes, P.M., Zielinski, G.A., Ram, M., Spinelli, G., Elder, B. (1997). Visual-stratigraphic dating of the GISP2 ice core: Basis, reproducibility, and application. *Journal of Geophysical Research*, **102** (C12), 26,367-26,381.

- An, Z., Bowler, J.M., Opdyke, N.D., Macumber, P.G., and Firman, J.B. (1986). Palaeomagnetic stratigraphy of Lake Bungunnia: A Plio-Pleistocene precursor of aridity in the Murray Basin, southeastern Australia. *Palaeogeography, Palaeoclimatology, Palaeoecology*, **54**, 219-239.
- Arakel, A.V. (1982). Genesis of calcrete in Quaternary soil profiles, Hutt and Leeman Lagoons, Western Australia. *Journal of Sedimentary Petrology*, **52** (1), 109-125.
- Arnold, L.D. (1995). Conventional radiocarbon dating. In: Rutter, N.W. and Catto, N.R. [Eds.] *Dating Methods for Quaternary Deposits*, Geological Association of Canada, St. John's, pp 107-116.
- Aziz-Ur-Rahman and McDougall, I. (1972) Potassium-argon ages on the Newer Volcanics of Victoria. *Proceedings of the Royal Society of Victoria*, **85**, 61-70.
- Bada, J.L. and Helfman, P.M. (1975). Amino acid racemization dating of fossil bones. *World Archaeology*, **7**, 160-173.
- Bada, V.L. and Shou, M-Y. (1980). Kinetics and mechanism of amino acid racemization in aqueous solution and in bones. In: Hare, P.E., Hoering, T.C., and King, K. (Eds.), *Biogeochemistry of amino acids*, Wiley, New York, pp 235-255.
- Banjeree, D.; Hildebrand, A.N.; Murray-Wallace, C.V.; Bourman, R.P.; Brooke, B.P.; Blair, M. (2003). New quartz SAR-OSL ages from the stranded beach dune sequence in south-east South Australia. *Quaternary Science Reviews*, **22**, 1019-1025.
- Barker, S., Knorr, G., Edwards, R.L., Parrenin, F., Putnam, A.E., Skinner, L.C., Wolff, E., Ziegler, M. (2011). 800,000 years of abrupt climate variability. *Science*, **334**, 347-351.
- Barnett, E.J. (1993). Recent sedimentary history of Lake Alexandrina and the Murray Estuary. *PhD Thesis*, Flinders University, South Australia.
- Barnett, E.J. (1993). A Holocene paleoenvironmental history of Lake Alexandrina, South Australia. *Journal of Paleolimnology*, **12**, 259-268.

Barnett, S. (1991). Murray Basin hydrogeological investigation drilling programme – Coastal plain progress report No 9. *Geological Survey South Australia*, Report Book **92/13**, Department of Mines and Energy South Australia, Adelaide.

Barrows, T.T. and De Deckker, P. (2007). Long records of climate in southern Australia. *PAGES News*, **15** (2), 15-16.

Barrows, T.T., Juggins, S., De Deckker, P., Calvo, E., Pelejero, C. (2007). Long-term sea surface temperature and climate change in the Australian-New Zealand region. *Paleoceanography*, **22**, PA2215.

Bateman, M.D., Carr, A.S., Dunajko, A.C.; Holmes, P.J., Roberts, D.L., McLaren, S.J., Bryant, R.G., Marker, M.E., Murray-Wallace, C.V. (2011). The evolution of coastal barrier systems: a case study of the Middle-Late Pleistocene Wilderness barriers, South Africa. *Quaternary Science Reviews*, **30**, 63-81.

Bathurst, R.G.C. (1978). Marine diagenesis of shallow water calcium carbonate sediments. *Annual Review of Earth and Planetary Sciences*, **2**, 257-274.

Behrensmeyer, A.K. and Kidwell, S.M. (1985). Taphonomy's contributions to paleobiology. *Paleobiology*, **11** (1), 105-119.

Belperio, A.P. (1985). Quaternary geology of the Sandy Point and Outer Harbor – St Kilda areas, Gulf St Vincent. *Quaternary Geological Notes, The Geological Survey of South Australia*, **96**, 2-6.

Belperio, A.P. (1988). *Fowlers Bay Rotary Drilling Report and Revision of the Quaternary Geology Around Fowlers Bay*. Department of Mines and Energy South Australia, Report Book **No. 88/93**, 63 pgs.

Belperio, A.P. (1995a): Introduction, Chapter 11, Quaternary. In, Drexel, J. F. and Preiss, W.V. [Eds.] *The Geology of South Australia. Vol. 2, The Phanerozoic*. Geological Survey of South Australia, Bulletin 54, pp 219.

Belperio, A.P. (1995b): Coastal and Marine Sequences, Chapter 11, Quaternary. In, Drexel, J. F. and Preiss, W.V. [Eds.] *The Geology of South Australia. Vol. 2, The Phanerozoic*. Geological Survey of South Australia, Bulletin 54, pp 220-240.

Belperio, A.P. and Bluck, R.G. (1990). Coastal palaeogeography and heavy mineral sand exploration targets in the western Murray Basin, South Australia. *AusIMM Proceedings*, **No. 1**, 5-10.

Belperio, A.P. and Cann, J.H. (1990). *Quaternary Evolution of the Robe-Naracoorte Coastal Plain: an Excursion Guide*, Department of Mines and Energy, South Australia, Report Book **90/27**.

Belperio, A.P., Smith, B.W., Polach, H.A., Nitttrouer, C.A., DeMaster, D.J., Prescott, J.R., Hails, J.R., Gostin, V.A. (1984). Chronological studies of the Quaternary marine sediments of northern Spencer Gulf, South Australia. *Marine Geology*, **61**, 265-296.

Belperio, A.P., Murray-Wallace, C.V., Cann, J.H. (1995). The last interglacial shoreline in southern Australia: morphostratigraphic variations in temperate carbonate setting. *Quaternary International*, **26**, 7-19.

Belperio, A.P., Harvey, N., Bourman, R.P. (2002). Spatial and temporal variability in the Holocene sea-level record of the South Australian coastline. *Sedimentary Geology*, **150**, 153-169.

Blackburn, G., Bond, R.D., Clarke, A.R.P. (1965). *Soil Development associated with Stranded Beach Ridges in South-east South Australia*. CSIRO, Melbourne, Soil Publication **No. 22**, 72 pgs.

Blakemore, Amy (2014). *Middle Pleistocene to Holocene sea-level changes and coastal evolution on the Mount Gambier coastal plain, southern Australia*. Doctor of Philosophy thesis, School of Earth and Environmental Sciences, University of Wollongong, <http://ro.uow.edu.au/theses/4243>.

Blakemore, A.G., Murray-Wallace, C.V., Lachlan, T.J. (2014). First recorded evidence of subaqueously-deposited late Pleistocene interstadial (MIS 5c) coastal strata above present sea level in Australia. *Marine Geology*, **355**, 377-383.

- Blakemore, A.G., Murray-Wallace, C.V., Westaway, K.E., Lachlan, T.J. (2015). Aminostratigraphy and sea-level history of the Pleistocene Bridgewater Formation, Mount Gambier region, southern Australia. *Australian Journal of Earth Sciences*, **62** (2), 151-169.
- Bond, G., Broecker, W., Johnsen, S., McManus, J., Labeyrie, L., Jouzel, J., Bonani, G. (1993). Correlations between climate records from North Atlantic sediments and Greenland ice. *Nature*, **365**, 143-147.
- Bourman, R.P. and Alley, N.F. (1990). Stratigraphy and environments of deposition at Hallett Cove during the Late Palaeozoic. *S.A. Dept. Mines and Energy. Mines and Energy Review*, **157**, 68-82.
- Bourman, R.P. and Alley, N.F. (1995). Late Palaeozoic glaciogene sediments at King Point southeastern Troubridge Basin, South Australia. *Geological Survey of South Australia Quarterly Geological Notes*, **128**, 2-7.
- Bourman, R. P. and Alley, N.F. (1999). Permian Glaciated Bedrock Surfaces and Associated Sediments on Kangaroo Island, South Australia: implications for local Gondwanan ice-mass dynamics. *Australian Journal of Earth Sciences*, **46**, 523 - 531.
- Bourman, R.P. and Harvey, N. (1983). The Murray mouth flood tidal delta. *Australian Geographer*, **15** (6), 403-406.
- Bourman, R.P. and Lindsay, J.M. (1989). Timing, extent and character of Late Cainozoic faulting on the eastern margin of the Mt. Lofty Ranges, South Australia. *Transactions of the Royal Society of South Australia*, **113**, 63-67.
- Bourman, R.P. and Murray-Wallace, C.V. (1991). Holocene evolution of a sand spit at the mouth of a large river system: Sir Richard Peninsula and the Murray Mouth, South Australia. *Zeitschrift für Geomorphologie*, **81**, 63-83.
- Bourman, R.P. and Barnett, E.J. (1995). Impacts of river regulation on the terminal lakes and mouth of the River Murray, South Australia. *Australian Geographical Studies*, **33** (1), 101-115.

Bourman, R.P., Martinaitis, P., Prescott, J.R., Belperio, A.P. (1997). The age of the Pooraka Formation and its implications, with some preliminary results from luminescence dating. *Transactions of the Royal Society of South Australia*, **121** (3), 83-94.

Bourman, R.P., Murray-Wallace, C.V., Belperio, A.P., Harvey, N. (2000). Rapid coastal geomorphic change in the River Murray estuary of Australia. *Marine Geology*, **170**, 141-168.

Bourman, R.P., Prescott, J.R., Banerjee, D., Alley, N.F., Buckman, S. (2010). Age and origin of alluvial sediments within and flanking the Mt Lofty Ranges, southern South Australia: a Late Quaternary archive of climate and environmental change. *Australian Journal of Earth Sciences*, **57**, 175-192.

Boutakoff, N. (1963). The geology and geomorphology of the Portland area. *Geological Survey of Victoria*, Memoir **22**.

Bowen, D.Q. and Gibbard, P.L. (2007). The Quaternary is here to stay. *Journal of Quaternary Science*, **22** (1), 3-8.

Bowler, J.M. (1976). Aridity in Australia: Age, origins and expression in aeolian landforms and sediments. *Earth-Science Reviews*, **12**, 279-310.

Bowler, J.M. (1982). Aridity in the late Tertiary and Quaternary of Australia. In: Barker, W.R. and Greenslade, P.J.M. [Eds.] *Evolution of the Flora and Fauna of Arid Australia*, Peacock Publications, Frewville, pgs. 35-45.

Bowler, J.M. and Sandiford, M. (2007). Dynamic Antarctic Ice: Agent for Mid-Pleistocene Transition. *PAGES News*, **15**, 16-18.

Bowler, J.M., Kotsonis, A., Lawrence, C.R. (2006). Environmental evolution of the Mallee Region, western Murray Basin. *Proceedings of the Royal Society of Victoria*, **118** (2), 161-210.

Brett, C.E. and Baird, G.C. (1986). Comparative taphonomy: A key to paleoenvironmental interpretation based on fossil preservation. *PALAIOS*, **1**, 207-227.

Broecker, W.S., Thurber, D.L., Goddard, J., Ku, T.-L., Matthews, R.K., Meselella, K.J. (1968). Milankovitch hypothesis supported by precise dating of coral reefs and deep-sea sediments. *Science*, **159**, 297-300.

Brooke, B. (2001). The distribution of carbonate eolianite. *Earth-Science Reviews*, **55**, 135-164.

Brooke, B.P., Olley, J.M., Pietsch, T., Playford, P.E., Haines, P.W., Murray-Wallace, C.V., Woodroffe, C. (2014). Chronology of Quaternary coastal aeolianite deposition and the drowned shorelines of southwestern Western Australia – a reappraisal. *Quaternary Science Reviews*, **93**, 106-124.

Brookes, J.D., Lamontagne, S., Aldrige, K.T., Bengner, S., Bissett, A., Bucater, L., Cheshire, A.C., Cook, P.L.M., Deegan, B.M., Dittmann, S., Fairweather, P.G., Fernandes, M.B., Ford, P.W., Geddes, M.C., Gillanders, B.M., Grigg, N.J., Haese, R.R., Krull, E., Langley, R.A., Lester, R.E., Loo, M., Munro, A.R., Noell, C.J., Nayar, S., Paton, D.C., Revill, A.T., Rogers, D.J., Roston, A., Sharma, S.K., Short, D.A., Tanner, J.E., Webster, I.T., Wellman, N.R., Ye, Q. (2009). *An Ecosystem Assessment Framework to Guide Management of the Coorong*. Final Report of the CLAMMecology Research Cluster. CSIRO: Water for a Healthy Country National Research Flagship, Canberra, 47 pgs.

Brown, C.M. (1983). Sea-level changes and Cainozoic sedimentation in the Murray Basin. *BMR Journal of Australian Geology and Geophysics*, **8**, (2), 171.

Brown, C.M. (1985). Murray Basin, Southeastern Australia: Stratigraphy and resource potential – A synopsis. *Bureau of Mineral Resources, Physics, Geology and Geophysics, Report 264*, 24 pgs.

Brown, C.M. and Stephenson, A.E. (1991). Geology of the Murray Basin, Southeastern Australia. *Bureau of Mineral Resources, Geology and Geophysics, Canberra, BMR Bulletin 235*, 430 pgs.

Brown, R.G. (1965). *Sedimentation in the Coorong Lagoon, South Australia*. Ph.D. Thesis, Department of Geology and Mineralogy, The University of Adelaide, South Australia, 223 pgs.

Bryant, E.A.; Young, R.W.; Price, D.M.; Short, S.A. (1994). Late Pleistocene dune chronology: Near-coastal New South Wales and eastern Australia. *Quaternary Science Reviews*, **13**, 209-223.

Bureau of Meteorology (2015). *Climate Data Online*, Australian Government. Data retrieved 16 July 2015 from <http://www.bom.gov.au/climate/data/>.

Bye, J.A.T. (1983). Physical Oceanography. In: Tyler, M.J., Twidale, C.R., Ling, J.K., Holmes, J.W. [Eds.] *Natural History of the South East*, Royal Society of South Australia, Northfield, pgs 75-84.

Candy, I. and Black, S. (2009). The timing of Quaternary calcrete development in semi-arid southeast Spain: Investigating the role of climate on calcrete genesis. *Sedimentary Geology*, **218**, 6-15.

Cann, J.H. (1978). An exposed reference section for the Glanville Formation. *Quaternary Geological Notes, The Geological Survey of South Australia*, **65**, 2-4.

Cann, J.H. and Gostin, V.A. (1985). Coastal sedimentary facies and foraminiferal biofacies of the St Kilda Formation at Port Gawler, South Australia. *Transactions of the Royal Society of South Australia*, **109**, 121-142.

Cann, J.H. and Clarke, D.A. (1993). The significance of *Marginopora vertebralis* (Foraminifera) in surficial sediments at Esperance, Western Australia, and in last interglacial sediments in northern Spencer Gulf, South Australia. *Marine Geology*, **111**, 171-187.

Cann, J.H. and Murray-Wallace, C.V. (2012). Interstadial age (MIS5c) beach-dune barrier deposits in the Coorong Lagoon, South Australia. *Australian Journal of Earth Sciences*, **59**, 1127-1134.

Cann, J.H., Belperio, A.P., Gostin, V.A., Murray-Wallace, C.V. (1988). Sea-Level history, 45,000 to 30,000 yr B.P., inferred from benthic foraminifera, Gulf St. Vincent, South Australia. *Quaternary Research*, **29**, 153-175.

Cann, J.H., De Deckker, P., Murray-Wallace, C.V. (1991). Coastal Aboriginal shell middens and their palaeo-environmental significance, Robe Range, South Australia. *Transactions of the Royal Society of South Australia*, **115**, 161-175.

Cann, J.H., Murray-Wallace, C.V., Belperio, A.P., Brenchley, A.J. (1999). Evolution of Holocene coastal environments near Robe, southeastern South Australia. *Quaternary International*, **56**, 81-97.

Cann, J.H., Bourman, R.P., Barnett, E.J. (2000). Holocene foraminifera as indicators of relative estuarine-lagoonal and oceanic influences in estuarine sediments of the River Murray, South Australia. *Quaternary Research*, **53**, 378-391.

Carlisle, D. (1983). Concentration of uranium and vanadium in calcretes and gypcretes. *Geological Society*, London, Special Publication **11**, 185-195.

Carter, A.N. (1985). A model for depositional sequences in the Late Tertiary of southeastern Australia. *Special Publication, South Australia Department of Mines and Energy*, Papers in Honour of Dr. Nell Ludbrook. **No. 5**, 13-27.

Cawood, P.A. (2005). Terra Australis orogen: Rodinia breakup and development of the Pacific and Iapetus margins of Gondwana during the Neoproterozoic and Paleozoic. *Earth Science Reviews*, **69**, 249-279.

Chappell, J. (1974). Geology of coral terraces, Huon Peninsula, New Guinea: A study of Quaternary tectonic movements and sea-level changes. *Geological Society of America Bulletin*, **85**, 553-570.

Chappell, J. and Polach, H.A. (1976). Holocene sea-level change and coral-reef growth at Huon Peninsula, Papua New Guinea. *Geological Society of America Bulletin*, **87**, 235-240.

Chappell, J. and Shackleton, N.J. (1986). Oxygen isotopes and sea level. *Nature*, **324**, 137-140.

Chappell, J., Omura, A., Esat, T., McCulloch, M., Pandolf, J., Ota, Y., Pillans, B. (1996). Reconciliation of late Quaternary sea levels derived from coral terraces at Huon

Peninsula with deep sea oxygen isotope records. *Earth & Planetary Science Letters*, **141**, 227-236.

Chen, X.Y. (2002). Introduction. In: Chen, X.Y., Lintern, M.J., Roach, I.C. [Eds.] *Calcrete: characteristics, distribution and use in mineral exploration*, Cooperative Research Centre for Landscape Environments and Mineral Exploration, CSIRO, Kensington / University of Canberra, ACT, pp 1-4.

Chen, X.Y. and Roach, I.C. (2002). Morphology and Occurrence. In: Chen, X.Y., Lintern, M.J., Roach, I.C. [Eds.] *Calcrete: characteristics, distribution and use in mineral exploration*, Cooperative Research Centre for Landscape Environments and Mineral Exploration, CSIRO, Kensington / University of Canberra, ACT, pp 5-7.

Chen, X.Y., McKenzie, N.J., Roach, I.C. (2002). Distribution in Australia: calcrete landscapes. In: Chen, X.Y., Lintern, M.J., Roach, I.C. [Eds.] *Calcrete: characteristics, distribution and use in mineral exploration*, Cooperative Research Centre for Landscape Environments and Mineral Exploration, CSIRO, Kensington / University of Canberra, ACT, pp 110-138.

Cirano, M. and Middleton, J.F. (2004). Aspects of the mean wintertime circulation along Australia's southern shelves numerical studies. *Journal of Physical Oceanography*, **34**, 668-684.

Clark, P.U., Archer, D., Pollard, D., Blum, J.D., Rial, J.A., Brovkin, V., Mix, A.C., Pisias, N.G., Roy, M. (2006). The middle Pleistocene transition: characteristics, mechanisms, and implications for long-term changes in atmospheric pCO₂. *Quaternary Science Reviews*, **25**, 3150-3184.

Clarke, S.J. and Murray-Wallace, C.V., (2006). Mathematical expressions used in amino acid racemisation geochronology – A review. *Quaternary Geochronology*, **1**, 261-278.

Coblentz, D.D., Sandiford, M., Richardson, R.M., Zhou, S., Hillis, R. (1995). The origins of the intraplate stress field in continental Australia. *Earth and Planetary Science Letters*, **133**, 299-309.

Coe, A.L. (2010). Sedimentary. In: Coe, A.L. [Ed.] *Geological Field Techniques*, Wiley-Blackwell, Oxford, pp 102-138.

Cohen, K.M. and Gibbard, P. (2011). *Global Chronostratigraphical correlation table for the past 2.7 Million Years*. Subcommission on Quaternary Stratigraphy (International Commission on Stratigraphy), Cambridge, England.

Cohen, K.M., Finney, S.C., Gibbard, P.L., Fan, J.-X. (2013). The ICS International Chronostratigraphic Chart. *Episodes*, **36**, 199-204.

Cohen, T.J. and Nanson, G.C. (2007). Mind the gap: an absence of valley-fill deposits identifying the Holocene hypsithermal period of enhanced flow regime in southeastern Australia. *The Holocene*, **17** (3), 411-418.

Cohen, T.J., Nanson, G.C., Jansen, J.D., Jones, B.G., Jacobs, Z., Treble, P., Price, D.M., May, J.-H., Smith, A.M., Ayliffe, L.K., Hellstrom, J.C. (2011). Continental aridification and the vanishing of Australia's megalakes. *Geology*, **39** (2), 167-170.

Colhoun, E.A. and Barrows, T.T. (2011). The glaciation of Australia. In: Ehlers, J., Gibbard, P.L., and Hughes, P.D. [Eds.] *Quaternary Glaciations – Extent and Chronology*, Developments in Quaternary Science, **15**, 1037-1045.

Collins, M.J. and Riley, M.S. (2000). Amino acid racemization in biominerals, the impact of protein degradation and loss. In: Goodfriend, G.A., Collins, M.J., Fogel, M.L., Macko, S.A., Wehmler, J.F. [Eds.] *Perspectives In Amino Acid and Protein Geochemistry*, Oxford University Press, pp 102-142.

Colwell, J.B. (1978). The late Cainozoic sequence of southeastern South Australia – lithology and mineralogy. *BMR Geology and Geophysics, Record 1978/105*, 26 pgs.

Commonwealth of Australia, Geoscience Australia (2009). *Geoscience Australia 1 second SRTM Derived Digital Elevation Models (DEM, DEM-S, DEM-H) Version 1.0*.

Commonwealth of Australia, Department of Agriculture (2013). *Elevation of the Pre-Tertiary Basement in the Murray Basin*. Creative Commons Attribution 3.0 Australia.

Retrieved 09 January 2014 from <https://data.gov.au/dataset/elevation-of-the-pre-tertiary-basement-in-the-murray-basin>

Cook, P.J., Colwell, J.B., Firman, J.B., Lindsay, J.M., Schwebel, D.A., Von der Borch, C.C. (1977). The late Cainozoic sequence of southeast South Australia and Pleistocene sea-level changes. *BMR Journal of Australian Geology & Geophysics*, **2**, 81-88.

Crocker, R.L. and Cotton, C. (1946). Some raised beaches of the lower south-east of South Australia and their significance. *Transactions of the Royal Society of South Australia*, **70** (1), 64-82.

Croll, J. (1875). *Climate and time in their geological relations: a theory of secular changes of the Earth's climate*. Daldy, Isbister, London, 577 pgs.

Crowell, J.C. and Frakes, L.A. (1971). Late Palaeozoic glaciation of Australia. *Journal of the Geological Society of South Australia* **17** (2), 115-155.

Damon, P.E.; Lerman, J.C.; Long, A. (1978). Temporal fluctuations of atmospheric ^{14}C : causal factors and implications. *Annual Review of Earth and Planetary Sciences*, **6**, 457-494.

Dansgaard W. and Oeschger, H. (1989). Past environmental long-term records from the Arctic. In: Oeschger, H. and Langway Jr., C.C. [Eds.] *The Environmental Record in Glaciers and Ice Sheets*, John Wiley & Sons Limited, Chichester, pgs 287-317.

De Mooy, C.J. (1959). Notes on the geomorphic history of the area surrounding Lakes Alexandrina and Albert, South Australia. *Transactions of the Royal Society of South Australia*, **82**, 99-118.

Department of Environment, Water and Natural Resources, South Australia (2012). *South Australian Topographic Data*.

Department for Manufacturing, Innovation, Trade, Resources and Energy (DMITRE) (2014). Geoscientific Data, The Government of South Australia, sourced on 20 August 2014, <https://sarig.pir.sa.gov.au/Map>

Dickinson, J.A., Wallace, M.W., Holdgate, G.R., Daniels, J., Gallagher, S.J., and Thomas, L. (2001). Neogene tectonics in SE Australia: Implications for petroleum systems. *APPEA Journal*, 37-51.

Dickinson, J.A., Wallace, M.W., Holdgate, G.R., Gallagher, S.J., Thomas, L. (2002). Origin and timing of the Miocene-Pliocene unconformity in southeast Australia. *Journal of Sedimentary Research*, **72** (2), 288-303.

Doutch, H.F. and Nicholas, E. (1978). The Phanerozoic sedimentary basins of Australia and their tectonic implications. *Tectonophysics* **48**, 365-388.

Duller, G.A.T. (2004). Luminescence dating of Quaternary sediments: recent advances. *Journal of Quaternary Science*, **19** (2), 183-192.

Dunham, R.J. (1962). Classification of carbonate rocks according to depositional texture. In: Ham, W.E. [Ed.] *Classification of Carbonate Rocks – A symposium*. American Association of Petroleum Geologists, Memoir 1, pp. 108-121.

Dutton, A., Bard, E., Antonioli, F., Esat, T.M., Lambeck, K., McCulloch, M.T. (2009). Phasing and amplitude of sea-level and climate change during the penultimate interglacial. *Nature Geoscience*, **2**, 355-359.

Eastburn, D. (1990). River Form and Flow. In: Mackay N. and Eastburn, D. [Eds.] *The Murray*, Murray Darling Basin Commission, Canberra, 3-16.

Emiliani, C. (1955). Pleistocene Temperatures. *The Journal of Geology*, **63** (6), 538-578.

Esteban, M. and Klappa, C.F. (1983). Chapter 1 Subaerial Exposure. In: Scholle, P.A., Bebout, D.G., Moore, C.H. [Eds.] *Carbonate Depositional Environments*, The American Association of Petroleum Geologists, Tulsa, pp 1-54.

Firman, J.B. (1963). Quaternary geological events near Swan Reach in the Murray Basin, South Australia. *Quaternary Geological Notes, The Geological Survey of South Australia*, **5**, 3-5.

Firman, J.B. (1964). The Bakara Soil and other Stratigraphic Units of Late Cainozoic Age in the Murray Basin, South Australia. *Quaternary Geological Notes, The Geological Survey of South Australia*, **10**, 2-5.

Firman, J.B. (1965). Late Cainozoic Lacustrine Deposits in the Murray Basin, South Australia. *Quaternary Geological Notes, The Geological Survey of South Australia*, **16**, 1-2.

Firman, J.B. (1966a). Stratigraphic units of Late Cainozoic age in the Adelaide Plains Basin, South Australia. *Quaternary Geological Notes, The Geological Survey of South Australia*, **17**, 6-9.

Firman, J.B. (1966b). Stratigraphy of the Chowilla area in the Murray Basin. *Quaternary Geological Notes, The Geological Survey of South Australia*, **20**, 3-7.

Firman, J.B. (1967a). Late Cainozoic stratigraphic units in South Australia. *Quaternary Geological Notes, The Geological Survey of South Australia*, **22**, 4-8.

Firman, J.B. (1967b). Stratigraphy of Late Cainozoic deposits in South Australia. *Transactions of the Royal Society of South Australia* **91**, 165-178.

Firman, J.B. (1969). Quaternary Period. In: Parkin, L.W. [Ed.] *Handbook of South Australian Geology*, A.B. James, Adelaide, pp 204-233.

Firman, J.B. (1973). Regional stratigraphy of surficial deposits in the Murray Basin and Gambier Embayment. *Geological Survey of South Australia, Report of Investigations*, **39**, 68 pgs.

Fitzsimmons, K.E. and Barrows, T.T. (2012). Late Pleistocene aeolian reactivation downwind of the Naracoorte East Range, southeastern South Australia. *Zeitschrift für Geomorphologie*, **56** (2), 225-237.

Flöttman, T. and Cockshell, C.D. (1996). Palaeozoic basins of southern South Australia: new insights into their structural history from regional seismic data. *Australian Journal of Earth Sciences*, **43**, 45-55.

- Flügel, E. (2010). *Microfacies of Carbonate Rocks Analysis, Interpretation and Application*. Springer, Heidelberg, 984 pgs.
- Folk, R.L. (1959). Practical petrographic classification of limestones. *Bulletin of the American Association of Petroleum Geologists*, **43** (1), 1-38.
- Folk, R.L. (1962). Spectral subdivision of limestone types. In: Ham, W.E. [Ed.] *Classification of Carbonate Rocks – A symposium*. American Association of Petroleum Geologists, Memoir 1, pp. 62-84.
- Forsström, L. (2001). Duration of interglacials: a controversial question. *Quaternary Science Reviews*, **20**, 1577-1586.
- Frébourg, G., Hasler, C-A., Le Guern, P., Davaud, E. (2008). Facies characteristics and diversity in carbonate aeolianites. *Facies*, **54**, 175-191.
- Frenchen, M., Dermann, B., Boenigk, W., Ronen, A. (2001). Luminescence chronology of aeolianites from the section at Givat Olga – Coastal Plain of Israel. *Quaternary Science Reviews*, **20**, 805-809.
- Fujioka, T. and Chappell, J. (2010). History of Australian aridity: chronology in the evolution of arid landscapes. In: Bishop, P. and Pillans, B. [Eds.] *Australian Landscapes*. Geological Society, London, Special Publications, **346**, 121-139.
- Fujioka, T., Chappell, J., Fifield, L.K., Rhodes, E.J. (2009). Australian desert dune fields initiated with Pliocene-Pleistocene global climatic shift. *Geology*, **37** (1), 51-54.
- Gaffey, S.J. and Bronnimann, C.E. (1993). Effects of bleaching on organic and mineral phases in biogenic carbonates. *Journal of Sedimentary Petrology*, **63**, 752-754.
- Gallagher, S.J. and Gourley, T.L. (2007). Revised Oligo-Miocene stratigraphy of the Murray Basin, southeast Australia. *Australian Journal of Earth Sciences*, **54**, 837-849.
- Gallagher, S.J., Greenwood, D.R., Taylor, D., Smith, A.J., Wallace, M.W., Holdgate, G.R. (2003). The Pliocene climatic and environmental evolution of southeastern Australia: evidence from the marine and terrestrial realm. *Palaeogeography, Palaeoclimatology, Palaeoecology*, **193**, 349-382.

Gao, S. and Collins, M.B. (2014). Holocene sedimentary systems on continental shelves. *Marine Geology*, **352**, 268-294.

Gatehouse, C.G., Barnett, S.R., and Lablack, K. (1991). Lake Alexandrina groundwater investigation and basement core project: well completion report. *South Australia Department of Mines and Energy*, Report Book **No. 91/26**, 10 pgs.

Gibbard, P.L., Head, M.J., Walker, M.J.C., and the Subcommission on Quaternary Stratigraphy (2010). Formal ratification of the Quaternary System/Period and the Pleistocene Series/Epoch with a base at 2.58 Ma. *Journal of Quaternary Science*, **25**, 96-102.

Gibson, D. (2004). An enhanced framework for the natural resource studies in the Angus-Bremer Plains area, South Australia. *Cooperative Research Centre for Landscape Environments and Mineral Exploration*, South Australia Government Open File Report, **172**, 218 pgs.

Gibson, H.J. and Stüwe, K. (2000). Multiphase cooling and exhumation of the southern Adelaide Fold Belt: constraints from apatite fission track data. *Basin Research*, **12**, 31-45.

Gibson, G.M., Morse, M.P., Ireland, T.R., Nayak, G.K. (2011). Arc-continent collision and orogenesis in western Tasmanides: Insights from reactivated basement structures and formation of an ocean-continent transform boundary off western Tasmania. *Gondwana Research*, **19**, 608-627.

Gillespie, R. (1990). The Australian marine shell correction factor. In: Gillespie, R. [Ed.] *Quaternary Dating Workshop*, Australian National University, Canberra, 59 pgs.

Gillespie, R. and Polach, H.A. (1979). The suitability of marine shells for Radiocarbon dating of Australian prehistory. In: Berger, R. and Suess, H. [Eds.] *Proceedings of the Ninth International Conference on Radiocarbon Dating*, University of California Press, Los Angeles, pp 404-421.

Gingele, F.X., De Deckker, P., Hillenbrand, C. (2004). Late Quaternary terrigenous sediments from the Murray Canyons area, offshore South Australia and their

implications for sea level change, palaeoclimate and palaeodrainage of the Murray-Darling Basin. *Marine Geology*, **212**, 183-197.

Glen, R.A. (2013). Refining accretionary orogen models for the Tasmanides of eastern Australia. *Australian Journal of Earth Sciences* **60** (3), 315-370.

Glennie, K.W. (1970). Desert sedimentary environments. *Developments in Sedimentology* **14**, Elsevier Publishing Company, Amsterdam, 222 pgs.

Godfrey, J.S. and Ridgway, K.R. (1985). The large-scale environment of the poleward-flowing Leeuwin Current, western Australia: Longshore steric height gradients, wind stresses and geostrophic flow. *Journal of Physical Oceanography*, **15**, 481-495.

Goede, A., Murray-Wallace, C.V., Turner, E. (1993). A diverse Holocene molluscan fauna, including *Anadara trapezia*, from Royal Park Launceston, Tasmania. *Papers and Proceedings of the Royal Society of Tasmania*, **127**, 17-22.

Goodfriend, G.A. and Weidman, C.R. (2001). Ontogenetic trends in aspartic acid racemization and amino acid composition within modern and fossil shells of the bivalve *Arctica*. *Geochimica et Cosmochimica Acta*, **65** (12), 1921-1932.

Gostin, V.A. and Jenkins, R.J.F. (1980). Possible western outlet for an Ancient River Murray in South Australia 1. An alternative viewpoint. *Search*, **11** (7-8), 225-226.

Gostin, V.A., Belperio, A.P., Cann, J.H. (1988). The Holocene non-tropical coastal and shelf carbonate province of southern Australia. *Sedimentary Geology*, **60**, 51-70.

Gray, D.R. and Foster, D.A. (2004). Tectonic evolution of the Lachlan Orogen, southeast Australia: historical review, data synthesis and modern perspectives. *Australian Journal of Earth Sciences*, **51**, 773-817.

Green, R.H. (1968). Mortality and stability in a low diversity subtropical intertidal community. *Ecology*, **49** (5), 848-854.

Grove, S.J. (2014). *A Guide to the Seashells and other Marine Molluscs of Tasmania website*. Taroona Scientific, sourced on 2 December 2014, <http://www.molluscsoftasmania.net/index.html>

Gupta, S.K. and Polach H.A., (1985). *Radiocarbon Dating Practices at ANU*. Handbook Radiocarbon Laboratory, Research School of Pacific Studies ANU, Canberra 173 pgs.

Hails, J.R., Belperio, A.P., Gostin, V.A. Sargent, G.A.G. (1984). The submarine Quaternary stratigraphy of northern Spencer Gulf, South Australia. *Marine Geology*, **61**, 345-372.

Hare, P.E. (1969). Geochemistry of proteins, peptides and amino acids. In: Eglinton, G. and Murphy MTJ [Eds.] *Organic geochemistry: Methods and Results*, Springer-Verlag, Berlin, pp 438-463.

Hare, P.E. and Mitterer, R.M. (1966). Nonprotein amino acids in fossil shells. *Carnegie Institute of Washington*, **65**, 362-364.

Hare, P.E. and Abelson, P.H. (1967). Racemisation of amino acids in fossil shells. *Carnegie Institute of Washington*, **66**, 526-528.

Hare, P.E. and Mitterer, R.M. (1968). Laboratory simulation of amino-acid diagenesis in fossils. *Carnegie Institute of Washington*, **67**, 205-208.

Hare, P.E. and Hoering, T.C. (1973). Separation of amino acid optical isomers by gas chromatography. *Carnegie Institute of Washington*, **72**, 690-694.

Hare, P.E., Miller, G.H. and Tuross, N.C. (1975). Simulation of natural hydrolysis of proteins in fossils. *Carnegie Institute of Washington*, **74**, 608-612.

Hare, P.E., Von Endt, D.W., Kokis, J.E. (1997). Protein and Amino Acid Diagenesis Dating. In: Taylor, R.E. and Aitken, M.J. [Eds.] *Chronometric Dating*, Plenum Press, New York, pp 261-296.

Harris, W.K., Lindsay, J.M.,; and Twidale, C.R. (1980). Possible western outlet for an Ancient River Murray in South Australia 2. A discussion. *Search*, **11** (7-8), 226-227.

Harvey, N. (1981). Coastal geomorphology of south east South Australia. *Taminga*, **18**, 1-15.

Harvey, N. (1996). The significance of coastal processes for management of the River Murray estuary. *Australian Geographical Studies*, **34** (1), 45-57.

Harvey, N. (2006). Holocene coastal evolution: barriers, beach ridges, and tidal flats of South Australia. *Journal of Coastal Research*, **22** (1), 90-99.

Harvey, N., Belperio, A.P., and Bourman, R.P. (2001). Late Quaternary sea-levels, climate change and South Australian coastal geology. In: Gostin, V.A. [Ed.] *Gondwana to Greenhouse: Australian Environmental Geoscience*, Geological Society of Australia Special Publication, **21**, 201-213.

Harvey, N., Bourman, R.P., James, K. (2006). Evolution of the Younghusband Peninsula, South Australia: new evidence from the northern tip. *South Australian Geographical Journal*, **105**, 37-50.

Hays, J.D., Imbrie, J., Shackleton, N.J. (1976). Variations in the Earth's Orbit: Pacemaker of the Ice Ages. *Science*, **194**, 1121-1132.

Head, M.J. and Gibbard, P.L. (2005). Early-Middle Pleistocene transitions: an overview and recommendation for the defining boundary. In: Head, M.J. and Gibbard, P.L. [Eds.] *Early-Middle Pleistocene Transitions: The Land-Ocean Evidence*, Geological Society, London, Special Publication 247, pp 1-18.

Head, M.J., Gibbard, P., Salvador, A. (2008). The Quaternary: its character and definition. *Episodes*, **31** (2), 234-238.

Hearty, P.J. (1998). The geology of Eleuthera Island, Bahamas: a Rosetta Stone of Quaternary stratigraphy and sea-level history. *Quaternary Science Reviews*, **17**, 333-355.

Hearty, P.J. and O'Leary, M.J. (2008). Carbonate eolianites, quartz sands, and Quaternary sea-level cycles, Western Australia: A chronostratigraphic approach. *Quaternary Geochronology*, **3**, 26-55.

Hearty, P.J., Vacher, H.L., Mitterer, R.M. (1992) Aminostratigraphy and ages of Pleistocene limestones of Bermuda. *Geological society of America Bulletin*, **104**, 471-480.

Hearty, P.J., Kindler, P., Cheng, H., Edwards, R.L. (1999). A +20 m middle Pleistocene sea-level highstand (Bermuda and the Bahamas) due to the partial collapse of Antarctic ice. *Geology*, **27** (4), 375-378.

Hearty, P.J., O'Leary, M.J., Kaufman, D.S., Page, M.C., Bright, J. (2004). Amino acid geochronology of individual foraminifer (*Pulleniatina obliquiloculata*) tests, north Queensland margin, Australia: A new approach to correlating and dating Quaternary tropical marine sediment cores. *Paleoceanography*, **19**, PA4022.

Hearty, P.J., Hollin, J.T., Neumann, A.C., O'Leary, M.J., McCulloch, M. (2007). Global sea-level fluctuations during the Last Interglaciation (MIS 5e). *Quaternary Science Reviews*, **26**, 2090-2112.

Helfman, P.M. and Bada, J.L. (1975). Aspartic acid racemization in tooth enamel from living humans. *Proceedings of the National Academy of Sciences of the United States of America*, **72** (8), 2891-2894.

Hesse, P. (2010). The Australian desert dunefields: formation and evolution in an old, flat, dry continent. In: Bishop, P. and Pillans, P. [Eds.] *Australian Landscapes*, Geological Society, London, Special Publications, **346**, 141-164.

Hesse, P. (2011). Sticky dunes in a wet desert: Formation, stabilisation and modification of the Australian desert dunefields. *Geomorphology*, **134**, 309-325.

Hill, P.J., De Deckker, P., von der Borch, C., Murray-Wallace, C.V. (2009). Ancestral Murray River on the Lacepede Shelf, southern Australia: Late Quaternary migrations of a major river outlet and strandline development. *Australian Journal of Earth Sciences*, **56**, 135-157.

Hollin, J.T. and Hearty, P.J. (1990). South Carolina Interglacial Sites and Stage 5 Sea Levels. *Quaternary Research*, **33**, 1-17.

Hossfeld, P.S. (1950). The late Cainozoic history of the south-east of South Australia. *Transactions of the Royal Society of South Australia*, **73** (2), 232-279.

Howchin, W. (1888). Notes on a geological section at the new graving dock, Glanville, with special reference to the supposed old land surface now below sea level. *Transactions of the Royal Society of South Australia*, **10**, 31-35.

Howchin, W. (1926). The geology of the Victor Harbour, Inman Valley, and Yankalilla Districts, with special reference to the Great Inman Valley glacier of Permo-Carboniferous age. *Transactions of the Royal Society of South Australia*, **50**, 89-119.

Huber, M. (2014). *Paphies elongata*. Data retrieved 17 February 2015 through: World Register of Marine Species at <http://www.marinespecies.org/aphia.php?p=taxdetails&id=505808>.

Hughen, K.A., Baillie, M.G.L., Bard, E., Beck, J.W., Bertrand, C.J.H., Blackwell, P.G., Buck, C.E., Burr, G.S., Cutler, K.B, Damon, P.E., Edwards, R.L., Fairbanks, R.G., Friedrich, M., Guilderson, T.P., Kromer, B., McCormac, G., Manning, S., Ramsey, C.B., Reimer, P.J., Reimer, R.W., Remmele, S., Southon, J.R., Stuiver, M., Talamo, S., Taylor, F.W., van der Plicht, J., Weyhenmeyer, C.E. (2004). Marine04 Marine radiocarbon age calibration, 0-26 Cal kyr BP. *Radiocarbon*, **46** (3), 1059-1086.

Huntley, D.J. and Prescott, J.R. (2001). Improved methodology and new thermoluminescence ages for the dune sequence in south-east South Australia. *Quaternary Science Reviews*, **20**, 687-699.

Huntley, D.J., Godfrey-Smith, D.I., Thewalt, M.L.W. (1985). Optical dating of sediments. *Nature*, **313**, 105-107.

Huntley, D.J.; Hutton, J.T.; Prescott, J.R. (1993a). The stranded beach-dune sequence of south-east South Australia: a test of thermoluminescence dating, 0-800 ka. *Quaternary Science Reviews*, **12**, 1-20.

Huntley, D.J.; Hutton, J.T.; Prescott, J.R. (1993b). Optical dating using inclusions within quartz grains. *Geology*, **21**, 1087-1090.

Huntley, D.J.; Hutton, J.T.; Prescott, J.R. (1994). Further thermoluminescence dates from the dune sequence in the southeast of South Australia. *Quaternary Science Reviews*, **13**, 201-207.

Huston D.L., Blewett, R.S., Champion, D.C. (2012). Australia through time; a summary of its tectonic and metallogenic evolution. *Episodes*, **35** (1), 23-43.

Idnurm M. and Cook, P. (1980). Palaeomagnetism of beach ridges in South Australia and the Milankovitch theory of ice ages. *Nature*, **286**, 699-702

Imbrie, J. (1985). A theoretical framework for the Pleistocene ice ages. *Journal of the Geological Society, London*, **142**, 417-432.

Imbrie, J., Hays, J.D., Martinson, D.G., McIntyre, A., Mix, A.C., Morley, J.J., Pisias, N.G., Prell, W.L., Shackelton, N.J. (1984). The orbital theory of Pleistocene climate: support from a revised chronology of the marine $\delta^{18}\text{O}$ record. In: Berger, A., Imbrie, J., Hays, J., Kukla, G., Saltzman, B. [Eds.] *Milankovitch and Climate, Part 1*, D.Reidal Publishing Company, Dordrecht, pp 269-305.

Jacobs, Z. and Roberts, R.G. (2007). Advances in optically stimulated luminescence dating of individual grains of quartz from archaeological deposits. *Evolutionary Anthropology*, **16** (6), 210-223.

James, K. (2004). Shifting sands at the Murray Mouth: evidence from historic surveys 1839-1938. *South Australian Geographical Journal*, **103**, 25-42.

James, K.F., Bourman, R.P., Harvey, N. (*in press*). Rapid evolution of a flood tidal deltaic island in River Murray estuary, South Australia: A canary in the cage of river management. *Journal of Coastal Research*.

James, N.P. and Choquette, P.W. (1983). Diagenesis 5. Limestones: Introduction. *Geoscience Canada*, **10** (4), 159-161.

James, N.P. and Choquette, P.W. (1984). Diagenesis 9. Limestones – The meteoric diagenetic environment. *Geoscience Canada*, **11** (4), 161-194.

James, N.P. and Bone, Y. (2011). *Neritic Carbonate Sediments in a Temperate Realm*. Springer, Dordrecht, 254 pgs.

James, N.P., Bone, Y., von der Borch, C.C., Gostin, V.A. (1992). Modern carbonate and terrigenous clastic sediments on a cool water, high energy, mid-latitude shelf: Lacepede, southern Australia. *Sedimentology*, **39**, 877-903.

James, N.P., Bone, Y., Hageman, S.J., Feary, D.A., Gostin, V.A. (1997). Cool-water carbonate sedimentation during the terminal Quaternary sea-level cycle: Lincoln Shelf, southern Australia. In: James, N.P. and Clarke, J.A.D. [Eds.] *Cool-water Carbonates*, Society for Sedimentary Geology Special Publication No. **56**, pp 53-75.

Jankowski, N.R., Jacobs, Z., and Goldberg, P. (2014). Optical dating and soil micromorphology at MacCauley's Beach, New South Wales, Australia. *Earth Surface Processes and Landforms*, **40** (2), 229-242.

Jayawardena, Chulantha Lakmal (2013). *Characteristics of neotectonic faulting in the Mount Lofty and Flinders Ranges, South Australia*. Doctor of Philosophy thesis, School of Earth and Environmental Sciences, University of Wollongong, <http://ro.uow.edu.au/theses/4093>.

Johnson, R.G. (1960). Models and methods for analysis of the mode of formation of fossil analysis. *Bulletin of the Geological Society of America*, **71**, 1075-1086.

Johnston, E.N. (1917). Report on the harbour for the River Murray Valley. *Parliamentary Papers Adelaide*, **No. 38**, pgs.71.

Jones, J.G. and Veevers, J.J. (1982). A Cainozoic history of Australia's Southeast Highlands. *Journal of the Geological Society of Australia*, **29**, 1-12.

Jones, A.R., Murray, A., Skilleter, G.A. (1988). Aspects of the life history and population biology of *Notospisula trigonella* (Bivalvia: Mactridae) from the Hawkesbury Estuary southeastern Australia. *The Veliger*, **30** (3), 267-277.

Jouzel, J., Masson-Delmotte, V., Cattani, O., Dreyfus, G., Falourd, S., Hoffman, G., Minster, B., Nouet, J., Barnola, J.M., Chappellaz, J., Fischer, H., Gallet, J.C., Johnsen, S., Leuenberger, M., Loulergue, L., Luethi, D., Oerter, H., Parrenin, F., Raisbeck, G., Raynaud, D., Schilt, A., Schwander, J., Selmo, E., Souchez, R., Spahni, R., Stauffer, B., Steffensen, J.P., Stenni, B., Stocker, T.F., Tison, J.L., Wemer, M., Wolff, E.W. (2007). Orbital and millennial Antarctic climate variability over the past 800,000 years. *Science*, **317**, 793-796.

Kanfoush, S.L., Hodell, D.A., Charles, C.D., Guilderson, T.P., Mortyn, P.G., Ninnemann, U.S. (2000). Millennial-scale instability of the Antarctic ice sheet during the last glaciation. *Science*, **288**, 1815-1818.

Kaufman, D.S. and Manley, W.F. (1998). A new procedure for determining DL amino acid ratios in fossils using reverse phase liquid chromatography. *Quaternary Geochronology*, **17**, 987-1000.

Kemp, E.M. (1978). Tertiary climatic evolution and vegetation history in the southeast Indian Ocean region. *Palaeogeography, Palaeoclimatology, Palaeoecology*, **24**, 169-208.

Kendrick, G.W., Wyrwoll, K-H., Szabo, B.J. (1991). Pliocene-Pleistocene coastal events and history along the western margin of Australia. *Quaternary Science Reviews*, **10**, 419-439.

Kidwell, S.M., Fursich F.T., Aigner, T. (1986). Conceptual framework for the analysis and classification of fossil concentrations. *PALAIOS*, **1**, 228-238.

Kimber, R.W.L. and Milnes, A.R. (1984). The extent of racemization of amino acids in Holocene and Pleistocene marine molluscs in southern South Australia: Preliminary data on a time-framework for calcrete formation. *Australian Journal of Earth Sciences*, **31**, 279-286.

Kimber, R.W.L. and Griffin, C.V. (1987). Further evidence of the complexity of the racemization process in fossil shells with implications for amino acid racemization dating. *Geochimica et Cosmochimica Acta*, **51**, 839-846.

Kimber, R.W.L., Griffin, C.V., Milnes, A.R. (1986). Amino acid racemisation dating: Evidence of apparent reversal in aspartic acid racemization with time in shells of *Ostrea*. *Geochimica et Cosmochimica Acta*, **50**, 1159-1161.

Kindler, P. and Hearty, P.J. (1996). Carbonate petrography as an indicator of climate and sea-level changes: new data from Bahamian Quaternary units. *Sedimentology*, **43**, 381-399.

King, D. (1960). The sand ridge deserts of South Australia and related aeolian landforms of the Quaternary arid cycles. *Transactions of the Royal Society of South Australia*, **83**, 99-108.

Kotsonis, A. (1999). Tertiary shorelines of the western Murray Basin: weathering sedimentology and exploration potential. In: Stewart, R. [Ed.] *Murray Basin Mineral Sands, Extended abstracts of Papers Presented at a Conference*, Australian Institute of Geoscientists, Bulletin No. **26**, 57-63.

Kriausakul, N. and Mitterer, R. (1978). Isoleucine epimerization in peptides and proteins: kinetic factors and applications to fossil proteins. *Science*, **21**, 1011-1014.

Krieg, G.W., Alexander, E.M., Alley, N.F., Armstrong, D., Farrand, M.G., Gatehouse, C.G., Gravestock, D.I., Hill, A.J., Kwitko, G., Morton, J.G.G., Rogers, P.A. (1995): Jurassic-Cretaceous Rift Basins, Chapter 9, Mesozoic. In, Drexel, J. F. and Preiss, W.V. [Eds.] *The Geology of South Australia. Vol. 2, The Phanerozoic*. Geological Survey of South Australia, Bulletin 54, pp 130.

Kuenen, Ph. H. (1960). Experimental Abrasion 4. Eolian Action. *The Journal of Geology*, **78** (4), 427-449.

Kuenen, Ph. H. and Perdok, W.G. (1962). Experimental abrasion 5. Frosting and defrosting of quartz grains. *The Journal of Geology*, **70** (6), 648-658.

Kvenvolden, K.A. (1975). Advances in the geochemistry of amino acids. *Annual Review of Earth and Planetary Science*, **3**, 183-212.

Kvenvolden, K.A., Blunt, D.J., Clifton, H.E. (1981). Age estimations based on amino acid racemization: reply to comments of J.F. Wehmiller. *Geochimica et Cosmochimica Acta*, **45**, 265-267.

Lachlan, T.J. (2011). *Aminostratigraphy and luminescence dating of the Pleistocene Bridgewater Formation, Kangaroo Island, South Australia: an archive of long term climate and sea-level change*. Doctor of Philosophy thesis, School of Earth and Environmental Sciences, University of Wollongong, <http://ro.uow.edu.au/theses/3503>

Lajoie, K.R., Wehmiller, J.F., Kennedy, G.L. (1980). Inter- and intrageneric trends in apparent racemization kinetics of amino acids in Quaternary Mollusks. In: Hare, P.E., Hoering, T.C., and King, K. [Eds.], *Biogeochemistry of Amino Acids*, Wiley, New York, pp 305-340.

Lambeck, K. and Chappell, J. (2001). Sea level change through the last glacial cycle. *Science*, **292**, 679-686.

Lambeck, K., Purcell, A., Dutton, A. (2012). The anatomy of interglacial sea levels: The relationship between sea levels and ice volumes during the Last Interglacial. *Earth and Planetary Science Letters*, **315-316**, 4-11.

Langway, Jr., C.C. and Oeschger, H. (1989). Introduction. In: Oeschger, H. and Langway Jr., C.C. [Eds.] *The Environmental Record in Glaciers and Ice Sheets*, John Wiley & Sons Limited, Chichester, pp 1-11.

Lawrence, C.R. (1966). Cainozoic stratigraphy and structure of the Mallee Region, Victoria. *Proceedings of the Royal Society of Victoria*, **79**, 517-553.

Lawrence, C.R. (1975). Geology, hydrodynamics and hydrochemistry of the southern Murray Basin. *Geological Survey of Victoria*, Memoir **30**, 359 pgs.

Lawrence, C.R. (1980). Aeolian landforms of the Lowan Sand and Woorinen Formation in north-western Victoria. In: Storrier, R.R. and Stannard, M.E. [Eds.] *Aeolian Landscapes in the Semi-arid Zone of Southern Australia*, Riverina Society of Soil Science, Wagga Wagga, pgs 57-64.

Lewis, S.E., Sloss, C.R., Murray-Wallace, C.V., Woodroffe, C.D., Smithers, S.G. (2013). Post-glacial sea-level changes around the Australian margin: a review. *Quaternary Science Reviews*, **74**, 115-138.

Li, Q., James, N.P., McGowran, B., Bone, Y., Cann, J. (1998). Synergetic influence of water masses and Kangaroo Island barrier on foraminiferal distribution, Lincoln and Lacepede shelves, South Australia: A synthesis. *Alcheringa*, **22** (2), 153-176.

Li, Q., Simo, J.A., McGowran, B., Holbourn, A. (2004). The eustatic and tectonic origin of Neogene unconformities from the Great Australian Bight. *Marine Geology*, **203**, 57-81.

Liritzis, I., Singhvi, A.K., Feathers, J.K., Wagner, G.A., Kadereit, A., Zacharias, N., Li, S-H. (2013). Luminescence dating protocols and dating range. In: Liritzis, I., Singhvi, A.K., Feathers, J.K., Wagner, G.A., Kadereit, A., Zacharias, N., Li, S-H. [Eds.] *Luminescence dating in Archaeology, Anthropology, and Geochronology An Overview*, Springer Briefs in Earth System Sciences, Cham, pp 5-20.

Lisiecki, L. and Raymo, M.E. (2005). A Pliocene-Pleistocene stack of 57 globally distributed benthic $\delta^{18}\text{O}$ records. *Paleoceanography*, **20**, PA1003.

Logan, B.W., Read, J.F., Davies, G.R. (1970). History of carbonate sedimentation, Quaternary Epoch, Shark Bay, Western Australia. In: Logan, B.W., Davies, G.R., Read, J.F., Cebulski, D.E. [Eds] *Carbonate Sedimentation and Environments, Shark Bay, Western Australia*, The American Association of Petroleum Geologists, Tulsa, pp 38-84.

Lomax, J., Hilgers, A., Radtke, U. (2011). Palaeoenvironmental change recorded in the palaeodunefields of the western Murray Basin, South Australia – New data from single grain OSL-dating. *Quaternary Science Reviews*, **30**, 723-736.

Lorius, C., Raisbeck, G., Jouzel, J., Raynaud, D. (1989). In: Oeschger, H. and Langway Jr., C.C. [Eds.] *The Environmental Record in Glaciers and Ice Sheets*, John Wiley & Sons Limited, Chichester, pgs 343-361.

Love, K.M. and Woronow, A. (1991). Chemical changes induced in aragonite using treatments for the destruction of organic material. *Chemical Geology*, **93**, 291-301.

Ludbrook, N.H. (1957). A reference column for the Tertiary Sediments of the South Australian Portion of the Murray Basin. *Journal of the Proceedings of the Royal Society of New South Wales*, **90**, 174-180.

Ludbrook, N.H. (1961). Stratigraphy of the Murray Basin in South Australia. *Geological Survey of South Australia*, SA Department of Mines, Bulletin No. **36**.

Ludbrook, N.H. (1967). Permian deposits of South Australia and their fauna. *Transactions of the Royal Society of South Australia*, **91**, 65-87.

Ludbrook, N.H. (1976). The Glanville Formation at Port Adelaide. *Quaternary Geological Notes, The Geological Survey of South Australia*, **57**, 4-7.

Ludbrook, N.H. (1984). Quaternary Molluscs of South Australia. Department of Mines and Energy, South Australia, Handbook **No. 9**, 327 pgs.

Luebbers, R.A. (1982). *The Coorong Report: An Archaeological Survey of the Northern Coorong*. Prepared for the South Australian Department for Environment and Planning, 85 pgs.

Lukasik, J.J. and James, N.P. (1998). Lithostratigraphic revision and correlation of the Oligo-Miocene Murray supergroup, western Murray Basin, South Australia. *Australian Journal of Earth Sciences*, **45**, 889-902.

Lukasik, J. and James, N.P. (2006). Carbonate sedimentation, climate change and stratigraphic completeness on a Miocene cool-water epeiric ramp, Murray Basin, South Australia. *Geological Society, London, Special Publications*, **255**, 217-244.

MacFadden, B.J., Whitelaw, M.J., MacFadden, P., Rich, T.H.V. (1987). Magnetic polarity stratigraphy of the Pleistocene section at Portland (Victoria), Australia. *Quaternary Research*, **28**, 364-373.

Macumber, P.G. (1978). Evolution of the River Murray during the Tertiary Period. Evidence from northern Victoria. *Proceedings of the Royal Society of Victoria*, **90**, 43-52,

Martin, H.A. (2006). Cenozoic climatic change and the development of the arid vegetation in Australia. *Journal of Arid Environments*, **66**, 533-563.

Martinson, D.G., Pisias, N.G., Hays, J.D., Imbrie, J., Moore, T.C., Shackleton, N.J. (1987). Age dating and the orbital theory of the Ice Ages: Development of a high resolution 0 to 300,000-year chronostratigraphy. *Quaternary Research*, **27**, 1-29.

Maslin, M., Seidor, D., Lowe, J. (2001). Synthesis of the nature and causes of rapid climate transitions during the Quaternary. *The Oceans and Rapid Climate Change: past, Present, and Future*, Geophysical Monograph **126**, 9-52.

Masson-Delmotte, V., Stenni, B., Pol, K., Braconnot, P., Cattani, O., Falourd, S., Kageyama, M., Jouzel, J., Landais, A., Minster, B., Barnola, J.M., Chappellaz, J., Krinner, G., Johnsen, S., Röthlisberger, R., Hansen, J., Mikolajewicz, U., Otto-Bliesner, B. (2010). EPICA Dome C record of glacial and interglacial intensities. *Quaternary Science Reviews*, **29**, 113-128.

Masters, P.M., Bada, J.L., Zigler Jr., J.S. (1977). Aspartic acid racemisation in the human lens during ageing and in cataract formation. *Nature*, **268**, 71-73.

McFadden, B.J., Whitelaw, M.J., McFadden, P., Rich, T.H.V. (1987). Magnetic polarity stratigraphy of the Pleistocene section at Portland (Victoria), Australia. *Quaternary Research*, **28**, 364-373.

McGowran, B., Li, Q., and Moss, G. (1997a). The Cenozoic neritic record in southern Australia: The biogeohistorical framework. In: James, N.P. and Clarke, J.A.D. [Eds] *Cool-Water Carbonate*, SEPM (Society for Sedimentary Geology) Special Publication **No. 56**, 185-203.

McGowran, B., Li, Q., Cann, J., Padley, D., McKirdy, D.M., Shafik, S. (1997b). Biogeographic impact of the Leeuwin Current in southern Australia since the late middle Eocene. *Palaeogeography, Palaeoclimatology, Palaeoecology*, **136**, 19-40.

McGowran, B., Holdgate, G.R., Li, Q., Gallagher, S.J. (2004). Cenozoic stratigraphic succession in southeastern Australia. *Australian Journal of Earth Sciences*, **51**, 459-496.

McKee, E.D. and Ward, W.C. (1983). Chapter 3 Eolian. In: Scholle, P.A., Bebout, D.G., Moore, C.H. [Eds.] *Carbonate Depositional Environments*, The American Association of Petroleum Geologists, Tulsa, pp 131-170.

McLaren, S. and Wallace, M.W. (2010). Plio-Pleistocene climate change and the onset of aridity in southeastern Australia. *Global and Planetary Change*, **71**, 55-72.

McLaren, S., Wallace, M.W., Pillans, B.J., Gallagher, S.J., Miranda, J.A., Warne, M.T. (2009). Revised stratigraphy of the Blanchetown Clay, Murray Basin: age constraints on the evolution of paleo Lake Bungunna. *Australian Journal of Earth Sciences*, **56**, 259-270.

McLaren, S., Wallace, M.W., Gallagher, S.J., Miranda, J.A., Holdgate, G.R., Gow, L.J., Snowball, I., Sandgren, P. (2011). Palaeogeographic, climatic and tectonic change in southeastern Australia: the Late Neogene evolution of the Murray Basin. *Quaternary Science Reviews*, **30**, 1086-1111.

Mee, A.C., Bestland, E.A., Spooner, N.A. (2004). Age and origin of Terra Rossa soils in the Coonawarra area of South Australia. *Geomorphology*, **58**, 1-25.

Miall, A.D. (2010). *The Geology of Stratigraphic Sequences*, Springer, Heidelberg, 522 pgs.

Miller, G.H. and Brigham-Grette, J. (1989). Amino acid geochronology: resolution and precision in carbonate fossils. *Quaternary International*, **1**, 111-128.

Miller, G.H. and Hare, P.E. (1975). Use of amino acid reactions in some arctic marine fossils as stratigraphic and geochronological indicators. *Carnegie Institute of Washington*, **74**, 612-617.

Miller, G.H. and Hare, P.E. (1980). Amino acid geochronology: Integrity of the carbonate matrix and potential of molluscan fossils. In: Hare, P.E., Hoering, T.C., and King, K. [Eds.], *Biogeochemistry of Amino Acids*, Wiley, New York, pp 415-443.

Miller, G.H., Hart, C.P., Roark, E.B., Johnson, B.J. (2000). Isoleucine epimerisation in eggshells of the flightless Australian birds *Genyornis* and *Dromaius*. In: Goodfriend, G.A., Collins, M.J., Fogel, M.L., Macko, S.A., Wehmler, J.F. [Eds.], *Perspectives in Amino Acid and Protein Geochemistry*, Oxford University Press, New York, pp 279-300.

Miller, J. McL., Phillips, D., Wilson, C.J.L., Dugdale, L.J. (2005). Evolution of a reworked orogenic zone: the boundary between the Delamerian and Lachlan Fold Belts, southeastern Australia. *Australian Journal of Earth Sciences*, **52**, 921-940.

Milnes, A.R. (1982). Calcretes in Southern Australia. In: Wasson, R.J. [Ed.] *Quaternary Dust Mantles of China, New Zealand and Australia*, Australian National University, Canberra, pp 161-165.

Milnes, A.R. and Bourman, R.P. (1972). A Late Palaeozoic glaciated granite surface at Port Elliot, South Australia. *Transactions of the Royal Society of South Australia*, **96** (3), 149-155.

Milnes, A.R. and Hutton, J.T. (1983). Calcretes in Australia. In: *Soils: an Australian Viewpoint*, Division of Soils CSIRO, Melbourne / Academic Press, London, pp 120-162.

Milnes, A.R. and Ludbrook, N.H. (1986). Provenance of microfossils in aeolian calcarenites and calcretes in southern South Australia. *Australian Journal of Earth Sciences*, **33**, 145-159.

Miranda, J.A., Wallace, M.W., McLaren, S. (2008). The Norwest Bend Formation: Implications for the evolution of Neogene drainage in southeastern Australia. *Sedimentary Geology*, **205**, 53-66.

Miranda, J.A., Wallace, M.W., McLaren, S. (2009). Tectonism and eustasy across a Late Miocene strandplain: The Loxton-Parilla Sands, Murray Basin, southeastern Australia. *Sedimentary Geology*, **219**, 24-43.

Mitterer, R.M. and Kriaušakul, N. (1989). Calculation of amino acid racemization based on apparent parabolic kinetics. *Quaternary Science Reviews*, **8**, 353-357.

Moore, C.H. (1989). *Carbonate Diagenesis and Porosity*. Developments in Sedimentology **46**, Elsevier, Amsterdam, 338 pgs.

Mount, J. (1985). Mixed siliclastic and carbonate sediments: a proposed first-order textural and compositional classification. *Sedimentology*, **32**, 435-442.

Muhs, D. (2002). Evidence for the timing and duration of the Last Interglacial Period from high-precision Uranium-series ages of corals on tectonically stable coastlines. *Quaternary Research*, **58**, 36-40.

Muhs, D.R., Pandolfi, J.M., Simmons, K.R., Schumann, R.R. (2012). Sea-level history of past interglacial periods from uranium-series dating of corals, Curaçao, Leeward Antilles islands. *Quaternary Research*, **78**, 157-169.

Munsell Soil Color Charts (1994 revised edition). Macbeth Division of Kollmorgan Instruments Corporation, New Windsor, NY.

Murray, A.S. and Wintle, A.G. (2000). Luminescence dating of quartz using an improved regenerative-dose protocol. *Radiation Measurements*, **32**, 57-73.

Murray-Wallace, C.V. (1995). Aminostratigraphy of Quaternary coastal sequences in southern Australia – An overview. *Quaternary International*, **26**, 69-85.

Murray-Wallace, C.V. (2000). Quaternary coastal aminostratigraphy: Australian data in a global context. In: Goodfriend, G.A., Collins, M.J., Fogel, M.L., Macko, S.A., Wehmler, J.F. [Eds.], *Perspectives in Amino Acid and Protein Geochemistry*, Oxford University Press, New York, pp 279-300.

Murray-Wallace, C.V. (2002). Pleistocene coastal stratigraphy, sea-level highstands and neotectonism of the southern Australian passive continental margin – a review. *Journal of Quaternary Science*, **17** (5-6), 469-489.

Murray-Wallace, C.V. (2014). The continental shelves of SE Australia. *Geological Society, London, Memoirs*, **41**, 273-291.

Murray-Wallace, C.V. and Kimber, R.W.L. (1987). Evaluation of the amino acid racemization reaction in studies of Quaternary marine sediments in South Australia. *Australian Journal of Earth Sciences*, **34**, 279-292.

Murray-Wallace, C.V. and Belperio, A.P. (1991). The last interglacial shoreline in Australia – A review. *Quaternary Science Reviews*, **10**, 441-461.

Murray-Wallace, C.V. and Kimber, R.W.L. (1993). Further evidence for apparent ‘parabolic’ racemization kinetics in Quaternary molluscs. *Australian Journal of Earth Sciences*, **40**, 313-317.

Murray-Wallace, C.V. and Belperio, A.P. (1994). Identification of remanié fossils using amino acid racemisation. *Alcheringa*, **18** (3), 219-227.

Murray-Wallace, C.V. and Cann, J. (2007). Quaternary history of the Coorong Coastal Plain, South Australia. *Excursion Guide (A6)*, XVII INQUA Congress, Cairns, Australia, 72 pgs.

Murray-Wallace, C.V. and Woodroffe, C.D. (2014). *Quaternary Sea-Level Changes: a Global Perspective*. Cambridge University Press, New York, 484 pgs.

Murray-Wallace, C.V., Kimber, R.W.L., Belperio, A.P. (1988). Geological Note: Holocene palaeotemperature studies using amino acid racemization reactions. *Australian Journal of Earth Sciences*, **35**, 575-577.

Murray-Wallace, C.V., Kimber, R.W.L., Belperio, A.P., Gostin, V.A. (1988). Aminostratigraphy of the last interglacial in southern Australia. *Search*, **19**, 33-36.

Murray-Wallace, C.V., Belperio, B.P., Picker, K., Kimber, R.W.L. (1991). Coastal aminostratigraphy of the last interglaciation in southern Australia. *Quaternary Research*, **35**, 63-71.

Murray-Wallace, C.V., Belperio, A.P., Cann, J.H., Huntley, D.J., Prescott, J.R. (1996). Late Quaternary uplift history, Mount Gambier region, South Australia. *Zeitschrift für Geomorphologie*, **106**, 41-56.

Murray-Wallace, C.V., Belperio, A.P., Cann, J.H. (1998). Quaternary neotectonism and intra-plate volcanism: the Coorong to Mount Gambier Coastal Plain, southeastern Australia: a review. In: Stewart, I.S. and Vita-Finzi, C. [Eds.] *Coastal Tectonics*. Geological Society, London, Special Publications, **146**, 255-267.

Murray-Wallace, C.V., Belperio, A.P., Bourman, R.P., Cann, J.H., Price, D.M. (1999). Facies architecture of a last interglacial barrier: a model for Quaternary barrier development from the Coorong to Mount Gambier Coastal Plain, southeastern Australia. *Marine Geology*, **158**, 177-195.

Murray-Wallace, C.V., Beu, A.G., Kendrick, G.W., Brown, L.J., Belperio, A.P., Sherwood, J.E. (2000). Palaeoclimatic implications of the occurrence of the arcoid bivalve *Anadara trapezia* (Deshayes) in the Quaternary of Australasia. *Quaternary Science Reviews*, **19**, 559-590.

Murray-Wallace, C.V., Brooke, B.P., Cann, J.C., Belprio, A.P., Bourman, R.P. (2001). Whole-rock aminostratigraphy of the Coorong Coastal Plain, South Australia: towards a 1 million year record of sea-level highstands. *Journal of the Geological Society*, **158**, 111-124.

Murray-Wallace, C.V., Banerjee, D., Bourman, R.P., Olley, J.M., Brooke, B.P. (2002). Optically stimulated luminescence dating of Holocene relict foredunes, Guichen Bay, South Australia. *Quaternary Science Reviews*, **21**, 1077-1086.

Murray-Wallace, C.V., Bourman, R.P., Prescott, J.R., Williams, F., Price, D.M., Belperio, A.P. (2010). Aminostratigraphy and thermoluminescence dating of coastal aeolianites and the later Quaternary history of a failed delta: The River Murray mouth region, South Australia. *Quaternary Geochronology*, **5**, 28-49.

Nanson, G.C., Price, D.M., Short, S.A. (1992). Wetting and drying of Australia over the past 300 ka. *Geology*, **20**, 791-794.

Norvick, M.S. and Smith, M.A. (2001). Mapping the plate tectonic reconstruction of southern and southeastern Australia and implications for petroleum systems. *APPEA JOURNAL*, 15-35.

O'Driscoll, E.P.D. (1960). The hydrology of the Murray Basin province in South Australia. *Geological Survey of South Australia*, SA Department of Mines, Bulletin no. **35**. 300 pgs.

Oliver, H.G. and Anderson, W.M. (1940). *The River Murray barrages at Mundoo, Boundary Creek, Ewe Island and Tauwitcherie Channels*. Engineering and Water Supply Document, Adelaide, 23 pgs.

Paul, E., Sandiford, M., Flöttman, T. (2000). Structural geometry of a thick-skinned fold-thrust belt termination: the Olary Block in the Adelaide Fold Belt, South Australia. *Australian Journal of Earth Sciences*, **47**, 281-289.

- Pell, S.D., Chival, A.R., Williams, I.S. (2001). The Mallee Dunfield: development and sand provenance. *Journal of Arid Environments*, **48**, 149-170.
- Penkman, K.E.H., Kaufman, D.S., Maddy, D., Collins, M.J. (2008). Closed-system behaviour of the intra-crystalline fraction of amino acids in mollusc shells. *Quaternary Geochronology* 3, pp 2-25.
- Perincek, D. and Cockshell, C.D. (1995). The Otway Basin: Early Cretaceous rifting to Neogene inversion. *APEA Journal*, 451-461.
- Petit, J-R., Briat, M., Royer, A. (1981). Ice age aerosol content from East Antarctic ice core samples and past wind strength. *Nature*, **293**, 391-394.
- Petit, J.R., Jouzel, J., Raynaud, D., Barkov, N.I., Barnola, J.-M., Basile, I., Bender, M., Chappellaz, J., Davis, M., Delaygue, G., Delmotte, M., Kotlyakov, V.M., Legrand, M., Lipenkov, V.Y., Lorius, C., Pépin, L., Ritz, C., Saltzman, E., Stievenard, M. (1999). Climate and atmospheric history of the past 420,000 years from Vostok ice core, Antarctica. *Nature*, **399**, 429-436.
- Pettijohn, F.J., Potter, P.E., Siever, R. (1987). *Sand and Sandstone*. Springer-Verlag, New York, 553 pgs.
- Phillips, S.E. and Self, P.G. (1987). Morphology, crystallography, and origin of needle-fibre calcite in Quaternary pedogenic calcretes of South Australia. *Australian Journal of Soil Research*, **25**, 429-444.
- Phillips, S.E. and Milnes, A.R. (1988). The Pleistocene terrestrial carbonate mantle on the southeastern margin of the St Vincent Basin, South Australia. *Australian Journal of Earth Science*, **35**, 463-481.
- Pilcher, J.R. (1991) Radiocarbon dating for the Quaternary scientist. In: J.J Lowe [Ed.] *Radiocarbon Dating: Recent Applications and Future Potential*, Quaternary Proceedings No. 1, John Wiley & sons, Chichester, pp 27-34.

Pilcher, J.R. (2003) Radiocarbon dating and environmental radiocarbon studies. In: Mackay, A.; Battarbee, R.; Birks, J.; Oldfield, F. [Eds.] *Global change in the Holocene*, Arnold, London, pp 63-74.

Pirazzoli, P.A., Radtke, U., Hantoro, W.S., Jouannic, C., Hoang, C.T., Causse, C., Borel Best, M. (1993). A one million-year-long sequence of marine terraces on Sumba Island, Indonesia. *Marine Geology*, **109**, 221-236.

Playford, P.E., Cope, R.N., Cockbain, A.E., Low, G.H., Lowry, D.C. (1975). Perth Basin. In: *Geology of Western Australia*, Geological Survey of Western Australia, Memoir 2, pp 227-259.

Playford, P.E., Cockbain, A.E., Low, G.H. (1976). *Geology of the Perth Basin*. Geological Survey of Western Australia, Bulletin **124**, 311 pgs.

Plint, A.G., Eyles, N., Eyles, C.H., Walker, R.G. (1992). Control of sea level change. In: Walker, R.G., James, N.P. [Eds.] *Facies Models Response to Sea Level Change*, Geological Association of Canada, Newfoundland, pp 15-25.

Preiss, W.V. (1995): Delamerian Orogeny, Chapter 7, Early and Middle Palaeozoic. In: Drexel, J. F. and Preiss, W.V. [Eds.] *The Geology of South Australia. Vol. 2, The Phanerozoic*. Geological Survey of South Australia, Bulletin 54, pp 45-54.

Preiss, W.V. (2000). The Adelaide Geosyncline of South Australia and its significance in Neoproterozoic continental reconstruction. *Precambrian Research*, **100**, 21-63.

Preiss W.V., Rutland, R.W.R., Murrell, B. (1981). The Stuart Shelf and Adelaide Geosyncline. In: Hunter, D.R. [Ed.] *Precambrian of the Southern Hemisphere*, Elsevier Scientific Publishing Company, Amsterdam, 327-360.

Prescott, J.R. and Hutton, J.T. (1994). Cosmic ray contributions to dose rates for luminescence and ESR dating: Large depths and long-term time variations. *Radiation Measurements*, **23** (2-3), 497-500.

Preusser, F., Degering, D., Fuchs, M., Hilgers, A., Katereit, A., Klasen, N., Krbetschek, M., Richter, D., Spencer, J.Q.G. (2008) Luminescence dating: basics, methods and application. *Eiszeitalter und Gegenwart*, **57** (1-2), 95-149.

Price, D.M. (2004). TL signatures of quartz grains of different origin. *Radiation Measurements*, **23** (2/3), 413-417.

Price, D.M.; Brooke, B.P.; Woodroffe, C.D. (2001). Thermoluminescence dating of aeolianites from Lord Howe Island and South-West Western Australia. *Quaternary Science Reviews*, **20**, 41-846.

Pufahl, P.K., James, N.P., Bone, Y., Lukasik, J.J. (2004). Pliocene sedimentation in a shallow, cool-water, estuarine gulf, Murray Basin, South Australia. *Sedimentology*, **51**, 997-1027.

Purdy, E.G. (1968). Carbonate diagenesis: an environmental survey. *Geologica Romana*, **7**, 183-228.

Quigley, M., Sandiford, M., Fifield, K., Alimanovic, A. (2007). Bedrock erosion and relief production in the northern Flinders Ranges, Australia. *Earth Surface Processes and Landforms*, **32**, 929-944

Quigley, M.C., Horton, T., Hellstrom, J.C., Cupper, M.L., Sandiford, M. (2010). Holocene climate change in arid Australia from speleothem and alluvial records. *The Holocene*, **20** (7), 1093-1104.

Raymo, M.E. (1992). Global climate change: a three million year perspective. In: Kukla, G.J. and Went, E. [Eds.] *Start of a Glacial*, Springer-Verlag, Berlin, pp. 207-223.

Raymo, M.E. and Mitrovica, J.X. (2012). Collapse of polar ice sheets during the stage 11 interglacial. *Nature*, **483**, 453-456

Raymo, M.E., Ruddiman, W.F., Backman, J., Clement, B.M., Martinson, D.G. (1989). Late Pliocene variation in northern hemisphere ice sheets and North Atlantic deep water circulation. *Paleoceanography* **4** (4), 413-446.

Reimer, P.J., Bard, E., Bayliss, A., Beck, J.W., Blackwell, P.G., Ramsey, C.B., Buck, C.E., Cheng, H., Edwards, R.L., Friedrich, M., Grootes, P.M., Guilderson, T.P., Haflidason, H., Hajdas, I., Hatté, C., Heaton, T.J., Hoffmann, D.L., Hogg, A.G., Hughen, K.A., Kaiser, K.F., Kromer, B., Manning, S.W., Niu, M., Reimer, R.W., Richards, D.A., Scott, E.M., Southon, J.R., Staff, R.A., Turney, C.S.M., van der Plicht, J. (2013). INTCAL13 and MARINE13 radiocarbon age calibration curves 0-50,000 years CAL BP. *Radiocarbon*, **55** (4), 1869-1887.

Reinson, G.E. (1992). 10. Transgressive Barrier Island and Estuarine Systems. In: Walker, R.G. and James, N.P. [Eds.] *Facies Models Response to Sea Level Change*, Geological Association of Canada, Newfoundland, pp 179-194.

Reissen, A. and Chappell, J.F. (1991). Murray Mouth Littoral Drift Study. Prepared for the Engineering and Water Supply Department of South Australia, 651-654.

Riordan, N.K., James, N.P., Bone, Y. (2012). Oligo-Miocene seagrass-influenced carbonate sedimentation along a temperate marine palaeoarchipelago, Padthaway Ridge, South Australia. *Sedimentology*, **59**, 393-418.

Rivers, J.M., James, N.P., Kyser, T.K., Bone, Y. (2007). Genesis of palimpsest cool-water carbonate sediment on the continental margin of southern Australia. *Journal of Sedimentary Research*, **77**, 480-494.

Rivers, J.M., James, N.P., Kyser, T.K., (2008). Early diagenesis of carbonates on a cool-water carbonate shelf, southern Australia. *Journal of Sedimentary Research*, **78**, 784-802.

Roberts, R.G., Galbraith, R.F., Olley, J.M., Yoshida, H., Laslett, G.M. (1999). Optical dating of single and multiple grains of quartz from Jinmium rock shelter, northern Australia, Part II: results and implications. *Archaeometry*, **41**, 365-395.

Rochow, K. (1969) Naracoorte 1:250 000 Geological Sheet. *Geological Survey of South Australia*, Department of Mines and Energy, Adelaide.

Rochow, K. (1971). The Padthaway Ridge. In: Wopfner, H. and Douglas, J.G. [Eds.] *The Otway Basin of Southeastern Australia*. Special Bulletin, Geological Surveys of South Australia and Victoria.

Rogers, P.A. (1979) Pinnaroo 1:250 000 Geological Sheet. *Geological Survey of South Australia*, Department of Mines and Energy South Australia, Adelaide.

Rogers, P.A. (1980) *Explanatory Notes for the Pinnaroo 1:250 000 Geological Map*. Department of Mines and Energy South Australia, Adelaide, Report Book **No. 76/69**, 43 pgs.

Rogers, P.A. (1995): Continental Sediments of the Murray Basin, Chapter 11, The Quaternary. In, Drexel, J. F. and Preiss, W.V. [Eds.] *The Geology of South Australia. Vol. 2, The Phanerozoic*. Geological Survey of South Australia, Bulletin 54, pp 252-254.

Rohling, E.J., Fenton, M., Jorissen, F.J., Bertrand, P., Ganssen, G., Caulet, J.P. (1998). Magnitudes of sea-level lowstands of the past 500,000 years. *Nature*, **394**, 162-165.

Rohling, E.J., Braun, K., Grant, K., Kucera, M., Roberts, A.P., Siddall, M., Trommer, G. (2010). Comparison between Holocene and Marine Isotope Stage-11 sea-level histories. *Earth and Planetary Science Letters*, **291**, 97-105.

Roy, P.S. and Whitehouse, J. (1999). In: Stewart, R. [Ed.] *Murray Basin Mineral Sands, Extended abstracts of Papers Presented at a Conference*, Australian Institute of Geoscientists, Bulletin **No. 26**, 90-92.

Ruddiman, W.F., Raymo, M., McIntyre, A. (1986). Matuyama 41,000-year cycles: North Atlantic Ocean and northern hemisphere decay sheets. *Earth and Planetary Science Letters*, **80**, 117-129.

Rutter, N.W. and Blackwell, B. (1995). Amino acid racemisation dating. In: Rutter, N.W. and Catto, N.R. (Eds.), *Dating methods for Quaternary Deposits*, Geological Association of Canada, St. John's, pp 125-164.

Sandiford, M. (2003). Neotectonics of southeastern Australia: linking the Quaternary faulting record with seismicity and *in situ* stress. *Geological Society of Australia Special Publication*, **No. 22** and *Geological Society of America Special Paper*, **372**, 107-119.

Sandiford, M. (2007). The tilting continent: A new constraint on the dynamic topographic field from Australia. *Earth and Planetary Science Letters*, **261**, 152-163.

Sandiford, M., Quigley, M., De Broekert, P., Jakica, S. (2009). *Australian Journal of Earth Sciences*, **56**, S5-S18.

Schellmann, G. and Radtke, U. (2004) Distribution and chronostratigraphy of fossil coral reef terraces on the south coast of Barbados. In: Schellmann, G. and Radtke, U. [Eds] *The Marine Quaternary of Barbados*, Selbstverlag Geographisches Institut der Universität zu Köln, pp 69-106.

Schellmann, G., Radtke, U., Potter, E.-K., Esat, T.M., McCulloch, M.T. (2004). Comparison of ESR and TIMS U/Th dating of marine isotope stage (MIS) 5e, 5c, and 5a coral from Barbados-implications for palaeo sea-level changes in the Caribbean. *Quaternary International*, **120**, 41-50.

Schroeder, R.A. and Bada, J.L. (1976). A review of the geochemical applications of the amino acid racemization reaction. *Earth Science Reviews*, **12**, 347-391.

Schwebel, D.A. (1984). Quaternary stratigraphy and sea-level variation in Southeast of South Australia. In: Thom, B.G. [Ed.], *Coastal Geomorphology in Australia*, Academic Press, Sydney, pp 291-311.

Scoffin, T.P. (1987). *An Introduction to Carbonate Sediments and Rocks*. Chapman and Hall, New York, 274 pgs.

Searle, D.J. and Semeniuk, V. (1988). Petrology and origin of beach sands along the Rottnest Shelf coast, southwestern Australia. *Journal of the Royal Society of Western Australia*, **70** (4), 119-128.

- Semeniuk, V. and Meagher, T.D. (1981). Calcrete in Quaternary coastal dunes in southwestern Australia: a capillary-rise phenomenon associated with plants. *Journal of Sedimentary Petrology*, **51** (1), 47-68.
- Semeniuk, V. and Glassford, D.K. (1988). Significance of aeolian limestone lenses in quartz sand formations: an interdigitation of coastal and continental facies, Perth Basin, southwestern Australia. *Sedimentary Geology*, **57**, 199-209.
- Shackleton, N.J. (1967). Oxygen isotope analyses and Pleistocene temperatures re-assessed. *Nature*, **215**, 15-17.
- Shackleton, N.J. (1987). Oxygen isotopes, ice volume, and sea level. *Quaternary Science Reviews*, **6**, 183-190.
- Shackleton, N.J. (2006). Formal Quaternary stratigraphy – What do we expect and need? *Quaternary Science Reviews*, **25**, 3458-3462.
- Shackleton, N.J. and Opdyke, N.D. (1973). Oxygen isotope and palaeomagnetic stratigraphy of Equatorial Pacific core V28-238: Oxygen isotope temperatures and ice volumes on a 10^5 year and 10^6 year scale. *Quaternary Research*, **3**, 39-55.
- Shepherd, M.J. and Price, D.M. (1990). Thermoluminescence dating of late Quaternary dune sand, Manawatu/Horowhenua area, New Zealand: a comparison with ^{14}C age determinations. *New Zealand Journal of Geology and Geophysics*, **33**, 535-539.
- Short, A.D. (1988). The South Australia coast and Holocene sea-level transgression. *Geographical Review*, **78** (2), 119-136.
- Short, A.D. and Hesp, P.A. (1984). *Beach and Dune Morphodynamics of the South East Coast of South Australia*. University of Sydney, Department of Geography, Coastal Studies Unit Technical Report **84/1**, 142 pgs.
- Siddall, M., Smeed, D.A., Hemleben, C., Rohling, E.J. (2004). Understanding the Red Sea response to sea level. *Earth and Planetary Science Letters*, **225**, 421-434.

Siddall, M., Chappell, J., Potter, E-K. (2007). Eustatic sea level during past interglacials. In: Sirocko, F., Claussen, M., Sánchez-Goñi, MF., Litt, T. [Eds]. *Developments in Quaternary Sciences, The Climate of Past Interglacials*, Elsevier, Volume **7**, pp 75-92.

Singleton, O.P., McDougall, I., Mallett, C.W. (1976). The Pliocene-Pleistocene Boundary in southeastern Australia. *Journal of the Geological Society of Australia*, **23** (3), 299-311.

Smith, G.G. and Evans, R.C. (1980). The effect of structure and conditions on the rate of racemization of free and bound amino acids. In: Hare, P.E., Hoering, T.C., and King, K. (Eds.), *Biogeochemistry of amino acids*, Wiley, New York, pp 257-282.

Smith, G.G., Williams, K.M., Wonnacott, D.M. (1978). Factors affecting the rate of racemization of amino acids and their significance to geochronology. *The Journal of Organic Chemistry*, **43**, 1-5.

Smith, P.C., Rogers, P.A., Lindsay, J.M., White, M.R., Kwitko, G. (1995): Gambier Basin, Chapter 10, Tertiary. In, Drexel, J. F. and Preiss, W.V. [Eds.] *The Geology of South Australia. Vol. 2, The Phanerozoic*. Geological Survey of South Australia, Bulletin **54**, pp 151-157.

Spooner, N.A. and Questiaux, D.G. (2000). Kinetics of red, blue and UV thermoluminescence and optically-stimulated luminescence from quartz. *Radiation Measurements*, **32**, 659-666.

Sprigg, R.C. (1952). The geology of the south-east province, South Australia, with special reference to Quaternary coast-line migrations and modern beach developments. *Geological Survey of South Australia*, South Australia Department of Mines, Bulletin No. **29**.

Sprigg, R.C. (1959). Stranded sea beaches and associated sand accumulations of the Upper South-East. *Transactions of the Royal Society of South Australia*, **82**, 183-193.

Sprigg, R.C. (1982a). Some stratigraphic consequences of fluctuating Quaternary sea level and related wind regimes in southern and central Australia. In: Wasson, R.J. [Ed.] *Quaternary Dust Mantles of China, New Zealand and Australia*, Australian National University, Canberra, pp 249.

Sprigg, R.C. (1982b). Alternating wind cycles of the Quaternary Era and their influences on aeolian sedimentation in and around the dune deserts of south-eastern Australia. In: Wasson, R.J. [Ed.] *Quaternary Dust Mantles of China, New Zealand and Australia*, Australian National University, Canberra, pp 211-240.

Stephenson, A.E. (1986). Lake Bungunnia – A Plio-Pleistocene megalake in southern Australia. *Palaeogeography, Palaeoclimatology, Palaeoecology*, **57**, 137-156.

Stephenson, A.E. and Brown, C.M. (1989). The ancient River Murray system. *BMR Journal of Australian Geology and Geophysics*, **11**, 387-395.

Stirling, C.H., Esat, T.M., Lambeck, K., McCulloch, M.T., Blake, S.G., Lee, D.-C., Halliday, A.N. (2001). Orbital forcing of the Marine Isotope Stage 9 Interglacial. *Science*, **291**, 290-292.

Stivala, J. (2005). *Statement of Management Arrangements for the Victorian Commercial Scallop (*Pecten fumatus*) Fishery*. Victoria Department of Primary Industries, 19 pgs.

Stocker, T.F. and Johnsen, S.J. (2003). A minimum thermodynamic model for the bipolar seesaw. *Palaeoceanography*, **18** (4), 1087.

Strasser, A. (1984). Black-pebble occurrence and genesis in Holocene carbonate sediments (Florida Keys, Bahamas, and Tunisia). *Journal of Sedimentary Petrology*, **54** (4), 1097-1109.

Sykes, G.A., Collins, M.J., Walton, D.I. (1995). The significance of a geochemically isolated intracrystalline organic fraction within biominerals. *Organic Geochemistry*, **23**, 1059-1065.

Szabo, B.J., Miller, G.H., Andrews, J.T., Stuvier, M. (1981). Comparison of uranium-series, radiocarbon, and amino acid data from marine molluscs, Baffin Island, Arctic Canada. *Geology*, **9**, 451-457.

Terasmae, J. (1984) Radiocarbon Dating: some problems and potential developments. In: W.C. Mahaney [Ed.] *Quaternary Dating Methods*, Elsevier, Amsterdam, pp 1-15.

Thiele, C. (1970). *Selected Verse*. Rigby, Adelaide, 178 pgs.

Thompson, W.G., Curran, H.A., Wilson, M.A., White, B. (2011). Sea-level oscillations during the last interglacial highstand recorded by Bahamas corals. *Nature Geoscience*, **4**, 648-687.

Thoms, M.C. and Walker, F. (1992). Channel changes related to low-level weirs on the River Murray, South Australia. In: Carling, P.A. and Petts, G.E. [Eds.] *Lowland Floodplain Rivers: Geomorphological Perspectives*, John Wiley & Sons Ltd., Brisbane, pp. 235-249.

Thomson, B.P. and Horwitz, R.C. (1962) Barker 1:250 000 Geological Sheet. *Geological Survey of South Australia*, Department of Mines and Energy, Adelaide.

Tian, J., Wang, P., Cheng, X., Li, Q. (2002). Astronomically tuned Plio-Pleistocene benthic $\delta^{18}\text{O}$ record from South China Sea and Atlantic-Pacific comparison. *Earth and Planetary Science Letters*, **203**, 1015-1029.

Tokarev, V., Sandiford, M., and Gostin, V. (1998). Landscape evolution in the Mount Lofty Ranges: Implications for regolith development. In: Taylor, G. and Pain, C. [Eds.] *Regolith '98 New Approaches to an Old Continent*, Cooperative Research Centre for Landscape Evolution and Mineral Exploration, 3rd Australian Regolith Conference.

Trumbore, S.E. (2000) Radiocarbon Geochronology. In: Noller, J.S.; Sowers, J.M.; Lettis, W.R. [Eds.] *Quaternary Geochronology Methods and Applications*, American Geophysical Union, Washington D.C., pp 41-60.

Tucker, M.E. (1991). *Sedimentary Petrology An Introduction to the Origin of Sedimentary Rocks*. Blackwell Science Ltd., Oxford, 260 pgs.

Twidale, C.R., Lindsay, J.M., Bourne, J.A. (1978). Age and origin of the Murray River and Gorge in South Australia. *Proceedings of the Royal Society of Victoria*, **90**, 27-42.

Twidale, C.R. (1994). Gondwana (Late Jurassic and Cretaceous) palaeosurfaces of the Australian craton. *Palaeogeography, Palaeoclimatology, Palaeoecology*, **112**, 157-186.

Twidale, C.R. (2000). Early Mesozoic (?Triassic) landscapes in Australia: evidence, argument, and implications. *The Journal of Geology*, **108** (5), 537-552.

Tzedakis, P.C., Andrieu, V., de Beaulieu, J.-L., Crowhurst, S., Follieri, M., Hooghiemstra, H., Magri, D., Reille, M., Sadori, L., Shackleton, N.J., Wijmstra, T.A. (1997). Comparison of terrestrial and marine records of changing climate of the last 500,000 years. *Earth and Planetary Science Letters*, **150**, 171-176.

Veeh, H.H. (1966). $\text{Th}^{230}/\text{U}^{238}$ and $\text{U}^{234}/\text{U}^{238}$ ages of Pleistocene high sea level stand. *Journal of Geophysical Research*, **71**, 3379-3386.

Veevers, J.J. (1982). Australian-Antarctic depression from the mid-ocean ridge to adjacent continents. *Nature*, **295**, 315-317.

Veevers, J.J. (2000). Chapter 10 Present and Past Tectonic State. In: Veevers, J.J. [Ed.] *Billion-year earth history of Australia and neighbours in Gondwanaland*, GEMOC Press, Sydney, 61-73

Veevers, J.J. (2006). Updated Gondwana (Permian-Cretaceous) earth history of Australia. *Gondwana Research*, **9**, 231-260.

Vézina, J., Jones, B., Ford, D. (1999). Sea-level highstands over the last 500,000 years: Evidence from the Ironshore Formation on Grand Cayman, British West Indies. *Journal of Sedimentary Research*, **69** (2), 317-327.

Von der Borch, C.C. (1975). The geological history of the Coorong Lagoon. In: Noye, J. [Ed.] *The Coorong*. The University of Adelaide, Department of Adult Education, Publication #39.

Von der Borch, C.C. and Altmann, M. (1979). Holocene stratigraphy and evolution of the Cooke Plains Embayment, a former extension of Lake Alexandrina, South Australia. *Transactions of the Royal Society of South Australia*, **103** (3), 69-78.

Von der Borch, C.C. and Lock, D. (1979). Geological significance of Coorong dolomites. *Sedimentology*, **26**, 813-824.

Von der Borch, C.C., Lock, D.E., Schwebel, D. (1975). Groundwater formation of dolomite in the Coorong region of South Australia. *Geology*, **3**, 283-285.

Von der Borch, C.C., Bada, J.L., Schwebel, D.L. (1980). Amino acid racemization dating of Late Quaternary strandline events of the coastal plain sequence near Robe, southern South Australia. *Transactions of the Royal Society of South Australia*, **104** (6), 167-170.

Walker, M. (2005) *Quaternary Dating Methods*, John Wiley & Sons, Chichester, 286 pgs.

Walker, M., Johnsen, S., Rasmussen, S.O., Popp, T., Steffensen, J-P., Gibbard, P., Hoek, W., Lowe, J., Andrews, J., Björck, S., Cwynar, L.C., Hughen, K., Kershaw, P., Kromer, B., Litt, T., Lowe, D.J., Nakagawa, T., Newnham, R., Schwander, J. (2009). Formal definition and dating of the GSSP (Global Stratotype Section and Point) for the base of the Holocene using the Greenland NGRIP ice core, and selected auxiliary records. *Journal of Quaternary Science*, **24** (1), 3-17.

Wallace, M.W., Dickinson, J.A., Moore, D.H., Sandiford, M. (2005). Late Neogene strandlines of southern Victoria: a unique record of eustasy and tectonics in southeast Australia. *Australian Journal of Earth Sciences*, **52**, 279-297.

Walton, D. (1998). Degradation of intracrystalline proteins and amino acids in fossil brachiopods. *Organic Geochemistry*, **28**, 389-410.

Ward, J.H. (1963). Hierarchical grouping to optimize an objective function. *Journal of the American Statistical Association*, **58** (301), 236-244.

Ward, W.T. (1966) *Geology, geomorphology and soil of the south-western part of County Adelaide, South Australia*. CSIRO Publication **23**.

Warren, J.K. (1983). Pedogenic calcrete as it occurs in Quaternary calcareous dunes in coastal South Australia. *Journal of Sedimentary Petrology*, **53**(3), 787-796.

Wasson, R.J. (1982). Landform development in Australia. In: Barker, W.R. and Greenslade, P.J.M. [Eds.] *Evolution of the Flora and Fauna of Arid Australia*, Peacock Publications, Frewville, pp. 23-33.

Wehmiller, J.F. (1980). Intergeneric differences in apparent racemization kinetics in mollusks and foraminifera: Implication for models of diagenetic racemization. In: Hare,

P.E., Hoering, T.C., and King, K. (Eds.), *Biogeochemistry of Amino Acids*, Wiley, New York, pp 341-355.

Wehmiller, J.F. (1982). A review of amino acid racemization studies in Quaternary mollusks: stratigraphic and chronologic applications in coastal and interglacial sites, Pacific and Atlantic coasts, United States, United Kingdom, Baffin Island and Tropical Islands. *Quaternary Science Reviews*, **1**, 83-120.

Wehmiller, J.F. (1984). Relative and absolute dating of Quaternary mollusks with amino acid racemization: evaluation, applications and questions. In: Mahaney, W.C. [Ed.] *Quaternary Dating Methods*, Developments in Paleontology and Stratigraphy 7, Elsevier, Amsterdam, p. 171-193.

Wehmiller, J.F. (2013a). United States Quaternary coastal sequences and molluscan racemization geochronology – what have they meant for each other over the past 45 years? *Quaternary Geochronology*, **16**, 3-20.

Wehmiller, J.F. (2013b). Interlaboratory comparison of amino acid enantiomeric ratios in Pleistocene fossils. *Quaternary Geochronology*, **16**, 173-182.

Wehmiller, J.F. and Hare, P.E. (1971). Racemization of amino acids in marine sediments. *Science*, **173**, 907-911.

Wehmiller, J.F. and Miller, G.H. (2000). Aminostratigraphic dating methods in Quaternary geology. In: Noller, J.S., Sowers, J.M., Lettis, W.R. (Eds.), *Quaternary Geochronology, Methods and Applications*, American Geophysical Union Reference Shelf 4, pp 187-222.

Wehmiller, J.F., Belknap, D.F., Boutin, B.S., Mirecki, J.E., Rahaim, S.D., York, L.L. (1988). A review of the aminostratigraphy of Quaternary mollusks from United States Coastal Plain sites. In: Easterbrook, D.J. [Ed.] *Dating Quaternary Sediments*, Geological Society of America, Special Paper **227**, pp 69-110.

Wehmiller, J.F., York, L.L., Bart, M.L. (1995). Amino acid racemization geochronology of reworked Quaternary mollusks on U.S. Atlantic coast beaches: implications for

chronostratigraphy, taphonomy, and coastal sediment transport. *Marine Geology*, **124**, 303-337.

Wehmiller, J.F., Stecher III, H.A., York, L.L., Friedman, I. (2000). The thermal environment of fossils: effective ground temperatures at aminostratigraphic sites on the U.S. Atlantic Coastal Plain. In: Goodfriend, G.A., Collins, M.J., Fogel, M.L., Macko, S.A., Wehmiller, J.F. [Eds.] *Perspectives in Amino Acid and Protein Geochemistry*, Oxford University Press, pp 219-250.

Wellman, P. and Greenhalgh, S.A. (1988). Flinders/Mount Lofty Ranges, South Australia their uplift, erosion, and relationship to crustal structure. *Transactions of the Royal Society of South Australia*, **112** (1), 11-19.

White, S. (2000). Thermoluminescence dating of dune ridges in western Victoria. *Helictite*, **36** (2) 38-40.

Wilcox, J.B. and Stagg, H.M.J. (1990). Australia's southern margin: a product of oblique extension. *Tectonophysics*, **173**, 269-281

Williams, G.E. (1985). Glacial age of piedmont alluvial deposits in the Adelaide area, South Australia. *Australian Journal of Earth Science*, **32** (6), 257.

Williams, G.E. and Goode, A.D.T. (1978). Possible western outlet for an ancient River Murray in South Australia. *Search*, **9** (12), 442-447.

Williams, K.M. and Smith, G.G. (1977). A critical evaluation of the application of amino acid racemization to geochronology and geothermometry. *Origins of Life*, **8**, 91-144.

Williams, M.A.J. (2000). Quaternary Australia: Extremes in the last glacial-interglacial cycle. In: Veevers, J.J. [Ed.] *Billion-year earth history of Australia and neighbours in Gondwanaland*, Gemoc Press, Sydney, pgs. 55-59.

Wintle, A.G. (1997). Luminescence dating: laboratory procedures and protocols. *Radiation Measurements*, **27**, 769-817.

Wintle, A.G. (2010). Future directions of luminescence dating of quartz. *Geochronometria*, **37**, 1-7.

- Wintle, A.G. and Huntley, D.J. (1982). Thermoluminescence dating of sediments. *Quaternary Science Reviews*, **1**, 31-53.
- Woodroffe, C.D. (2002). *Coasts: form, process, and evolution*. Cambridge University Press, Cambridge, 623 pgs.
- Woodroffe, C.D. and Webster, J.M. (2014). Coral reefs and sea-level change. *Marine Geology*, **352**, 248-267.
- Woods, J.A. (1862). *Geological Observations in South Australia: Principally in the District South-East of Adelaide*. Spottiswoode and Co., London, 404 pgs.
- Wopfner, H. (1972). Depositional history and tectonics of South Australian sedimentary basins. *Mineral Resources Review South Australia*, **133**, 32-50.
- Wright, V.P. and Tusker, M.E. (1991). Calcretes: An Introduction. In: Wright, V.P. and Tucker, M.E. [Eds.] *Calcretes*. Blackwell Scientific Publications, Oxford, pp 1-22.
- Yokoyama, Y., Esat, T.M., Lambeck, K. (2001). Coupled climate and sea-level changes deduced from Huon Peninsula and coral terraces of the last ice age. *Earth and Planetary Science Letters*, **193**, 579-587.
- Young, P.C., West, G.J., McLoughlin, R.J., Martin, R.B. (1999). Reproduction of the commercial scallop, *Pecten fumatus*, Reeve, 1852 in Bass Strait, Australia. *Marine & Freshwater Research*, **50**, 417-425.
- Yung, Y.L., Lee, T., Wang, C.-H., Shieh, Y.-T. (1996). Dust: A diagnostic of the hydrological cycle during the Last Glacial maximum. *Science*, **271**, 962-963.
- Zachos, J., Pagani, M., Sloan, L, Thomas, E., Billups, K. (2001). Trends, rhythms, and aberrations in global climate 65 Ma to present. *Science*, **292**, 686-693.
- Zhang, X., Lohmann, G., Knorr, G., Purcell, C. (2014). Abrupt glacial climate shifts controlled by ice sheet changes. *Nature*, **512**, 290-294.
- Zhou, L., Williams, M.A.J., Peterson, J.A. (1994). Late Quaternary aeolianites, palaeosols and depositional environments on the Nepean Peninsula, Victoria, Australia. *Quaternary Science Reviews*, **13**, 225-239.

APPENDIX 1:
Digital Elevation Model (DEM)
Methodology of Construction

A1.1 Introduction

A digital elevation model (DEM) was created using the ESRI suite of ArcGIS products during this research to aid in conceptualising the complexity of the landscape and to demonstrate the stratigraphic relationships observed in the field to topography. The DEM shown in figures throughout the thesis is a mosaic of smaller, individual DEMs. This was necessary due to the size of the spatial data files and processing capabilities required to develop the models. Spatial data used in the construction of the DEMs was provided by the Department of Environment, Water and Natural Resources (DEWNR), South Australia (2012). A list of the spatial data layers provided by DEWNR (2012) and used in the construction of the DEMs is provided below. It was also necessary to digitise the coastline of the study area due to artefacts in the data. The methodology for digitising the coastline is provided below.

A1.2 List of spatial data layers provided by DEWNR (2012) and used in DEM construction

Layer Type	Scale	Source	Errors
Elevation Layers			
Contours	1:2500 (2 metre interval)	vectorised ground controlled aerial photography	90% of features are within 1 m of true position
Spot Heights	1:2500	vectorised ground controlled aerial photography	90% of features are within ± 1.25 m of true position
Contours	1:10000 (5 metre interval)	vectorised ground controlled aerial photography	90% of features are within ± 2.5 m of true position
Spot Heights	1:10000	vectorised ground controlled aerial photography	90% of features are within ± 2.5 m of true position
Hydrographical Layers			
Water Bodies	1:50000	vectorised ground controlled aerial photography	equal to or better than within ± 100 m of true position
Marine Layers			
Bathymetric Contours	varying scales 1:2500, 1:10000, 1:50000	digitised from Australian Navigation charts for South Australian State Waters (out to the 3 nautical mile limit)	dependent upon scale of map, e.g. 1:2500 ± 0.2 m, 1:10000 ± 1.2 m, 1: 50000 ± 5 m

Both 1:2500 and 1:10000 scale elevation layers were necessary as the higher resolution spatial data was limited to built-up areas, e.g. Victor Harbor, Goolwa and Meningie. The bathymetric contours extend to a depth of 76 m. The extent of the

elevation layers provided did not cover the entire study area and limited the DEM to the east.

A1.3 Digitisation of study area coastline

Digitisation of the coastline was found to be necessary due to artefacts within the data creating topographical errors within Encounter Bay. The coastline was digitised using expert knowledge from the western end of Parsons Beach (~3.5 km southwest of the Waitpinga field site on Fleurieu Peninsula) to the Younghusband Peninsula beach ~5.5 km directly west of the Stratland field site. Digitisation ceased at the most eastern extent of available elevation spatial data and the limit of possible DEM construction.

ESRI satellite imagery was used in conjunction with the contour layers (including bathymetric) as a guide in coastline digitisation. The rocky coastline along Fleurieu Peninsula was generally digitised at a scale of 1:1000. Due to the steepness of the Fleurieu Peninsula coastline there are very few beaches and the contact between the land and water was defined as the coastline. The beaches of Sir Richard and Younghusband Peninsulas are broad (10s of metres) and cusped. To acquire the coastline, digitisation took place at a scale of 1:5000 and followed the general trend of the top of the beach swash.

A1.4 Methodology of DEM Construction

Although the elevation spatial data provided by DENWR (2012) did not cover the entire study area, the spatial data extent for all layers provided far exceeded the size of the study area; for example, the elevation data covered the entire Mount Lofty-Flinders Ranges. To reduce the processing time created by using such large data files, all feature layers provided were initially extracted to the area of interest. This smaller dataset could then be managed more efficiently and further extracted in the creation of individual DEMs. The 1:10000 contour layer was also combined with the bathymetric contours to produce one layer before deriving the models.

Individual DEMs were created with spatial data extracted to a boundary specific to the individual DEM extent. The size of individual DEMs was dependent on the quantity of spatial data which went into the DEM construction. The spatial layers (e.g.

water body, digitised coastline) used in the creation of an individual DEM was dependent upon the location within the study area. For example, a DEM inland from the coastline would not require the coastline spatial layer for its creation but may require the water body spatial layer. Once DEMs were derived the mosaic could be presented as a seamless DEM which covered the southern Fleurieu Peninsula, the eastern margin of the Mount Lofty Ranges and the region immediately surrounding the Lakes Alexandrina and Albert.

APPENDIX 2:
All Particle Size Analysis Results
Malvern Mastersizer 2000

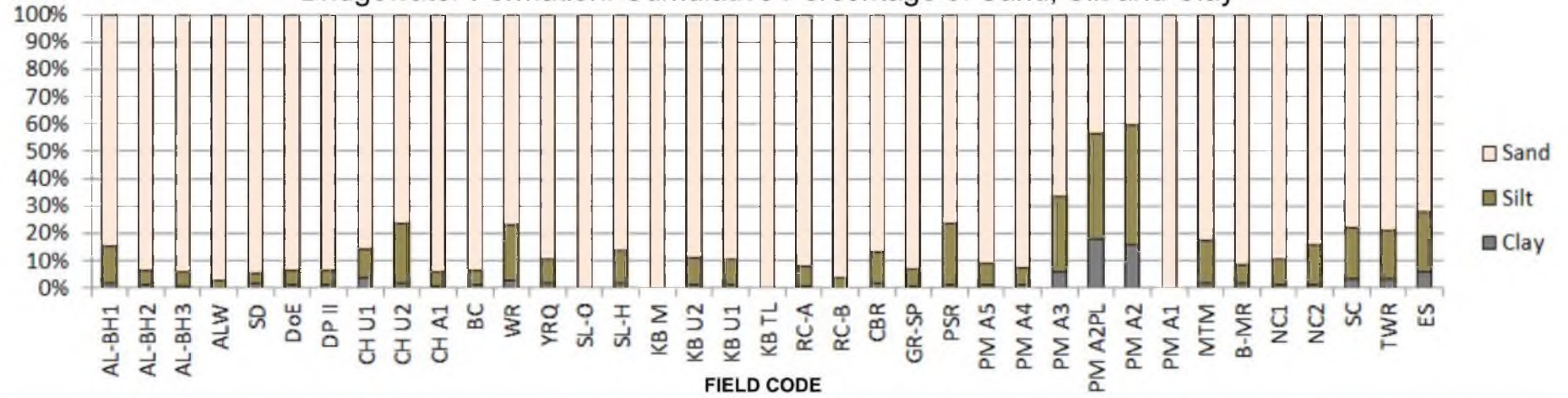
Table A2.1: Summary of all particle size results for Bridgewater Formation sedimentary successions. Field codes correspond to x-axis in below bar graphs. Table A2.1 continues on the following page.

Field Site	Field Code	Locality	Marine Isotope Stage	Clay	Silt	Sand	very fine	fine	medium	coarse	very coarse
Annie Lucas Drillhole 1 m	AL-BH1	Hindmarsh Island	1	1.9	13.2	85.0	24.2	46.3	14.4	0.0	0.0
Annie Lucas Drillhole 5 m	AL-BH2	Hindmarsh Island	1	0.9	5.6	93.6	7.3	50.2	32.9	1.0	2.1
Annie Lucas Drillhole 9 m	AL-BH3	Hindmarsh Island	1	0.8	4.9	94.3	12.2	56.9	25.2	0.0	0.0
Annie Lucas Well	ALW	Hindmarsh Island	1	0.0	2.5	97.5	19.6	62.5	15.3	0.0	0.0
Surfer Dune	SD	West of Goolwa	5c	1.5	3.7	94.8	19.2	58.3	17.1	0.0	0.2
Denver DoE	DoE	Hindmarsh Island	5e	1.0	5.4	93.6	10.3	57.2	26.0	0.0	0.0
Denver P2	DP II	Hindmarsh Island	5e	1.0	5.5	93.5	8.2	54.6	30.5	0.2	0.0
Chart House Unit 1	CH U1	Goolwa	5e	3.9	10.3	85.8	9.2	35.0	35.2	6.4	0.0
Chart House Unit 2	CH U2	Goolwa	5e	1.7	21.7	76.6	12.7	25.6	28.9	9.4	0.0
Chart House Aeolianite 1	CH A1	Goolwa	5e	0.6	5.1	94.3	0.2	19.6	54.9	19.5	0.0
Goolwa Bridge Calcrete	BC	Goolwa	7	1.3	5.2	93.5	0.0	8.2	74.5	10.8	0.0
Woolshed Road	WR	SE Lake Albert	5e	2.9	20.1	77.0	10.1	43.3	23.5	0.0	0.0
Yarindale Road	YRQ	SE Lake Albert	5e	1.6	8.8	89.7	17.6	46.0	21.8	2.0	2.2
Stratland Orange	SL-O	SE Lake Albert	5e	0.0	0.0	100.0	3.1	32.5	34.1	19.3	11.1
Stratland Hash	SL-H	SE Lake Albert	5e	1.8	11.8	86.4	7.8	25.8	28.3	10.4	14.1
Knights Beach Modern	KB M	Fleurieu Peninsula	1	0.0	0.0	100.0	0.0	21.5	66.0	12.5	0.0
Knights Beach Unit 2	KB U2	Fleurieu Peninsula	7	0.8	10.0	89.2	3.6	5.2	13.3	38.6	28.5
Knights Beach Unit 1	KB U1	Fleurieu Peninsula	7	1.2	9.4	89.4	3.5	16.7	44.7	24.4	0.1
Knights Beach TL	KB TL	Fleurieu Peninsula	7	0.0	0.0	100.0	0.0	20.0	60.6	19.5	0.0
Riverside Calcrete A (east)	RC-A	Hindmarsh Island	7	0.5	7.1	92.3	20.2	50.7	21.4	0.0	0.0
Riverside Calcrete B	RC-B	Hindmarsh Island	7	0.2	3.7	96.1	15.2	47.7	26.9	3.9	2.4
Clayton Bay Road	CBR	Sturt Peninsula	7	1.8	11.1	87.0	6.4	29.3	35.4	13.0	3.0
Griffin Road	GR-SP	Sturt Peninsula	7	0.8	6.0	93.2	5.8	42.2	41.5	3.7	0.0
Point Sturt Road	PSR	Sturt Peninsula	9?	1.3	22.1	76.6	13.0	26.6	27.1	9.6	0.3
Point McLeay A5	PM A5	Point McLeay	1	1.1	8.0	91.0	27.3	58.7	14.0	0.0	0.0
Point McLeay A4	PM A4	Point McLeay	5e	1.1	6.3	92.7	11.4	49.9	30.7	0.7	0.0
Point McLeay A3	PM A3	Point McLeay	9?	5.7	27.6	66.7	29.2	29.1	8.4	0.0	0.0
Point McLeay A2PL	PM A2PL	Point McLeay	9?	18.0	38.6	43.5	16.1	17.5	9.3	0.5	0.0
Point McLeay A2	PM A2	Point McLeay	9?	15.7	43.7	40.6	15.7	20.5	4.4	0.0	0.0
Point McLeay A1	PM A1	Point McLeay	11	0.0	0.0	100.0	0.0	24.9	68.0	7.1	0.0

Table A2.1 *continued*: Summary of all particle size results for Bridgewater Formation sedimentary successions. Field codes correspond to x-axis in below bar graphs.

Field Site	Field Code	Locality	Marine Isotope Stage	Clay	Silt	Sand	very fine	fine	medium	coarse	very coarse
Mount Misery	MTM	Inland	11?	1.8	15.5	82.7	11.9	39.2	28.3	2.8	0.5
B-McIntosh	B-MR	Inland	eP	1.5	6.9	91.7	12.5	49.0	26.5	3.4	0.3
North Coonalpyn 1	NC1	Inland	eP	1.2	9.1	89.7	1.1	26.7	48.1	13.8	0.0
North Coonalpyn 2	NC2	Inland	eP	1.0	14.7	84.3	6.8	18.8	35.3	22.7	0.8
South Coonalpyn	SC	Inland	eP	3.0	18.7	78.3	15.3	29.6	26.8	6.5	0.0
Tauragut Well	TWR	Inland	eP	3.0	18.2	78.8	7.8	30.3	32.9	7.8	0.0
Emu Springs	ES	Inland	eP	5.8	21.9	72.2	21.2	37.0	14.0	0.0	0.0
Marine Isotope Stage designation 'eP' = early Pleistocene											

Bridgewater Formation: Cumulative Percentage of Sand, Silt and Clay



Bridgewater Formation: Cumulative Percentage of Sand-sized Grains

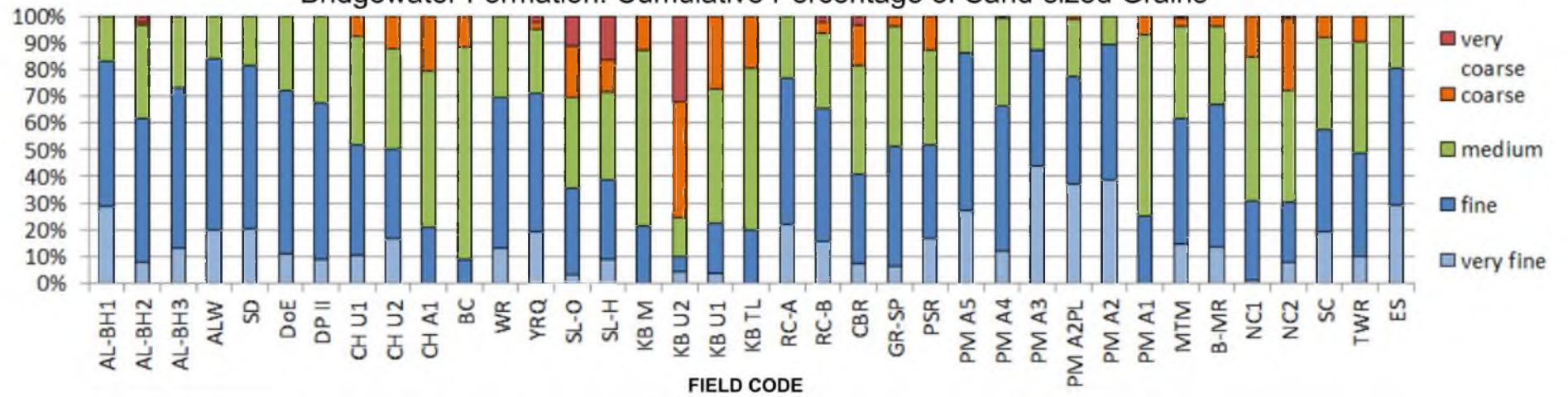
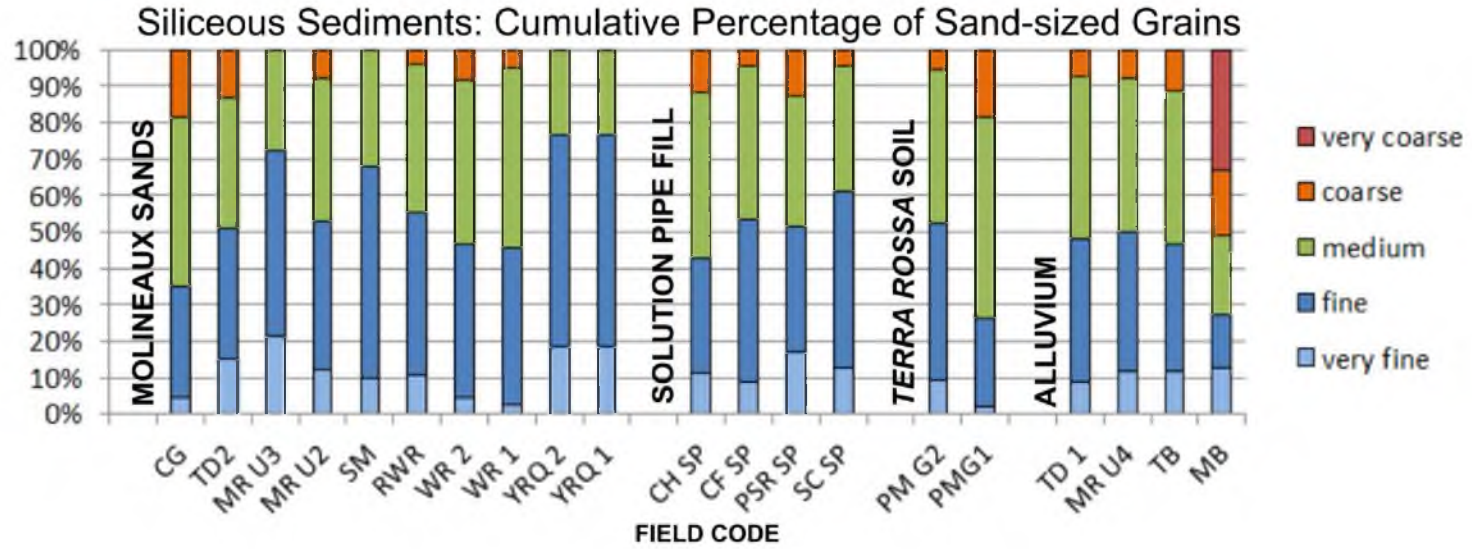
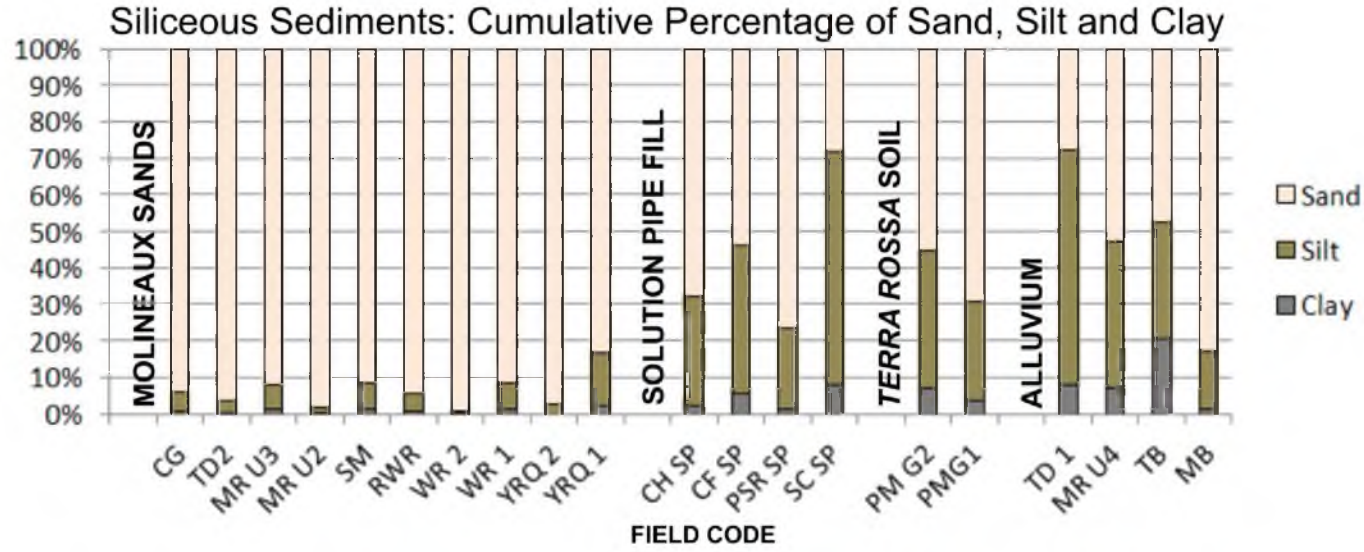


Table A2.2: Summary of all particle size results for siliceous sedimentary successions. Field codes correspond to x-axis in below bar graphs.

Field Site	Field Code	Locality	Clay	Silt	Sand	very fine	fine	medium	coarse	very coarse
Molineaux Sands										
Carcuma	CG	Inland	0.6	5.4	94.0	4.2	30.7	46.5	18.5	0.0
The Drain Recent	TD2	Goolwa	0.4	3.5	96.1	15.2	35.9	35.8	13.1	0.0
Myrtlegrove Unit 3	MR U3	Currency Creek	1.2	6.9	91.9	21.4	51.0	27.6	0.0	0.0
Myrtlegrove Unit 2	MR U2	Currency Creek	0.2	1.5	98.2	12.2	40.4	39.6	7.8	0.0
Sturt Monument	SM	Hindmarsh Island	1.1	7.3	91.6	9.7	57.9	32.2	0.2	0.0
Riverside Recent	RWR	Hindmarsh Island	0.5	5.1	94.4	10.6	44.7	40.5	4.2	0.0
Woolshed Recent	WR 2	SE Lake Albert	0.2	0.5	99.3	4.4	42.1	45.2	8.4	0.0
Woolshed Glacial	WR 1	SE Lake Albert	1.4	7.3	91.3	2.6	42.8	49.3	5.3	0.0
Yarindale Recent	YRQ 2	SE Lake Albert	0.0	2.6	97.4	18.6	57.9	23.5	0.0	0.0
Yarindale Glacial	YRQ 1	SE Lake Albert	2.0	14.9	83.1	18.6	57.9	23.5	0.0	0.0
Solution Pipes										
Chart House	CH SP	Goolwa	2.3	29.9	67.9	11.4	31.3	45.3	12.0	0.0
Cheese Factory	CF SP	Hindmarsh Island	5.6	40.5	53.9	9.0	44.5	41.7	4.8	0.0
Point Sturt Road	PSR SP	Sturt Peninsula	1.3	22.1	76.6	16.9	34.7	35.4	12.6	0.4
South Coonalpyn	SC SP	Inland	8.2	63.4	28.4	12.5	48.5	34.5	4.5	0.0
Terra Rossa										
Point McLeay G2	PM G2	Point McLeay	6.9	38.0	55.1	9.3	42.9	42.5	5.3	0.0
Point McLeay G1	PMG1	Point McLeay	3.7	26.8	69.5	1.9	24.1	55.6	18.4	0.0
Alluvium										
The Drain Glacial	TD 1	Goolwa	7.8	64.6	27.5	8.9	39.4	44.3	7.5	0.0
Myrtlegrove Road	MR U4	Currency Creek	7.2	40.0	52.7	6.1	20.3	22.3	4.2	0.0
Tailem Bend	TB	Tailem Bend	20.6	32.0	47.3	11.5	35.0	42.3	11.2	0.0
Murray Bridge	MB	Murray Bridge	1.4	15.9	82.7	12.8	14.3	21.8	18.0	33.1



APPENDIX 3:
All X-ray Diffraction Results

Table A3.1: Summary of all XRD results for Bridgewater Formation sedimentary successions. Field codes correspond to x-axis in below bar graphs. Table A3.1 continues on the following page.

Field Sites	Field Code	Locality	Marine Isotope Stage	Calcium Carbonate Cements						Quartz	Feldspar Group				Clays			Other	
				Aragonite	High-Mg Calcite	Low-Mg Calcite	Dolomite	Siderite	Ankerite		Albite	Labradorite	Orthoclase	Microcline	Kaolin	Illite	Chlorite	Sodium Chloride	Gypsum
Richard Owens Beach	ROB	Hindmarsh Island	1	7.2	19	18.3	0.4	-	2.8	36.9	3.1	2.4	-	7.2	0.3	1.2	-	1.3	-
Yilki Beach	YB	Fleurieu Peninsula	5	10.9	16	42.1	-	0.1	-	13.3	-	4.9	0.7	3.8	0.5	1.5	1.6	0.9	3.6
Chart House A2	CH A2	Goolwa	5e	-	1.9	23	-	-	-	61.8	12.3	-	0.3	0.3	0.2	-	-	0.1	-
Chart House A1	CH A1	Goolwa	5e	-	4.3	19.4	0.3	0.2	-	74.1	-	0.1	-	-	0.2	1	-	0.3	-
Chart House Unit 2	CH U2	Goolwa	5e	3.4	6.1	56.7	-	0.6	-	20.5	-	3	-	2.2	0.5	2.9	-	3.4	0.6
Chart House Unit 1	CH U1	Goolwa	5e	9.1	4.6	46	-	-	-	27.1	-	2.7	-	4.5	1.2	0.8	1.3	0.2	2.6
Griffin Road	GR-SP	Sturt Peninsula	7	3.9	3.2	42.2	0.4	-	0.5	38.3	4.4	-	0.9	4.8	0.3	-	1.1	-	-
Point McLeay A5	PM A5	Point McLeay	1	0.8	1.8	11.2	-	-	-	73.9	2.1	1.6	1.6	6.1	0.3	0.7	-	0.1	-
Point McLeay A4	PM A4	Point McLeay	5e	2.7	5.3	26.2	0.8	-	3.5	55.2	0.5	1.6	0.3	-	0.5	3.5	-	-	-
Point McLeay A3	PM A3	Point McLeay	9?	-	0.8	12.6	-	0.2	-	70	6.1	1.1	1.5	2.2	1.2	2.9	-	1.4	-
Point McLeay A2	PM A2	Point McLeay	9?	-	2.1	8.1	13.5	0.3	12.9	48	0	4.9	2.7	0.6	1	4.6	0	0.7	-
Point McLeay A1	PM A1	Point McLeay	11	-		5.8	-	-	0.1	85.2	-	1.2	5.2	2.2	0.2	-	-	-	-
Mount Misery	MTM	Inland	11?	2	6	47.4	-	0.4	-	32	-	3.3	4.1	3.9	0.8	0.1	-	-	-

Table A3.1: Summary of all XRD results for Bridgewater Formation sedimentary successions. Field codes correspond to x-axis in below bar graphs.

Field Sites	Field Code	Locality	Marine Isotope Stage	Calcium Carbonate Cements						Quartz	Feldspar Group				Clays			Other	
				Aragonite	High-Mg Calcite	Low-Mg Calcite	Dolomite	Siderite	Ankerite		Albite	Labradorite	Orthoclase	Microcline	Kaolin	Illite	Chlorite	Sodium Chloride	Gypsum
B-McIntosh Road	B-MR	Inland	eP	-	1.2	38	-	0.2	-	52.7	1.8	-	2.9	2.4	0.6	0.2	-	0.1	-
North Coonalpyn 1	NC IG1	Inland	eP	0.5	2.6	33.9	0.2	0.6	0.8	45.4	2.2	2.1	1.4	3.1	0.7	4.3	2.1	0.3	-
North Coonalpyn 2	NC IG2	Inland	eP	3.3	1.1	24.8	5.1	0.1	4.3	58.2	1.3	-	0.8	0.3	0.2	0.5	-	0.1	-
South Coonalpyn	SC-B	Inland	eP	0.4	2.3	53.3	-	-	0.5	30	2	-	4	5.8	0.3	-	-	1.4	-
Tauragut Well	TW	Inland	eP	0.5	2	25.4	-	-	-	58.1	0.3	0.5	1.4	9.5	0.3	0.4	1.5	0.1	-
Emu Springs	ES	Inland	eP	1.3	2.3	79.4	-	0.3	0.1	10	1.2	1.7	2.7	-	0.8	-	0.2	-	-

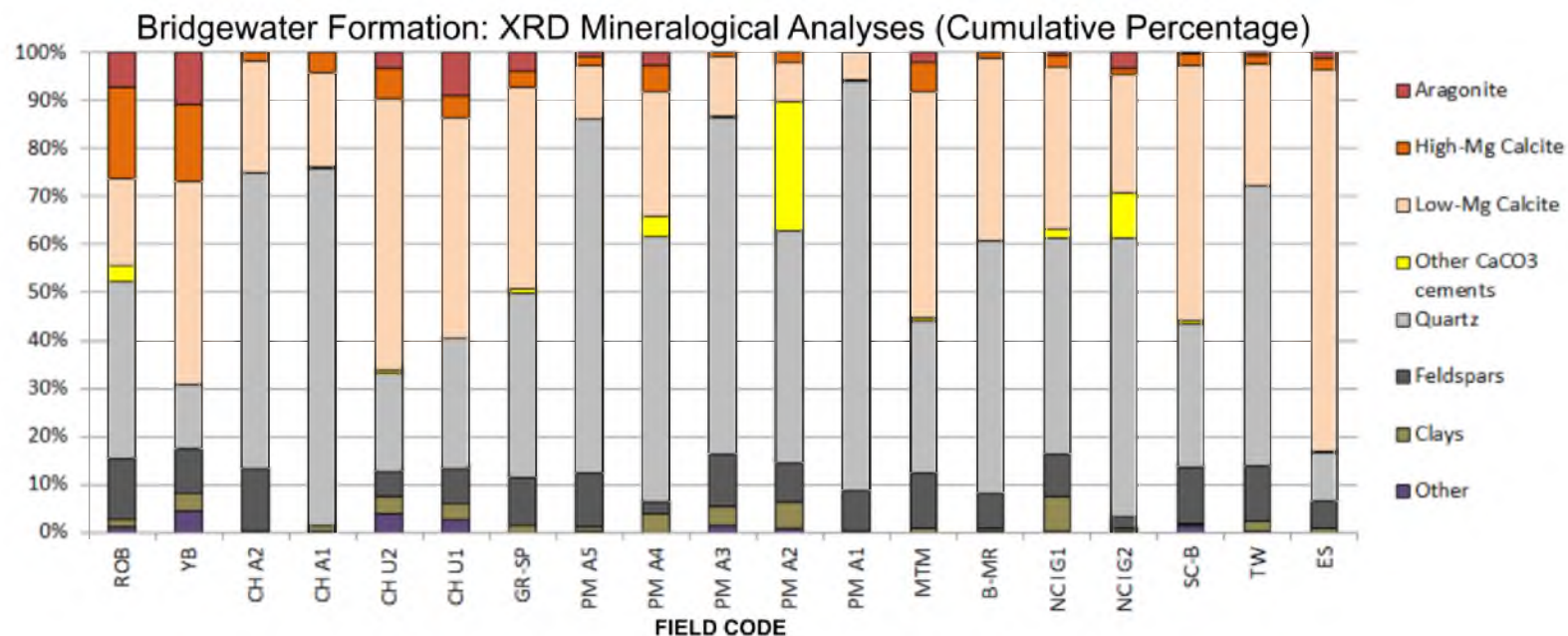
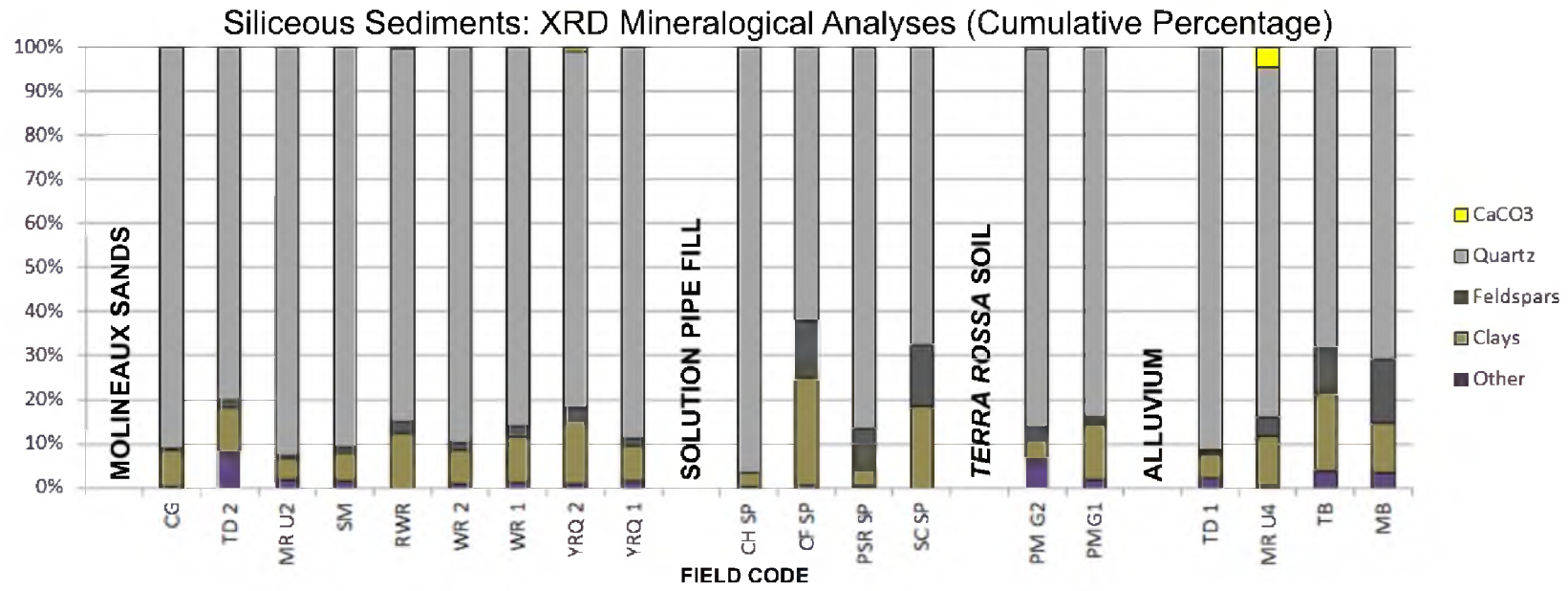


Table A3.2: Summary of all XRD results for siliceous sand sedimentary successions. Field codes correspond to x-axis in below bar graphs. Table A3.2 continues on the following page.

Field Sites	Field Code	Locality	Calcium Carbonate Cements	Quartz	Feldspar Group				Clays			Other		
					Albite	Labradorite	Orthoclase	Microcline	Kaolin	Illite	Chlorite	Sodium Chloride	Gypsum	Pyrite
Molineaux Sands														
Carcuma	CG	Inland		91.2	-	-	-	0.1	4.6	3.5	0.5	-	0.1	-
The Drain Recent	TD 2	Goolwa		80.2	0.1	-	-	1.4	3.9	2.1	4.4	7.9	-	-
Myrtlegrove Unit 2	MR U2	Currency Creek		92.6	0.2	-	0.2	0.5	2.3	1.5	0.8	1.4	0.1	0.4
Sturt Monument	SM	Hindmarsh Island		90.8	-	-	0.3	0.9	4.6	1.3	0.6	1.3	0.1	-
Riverside Recent	RWR	Hindmarsh Island	0.3 High-Mg Calcite	84.8	0.2	-	0.3	2.1	7.7	4.4	0.2	-	-	-
Woolshed Recent	WR 2	SE Lake Albert		89.6	-	0.1	0.6	1	5.3	2.4	0.2	0.7	-	-
Woolshed Glacial	WR 1	SE Lake Albert		85.9	0.4	0.7	1.4	-	5.4	3.8	1.3	1.1	-	-
Yarindale Recent	YRQ 2	SE Lake Albert	0.9 Low-Mg Calcite	81	0.5	0.8	2.1	-	7.6	4.6	1.9	0.8	-	-
Yarindale Glacial	YRQ 1	SE Lake Albert		88.2	-	-	0.5	1	5.1	2.3	0.6	1.4	-	-
Solution Pipes														
Chart House	CH SP	Goolwa		96.5	-	-	-	-	0.5	2.8	-	0.1	-	-
Cheese Factory	CF SP	Hindmarsh Island		62	-	4.2	4.3	4.5	5.8	5	13.7	-	-	0.5
Point Sturt Road	PSR SP	Sturt Peninsula		86.3	0.9	0.8	3.3	4.3	1	2.9	-	0.1	-	-
South Coonalpyn	SC SP	Inland		67.2	1.3	1.2	5.4	5.7	5.1	9.6	3.7	-	-	-

Table A3.2: Summary of all XRD results for siliceous sand sedimentary successions. Field codes correspond to x-axis in below bar graphs.

Field Sites	Field Code	Locality	Calcium Carbonate Cements	Quartz	Feldspar Group				Clays			Other		
					Albite	Labradorite	Orthoclase	Microcline	Kaolin	Illite	Chlorite	Sodium Chloride	Gypsum	Pyrite
<i>Terra Rossa</i>														
Point McLeay G2	PM G2	Point McLeay	0.5 Aragonite 0.6 High-Mg Calcite	85	0.2	-	2.6	0.1	0.5	1.2	2.9	5.1	0.2	0.9
Point McLeay G1	PMG1	Point McLeay		83.5	-	-	0.4	1.6	7.6	4	1.1	1.7	-	-
<i>Alluvium</i>														
The Drain Glacial	TD 1	Goolwa		92.3	-	-	0.8	-	2.6	2.8	0.2	1.3	0.1	0.8
Myrtlegrove Road	MR U4	Currency Creek	3.6 Low-Mg Calcite 0.5 High-Mg Calcite 0.2 Siderite	79.7	-	1.9	0.5	1.7	4.1	7.3	-	0.1	0.4	-
Tailem Bend	TB	Tailem Bend		68.1	0.9	1.7	4.3	3.4	4.3	10	3.6	0.9	2.8	-
Murray Bridge	MB	Murray Bridge		70.8	-	-	14.4	0.2	5.6	3.2	2.3	2.6	-	0.9



APPENDIX 4:
Amino Acid Racemisation
analytical methods

A4.1 Introduction

This appendix outlines the amino acid racemisation analytical methods for the preparation and analysis of mollusc shell, whole-rock and individual foraminifera. This outline will begin with the mollusc shell procedure and describe any variations to that procedure for whole-rock and individual foraminifers in the following sections.

A4.2 Mollusc Shell

Cleaning

Mollusc shells were mechanically cleaned the shell using a dentist drill to remove any adhering cements, sediments or algae. Cleaning by the dentist drill removed the outer layer of the shell where foreign matter was likely to reside. In order to reduce the potential of induced racemisation by this process, the dentist drill and sample were periodically submerged in a water bath to keep the sample wet and to keep temperature of the sample and drill low. Following cleaning, shell could be cut into smaller sub-samples for analyses. Bivalve shells were commonly sub-sampled unless they were juveniles or under 100 mg.

The gastropod shells of *Coxiella striata* and *Hydrococcus brazieri* were too small (<10 mg) and delicate for cleaning by the dentist drill. Any adhering sediments were removed with a probe and the shell could be broken down to release any trapped sediments.

Following mechanical cleaning, individual samples were placed in separate sterile test tubes and covered with distilled water. The test tubes were then placed in an ultrasonic bath for ten minutes to remove any adhering cements. Samples were then flushed with distilled water at least three times to remove any disaggregated sediment. Samples were then allowed to dry in plastic trays.

Acid Etch

Following cleaning and drying samples were subject to an acid etch to remove non-indigenous amino acids or leached material, ~33% of the sample mass. Samples were weighed to the nearest mg and placed into separate sterile test tubes and covered

with distilled water. To this, 0.0033 mL of 2 M hydrochloric acid (HCl) for every 1 mg of sample mass was added. For example, a sample weighing 100 mg would require:

$$2 \text{ M HCl} = 0.0033 \text{ mL} \times 100 \text{ mg} = 0.330 \text{ mL (330 } \mu\text{L of 2 M HCl)}$$

The sample was left in the acid etch until the acid-carbonate reaction was no longer visible or at most, twenty minutes to prevent excessive or complete dissolution. Following the acid etch the sample was washed 3 to 5 times to with distilled water to remove any acid.

Samples were then covered by 3% hydrogen peroxide (H₂O₂) (using a Pasteur pipette) and left to soak for a minimum of two hours to remove any non-indigenous organic matter. The peroxide soak was the final step in the cleaning process and samples were then considered sterile. Samples were then rinsed 3 to 5 times by Millipore water, placed in sterile plastic trays, covered by sterile tissue (Kimwipes) to prevent contamination and left to dry.

Note, for the bleaching experiment (section 5.2.3.2), the peroxide soak was substituted for with a 24 hour bleach soak.

Hydrolysis

Following drying samples were again weighed in preparation for hydrolysis and placed into sterile 4 mL vials. Hydrolysis of samples was achieved by dissolving the sample in 8 M HCl and placing the resulting 7 M HCl solution into a 110°C oven for 22 hours. The determination of the appropriate amount of 8 M HCl to add is also. For example, a sample weighed 100 mg following the 2 M HCl etch would require:

$$0.02 \text{ mL} \times 100 \text{ mg} = 2 \text{ mL (2000 } \mu\text{L of 8 M HCl)}$$

The 8 M HCl was added to the 4 mL vials by Pasteur pipette and samples were allowed to dissolve completely. Samples were dissolved and hydrolysed in the same vials to minimise loss and contamination. Prior to placement in the oven, the 4 mL vials were flushed with N₂ for approximately 15 to 20 seconds, to prevent oxidation of the protein residue in the acid solution, and then securely capped. The caps were tightened following the first 30 minutes in the oven.

The samples were removed from the oven following 22 hours and allowed to cool. A 50 μ L sub-sample was drawn and placed into a 2 mL vial and dried in a vacuum desiccator. After complete desiccation the samples were rehydrated to 50 mL by a rehydration solution of 0.01 mM L-homoarginine + 0.01 M HCl and 0.77 mM sodium azide. The L-homoarginine is the internal standard by which the concentration of amino acids can be determined. The samples were capped with septa and mixed thoroughly on a vortex mixer. The samples were then fully prepared for analysis in the RP-HPLC Autosampler.

Note, free amino acid sub-samples (50 μ L) were taken from the 4 mL vials following dissolution but prior to oven hydrolysis and placed into 2 mL vials for vacuum desiccation before analysis in the RP-HPLC Autosampler.

A4.2 Whole-rock

Depending upon the consolidation of the whole-rock sample, the samples could require the grinding down by use of mortar and pestle to separate grains. This was done in gentle manner so as to not grind or break down the skeletal carbonate grain contained within the sample. The sample was then sieved with the 250 – 500 μ m used for analysis.

Cleaning

Samples were then placed in a beaker with water and rinsed at least five times. The sample was again placed under water and into the ultrasonic bath for 10 minutes and rinsed again. This was done to remove any silt, clay or adhering organic material within the sample. Samples were then placed in plastic trays to dry.

Whole-rock analysis required the additional step to mollusc shell preparation of determining the percentage of calcium carbonate within the whole-rock sample for accurate determination of the appropriate quantity of 2 M and 8 M HCl necessary for the acid etch and hydrolysis. The percentage of calcium carbonate was determined by placing a measured weight of the whole-rock sample (250 – 500 μ m) in a beaker and adding enough 8 M HCl to dissolve all carbonate; this was judged to be complete when the acid-carbonate reaction stopped. The acid was washed off by rinsing with water 3 to

5 times. The sample was then dried in the oven at 110°C before the sample was reweighed. The difference in mass (net loss) was interpreted as reflecting the carbonate content of the sample.

Stoichiometric calculations

The equations to determine the appropriate quantity of 2 M and 8 M HCl necessary for the acid etch and hydrolysis differed slightly for whole-rock analysis by taking into account the percentage of calcium carbonate.

Acid etch example:

$$2 \text{ M HCl} = [(\text{initial mass of sample} \times \% \text{ calcium carbonate of sample}) \times 0.0033] \times 1000$$

If a sample weighed 100 mg with a calcium carbonate content of 90% then,

$$2 \text{ M HCl} = [(100 \times .9) \times 0.0033] \times 1000 = 297 \text{ } \mu\text{L of 2 M HCl}$$

Hydrolysis example:

$$8 \text{ M HCl} = [(\text{mass of sample following acid etch} \times \% \text{ calcium carbonate of sample}) \times 0.02] \times 1000$$

If a sample weighed 100 mg following the acid etch with a calcium carbonate content of 90% then,

$$8 \text{ M HCl} = [(100 \times .9) \times 0.02] \times 1000 = 1800 \text{ } \mu\text{L of 8 M HCl}$$

Filtering

Whole-rock samples were processed in a similar manner to mollusc shell through acid etch and hydrolysis. However, following hydrolysis and before 50 μL sub-sampling for vacuum desiccation, each whole-rock sample was filtered to remove any non-carbonate portion of the sample that had not dissolved. Following this step, processing was the same as for mollusc shell.

Also, whole-rock samples with a low percentage of calcium carbonate were sub-sampled at a higher volume than 50 μL before desiccation but rehydrated to 50 μL in order to increase the concentration of amino acids within sample for RP-HPLC analysis.

Whole-rock samples with less than 50% calcium carbonate were sub-sampled at 100 μL and samples with less than 25% calcium carbonate were sub-sampled at 150 μL .

A4.3 Foraminifer

Processing of foraminifers was generally followed the process outlined for mollusc shell but due to the small size of individual tests, some steps were omitted.

Foraminifers could not be mechanically cleaned. Following hand-picking of foraminifers from sediment samples, they were placed within a test tube, covered with water and placed in the ultrasonic bath for 10 minutes.

The samples were not subjected to the 2 M acid etch as they were likely to be dissolved and were too light for weighing. Instead, the samples were placed in a test tube and soaked in 3% H_2O_2 for 2 hours. The samples were flushed with water and left to dry in plastic trays.

Individual tests were placed in 0.1 mL micro-vials in preparation for hydrolysis. As it was not possible to weigh the individual foraminifers accurately, each sample was dissolved using 5 μL of high purity 6 M HCl. Processing continued as with mollusc shell through desiccation. Samples were rehydrated by 5 μL of L-homoarginine.

Sub-sampling of foraminifers for free amino acids was not possible due to their small mass.